A multiproxy approach to studying lake ecosystems in the Mesozoic

der Naturwissenschaftlichen Fakultät

der Friedrich-Alexander-Universität

Erlangen-Nürnberg

zur

Erlangung des Doktorgrades Dr. rer. nat.

vorgelegt von

Manja Hethke

aus Greifswald

A multiproxy approach to studying lake ecosystems in the Mesozoic

Rekonstruktion mesozoischer Seeökosysteme: Ein Multiproxyansatz

der Naturwissenschaftlichen Fakultät

der Friedrich-Alexander-Universität

Erlangen-Nürnberg

zur

Erlangung des Doktorgrades Dr. rer. nat.

vorgelegt von

Manja Hethke

aus Greifswald

Als Dissertation genehmigt

von der Naturwissenschaftlichen Fakultät

der Friedrich-Alexander-Universität Erlangen-Nürnberg

Tag der mündlichen Prüfung: 11.12.2014

Vorsitzender des Promotionsorgans: Prof. Dr. Jörn Wilms

Gutachter: Prof. Dr. Franz T. Fürsich

Prof. Dr. Alexander Nützel

Abstract

The lake sediments of the Barremian to Aptian Yixian Formation of western Liaoning, China, have received worldwide attention for their outstanding fossil preservation and evolutionary significance. Previous work on this Mesozoic fossillagerstätte has centred on feathered dinosaurs, early birds, and early angiosperms. However, the physico-chemical conditions that led to its formation and the response of palaeocommunities to varying environmental conditions, necessary to establish it as an important window on Mesozoic lake evolution, are poorly understood. The state-of-the-art palaeoenvironmental interpretation of the so-called Lake Sihetun is a shallow, eutrophic setting governed by seasonal anoxia and synsedimentary volcanism.

Considering the proposed lake duration of 0.7 to 1.5 Ma, it is hypothesized that the lake underwent several evolutionary phases in response to climate change and ecological disturbances, each marked by distinct palaeoenvironmental conditions. The difficulty of reconstructing the ecosystem evolution of Lake Sihetun results from the general absence of seasonally-responsive marker organisms, which is characteristic of Mesozoic lake deposits in general. The lake is, however, characterized by an abundance of clam shrimps, branchiopod crustaceans of the suborder Spinicaudata, which experienced a diversification during Mesozoic times and a characteristic decline during the Cenozoic. The main goal of this thesis is to establish this group as one of the most important proxies for the reconstruction of Mesozoic lake ecosystems. This can only be achieved by a highly resolved study of the lake development, a comprehensive taxonomic revision, multiple morphometric studies of its spinicaudatan fauna, and a palaeocommunity analysis.

Lake evolution has been subdivided into four developmental phases. While phases 1 and 4 mark the formation and the eventual siltation of the lake, respectively, phases 2 and 3 represent the bulk of the time of its existence. The latter are in focus due to their excellent fossil preservation. The sedimentological evidence points to a change in climate from dry to humid between both phases, which is accompanied by a deepening of lake waters and an increased fluvial influx at the onset of Phase 3. Rare chrysophycean cyst accumulations in Phase-2 sediments indicate annual sedimentation (varves), and they represent the earliest unambiguous appearance of this seasonally-responsive algal group in lake deposits. The redox state of the lake has been resolved using pyrite framboid size distributions. Phase 2 was governed by dysoxic bottom waters with spells of anoxia. The lake was therefore characterized by mainly holomictic conditions that episodically alternated with meromictic intervals. Spatial variations in redox state were pronounced. Conversely, Phase 3 was marked by oxic conditions and an entirely holomictic lake.

Clam-shrimp taxonomy of eastern Asia suffers from extreme oversplitting as phenotypic and ontogenetic variation has repeatedly been neglected. We herein comprehensively revise the existing taxonomic framework for Lake Sihetun by integrating all representatives of ontogenetic stages and sexes. During one study that investigates the taxonomic validity of the ten alleged clam-shrimp species occurring within the Yixian Formation of Western Liaoning, it could be demonstrated that clam-shrimp diversity was considerably overestimated. The number of valid species has been reduced to five, potentially even four.

The key to pinpointing the clam-shrimp species governing Lake Sihetun has been the identification of size and shape diversity within the dominating species (*Eosestheria middendorfii*). This marks the first morphometric study on clam shrimps that takes allometric relationships among characters into account. The three main objectives, which have been investigated in two interlinked studies, have been (1) to inspect possible sexual dimorphism in adult carapaces, (2) to identify ontogenetic and phenotypic variation within *E. middendorfii*, and (3) to estimate the influence of environmental parameters on carapace shape.

(1) Clam shrimps rival many other animals regarding the diversity of their sexual systems, which ranges from obligate sexual reproduction over self-fertilization with the occasional presence of males to unisexuality, rendering the Spinicaudata a model clade for the study of reproductive system evolution. Obligate sexuality ("dioecy") is the inferred reproductive system for *Eosestheria middendorfii*. Sexual dimorphism accounts for about 10% of the adult shape variation. Carapace shape variation resulting from malformation and deformation is more pronounced than the underlying sexual dimorphism. A discriminant function that uses linear measurements has been proposed for the classification of adult individuals of *E. middendorfii* as female or male.

(2) Numerous horizons of Phase 3 yield very small clam shrimps that have barely completed their naupliar phase, rendering them unidentifiable with existing methods. The analysis of ontogenetic shape variation shows that *Eosestheria middendorfii* is a strongly allometric species. Importantly, all individuals (juveniles and adults) fit a single allometric model (no divergence in the ontogenetic trajectory), supporting the presence of a single species within Lake Sihetun. This identification of growth-related variation has led to an emendation of the species diagnosis of *E. middendorfii*.

(3) Subsequently, ecophenotypic variation in *Eosestheria middendorfii* has been analysed, using an approach that minimizes ontogenetic variation. Three distinct phenotypic morphogroups corresponding to different lake phases and excavation areas have been recognized, implying that palaeoenvironmental changes had a great effect on carapace size and shape. Ecophenotypic differences are most pronounced between phases 2 and 3 of Lake Sihetun.

In addition to morphological disparity, the mineralogical and microstructural cuticle preservation of clam shrimps is introduced as a proxy for palaeoenvironmental conditions. Biominerals have been confirmed within two of the three extant spinicaudatan families: Cyzicidae build in calcium phosphate biominerals and possibly calcite. Leptestheriidae biomineralize with calcite, and carapaces of the Limnadiidae are either hardly mineralized or they lack biominerals. Calcium phosphate biomineralization is a prerequisite for fluorapatite preservation, which is widespread in fossil clam shrimps. Important additional fossil minerals are carbon residues, dolomite, quartz, and silicates, which carry environmental instead of genetic signals. Calcite has not been detected in fossil material. Excellent microstructure preservation implies oxygen deficient, alkaline lake waters (Phase 2). In turn, oxygenated conditions are identified by an amalgamation of growth increments and the precipitation of silica and silicates.

In the final study, a partial response of lake communities to the proposed abiotic changes in the palaeoenvironment between phases 2 and 3 has been demonstrated. The studied section of Lake Sihetun yields three arthropod-dominated associations as well as two assemblages. Response curves to environmental gradients indicate that components of associations 1 and 2 (*Eosestheria middendorfii* and mayfly larvae) were generalists, explaining their presence in both phases 2 and 3. In turn, the so-called Transitional Fauna (Association 3 and the two assemblages) is dominated by a more specialized fauna that was restricted to the early Phase 3, which was marked by comparatively deep waters. Carapace size distributions point to environmentally-induced mass mortality events of juvenile clam shrimps triggered by lethally high temperatures in shallower waters of the late Phase 3 (Association 1). In contrast, clam shrimps of most other horizons died due to senescence instead of ecological disturbance.

In summary, the combination of sedimentary and biotic proxies shows that Lake Sihetun was governed by an oxygen-controlled Phase 2 and a temperature-controlled Phase 3. The dioecious *Eosestheria middendorfii* was a generalist adapted to life in permanent waters. Its high tolerance towards environmental gradients is expressed in a pronounced ecophenotypic variability. This indicates that careful analyses of carapace size and shape in combination with sedimentological proxies and a palaeocommunity analysis can establish clam shrimps as important marker organisms for ecosystem changes in Mesozoic lakes.

Zusammenfassung

Die Seesedimente der Yixian Formation (Barreme bis Apt) aus West-Liaoning, China, erlangten weltweit Bekanntheit als eine der wichtigsten mesozoischen Fossillagerstätten, welche Einblick in die Evolution gefiederter Dinosaurier und früher Vögel erlaubt. Im Gegensatz zu der terrestrischen Fauna sind die physikalisch-chemischen Bedingungen des Sees sowie die Reaktionen der aquatischen Fauna auf schwankende Umweltbedingungen bislang wenig erforscht. Der sogenannte Sihetunsee wurde bisher als flacher, eutrophischer See beschrieben, welcher durch Sauerstoffarmut während der Sommerstagnation und synsedimentärem Vulkanismus geprägt wurde.

In Anbetracht seiner verhältnismäßig langen Existenz (0,7 bis 1,5 Ma) kann angenommen werden, dass der See auf größere Ereignisse wie Klimawandel oder ökologische Einschnitte durch vulkanische Aktivität reagierte und daher mehrere Entwicklungsphasen durchlief, die durch spezifische Paläoumweltbedingungen gekennzeichnet waren. Schwierigkeiten in der Ökosystemrekonstruktion des Sihetunsees ergaben sich aus dem Fehlen von Organismen, die als jahreszeitliche Indikatoren fungieren, was generell für mesozoische Seeablagerungen gilt. Die bei Weitem individuenreichste Fossilgruppe des Sihetunsees ist die der Spinicaudata, branchiopode Krebstiere, welche im Vergleich zum Känozoikum durch eine hohe Diversität während des Mesozoikums gekennzeichnet war. Das Ziel dieser Arbeit ist es die Spinicaudata als einen der wichtigsten Proxies für die Rekonstruktion mesozoischer Seeökosysteme zu etablieren. Dies kann nur durch die Kombination von hochauflösender Betrachtung der Seeentwicklung, umfassender taxonomischer Revision und morphometrischer Analyse der Spinicaudaten, sowie der Untersuchung der Entwicklung benthischer Faunenvergesellschaftungen geschehen.

Die Evolution des Sihetunsees weist vier Entwicklungsphasen auf. Phasen 1 und 4 markieren die Entstehung und Verlandung des Sees. Der Großteil der Seeentwicklung fand jedoch während der Phasen 2 und 3 statt, deren Paläomilieu unter anderem Weichteilerhaltung begünstigte. Der Übergang von Phase 2 zu Phase 3 wurde durch einen Klimawandel von trocken zu humid hervorgerufen, was zu einer Vertiefung des Sees und vermehrtem fluviatilen Eintrag führte. In Ablagerungen aus Phase 2 gelang es vereinzelt Varven nachzuweisen, welche durch Zysten goldbrauner Algen (Herbstlagen) angezeigt wurden. Diese stellen die frühesten eindeutigen Vorkommen dieser Fossilgruppe im Süßwasser dar. Die Sauerstoffbedingungen im See wurden mittels Größenverteilungen von Pyritframboedern untersucht. Das Hypolimnion der Phase 2 war generell durch sauerstoffarme Verhältnisse gekennzeichnet, welche episodisch mit sauerstofffreien Bedingungen abgewechselten. Dementsprechend war der See während dieser Phase zumeist holomiktisch; temporär kam es zur Etablierung eines sauerstofffreien, teils euxinischen Tiefenwasserbereichs (Meromixis). Hingegen war der See während der Phase 3 ausnahmslos durch oxische Bedingungen am Seeboden gekennzeichnet. Jahreszeitliche Stagnation führte zwar zur Abnahme des Sauerstoffgehalts, ermöglichte jedoch die Besiedlung durch an niedrige Sauerstoffbedingungen angepasste Seeorganismen, vornehmlich Spinicaudaten.

Die Taxonomie der fossilen Spinicaudaten Ostasiens ist durch eine hohe Anzahl künstlicher Arten geprägt, was von der Beschreibung verschiedener ontogenetischer Stadien und Erhaltungszustände sowie von einer hohen morphologischen Variabilität herrührt. Die Revision der Artzusammensetzung der Yixian Formation West-Liaonings ergab, dass die Region durch eine weitaus geringere Spinicaudatendiversität gekennzeichnet war als bisher angenommen. Die Zahl der gültigen Taxa konnte von zehn auf fünf reduziert werden, potentiell sogar auf vier sobald das entsprechende Typusmaterial zur Verfügung steht. Der Sihetunsee wird von *Eosestheria middendorfii* (Jones, 1862) geprägt.

Der Schlüssel zur Erforschung des Potentials von *Eosestheria middendorfii* als Paläoumweltindikator liegt in der morphometrischen Analyse seiner Carapaxmerkmale, welche drei Fragestellungen folgt. Es wurde untersucht, (1) ob *E. middendorfii* einen Sexualdimorphismus aufweist, (2) ob ontogenetische und phänotypische Variabilität eingegrenzt werden können, und (3) ob und in welchem Ausmaß eine Änderung abiotischer Umweltfaktoren die Carapaxmorphologie beeinträchtigte.

(1) Rezente Spinicaudatenarten sind durch eine Vielfalt von Fortpflanzungsstrategien gekennzeichnet, was sie zu einer Modellgruppe für die Evolution von Fortpflanzungssystemen macht. Sexualdimorphismus bestimmt etwa 10% der morphologischen Variabilität erwachsener Individuen von *Eosestheria middendorfii*, wobei Carapaxfehlbildungen und ab-

lagerungsbedingte Verformungen eine wesentlich höhere Variabilität bedingen. Geschlechter sind zahlenmäßig gleich unter den Individuen verteilt, weshalb sich diese Art geschlechtlich über Fremdbefruchtung fortpflanzte.

(2) Zahlreiche Horizonte der Phase 3 weisen juvenile Individuen auf, welche gerade erst ihr Naupliusstadium durchlaufen haben und mit etablierten Mitteln nicht bestimmbar sind. *Eosestheria middendorfii* weist eine starke Wachstumsallometrie auf und juvenile sowie adulte Spinicaudaten des Sihetunsees können einem einzigen allometrischen Modell zugeordnet werden (einfache Allometrie). Der Sihetunsee wurde offenbar von nur einer Spinicaudatenart dominiert.

(3) Morphologische Variabilität hervorgerufen durch Schwankungen in den Paläoumweltbedingungen wurde mittels einer Methode untersucht, welche den Einfluss der ontogenetischen Variabilität minimiert. Drei morphologische Phänotypen konnten unterschieden werden, die jeweils den Phasen 2 und 3 der Seeentwicklung sowie verschiedenen Lokalitäten des Sees entsprechen.

Zusätzlich zu morphologischen Merkmalen spiegelt die mineralogische und mikrostrukturelle Erhaltung des Carapax die Paläoumweltbedingungen wider. Im Vordergrund der Untersuchungen zur Fossilisation stand die Fragestellung welche Biominerale die drei rezenten Familien der Spinicaudata einbauen. Cyzicidae biomineralisieren mit Calciumphosphat und möglicherweise Kalzit. Leptestheriidae bauen Kalzit ein, während in Limnadiidae keine Biominerale festgestellt wurden. Das Auftreten von Calciumphosphaten scheint eine Voraussetzung für die Kristallisation von Fluorapatit während der Fossilisation zu sein, welcher häufig in fossilen Carapaces zu finden ist. Kalzit konnte in fossilen Spinicaudaten nicht nachgewiesen werden. Stattdessen kommen je nach Ablagerungsmilieu und Familie wahlweise kohlige Rückstände, Dolomit, Quarz, und Silikate vor. Die detaillierte Erhaltung der einzelnen Häutungsstadien in der Carapaxcuticula setzt Sauerstoffarmut sowie eine erhöhte Alkalinität voraus (Phase 2), während ein sauerstoffgesättigtes Hypolimnion zur Auflösung der Carapaxmikrostruktur sowie der Bildung von Sekundärmineralen führt (Phase 3).

In einer abschließenden Studie wird gezeigt, dass die benthischen Faunen des Sihetunsees nur teilweise die Veränderungen der Paläoumweltbedingungen zwischen Phase 2 und Phase 3 widerspiegeln. In der untersuchten Grabung ließen sich drei Assoziationen und zwei Vergesellschaftungen benthischer Faunen dokumentieren. Dominierende Arten der Assoziationen 1 und 2 (*Eosestheria middendorfii* und Eintagsfliegenlarven) waren tolerant gegenüber Umweltschwankungen, was ihr Vorkommen sowohl in Phase 2 als auch Phase 3 erklärt. Demgegenüber wurde die sogenannte Übergangsfauna (Assoziation 3 und beide Vergesellschaftungen) von spezialisierteren Faunen dominiert, welche ausschließlich in der frühen Phase 3 vorkamen (Oligochaeten und Ruderwanzen), die durch eine Vertiefung des Sees bestimmt war. Carapaxgrößenverteilungen juveniler Individuen aus Phase 3 zeigen Massensterbeereignisse an, welche durch hohe Temperaturen im flachen Wasser während der Sommerstagnation ausgelöst wurden. Hingegen liefern adulte Individuen, welche die Phase 2 sowie die Übergangsfauna prägten, keinen Hinweis auf Spinicaudaten-Massensterbeereignisse. *Eosestheria middendorfii* war besonders tolerant gegenüber Sauerstoffarmut.

Zusammenfassend war der Sihetunsee von Sauerstoffarmut (Phase 2) und kritisch hohen Temperaturen (Phase 3) geprägt. Die hohe Toleranz von *Eosestheria middendorfii* gegenüber abiotischen Umweltschwankungen spiegelte sich in einer hohen morphologischen Variabilität wider. Verschiedene Morphotypen können spezifischen Umweltbedingungen zugeordnet werden. Dies zeigt, dass die Spinicaudata durch die Analyse der morphologischen Variabilität in Kombination mit sedimentologischen Proxies und Faunenvergesellschaftungen wichtige Indikatoren für die Rekonstruktion mesozoischer Seeökosysteme sind.

Statement

I certify that this thesis entitled

"A multiproxy approach to studying lake ecosystems in the Mesozoic"

has not been previously submitted for any degree, nor has it been submitted as part of the requirements for a degree to any other university or institution other than the Friedrich-Alexander-Universität Erlangen-Nürnberg.

It is a new and original piece of research that has been written by me, Manja Hethke. Any help that I have received during the preparation of this work has been appropriately acknowledged.

I also certify that all sources of information and literature used are specified in this thesis.

This thesis contains material that has been published or that is in preparation for submission in peer-reviewed journals. Already published works will be referenced as "Chapter 1" and "Chapter 2" in this thesis for reasons of consistency. Each chapter represents an independent study and all are linked by the main theme of this thesis stated above. They have been prepared in collaboration with colleagues, as follows:

Chapter 1: "Seasonal to sub-seasonal palaeoenvironmental changes in Lake Sihetun (Lower Cretaceous Yixian Formation, NE China)" has been published in *International Journal of Earth Sciences* in 2013. My contribution to this paper consisted of field work, sample preparation, analytical work, data interpretation, and writing, resulting in a total contribution of 85%. (**Hethke, M.**, Fürsich, F.T., Jiang, B., Pan, Y. 2013. Seasonal to sub-seasonal palaeoenvironmental changes in Lake Sihetun (Lower Cretaceous Yixian Formation, NE China). – *International Journal of Earth Sciences* **102**: 351-378.)

The first chapter forms the "sister-publication" to Jiang et al. (2012), which does not form a separate chapter in this thesis: Jiang, B., Fürsich, F.T., **Hethke, M.** 2012. Depositional evolution of the Early Cretaceous Sihetun Lake and implications for regional climatic and volcanic history in western Liaoning, NE China. – *Sedimentary Geology* **257-260**: 31-44.

Chapter 2: "Oxygen deficiency in Lake Sihetun – Formation of the Lower Cretaceous Liaoning Fossillagerstätte (China)" has been published in *Journal of the Geological Society* in 2013. My contribution to this paper consisted of field work, sample preparation, thin-section microscopy, analytical work, data interpretation, and writing, resulting in a total contribution of 85%. (**Hethke, M.**, Fürsich, F.T., Jiang B., Klaus R. 2013. Oxygen deficiency in Lake Sihetun; formation of the Lower Cretaceous Liaoning Fossillagerstätte (China). – *Journal of the Geological Society, London* **170**: 817-831.)

Chapter 3: "Clam-shrimp biomineralization (Branchiopoda: Spinicaudata) and its implications for the classification of the group" has been prepared in collaboration with Carys Bennett, Leicester, Franz T. Fürsich, Erlangen, Baoyu Jiang, Nanjing, Frank Scholze, Freiberg, Sebastian Dittrich, Erlangen, and Jürgen Neubauer, Erlangen. Additional data have been provided by C. Bennett. My contribution to this manuscript consisted of sample preparation, dissection of extant clam shrimps, analytical work, data interpretation, and writing of the manuscript, resulting in a total contribution of 75%.

Chapter 4: "Taxonomic revision of Early Cretaceous clam shrimps from the Yixian Formation of western Liaoning" is based on the microscopy of type material of the collection of the Nanjing Institute of Geology and Palaeontology carried out by myself. Further contributions of mine were analytical work and writing, resulting in a total contribution of 95%. Valuable contributions to the discussion were received from Franz T. Fürsich and Baoyu Jiang.

Chapters 5-7: The remaining four chapters are products of the work group Hethke, Fürsich, and Jiang. Chapters 6 and 7 profited from discussions with Simon Schneider and Patrick Chellouche, respectively. Golda Schugmann was a great support during the data collection for Chapter 7. My contribution to either chapter consisted of field work, sample preparation, analytical work, data interpretation, and writing, resulting in estimated contributions of 90% for chapters 5 and 6 and 85% for chapter 7.

Erlangen, 27.10.2014

Manja Hethke

Acknowledgements

I would like to thank my supervisor *Franz T. Fürsich* for his support, scientific discussions, and patience. His enthusiasm for geology and palaeontology during field trips is contagious and it sparked my interest in palaeoecology.

The next person I am thanking is *Baoyu Jiang*, whose energy in the field as well as in front of the computer during discussions is unbeatable. The field campaigns we have carried out were mainly organized by him.

I am grateful to *Wolfgang Kießling* for funding me during my last year in Erlangen and for bringing new ideas to the Erlangen palaeontological group.

I thank *Alexander Nützel* for reviewing my thesis.

Special thanks go to *Michael Heinze*, who introduced fossils to me when I was a student back in Würzburg.

I thank my officemates *Patrick Chellouche*, who is an expert in thinking outside the box, and *Li Qi-jian*, who is always in good spirits and eager to help with translations and green tea.

A big thank you goes to *Christian Schulbert* for fixing my computer whenever something was wrong with it and for helping me with InDesign and countless other things.

Yazhuo Niu, *Larry*, and *Kerry* accompanied us during field work and were always very helpful when it came to finding Chinese literature.

I would also like to thank the technical staff of our institute. *Birgit Leipner-Mata* helped with the preparation of thin-sections. *Gabriele Schönberger*, *Cristina Krause*, and *Sabine Wolf* managed the bulk of my administrative workload.

I thank all of my fellow scientists of the Loewenichstraße, Fichtestraße, and the LUA for scientific discussions and general support.

Claire Mellish, curator at the Natural History Museum in London, coordinated the virtual loan of a syntype series I urgently needed to get my hands on. I thank *Andy Grass*, University of Iowa, for taking pictures of it. *Stefan Friedrich*, Bavarian State Collection of Zoology, assisted with the selection of modern clam shrimps as well as their dehydration and critical point drying. *Eckhard Mönnig*, Naturkunde-Museum Coburg, supplied Late Triassic material from the museum collection. He also toured me around his museum, which added up to a fine day.

There are many people who have spent vast amounts of time discussing my work; all are surpassed by *Simon Schneider*, who has always been content with setting aside his work for a good conversation. I also acknowledge valuable contributions to discussions by *Kenneth De Baets*, *Friedlinde Götz-Neunhoeffer*, *John Huntley*, *Edmund Jarzembowski*, *Patrick Orr*, *Jörg Schneider*, and *Frank Scholze*.

This last paragraph is reserved for my family and friends, whose support and love I can always count on. I deeply appreciate all the support from my parents *Helga* and *Uwe*, my sister *Katrin* and her husband *Jörg*, my nephew *Lennsen*, my grandparents *Linda* and *Georg* as well as *Ilse* and *Heinz*. I am very grateful to *Tobi*, who is always watching my back, and to his family *Sabine*, *Horst*, and *Gudrun*. My time in Erlangen would not have been the same without my friends: *Matze*'s barbecues, the hospitality of *Melli*, *Anne*, *Henning*, and *Habbe* during my last months of writing, *Ste*'s and *Larsi*'s good nature, and *Mona*'s evening-tea sessions, to name a few. There are a lot more people to list, whom I herewith invite to feel addressed.

Contents

Abbreviations

a	slope of a straight line
ACP	amorphous calcium phosphates
BSE	back-scattered electrons
C	concentrated framboids
CA	correspondence analysis
CVA	canonical variate analysis
E2-4	excavation sites 2 to 4
EDS	energy-dispersive X-ray spectroscopy
EMP	electron microprobe
En	endocuticle
Ep	epicuticle
EVA	software used for the qualitative phase analysis of XRD patterns
Ex	exocuticle
H'	Shannon-Wiener index
H_0	null hypothesis
JSG	Jianshangou (excavation site E4); horizons AP (base) – A (top)
LXBE	Erdaogou (excavation site E3); horizons S1 (base) – A (top)
M	matrix framboids
MANOVA	multivariate analysis of variance
Mf 1-6	microfacies 1-6
n	number of observations
NHM	Natural History Museum, London
OCP	octacalciumphosphate
p	probability under the assumption the null hypothesis is true
PC1, 2	first principal component, second principal component
PCA	principal component analysis
r^2	Pearson's coefficient squared

R	length of the resultant vector after vector addition
$\overline{R}$	mean resultant length
RMA	reduced major axis
S	species richness
SEM	scanning electron microscope
SE	secondary electrons
T^2	Hotelling's test statistic
U	test statistic for Rao's spacing test
WW	Wangjiawan section
XRD	X-ray diffraction
ZJG	Zhangjiagou (excavation site E2); horizons T (base) – A (top)

Carapace characteristics (Refer to Figs. 4.2, 6.6 for illustrations of the linear variables)

A – most anterior point of the valve
B – most posterior point of the valve
C – most ventral point of the valve
D – anterior extremity of the dorsal margin
E – posterior extremity of the dorsal margin
U – midpoint of the larval valve
a – vertical distance of A to A'
b – vertical distance of B to B'
c – horizontal distance of C to A"
Arr – horizontal distance of E to B'
Av – horizontal distance of D to A'
Ch – length of the dorsal margin
Cr – horizontal distance of U' to A'
L – valve length
H – valve height

Introduction to "A multiproxy approach to studying lake ecosystems in the Mesozoic"

*** This thesis is composed of seven chapters, each of which constitutes an independent work that either has already been published or will be submitted in the near future. All chapters are connected by the governing theme of this thesis, which is unravelling the biotic and abiotic components of the ancient **Mesozoic ecosystem** of **Lake Sihetun** of western Liaoning, China. The lake sediments accumulated in the Sihetun area as part of the volcanically influenced **Yixian Formation** (Barremian to Aptian; Chang et al., 2009) at a palaeolatitude of about 41.9°N (Enkin et al., 1992; Zhou et al., 2003; Amiot et al., 2011). They are represented by the Jianshangou Unit (Fig. I.1). ***

During the past 15 years the Yixian Formation has received worldwide attention for its outstanding fossil preservation and the evolutionary significance of its fossil riches (e.g., Barrett, 2000; Zhou et al., 2003; Wang and Zhou, 2006; Pan et al., 2013). Among other things, these fossils mark a major step towards understanding the link between dinosaurs and birds or the behaviour of early mammals. We are now aware of the extent to which dinosaurs were covered in feathers and how they evolved (Xu et al. 1999a, b, 2001), how the smallest known non-avian theropod dinosaur looked like (*Microraptor*; Xu et al., 2000), that the earliest known unquestionable tyrannosauroid bore proto-feathers (*Dilong*; Xu et al., 2004), and that Mesozoic mammals were not only prey to dinosaurs, but also fed on juvenile ceratopsians (*Repenomamus*; Hu et al., 2005). In addition, floral novelties are recorded in form of putative basal flowering plants (*Archaefructus*; Sun et al., 2002). The evolutionary significance of these fossil finds and their excellent preservation renders the Yixian Formation one of the most important **Mesozoic fossillagerstätten**.

It was only in 2006 that attention turned towards the lake's ecosystem and its general sedimentological evolution (Jiang and Sha, 2007; Fürsich et al., 2007; Jiang et al., 2011; Jiang et al., 2012; Pan et al., 2012; Hethke et al., 2013a, b). For this purpose, three excavations were carried out in the Sihetun area near Zhangjiagou (ZJG), Erdaogou (LXBE), and Jianshangou (JSG; Fig. I.1). The results of the first excavation (ZJG) indicate that Lake Sihetun suffered from seasonal hypoxia, which led to recurrent mass mortality events of the benthic fauna, followed by winter mixing and re-oxygenation (Fürsich et al., 2007). This hypothesis will be developed further in this thesis, based on data gathered from all three excavations.

Ecosystem reconstructions are generally complex and with progressive work on this thesis it became clear that there are profound differences in the analytical approaches to the ecosystems of Mesozoic and Cenozoic lakes. The trajectory of Lake Sihetun's ecosystem will be identified by a **multiproxy approach**, designed to delimit the major physicochemical processes and biotic changes that shaped this Mesozoic lake.

Of all the surface water on our planet, **lakes** hold less than 0.01 %, but they contain more than 98 % of the liquid surface freshwater (Hairston and Fussmann, 2014). Freshwater habitats are biodiversity hotspots; although they cover only 0.8 % of our planet's surface, about 9.5 % of all known extant animal species described dwell in such habitats (Balian et al., 2008; Strayer and Dudgeon, 2010). They are often marked by a high rate of **endemicity** with sometimes relatively little faunal exchange and overlap between two closely adjacent lakes (Albrecht and Wilke, 2008). Hence, they are model examples for speciation and the mechanisms that drive biodiversity.

Humans depend on lakes in many ways. They are sites for fisheries, recreation, or used as water sources for agricultural irrigation, industrial use, and for drinking water. However, the consequences of this increasing anthropogenic pressure – habitat degradation, pollution, and the introduction of alien species – are severely endangering lake biodiversity as well as ecosystem functioning (Strayer and Dudgeon, 2010). The International Union for Conservation of Nature and Natural Resources (IUCN) Red List of Threatened Species named the freshwater system the **most endangered** of all ecosystems (IUCN, 2013). One of the reasons for this is the high fragmentation of freshwater habitats that reduces the ability of species to migrate and potentially re-establish locally extinct populations. As a consequence, this fragmentation severely affects the ability of organisms to respond to climate change (Strayer and Dudgeon, 2010). Biodiversity

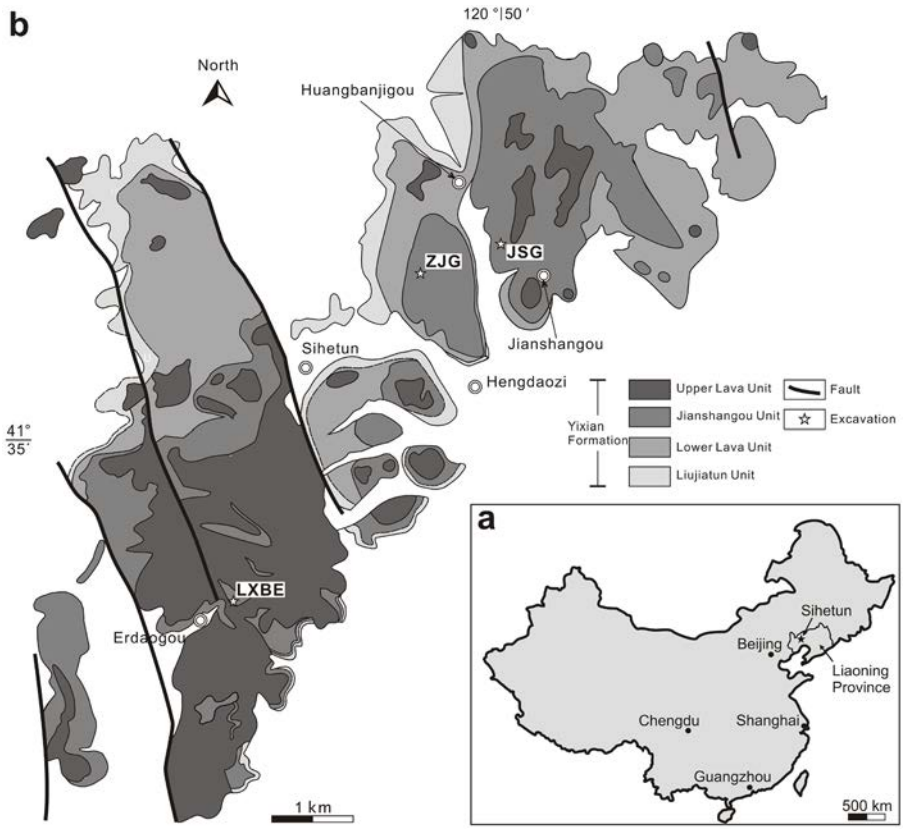

← **Fig. I.1.** (a) Location and (b) geological map of the Sihetun area. The Yixian Formation is subdivided into four units and the lake sediments are represented by the Jianshangou Unit (125.7 ± 2.6 Ma to 124.2 ± 2.5 Ma; Zhu et al. 2007), which is under- and overlain by lava units. The three excavations Jianshangou (JSG), Erdaogou (LXBE), and Zhangjiagou (ZJG) are marked. Modified after Jiang et al. (2011).

conservation areas are being set up worldwide and species are monitored by the IUCN to counteract this trend. Conservation action targets the **abiotic environment**, commonly habitat degradation, as well as **community aspects**, such as a reduction in the prey of an animal. Considering a community of organisms and its response to their abiotic environment is the fundamental concept behind the term "**ecosystem**" (Tansley, 1935; Townsend et al., 2008).

We need to understand how lake ecosystems evolved in deep time to anticipate ecological responses to future climate change or other anthropogenic influences. A lack of such knowledge can lead to the extinction of taxa. One unfortunate example is the Clear Lake Splittail, an endemic fish to the Clear Lake (California) and its watershed, which quickly declined after the introduction of an alien competing species. It has not been observed since 1970 and is now rated extinct by the IUCN (IUCN, 2013). In addition, modern geographic shifts of isotherms due to climate change entail complex community range shifts of several kilometres per decade (e.g., Parmesan and Yohe, 2003; Chen et al., 2011; Burrows et al., 2011; Poloczanska et al., 2013), as must have been the case for past climate-change events. Due to the insular nature of lake habitats, communities will not be able to freely establish populations elsewhere. This, in combination with high endemism, renders lake ecosystems especially **sensitive to extinction** (Strayer and Dudgeon, 2010). With respect to geological time scales most modern lakes are short-lived (postglacial) and typically marked by a non-diverse and non-endemic biota. There are, however, the so-called **ancient lakes** (not be confused with the term 'palaeolake'), which date back several million years and which are characterized by an unusual biodiversity and high levels of endemicity (Martens, 1997; Martens and Schön, 1999). Famous modern examples are Lake Kivu, Lake Tanganyika (both East Africa), Lake Ohrid (central Balkans), and Lake Baikal (Siberia). The latter is the oldest modern lake with an age of 25-30 Ma (Martens, 1997). The Early Cretaceous **Lake Sihetun** also falls into the ancient lake category with a proposed duration of 0.7 Ma to 1.5 Ma (Zhu et al., 2007; Wu et al., 2013). An existence over such long time intervals always leads to rather complex lake evolutions. For example, the onset of hydrothermal events and sub-lacustrine volcanism in Lake Kivu during mid-Holocene times has led to an impoverished modern fauna. The event is recorded by dramatic sedimentological and biotic changes (Haberyan and Hecky, 1987). This shows that modern lake conditions represent mere snapshots of their evolution. Climatic changes and other major forces, such as volcanism, are recorded by their sedi-

ments, which form one of the best continental archives for the high-resolution reconstruction of lake evolution. By tapping this archive we may be able to predict how existing ecosystems will behave in the future.

Lake Sihetun as a model Mesozoic ecosystem

Despite the huge attention the Yixian Formation has received (e.g., Xu et al. 1999a, b, 2000, 2001, 2004; Barrett, 2000; Sun et al., 2002; Zhou et al. 2003; Hu et al., 2005; Wang and Zhou, 2006), the evolution of the ecosystem of **Lake Sihetun** has not been fully resolved to date, owing to knowledge gaps in stratigraphy, microfacies, and in the taxonomic and ecological information on its most abundant faunal group, the Spinicaudata ("clam shrimps"; Fig. I.2). All of these aspects are tackled in this thesis, which is subdivided into **three main sections** for convenience sake. The first is dealing with the reconstruction of abiotic components by using sedimentological proxies (*chapters 1* and *2*), the second is concerned with fossilization processes and a taxonomic revision of clam shrimps (*chapters 3* and *4*) and the third is centering its attention on the biotic components by placing a strong focus on clam shrimps (*chapters 5-7*). The concluding *Chapter 7* examines how abiotic and biotic factors combine to determine the dynamics of clam-shrimp populations.

Generally, facets of lake ecosystems are closely connected to their thermal structure, their main habitats (pelagic, littoral, profundal, and benthic), the availability of nutrients for phytoplankton growth (oligo-, meso-, and eutrophic), and the trophic control of the food chain (Hairston and Fussmann, 2014). Lakes undergo a continuous evolution. Changes in primary productivity, for example, affect the food web in its total, and the replacement of an oligotrophic with a eutrophic benthic association represents a change of the lake morphometry, with the hypolimnion being successively obliterated by sediments (Deevey, 1984). **Four** main **developmental phases** have been identified for Lake Sihetun by Jiang et al. (2012): Water levels were fluctuating but gradually on the rise during Phase 1. Sediments of Phase 2 are subdivided into a marginal beach to nearshore facies and a suspension-derived lake floor facies, while turbiditic flows governed Phase 3. Eventually, Lake Sihetun silted up due to a prograding fan delta during Phase 4. With this characterization of the main developmental phases, Jiang et al. (2012) set the framework for further analyses.

One of the main tasks of a limnologist is the identification of **seasonalities**. While it is comparatively easy to identify **annual lamination** (*Chapter 1*) in Cenozoic lakes (e.g., Anderson and Dean, 1988; Lotter, 1989; Lindqvist and Lee, 2009), pre-Cenozoic varve reconstructions are tricky and rare (e.g., Anderson and Kirkland, 1960; Smith, 1986; Olsen, 1986; Kirkland, 2003; Andrews et al., 2010; Hethke et al., 2013a). Various combinations of varve components exist; perhaps best known are dark, diatom-rich winter and spring layers that alternate with light, calcitic summer layers (Lotter, 1989). In addition, annual lamination may be recognized with the help of diverse other proxies such as pollen, spores, leaves, insects, or even sunspot cycles (Anderson and Kirkland, 1960; Anderson and Dean, 1988; Andrews et al., 2010).

Even though pollen have been reported from the Jianshangou Unit in the Sihetun area, they are rare and poorly preserved (Li and Liu, 1999). The main reason for the difficulty to identify varves in Mesozoic lake deposits is undoubtedly the general **absence** of **marker organisms**, mainly seasonally-responsive phytoplankton such as diatoms (spring) or chrysophycean cysts (autumn). Diatoms became established in lakes during the Oligocene (Anderson and Dean, 1988) and freshwater chrysophycean cysts had been known only from the Cenozoic (Tappan, 1980), until our group (Hethke et al., 2013a) proved otherwise (*Chapter 1*). Therefore, most of the pre-Cenozoic varves described in the literature are chemical varves (carbonate-organic claystone couplets). But strictly speaking, chemical varves only signal climatic seasonality instead of annual depositions in the absence of marker organisms (Smith, 1986). The annual interpretation is only valid, when such couplets are successfully correlated with orbital cycles, as has been done for the early Mesozoic Newark Supergroup (Olsen, 1986). Furthermore, exclusively clastic modern varves are essentially driven by strongly seasonal precipitation (Anderson and Dean, 1988), which may or may not be annual. Therefore, in lack of marker organisms or clear orbital cycles, varve interpretations are unsubstantiated. The sedimentological analysis of *Chapter 1* aims at identifying seasonalities and the major physico-chemical properties of the lake.

One of the major factors put forward for larger-scale biotic crises is **oxygen depletion** (e.g., Bond et al., 2004; Wignall et al., 2010; *Chapter 2*). Lake Sihetun was afflicted by repeated mass mortality

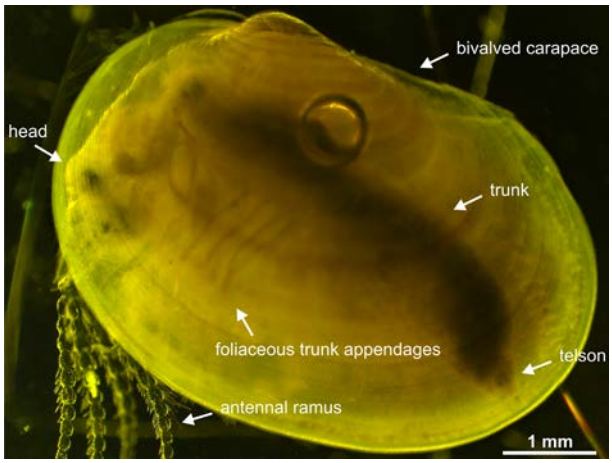

Fig. I.2. Example of a modern spinicaudatan ("clam shrimp", *Cyzicus*) that was raised in captive breeding in Erlangen. The main anatomical features are indicated. Spinicaudatan branchiopods are bivalved crustaceans that are taxonomically aligned with water fleas, fairy shrimps, and tadpole shrimps. "Conchostraca" as a taxonomic unit has been abandoned and Spinicaudata, along with the Laevicaudata, elevated to (sub-)ordinal level (Fryer, 1987; Martin and Davis, 2001; Braband et al., 2002). The antennae are modified to swimming organs, but they may also be used for burrowing (Tasch, 1969). Maxillae are represented by small lobes (Martin, 1992). Spinicaudatans own a maximum of 32 somites and according pairs of foliaceous trunk limbs, each equipped with a respiratory epipod. There is a U-shaped food groove between the gnathobases. Male specimens are marked by modified first and second trunk limbs, so-called claspers. Female limbs 9-11 bear filaments that carry eggs. Openings of the genital ducts are located at the base of the 11th pair of limbs in males as well as females (Martin, 1992). Clam shrimps are generally non-selective detritus feeders with adaptations to temporary freshwater environments, resulting in high-density and low-diversity communities (Webb, 1979; Orr and Briggs, 1999). However, there are exceptions to this stereotypic environmental interpretation.

events, which have frequently been attributed to synsedimentary volcanism and oxygen deficiency (e.g., Wang, 1999; Fürsich et al., 2007). However, the distinction between anoxia and dysoxia has important implications for the overall interpretation of **lake stratification** (holomictic versus meromictic). Oxygen depletion is recognized by the laminated sedimentation of Lake Sihetun (Fürsich et al., 2007), but both lower dysoxic and anoxic conditions may have generated them (Wignall and Hallam, 1991). Geochemical indices for the distinction of ancient redox levels, such as the degree of pyritization (Jones and Manning, 1994), have been considered. However, the sediments of Lake Sihetun are heavily weathered, which is why a method that is robust to alteration processes will have to serve as a proxy, such as size distributions of pyrite framboids (Wilkin et al., 1996, 1997; Wignall and Newton, 1998; Bond and Wignall, 2005; Wignall et al., 2010). In essence, *Chapter 2* is designed to identify palaeoredox conditions in space (excavations ZJG, LXBE, and JSG) and time (different horizons and lake phases) in order to predict the prominent lake type that governed Lake Sihetun during phases 2 and 3.

Clam shrimps as Mesozoic marker organisms

Because of the lack of marker organisms in Mesozoic lake deposits, the focus invariably shifts away from phytoplankton towards **clam shrimps** (**Spinicaudata**), mm- to cm-sized branchiopod crustaceans (Fig. I.2). The taxon Spinicaudata was declared a monophylum by Braband et al. (2002) based on nuclear and mitochondrial markers, rendering the historic taxon "Conchostraca" (Spinicaudata and Laevicaudata; Linder, 1945; Tasch, 1969) paraphyletic. The most obvious difference between the two traditional conchostracan groups is a lack of growth lines in laevicaudatan carapaces. The closest relatives to the spinicaudatans are in fact the Cladoceromorpha (Cladocera, "water fleas", and Cyclestherida), with whom the Spinicaudata form a monophylum (Braband et al., 2002).

Clam shrimps are by far the most abundant faunal component in Lake Sihetun and they are encountered along with malacostracan crustaceans and insects (Fürsich et al., 2007). Such low diversity, arthropod-dominated associations are a recurrent phenomenon in terrestrial freshwater deposits (Vannier et al., 2003). Notable arthropod-dominated faunas are the Late Carboniferous Montceau Lagerstätte (France; spinicaudatans, ostracods, isopods, syncarids, and insects; Vannier et al., 2003), the Late Carboniferous freshwater Braidwood fauna of Mazon Creek (Illinois, USA; Baird et al., 1985), the Late Carboniferous Castlecomer fauna (Ireland; Orr and Briggs, 1999), or the early Middle Triassic Grès à Voltzia fauna (France; Gall and Grauvogel-Stamm, 2005). The Early Cretaceous arthropod fauna of **Lake Sihetun** (western Liaoning, China) is made up of three low diversity associations, dominated by spinicaudatans, insect larvae, and malacostracan crustaceans, respectively (Fürsich et al., 2007). Thus far, palaeocommunity analyses for Lake Sihetun had only been carried out for higher-rank taxa (Pan et al., 2012), because of fundamental

taxonomic uncertainties of the clam-shrimp species from the Yixian Formation in western Liaoning.

There is **no consensus** on a **classification scheme** to be adopted for fossil clam shrimps. Even though the Treatise on Invertebrate Paleontology (Tasch, 1969) presents a comprehensive scheme of fossil and modern taxa, it is out-of-date regarding recently published molecular data and the numerous fossil families erected after it was printed. Moreover, this thesis concentrates on species of Eastern Asia, which were erected subsequent to the publication of the Treatise in 1969 by Zhang et al. (1976). However, 275 new species of a total of 399 described species shed some doubt on the validity of the proposed scheme of Zhang et al. (1976), which is most likely heavily biased by oversplitting of taxa. *Chapters 3* and *4* tackle different aspects of clam-shrimp taxonomy, which will be valuable assets for the erection of a new classification scheme.

In a way *Chapter 3* links considerations on abiotic components of the ecosystem with the introduction of the most abundant faunal group of Lake Sihetun: clam shrimps. Currently, the fossilization of clam shrimps is not well understood and almost nothing is known about the **biomineralization** of their cuticles. The main objective is to identify biominerals in extant clam-shrimp cuticles and to predict how they are being altered when exposed to various environments. Ultimately, environmental conclusions will be drawn for Lake Sihetun based on the microstructural preservation of fossil carapaces in thin-section. Structural and chemical preservation of clam-shrimp cuticles will also be introduced as a diagnostic feature for family-level systematics.

While data on vertebrates seem credible, the **apparent high clam-shrimp diversity** with ten reported species for the **Yixian Formation** of western Liaoning (Chen, 1999a) is puzzling, considering that only little more than ten extant spinicaudatan species are reported for the entire continent of Europe (Brtek and Thiéry, 1995). There are, of course, records with up to 11 species in a comparatively confined space, but it can be divided into a number of sub-environments each of those species is adapted to (Paroo catchment, Australia; Timms and Richter, 2002). The palaeocommunity analysis of Lake Sihetun will therefore heavily profit from a taxonomic revision of the ten alleged clam-shrimp species occurring within the Yixian Formation of western Liaoning (*Chapter 4*).

Palaeoenvironmental conclusions are often uncritically drawn from the mere presence of clam shrimps in a sample, based on an analogue with the ecology of extant taxa (e.g., Wang, 1999). In this thesis, the population ecology of the resultant clam-shrimp species *Eosestheria middendorfii* will be based entirely on sedimentological, morphometric, and palaeocommunity evidence (*chapters 5–7*).

Representatives of clam shrimps seem to be characterized by a conservative morphology across wide geographic ranges and over long time intervals. Nevertheless, we attempt to isolate the ecophenotypic variation in a single species for the first time, concentrating on the ecosystem of Lake Sihetun. This is important, because **phenotypic variation** in a taxon is what selection acts upon (Zelditch et al., 2004) and isolating it may shed light on varying environmental parameters. However, in order to isolate the phenotypic variation of *E. middendorfii*, **ontogenetic variation** and **sexual dimorphism** have to be assessed (Zelditch et al., 2004), along with variation resulting from malformation and fossil alignment as well as deformation during compaction. *Chapter 5* concentrates on a single developmental stage of *E. middendorfii*, by assessing how much of the adult shape variation can be attributed to sexual dimorphism. *Chapter 6* will then consider the full spectrum of carapace growth with the main objectives to clarify the diversity of shape within *E. middendorfii* and to assess whether phenotypic variation is driven primarily by growth or by environmental parameters in this fossil species.

The analysis of sexual dimorphism is not straightforward, because the sexual systems of clam shrimps are diverse and include: (1) obligate sexual reproduction (dioecy), (2) self-fertilization with the occasional presence of males (androdioecy), and (3) unisexuality (self-fertilization or parthenogenesis; Sassaman and Weeks, 1993; Sassaman, 1995; Weeks et al., 2009). Therefore, the analysis of sexual dimorphism in a species is in fact asking for its **sexual system**, as there will be no dimorphism in unisexual species. This thesis will propose a new morphometric approach to the identification of the reproductive system of fossil clam-shrimp taxa (*Chapter 5*).

While *chapters 5* and *6* concentrate on clam-shrimp populations, they will be viewed on community-level within the context of the palaeocommunity analysis of the concluding *Chapter 7*. Population dynamics reflect a combination of changes in habitat conditions, intra- and interspecific competition, and predation (Townsend et al., 2008).

The palaeoenvironmental interpretation of clam-shrimp bearing strata is frequently based on faunal similarities with modern temporary freshwater habitats (Vannier et al., 2003), so the presence of

fossil clam shrimps often leads to a stereotypic environmental interpretation that can be summarized as "small temporary freshwater pools" (e.g., Olempska, 2004). The "freshwater" interpretation may work as an environmental assumption, albeit there are exceptions. Extant species are in fact adapted to different salinity ranges of up to 15 g/l salinity (Timms and Richter, 2002), however the vast majority of species lives in fresh- to subsaline waters (Timms and Richter, 2002; Vannier et al., 2003). Clam shrimps are therefore generally good indicators of freshwater conditions from the Late Carboniferous to the Recent (Petzold and Lane, 1988; Vannier et al., 2003). However, strong doubts are herein placed on the "**temporary**" nature of the ancient water bodies, as the associated sedimentological features present conflicting evidence. This controversy will be tackled as part of the final **ecosystem characterization** of Lake Sihetun (*Chapter 7*). For this purpose, the community relicts of 43 horizons of excavation JSG were quantitatively documented, comprising both phases 2 and 3. It involves (1) a species-level **palaeocommunity analysis** based on more than 33,000 specimen counts of an arthropod-dominated fauna, (2) the identification of environmental gradients, and (3) the identification of the responses of each of the benthic species to those gradients.

Judging from the high abundance of clam shrimps in Mesozoic lake deposits, a similar dominance might be expected from Cenozoic lakes. But **post-Mesozoic** (Kobayashi, 1972) **occurrences** of clam shrimps are comparatively **rare**. Only five species of large branchiopods are confirmed for Denmark, **none** of them are spinicaudatans, despite earlier reports (Damgaard and Olesen, 1998). In a compilation of the geographic distribution of European branchiopods, only a handful of spinicaudatan occurrences are marked for Germany (Brtek and Thiéry, 1995). The general lack of commonly used marker organisms, such as freshwater diatom floras, results in a loss of "climatic accuracy" in the reconstruction of **Mesozoic** lake ecosystems. So these reconstructions will have to be based on somewhat different **proxies**. The diversification and general abundance of **clam shrimps** during the Mesozoic may establish this group as one of the most important marker organisms in pre-Cenozoic lakes. Also, species that are dominant can be expected to have a large impact on ecosystem functioning. The fact that clam shrimps are markedly rare in Cenozoic lake sediments implies a shift in lake communities from the Mesozoic to the Cenozoic, which needs to be understood and clam shrimps ought to be recognized as a key to Mesozoic limnological studies.

Chapter 1: Seasonal to sub-seasonal palaeo-environmental changes in Lake Sihetun (Lower Cretaceous Yixian Formation, NE China)

Chapter 1 has previously been published:

Hethke, M., Fürsich, F.T., Jiang, B., Pan, Y. 2013. Seasonal to sub-seasonal palaeoenvironmental changes in Lake Sihetun (Lower Cretaceous Yixian Formation, NE China). – *International Journal of Earth Sciences*, **102**: 351-378.

Texts, tables, and figures are reformatted in the style of this thesis. There are minor orthographic changes in the text.

Introduction

Although the fossils of the famous Lower Cretaceous Jehol Biota of western Liaoning have been studied intensively, the same cannot be said for the lacustrine sediments in which they occur. As a result, the palaeoenvironment that led to the deposition of the Jianshangou Unit (Yixian Formation) and its excellent fossil preservation has not yet been satisfactorily resolved. Here, we focus on a Lower Cretaceous lake system of about 20 km^2 in area that is exposed around Sihetun village (Fig. 1.1), and for which the name Lake Sihetun has been proposed (Pan et al., 2012), in an attempt to gain a comprehensive picture of the palaeoenvironment of this important Mesozoic *fossillagerstätte*.

The strata of the Yixian Formation allow unique glimpses into an ancient ecosystem, of which a rich biota has been preserved that has received widespread attention in the media of late. Among the most spectacular fossils range feathered dinosaurs and the putative early flowering plant *Archaefructus* (Sun et al., 2002). Diverse other vertebrate and invertebrate fossils have been retrieved from Lake Sihetun. They provide important clues about the evolution of major clades (e.g., the origin of angiosperms and radiation of birds) and of anatomical features such as feathers during Early Cretaceous times (e.g., Barrett, 2000; Xu et al., 2001). Commonly, these fossils are remarkably well preserved, as documented by soft-tissue impressions and articulated vertebrate skeletons (e.g., Xu et al., 1999a, b; Zhou et al., 2003).

In contrast to these well-studied fossils, our knowledge of the sedimentary environments of Lake Sihetun is far from complete and the underlying mechanisms that made Lake Sihetun so special are not yet understood. Our overall goal is to understand the small-scale palaeoenvironmental and palaeocommunity changes, which can only be explained by a preceding, high-resolution sedimentological analysis that should form the basis of any palaeoecological study.

It is general practise to claim that active synsedimentary volcanism, evident from numerous conformable tuff layers throughout the investigated sedimentary succession, led to episodic catastrophic mass mortality events and ultimately to the excellent preservation of fossils (e.g., Liu et al., 2002). The synsedimentary volcanism resulted from tectonic activity along the Pacific Rim that culminated during the deposition of the Yixian Formation (Wang et al., 1983). Beyond this plausible claim, no further clarification about the abiotic components of the water column within Lake Sihetun has been put forward so far. Apart from the fact that this might be true for the vertebrate fauna, mass mortality events of the much more abundant aquatic invertebrate fauna suggest additional causes. First attempts to understand the ecosystem of Lake Sihetun based on fossil community data were made by Fürsich et al. (2007) and Pan et al. (2012), who proposed seasonal oxygen fluctuations at the lake bottom to account for recurrent mass mortality events documented by the benthic and occasionally nektonic lake fauna.

The study of the various depositional environments of the Yixian Formation has been initiated by Jiang and Sha (2007) and Jiang et al. (2011). Jiang et al. (2012) recognised four facies associations in the lake sediments: (1) beach to nearshore, (2) lacustrine floor type A, (3) lacustrine floor type B, and (4) fan delta. Based on the spatio-temporal distribution pattern of these facies associations, four phases in the evolution of Lake Sihetun can be distinguished. In contrast to phases 1, 3, and 4, the lake waters were stratified during Phase 2. As a result, the sediments deposited during Phase 2 are finely laminated.

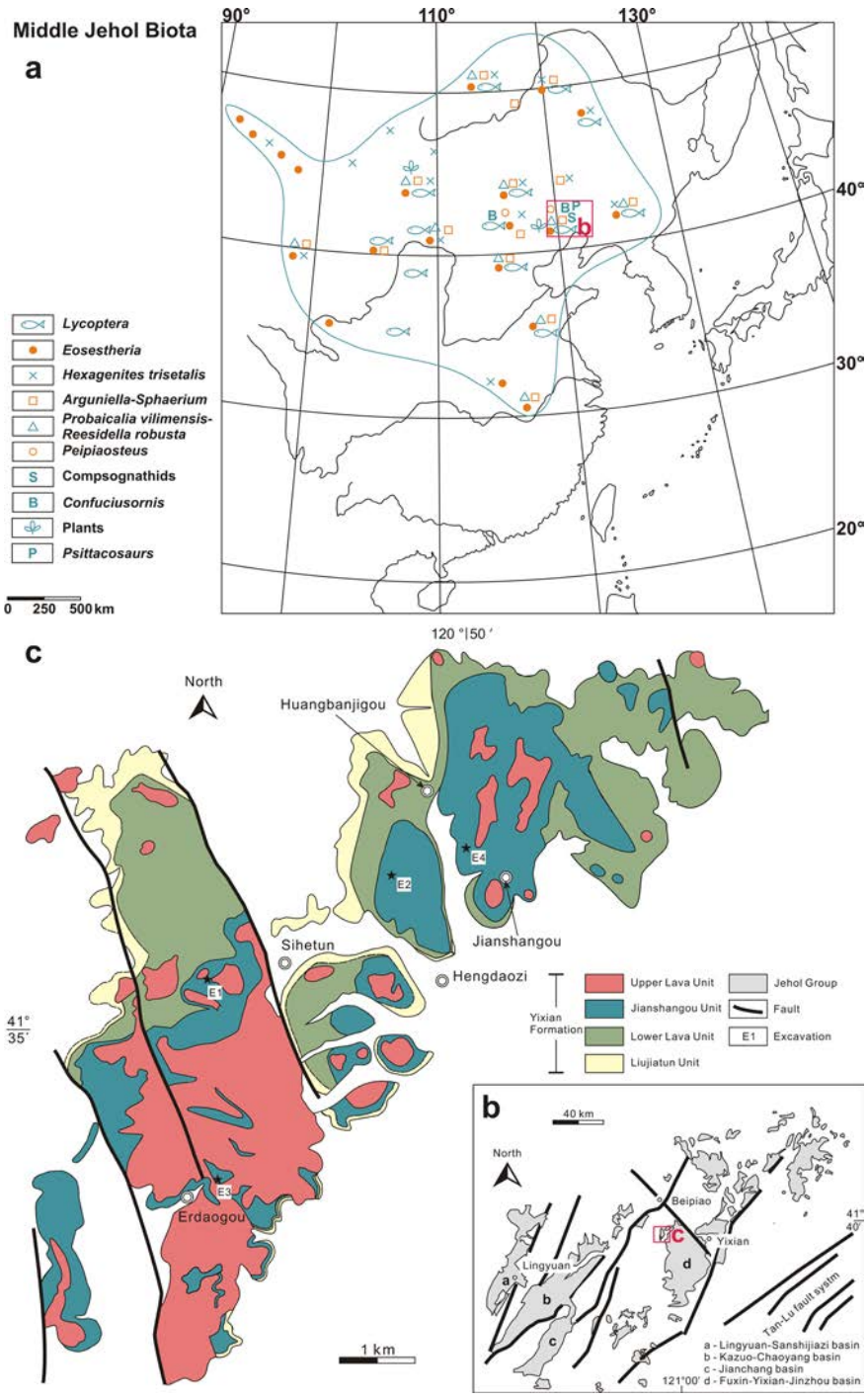

Fig. 1.1. (a) Distribution of the middle Jehol Biota in China (modified after Chen, 1999). (b) Distribution of the Jehol Group in the Sihetun area, which is marked with a red box (modified after Jiang and Sha, 2006). (c) Geological map of the Sihetun area, showing the outcrop pattern of the four units of the Yixian Formation. The positions of the three excavations studied in this paper (E2-4) as well as the Sihetun fossil site (E1) are indicated (modified after Jiang et al., 2011).

This paper concentrates on the sediments of the central lake floor deposited during phases 2 and 3, which comprise the most fossiliferous part of the formation and which represent environments that led to exceptional preservation of fossils. The sedimentological processes governing the development of the lake are still poorly understood. Liu et al. (2002), for instance, interpreted the laminations as varves, although stating that "no independent evidence was discovered to demonstrate that the laminations are annually deposited". Thus, do the lake sediments represent actual non-glacial varves? Are there prominent changes in laminae thickness? Does a change in laminae pattern coincide with climatic events? And what effects did seasonal forcing have on the physico-chemical properties of Lake Sihetun? Another unsolved question is why only a handful layers of the investigated sediments yield aquatic invertebrates compared to the high number of layers completely devoid of fossils (see also Pan et al., 2012).

The high-resolution analysis presented in this paper reveals new insights into the physical and chemical evolution of Lake Sihetun and contributes

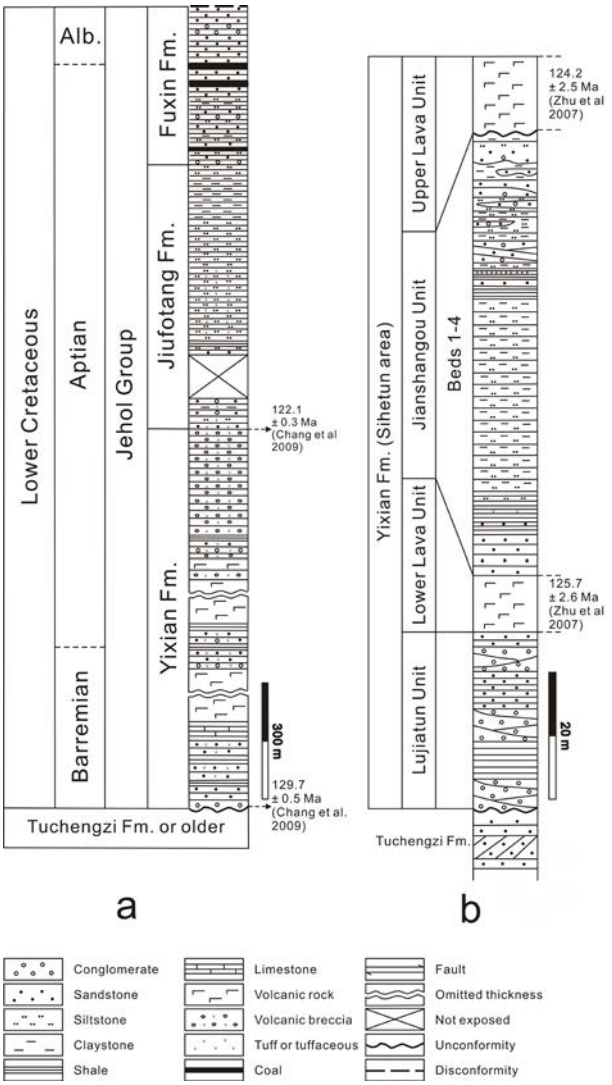

Fig. 1.2. (a) Jehol Group of western Liaoning and (b) the Sihetun area (modified after Jiang et al., 2012).

towards a better understanding of the underlying processes that ultimately led to the formation of the famous *fossillagerstätte*.

Geological and palaeontological setting

The Lower Cretaceous Jehol Group (Figs. 1.1, 1.2) of western Liaoning includes the Yixian, Jiufotang, and Fuxin formations (Jiang and Sha, 2006). The depositional age for the base of the Yixian Formation is 129.7 ± 0.5 Ma ($^{40}Ar/^{39}Ar$; Chang et al., 2009). The lowermost part of the overlying Jiufotang Formation was deposited about 122.1 ± 0.3 Ma ago, implying that the Yixian Formation was deposited within a time-interval of 7 Ma and entirely within the Lower Cretaceous (Swisher III et al., 1999; Chang et al., 2009).

Estimates about lake duration were obtained from $^{40}Ar/^{39}Ar$ ages taken from the Lower Lava Unit and the Upper Lava Unit, respectively, which suggest a period of 1.5 Ma for the deposition of the Jianshangou Unit (125.7 ± 2.6 Ma – 124.2 ± 2.5 Ma; Zhu et al., 2007). Palaeomagnetic data proposes an even shorter duration of 0.7 Ma or less (Zhu et al., 2007). Furthermore, studies agree on the depositional age of a tuff located beneath the feathered dinosaur-bearing bed that varies around 124.5 Ma (124.6 ± 0.2 Ma Swisher III et al. 1999; 124.7 ± 2.7 Ma, Yang et al., 2007; 124.1 ± 0.3 Ma, Chang et al., 2009) and that is matching the time interval for the existence of Lake Sihetun.

Hence, radiometric ages approximately agree regarding the top of the Yixian Formation and the time of deposition of the lake sediments, but they are diverging about the onset of the Yixian Formation by several million years. Yang et al. (2007) suggest that in Huangbanjigou, the Yixian Formation (Fig. 1.1) was deposited within a short time interval of 2 Ma (124.9 ± 1.7 Ma – 122.8 ± 1.6 Ma), the oldest age coming from a tuff horizon. Conversely, the lower Barremian age for the onset of the Yixian Formation by Chang et al. (2009) was obtained from the base of a 50 m-thick lava, whose upper part was dated to be 3.5 Ma younger, implying several eruption events with considerable time hiatuses within this lava.

Liaoning was located at a palaeolatitude of about 41.9° ± 6.6° N (Enkin et al., 1992; Zhou et al., 2003; Amiot et al., 2011) during the time of deposition of the Yixian Formation.

The ecosystem of the Jehol Biota is distributed in eastern and central Asia (Fig. 1.1a) and characterized by the *Eosestheria-Ephemeropsis-Lycoptera* assemblage (Grabau, 1928; Gu, 1962). The Yixian Formation can be assigned to the middle Jehol Biota (Chen, 1999b). Wetlands and numerous lakes were dominating the environment under temperate climates (Amiot et al., 2011). Palynological evidence points to a *warm* and *dry* climate with seasonal rainfall (Li and Batten, 2007). In contrast, hygrophilous and thermophilous plants indicate generally *warm* and *wet* habitats, but with seasonal arid or semi-arid conditions (Ding et al., 2003).

The Yixian Formation in the Sihetun area comprises, from bottom to top, four units: Lujiatun Unit, Lower Lava Unit, Jianshangou Unit, and Upper Lava Unit (Fig. 1.1c, Jiang and Sha, 2007). The Lujiatun Unit, which unconformably overlies the Upper Jurassic-Lower Cretaceous aeolian Tuchengzi Formation (Cheng et al., 1997), consists

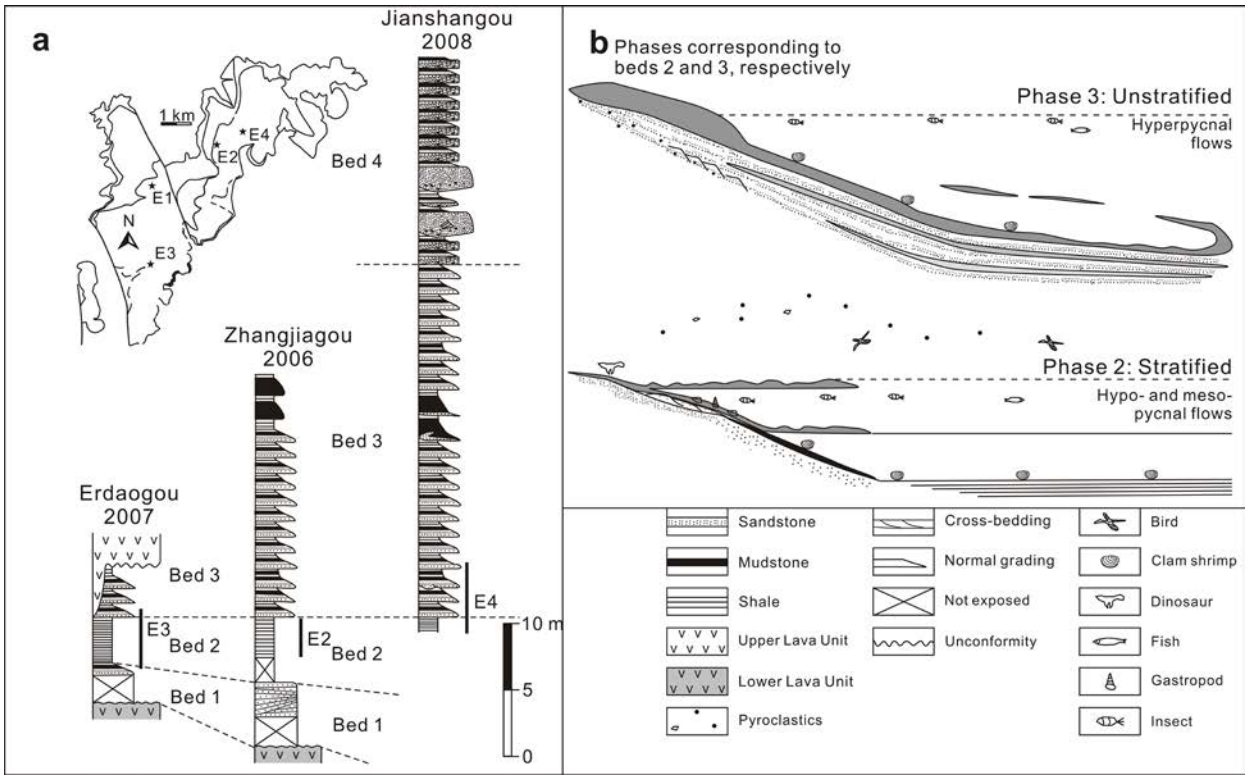

Fig. 1.3. (a) Schematic lithologs of excavations 2-4 (E2-4). Beds 1-4 of the Jianshangou Unit are designated. E2-4 were carried out within beds 2 and 3. (b) Palaeoenvironmental model of phases 2 and 3 that correspond to beds 2 and 3, respectively (Jiang et al., 2012). Phase 2 is characterized by a stratified lake with meso- and hypopycnal flows, whereas in Phase 3 the lake was unstratified and hyperpycnal currents frequently reached the distal lake floor.

of volcanic conglomerates to sandstones as well as of lapilli-tuffs. Basaltic andesites, olivine basalts, and trachyandesites of the Lower Lava Unit disconformably overlie the Lujiatun Unit. The following Jianshangou Unit is composed of finer siliciclastics and tuffs, with intercalated calcareous marl and gypsum. It contains an abundant flora and fauna. The extrusive-intrusive Upper Lava Unit is made up of intermediate-basic lava and intrusive rocks (Jiang and Sha, 2007). An analysis of the depositional environments of the Yixian Formation yielded a succession of volcanic complexes (Jiang et al., 2011): a shield volcano, an intermediate multi-vent centre, a volcanic lake, and lava domes. Fig. 1.1c illustrates the distribution of the volcanic lake sediments (Jianshangou Unit), which can further be subdivided into four beds (Fig. 1.3a): Bed 1 is made up of coarser, horizontally or cross-bedded, tuffaceous siliciclastics (beach to nearshore), Bed 2 consists of paper-thin laminae of fine tuffaceous siliciclastics and some evaporates (lake floor type A), Bed 3 yields a succession of normal-graded fine sandstones to siltstones (lake floor type B), and Bed 4 composes tuffaceous conglomeratic sandstones and tuffs that are interbedded with finer siliciclastics (fan delta; Jiang et al., 2012). The lithostratigraphic units of beds 1-4 correspond to four phases of lake evolution (Fig. 1.3b): During the first phase, the water level of the lake fluctuated but was generally on the rise resulting in subaerial and shallow-water deposits. The second phase is characterized by beach to nearshore facies in marginal areas and a central lake floor with suspension-derived deposits. During the third phase, lake-floor sedimentation occurred mainly by hyperpycnal flows, whereas the fourth phase is characterized by progradation of a fan delta (Jiang et al., 2012).

Material and methods

Sediment and fossil samples have been retrieved in the course of three excavations in the Sihetun area (Figs. 1.1c, 1.3a) near Zhangjiagou (ZJG; E2), Erdaogou (LXBE; E3), and Jianshangou (JSG; E4), 3.5 m, 4.5 m, and 5 m deep, respectively. They correspond to two of the four phases recognized in the evolution of Lake Sihetun (Jiang et al., 2012).

The laminated rocks were fixed with epoxy resin and some of the sediment samples were impregnated with dyed epoxy resin to reveal porosity. Petrographic thin-sections were prepared and thoroughly examined with both traditional optical microscopic

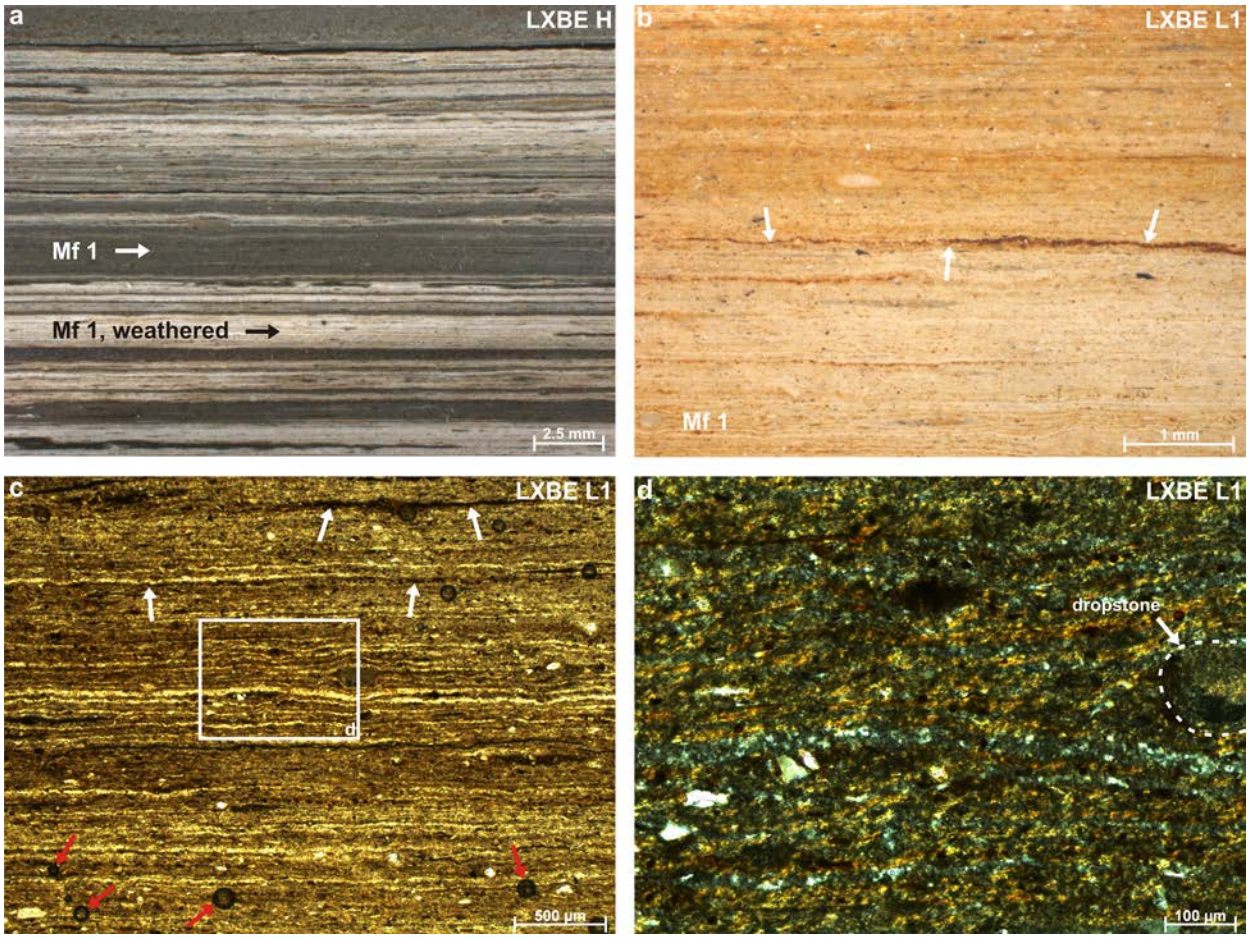

Fig. 1.4. Microfacies 1. (a, b) Reflected light. (c) Plane-polarized light. (d) Crossed polars. (a) Original dark-grey colour of Bed 2 (Mf 1) and the formation of "apparent laminae" due to weathering. (b) The weathered Bed 2 is generally light-coloured with distinct red stains in the vicinity of framboids (pyrite pseudomorphs). Arrows point towards a red layer composed of concentrated framboids. Tiny red "dots" scattered all over the sediment represent single framboids. (c) Overview of Microfacies 1-lamination. White arrows designate pyrite framboids, whereas red arrows point towards artificial bubbles produced during preparation. (d) Under crossed polars the brown colour observed under plane-polarized light is being retained.

methods and raster scan using the VEGA\\ scanning electron microscope (SEM). The optical microscope was equipped with the Zeiss AxioVision Software (Release 4.8.1) that enabled high-precision measurements of structures observed in thin-section.

Back-scattered electrons (BSE) were detected for compositional imaging. Brightness in a BSE image is dependent on the mean atomic numbers of different phases, which were obtained from Reed (2005). Note that mean atomic numbers of Fe oxides and sulphides are comparatively high. Consequently, these minerals appear much brighter on BSE images than silicates. The order of mean atomic numbers of relevant minerals from higher to lower appearing brighter and darker, respectively, is: calcite > anorthite and orthoclase > albite > quartz.

The SEM (TESCAN Model Vega\\xmu) was equipped with an energy-dispersive X-ray spectroscopy (EDS) system (Programm: INCA), which allowed further elemental analyses. At least 250 000 counts were detected for a statistically significant output, but they usually ranged around 400 000. Gold and carbon were used for conductive coatings and sputtered upon the specimens with the "Cressington Sputter Coater 108 auto".

A preliminary whole rock X-ray analysis was carried out on a rock sample collected from Bed 2 of the Jianshangou Unit, about 1 m above the bird-bearing horizons from the site of the Sihetun Fossil Museum (E1 in Fig. 1.1c).

The reference material is deposited at the Paläoumwelt Section of the GeoZentrum Nordbayern, University of Erlangen-Nürnberg, Germany.

Thin-section analysis

Beds 2 and 3 (Fig. 1.3a) of the Jianshangou Unit (Yixian Formation) are mostly siliciclastic with intermittent chemical precipitate-dominated intervals. The layering is frequently interrupted by tuff layers. A total of five microfacies is recognized within Bed 2 (Mf 1-5) and one microfacies is dominant in Bed 3 (Mf 6). They are allochthonous, siliciclastic laminae (Mf 1), chrysophycean cyst accumulations (Mf 2), tuffaceous silt (Mf 3), lacustrine chemical precipitates (Mf 4), tuff (Mf 5), and normal-graded, sandy to silty siliciclastics (Mf 6). Different forms of biofilms are recognized within both beds. A list of the various microfacies present within the examined horizons can be found in Supplementary 1.1.

The lithological analyses are expected to answer questions about processes of lamina or non-glacial varve formation and counteracting processes, such as water circulation and bioturbation. Special interest is placed in finding temporal successions of sediment components and seasonally responsive organisms to identify potential varve depositions.

Microfacies

Microfacies 1: Allochthonous, siliciclastic laminae

Mf 1 (Figs. 1.4-1.6) is characterised by light-brown, parallel to sub-parallel couplets of mainly clay and argillaceous silt laminae. Average couplet thicknesses differ according to their location within the lake (Fig. 1.3a; E2 ~ 39.5 μm; E3 ~ 25.3 μm; E4 ~ 13.4 μm). Apparent "laminae" of light and dark colours observed with magnifying glasses in the field (Fig. 1.4a) do not reflect the true lamination, as they show little relation to compositional differences or grain-size variations. Instead, alteration processes led to an apparent increase in lamina thickness (Figs. 1.4a, 1.5e, f). The light colour of the sediments in Fig. 1.4a is prevalent in outcrops and resulted from extensive bleaching during weathering, whereas the darker colour represents less altered sediments. Therefore, only thorough thin-section analyses reveal a refined picture of small-scale depositional units. Two stages of alteration are distinguished: lightly to moderately altered (Mf 1.1) and profoundly altered (Mf 1.2).

Generally, Mf 1 consists of varying amounts of quartz (main component), alkali feldspar, plagioclase, and volcanic rock fragments as well as their alteration products, mainly smectite and hydromica with mixed-layer smectite. Accessory volcanic minerals such as biotite occur. Dropstone lapilli (Fig. 1.4d), which are generally made up of volcanic rock fragments, are common. Furthermore, two types of opaque phases are present. They are pseudomorphs of pyrite framboids found in Mf 1.1 and, occurring within the heavily weathered Mf 1.2, pearl-string-like aligned grains that are forming delicate layers (white arrows in Fig. 1.5f). The presence of pyrite framboids in Mf 1 produced a distinct red stain after having been almost entirely altered to iron oxide-hydroxides. Framboids occur concentrated and scattered as distinct red "dots" (Fig. 1.4b). The main biogenic components observed in thin-section are clam-shrimp carapaces, fish remains, and plant debris.

Thicknesses of the examined laminae generally range from several μm to maximum thicknesses of 102 μm (E2), 66.2 μm (E3), and 19.3 μm (E4). Light and brown laminae are indistinct (Figs. 1.4c, d; 1.5), but a difference in grain size and composition between the sediments of either colour can be observed (Fig. 1.5c). The light layers traced in Fig. 1.5c are generally finer-grained, containing a smaller amount of feldspar than those layers exhibiting a diffuse brown coating, which comprise mostly silt-sized particles and are compositionally more immature. Hence, silty laminae are coupled with clay. The deposition of Mf 1.1-laminae (Fig. 1.5c) is also marked by thin dark layers deposited between the light-brown laminae and composed of fine organic detritus, most likely of algal and to a lesser degree of higher plant origin. Conditions also led to the establishment of biofilms that are marked by a much more pronounced organic layer (Fig. 1.11a, b).

The sediment of the *light layer* is made up of angular to subrounded detrital material, which exhibits a typical grain-size range of 0.6 to 2.3 μm (Fig. 1.13c). The grains of the matrix reveal a near homogeneous orientation of extinction under crossed polarizers, suggesting crystal orientations parallel to the bedding (Fig. 1.4d). Occasionally, silty to fine sandy grains are embedded within this fine matrix. It is not clear yet, whether the sediment contains any amorphous to cryptocrystalline autochthonous silica precipitates, which could be expected, as silica is commonly released during the alteration of volcanic glass. The brown coating of the silt layer is thought to result from diagenetic iron oxide-hydroxide coatings that formed because iron-laden pore waters preferred as pathways the coarser, more porous and supposedly more permeable material.

Epoxy staining (blue) reveals a high secondary porosity in parts of thin-section JSG AP (Fig. 1.5d). These highly porous areas labelled as Mf 1.2

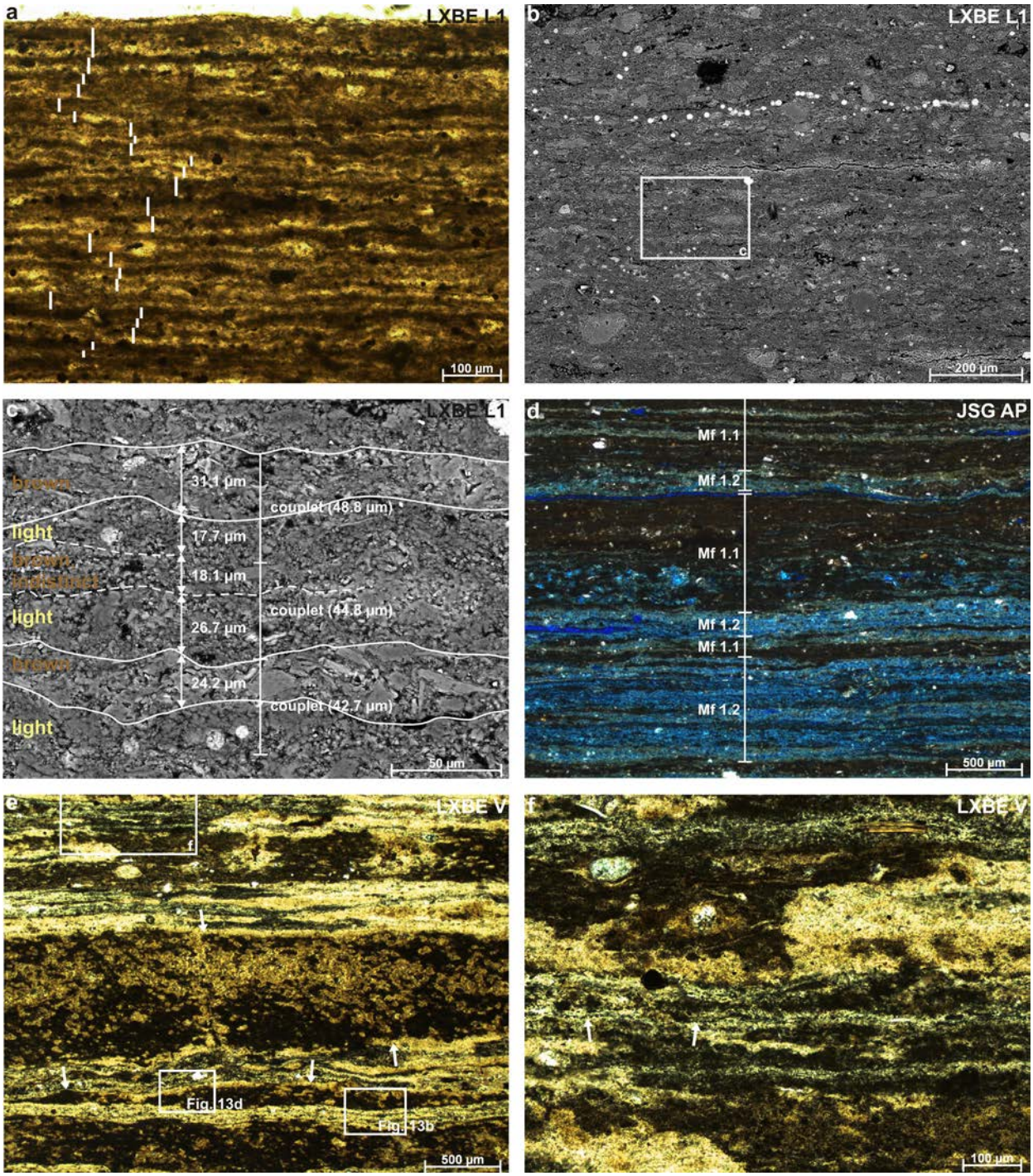

Fig. 1.5. Microfacies 1 (Mf 1): Allochthonous siliciclastic laminae. (a, d-f) Plane-polarized light. (b, c) BSE images. (a) Example of lamina-thickness measurements using a 574 µm-thick transect, in which overall lamina thickness ranges from 12.2 µm to 51.7 µm with an average of 23.9 µm. Elsewhere in the same thin-section, average lamina thickness drops to as low as 18 µm. (b) The bright spheres in this BSE image are altered pyrite framboids. (c) Detail of (b) showing coupled light and brown laminae, which are traced. Light layers are generally finer-grained with less feldspar, while brown layers are compositionally more immature. (d) Dyed epoxy resin stained the altered clear-yellow parts blue (Mf 1.2), revealing a much higher porosity than less altered, darker parts (Mf 1.1). (e) Lamination is indistinct to non-distinguishable. Arrows point towards the patchy distribution of dark-brown layers, whose underlying microfacies cannot clearly be resolved. (f) The light matrix is streaked with filaments composed of black nodules (arrowed, ø ~ 1 µm).

correspond to bleached, lighter areas in non-stained thin-sections. Weathering processes have been so severe in parts that the lamination was eventually rendered indistinct to non-distinguishable (Fig.

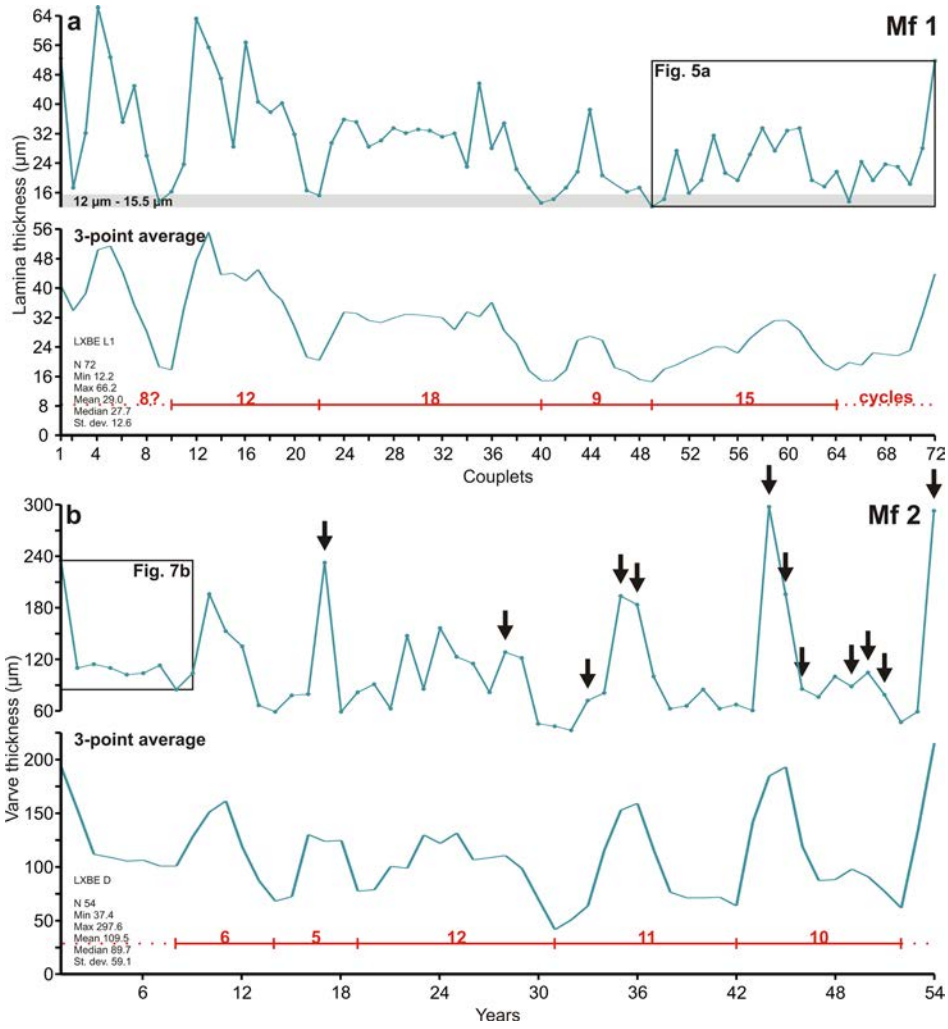

Fig. 1.6. Lamina-thickness measurements for Microfacies 1-couplets and Microfacies 2-varves. (a) The upper graph shows total lamina thickness for a transect of 72 couplets. A micrograph of the upper part of the measured transect is depicted in Fig. 1.5a. The thickness range of 12 µm to 15.5 µm has been shaded grey. Measurements falling into it correspond to cycle boundaries. The 3-point average reveals four consecutive cycles of 9 to 18 couplets per cycle, which are interpreted to represent annual changes in humidity. (b) Varve-thickness measurements of Microfacies 2-varves. Arrows signal deposition of tuffaceous silt (Microfacies 3). The 3-point average reveals suggestive varve-thickness cycles of 5 to 12 years.

1.5e, f). Hence, Mf 1 can be divided into two stages of alteration. Mf 1.2 is thought to be an altered Mf 1.1 and discussed separately in the paragraph about sediment alteration.

Depositional structures are characterised by very thin, undisturbed laminae owing to lack of bioturbation (Fürsich et al., 2007). The lamination is usually continuous, except for a few microfractures. Occasionally, microfracturing was so severe that several 100-µm-wide sediment blocks were rotated. This rotation took place synsedimentarily, as such levels are overlain on top by undisturbed laminae. Likely causes are synsedimentary tremors as they occur during volcanic eruptions.

The layering of Mf 1 is difficult to assess, because the sediments consist of mainly allochthonous material. As laminae are assumed to represent rhythmic bedding forming light-brown couplets and as brown layers tend to be indistinct at their bases and distinct at their tops, couplet-thickness measurements were carried out from the base of a light layer to the top of the corresponding brown layer (Figs. 1.5a, 1.6a; Table 1.1). Couplet thickness of the segment depicted in Fig. 1.6a (12.2-66.2 µm, ø 29 µm) varies only little, but smoothing of the total-thickness curve using the 3-point average suggests the presence of cycles composed of 9 to 18 couplets each.

Interestingly, the thickness of an average Mf 1-cycle (392 µm) falls into the thickness range of Mf 4-varves (Fig. 1.9). If the siliciclastic components of Mf 4 are equivalent to Mf 1-sedimentation, then the thickness of Mf 1-cycles determined in Fig. 1.6a can be compared to the thickness of Mf 4-varves, not taking the extra amount of precipitated carbonates into account. This would imply that one Mf 1-cycle represents one year.

Microfacies 2: Chrysophycean cyst accumulations

Characteristic for Phase 2, but rare, are dark layers labelled as Mf 2 in Fig. 1.7. They consist of allochthonous siliciclastic material, organic detritus, and chrysophycean stomatocysts. A rhythmic occurrence of Mf 2-laminae can be observed, in which one Mf 2-lamina typically alternates with Mf 1-laminae, altogether forming one varve (Fig. 1.7a).

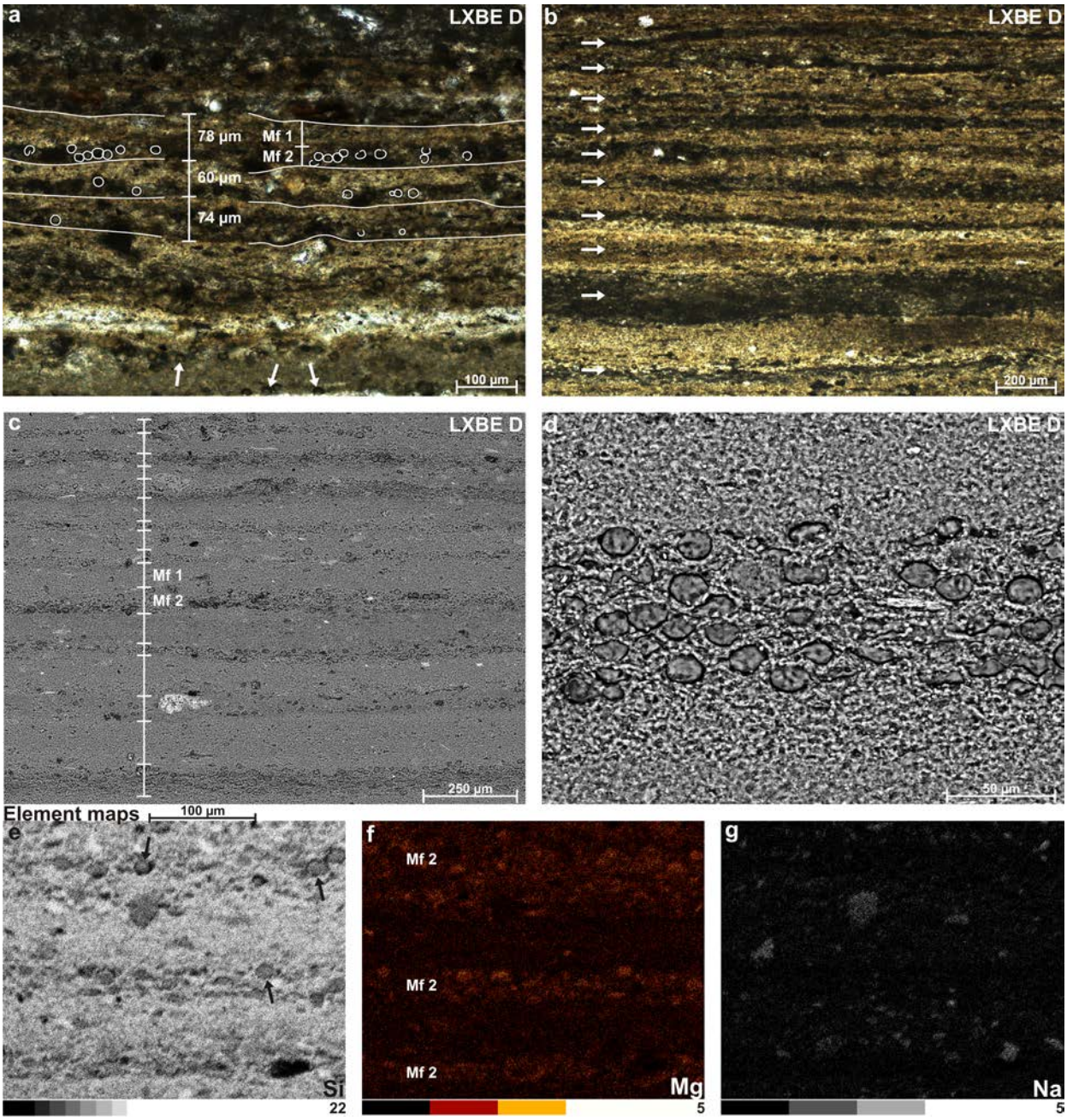

Fig. 1.7. Microfacies 2 (Mf 2): Chrysophycean cyst accumulations. (a, b) Plane-polarized light. (c, d) BSE images. (e-g) Element maps. (a) The three consecutive varves traced are composed of Mf 2- and Mf 1-laminae. The dark-coloured laminae of Mf 2 comprise mostly finer siliciclastics and are enriched in organic matter consisting of organic debris as well as chrysophycean cysts, some of which are traced in white or arrowed. (b) Part of the transect measured in Fig. 1.6b. Chrysophycean cyst accumulations are marked with arrows. (c, d) The rhythmic bedding produced by Mf 2-deposition is easiest to detect using BSE imaging. The diameters of the chrysophycean cysts shown in (d) range from 10 to 17 µm. (e-g) Chrysophycean-cyst infills are depleted in Si and enriched in Mg, likely corresponding to Mg-rich clay minerals such as the weathering product of volcanic ash, smectite. Na-silicates are more abundant in the layers adjacent to Mf 2.

Overall Mf 2-laminae thickness varies profoundly from several 10 µm to more than 1 mm, depending on the addition of tuffaceous silt (Mf 3) to the Mf 2-varve-forming process (arrowed in Fig. 1.6b). Even though Mf 2 could unambiguously be recognized in only one thin-section, this microfacies is of great importance for the main interpretation. Mf 2 provides a depositional scenario for Mf 3-events, which occur throughout all sections studied (see discussion), and it represents the only unmistakable evidence for annual deposition within all the Early Cretaceous lake deposits studied in this thesis.

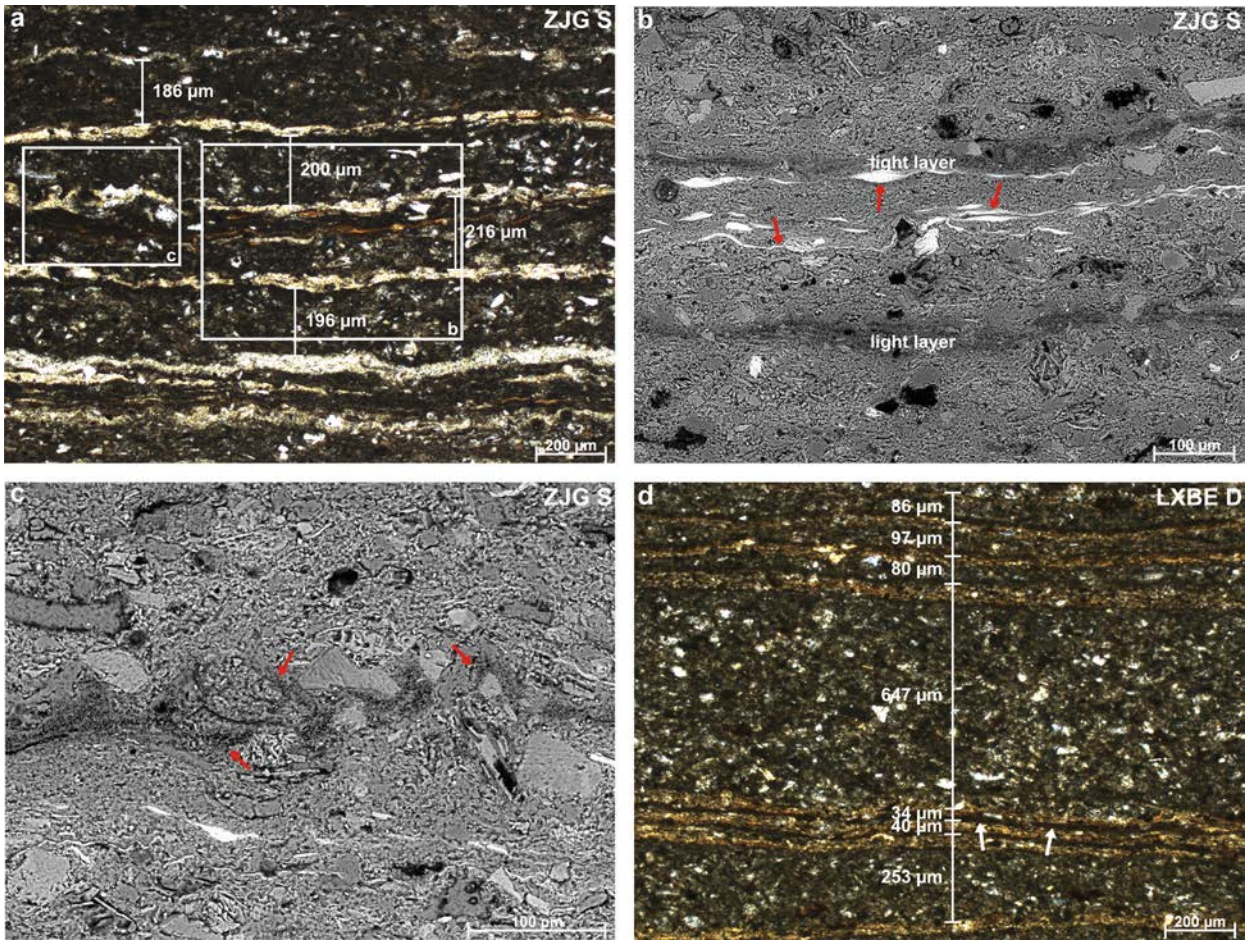

Fig. 1.8. Microfacies 3 (Mf 3): Tuffaceous silt. (a, d) Plane-polarized light. (b, c) BSE images. (a) Alteration of light clay and dark tuffaceous silt. (b, c) Close-ups of (a). Indicative of a hyperpycnal-flow origin of Mf 3 are (b) broken clam-shrimp carapaces scattered throughout some layers and (c) the disturbance of underlying light clay layers. (d) Mf 3 incorporated into the varve-forming process. Varve thickness highly fluctuates depending on the occurrence of Mf 3-events. There is no or only little evidence of scouring at the base of Mf 3 in this case. This corresponds to a depositional mechanism of siliciclastics settling from hypopycnal flows. At times when no deposition occurred, the resultant thicknesses of depositional events are similar to those of Mf 1-layers, that is, 40 and 34 µm, respectively.

Characteristic for Mf 2 are spherical structures traced and arrowed in Fig. 1.7a, which exhibit dark walls under plane-polarized light. Each sphere displays a pore and BSE images reveal that its wall has been decomposed to small cavities (Fig. 1.7d). The taxonomically important pore morphology cannot be discerned. These spheres probably represent endogenous cysts of golden algae (Chrysophyceae), which are exclusively made up of silica bound to pectic substances in extant forms containing a single pore (Bourrelly, 1963; Duff et al., 1995). These original substances have been degraded leaving cavities. The cysts are commonly around 15 µm in diameter and more or less distinct, as preservation mostly depends on the grain size of the surrounding sediment. The infillings of the cysts are depleted in Si and enriched in Mg (Fig. 1.7e-g), which is suggestive of clay minerals (mainly Mg-rich smectites). Na-silicates are more abundant in Mf 1-laminae than in the finer-grained parts of Mf 2.

The chrysophycean deposits reported from Lake Sihetun are probably the oldest recorded from freshwater deposits. Apart from "chrysophycean-like" Proterozoic forms (Cloud, 1976), they have been recognized in marine sediments from the Cretaceous to the Holocene and in freshwater deposits only from the Cenozoic (Tappan, 1980).

The chrysophycean cysts of Mf 2 occur in separate layers emphasizing their seasonal nature. Encystment occurs during asexual as well as sexual reproduction, rendering morphologically identical stomatocysts in both modes. According to Duff et al. (1995), sexual cyst formation in extant species does not seem to be triggered by environmental stress but is density dependent. Asexual encystment is not well understood. Generally, cyst formation is

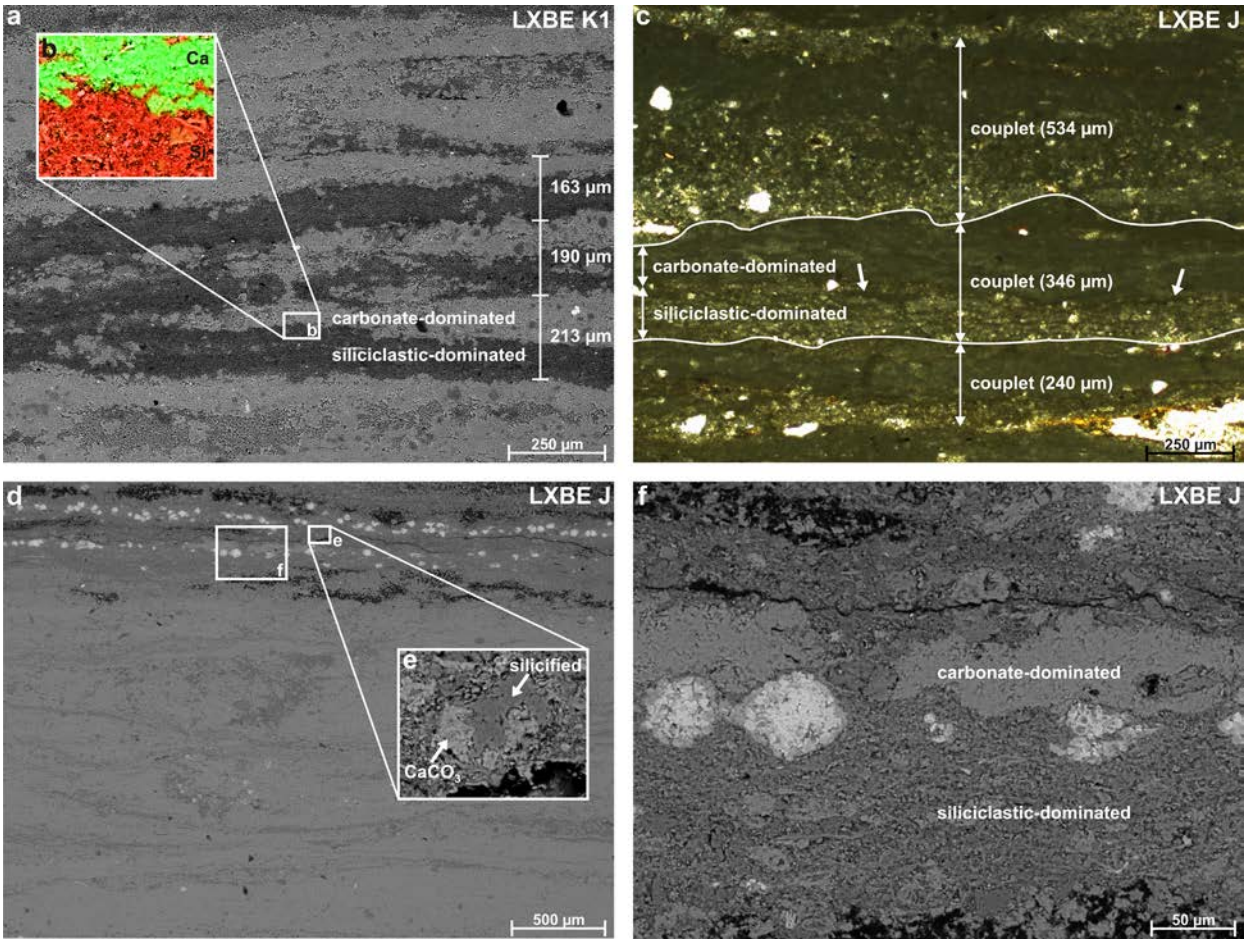

Fig. 1.9. Microfacies 4 (Mf 4): Lacustrine chemical precipitates. (a, d-f) BSE images. (b) Element map. (c) Plane-polarized light. (a, b, d-f) Light-grey and darker grey areas are indicative of $CaCO_3$ and siliciclastic material, respectively. Calcium carbonate exhibits a patchy distribution that is due to dissolution and re-precipitation during diagenesis. (e) Silica replacement of calcium carbonate occurs. (c) Mf 4-constituents form couplets composed of siliciclastic material in the lower part and argillaceous carbonates in the upper part. White arrows point towards a prominent organic horizon that loosely separates siliciclastic- and carbonate-dominated layers. Couplet thickness ranges from 100 to several 100 µm.

thought to be a survival adaptation for the seasonally restricted golden algae. Although winter taxa exist, chrysophyte biomass is highest in the warm season from July to September (Eloranta, 1995). Unfortunately, much environmental information is lost, as the taxonomic identities of the cysts of Lake Sihetun are unknown.

Microfacies 3: Tuffaceous silt

Mf 3 (Fig. 1.8) is composed of tuffaceous fine-sandy silt (dark) that is interbedded with well-sorted clay (light, Fig. 1.8a-c) or Mf 1-couplets (Fig. 1.8d). The dark Mf 3-layers are compositionally immature, containing pyroclastics. Grading is generally not discernable, except in thicker Mf 3-layers. Broken clam-shrimp carapaces occur scattered within layers (Fig. 1.8a-b). Framboids are scarce in Mf 3, but some occur in discontinuous Mf 3-lenses, which are mantled by framboid-yielding Mf 1.

Distinguishing Mf 3 from other microfacies can be tricky. In general, Mf 3 is related to Mf 1 as both contain similar fine-grained background sedimentation (light clay layer, Fig. 1.8a). Mf 3 can be distinguished from coarser tuff layers (Mf 5) by partial mixing of the tuffaceous material with the underlying background sedimentation (red arrows in Fig. 1.8c) and the incorporation of clam shrimps. Also, ashfall pyroclastics of Mf 5-tuffs only indent the underlying sediment instead of rupturing and incorporating them partly. Distinction between Mf 3- and Mf 5-tuffs is impossible when pyroclastic particle size passes a threshold value, commonly fine ash. Distinction between Mf 3 and Mf 6 is based on the generally graded and more mature sediments of Mf 6.

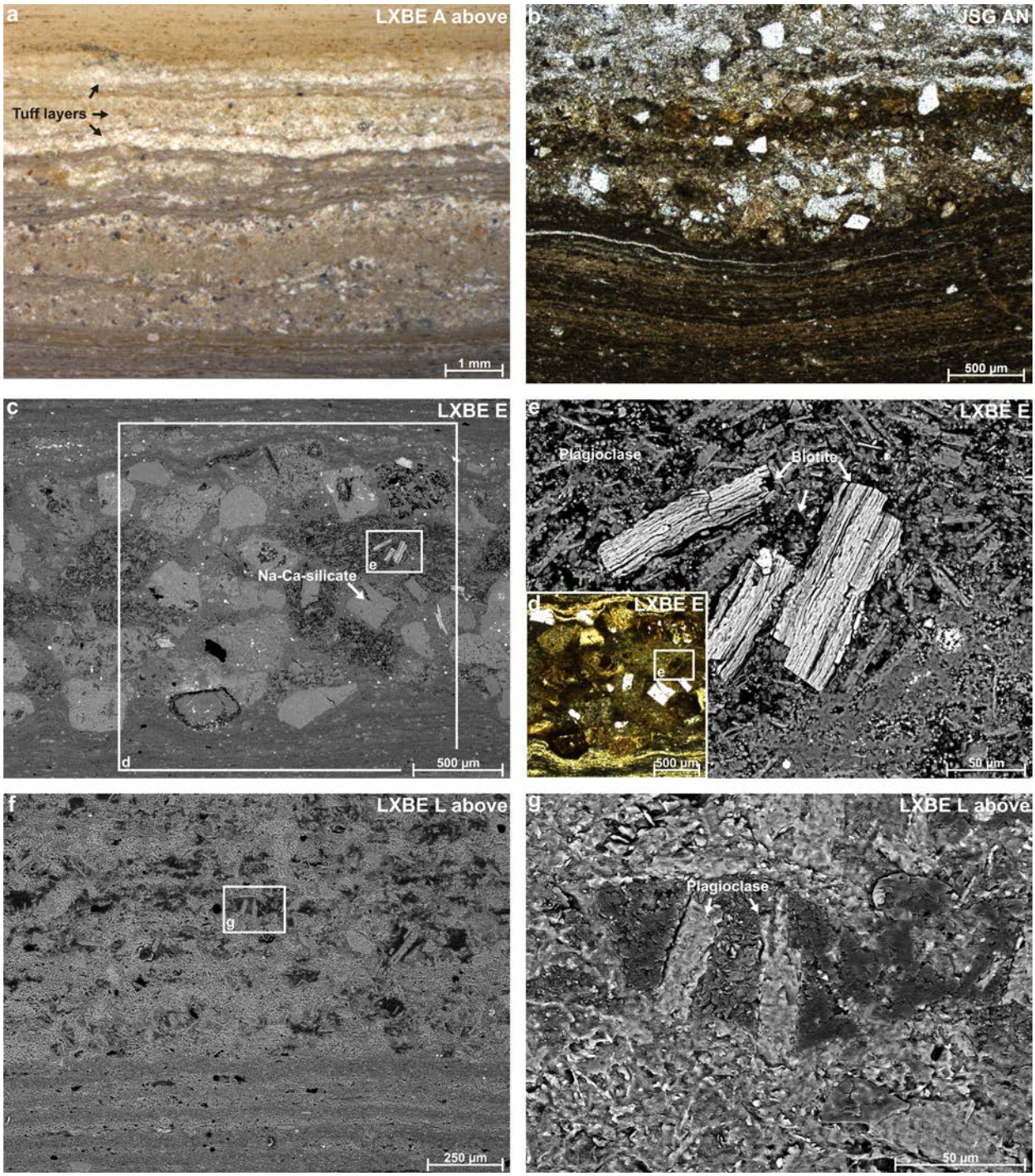

Fig. 1.10. Microfacies 5 (Mf 5): Tuff. (a) Reflected light. (b, d) Plane-polarized light. (c, e-g) BSE images. (a, b, d) Ash-tuff layers (arrowed) regularly interrupt the background sedimentation and, depending on thickness and grain size, often distort the underlying lamination. (c-e) Major components of the LXBE E-ash-tuff layer are rock fragments (~ 50 %) and feldspar (40 %). Accessory minerals, such as biotite, occur. (f, g) Most of the pyroclastic crystals in Mf 4 are made up of plagioclase.

Conversely, only small-scale scouring, if at all, can be observed at the base of Mf 3-laminae in Mf 1-yielding sediments, but usually underlying laminae are left undisturbed (Fig. 1.8d). This suggests that Mf 1-couplets must have been somehow stabilized (e.g. by biofilms) or that, at times, the deposition of tuffaceous silt occurred through hypo- or mesopycnal inflow. This would explain the smaller grain size of Mf 3 in Fig. 1.8d, as the bed load of the sediment influx was probably deposited in more proximal regions of the lake. As tuffaceous silt was incorporated into the varve-forming process (arrows Fig. 1.6b, Fig. 1.8d), varve thickness highly fluctuates depending on the occurrence of Mf 3-events.

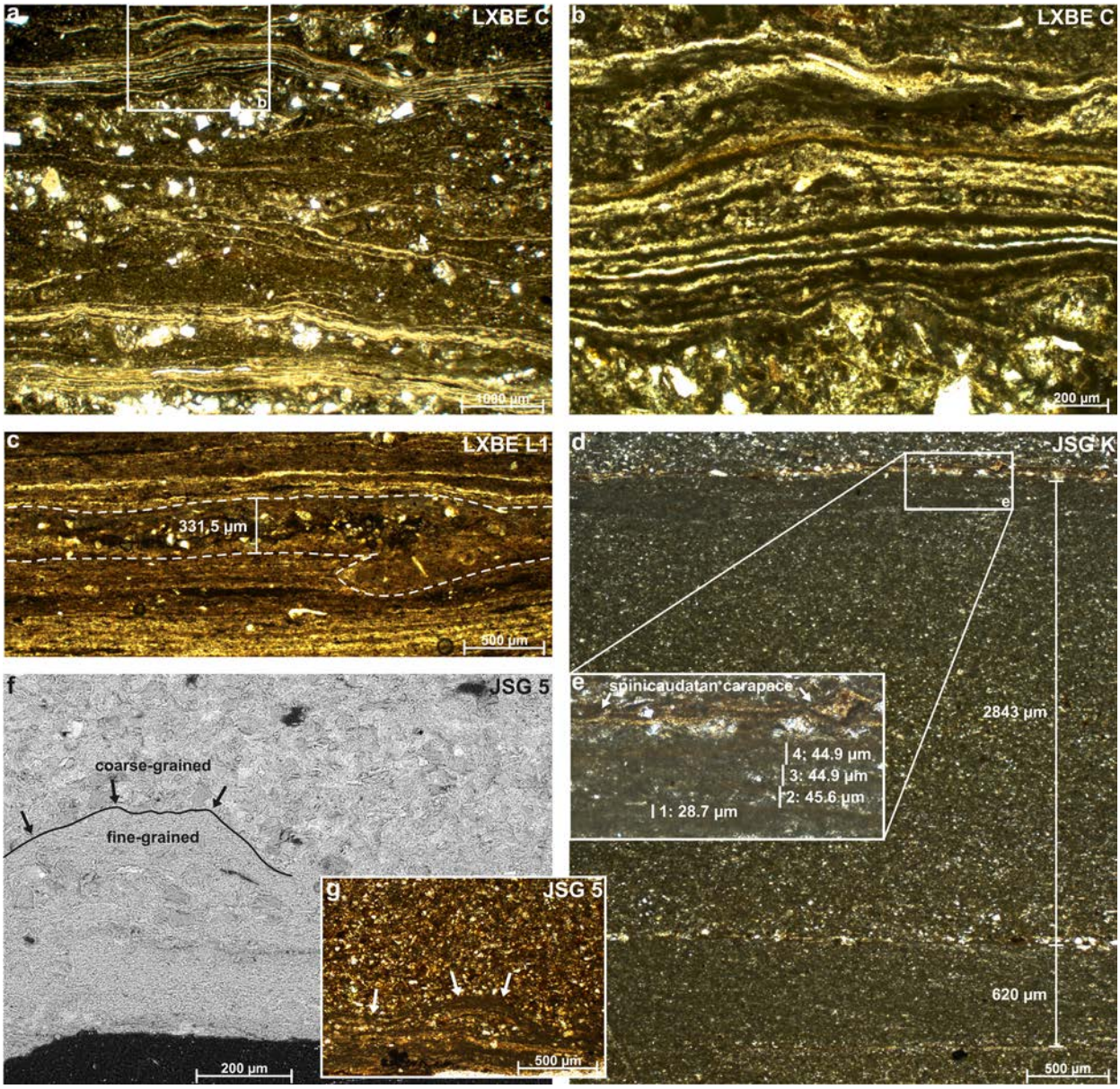

Fig. 1.11. Biofilms and Microfacies 6 (Mf 6): Normal-graded, sandy to silty siliciclastics of Phase 3. (a-e, g) Plane-polarized light. (f) BSE image. (a, b) Irregular lamination overlying tuffaceous material of Phase 2 is probably indicative of biofilm stabilization. (c) ~5 mm long (left and right ends not on the picture) and up to 331.5 µm thick microbially stabilized patch with depositional folding at its right end. The laminae overlying the cohesive patch and those directly underlying it meet at the edges of the patch, implying that it was transported for some distance. (d, e) Typical Bed 3-deposit of thicker, normal-graded units that are overlain by several minor, organic-rich layers. Clam-shrimp carapaces are commonly found on top of depositional units. (f, g) Biofilms (arrowed) are also found in Phase 3 deposits. In BSE images they are marked by fissures. The microbial structure is mound-like and accommodates fine-grained siliciclastic material that has been deposited during an equally tranquil period as the four laminae shown in (e).

Microfacies 4: Lacustrine chemical precipitates

Mf 4 consists of siliciclastic layers grading upward into layers rich in lacustrine chemical precipitates, which are recurrent throughout Phase 2 and composed of predominantly calcium carbonates. Fibrous gypsum, a second chemical precipitate that occurs in several mm to cm-thick layers, is associated with cm-thick coal layers of Bed 2 and thought to be secondary as a product of sulphide oxidation (see pyrite framboids below). The BSE images in Fig. 1.9 show light-grey and darker grey areas that are indicative of $CaCO_3$ and siliciclastic material, respectively, as the mapping in Fig. 1.9b confirms. The patchy distribution of micritic calcium carbonate (light areas) is especially apparent in the BSE image of Fig. 1.9d and accounts for its intensive diagenetic dissolution. Replacement of calcium carbonates by silica has been observed (Fig. 1.9e).

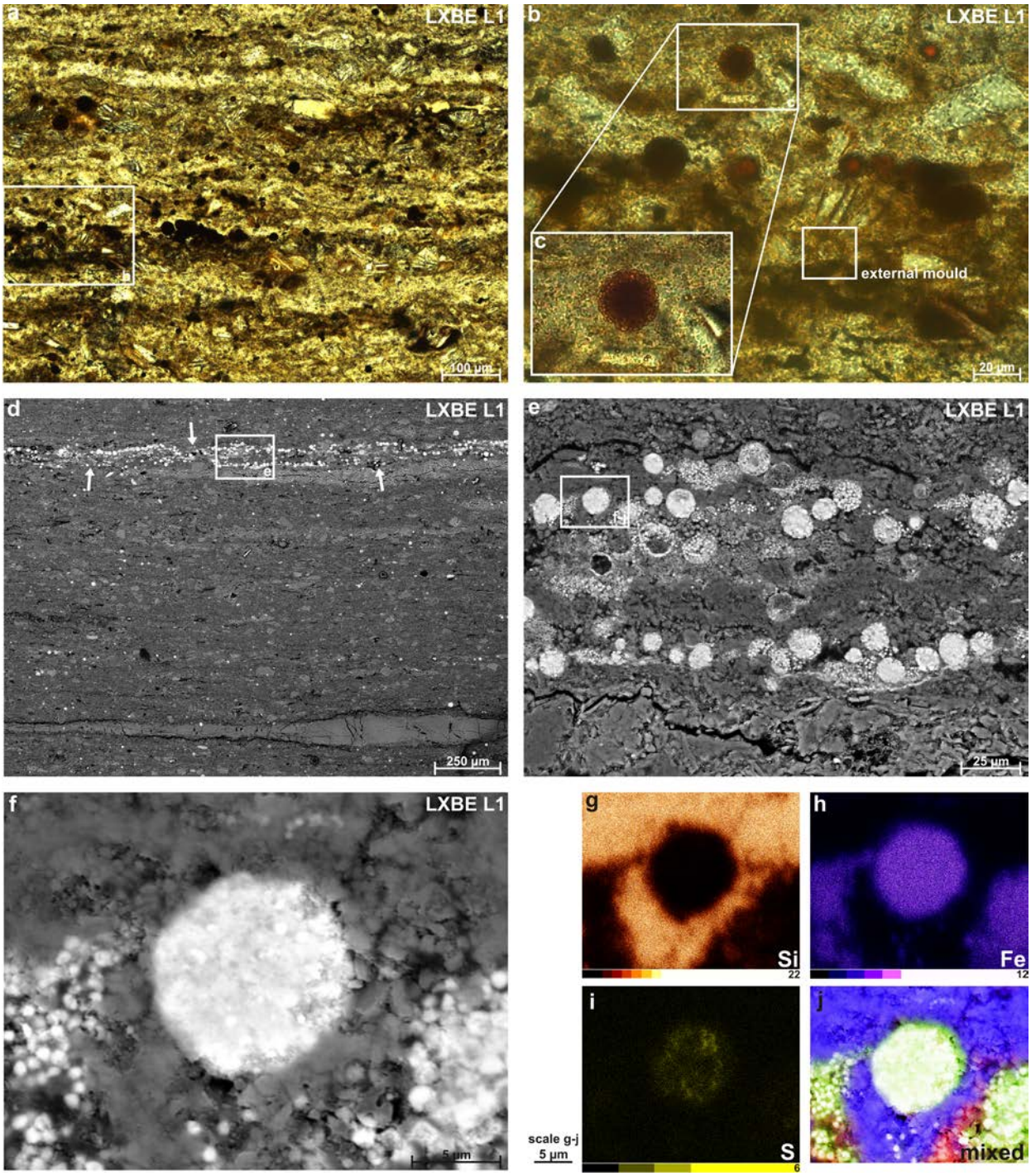

Fig. 1.12. (a, b) Plane-polarized light. (d-f) BSE images. (g-j) Element maps. (a, d) Overview of framboids (pyrite pseudomorphs) in Microfacies 1. They occur scattered within the matrix as well as concentrated in layers (arrowed). (b, c) The colour of framboids is commonly altered to a distinct red. External moulds occur. (e) Close-up view of two framboid concentrations forming discontinuous layers adjacent to each other. Note the different stages of preservation from framboidal to disintegrated. (f) Detail used for element mapping. (g) Element maps obtained with an ED spectrometer revealing the spatial distribution of Si, Fe, and S. Mixed: Si = blue, Fe = green, and S = red. Note that remnant sulphur is preserved in the centre of the framboid as well as in the microcrystals adjacent to it.

EDS spectra do not show any Mg peaks, implying low Mg/Ca ratios in the lake during precipitation. According to Müller et al. (1972), low Mg/Ca ratios favour the formation of primary calcite and/or high-Mg calcite (rarely aragonite).

Mf 4 constituents form couplets, consisting of a siliciclastic-dominated layer that is overlain by a more carbonate-rich layer towards the top (Fig. 1.9c). In the upper part of the couplets, argillaceous carbonates are prominent. The carbonates are always

mixed with a fair amount of siliciclastic material, supporting the hypothesis of ongoing Mf 1-sedimentation proposed above in the paragraph about Mf 1-layering (Fig. 1.6a, Table 1.1). Both materials are more or less distinctly separated by a prominent, dark, organic-rich layer (arrowed in Fig. 1.9c). Next to this prominent layer, many additional streaks of sub-seasonal dark organic laminae can be identified. Concentrated layers of framboids occur (Fig. 1.9d, f), which are curiously disintegrated and confined to exclusively siliciclastic horizons, but they may be topped by calcium carbonates (Fig. 1.9d, f). Mf 4-couplet thickness measured in several thin-sections ranges from 107 to 534 µm.

Microfacies 5: Tuff

The very fine rhythmic lamination occurring in Phase 2 is often interrupted by generally much thicker ash-tuff layers (Fig. 1.10). A typical ash-tuff horizon starts with basal ballistics forming craters (Fig. 1.10c, d), followed usually but not necessarily by finer-grained material, mainly irregularly distributed plagioclase (Fig. 1.10e, f, g) and smaller volcanic rock fragments (Fig. 1.10c, d). General components are rock fragments, plagioclase, alkali feldspar, biotite (Fig. 1.10e), and quartz.

Volcanic eruptions frequently interrupted the ongoing deposition of detrital material, as several consecutive tuff layers in Fig. 1.10a show. At least four eruption events are depicted. The pre-eruption deposits are dark, whereas the post-eruption lake deposits are lighter-coloured. This might either be a result of a post-eruption excess supply of light tephra in the vicinity of the lake or of tuff layers acting as seals sheltering the underlying laminae from weathering. The deposition of thicker tuff horizons led to indentations into the lamination (Fig. 1.10b). Several authors (e.g., Liu et al., 2002; Leng and Yang, 2003; Fürsich et al., 2007) suggested that eruption events might have had an impact on overall lake ecology and fossil preservation.

Microfacies 6: Normal-graded, sandy to silty siliciclastics (Bed 3)

Typical for Bed 3 are comparatively coarse siliciclastics (Fig. 1.11 d-g) made up of beige, normal-graded silty fine sand to silty clay, which are finely bedded. The thickness of individual layers is several mm to few cm. There is also evidence of biofilms, producing mound-like structures within the finer-grained fraction. They occur in the upper part of depositional units and are succeeded by new pulses of coarser-grained sediments (Fig. 1.11f, g).

Casts consisting of opaque minerals on bedding planes are common. They also affected clam-shrimp carapaces, which occur preferentially on top of depositional units (Fig. 1.11e). Soft-sediment deformation, such as slumpings, is common within Bed 3. Occasionally, Mf 6-deposits disrupted the sedimentation process in horizons of Bed 2.

Biofilms

The presence of many cycles of undisturbed, very fine Mf 1-lamination suggests biological forcing, but cannot be used as evidence by itself. However, four features of beds 2 and 3 imply the presence of biogenic sedimentary structures. (1) Unusually irregular laminations observed in several horizons have likely been produced by microbial activity (Fig. 1.11a, b). (2) Transported fragments of microbially stabilized laminae occur as laterally discontinuous patches (Fig. 1.11c). (3) Small-scale wrinkled and folded patterns on bedding planes, which are also known from bedded cherts of Lake Magadi (Behr, 2002), are interpreted to originate from sliding of sediment layers on mucilaginous bacterial films caused by seismic tremors. (4) Mound-like structures are evidence of microbial activity that occurred during the deposition of finer siliciclastics within Phase 3 (Fig. 1.11f, g).

Pyrite framboids

Pyrite framboids are common in Bed 2 (especially Mf 1). The structures are composed of aggregates of euhedral crystals forming framboidal spheres (Fig. 1.12). They occur concentrated in discontinuous layers and scattered (diameter = 2.5-35 µm) and their colour is predominantly red, which is often only revealed under plane-polarized light by overexposure. There are transitions in colour from colourless to orange and black. The latter often goes along with a bigger sphere diameter of > 20 µm. Colourless framboids, which represent external moulds, are blending in with the surrounding sediment, rendering them hard to discern (Fig. 1.12b). These transitions signal that colour is a secondary feature.

Element maps (Fig 1.12g-j) show that Fe is clearly dominating and that remnant sulphur is preserved within the framboid as well as in the microcrystals adjacent to it. Hence, these framboids represent pseudomorphs of pyrite micro-concretions altered to iron oxides and hydroxides, as EDS spectra show predominantly Fe and O peaks. Many framboids appear hollow inside (Fig. 1.12e). Framboid formation undergoes a succession of initial precipitation of phases such as mackinawite ($Fe_{1+x}S$)

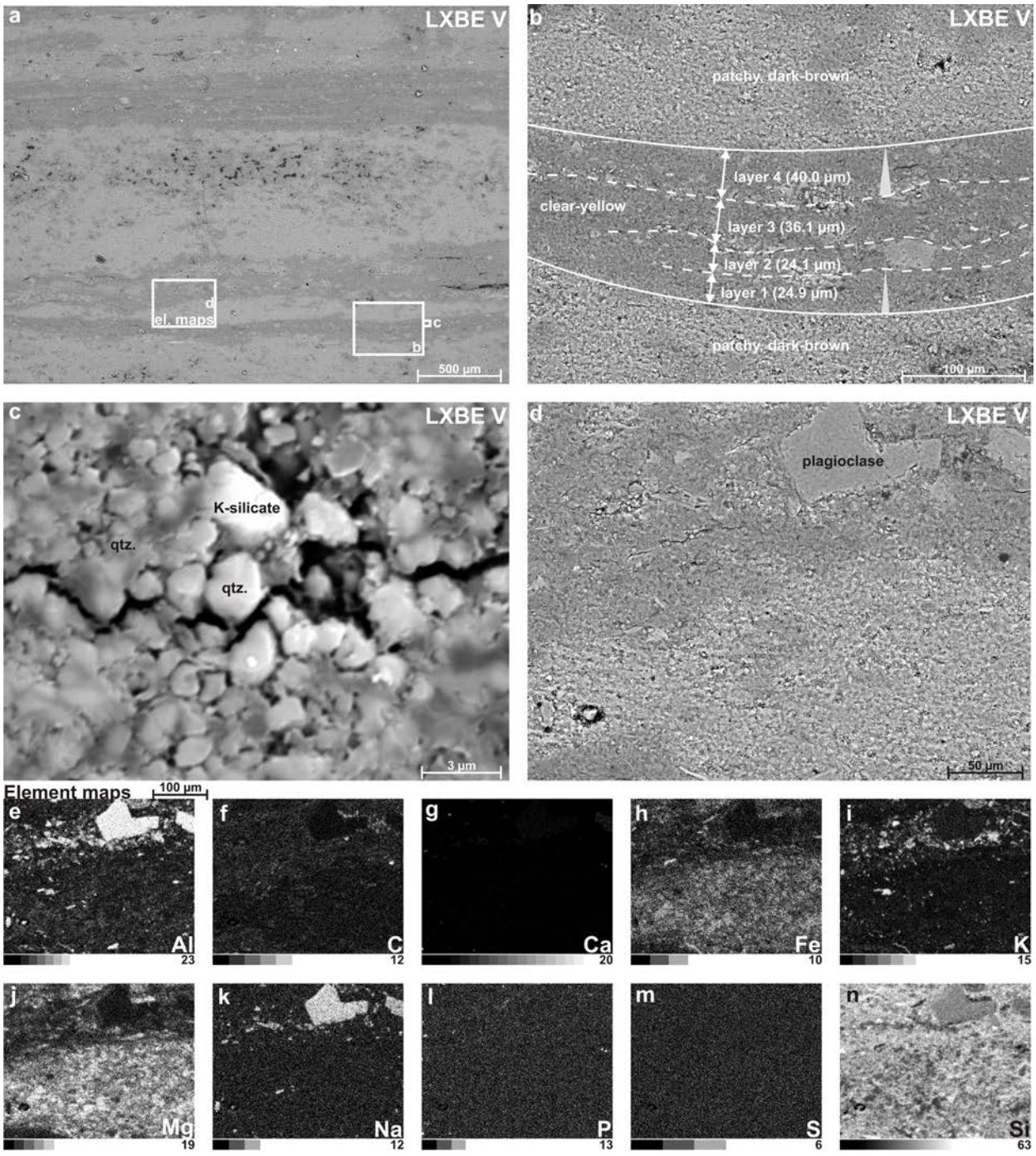

Fig. 1.13. Sediment alteration. (a-d) BSE images. (e-n) Element maps. (a) BSE image of Fig. 1.5e. (b) The three filaments of black nodules visible in Fig. 1.5e appear as diffuse bright streaks that are traced with dashed lines. They follow lines of weaknesses that enabled water migration and precipitation of an Fe- and Mg-rich veneer. Hence, the filaments trace actual laminae boundaries. Normal grading can be inferred in layers 1 and 4. (c) Close-up of lamina boundary and Fe-Mg-stained grains. (d) BSE image corresponding to the element maps (e-n) with partly dark-brown materials (lower part) and partly clear-yellow materials (upper part, Fig. 1.5e). There is a difference in composition between the two, as elements such as K and Al are enriched in the upper, clear-yellow region, whereas Fe and Mg, which possibly belong to smectites, are concentrated within the dark-brown area that exhibits only very low concentrations of C. Note that the detection of C with the EDS is much more imprecise than that of the other elements listed. Clear-yellow layers belong to altered Microfacies 1, whereas dark-brown materials could represent the weathering product of either Microfacies 2, 3, or 5.

or amorphous iron sulphide (Sweeney and Kaplan, 1973) and subsequent transformation to ferrimagnetic greigite (Fe_3S_4), which is unstable under excess H_2S. This ultimately leads to the formation

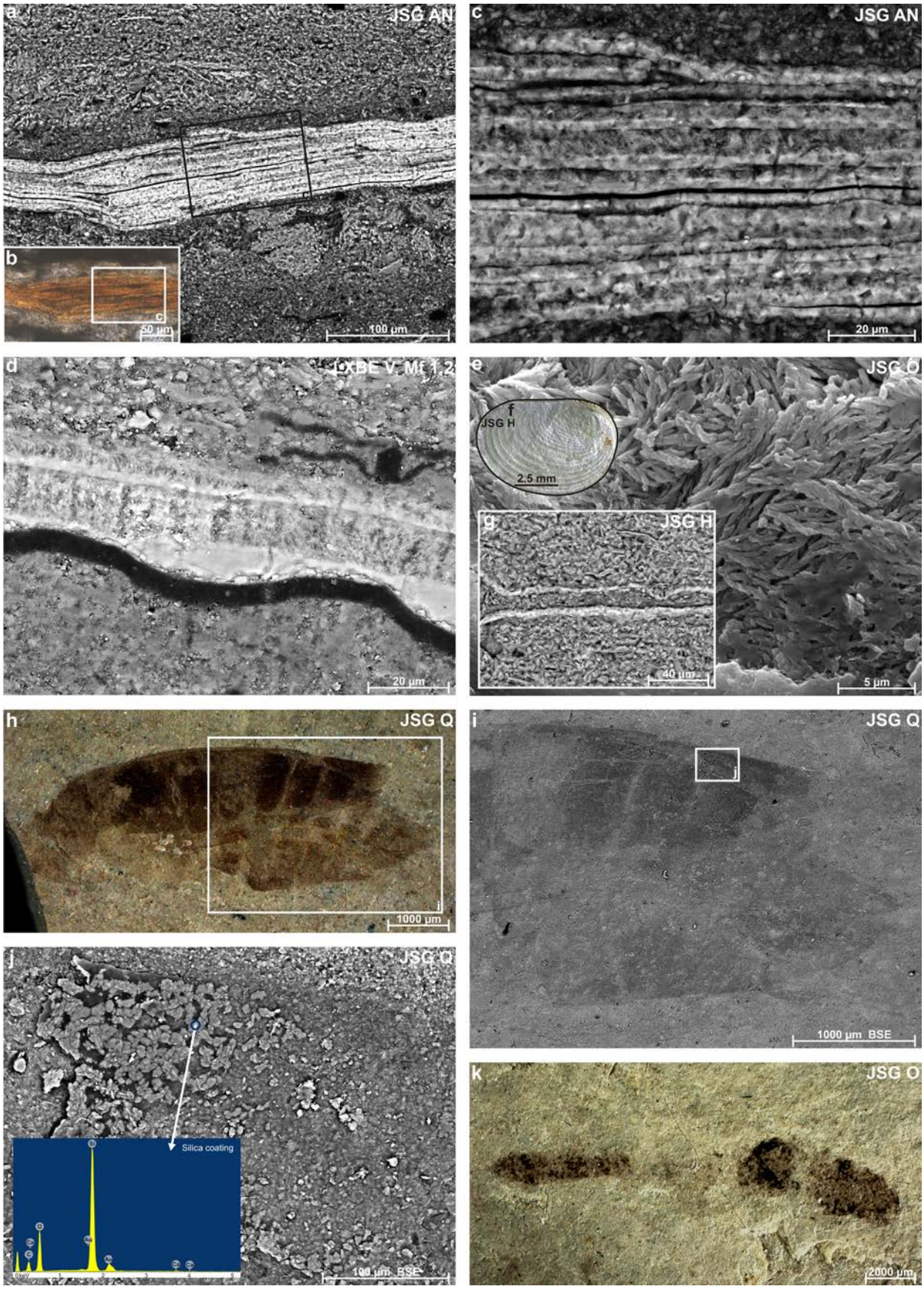
a
JSG AN
b
c
50 µm
100 µm
c
JSG AN
20 µm
d
JXBE V, Mf 1,2
20 µm
e
JSG O
f
JSG H
2.5 mm
g
JSG H
40 µm
5 µm
h
JSG Q
i
1000 µm
i
JSG Q
j
1000 µm BSE
j
JSG Q
Silica coating
100 µm BSE
k
JSG O
2000 µm

← **Fig. 1.14.** Fossil preservation. (a, c-e, g, i, j) BSE images. (b) Plane-polarized light. (f, h, k) Reflected light. (a-g) Comparison of clam-shrimp preservation between Phase 2 (a-d) and Phase 3 (e-g). (a-c) Growth increments are well distinguishable in cross-sections of clam-shrimp carapaces preserved in Phase 2. (d) Diagenetic overprint as observed in Microfacies 1.2 of Phase 2 led to dissolution and successive loss of detail. (e-g) The internal structure of Phase 3 clam-shrimp carapaces is no longer preserved and usually much thinner owing to dissolution. Fluorapatite crystals are about 450-650 nm wide. (h-k) Soft parts of aquatic invertebrates from Phase 3 are preserved as a dark stain covered by a silica coating.

of pyrite (Berner, 1981). Greigite forms spherules that form the nuclei for pyrite framboids (Sweeney and Kaplan, 1973). Framboid formation requires a higher pH, otherwise the metastable pyrite precursors important for framboid formation would not form (Farrand, 1970; Sweeney and Kaplan, 1973). The fastest rates of experimental framboid formation are achieved when air is periodically bubbled into the reaction vessel (Wilkin and Barnes, 1996). Therefore, there are steps within framboid formation that require weakly oxidizing conditions.

Sediment alteration

Alteration of sediment led to severe modifications in sediment appearance. A pervasive overprint is expressed in a jumble of clear-yellow and dark-brown irregular colours (white arrows in Fig. 1.5e, f). These patchy, dark-brown phases overprint lighter, less flamboyant colours, obscuring large portions of the lamination and rendering precise diagnoses of microfacies impossible. Pyrite framboids disappear within these altered parts, leaving only dark remnants behind, if at all. Bleaching along fissures is also common. The dark-brown and clear-yellow regions differ compositionally (Fig. 1.13e-n), as elements such as K and Al (indicative of feldspars) are dominant in the upper, clear-yellow regions, whereas Fe and Mg are concentrated within the sediment covered by the dark-brown stain, signalling the presence of Mg-rich clay minerals (smectites). This region is curiously devoid of C, excluding organic debris as reason for the dark-brown colour. High values of Si underline the general predominance of quartz grains and silicates. However, Si is not distributed evenly, as its concentration is slightly lower where Mg is especially common, which is most likely incorporated into smectites. The nodule-like element-map pattern of the dark-brown layer is similar to that of Mf 2-element maps (Fig. 1.7), but these nodules could also represent feldspar grains of tuffaceous silts (Mf 3) or tuffs (Mf 5) altered to clay minerals. Therefore, it is not possible to identify a distinct microfacies for the dark-brown layers.

Clear-yellow regions (Mf 1) are easier to assess, as they are streaked with delicate filaments of opaque phases (ø ~ 1 μm, arrowed in Fig. 1.5f). These pearl-string arrangements observed under transmitted light do not show on BSE images (Fig. 1.13a), where they appear as diffuse bright layers that are traced with dashed lines in Fig. 1.13b. The formation of the black nodules is possibly associated with staining of the matrix with Mg- and Fe-rich minerals along lines of weaknesses that are observed as delicate cracks (Fig. 1.13c) corresponding to boundaries between different laminae. The thicknesses of the inferred four layers in Fig. 1.13b range between 24.1 and 40.0 μm, which lies well within the thickness range of Mf 1-laminae (Figs. 1.5a, 1.6a).

Fossil preservation

Beds 2 and 3 both yield well-preserved fossils, but their mode and/or detail of preservation differ (Fig. 1.14). Excellently preserved fossil groups of Bed 2 are often less well preserved in Bed 3 and vice versa. Hence, fossil preservation in different beds of Lake Sihetun is group-specific. The following account is not meant to be complete. It should rather point out differences between the two beds analysed.

Bed 2

The preservation of fossils within Bed 2 is generally excellent and dominated by replacement of plant tissue by iron sulphides represented by concentrated framboid layers (Fig. 1.12d, e). Preliminary taphonomic studies on three fossil plants and two feathers from the Dawangzhangzi Bed and the Jianshangou Bed led Leng and Yang (2003) to propose a fossil-envelop model with a micro-environment, in which pyrite framboids formed. Most framboids observed formed on the surface of plant fossils, whereas they were only sporadically found in feather samples. According to Leng and Yang (2003), replacement of fossil tissue occurred by precipitation of pyrite microcrystals and only subordinately by framboids. However, only a statistically small number of fossils had been studied by them.

The original structure of clam-shrimp carapaces, which are not shed during ecdysis, was retained for those spinicaudatans that biomineralized with biologically relevant calcium phosphates, such as hydroxyapatite and amorphous calcium phosphates (Fig. 1.14a-c). The calcium phosphates diageneti-

cally recrystallized to flour-apatite crystals that are 650 nm wide on average and several μm long. Bed 2 of the Jianshangou Unit yielded mostly excellent preservation with 5-7 growth increments per valve observed in thin-sections and only traces of dissolution features, which are commonly very pronounced in many clam-shrimp occurrences of other lake sediments studied by the authors. Dissolution led to a loss of detail within the internal structures of clam-shrimp carapaces that occur in the intensively altered horizons of Mf 1.2 (Figs. 1.5e, f, 1.14d).

Bed 3

Clam shrimps of Bed 3 show the same overall mineralogy as those from Bed 2, but internal structures within the valves have been completely obscured by dissolution and re-crystallization processes (Fig. 1.14e-g). This cannot be a function of crystal size, as it is similar (450 nm wide on average) to that observed in Bed 2-carapaces. Rather, this might be an effect of the coarser grain size and higher porosity and permeability within Bed 3. In addition, ash-tuff layers frequent in Bed 2, which shelter fossils from degradation, are not common.

In contrast, Bed 3-insect fossils are very well preserved (Fig. 1.14h-j). Preservation has been tested on an aquatic insect of the order Hemiptera that is preserved as a dark imprint, showing Fe- and Mg-peaks in EDS spectra, and protected by a silica coating on top. The same mode of preservation has been observed for a possible oligochaete (Fig. 1.14k).

Discussion

The main questions stated in the introduction revolve around climate and its effects on the physicochemical properties of Lake Sihetun. Indicators to look for are different types of microfacies and lamination (Fig. 1.15), as well as sediment yield. Precipitation is used as the main climatic factor when assessing sediment yield as it has great effect on vegetative ground cover and runoff.

So, do the sediments of Lake Sihetun reflect an underlying seasonality? Do all rhythmites observed represent varves, i.e. annual groupings of seasonal laminations forming in quiet, deeper waters? Liu et al. (2002) found no evidence that could demonstrate that the laminations are varves, but still interpreted them as such using modern-day analogues. As a general rule, non-glacial varves must contain two components that set each other off, including at least one autochthonous constituent that usually creates a more predictable annual signal than the allochthonous siliciclastic component by itself (Anderson and Dean, 1988). The following paragraphs are revolving around the question whether the laminations observed can or cannot be interpreted as non-glacial varves. This analysis then leads to an assessment of the underlying environmental signals found in the laminated sediments of Lake Sihetun.

Phase 2

Phase 2 is governed by Mf 1-laminations, but sporadic intervals of Mf 4-carbonate precipitates occur. Chrysophycean cyst accumulations (Mf 2) are rare. All are frequently interrupted by tuffaceous silt (Mf 3) and tuff layers (Mf 5), which are often proposed to have been responsible for the excellent preservation of vertebrates (e.g., Liu et al., 2002; Leng and Yang, 2003; Fürsich et al., 2007).

Mf 1

Mf 1-laminations mainly consist of allochthonous siliciclastic material forming paper-thin laminae that lack any preserved autochthonous carbonate precipitates (Fig. 1.5). Such regular siliciclastic laminations cannot have been produced during continuous influx of siliciclastics. Therefore, breaks in deposition must have been present to provide time for settling of suspended material and stabilization processes, such as microbial overgrowth (Fig. 1.11a-c). During these breaks, organic accumulation occurred. Mf 1-thickness changes correspond to cycles of 9 to 18 couplets each (Fig. 1.6a; Table 1.1). As the major components are siliciclastic, the thickness changes of these cycles denote differences in humidity or storminess (Anderson 1964) and ground cover (Anderson and Dean, 1988).

Argillaceous silt was flushed into Lake Sihetun during the onset of heavier rain, which frequently interrupted otherwise dry conditions. Since grading within the corresponding deposits is indistinct to absent, a hypopycnal to homopycnal-flow origin and moderately prolonged siliciclastic influx can be inferred. Influx that occurred during stratification of the lake led to trapping of clay-sized particles within the surface waters, but allowed deposition of the silt fraction (brown layer). When the water column became destratified during overturn or the surface waters too sediment-laden (i.e. denser), deposition of clay-sized particles increased (light layer). During these times of destratification, which also led to rare colonization events of benthic invertebrates, settling of particles of all grain sizes was possible so that newly introduced coarser silt particles could settle time-equivalent to clay-sized grains previous-

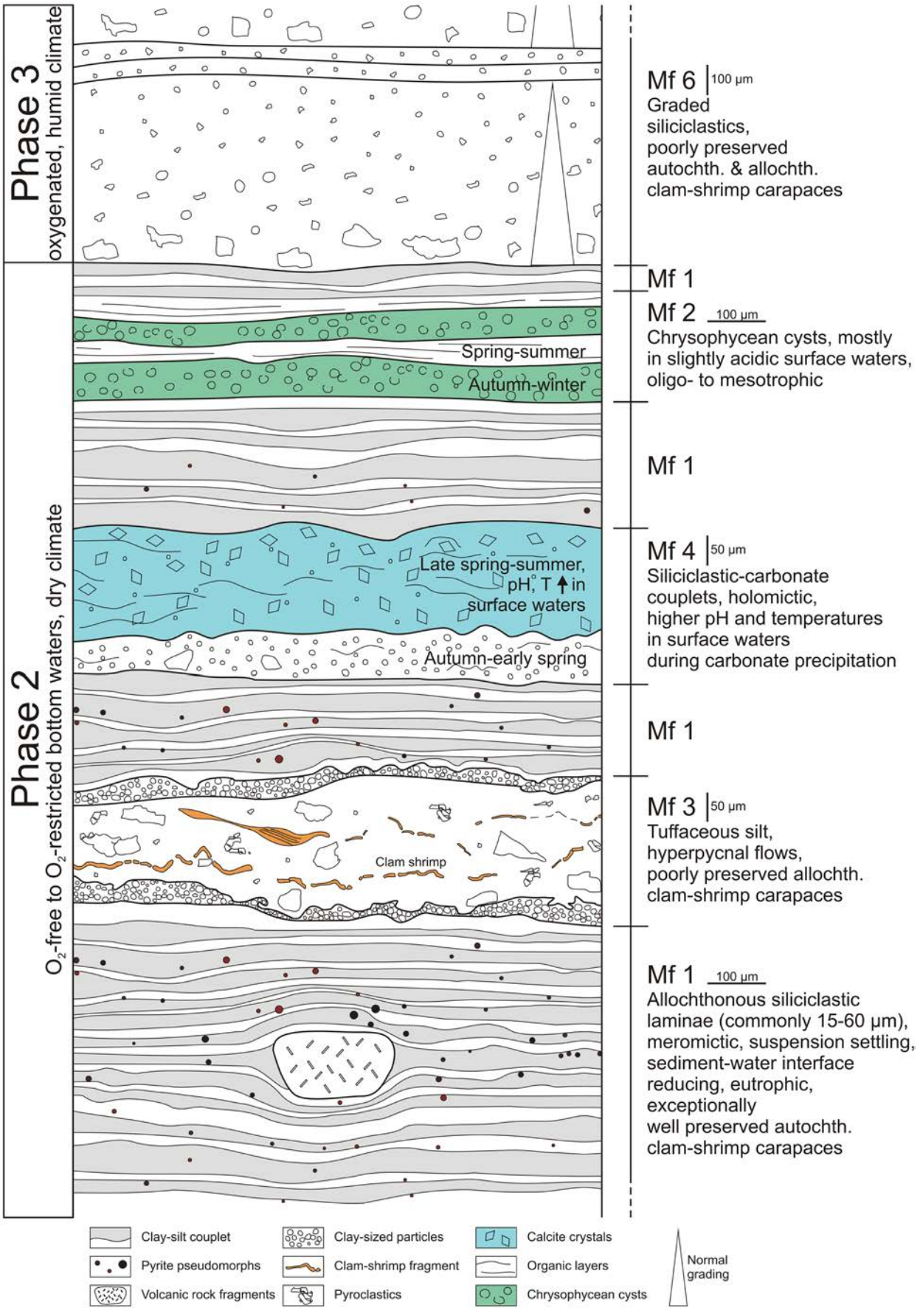

Fig. 1.15. Schematic representation of Phase 2 and Phase 3 deposits and their characteristic microfacies. Horizontal scales are applicable for components as well as lamina thickness. Vertical scales refer only to lamina thickness. Tuff layers (Microfacies 5), which are common in Phase 2-deposits, are not included in the figure.

ly trapped within the epilimnion (compare Sturm, 1979).

According to Sturm's (1979) idealized sedimentary features deferred from two hydrological parameters (stratification and influx of suspended matter), Mf 1 partly fits the model of influx of suspended matter being introduced to a stratified as well as to a mixed water column. Evidence for this model are sporadic silty to fine sandy particles occurring within some of the clay-dominated light layers. In truth, it cannot be safely reconstructed from Mf 1 how often the lake overturned, because complete mixing is not needed to explain the deposition of those light clay layers that do not contain any notably coarser grains. Therefore, it is possible that the lake remained stagnant during most of Phase 2. This is in agreement with the overall Phase 2-depositional model of a mostly stratified lake (Fig. 1.3b; Jiang et al., 2012). However, some degree of overturn must have occurred to account for the presence of invertebrates such as clam shrimps and aquatic insects during short recurrent intervals. This combined model of mostly stagnant conditions with discontinuous influx and occasional times of overturn might answer the question of why only some layers in Phase 2 yield aquatic invertebrates compared to the number of layers completely devoid of fossils. Hence, the model of summer stagnation and winter mixing proposed by Fürsich et al. (2007) has to be revised.

In summary, the constituents of Mf 1-couplets document a succession of (1) a flush of siliciclastic material reaching distal parts of the lake through hypo- or homopycnal flows, with possible sediment trapping of clay-sized particles in the surface waters and settling of silty grains, (2) deposition of clay-sized particles, and (3) organic-ooze formation. An annual signal cannot be inferred for single Mf 1-couplets. The low overall sediment yield might be related to dry conditions or, conversely, to dense ground vegetation, implying humid conditions (Langbein and Schumm, 1958; see discussion of precipitation and sediment yield below). Thus, Mf 1-rhythmites cannot be interpreted as varves, rendering any calculations about lake duration carried out in earlier papers pointless.

Mf 2 and Mf 3

A modification of the sedimentation process and changes in lake chemistry led to ecological changes, the addition of chrysophycean-cyst accumulations, and the introduction of coarser siliciclastic material to the Mf 1-lamination known from Phase 2. Mf 2 is a sub-seasonal phenomenon, as it contains seasonally responsive golden algae (Chrysophyceae) living as plankton in Lake Sihetun and providing evidence for non-glacial varve formation (Fig. 1.7).

The tops and the bases of Mf 2-varves are distinct, in contrast to Lake Soppen (Switzerland), where the base is sharp, while the upper boundary is indistinct due to a gradual increase in the amount of diatoms (Lotter, 1989). However, freshwater diatom floras, which are commonly studied in varve analyses of Recent lakes (e.g., Lotter, 1989), were not present during the Lower Cretaceous, as diatoms established themselves in lacustrine systems much later during the Oligocene (Anderson and Dean, 1988). The varves from Lake Soppen contain four constituents: Autumn chrysophycean cysts, spring diatoms, a late spring/early summer onset of calcite crystals, and fine calcite crystals during summer. Mf 2-varves of Lake Sihetun are different in lacking diatoms and the carbonate component, rendering chrysophycean cysts, which are commonly found in organic layers, their most important marker. Chrysophycean cyst layers were deposited during late winter and early spring in two eutrophic maar lakes of the Eifel Mountains, Germany (Zolitschka, 1989). But Eloranta (1995) showed, in a study of 329 lakes, that golden algae exhibit a clear summer biomass maximum, despite the occurrence of such winter taxa. As encystment occurs after the peak of blooming, one annual Mf 2-cycle of Lake Sihetun contains (1) a dark layer with a sharp base and top that is made up of allochthonous siliciclastics (in varying amounts), organic detritus, and chrysophycean cysts (autumn and winter) and (2) a lighter layer of Mf 1-siliciclastics (?spring and summer).

Fig. 1.8d is special, as the section depicted belongs to the chrysophyte-bearing horizon LXBE D and is located only few mm above the Mf 2-varve section measured in Fig. 1.6b, where incorporation of Mf 3 becomes progressively more abundant within its upper part (arrows in Fig. 1.6b). Chrysophytes have been identified within the basal parts of some Mf 3-deposits, suggesting that the deposition of both, Mf 2 and Mf 3, occurred during the same season (autumn). Hence, it is safe to assume that the measurements in Fig. 1.8d belong to annual cycles and that Mf 3-deposition occurred seasonally instead of continuously. During dryer times, in which siliciclastic inflow leading to the deposition of Mf 3 did not occur, the resultant layer only consisted of a dark lamina of organic detritus that is especially apparent at the base of the 34 μm-thick layer pointed out by arrows in Fig. 1.8d.

Generally, Mf 3 represents volcanic epiclastics, which were deposited throughout Phase 2, commonly decoupled from Mf 2. Volcanic ash was carried into the lake by surface runoff and reached the distal lake floor through hyperpycnal flows. Turbulence led to disturbance of the light-coloured background sedimentation (Fig. 1.8c). A remobilisation of pyroclastic-fall deposits becoming unstable at the lake margin is also likely. The presence of scattered broken clam-shrimp carapaces (red arrows in Fig. 1.8b) implies transportation of the crustaceans from more marginal areas, which must have been colonized at the time of deposition of Mf 3. It will be interesting to see whether species from this microfacies are different from autochthonous ones that colonized the more distal lake floor.

Depositional rates started to increase in the upper part of Phase 2. The change from the stratified lake interval of Phase 2 with mainly hypo- and homopycnal inflow to hyperpycnal inflow in Phase 3 (Jiang et al., 2012) may be represented by an increase of Mf 3-deposition induced by storms and floods. Since varves calibrate the rate of change (Anderson, 1964), it would be possible to establish time relations for Mf 3-occurrences. Continuous lamina counts, which are beyond the scope of this study, would be necessary to confirm this.

Mf 4

A second type of varve can be reported from Phase 2 through the seasonal formation of carbonate oozes at the lake floor (Mf 4). The primary formation of calcium carbonates can be inferred from a low Mg/Ca ratio in the lake waters (Müller et al., 1972). The amount precipitated was a result of seasonal changes, most likely in temperature as the most critical factor, but plankton production as well as dilution and precipitation might also have been important influences (Anderson, 1964). The precipitation of carbonates is associated with a decrease in dissolved CO_2 that is accomplished during the warm season and through a binding of CO_2 during increased photosynthesis rates, which are high in late spring and summer (Kelts and Hsü, 1978; Anderson and Dean, 1988). Furthermore, $CaCO_3$-precipitation can also be a result of calcium-rich waters flowing into a carbonate-rich lake or vice versa. The processes described are abundant in surface waters and it is possible that dissolution occurring as the crystals settled might have obscured this autochthonous signal in the sedimentary record. In other words, precipitation of carbonates during the deposition of Mf 1, where no clear signal indicates annual layering, might have occurred but no trace of it is left.

Calcium carbonate most likely formed during the warm and dry seasons. The siliciclastic-dominated layer (Fig. 1.9c) therefore represents autumn to early spring, while the carbonate-dominated layer was deposited during late spring and summer. The former is often not laminated (Fig. 1.9c), implying the presence of meiofaunal bioturbation and, at least, oxygen-restricted instead of oxygen-free conditions within the hypolimnion. This scenario describes a monomictic lake with overturn once a year, which, for example, occurs from late autumn to early winter in the monomictic Obersee (Lake Constance; Schäfer, 2005). Mf 4-varves were deposited in the deeper part of the lake with average rates of deposition of about 200 µm/a. These rates are on the lower end of the average rates proposed by Anderson (1964), which are 0.1-1 mm. According to Anderson (1964), third-order stratification (100-300+ a) accounts for climatic changes sufficient to induce the modifications in composition observed in Phase 2 from Mf 1-siliciclastics to Mf 4-varves. An important second impulse for the precipitation of chemical sediments in Lake Sihetun might have been an unusually high geothermal heat flow (see discussion of temperature below).

These intervals of Mf 4-deposition during Phase 2 (Fig. 1.9) may offer an explanation for the nature of Mf 1-laminations, assuming that Mf 1-deposition was taking place without interruption as a background signal. Proof of this are (1) sub-seasonal dark organic layers (arrows in Fig. 1.9c), which are recurring throughout one Mf 4-varve and possibly are analogous to Mf 1-organic layers, and (2) the ongoing siliciclastic deposition in the carbonate-bearing horizons. If this assumption proves to be true, Mf 4-varve thicknesses can be correlated with those of Mf 1-cycles. Then, one cycle consisting of several Mf 1-couplets would represent an annual layer with waxing and waning amounts of siliciclastic material related to more humid and dryer conditions.

Phase 3

The change to thicker, normal-graded laminae (Mf 6) represents a change from a mostly stratified, meromictic lake that prevailed during most of Phase 2 to a holomictic lake with oxygenated bottom waters, in which deposition by hyperpycnal flows was predominant. This change occurred across the lake basin.

The transition from Phase 2 to Phase 3 is marked by a dramatic increase in the input of siliciclastic material into the lake related to changes in the drainage basin, such as a shift in vegetative ground cover associated with climate change. In sediment cores of Elk Lake, Minnesota, the deposition of siliciclastic material became more pronounced during the mid-Holocene dry climatic interval that led to a shift from coniferous forests to prairie vegetation (Anderson et al., 1993). Hence, it is clear that climate change must have triggered the change in sedimentation from Phase 2 to 3. Whether conditions became dryer, providing more erodable siliciclastic material, or more humid, which would have led to a greater amount of discharge, is discussed below under precipitation and sediment yield.

Palaeoenvironment

Information on some environmental parameters governing ancient Lake Sihetun can be deduced from the results presented above. They concern precipitation and sediment yield, trophic state, temperature and depth, and chemical factors, mainly alkalinity and oxygen concentration.

Precipitation and sediment yield

Langbein and Schumm's (1958) study of mean annual precipitation in relation to sediment yield in drainage basins determined a maximum annual sediment yield at 254-356 mm effective precipitation. Erosion is a function of vegetal density throughout the climatic range and the direction of change in sediment yield is dependent on the amount of mean annual precipitation before the change (Langbein and Schumm, 1958). There are three scenarios for sediment-yield responses to a change in humidity. (1) An increase in annual rainfall would be followed by an increase in erosion within the 0-305 mm precipitation zone. (2) Higher rainfall within the precipitation zone 305-1143 mm results in decreased erosion. (3) Above 1143 mm, erosion remains more or less constant with an increased amount of rainfall.

So, the change from low (Phase 2) to significantly higher sediment yield (Phase 3) can be connected to an increase in rainfall (wetter conditions), if climatic conditions during Phase 2 were dry (scenario 1). Alternately (scenario 2), if the climate had been slightly humid during Phase 2, a change to an either wetter or dryer climate would have resulted in a decrease in erosion and lower sediment yield in either case due to increased vegetative ground cover or decreased runoff, respectively. Therefore, scenario 2 can be ruled out, as sediment yield increased significantly in Phase 3. Scenario 1 is proposed here, assuming *dry* conditions during Phase 2, which changed to *wetter* conditions that triggered the onset of Phase 3.

Also, sediment yield is commonly increased during the loss of vegetation in the course of eruption events (Anderson and Dean, 1988), which do not correspond to any particular season. Therefore, also of prime importance for the deposition in Lake Sihetun was the availability of volcanic detritus from the surrounding area.

Trophic state

Lake Sihetun was generally eutrophic during Phase 2. Eutrophic conditions favour the formation of pyrite, which requires ample amounts of organic matter for bacterial sulphate reduction (Berner, 1984).

However, oligotrophic to mesotrophic lake intervals are also recorded from Phase 2, which are connected to the deposition of chrysophycean cysts (Mf 2). The highest number of chrysophyte taxa occurs in mesohumic, mesotrophic lakes (Eloranta, 1995). Naturally, the highest chrysophyte biomass is measured in mesotrophic to moderately eutrophic lakes (Eloranta, 1995), but the amount of chrysophytes decreases significantly at higher levels of eutrophy (> 5 gm^{-3} biomass). Other sources indicate that chrysophytes are most important in oligotrophic lakes, where they often dominate the phytoplankton biomass (Siver, 1995). Hence, arguments point to an oligotrophic to mesotrophic Lake Sihetun during times of Mf 2-varve formation in Phase 2.

Temperature and depth

Heat exchange processes in lakes include solar radiation, sensible heat transfer, heat loss during evaporation, and conductive heat flow from geothermal sources (Ragotzkie, 1978). The Yixian Formation of the Sihetun area was located well within temperate latitudes (Enkin et al., 1992; Zhou et al., 2003; Amiot et al., 2011) and mean air temperatures estimated for the Barremian-Early Aptian are assumed to have ranged around 10 ± 4°C at mid-palaeolatitudes of about 41.9° (±6.6°) N, indicating an icehouse event during the Early Cretaceous (Amiot et al., 2011). Therefore, cooling must have occurred to some extent in Lake Sihetun from late summer to winter.

During the holomictic Phase 3, temperature was mainly governed by heating of the lake surface from solar radiation, creating a buoyant epilimnion during summer leading to the development of a ther-

mocline in a thermally stratified lake. As Phase 2 is interpreted to have been meromictic most of the time, temperature assessments are not as easily performed.

Lake depth has a great effect on the heat budget, since the heat storage capacity is much higher for larger, and usually also deeper, lakes. So far, Lake Sihetun was interpreted to have been shallow, explaining the presence of a shallow-water invertebrate fauna (Fürsich et al., 2007), but there are strong arguments for a moderately deep Lake Sihetun. Bounding faults account for steep lake margins (Jiang et al., 2011) and a certain depth was needed to keep the lake stratified, so that mixing would not reach the lake floor. Was Lake Sihetun subject to ice-sheet formation at some point during winter? Holomictic conditions, which were comparatively rare during Phase 2, would have been a prerequisite for ice-sheet formation during winter, since isothermal conditions were needed within the lake prior to ice formation. Especially in lakes with a moderate to large fetch, like Lake Sihetun, temperature needs to reach 1°C or less before freezing occurs (Ragotzkie, 1978). Lake Sihetun was subject to a temperate climate, yet signs of ice-sheet formation are vague. Dropstones are thought to have resulted from driftwood. Usually, the primary heat source in lakes is solar radiation, but in case of Lake Sihetun heat flow from geothermal sources should also be taken into account, since the sediments were deposited during a time of ongoing volcanic activity as documented by synsedimentary microfracturing and numerous tuff layers.

Alkalinity

During Phase 2, alkalinity near the sediment-water interface has probably been high as such conditions were needed for the formation of early diagenetic pyrite framboids. According to Sweeney and Kaplan (1973), pyrite framboids do not form in systems with a low pH, which would inhibit the formation of precursory metastable iron sulphide phases. If truly present, the alkaline, probably early diagenetic waters must have been the agent for the decomposition of the pyroclastics present within Lake Sihetun during Phase 2, creating silica-enriched waters, which in Lake Magadi (Kenya) led to the formation of colloidal silica sols (Behr, 2002).

Oxygen. – While the hypolimnion of the holomictic Phase 3 was oxygenated, bottom waters of the mainly meromictic Phase 2 remained mostly anoxic. However, the water column of the latter must have become completely mixed to some extent to account for short-lived colonization events by a benthic invertebrate fauna consisting of mayfly larvae, clam shrimps, and malacostracan crustaceans. During these overturn events and throughout Phase 3, the oxygen-deficiency model by Fürsich et al. (2007) with seasonal oxygen-depletion and reoxygenation of bottom waters explaining recurrent invertebrate mass mortality events can be applied.

Summary of environmental parameters during Mf 2 and Mf 4–varve deposition

During the late Phase 2, Lake Sihetun underwent considerable changes in its environmental parameters. Some of these are inferred from the presence of benthic chrysophycean resting cysts. Extant Chrysophyceae prefer oligotrophic waters of low specific conductance and slightly acidic conditions (Siver, 1988). This contrasts with other times of Phase 2, when carbonate precipitation (Mf 4) occurred and pH was elevated within the surface waters due to an increase in supersaturation that was caused by a decrease of dissolved CO_2 (Kelts and Hsü, 1978). However, Dixit and Dixit (1989) were able to record some chrysophyte taxa from lakes that are circumneutral to alkaline in pH. Temperature approximations can be inferred, as Recent populations bloom mostly during summer at temperatures of about 20°C with a minimum requirement of 13°C for the particular species studied by Siver (1988). As chrysophytes are ecologically diverse (Duff et al., 1995), more precise environmental information can only be given with proper taxonomic identification. The siliciclastics of Mf 2-varves are laminated, indicating oxygen-free bottom waters in a meromictic lake. Conversely, the presence of meiofaunal bioturbation in Mf 4 implies oxygen-restricted conditions in the hypolimnion of a monomictic lake.

Environmental parameters govern species diversity and have a large impact on the evolution of species. The response of the fauna to the proposed environmental changes will be analysed with statistical methods in subsequent studies.

Conclusions

Of the four phases of lake evolution recognized in Lake Sihetun (Jiang et al., 2012), Phase 2 (stratified lake interval) and Phase 3 (unstratified lake interval) are documented and interpreted in detail (Fig. 1.15), as they yield most of the spectacular fossils described from the Yixian Formation.

Phase 2

The main microfacies of Phase 2 is exceptionally finely laminated (only several 10 μm, Mf 1) and cannot be attributed to varves. In contrast, carbonate oozes that formed repeatedly towards the top of Phase 2 led to the formation of recognizable varves with a thickness range of 107 to 534 μm (Mf 4). A second varve-type (Mf 2), which is rare, is inferred from golden algae that exhibit a seasonal growth pattern forming cysts most likely during autumn. These chrysophycean cysts are probably the oldest reported from freshwater deposits. Coarser-grained siliciclastic inflows connected to events of heavy rain (Mf 3) were sometimes part of the varve-forming process. Due to correlation of Mf 3-deposits with Mf 2-varves, a synchronous occurrence of heavy rains and chrysophycean-cyst accumulations during autumn can be assumed. In some cases consecutive pulses of Mf 3, indicating several storms within one season, occurred. Lake Sihetun remained stratified throughout most of Phase 2 and convective mixing was rare. These meromictic conditions probably arose because the lake basin was moderately deep compared to its surface area. The lake experienced recurrent monomictic intervals, especially during the deposition Mf 4-varves.

Phase 3

General depositional rates culminated during Phase 3. The transition from Phase 2 to Phase 3 documents a period of climate change from dry to humid climates that led to a significant increase in sediment yield, which can be connected to increased runoff. The stratified water column finally broke down with the onset of Phase 3, when holomictic conditions had finally been re-established, rendering the lake floor more habitable for freshwater invertebrates.

Environmental parameters

The meromictic, eutrophic Lake Sihetun of Phase 2, which existed under prevailing dry conditions, was characterized by a moderate depth and alkaline conditions near the sediment-water interface. A significant heat source is postulated to have come from a strong geothermal heat flow. During Mf 2-varve deposition, the conditions of the surface waters must have changed to provide suitable living conditions for golden algae, most of whom prefer slightly acidic waters. Bottom waters during Phase 2 remained anoxic, except for recurrent events of overturn leading to oxygen-restricted bottom waters and conditions suitable for short-lived colonization events. At the onset of Phase 3, which was characterized by a more humid climate, the hypolimnion was fully oxygenated. This dramatically altered modes of preservation.

Fossil preservation

Phases 2 and 3 are governed by very different modes of preservation. Plant tissue in Phase 2 is characterized by iron-sulphide replacement, which subsequently became oxidized to a red stain. Preservation of clam-shrimp carapaces in Phase 2 is excellent, as growth increments are preserved. Clam shrimps preserved in Phase 3 exhibit the same mineralogy, but their internal structures are completely obscured by dissolution processes. Organic tissues of insects in Phase 3 are well preserved as dark stains that are sealed by silica coatings.

Acknowledgements

Research was supported by the 973 program grant (2012CB821905) and the National Science Foundation of China (grants 406032010, 40672077, 41172033). The authors benefited from discussions with R. Schöner, J. Sha, R. Koch, M. López Correa, J. Rust, and B. Kremer. Y. Niu and C. Wu assisted us in the field. B. Leipner-Mata helped with the preparation of thin-sections.

Chapter 2: Oxygen deficiency in Lake Sihetun – Formation of the Lower Cretaceous Liaoning Fossillagerstätte (China)

Chapter 2 has previously been published:

Hethke, M., Fürsich, F.T., Jiang B., Klaus R. 2013. Oxygen deficiency in Lake Sihetun; formation of the Lower Cretaceous Liaoning Fossillagerstätte (China). – *Journal of the Geological Society, London*, **170**: 817-831.

Texts, tables, and figures are reformatted in the style of this thesis. There are minor orthographic changes in the text.

Introduction

Oxygen depletion ranks among the major causes for mass mortality events and larger-scale biotic crises (e.g., Wignall and Twitchett, 1996; Bond et al., 2004; Wignall et al., 2010) and is one of the main factors leading to the formation of Konservat-Lagerstätten, when reducing conditions become established during stagnation, promoting early diagenetic precipitation (Seilacher et al., 1985; Allison, 1988). Identification of ancient redox levels can be achieved through a series of techniques. In addition to geochemical indices such as the degree of pyritization (Jones and Manning, 1994), oxygen depletion is best identified through the presence of laminated sediments. However, both lower dysoxic and anoxic conditions generate finely laminated sediments and only the existence of a low-diversity benthic fauna sets them apart (Wignall and Hallam, 1991). The distinction between ancient redox levels becomes very challenging when a great extent of sediment alteration is involved, as is the case for the famous Lower Cretaceous palaeolake deposits of western Liaoning, for which a technique that is robust towards such alteration processes is required. Wilkin et al. (1996) have shown that the size distributions of pyrite framboids (spheroidal clusters of equidimensional and equimorphic pyrite crystals; Rickard, 1970; Ohfuji and Rickard, 2005) correlate with bottom-water redox conditions in modern euxinic, dysoxic, and oxic settings. Small diameters and decreased framboid-size variabilities correspond to their formation above the sediment-water interface. Pyrite framboid analysis has become a powerful proxy for palaeoredox conditions with case studies performed for the Black Sea (Wilkin et al., 1997), Late Devonian anoxic events (Bond and Wignall, 2005), Permo-Triassic boundary sections (Bond and Wignall, 2010), Permian-Jurassic pelagic sediments (Wignall et al., 2010), submarine chimneys of the Gulf of Cadiz (Merinero et al., 2009), the Kimmeridge Clay (Wignall and Newton, 1998), for Upper Permian black shales of the East Greenland Basin (Nielsen and Shen, 2004), and for end-Permian deep-water sediments of Kashmir (Wignall et al., 2005). All are marine settings with the exception of a Pleistocene to Early Holocene freshwater phase in the Black Sea, which is now permanently anoxic (Ross and Degens, 1974; Wilkin et al., 1997).

Here we present a palaeoredox study on Lake Sihetun of the Lower Cretaceous Yixian Formation that is famous for its outstanding fossil preservation. Especially feathered dinosaurs, (e.g., Xu et al., 1999a, 2001) and the putative early flowering plant *Archaefructus* (Sun et al., 2002) roused widespread interest. Countless other exceptionally well preserved vertebrate and invertebrate fossils have been discovered. They represent a time during which the evolution of major clades such as birds and angiosperms took place (Barrett, 2000). The evolutionary significance, in combination with the superb preservation, renders the Yixian Formation one of the most important Mesozoic fossillagerstätten.

Somewhat surprisingly, palaeoenvironmental studies have long been neglected. Fürsich et al. (2007) and Pan et al. (2012) described Lake Sihetun as a shallow eutrophic lake system controlled by fluctuations of oxygen levels, but these studies were mainly based on fossil assemblages. Sedimentological evidence was put forward by Jiang et al. (2012), who recognized four different phases of lake evolution. Hethke et al. (2013a) added a high-resolution microfacies analysis by focussing on two of these phases (2 and 3), which yield most of the excellently preserved fossils mentioned above.

Oxygen deficiency has been suggested to cause recurrent mass mortality events of Phase-2 invertebrate fossils. Fürsich et al. (2007) proposed seasonal dysoxia during summer due to the consumption of oxygen by respiration processes coupled with winter mixing and re-oxygenation. Jiang et al. (2012) and Hethke et al. (2013a) refined this model by proposing a mainly stratified water column during Phase

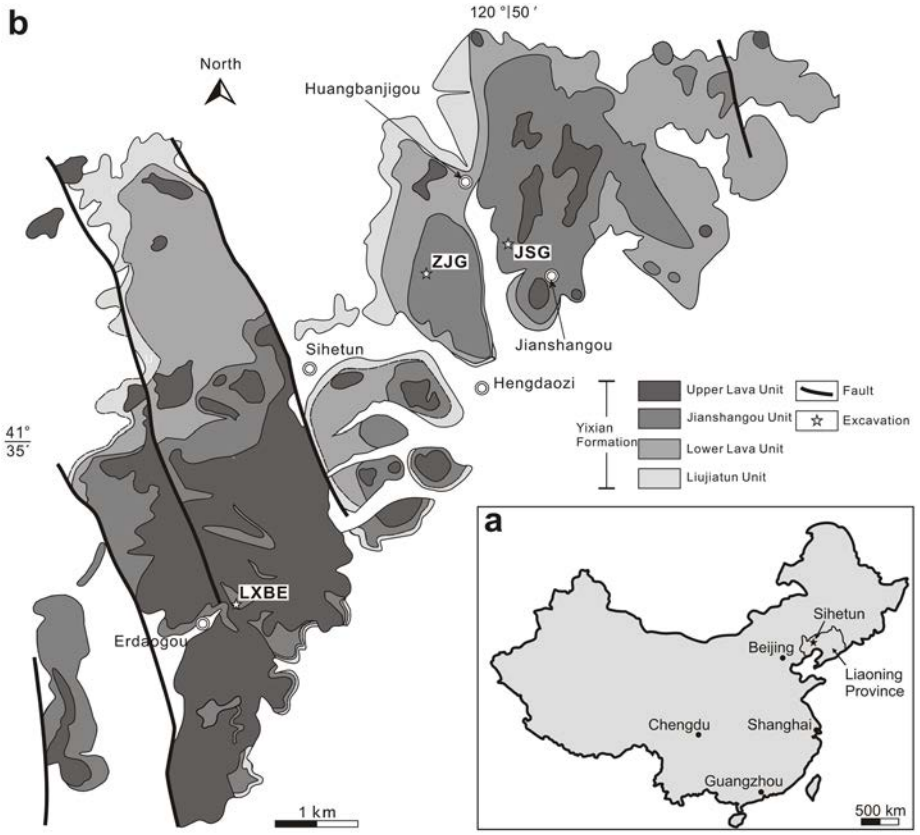

← **Fig. 2.1.** (a) Location and (b) geological map of the Sihetun area. Excavations Jianshangou (JSG), Erdaogou (LXBE), and Zhangjiagou (ZJG) are marked. Modified after Jiang et al. (2011).

Table 2.1. Units of the Yixian Formation in the Sihetun area, four beds of the Jianshangou Unit from oldest (Bed 1) to youngest (Bed 4), and microfacies present within beds 2 and 3.

Unit	Description
Units of the Yixian Formation (Jiang et al., 2011)	
Upper Lava	Intermediate-basic lava and intrusive rocks
Jianshangou	Fine siliciclastics and tuffs, with intercalated calcareous marl
Lower Lava	Basaltic andesites, olivine basalts, and trachyandesites
Lujiatun	Volcanic conglomerates, sandstones and lapilli-tuffs
Jianshangou Unit (Jiang et al., 2012)	
Bed 4	Tuffaceous conglomeratic sandstones and tuffs interbedded with finer siliciclastics
Bed 3	Normal-graded fine sandstones to siltstones
Bed 2	Paper-thin laminae of fine tuffaceous siliciclastics and some evaporates
Bed 1	Comparatively coarse, horizontally or cross-bedded, tuffaceous siliciclastics
Microfacies occurring in beds 2–3 (Hethke et al., 2013a)	
Mf 1	Allochthonous, siliciclastic laminae that are 26 μm thick on average
Mf 2	Chrysophycean cyst accumulations
Mf 3	Tuffaceous silt
Mf 4	Lacustrine calcium carbonate-rich laminae
Mf 5	Tuff
Mf 6	Comparatively coarse, normal-graded siliciclastics

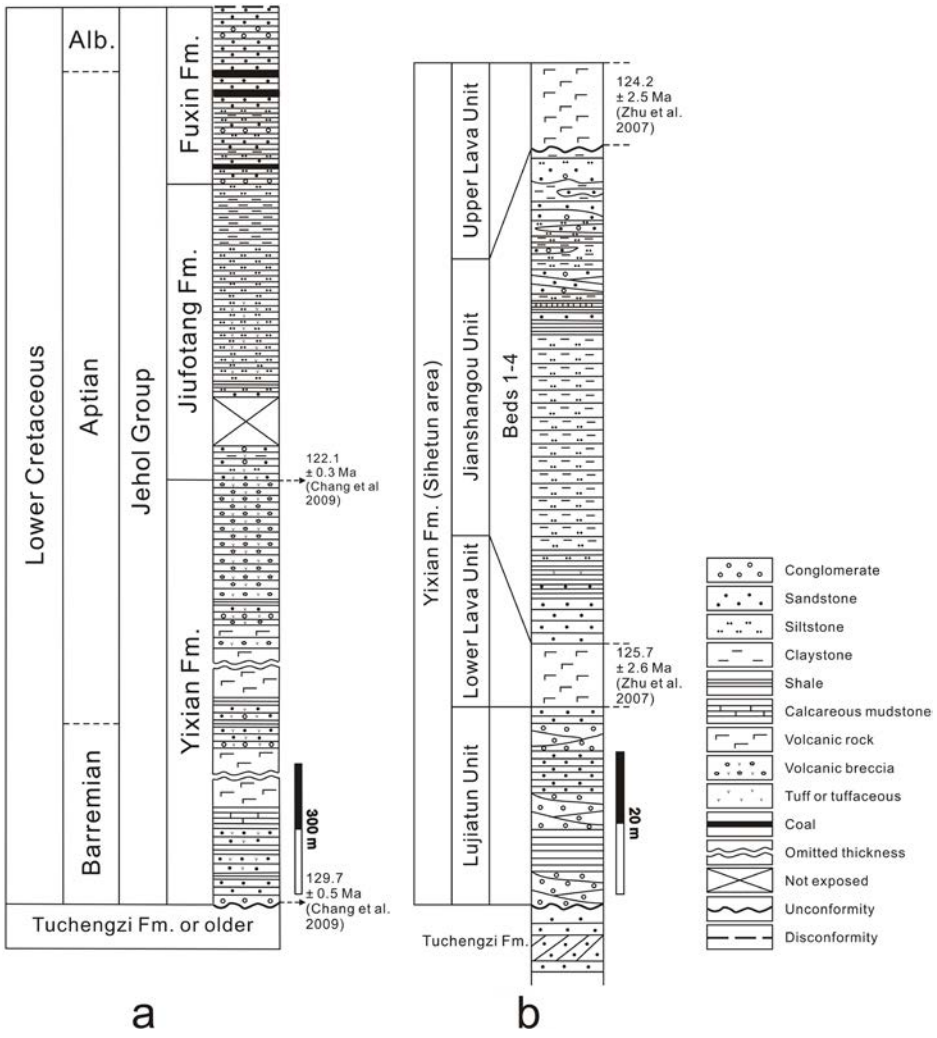

← **Fig. 2.2.** (a) Jehol Group of western Liaoning and (b) the Sihetun area (modified after Jiang et al., 2012). Lines schematically refer to the boundaries between the four units of the Yixian Formation.

2 with convective mixing seldom reaching the lake floor and leading to short-lived oxygenation events.

Pyrite-framboid pseudomorphs are widespread in the sediments of Phase 2 (Hethke et al., 2013a). The depositional environment proposed for Phase 2 will be developed further in this study through the determination of ancient redox levels using quantitative methods. Further identification of the main factors that controlled iron sulphide formation in Lake Sihetun will lead to a comprehensive lake model.

Geological setting

The Jehol Group of western Liaoning is Early Cretaceous in age and comprises three formations: Yixian, Jiufotang, and Fuxin (Figs. 2.1, 2.2; Jiang and Sha, 2006). It has been proposed that the Yixian Formation was deposited between 129.7 ± 0.5 Ma and 122.1 ± 0.3 Ma, within an interval of 7 Ma ($^{40}Ar/^{39}Ar$; Chang et al., 2009). At the time, Liaoning was located at a palaeolatitude of 41.9° (±6.6°) N (Enkin et al., 1992; Zhou et al., 2003; Amiot et al., 2011).

In the Sihetun area, the Yixian Formation is made up of four units (Fig. 2.2b; Table 2.1). They are the Lujiatun Unit, Lower Lava Unit, Jianshangou Unit, and Upper Lava Unit (Jiang and Sha, 2007). The lowermost Lujiatun Unit is unconformably overlying the Upper Jurassic-Lower Cretaceous aeolian Tuchengzi Formation (Cheng et al., 1997). Radiometric ages suggest a contemporaneous deposition of the Lujiatun Unit with the Jianshangou Unit (He et al., 2006), but extensive field investigations in the Sihetun area proved that the Lujiatun Unit is underlying the Lower Lava Unit and the Jianshangou Unit in more than ten sections. Furthermore, the Lujiatun Unit might be absent at a few localities, where the Lower Lava Unit and the Jianshangou Unit unconformably overlie the Tuchengzi Formation directly. The Jianshangou Unit is unconformably overlain by the Upper Lava Unit, which also intruded into the lake sediments (Jiang et al., 2011).

Lake Sihetun (Jianshangou Unit) has been proposed to have existed for 1.5 Ma (125.7 ± 2.6 Ma to

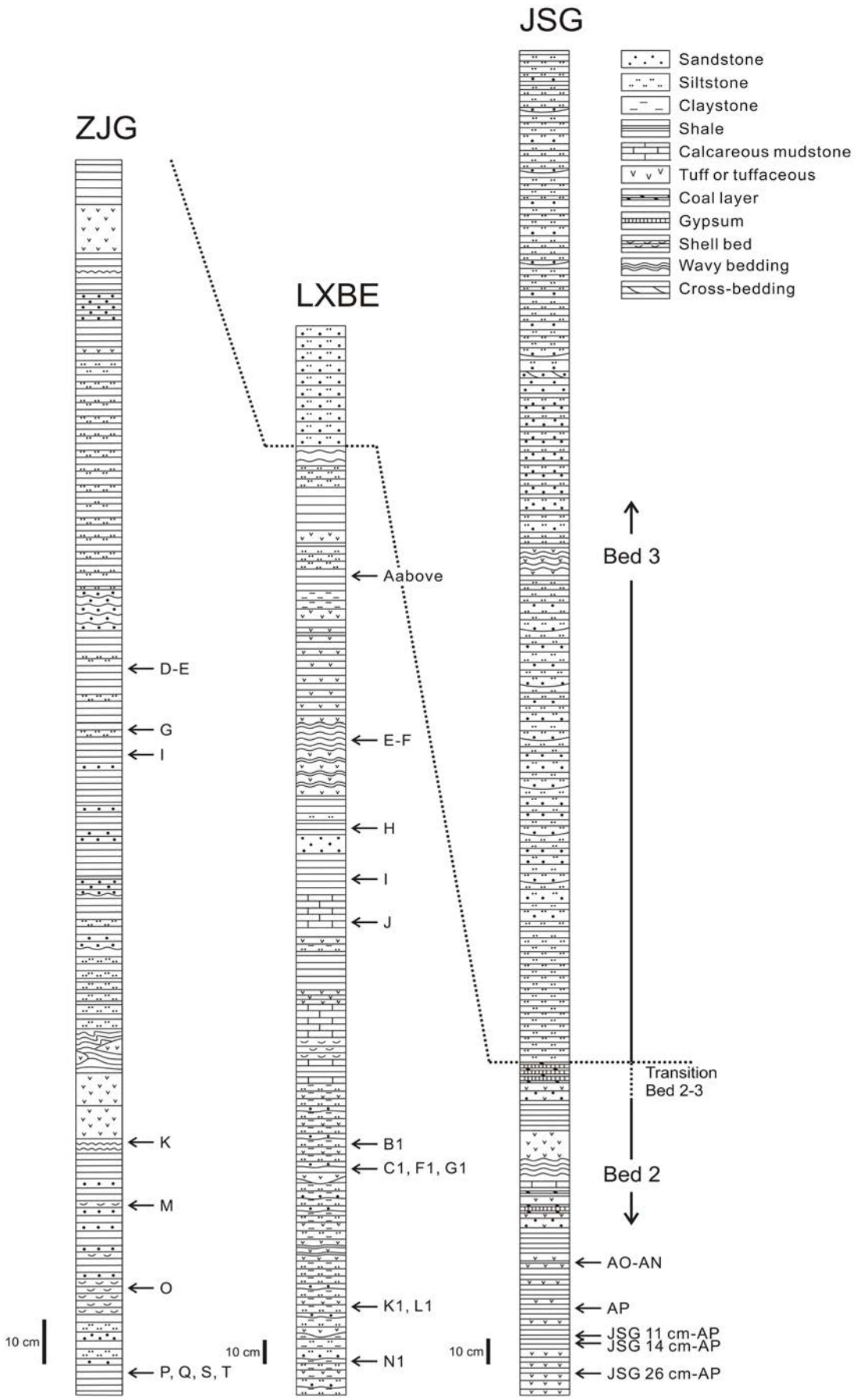

Fig. 2.3. Lithologs of excavations ZJG, LXBE, and JSG. Framboid yielding horizons analyzed in this study are marked. Beds 2 and 3 of the Jianshangou Unit are separated by a dotted line.

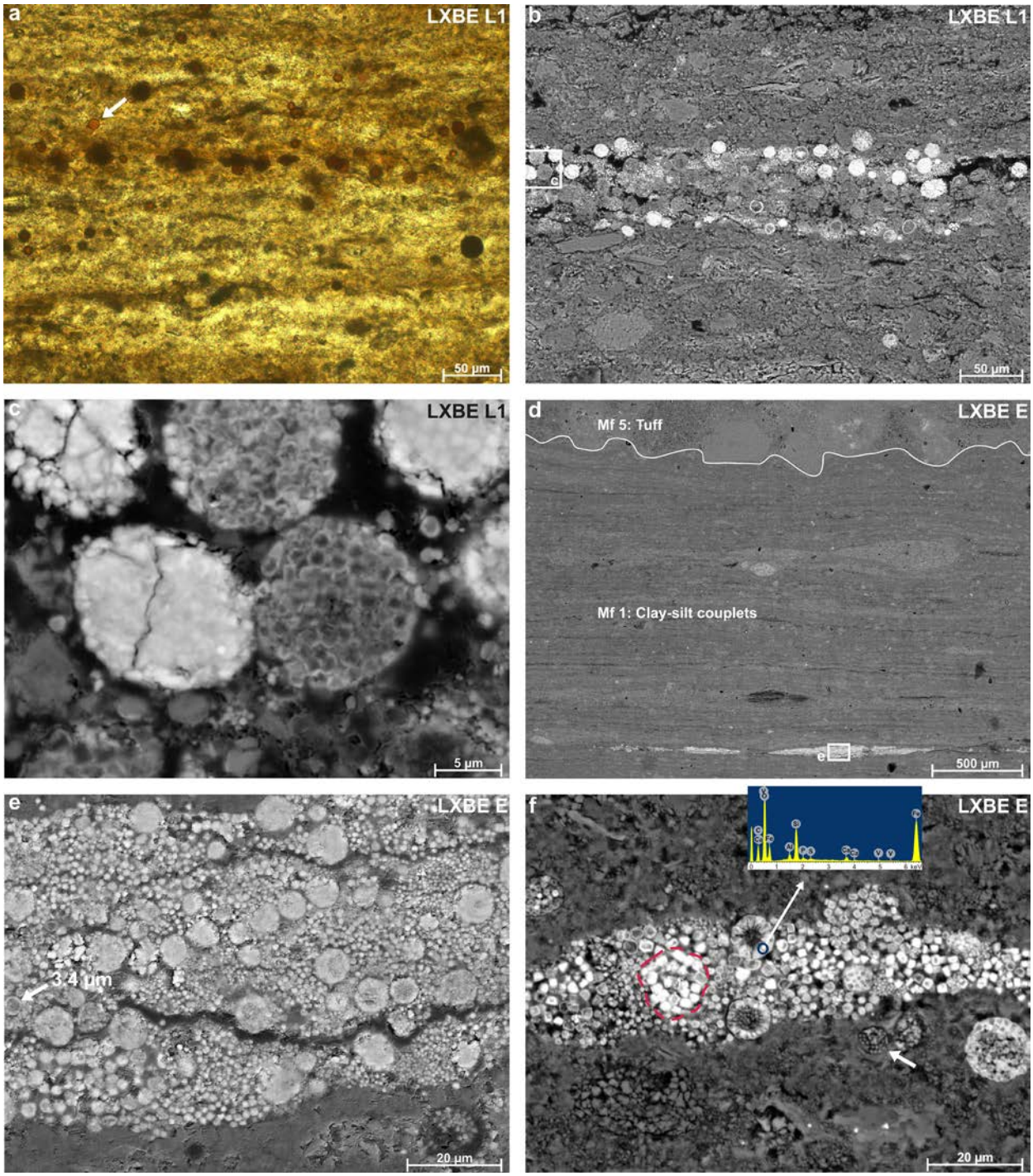

Fig. 2.4. Phase-2 sediments of allochthonous clay-silt couplets (Mf 1) and intercalated tuff layers (Mf 5). (a) Plane-polarized light. (b-f) BSE images. (a) Framboids appear red (arrowed) to dark under plane-polarized light. (b, c) Original framboid structures are retained in thin-section LXBE L1 and single microcrystalites exhibit reaction rims made up of iron oxide-hydroxides. This thin-section was used for a case study (see Fig. 2.7) that aimed at discriminating between concentrated and matrix framboids. (d) Overview of the profoundly altered sediment of thin-section LXBE E and (e) close-up of a concentrated iron-sulphide horizon made up of framboids as well as single microcrystals. Smaller framboids (arrowed) have likely been overlooked during size measurements, as concentrated layers often merge to one dark-red layer under plane-polarized light. (f) Progressive alteration is expressed by the formation of hollow, lobate (EDS spectrum) or meniscus-like structures (arrowed) that surround remnants of framboidal structures. An almost completely disintegrated structure is traced (13.9 µm).

124.2 ± 2.5 Ma; $^{40}Ar/^{39}Ar$), but there are even shorter estimates about lake duration (0.7 Ma or less) that are based on palaeomagnetic data (Zhu et al., 2007).

The Jianshangou Unit can be subdivided into four beds that correspond to four phases of lake evolution (Table 2.1; Fig. 2.3; Jiang et al., 2012). Phase 1 is characterized by fluctuating but gradually rising water levels. During Phase 2, a marginal beach to nearshore facies and a suspension-derived lake floor facies were deposited, whereas hyperpycnal flows were typical for Phase 3. A fan delta prograded into the lake during Phase 4. Hethke et al. (2013a) distinguished six microfacies (Mf 1-6) that occur within the most fossiliferous beds 2 and 3 of the Jianshangou Unit (Table 2.1). They are: (1) allochthonous, siliciclastic laminae with an average thickness of 26.1 μm, (2) chrysophycean cyst accumulations, (3) tuffaceous silt, (4) lacustrine chemical precipitates, (5) tuff, and (6) normal-graded sandy to silty siliciclastics. Pyrite framboids are restricted to Phase 2 and reported from Mf 1, associated tuffs as well as tuffaceous sediments (Mf 3 and Mf 5) and, to a lesser degree, from Mf 4.

Material and methods

Data are based on three excavations carried out in the Sihetun area several kilometres apart to identify spatial variations in redox state within the lake: Jianshangou (JSG), Erdaogou (LXBE), and Zhangjiagou (ZJG; Figs. 2.1, 2.3). Excavations LXBE and ZJG covered Bed-2 sediments, while excavation JSG focussed on sediments of Bed 3 with fewer samples retrieved from Bed 2, explaining the smaller amount of framboid-yielding thin-sections from JSG.

Traditional optical microscopic methods were used to examine 29 framboid-yielding petrographic thin-sections. Quantitative measurements (± 0.5 μm) of framboid diameters were taken under transmitted light using the Zeiss AxioVision Software (Release 4.8.1).

Back-scattered electrons (BSE) were detected for compositional imaging using the scanning electron microscope (TESCAN Model Vega\\xmu). Compositional changes were revealed by identifying differences in brightness, which are determined by the mean atomic numbers of phases (Reed, 2005). Mean atomic numbers relevant for this study from higher to lower are as follows: iron oxides and sulphides > calcite > anorthite and orthoclase > albite > quartz. Therefore, iron oxides and sulphides appear much brighter than quartz. Energy-dispersive X-ray spectroscopy (EDS; Programm: INCA) allowed further qualitative elemental analyses. Conductive coatings for the thin-sections were gold or carbon.

The reference material is stored at the Paläoumwelt section of the GeoZentrum Nordbayern, University of Erlangen-Nürnberg.

Results

Observations

Pseudomorphs of iron sulphide framboids are especially common in the clay-silt couplets of Mf 1 (Fig. 2.4), the dominant microfacies of Bed 2, and in associated tuffs and tuffaceous sediments. Pyrites of calcium carbonate-rich laminae (Mf 4; Fig. 2.5a, b) form aggregates that are only crudely spherical and termed clustered pyrite (Canfield and Raiswell, 1991). They are larger (< 50 μm) and made up of octahedral microcrystalites of variable sizes (< 12 μm). Framboids are defined by an arbitrary maximum ratio of microcrystalite size to spheroid diameter of 1:10 (Rickard, 1970). This ratio is sometimes higher for Mf-4 clustered pyrites. However, since most of these are nevertheless spheroidal (Fig. 2.5a), diameters of comparatively well defined spheroids have also been measured.

Framboids occur (1) concentrated in discontinuous iron sulphide layers and (2) scattered throughout the matrix. Concentrated framboids are often associated with microcrystals, which exhibit maximum diameters of 2.5 μm in Mf 1 (Figs. 2.4e, 2.5c-e). These microcrystals may dominate over framboids in iron sulphide layers and their sizes characteristically increase towards the centre of such layers (Fig. 2.5e). EDS spectra of framboids show predominantly Fe and O peaks, but element maps (Hethke et al., 2013a, fig. 12) confirm that remnant sulphur is preserved within framboids and the single euhedral microcrystals adjacent to them.

There are two processes that obscure pyrite preservation: (I) oxidation and (II) extensive silica replacement (Fig. 2.5b-e). Fast oxidation rates can be expected, because of the high specific surface area of framboids. Original mineralogies are usually better preserved in bigger, euhedral pyrite crystals (Merinero et al., 2009). Generally, the alteration process (Fig. 2.6a) involves (1) the formation of comparatively thin reaction rims made up of iron oxide-hydroxides, (2) the dissolution of interior iron sulphides to a great extent and, in some cases, (3) silicification (spectrum of Fig. 2.5b). Similar alteration structures have been observed within greigite framboids from methane seep carbonates (Bailey et al., 2010). (4-5) Lobate alteration rinds formed by outgrowth may occur (Figs. 2.4f, 2.6b). Their inte-

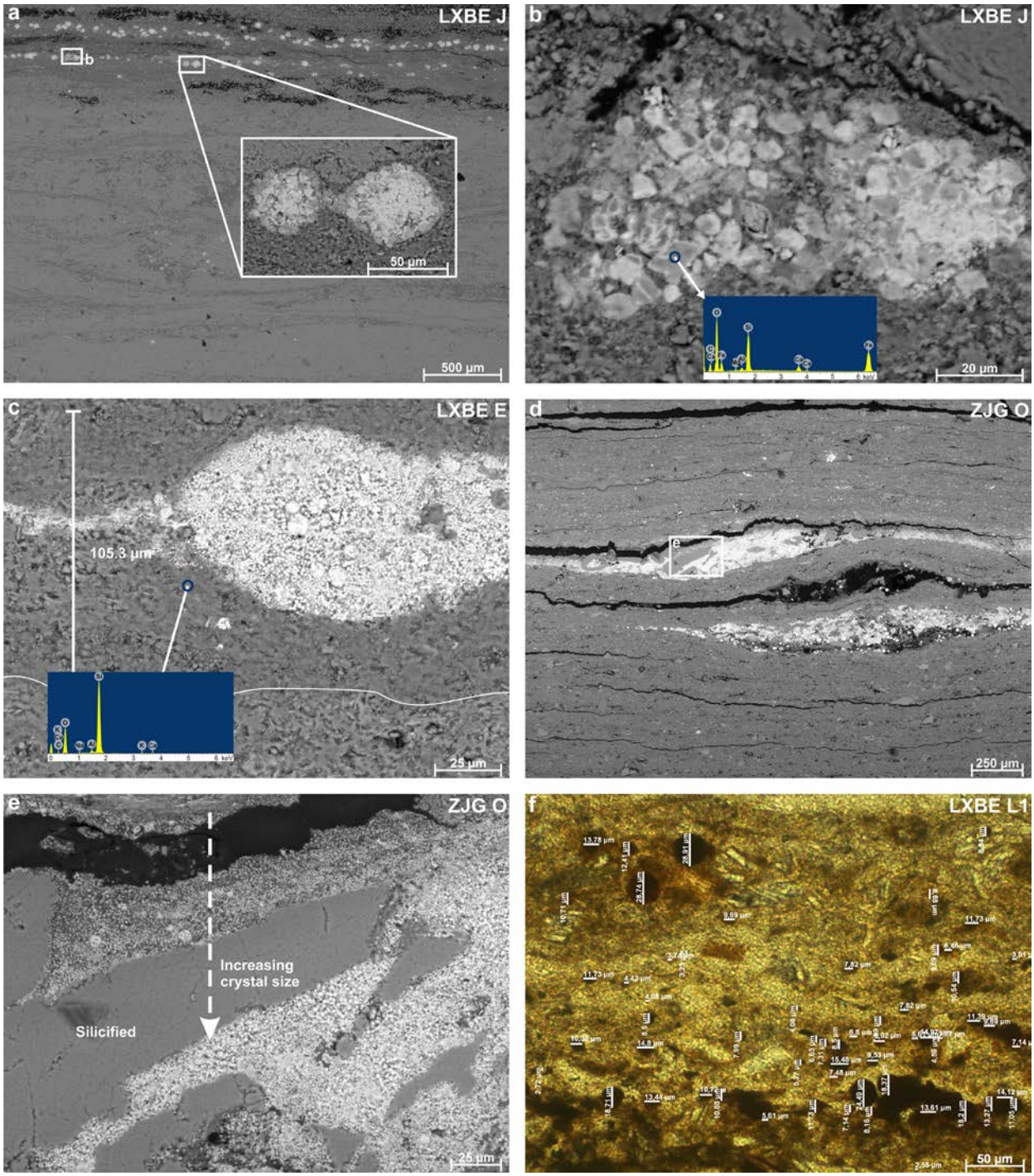

Fig. 2.5. Phase-2 sediments of lacustrine carbonate precipitates (Mf 4) and allochthonous clay-silt couplets (Mf 1). (a-e) BSE images. (f) Plane-polarized light. (a, b) Mf-4 clustered pyrites are more readily disintegrated and the octahedral microcrystalites are much larger than Mf-1 framboids. (c-e) Extensive silicification affected many iron-sulphide horizons and concealed them. The suggested boundary between "iron-sulphide sediment" and detrital sediment is traced in white (c), revealing an original lamina thickness of more than 100 µm. Such layers are proposed to have resulted from the establishment of biofilms at the lake floor or from microenvironments around animals and plants retaining reactive organic matter, corroborated by increasing microcrystal sizes towards the centres of iron sulphide layers (e). (f) Example of quantitative framboid-size measurements. Concentrated as well as matrix framboids are often hard to distinguish and measurements led to distribution overlap (see Fig. 2.7).

rior is hollow and once comprised parts of the original framboid that has readily been dissolved (compare with fig. 3p, Bailey et al., 2010). Virtasalo et al. (2010) described similar alteration rinds as radially arranged laths reminiscent of marcasite. Extensive silica replacement resulted in silicified patches (Fig.

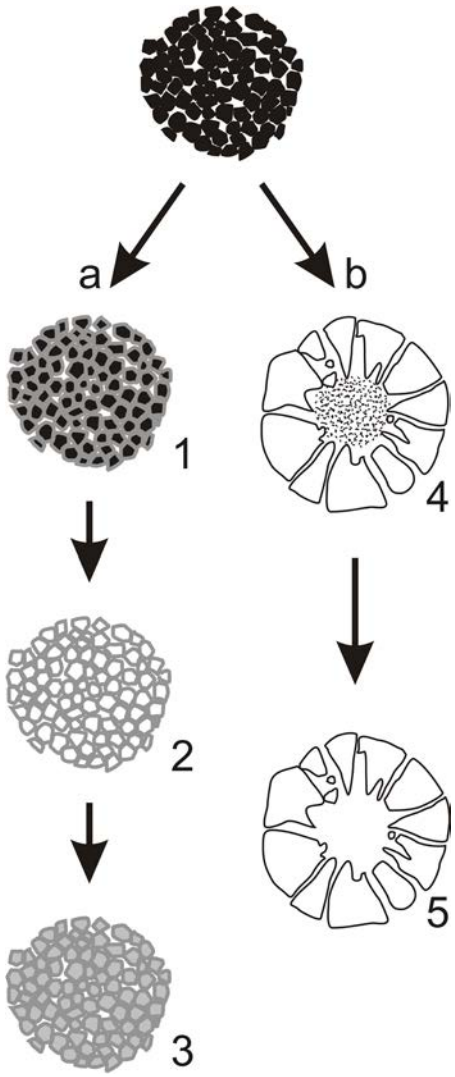

Fig. 2.6. Framboid alteration underwent oxidation as well as silicification. (a) In a first step, comparatively thin reaction rims made up of iron oxide-hydroxides form (1). Dissolution of interior iron sulphides led to the formation of hollow structures (2) and silica replacement of iron sulphides (3) took place within the interior of framboid microcrystalites. Alteration usually underwent a combination of steps 2 and 3, though both extremes have been observed within Lake Sihetun. Silicification is pervasive, but may be incomplete as demonstrated by the EDS spectrum of Fig. 2.5b. (b) Spherical, hollow structures occur that represent lobate alteration rinds (4 & 5), which grew around framboids that have completely been dissolved (compare with Fig. 2.4f).

2.5d, e) and led to widespread concealment of iron sulphide layers. Silicification was so severe in Fig. 2.5c that most of the original iron sulphide signature has completely been obscured.

Size measurements

Principally, there are differences in framboid formation between anoxic, dysoxic, and oxic bottom waters that result in distinct size distributions (Wilkin et al., 1996; Muramoto et al., 1991). The analysis of framboid diameters involves descriptive statistics summarized in Figs. 2.7-2.10. Measurement bias may come from overlooking smaller framboids within concentrated layers that are generally harder to discern under transmitted light (arrowed in Fig. 2.4e), possibly shifting the spectrum towards larger sizes. Such shifts are compensated for, as framboid diameters tend to be underestimated, because spheres are usually not exactly cut in half. Generally, framboids embedded within Mf 1 and associated tuffs exhibit smaller average diameters than clustered pyrites that are associated with carbonate precipitates (Mf 4).

Concentrated framboids are often hard to separate from matrix framboids in bulk measurements (e.g., Fig. 2.5f upper left region). To check for discrepancies between diameters of both statistical populations, framboids concentrated in a layer as well as matrix framboids in its vicinity have been measured independently (Fig. 2.7). Framboid diameters from the concentrated layer in Fig. 2.7a are distributed around a mean diameter of 10.5 µm and are thus distinctly larger than those that are scattered in the matrix (ø 6.9 µm on average). Concentrated framboids tend to be normally distributed, whereas scattered framboids exhibit positively-skewed distributions. Quantitative measurements often reveal polymodal distributions (Fig. 2.8) that are evidence of overlap of these two statistical populations.

Average diameters and standard deviations (Fig. 2.9) are smallest in horizons ZJG E and ZJG D (ø 5.5 µm; sd = 2.0 µm) and largest in horizons LXBE K1 and LXBE J (ø 25.7 µm; sd = 6.7 µm), which are characterized by carbonate precipitates (Mf-4 clustered pyrites). The relationship between mean diameter and standard deviation (Fig. 2.10) reveals that there are distinct differences between the three excavations. Framboid diameters of LXBE are generally larger and more dispersed, due to a larger number of thin-sections yielding only concentrated framboids within this particular excavation. ZJG framboids are smaller and their sizes are less dispersed. JSG framboids plot at an intermediate position.

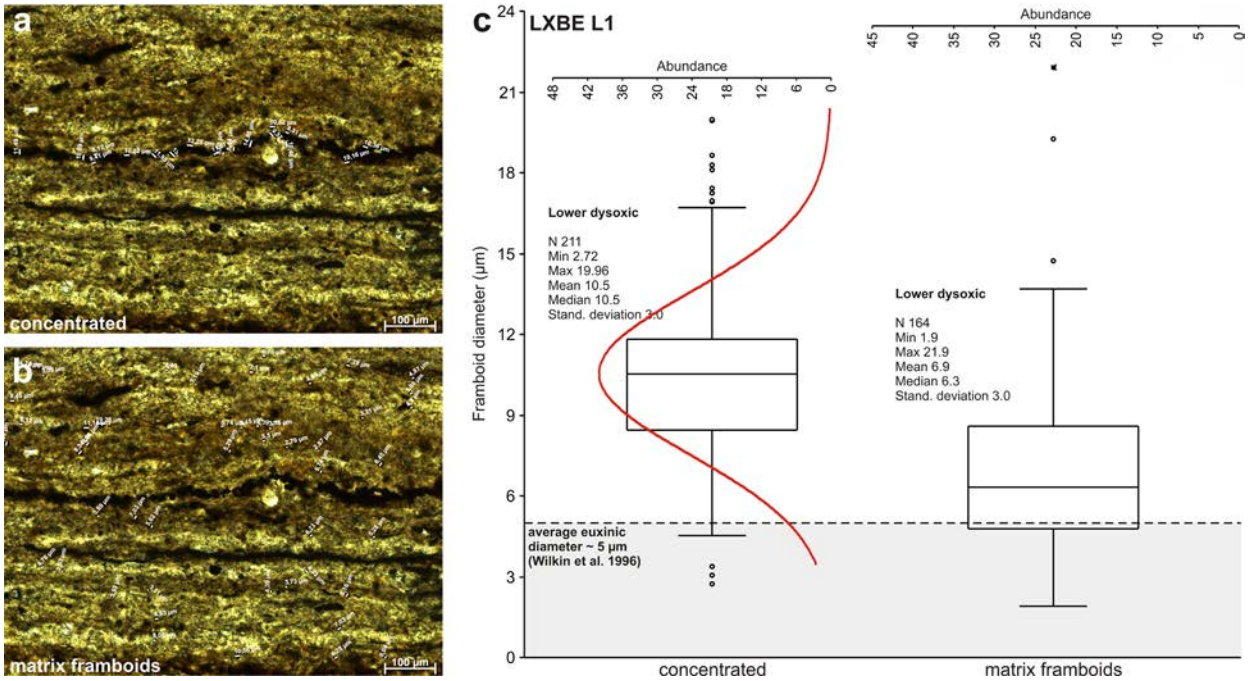

Fig. 2.7. Framboid diameters have been measured within a concentrated layer (a) and from the matrix in the immediate proximity of the concentrated layer (b), no more than 300 µm above and below. (c) Box plot of concentrated and matrix framboid diameters. A normal distribution (in red, parametric estimation) is fitted to the concentrated diameters (Shapiro-Wilk W = 0.98). Both exhibit the same standard deviation, but average diameters differ by several µm. The box (25-75 percent quartiles) for the scattered framboids scratches the dashed line that indicates average euxinic diameters of Black Sea pyrite framboids, but a standard deviation of 3.0 points to lower dysoxic bottom waters. Both distributions derived from framboid populations that originated from early diagenetic growth, but while matrix framboids formed in an open system under lower dysoxic bottom waters, concentrated framboids stem from growth in a confined microenvironment.

Discussion

Pyrite framboid formation and control parameters

The sediments of Lake Sihetun yield concentrated framboids, which are often associated with iron sulphide microcrystals, as well as matrix framboids of different size distributions. All have been altered to iron oxide-hydroxides. Iron sulphides are usually referred to as early diagenetic products that form in shallow sediment depths under oxic bottom waters through the reaction of detrital iron minerals with H_2S, but syngenetic iron sulphides precipitating directly from a euxinic water column have also been reported (e.g., Degens et al., 1972; Muramoto et al., 1991). Stable iron minerals under reducing conditions are pyrite, siderite and magnetite, depending on carbonate and sulphur concentrations. Higher concentrations of dissolved sulphur and lower dissolved carbonate concentrations extend the stability field of pyrite (Krauskopf and Bird, 1995).

Experimental synthesis of pyrite framboids can be achieved at high supersaturation and rapid nu-

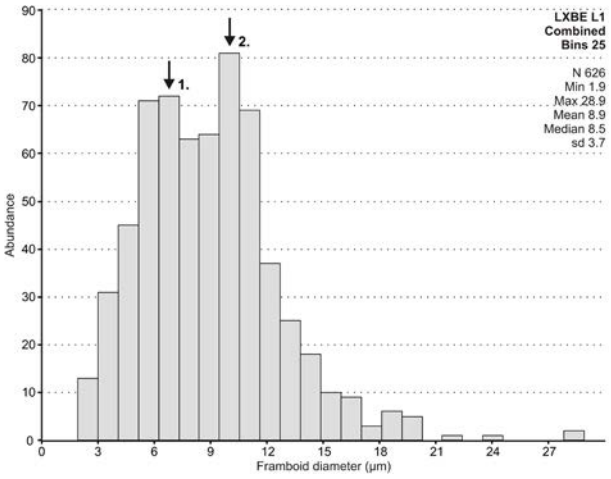

Fig. 2.8. Composite framboid-size distribution of four different horizons from the same thin-section. Framboids occurring within a thin-section have been measured quantitatively, because concentrated as well as matrix framboids are often hard to discriminate (e.g., Fig. 2.5f); consequently distributions are superimposed. The resultant positively skewed distribution is bimodal and arrows point to the two main framboid populations, delineating concentrated (2) and matrix framboid (1) signatures.

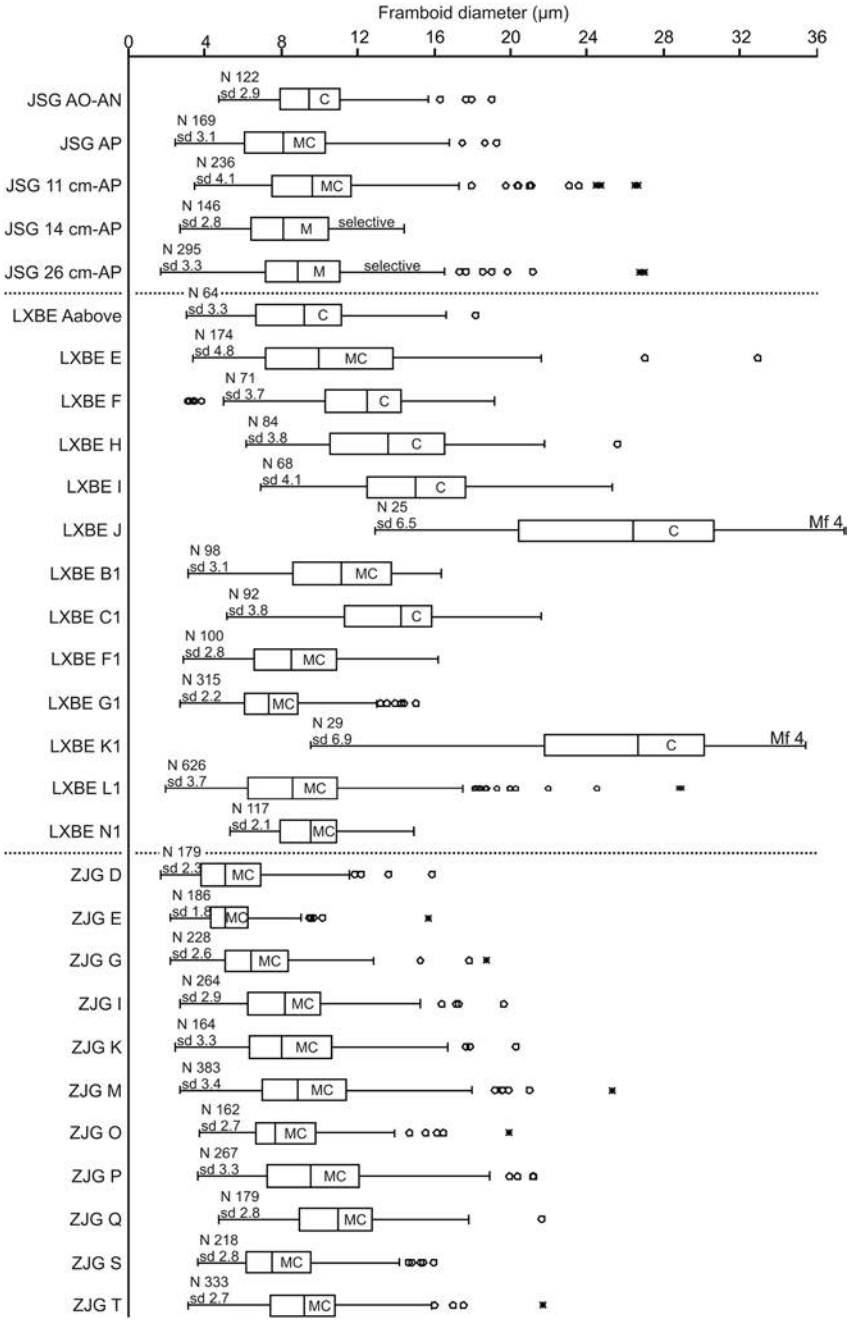

← **Fig. 2.9.** Boxplot of 29 horizons from three different excavations near Jianshangou (JSG), Erdaogou (LXBE), and Zhangjiagou (ZJG). The box plots are in stratigraphic order for each excavation from oldest to youngest. C – concentrated framboids, M – matrix framboids. Average diameters and standard deviations are smallest for horizons ZJG E and ZJG D, indicating the lowest oxygen levels at the lake bottom, perhaps even euxinic conditions. Highest average diameters occur in horizons LXBE K1 and LXBE J, which are characterized by carbonate precipitates (Mf 4). Mf-4 clustered-pyrite size distributions are slightly negatively skewed, pointing towards a longer interval of closed-system growth through Ostwald ripening. Log-normal distributions, as observed for Mf-1 framboid diameters, point towards growth in open systems.

cleation rates. Suitable environments are realized by the addition of sulphur, oxygen, or by increasing temperature (Butler and Rickard, 2000; Ohfuji and Rickard, 2005). Workers argue for the formation of metastable pyrite precursors that precede pyrite framboid formation (Farrand, 1970; Sweeney and Kaplan, 1973; Wilkin and Barnes, 1996). Those precursor iron monosulphides may rapidly convert to pyrite or be transformed to ferrimagnetic greigite (Fe_3S_4). Experimental evidence that framboid formation may be independent of greigite precursors has also been put forward (Butler and Rickard, 2000; Soliman and Goresy, 2012). Variables leading to single microcrystal growth instead of framboidal textures, which is the case for a number of concentrated iron sulphide layers in Lake Sihetun (Fig. 2.5c-e), include slower nucleation rates and lower oxidation-reduction potential (Eh) (Butler and Rickard, 2000), conditions that were realized in pore spaces of postglacial lacustrine clays of the northern Baltic Sea that were not enriched in reactive organic matter (Virtasalo et al., 2010). Butler and Rickard (2000) argue that texture is a function of Eh. At a pH of 6 and under the exclusion of oxygen, framboidal pyrite forms at Eh > -250 mV, whereas small octahedra are predominant at lower Eh-values of -400 mV. Note that reaction temperatures were set between 60 °C and 140 °C. Under

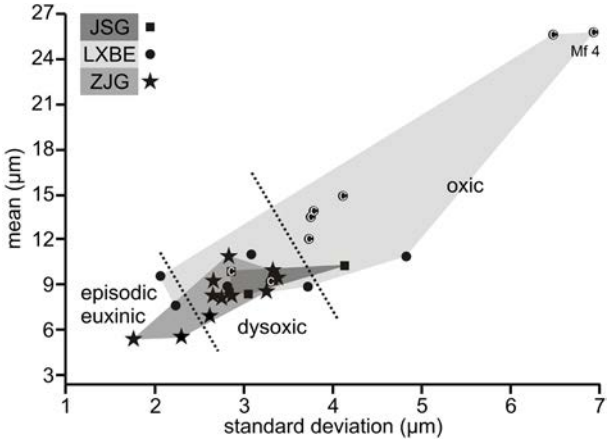

Fig. 2.10. Mean versus standard deviation of Phase-2 framboid diameters. Convex hulls around samples of each excavation (JSG, LXBE, and ZJG) are shaded and thin-sections characterized by concentrated framboids are highlighted with the letter "c". The boundaries between redox states have been inferred from modern data by Wilkin et al. (1996), but distribution overlap between concentrated and matrix framboids has also been taken into consideration. Generally, framboid means and standard deviations are lowest for excavation ZJG and oxygen concentrations were higher in bottom waters overlying LXBE. Pronounced spatial variations in redox state are inferred for Lake Sihetun, possibly related to water depth.

these conditions, greigite intermediates, molecular oxygen, or biological forcing are not involved.

According to Wilkin and Barnes (1996), fastest rates of experimental framboid formation are achieved when air is periodically bubbled into the reaction vessel. Therefore, there are steps within framboid formation that involve weakly oxidizing conditions under non-excessive amounts of H_2S. Maximum simultaneous production rates of the reactants required (dissolved sulphide, ferrous iron, and an oxidant) are found directly subjacent to redox interfaces (Wilkin et al., 1996; Wignall and Newton, 1998).

The role bacteria play in iron sulphide precipitation is being debated. Though it has been proven that framboidal sulphides may form in vitro from suspension in the absence of bacteria (Farrand, 1970; Butler and Rickard, 2000), we are dealing with a natural environment, where bacteria are likely to be an important factor. Iron sulphides may result from anaerobic biologically mediated processes of sulphate-reducing bacteria, which raise the H_2S concentration. There are also arguments that framboids are pseudomorphic after pre-existent organic spherules such as organic coacervates or gaseous vacuoles (e.g., Rickard, 1970). Other workers point out that diagenetically altered framboids only mimic the morphology of syntrophic archaebacterial consortia, implying acellular framboids (Bailey et al., 2010), similar diagenetically altered framboids have also been observed within the sediments of Lake Sihetun (Figs. 2.4f, 2.6b). Another possibility for bacterial involvement would be the formation of intracellular iron sulphides reported from magnetotactic bacteria living in freshwater and in brackish as well as marine environments (Blakemore, 1975; Frankel et al., 1981; Farina et al., 1990; Mann et al., 1990) or even soils (Fassbinder et al., 1990). However, individual microcrystals prominent within iron sulphide layers of Lake Sihetun (Figs. 2.4e, 2.5c, e) are too large to have derived from such intracellular biogenic greigite particles, which are only 75 nm on average.

Therefore, biologically mediated processes are favoured in case of Lake Sihetun, i.e., H_2S formed by bacterial reduction of dissolved sulphate with organic matter. Hence, there are three main controls on pyrite formation (Fig. 2.12), which are (1) organic matter and grain size, (2) dissolved sulphate, and (3) reactive iron minerals. However, the importance of each of them varies.

(1) Bacterial sulphate reduction is involving the breakdown of biopolymeric organic matter by fermentative micro-organisms and subsequent sulphate reduction by sulphate-reducing bacteria, a process that occurs only under anoxic conditions. The overall process is expressed by the following reaction: $2CH_2O + SO_4^{2-} \rightarrow H_2S + 2HCO_3^-$ (Westrich and Berner, 1984). Anoxic conditions are common within most subaqueous sediments that contain enough organic matter, and high proportions of clay particles support the development of reducing conditions within sediments (Baas Becking et al., 1960). Sedimentation during Phase 2 of Lake Sihetun was governed by clay and silt. Therefore, an "oxygen-consuming barrier" must have established at shallow depths within the sediments of the lake through the consumption of oxygen by oxic bacteria living within the upper few centimetres of the sediment (Fig. 2.11). There, organic matter was converted to CO_2 and oxygen consumed, creating anoxic conditions beneath.

(2) Freshwater pyrite formation is usually limited by dissolved sulphate concentrations, which are significantly lower than in marine waters, where in turn pyrite formation is mainly controlled by the amount of organic matter (Berner, 1984). In freshwater environments, sulphate is being rapidly consumed via

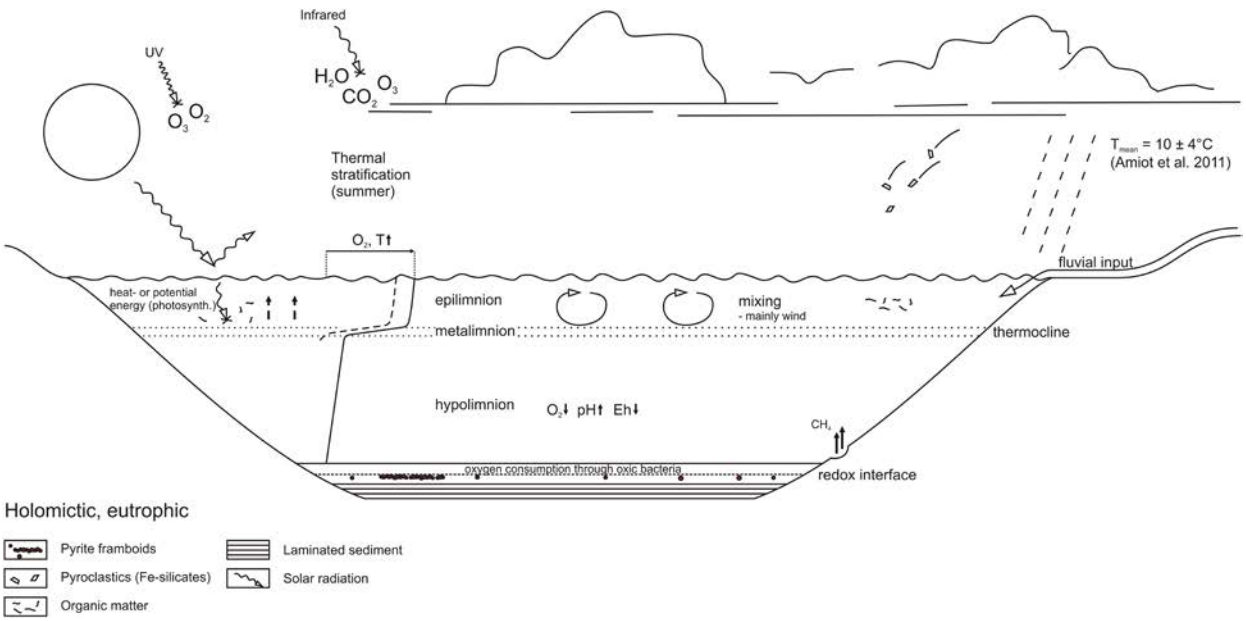

Fig. 2.11. Phase 2, holomictic setting. Dysoxia within eutrophic Lake Sihetun was most pronounced during summer stratification. Holomictic conditions in Lake Sihetun were governed by heating from solar radiation, creating seasonal thermal stratification. After turnover (isothermal conditions, not depicted), the thermocline (plane of maximum rate of temperature decrease) rose and stabilized, isolating the hypolimnion from the epilimnion. Stratification was lost again as a consequence of loss of heat through cooling of the epilimnion, sinking of the thermocline and subsequent rapid turnover. Eutrophic waters are inferred for Lake Sihetun to explain lower dysoxic conditions that are deduced from the lack of bioturbation and from framboid size distributions. This results in a clinograde O_2-profile (dashed line), where the hypolimnion was regulated by biological processes, mainly the consumption of O_2 through oxidative processes: respiration and decomposition of organic matter. A decrease in O_2-concentrations led to a decrease in redox potential, as did an increase in pH. Pyrite framboids formed early diagenetically immediately below the redox interface, if the supply of sulphate permitted it.

sulphate reduction in shallow sediment depths of only several centimetres. Therefore, in contrast to marine sediments, sulphate is the dominant control for pyrite formation in freshwater lake sediments and the carbon to sulphur ratio (C/S), which might serve as a palaeosalinity indicator, is high (Berner, 1984). Unfortunately, Phase-2 sediments of Lake Sihetun are heavily oxidized, so the C/S ratio will yield no further information. However, Lake Sihetun was volcanically influenced (Jiang et al., 2011; Hethke et al., 2013a), so dissolved sulphates or sulphides might have well been present in higher concentrations. Iron sulphides are soluble at pH levels of around 6 and lower, though sulphate reduction occurs at a pH as low as 4.2. The upper limit of sulphate reduction is at pH 9.9. Eh is commonly low (Baas Becking et al., 1960). Therefore, decreasing Eh and increasing pH values can be expected for the hypolimnion of Lake Sihetun (Fig. 2.11).

(3) Detrital iron minerals should not have limited iron sulphide formation in Lake Sihetun, as reactive iron minerals were abundant in the synsedimentary volcanic deposits.

Secondary controls on pyrite formation include sedimentation rate and nutrient concentration. Considering the low sedimentation rates of Phase 2 and assuming an environment with oxic to dysoxic bottom waters, then more reactive organic compounds must have been readily destroyed and only resistant organic compounds should have remained for sulphate reduction (Berner, 1984). Therefore, nutrient concentrations must have been high within eutrophic Lake Sihetun to compensate for the low sedimentation rate by generating a high amount of organic matter. Nevertheless, rare oligotrophic to mesotrophic intervals occurred during Phase 2 as well, which are inferred from the presence of chrysophycean cysts and a general absence of iron sulphides within the corresponding sediments (Hethke et al., 2013a).

When mixing of the water column is limited and organic matter supply is high, the redox interface rises above the bottom sediments. In the Black Sea, anoxic, sulphidic waters are present in 100 m depth and greigite concentrations in the water column are highest at a depth of 125 m (1988 R.V. Knorr cruise). Maximum concentrations of total dissolved

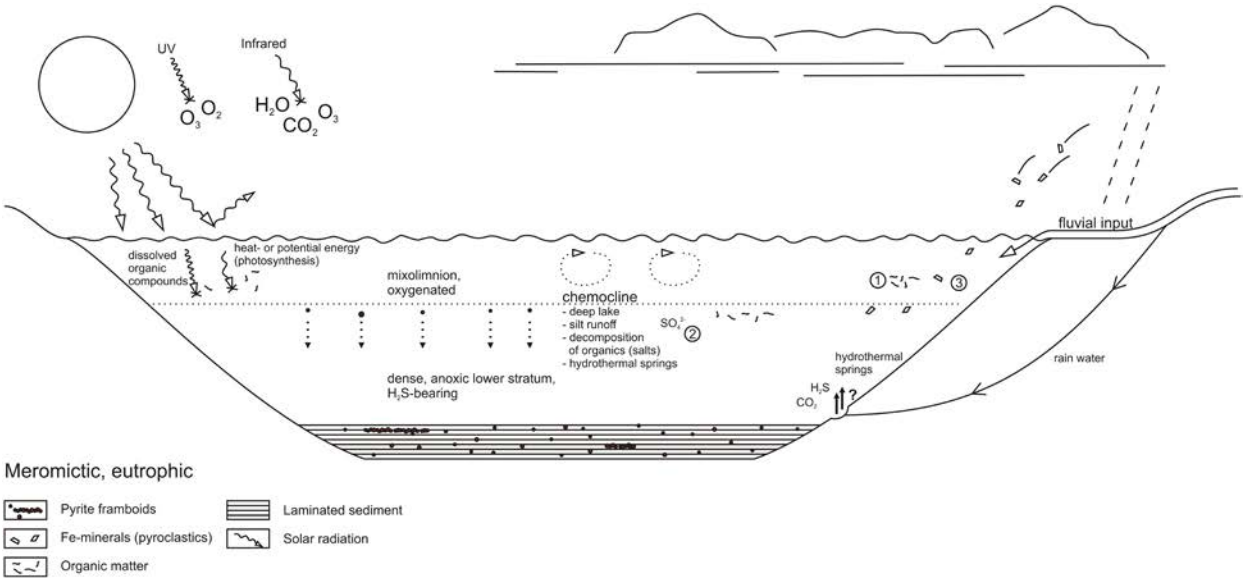

Fig. 2.12. Phase 2, meromictic setting. Meromictic conditions in a chemically stratified Lake Sihetun with syngenetic iron sulphide framboids precipitating immediately below the redox interface, which had moved into the water column. The three main controls on pyrite formation are numbered: (1) organic matter, (2) sulphate, and (3) detrital iron minerals. Different causes of meromixis are proposed for Lake Sihetun. (I) Meromixis probably arose due to extensive decomposition of organic matter in combination with a moderately deep to deep Lake Sihetun, where mixing was limited to the upper water column. Climates were dry. (II) As the lake was volcanically influenced, it might have been subjected to hydrothermal events, which corresponded to wetter climates when local rain waters became activated with CO_2 and H_2S. The chemical stratification must have been delicate, as it was almost offset by increasing temperatures with depth, and catastrophic outgassing of CO_2 might have led to major mass mortality events during times of reduced rainfall.

iron were found at 180 m depth, decreasing below it. The depth interval immediately below the redox interface in the Black Sea is a zone of net consumption of dissolved sulphide by oxidation and precipitation (Muramoto et al., 1991). Furthermore, the average $\delta^{34}S$ composition of dissolved sulphide from the uppermost 70-100 m of the sulphide zone of the Black Sea is similar to that of particulate sulphur fluxes and of sediment sulphides, corroborating their place of origin from immediately below the oxic-anoxic interface within the water column (Fry et al., 1991; Muramoto et al., 1991). Shifts to positive isotopic values as observed within the lacustrine beds of the Black Sea (25,000 - > 7,000 years BC; Ross and Degens, 1974) indicate freshwater conditions and even closed-system growth (Calvert et al., 1996).

Framboid size distributions

Intense diagenetic alteration and weathering within the sediments of Lake Sihetun led to the formation of characteristic reaction rims made up of iron oxide-hydroxides around numerous microcrystals (Figs. 2.4c, 2.5b, 2.6a) as well as to alteration rinds (Figs. 2.4f, 2.6b). Provided that primary iron sulphide textures are preserved (Fig. 2.6a), framboid size distributions can be used to discriminate between oxic, dysoxic, and anoxic conditions within the bottom waters. Wilkin et al. (1996) surveyed framboids in modern (1) anoxic-sulphidic (euxinic), (2) dysoxic, and (3) oxic environments.

(1) Euxinic framboids are small and less variable in size, being subjected to shorter growth times, because nucleation occurs syngenetically within the anoxic water column. As the zone of framboid formation is limited (immediately subjacent to the redox interface and above the sulphidic zone), syngenetic framboid growth is restricted by size. Since settling velocity varies with the square of the particle radius, standard deviations are small, corresponding to narrow size distributions (Stokes' law; Muramoto et al., 1991; Wilkin et al., 1996). Overall syngenetic diameters are smaller than those produced by diagenetic growth (Wignall et al., 2005). Importantly, syngenetic framboids of the Black Sea were not observed in larger clusters, but as single occurrences (Muramoto et al., 1991), which is also true for matrix framboids of Lake Sihetun deposits.

(2) and (3) Framboids forming within sediment pore waters that underlie dysoxic and oxic water columns have more time for nucleation and growth, and consequently yield larger diameters. Lower dysoxic conditions are indicated by framboids be-

ing similarly small as euxinic ones, but occasional larger diameters occur. Higher oxygen saturation is revealed by larger framboids exhibiting a broader size distribution (upper dysaerobic; Wignall and Newton, 1998).

These findings have been tested (Wignall and Newton, 1998), and a close correlation between framboid diameter and the degree of oxygen deficiency determined by other palaeoecological parameters has been discovered. A unique opportunity of application is provided by Holocene deep-water sediments of the Black Sea (Wilkin et al., 1997), which are subdivided into three units (Ross and Degens, 1974): Pleistocene-early Holocene lacustrine, organic carbon-poor layers (Unit 3), a sapropel (Unit 2), and the most recent carbonate-rich sediments (Unit 1). The development of water-column anoxia in the Black Sea, which coincided with the beginning of Unit 2, resulted in a drop in mean framboid diameters from 10 µm to 5 µm (Wilkin et al., 1997). Hence, a mean of 10.5 µm for the concentrated framboids of ancient Lake Sihetun (Fig. 2.7) implies growth within anoxic sediment pore waters, similar to Unit 3 of the Black Sea. Co-occurring matrix framboids, however, carry a lower dysoxic signal.

Mf-1 framboids

Crystal size distributions can be related to crystal growth mechanisms (Kile et al., 2000). Log-normal distributions of Mf-1 framboids (Fig. 2.9) indicate initial growth by surface control and subsequent supply-controlled growth suggestive of open-system growth (Kile et al., 2000; Merinero et al., 2009).

Diameter means of euxinic Black-Sea and Framvaren framboids range between 4.3 and 6.1 µm with standard deviations of 1.4 to 2.0 µm (Wilkin et al., 1996). According to these criteria, euxinic conditions were established in Lake Sihetun during the deposition of horizons ZJG E and ZJG D, which yield mean diameters of 5.4 and 5.6 µm, respectively. Two other thin-sections (LXBE N1 and LXBE G1) might yield an episodically anoxic signal, considering the distribution overlap between concentrated and matrix framboids (Figs. 2.9, 2.10). The existing discrepancy between euxinic framboids of the Black Sea and those of Lake Sihetun results from parameters that affect the settling rate, e.g., density differences, thermal motions, turbulence, and particle-particle interactions (Wilkin et al., 1996). Euxinic framboids of the Black Sea, for example, frequently adhere to biogenic particles (Muramoto et al., 1991).

A similar case is the size discrepancy between euxinic framboid diameters of the modern Black Sea and those of the Kimmeridge Clay (5.0 and 3.0 µm, respectively; Wilkin et al., 1996; Wignall and Newton, 1998). This discrepancy was suggested to result from more rapid settling rates of Kimmeridge Clay framboids compared to those of the Black Sea, where framboids form directly subjacent to the redox interface for several months until they reach a critical size and begin to settle. The Kimmeridge Clay sea exhibited a less pronounced density contrast, because it was thermally stratified in contrast to the salinity-stratified Black Sea (Wignall and Newton, 1998).

Dysoxic distributions, in turn, are characterized by the addition of large diameters to the spectrum (Wignall and Newton, 1998). Standard deviations of most Mf 1-framboids range around 3.1 µm (Fig. 2.9), which is similar to those of framboids recovered from the dysoxic Peru margin (Wilkin et al., 1996). However, Figs. 2.6 and 2.7 demonstrate that there is a considerable distribution overlap between concentrated and matrix framboids that raises standard deviations significantly. It can therefore be assumed that some distributions contain an anoxic signal, especially those of excavation ZJG.

Mf-4 clustered pyrites

Secondary pyrite overgrowth resulted in higher mean diameters and standard deviations of Mf-4 clustered pyrites (LXBE K1 and J; Fig. 2.5a, b). It is the more pronounced the longer pyrite is subjected to solutes such as Fe^{2+} or HS^{-}. Bioturbation promotes transportation of these by sediment remixing (Wilkin et al., 1996). Hethke et al. (2013a) noted the presence of meiofaunal bioturbation in Mf 4. Furthermore, Mf-4 standard deviations are similar to oxic environments of salt marshes (Wilkin et al., 1996), but the mean diameters of the Lake Sihetun clustered pyrites are significantly larger (Fig. 2.9).

The negatively skewed framboid size distribution of LXBE K1 is indicative of an eventual formation of a closed system. As saturation was being reduced, small pyrite crystals and clusters became unstable, while larger clusters grew at their expense due to their large surface free energy (Ostwald ripening; Kile et al., 2000; Merinero et al., 2009). However, Merinero et al. (2009) mentioned low values of size variance for closed-system conditions, which is not true of Mf-4 distributions. This might be a measurement artefact due to the general disintegration of most Mf-4 clustered pyrites or a result of a combined open system-closed system growth. Never-

theless, the general evidence strongly implies early-diagenetic, intergranular formation of Mf-4 pyrites and an oxic water column.

Methane-derived carbonates?

Methanogenic fermentation of buried organic matter leads to methane accumulation within organic-rich sediments. In view of the ongoing syn-sedimentary volcanism within Lake Sihetun, thermogenic methane may also be considered. Seepage of methane-rich fluids causes carbonate precipitation (Peckmann et al., 2001). Such methane-derived carbonates are induced by methane oxidation that is coupled to bacterial sulphate reduction. Increased alkalinity is held responsible for carbonate formation. Carbonates (Mf 4) are layered within the sediments of Lake Sihetun. In the Black Sea, flat crusts develop under oxic bottom waters instead of chimney-like structures, which are found within the anoxic zone. Iron sulphides accompany these microbial carbonates. The diameters of individual framboids reported from Black Sea methane seeps are 20 to 30 μm (Peckmann et al., 2001), similar to those of Mf-4 clustered pyrites. Therefore, in addition to the seasonal interpretation of Mf-4 deposits put forward by Hethke et al. (2013a), there might be a second cause involving the formation of methane-derived carbonates (Mf 4) induced by methane oxidation (Fig. 2.11).

Environmental inferences

There are three major environmental settings leading to pyrite formation that intermittently dominated Lake Sihetun during Phase 2. They are oxic, dysoxic, and anoxic bottom waters. Generally, palaeoecological evidence points towards anoxic to lower dysoxic bottom waters in Lake Sihetun, expressed by a general lack of bioturbation that left the laminated sediments undisturbed as well as by very low faunal diversities with abundant mono- to paucispecific assemblages of opportunistic taxa (Wignall and Hallam, 1991; Fürsich et al., 2007).

Setting 1: euxinic

This setting implies oxygen-free and H_2S-bearing bottom waters in a permanently stratified water column. Evidence for such conditions has been found within two horizons of excavation ZJG (Fig. 2.10). There are several causes for the establishment of such meromictic conditions in Lake Sihetun (Fig. 2.12):

(1) Stagnation due to minimal circulation might have arisen as Lake Sihetun was comparatively deep in contrast to its surface area. It may have led to an occurrence of H_2S above the sediment-water interface, so that iron sulphides could precipitate from the water column, usually through high rates of organic matter sedimentation as a result of eutrophic conditions. "Fresh" and more reactive organic compounds were retained and accumulated, which would have otherwise been rapidly destroyed. Bacterial sulphate reduction was extensive in both bottom waters and sediments, and pyrite formation was possible even during sedimentation (Berner, 1984). Detrital iron minerals were present in ample amounts during Phase 2, as most of the sediments are tuffaceous. Matrix framboids (Fig. 2.7) are proposed to be syngenetic in such a setting. Concentrated framboids and associated single euhedral microcrystals occurring adjacent to matrix framboids formed diagenetically within the sediment at a different time, maybe even underneath oxic to dysoxic bottom waters (e.g., Fig. 2.5e).

(2) As Lake Sihetun was volcanically influenced, hydrothermal spring activity might have occurred (Fig. 2.12) and led to high concentrations of dissolved gasses, specifically CO_2, CH_4, and H_2S. Hydrothermal events correspond to wetter climates, as rain waters become activated with CO_2 and H_2S (Degens et al., 1972), leading to a delicate temperature and salinity stratification, in which the chemical stratification is almost offset by increasing temperatures with depth. Such conditions were constantly at risk of sudden, catastrophic outgassings of CO_2 that might have happened during times of reduced rainfall, leading to major mass mortality events within the waters of Lake Sihetun as well as on land.

Settings 2 and 3: dysoxic and oxic

During most of Phase 2, lower dysoxic conditions were established within the bottom waters of Lake Sihetun, leading to a lack of bioturbation and to the absence of fossils on most bedding planes with only few fossil-bearing layers of very low diversity (Fürsich et al., 2007; see also Wignall and Hallam, 1991). Pyrite formation occurred during early diagenesis below the sediment-water interface. Setting 3 assumes oxic bottom waters, which is mainly applicable to Mf-4 clustered pyrites.

Concentrated iron-sulphide layers. – Considering the low rates of sedimentation present within Phase 2, highly reactive organic compounds must have been readily destroyed in the water column above the sediment-water interface and the top sediment layers and only more resistant compounds were able to survive for sulphate reduction. However, the

presence of biofilms at the bottom of Lake Sihetun may have provided favourable conditions for framboid formation. Concentrated framboid layers similar to Fig. 2.4b, c are stratiform and the grain fabric is loose, meeting the criteria described by Schieber (2002) for the presence of an organic slime matrix, which is a favourable culture medium for sulphate reducing bacteria. Pyrite concretions with framboid-dominated textures in Holocene lacustrine clays of the northern Baltic Sea, for example, formed within burrows by the decomposition of mucous coatings on the burrow walls (Virtasalo et al., 2010).

Several contradicting explanations are possible for the comparatively thick irregular layers dominated by euhedral microcrystals (Fig. 2.5c-e). (1) Masses of euhedral microcrystals similar to those observed in Lake Sihetun are known from Holocene lacustrine clays of the Baltic Sea, where they crystallized in organic-poor pore spaces (Virtasalo et al., 2010; Virtasalo et al., 2013). Pore spaces in the sediments of Lake Sihetun may have resulted from gases forming during the decomposition of biofilms, as observed in the Solnhofen Plattenkalk (Link and Fürsich, 2001).

(2) There might be a purely chemical explanation for the dominance of microcrystals, as texture is also a function of Eh and euhedral microcrystals are formed at an Eh lower than that for framboid formation (Butler and Rickard, 2000). Mixed textures of framboids and euhedra have also been observed by Butler and Rickard (2000).

(3) Furthermore, the establishment of microenvironments around and within plant and animal remains might have preserved reactive organic compounds and led to iron sulphide replacement (Briggs et al., 1996) that can be observed in many fossils of Bed 2 (Leng and Yang, 2003). Microcrystals similar to those of the iron sulphide layers observed in Bed 2 have been reported from pyritized insect fossils of the Middle Jurassic of Daohugou, Inner Mongolia (Wang et al., 2009).

With the onset of Phase 3, conditions in Lake Sihetun became moderately to strongly oxidizing at the sediment-water interface. This was accompanied by a cessation of extensive iron sulphide formation. Coarser sediments, as deposited during Phase 3, are usually much better oxidized than clay-sized particles (Baas Becking et al., 1960).

Lake analogue for setting 1

Volcanic and meromictic Lake Kivu (DR Congo and Rwanda) may be viewed as a lake analogue to Lake Sihetun in some respects. It is permanently stratified and anoxic below depths of 50-80 m. Evidence for lacustrine, syngenetic pyrite framboids has been reported by Degens et al. (1972), who found pyrite framboids (5-10 μm in diameter) suspended within the H_2S zone of the lake. Hydrothermal events lead to a temperature and salinity stratification in Lake Kivu. According to Degens et al. (1972), the water discharge through hydrothermal springs is so high that the lake would fill up in only 100 years. Hydrothermal solutions originate from rain waters that become activated with CO_2 and H_2S. Accordingly, concentrations of CO_2 and CH_4 increase with lake depth (Tassi et al., 2009). Sedimentary properties of Lake Sihetun deposits are very similar to those of Lake Kivu, except that the H_2S-zone in Lake Kivu is marked by sphalerite (ZnS), which has not been found in Lake Sihetun. This is a matter of zinc availability within the adjacent rock formations the hydrothermal solution is passing through.

To sustain meromictic conditions, prolonged hydrothermal input is needed. Haberyan and Hecky (1987) note that Lake Kivu's modern chemical stratification is almost offset by increasing temperatures with depth. The surface waters have to be constantly diluted to prevent lake overturn. Overturn would increase deep water pH through the release of CO_2, allowing for carbonate to precipitate. Therefore, carbonate precipitation occurs during strongly reduced inflow (Haberyan and Hecky, 1987). Evidently, pyrite must be scarce during severely high CO_2-concentrations leading to low pH levels. Nevertheless somewhat surprisingly, pyrite framboids have been reported from Lake Kivu (Degens et al., 1972).

One of the most striking similarities to Lake Sihetun is that Lake Kivu has endured massive mass mortality events triggered by extreme hydrothermal events that account for the mortality of plankton as well as the elimination of higher trophic levels, explaining the modern low fish diversity (Haberyan and Hecky, 1987). Lake-overturn events could potentially devastate terrestrial communities (Nayar, 2009) and have recently occurred in two other lakes from Cameroon. Sudden outgassings of CO_2 are known from Lake Monoun (1984) and Lake Nyos (1986), creating acidic clouds that erupted from the lakes and suffocated villagers and animals in the low-lying areas. It is possible that similar catastrophic overturn was responsible for mass mortality events in Lake Sihetun and its surroundings.

Conclusions

Phase 2 of Lake Sihetun, which is known for its excellently preserved vertebrate and invertebrate fossils, is characterized by predominantly dysoxic bottom waters, but intermittent euxinic spells occurred. Rarely, oxic bottom waters existed, mainly during the deposition of calcium carbonate-rich sediments, which were possibly methane-derived. Marked spatial variations in redox state across the lake floor are probably related to changing water depths. Phase 3 is characterized by a fully oxygenated lake and iron sulphides have not been observed within this lake interval.

Stagnation during Phase 2 episodically led to the establishment of meromictic conditions and reducing bottom waters provided environments suitable for syngenetic framboid formation taking place immediately below the redox interface in the water column. Framboids sank to the lake floor and became scattered throughout the matrix. Such euxinic conditions have been triggered by minimal circulation, eutrophy, and, since Lake Sihetun was volcanically influenced, possibly also by hydrothermal events, which may have led to high concentrations of dissolved gasses. Recurrent sudden outgassing events are proposed as a cause for vertebrate and invertebrate mass mortality events within the lake.

Framboids occurring in concentrated layers are often associated with iron sulphide microcrystals. A dominance of microcrystal textures within such layers reveals formation in organic-poor pore spaces or a decrease in Eh. Concentrated framboid layers represent the formation of early diagenetic restricted microenvironments around mucous biofilms at the lake floor or around other organic remains. Highly reactive organic matter was preserved and eventually oxidized, leading to suitable geochemical conditions for iron sulphide formation and ultimately excellent fossil preservation.

Acknowledgements

We would like to thank Matthias Alberti, Patrick Chellouche, Yanhong Pan, and Simon Schneider for helpful discussion. Valuable suggestions were provided by David Bond and one anonymous reviewer. Scientific editor Jim Hendry is thanked for his support during the review process. Technical guidance was received by Christian Schulbert. This study was supported by the BMBF (FKZ: 01DO12016), the 973 program grant (2012CB821905) and the National Science Foundation of China (grants 406032010, 40672077, 41172033).

Chapter 3: Clam-shrimp biomineralization (Branchiopoda: Spinicaudata) and its implications for the classification of the group

Chapter 3 is a joint project of the following authors:

Manja Hethke[1], Carys E. Bennett[2], Franz T. Fürsich[1], Baoyu Jiang[3], Frank Scholze[4], Sebastian Dittrich[5], Jürgen Neubauer[5]

[1]*GeoZentrum Nordbayern, FG Paläoumwelt, Germany*
[2]*Department of Geology, University of Leicester, UK*
[3]*School of Earth Sciences and Engineering, Nanjing University, China*
[4]*Institut für Geologie, Technische Universität Bergakademie Freiberg, Germany*
[5]*GeoZentrum Nordbayern, FG Angewandte Geowissenschaften, Germany*

Introduction

The Crustacea are the most morphologically diverse taxon on our planet and the Branchiopoda is one of its most diverse classes (Martin, 1992). As one major branchiopod group, the Spinicaudata ("clam shrimps") have an extensive fossil record that dates back at least to the Devonian (e.g., Raymond, 1946; Astin, 1990). One recurrent anatomical feature of the Spinicaudata is a carapace that originates from the back of the head as a dorsal fold (Barnes and Harrison, 1992), and the classification of fossils is almost entirely based on carapace morphology. Spinicaudatans are widely used as biostratigraphic markers in inland basins, such as the Mesozoic basins of Eastern Asia (e.g., Chen, 2003) or the Germanic Basin (e.g., Kozur and Weems, 2010). Despite this biostratigraphic importance, fossil spinicaudatan classification is not well resolved, as it suffers from pronounced regional influences. This lack of a comprehensive classification scheme causes workers to mix several schemes, by for instance placing a family of one scheme into an obsolete superfamily of another (Table 3.1; Raymond, 1946; Kobayashi, 1954, 1972; Novojilov, 1960; Defretin-Lefranc, 1965; Tasch, 1969, 1987; Zhang et al., 1976; Kozur, 1982). Moreover, several classification schemes do not include extant forms. Hence, there is a great need for a reassessment of the classification of fossil forms and a harmonization with that of modern spinicaudatans (e.g., Martin and Davis, 2001; Schwentner et al., 2009). We argue that one of the reasons for this confusion is that clam-shrimp fossilization is not well understood to date, in particular whether or not biominerals are present in extant cuticles and how these relate to the structural and chemical preservation of fossil cuticles.

While it is generally accepted that the multilamellar shell microstructure of fossil forms is similar to that of modern spinicaudatans (Kozur, 1982; Olempska, 2004), there are several different assertions about carapace mineralogy: Stigall et al. (2008) recognized that fossil spinicaudatans were preserved in calcium phosphates and, to a lesser degree, in silica. Up to then, it was promoted in the literature that fossil carapaces were preserved in calcium carbonate (e.g., Ziegler, 1998; Olempska, 2004). Such statements often lacked citations, however. Spinicaudatans may also be preserved as organic carbon residues, and, if present, appendages are infilled with phyllosilicates (Orr and Briggs, 1999). The literature on the biomineralization of Recent spinicaudatans is contradictory. Kobayashi (1954), for example, stated that "in living Conchostracans it was known that the chitinous carapace was somewhat calcified" without citing any sources. In the Treatise on Invertebrate Paleontology, Tasch (1969) avoided the issue by referring to Mathias (1937), who stated that "the corneous modern carapace was never strongly calcified". Vannier et al. (2003) mentioned that the modern spinicaudatan carapace was thin, flexible and unmineralized, though resistant to decay. Considering these numerous mineralogies in extant carapaces, there is a need for clarification.

Generally, the preservation potential of the original chemistry of the arthropod cuticle is determined by its thickness and degree of sclerotization, as well as the presence of biominerals (Briggs, 1999; Orr et al., 2008). Taphonomic studies on spinicaudatan crustaceans hint at selective preservation of certain appendages and of the carapace related to differences in cuticle recalcitrance (Orr et al., 2008). This preservational disparity might be accentuated by the

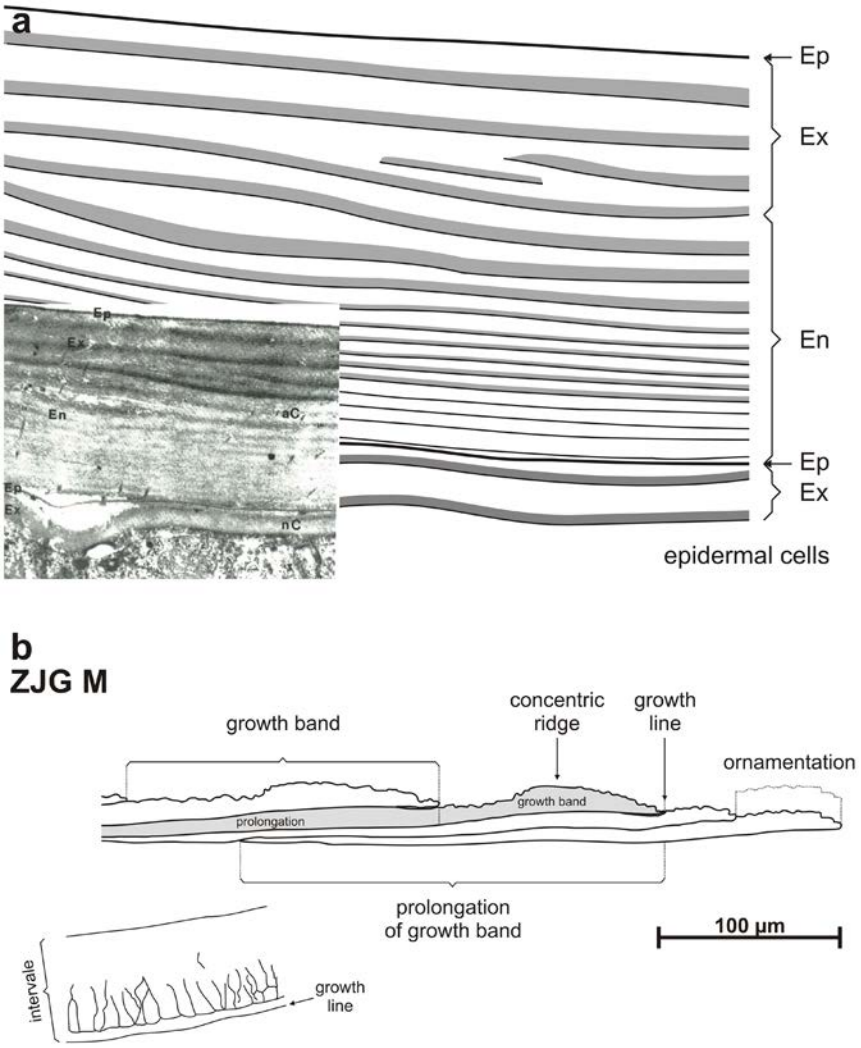

← **Fig. 3.1.** (a) Cross-section of the integument of the spinicaudatan *Leptestheria dahalacensis* near the carapace margin (nC – new cuticle, aC – old cuticle). The spinicaudatan cuticle is made up of three units: epicuticle (Ep), exocuticle (Ex), and endocuticle (En). The lamellar structure of the exo- and the endocuticle is apparent. The newly formed cuticle underneath the older cuticle thus far consists only of the epicuticle and the upper layer of the exocuticle. Scale unknown. Modified after Rieder et al. (1984). (b) Features of spinicaudatan growth bands, exemplified by the Early Cretaceous *Eosestheria middendorfii* as a model organism. Scale bar only applies to cross-section.

presence of biominerals in certain parts of the cuticle. Apart from these biological constraints on cuticle preservation, abiotic constraints in the form of the prevalent palaeoenvironment may lead to drastic alteration of the carapace. Hence, we are confronted with four main questions regarding cuticle preservation of spinicaudatan carapaces. (1) Do extant spinicaudatans biomineralize and, if yes, does that apply to all three extant families? (2) How are fossil clam shrimps preserved? (3) What happens to carapaces of species that biomineralize and to those that do not during fossilization? (4) How do different depositional environments affect the preservation of biomineralized material and what does the associated carapace microstructure look like?

This paper takes a major step towards clarifying the mineralogy of spinicaudatan carapaces, extant and fossil, relating cuticle preservation to depositional settings and considering the implications for family-rank taxonomy.

Carapace microstructure of modern spinicaudatans

The cuticle of spinicaudatans is designed like that of most other crustaceans (Fig. 3.1a), as it consists of two layers: a thin outer epicuticle made up of protein, lipids, and calcium salts, and an internal procuticle, which is much thicker than the epicuticle. The internal procuticle is differentiated into an outer preecdysial layer (exocuticle) and an inner postecdysial layer (endocuticle; Rieder et al., 1984; Stevenson, 1985; Martin, 1992; Vannier et al., 2003).

The typical branchiopod cuticle is very thin with no calcification of the exocuticle and little sclerotization (Martin, 1992) and the cuticle of spinicaudatan branchiopods is similar to that of *Daphnia* and *Artemia* for most parts of the body (Rieder et al., 1984). By contrast the presence of growth lines indicate that the cuticle of the spinicaudatan carapace is not shed during ecdysis (Fig. 3.1b). Consequently, the number of cuticle layers, retained after ecdysis, accumulates with age (Martin, 1992). A new, larger

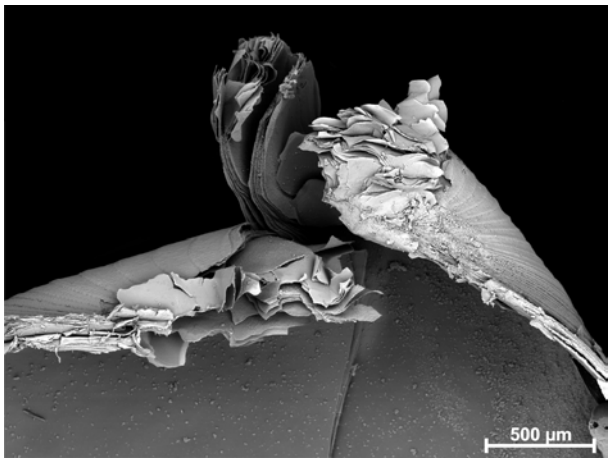

Fig. 3.2. SEM micrograph. Umbonal region of modern *Caenestheriella donaciformis* in cross-section displaying loosely connected cuticle layers.

cuticle typically develops beneath an older, smaller cuticle, adhering to the latter forming growth bands. The cuticle of the soft parts is shed.

The thickness and number (3-10 in *Leptestheria dahalacensis*; Fig. 3.1a) of lamellae of the exocuticle are different for the various body parts. The maximum thickness of exocuticle lamellae is reached at the ventral carapace margin (Rieder et al., 1984). The endocuticle is less sclerotized ("tanned") than the exocuticle (Rieder et al., 1984). Rieder et al. (1984) claim that no distinct contacts could be identified, suggesting that lamellae are only loosely connected and larger gaps may occur between them. According to this theory, the number of cuticle layers corresponds to the number of moults at the umbo and this region should become successively thicker with accumulated layers of unshed integument (Fig. 3.2; Rieder et al., 1984; Martin, 1992).

Material and methods

Numerous spinicaudatan crustaceans have been collected during field campaigns carried out in Germany, Morocco, and Russia, and in the Chinese provinces of Liaoning, Gansu, and Shaanxi. Mineralised fossil material was analysed from the collections of the British Geological Survey and the Natural History Museum, London. The Naturkunde-Museum Coburg provided Upper Triassic material from northern Bavaria, Germany. In total, specimens from eight different stratigraphic levels have been analysed. They are: Early Carboniferous, Late Carboniferous, Early Triassic, Middle Triassic, Late Triassic, Middle-Late Jurassic, Early Cretaceous, and the Recent (Fig. 3.3). An overview of specimens employed in this study is given in Table 3.2. The environmental framework of the fossil locations (where known) has been documented in detail (Table 3.4).

Modern spinicaudatans collected and studied from freshwater environments are: (a) *Limnadia lenticularis* collected in the Margraviate Brandenburg in 1956, (b) *Leptestheria dahalacensis*, female specimens collected in Altenburg near Vienna in 1959, (c) *Caenestheriella donaciformis* collected in Kordofan (central Sudan) before 1911, (d) *Cyzicus* sp. A from our own aquarium, and (e) captive breeding of eggs of *Cyzicus* sp. B collected from the Azraq Playa, Jordan, in 1998. Each of the modern specimens was chosen to represent one of the modern families: Limnadiidae (a), Leptestheriidae (b), and Cyzicidae (c-e). A number of modern spinicaudatans come from captive breeding in freshwater at the GeoZentrum Nordbayern of the University of Erlangen-Nürnberg as well as the Geological Institute of Freiberg University. These specimens had been air-dried for further analysis. Note that all material from the Bavarian State Collection of Zoology (a-c) had been kept in the same liquid preservative, so differences in carapace preservation resulting from conservation can be ruled out. Modern clam shrimps provided by the Bavarian State Collection of Zoology had been dissected to remove the soft parts from the carapace and subsequently dried in preparation for examination under the Scanning Electron Microscope (SEM). This involved a stepwise dehydration to acetone (30% → 100%) and subsequent critical point drying with CO_2 as a medium for the procedure.

Analytical techniques involved Energy-dispersive X-ray spectroscopy (EDS, using INCA analytical software) to identify the elemental composition of a sample using gold or carbon as conductive coatings. For comparison, one quantitative measurement of the chemical composition was taken with the Electron microprobe (EMP; Jeol Superprobe). Qualitative phase analyses were carried out using the General Area Detection Diffraction System (GADDS by Bruker AXS) equipped with a HI-STAR area detector. At the chosen working distance of 15 cm, a 2 theta range of 34° is covered by the detector. The XRD tube of the diffractometer was operated at 40 mA and 40 kV using Cu Kα radiation. The spot size of the incident X-ray beam on the sample was defined by the use of a collimator (diameter 300 µm) and an incident beam angle of 15°. EVA (Bruker, AXS) software was used for the qualitative phase analysis of the obtained XRD patterns. Mod-

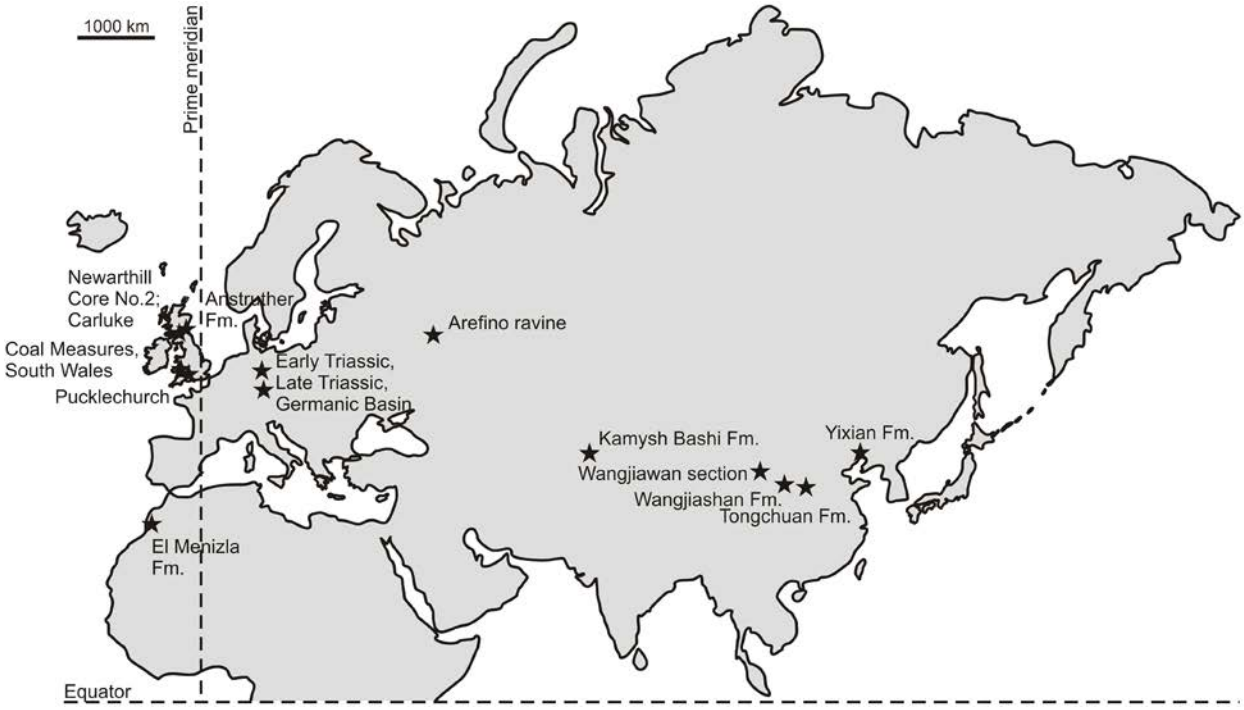

Fig. 3.3. Outcrop localities of the studied specimens. Localities not pictured are Warner's Bay, Lake Macquarie, New South Wales and Carapace Nunatak, Victoria Land, Transantarctic Mountains.

ern samples were pulverized by hand (agate mortar) and the powder was then prepared on a single silicon crystal sample holder using 2-propanol. As the silicon single crystal is cut along a defined crystallographic plane section, no intensity contribution to the XRD pattern is generated by the sample holder. This is important, because only a small amount of sample material was available, too little to keep the X-ray beam from hitting the sample holder. The fossil carapaces were very thin and powder preparation would often result in a carapace-sediment mix. To avoid this problem and to avoid destroying the samples, the X-ray investigation was carried out on the surfaces of complete carapaces embedded in the sedimentary host rock. Hence, effects resulting from surface roughness have to be considered when interpreting the XRD profiles. For a better presentation of the obtained XRD data, a linear background was subtracted from each pattern.

Reference materials are stored at the GeoZentrum Nordbayern in Erlangen, Germany, the Geological Institute of Freiberg University, Germany, the Naturkunde-Museum Coburg, Germany, the British Geological Survey, and the Natural History Museum, London UK.

Taxonomic framework

Classification of extant taxa

In this paper we adopt the branchiopod classification scheme put forward by Braband et al. (2002), declaring Spinicaudata a monophylum that is most closely related to the Cladoceromorpha (Cladocera and Cyclestherida). The historic taxon "Conchostraca" (Spinicaudata, Cyclestherida, and Laevicaudata) is paraphyletic (Braband et al., 2002), comprising groups that possess a laterally compressed body enclosed in a bivalved carapace (Tasch, 1969). Taxa belonging to the Cyclestherida or Laevicaudata are given in square brackets in Table 3.1. The monophyletic suborder Spinicaudata (Martin and Davis, 2001; Braband et al., 2002) contains three families: Cyzicidae, Leptestheriidae, and Limnadiidae (Martin and Davis, 2001), with distinctions based mostly on soft part anatomy and some carapace characteristics as well as on molecular markers. Limnadiidae are monophyletic (Hoeh et al., 2006). Cyzicidae become monophyletic by the exclusion of the genus *Eocyzicus* and the Leptestheriidae are either a sister group to the Cyzicidae or to *Eocyzicus* (Fig. 3.4; Schwentner et al., 2009).

Classification of fossil taxa

There is a lack of consistency in the classification of fossil spinicaudatans, not only at the generic rank

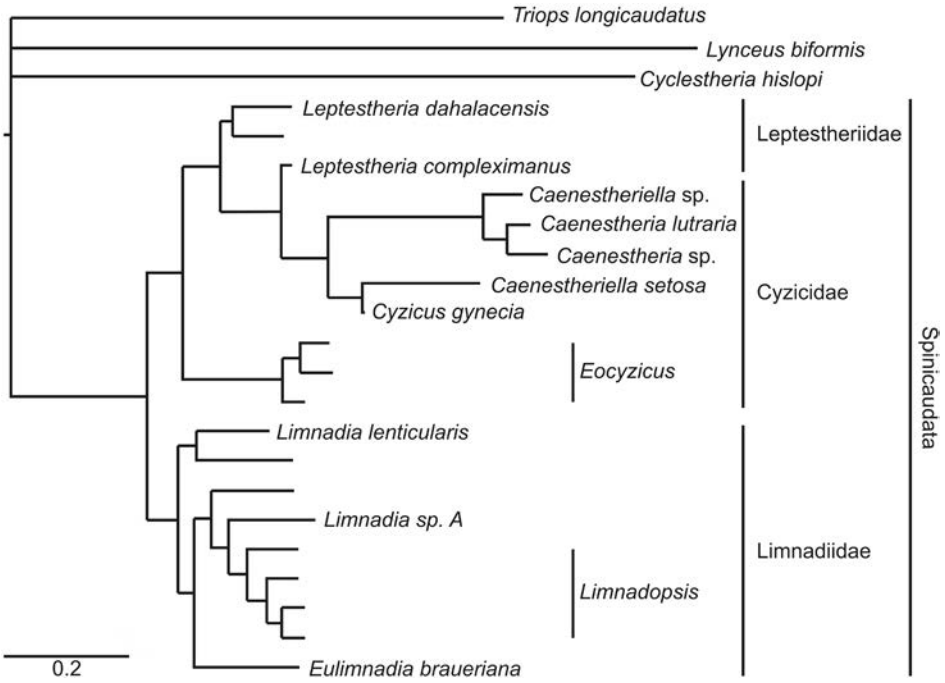

← **Fig. 3.4.** Spinicaudatan systematics after Schwentner et al. (2009) with the inclusion of related branchiopod taxa *Triops*, *Lynceus*, and *Cyclestheria*. The scale bar refers to genetic distance.

but also for higher-rank taxa (Table 3.1). While it may seem counterintuitive, the taxonomy of fossil spinicaudatans may suffer from either extensive splitting or lumping, depending on taxonomic scheme. Lumping is especially common in groups displaying only few characters, although morphological simplicity does not necessarily lead to taxonomic under-resolution (Kowalewski et al., 1997). It is clear that the main problem leading to lumping in clam shrimp taxonomies is poor descriptions, a notable example being that of *Euestheria* in Tasch (1969). There are several more biases that led to splitting and lumping in spinicaudatans; this study also broaches the issue of the often poor preservation of holotypes and syntypes.

For convenience and as a working basis, higher-rank taxa will relate to the "Treatise on Invertebrate Paleontology" (Tasch, 1969). Where applicable, generic names have been adapted to now commonly accepted taxa. For example, the Treatise lists *Euestheria* as a subgenus of *Cyzicus*, although most workers treat it as a genus. This genus has been allocated to various families by different authors, including Lioestheriidae, Leptestheriidae, Cyzicidae, and Euestheriidae, all of which are underlined in Table 3.1. In this study, *Euestheria* is regarded as of generic rank and assigned to the family Cyzicidae (Treatise classification; Tasch, 1969). One last issue taken into account is that many new taxon names have been erected subsequent to the publication of the Treatise, mainly including groups from Eastern Asia.

In accordance with Tasch (1969) and Martin and Davis (2001), five groups have been checked for biominerals in the course of this study: Limnadiidae, Cyzicidae *sensu lato*, Leptestheriidae, Estheriellidae†, and Leaiidae†. For the purpose of this study, the group "Cyzicidae" *sensu lato* was erected. The allocation of the genera listed below to this group is based on facts given in Table 3.3. Fossil specimens of the Limnadioidea have been studied by Orr and Briggs (1999). Genera analyzed herein are:

Suborder Spinicaudata Linder, 1945

Family Limnadiidae Baird, 1849
Genus *Limnadia* Brongniart, 1820 (modern)

Group "Cyzicidae" *sensu lato*
Genus *Carapacestheria* Shen, 1994
Genus *Eosestheria* Chen, 1976
Genus *Euestheria* (Depéret and Mazeran, 1912)
Genus *Laxitextella* Kozur, 1982
Genus *Liograpta* Novojilov, 1954
Genus *Triglypta* Wang, 1984
Genus *Yanjiestheria* Chen, 1976
Genus *Caenestheriella* Daday de Deés, 1913 (modern)
Genus *Cyzicus* Audouin, 1837 (modern)

Family Leptestheriidae Daday, 1923
Genus *Leptestheria* Sars, 1898 (modern)

Family Estheriellidae Kobayashi, 1954
Genus *Estheriella* Weiss, 1875

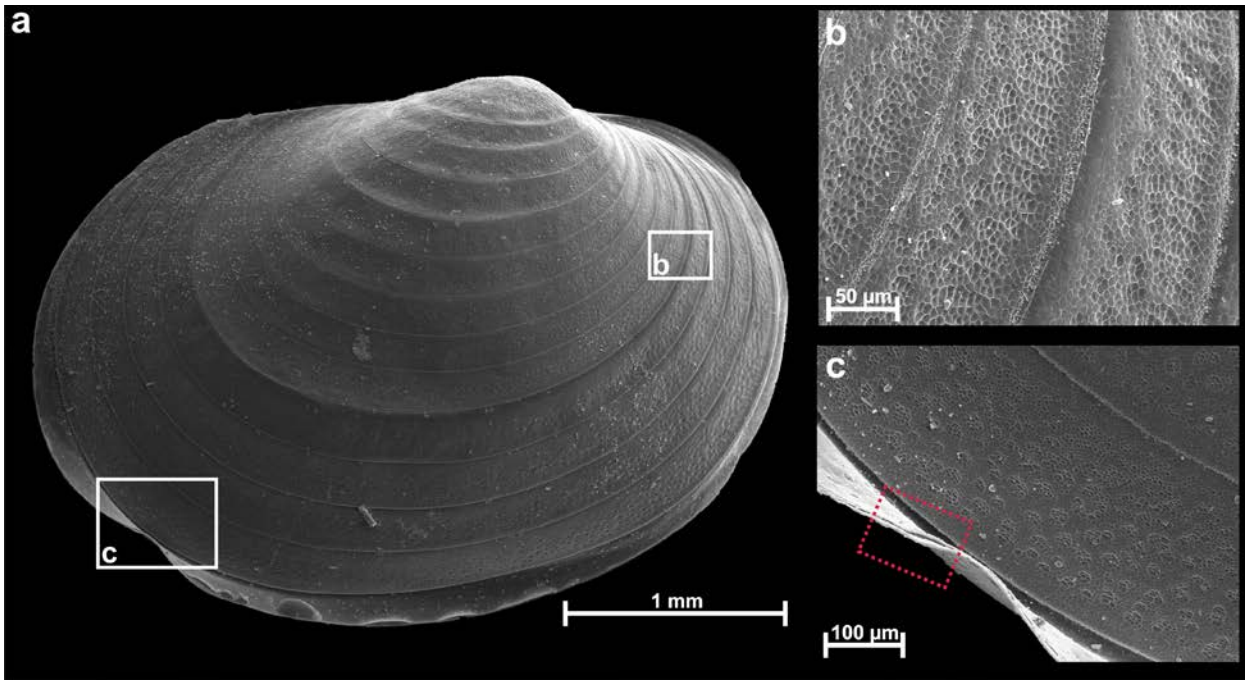

Fig. 3.5. SEM micrographs of (a) the carapace of modern *Cyzicus* and (b) its ornamentation. An apparent two-layered structure of the carapace is highlighted with a red box (c).

Family Leaiidae Raymond, 1946
Genus *Leaia* Jones, 1862

Family unknown
Genus *[Estheria]* Rüppell 1837

Biominerals

The modern spinicaudatans analysed have carapaces composed of either calcium phosphates or calcium carbonates. Which mineral is utilized seems genus-specific (Table 3.5; Figs. 3.6, 10). Dried modern cyzicid carapaces exhibit a two-layered structure (Fig. 3.5). An EDS transect through one growth increment of *Cyzicus* (Fig. 3.6b, c) implies an apatitic composition of the exterior biomineralized zone, which corresponds to the exocuticle. This was verified using X-ray diffraction. The XRD-profile of a second cyzicid species from the Azraq Playa supports biomineralization of the cyzicid carapace with calcium phosphates (Fig. 3.7b). The most important calcium phosphate is probably hydroxylapatite ($Ca_{10}(PO_4)_6(OH)_2$), which plots very close to apatite in XRD-profiles so that the two minerals cannot easily be differentiated using this method. According to Elliott (2002) hydroxylapatite forms the inorganic component in teeth and bones, occurring in an impure, carbonate-containing form (CO_3Ap). Other phosphate biominerals might be octacalciumphosphate ($Ca_8H_2(PO_4)_6x5H_2O$; OCP) and amorphous calcium phosphates (ACP). OCP is not listed in the database of the EVA software, so we were not able to check for it directly. There is also evidence for a mix of calcite and calcium phosphates, picked up by XRD of powdered samples of *Caenestheriella donaciformis* (Cyzicidae).

A specimen of the Leptestheriidae (Fig. 3.7a) builds in calcite, while the Limnadiidae (Fig. 3.7c) do not biomineralize. Their carapace is solely made up of chitin, a polysaccharide, and proteins. Nonetheless, sclerotization, the cross-linking of protein molecules, adds resilience to the carapaces towards physical stress, increasing the chances of preservation.

Structural and chemical clam-shrimp fossil preservation

Carapace preservation involves an assessment of both carapace mineralogy and microstructure. Adult-stage growth bands are usually much better preserved than those near the larval valve. Their orientation is easily distinguished in cross-section through concentric ridges that often form at the ventral end of growth bands. Ridges of older growth increments overlie the dorsal (proximal) ends of younger increments (Figs. 3.1b, 3.8b, c).

A total of four types of fossil clam-shrimp preservation can be distinguished from this study. They are: (1) silicified (Fig. 3.12a), (2) carbonised,

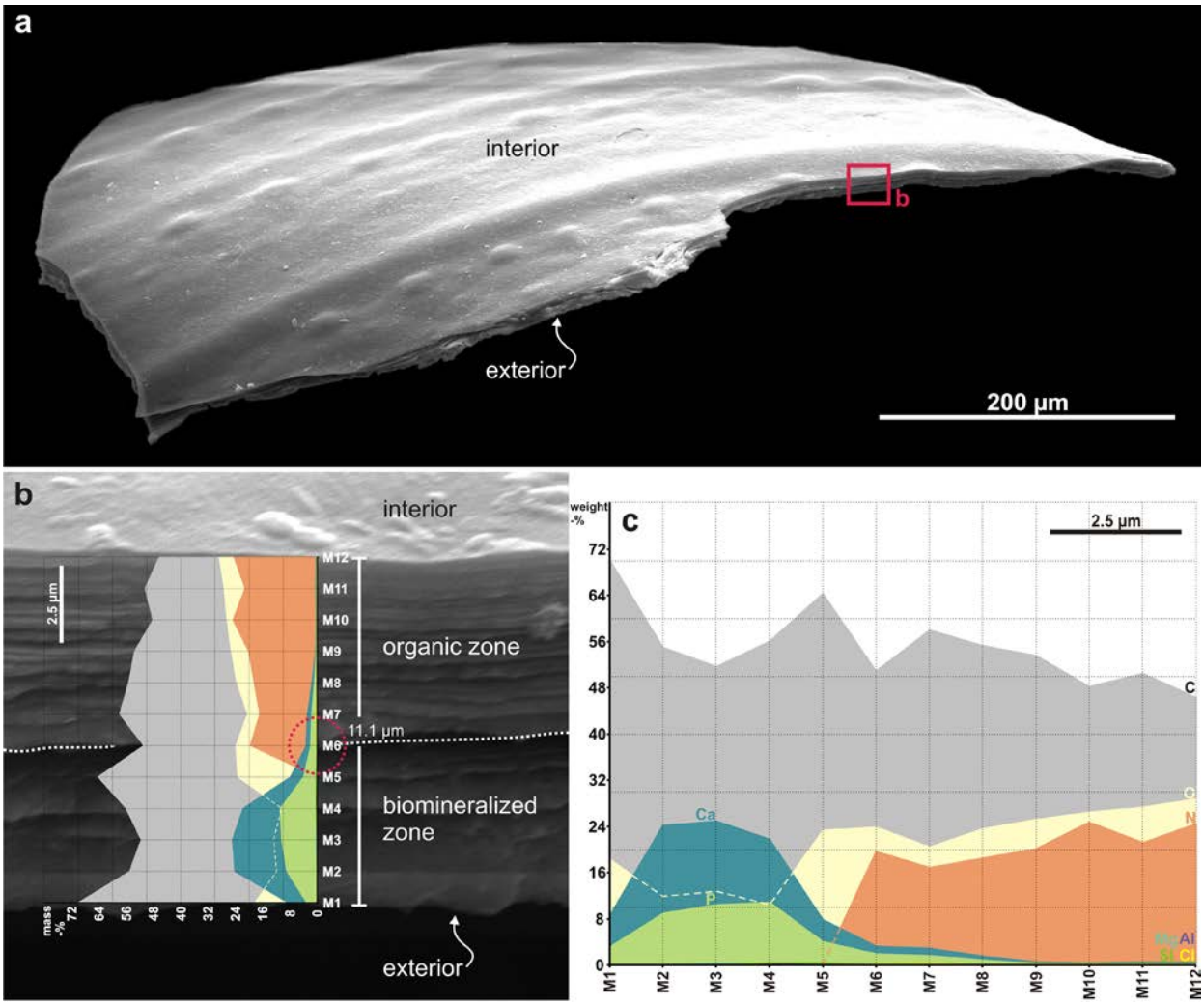

Fig. 3.6. EDS transect through the carapace of one growth increment of *Cyzicus* with twelve measurements (M1-M12). The modern cyzicid carapace can be subdivided into an outer biomineralized and an inner organic zone, which should correspond to the exo- and the endocuticle, respectively. According to (c), biominerals are of apatitic composition. The organic zone is made up of chitin and proteins. Note that the diameter of the electron beam is leading to a transitional zone of mixed composition (red dotted circle in b). M1 represents a mix of the biomineralized carapace and the carbon sticker the specimen is attached to. The raw data are listed in Supplementary 3.2.

(3) fluorapatite (Fig. 3.12b, d), and (4) a mix of fluorapatite and dolomite (Fig. 3.12c).

The most common preservation for fossil specimens is as organic carbon residues or fluorapatite. Carboniferous Leaiidae are commonly preserved as organic carbon residues (Table 3.2). Carboniferous Estheriellidae, Limnadiidae, *[Estheria]* and some Cyzicidae are also preserved as organic carbon residues. The majority of cyzicid specimens (spanning the Carboniferous, Triassic, Jurassic and Cretaceous) are composed of fluorapatite.

Type 1: Silicified

In this study, type-1 preservation is restricted to one Carboniferous specimen of the Leaiidae and one Early Triassic specimen of the Estheriellidae (Table 3.2). Growth lines are observed in most specimens, but fine ornamentation is not preserved, indicating rapid carapace degradation, the absence of biominerals, or a lack of fine ornamentation in the first place.

Type 2: Carbonised

Type-2 preservation is most commonly seen in the Carboniferous Leaiidae, but also occurs in some specimens of Cyzicidae, Limnadiidae and Estheriellidae (Table 3.2). Carbonised specimens are identified by a black coloured carbon-rich carapace, which is thin and flattened. Preservation is poor, the carapace is often partially degraded to reveal the underlying external mould of the specimen.

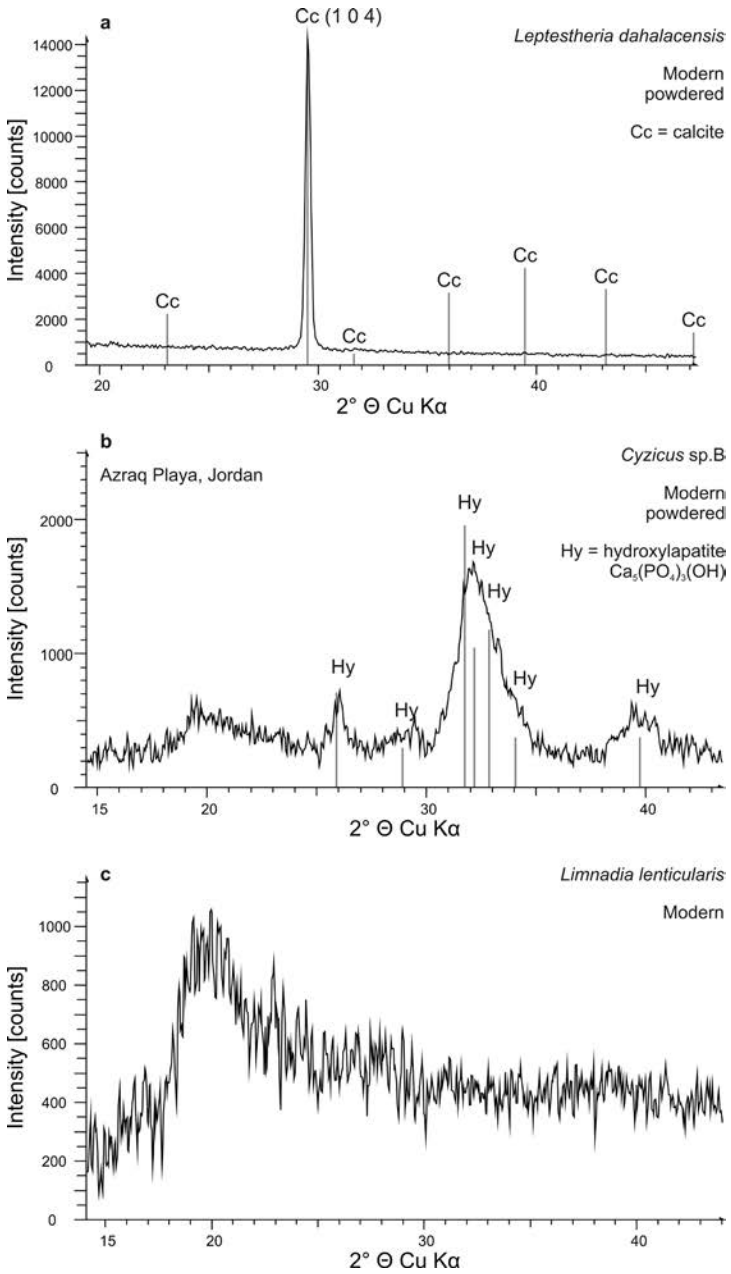

← **Fig. 3.7.** X-ray diffraction profiles for specimens belonging to each of the three extant families. (a) Leptestheriidae, (b) Cyzicidae, and (c) Limnadiidae. XRD-profiles (b) and (c) indicate the presence of amorphous material, represented by an elevated background in the profiles. *Leptestheria dahalacensis* biomineralizes with calcite; the profile shows a strong preferred orientation on (104) plane, owing to a planar crystal orientation assumed when the powdered sample was prepared with 2-propanol on the single crystal sample holder. The carapace of a cyzicid from the Azraq Playa, Jordan, yields calcium phosphates. *Limnadia lenticularis* does not biomineralize.

Type 3: Fluorapatite

An example of fluorapatite preservation is given in Fig. 3.9, where growth increments composed of fluorapatite are easily distinguished from the sediment because they are bright under the SEM using a back-scattered electron beam (Fig. 3.9b). Single fluorapatite crystallites are arranged in chords that are planar-oriented along thin barriers (arrows in Fig. 3.9c), which possibly correspond to the exterior sides of single growth increments (Figs. 3.9c; 3.10e). The interior parts of growth increments are softer and more susceptible to replacement by secondary minerals, such as silicates and iron sulphide framboids (box in Fig. 3.9b). This should not be confused with the input of detrital sediment between two carapace valves. In Fig. 3.9b, both valves are separated by a fissure (traced). Fractures indicate that recrystallization occurred soon after burial but before compaction.

Two sub-types can be distinguished by means of microstructure preservation. Type 3.1 involves exceptionally well preserved microstructures, whereas microstructures of the more common type 3.2 are obscured.

Type 3.1: Fluorapatite with excellent microstructural preservation

Type 3.1 preservation has been observed within Bed 2 of volcanic Lake Sihetun (Early Cretaceous, Sample 6). The mode of preservation in the sediments of Lake Sihetun differs between Bed 2 and Bed 3 according to the palaeoenvironment that

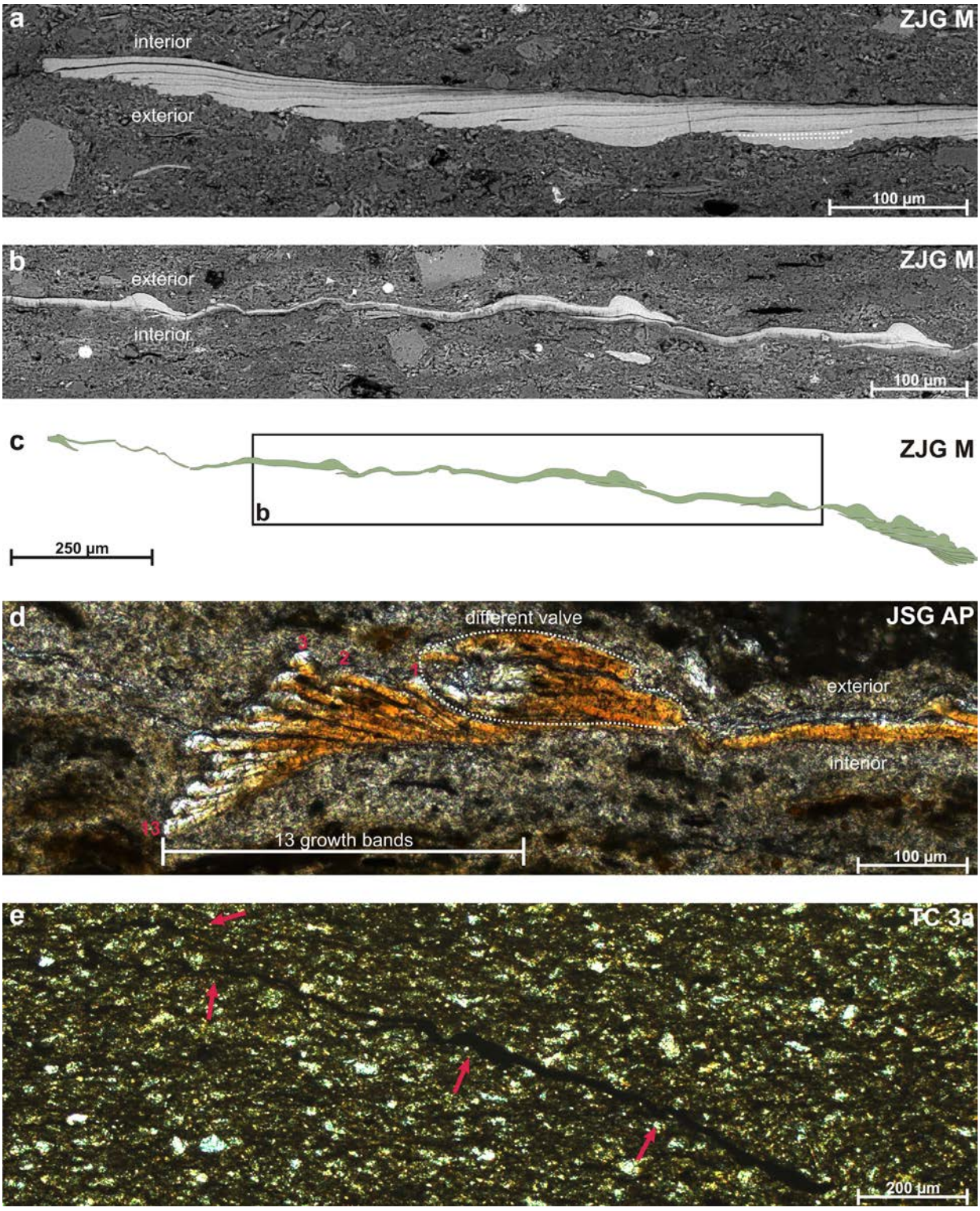

Fig. 3.8. Fossil carapaces in cross-section. Thin-sections from the Yixian Fm. (a-d), and the Tongchuan Fm. (e). (a, b) BSE images, (d, e) photographs taken under plane-polarized light. Carapace preservation (a) excellent, (b-d) good, and (e) poor. (a) Carapace margin (left) with overlap of growth increments (at most seven). Increment prolongations are thinning dorsally. Internal lamellae are discernable in part and two examples are traced. Here, they correspond to secondary ridges that are imprinted on top of the concentric ridges. (b) Three growth increments that are connected by only very short overlap. Single lamellae are not visible. (c, d) Several growth bands may remain entirely subjacent the older cuticle due to crowding of increments. Growth band counts should therefore be treated with care. (e) Microstructure preservation from most lakes examined usually appears welded so that growth increments are indiscernible in cross-section (compare Fig. 3.11).

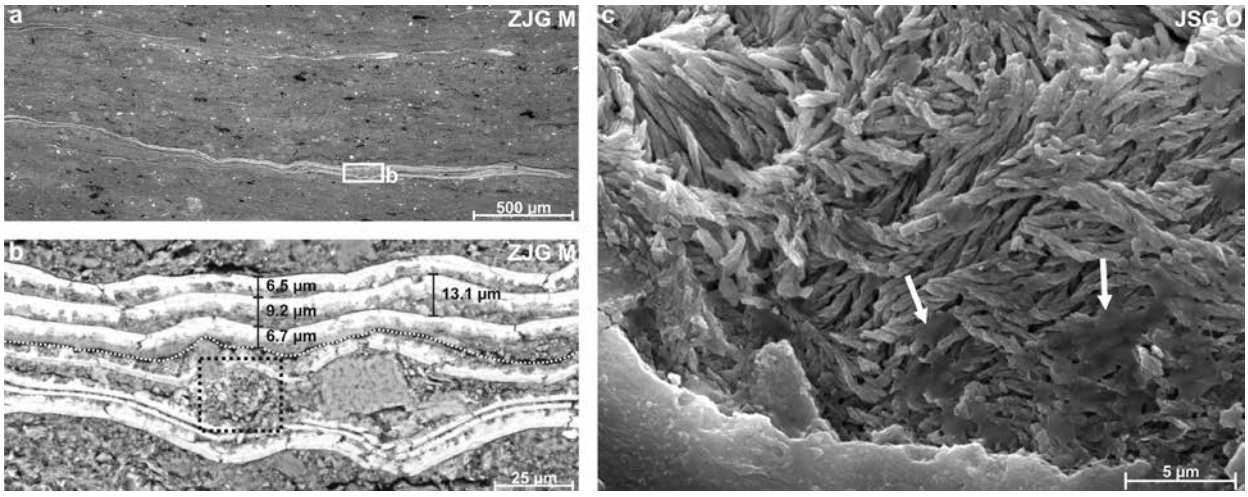

Fig. 3.9. Spinicaudatan preservation in the Early Cretaceous Yixian Formation. (a, b) BSE images, Bed 2, growth increments preserved (Type 2.1); (c) SEM micrograph, Bed 3, welded (Type 2.2). (a, b) Carapace valves were compacted to the same plane as the soft parts of the clam shrimp. Both valves are separated by a fissure (dotted line). Fossil growth increments are of similar scale as modern ones (compare with Fig. 3.6), but there is considerable variation in thickness even within the same increment. Three growth increments on the upper valve are opposed to five growth increments on the lower valve, most likely due to rotation of one valve relative to the other. Differential fossilization of clam-shrimp growth increments is well documented here, with a more compact exterior part and a softer interior part that is replaced by silicates, silica, and iron sulphide framboids (dotted box). (c) Fluorapatite crystals are arranged in nm-thick chords that are separated by horizontal planes (arrowed), which possibly correspond to the exterior surfaces of single growth increments.

prevailed during their deposition (Hethke et al., 2013a). Bed-2 clam shrimps (Figs. 3.8a-d, 3.9a, b) are generally very well preserved yielding growth increments as well as lamellae in cross-section (traced in Fig. 3.8a).

Pyrite framboids are often present marginal to carapaces in Bed 2, but they do not necessarily enhance preservation. Rather, their environmental implications, i.e. oxygen deficiency and raised alkalinity (Hethke et al., 2013b), explain the high degree of microstructural detail.

Wrinkling is not common within these specimens. Clam shrimps of facies C of the Middle-Late Jurassic Wangjiashan Fm. are preserved three-dimensionally and are therefore not affected (Fig. 3.10a-c), maintaining an incredible amount of detail with faint reticulations on the larval valve. Cyzicidae specimens from the Jurassic of England and Antarctica (Table 3.2) also exhibit 3D preservation.

Type 3.2: Fluorapatite with poor microstructural preservation

Type 3.2 preservation is marked by "welding" of growth increments (Fig. 3.11a, b). Carapace microstructure disappeared entirely during the process, leaving a homogeneous, single-layer appearance. An EMP measurement of a carapace in thin-section (Bed 3, Jianshangou Unit) confirms the presence of fluorapatite (Table 3.6). Inclusions of minerals other than fluorapatite are common; mostly quartz or clay minerals visible as dark spots in Fig. 3.11b. Ornamentation is commonly lost due to the delamination of the outermost ornamented layer (Fig. 3.10d, e), but ornaments occasionally remain intact in type-3.2 preservation, as the outermost layer is generally more resistant to decay. Valve thickness fluctuates heavily due to dissolution processes and fracturing (Fig. 3.11a). The carapaces tested are composed of fluorapatite with varying amounts of sulphur, sodium, iron, cerium, and other elements (Fig. 3.11d; Supplementary 3.1). Because of this profound alteration, type-3.2 clam shrimps are not suitable for stable isotope analyses, an approach which had previously been contemplated.

Wrinkling (Fig. 3.11c) is evident in clam shrimps of both analyzed Middle-Late Jurassic lakes and shells are usually compressed parallel to their commissural plane. Fresh carapaces initially remained elastic, but deformation subsequent to recrystallization led to microfracturing (Fig. 3.11a). Orr and Briggs (1999) attributed wrinkling observed in a specimen of the Cyzicidae to compaction and pronounced lateral convexity. Note that wrinkling is less common in Bed 3 of Lake Sihetun (Sample 6) than within the Middle-Late Jurassic lake deposits (Sample 5). Scottish Late Carboniferous specimens

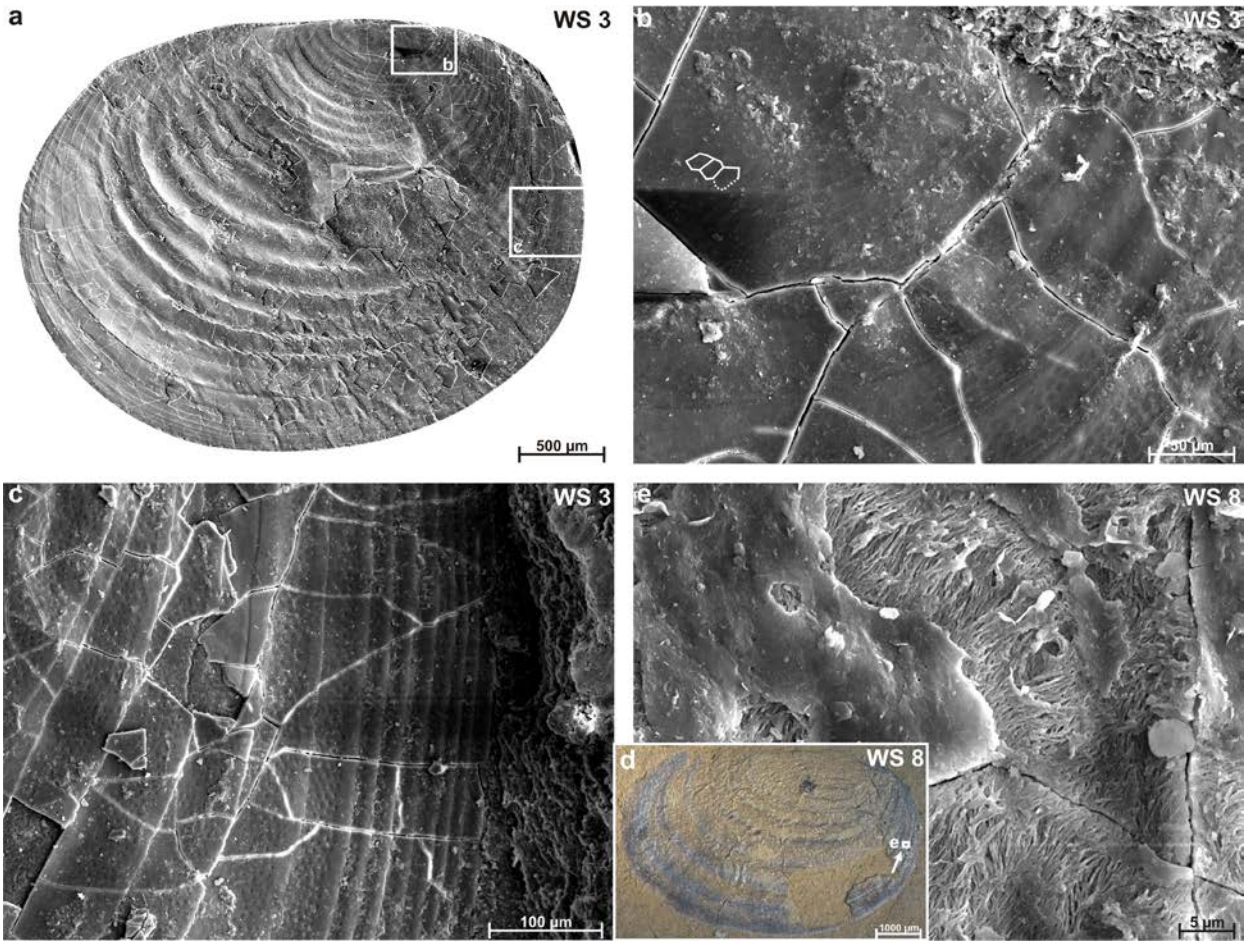

Fig. 3.10. Spinicaudatan preservation in the Middle Jurassic Wangjiashan Formation. All are SEM micrographs. (a-c) Right valve. Due to the close packing of fluorapatite crystals at the exterior side of growth increments (compare Fig. 3.9b), ornamentation such as fine reticulation near the umbo and anterior punctae is preserved. (d, e) Right valve. The outer ornamented layer is occasionally delaminated, meaning that one of the most diagnostic taxonomic characters is sometimes missing. Chord-like crystal aggregates of nm-scale are revealed underneath.

of *Euestheria* and *Estheria tenella* both exhibit type 3.2 preservation (Table 3.2). The carapaces are flattened and wrinkled and there is a variation in the concentration of fluorapatite across the carapace, which may indicate the incorporation of other minerals during diagenesis.

Type 4: Mixed composition of fluorapatite and dolomite

Laxitextella (Late Triassic, Sample 4.2) is composed of fluorapatite and dolomite (Fig. 3.12c). EDS measurements of the surface are purer than those of cross-sections (see supplementary data), presumably since microcrystals are more densely packed at the exterior side. Wrinkling has not been detected for the type 3 specimen.

Because the analysed specimen of *Laxitextella* is from a museum collection, it was not possible to check for microstructure preservation. However, its three-dimensionality hints at superb preservation of consecutive growth increments. In addition, different growth increments have been observed in *Laxitextella* from the Polish part of the Germanic Basin (Olempska, 2004). Though the mineralogy was not examined by Olempska (2004), brittleness and carapace appearance indicate a similar mineralogy as its Bavarian counterpart.

A specimen of *Estheria* from the Late Carboniferous (Table 3.2) is composed of ferroan dolomite, with euhedral pyrite crystals adhering to the surface of the specimen and patches that appear recrystallised. No fluorapatite content has been detected by EDS analysis. The specimen is flattened and wrinkled, with poor microstructural preservation.

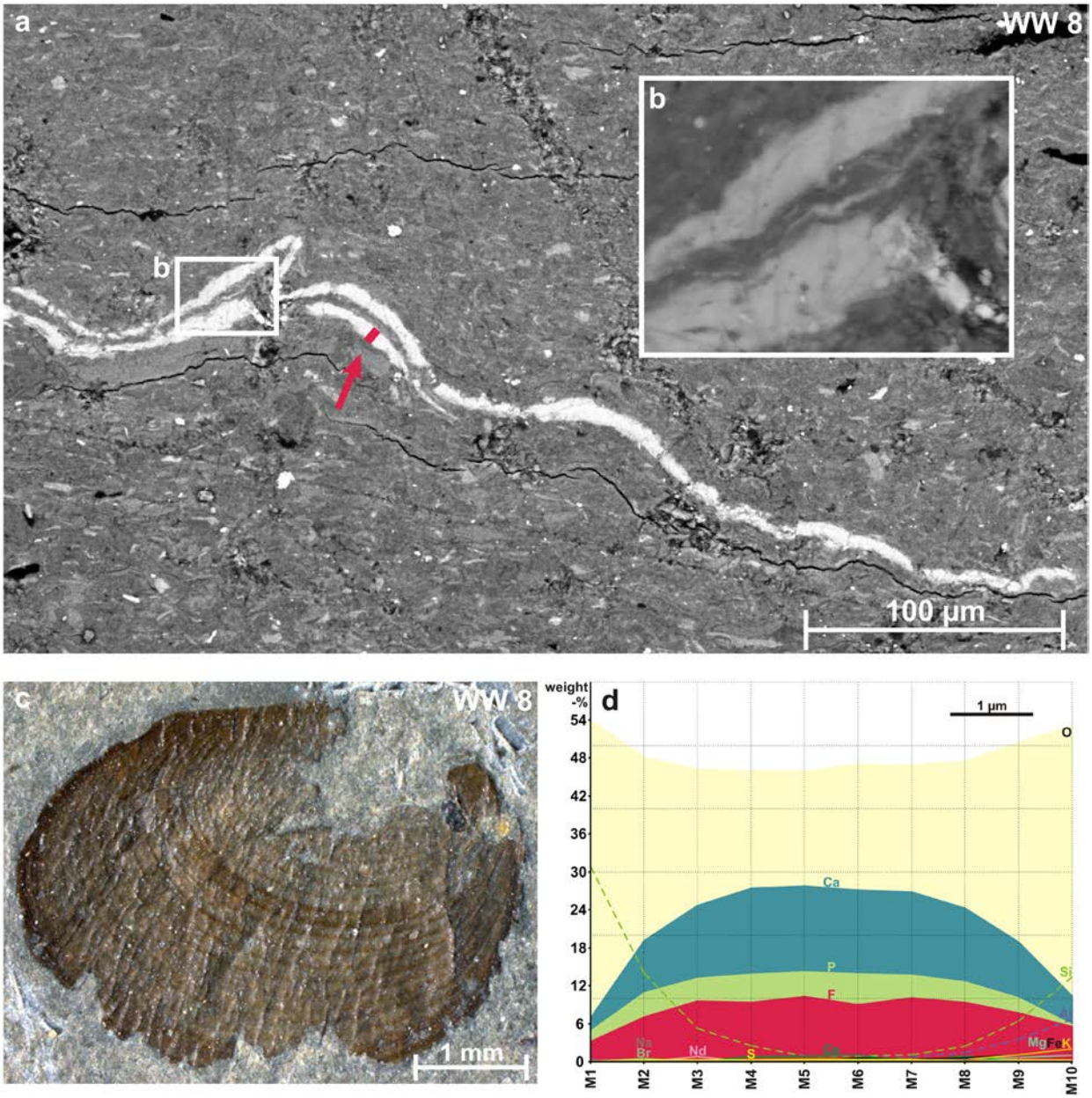

Fig. 3.11. *Triglypta* from the Middle Jurassic of China. (a, b) Profound recrystallization and dissolution have destroyed all growth increments. Clay minerals and silica cement are infilling the voids. (c) Wrinkling is common in the Middle Jurassic material. (d) The EDS transect, arrowed in (a), yields a uniform apatitic composition. The presence of Si and Al at the edges of the carapace are explained by the electron beam picking up a mixed signal of carapace and matrix minerals. The raw data are listed in Supplementary 3.3.

Discussion

Carapace microstructure

Comparison of modern and ancient carapace microstructure

Consecutive growth increments within a carapace have often been observed in fossil spinicaudatans (Kozur 1982, tab. 11; Olempska 2004, figs. 5, 6). According to Rieder et al. (1984), exocuticle lamellae reach their maximum thickness at the ventral carapace margin. In combination with the crowding of growth increments at the carapace margin, this leads to a preservation gradient that ranges from commonly poor near the umbo to good at the carapace margin.

Reliability of growth line counts

The number of growth lines is commonly used as a diagnostic character of taxa, but there are shortcomings that might affect such counts severely. Crowding of growth increments at the carapace

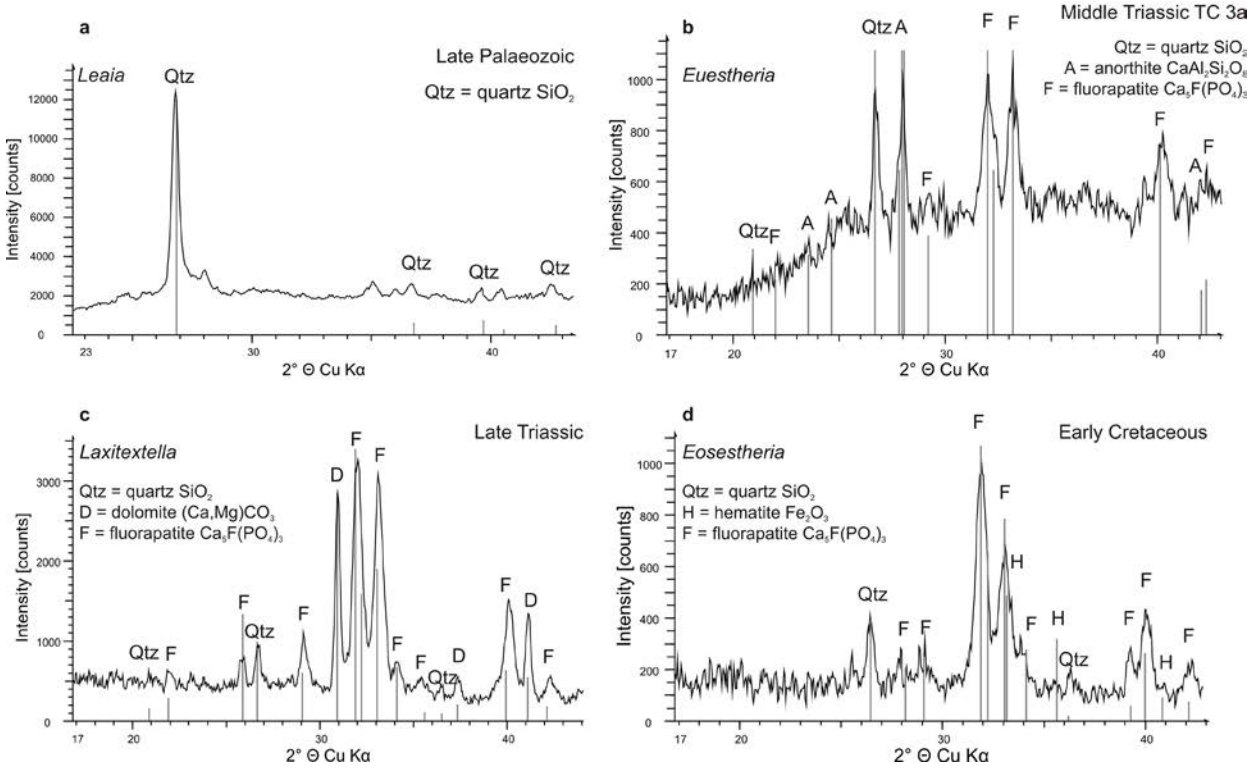

Fig. 3.12. X-ray diffraction profiles for selected environmental settings: Lake environment (Sample 1.2), lacustrine foreshore (sample 3), increased salinities (Sample 4.2), and oxygen deficient volcanic lake (sample 6). (a) *Leaia* is preserved as a silicified dark stain. Carapaces of all other fossil families investigated are primarily made up of fluorapatite, but secondary minerals such as quartz or dolomite are common. They often carry an environmental signal. (b) *Euestheria* from the Middle Triassic of Shaanxi is made up of fluorapatite, feldspar, and quartz. The elevated background in the XRD pattern from 20° 2θ on, only present in this fossil sample, accounts for amorphous material within the carapace. The sediment is marked by a high organic content, which may be responsible for the elevated background in the observed pattern. An impregnation with organics may account for the dark colouring of the carapace (compare with Fig. 3.8e). (c) The carapace of *Laxitextella* from Northern Bavaria, Germany, is made up of fluorapatite, dolomite, and minor amounts of quartz. The presence of dolomite is a purely sedimentary signal (marl). (d) *Eosestheria* from the Yixian Formation of western Liaoning comprises fluorapatite, quartz and traces of iron oxide minerals that stain the carapace distinctly red (compare with Fig. 3.8d).

margin may be problematic (Fig. 3.8). New growth increments may be smaller than their predecessors; for example, three growth increments remained beneath the older cuticle in the individual of Fig. 3.8c. In Fig. 3.8d there are actually five growth increments that would not be visible in lateral aspect.

Apart from the ubiquitous ontogenetic bias that leads to different growth line counts and splitting of taxa, sexual dimorphism and environmental forcing have a significant effect on carapace development. Males of *Limnadia grobbeni*, for instance, have ten growth lines less than females do (Tasch, 1969). A high amount of precipitation can result in higher food supplies and larger, more permanent pools, allowing individuals of *Cyzicus gynecia* (formerly *Caenestheriella gynecia*) to grow distinctly larger (as long as 10.6 mm as opposed to 7.3 mm in dryer years), yielding higher numbers of growth lines (Mattox, 1950). To conclude, the number of growth lines is not a diagnostic character of fossil taxa per se.

Carapace mineralogy – modern and fossil

Modern

According to literature, modern spinicaudatans are either "somewhat calcified" or unmineralized (e.g., Vannier et al., 2003). This may prove to be only part of the story. The present study shows that a set of biominerals is involved and that they seem to be group-specific (Fig. 3.7): Leptestheriidae build in calcite, Limnadiidae do not biomineralize, and Cyzicidae build in calcium phosphate biominerals and possibly calcite. XRD-profiles of powdered samples of *Caenestheriella donaciformis* (Cyzicidae) suggest a mix of calcite and calcium phosphates, while a calcite signal has not been picked up for a second cyzicid specimen from the Azraq Playa. EDS-spectra of

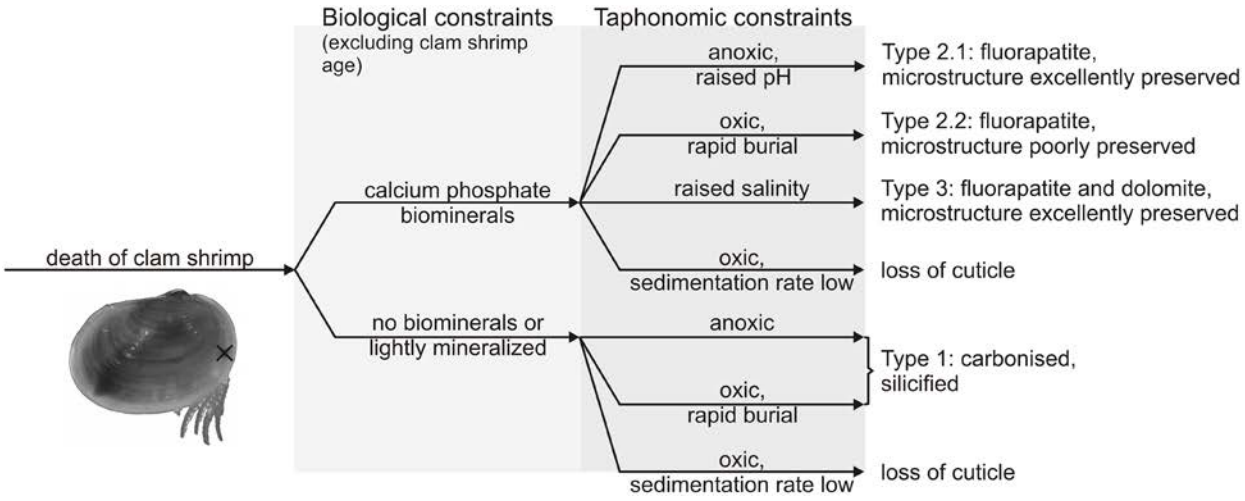

Fig. 3.13. Taphonomic pathway for carapace preservation. The driving factors are presence of biominerals, redox state, alkalinity, and sedimentation rate.

Limnadia resemble those of *Leptestheria*, signalling a small amount of Ca, its weight-% being lower than that of Cl, though (Table 3.3). However, calcite has not been picked up for *Limnadia* (Fig. 3.7c) in the XRD-profiles. There are two possible explanations: (1) the specimen did not biomineralize or (2) the carapace is only lightly mineralized and the amount of biominerals in the sample was too small for XRD to pick up. *Limnadia* was not powdered for XRD.

The results of this study partly diverge from those presented by Stigall et al. (2008), who realized that fossil spinicaudatans were primarily preserved in calcium phosphates, in line with our results. They deduced a calcium phosphate composition for all three modern families using EDS and consequently argued that the presence of calcium phosphates were likely a symplesiomorphy of the Spinicaudata. This would prove true, if they were present across the clade, but the data presented herein confirms calcium phosphates only for the Cyzicidae.

Evidently, a larger-scale study is needed to resolve this controversy with the data for modern specimens presented herein. Only once it is clear whether the lack of evidence for calcium phosphates in *Leptestheria* and *Limnadia* in this study is primary or secondary, can evolutionary questions be addressed. Environmental effects that impede biomineralization with calcium phosphates should also be considered.

Fossil

Fossil minerals reported for clam shrimps are calcium phosphates (Stigall et al., 2008), calcite (Kobayashi, 1954; Ziegler, 1998; Olempska, 2004), silica (Stigall et al., 2008), organic carbon residues, and phyllosilicates infilling appendages (Orr and Briggs, 1999). Until Stigall et al. (2008), statements about carapace mineralogy had been ambiguous. For example, Late Triassic spinicaudatans are allegedly "weakly calcified ("chitinous") of light amber to brownish-black colour" (Olempska, 2004), a statement that had probably been biased by previous reports, as it seems to mix fossil and modern evidence on carapace mineralogy. Admittedly, the main objective of that particular study was systematics and the description of the shell microstructure. Early Jurassic cyzicid carapaces from Utah are supposed to have been replaced by carbonates (Lucas and Milner, 2006). However, a closer inspection of their figures suggests complete dissolution of the carapaces along with or prior to carbonate precipitation, so this cannot be representative of carapace mineralogy either.

XRD-analyses of the present study do not support calcite in fossil valves, but indicate a mixed composition of dolomite and fluorapatite (type 4). The presence of dolomite seems to be associated with a carbonate-yielding lithology that provided chemicals for dolomite crystallization within the interstitial spaces of the existent fluorapatite framework, which formed in the course of fossilization of a carapace containing calcium phosphates. Stigall et al. (2008) pointed out that microbial mats enhanced silicification in spinicaudatan carapaces, leading to detailed preservation of the micro-ornamentation that might otherwise have been lost. Additionally, they mentioned that phosphatic mineralization of the fossil material was commonly coarse, obscuring microstructural details. This does not agree with the findings of this study. Though beneficial, silicifica-

tion is not a prerequisite for retaining a high degree of detail in outer moulds, as observed in many specimens from Mesozoic lakes of China. In summary, the following fossil mineralogies can be verified: fluorapatite (mainly associated with Cyzicidae, signalling biomineralization), dolomite (environmental signal), silica (Cyzicidae, Estheriellidae, Leaiidae; environmental signal), organic carbon residues (Leaiidae, Limnadiidae, some Cyzicidae; biological signal of a lack of biominerals or lightly mineralized carapaces), phyllosilicates (according to Orr and Briggs, 1999; biological signal of a lack of biominerals or lightly mineralized cuticle), and traces of iron oxides (environmental signal) that account for a distinct red-brown colouring of the carapace (Lake Sihetun, Bed 2).

Environmentally controlled diagenetic modifications

The mode of carapace preservation is mostly determined by environmental factors. In general, the cuticles of arthropods consist of chitin linked by a catechol moiety to protein, often strengthened by cross-linking, "sclerotization" (Briggs, 1999). Therefore, the usual arthropod cuticle should be considered organic, but it can act as a framework for biomineralization (Dalingwater and Mutvei, 1990). It is vital to consider the preservation potential of biopolymers, which are susceptible to hydrolysis and oxidation to different degrees. Nucleic acids as well as proteins decay rapidly and are commonly gone in fossils older than 100,000 years. Polysaccharides such as chitin, that form structural tissues through cross-linking with other molecules, may be preserved for several million years (Briggs, 1999). The earliest known traces of chitin are from the Oligocene (Stankiewicz et al., 1997).

The sedimentary context imposes a major control on cuticle preservation (Briggs, 1999). Briggs et al. (1998) noted that the degree of chitin preservation varied in Pliocene lake sediments from good in anoxic marl near the lake centre to less so in proximal sediments deposited under oxygenated conditions. According to this, the major control on preservation is environment, not age (Briggs, 1999). Chitin degrades much more readily in peat horizons than in silty lithologies, suggesting that contrasts in pH can also play a major role. Briggs (1999) assumed acidic environments to enhance chitin degradation through acidic hydrolysis.

Therefore, with raised alkalinity and oxygen deficiency at the sediment-water interface during Phase 2 of Lake Sihetun (= Bed 2, Sample 6), environments were favourable for chitin preservation (type 3.1; Hethke et al., 2013a, b). And in fact, carapace microstructure was conserved by recrystallization of calcium phosphate biominerals to fluorapatite during fossilization, tracing microstructural features, such as successive growth increments (Fig. 3.9a, b; fig. 13a-c in Hethke et al., 2013a), resulting in the absence of wrinkling.

While external ornamentation is well preserved, carapace microstructure is lost in Bed 3 of Lake Sihetun and in most other Mesozoic specimens that lived in well-oxygenated lake environments (type 3.2). The layered cuticle was replaced by a homogeneous amalgamation of fluorapatite, silicates, and quartz (Fig. 3.11b), rendering a less pure fluorapatite signal than that of type 3.1 preservation. As wrinkling is common in Middle to Late Jurassic lakes (Sample 5), environments must have been somewhat less alkaline, facilitating rapid degradation of chitin (Fig. 3.11). The fact that wrinkling is less common in Bed 3 of Lake Sihetun (Sample 6) might be a result of abiotic components that are intermediate between the Jurassic lakes and Bed 2 of the same lake.

Early diagenetic intra-carapace carbonate precipitation (type 4) stabilized the growth increments of clam shrimps from the Germanic Basin (Fig. 3.12c; for a picture see plate 11 of Kozur, 1982). Transverse sections reveal excellent preservation of the carapace microstructure of *Laxitextella* specimens from Poland (Olempska, 2004). In addition, the presence of sulphur in *Laxitextella* (specimen Coburg 14612; Supplementary 3.1) points to the occurrence of gypsum, either as a primary-evaporitic or as a secondary product of, for instance, pyrite.

Another form of preservation occurs in brown sideritic concretions from the Carboniferous (Vannier et al., 2003), each containing a single carapace. Carapaces and soft parts show three-dimensional preservation, which was facilitated by early mineralization and the rapid formation of concretions.

Organic carbon residues (type 2) may be explained by only lightly mineralized carapaces or even by an *a priori* absence of biomineralization. Decay experiments on clam shrimps (Orr et al., 2008) show that cuticle preservation is a function of its recalcitrance as well as the time spent at the lake floor before burial. This last factor, determined by sedimentation rate, is a crucial variable for carapace preservation, especially in oxic environments (Fig. 3.13). The presence of biominerals may add

resilience to the carapace, gaining an advantage over only lightly or non-mineralized taxa.

Implications for spinicaudatan systematics

We propose that the presence of calcium phosphate biominerals in clam-shrimp carapaces is a prerequisite for fluorapatite preservation. Consequently, a lack of fluorapatite in fossil carapaces may be indicative of three scenarios: (1) The original carapace yielded a comparatively low quantity of calcium phosphate biominerals that became rapidly dissolved. (This may be either taxon-specific or a result of adverse environmental conditions during the crustacean's life that impede the ability to biomineralize calcium phosphates.) (2) The diagenetic environment was not suitable for fluorapatite recrystallization and led to the dissolution of all biominerals. (3) The animal did not biomineralize in the first place. Scenarios 1 and 2 are based on the dissolution of biominerals, but there would be multiple consequences for family-rank systematics, if scenario 3 was correct and the mode of biomineralization was taxon-specific. For example, all Carboniferous Leaiidae investigated here are partly carbonised, silicified or preserved as external moulds, implying the presence of only lightly biomineralized carapaces or even the absence of biominerals. So, as long as fluorapatite is not reported from leaiid specimens, we may assume that this family did not biomineralize with calcium phosphates. On the basis that the presence of fluorapatite in fossil spinicaudatans is an immediate consequence of biomineralization with calcium phosphates, the following hypotheses can be proposed:

- A close phylogenetic relationship of Eosestheriidae, Polygraptidae, and Cyzicidae (*sensu stricto*) can be assumed, as the majority of specimens tested are composed of fluorapatite (Table 3.2). Members of the families studied herein have been allocated to Cyzicidae (*sensu lato*) through a taxonomic discussion in section 5.2.

- A lack of biominerals is an ancestral trait, displayed by Leaiidae†. Due to the disagreement with the data provided by Stigall et al. (2008), Limnadiidae cannot entirely be placed into this category, despite the absence of biominerals in all limnadiids checked herein (Fig. 3.7c; Table 3.5; Supplementary 3.1).

- The presence of biominerals is a derived trait.

Several taxonomic classification schemes are in use for fossil spinicaudatans, which are based on the preferences of authors regarding particular diagnostic features and working areas (e.g., Raymond, 1946; Kobayashi, 1954, 1972; Novojilov, 1960; Defretin-Lefranc, 1965; Tasch, 1969, 1987; Zhang et al., 1976; Holub and Kozur, 1981; Kozur, 1982). No consistent (super-)family-rank taxon names exist (Table 3.1). As a result, workers are forced to tentatively assign family names by adding question marks (e.g., Vannier et al., 2003).

An up-to-date classification scheme is needed that includes Recent material, which by itself is comparatively well documented (Fig. 3.4). It should build upon Tasch (1969), because the Treatise of Invertebrate Paleontology is widely distributed and usually the first reference for researchers. Taphonomic studies are a means of identifying whether a specimen biomineralized, a valuable biological trait that might be important for family-rank considerations.

Conclusions

- Modern Cyzicidae biomineralize with calcium phosphates and possibly calcite, Leptestheriidae build in calcite, and Limnadiidae do not biomineralize. Fossil minerals include fluorapatite, dolomite, quartz, organic carbon residues, silicates, and traces of iron oxides. The presence of fluorapatite is a consequence of calcium phosphate biomineralization and secondary replacement by minerals other than fluorapatite occurs preferentially on the softer, less mineralized interior sides of consecutive growth increments.
- A high degree of biomineralization renders the carapace more recalcitrant than only lightly or non-mineralized taxa, hinting at a possible underrepresentation of the latter taxa within the fossil record.
- The presence of specific fossil minerals depends on (1) the mode of biomineralization and (2) environmental parameters. Carapace microstructure preservation is enhanced in lakes characterized by oxygen deficiency and raised alkalinities.
- Biominerals seem to be diagnostic for modern families. As a result, the identification of fossil carapace mineralogies may indicate whether specimens biomineralized. Carboniferous Limnadiidae and Leaiidae are preserved as organic carbon residues, as are some Cyzicidae. Conversely, Mesozoic "cyzicid-related" families are all composed of fluorapatite. The evidence for the modern Limnadiidae is ambiguous and needs further investigation. The oldest evidence of calcium phosphate biominerals in cyzicid carapaces is from the Late Carboniferous.

Chapter 4: Taxonomic revision of Early Cretaceous clam shrimps from the Yixian Formation of western Liaoning

Chapter 4 is a joint project of the following authors:

Manja Hethke[1], Franz T. Fürsich[1], Baoyu Jiang[2]
[1]*GeoZentrum Nordbayern, FG Paläoumwelt, Germany*
[2]*School of Earth Sciences and Engineering, Nanjing University, China*

Introduction

The discovery of feathered dinosaurs and early birds (e.g., Xu et al., 1999a, b, 2001; Zhou et al., 2003; Zhou, 2006) has sparked a worldwide interest in the Jehol Biota, an early Cretaceous terrestrial biota of lakes and their adjacent forest environments (Zhou, 2006). Together they form one of the most extensively studied Early Cretaceous terrestrial ecosystems. Clam shrimps are among the most abundant preserved faunal elements of this ecosystem, but compared to their high abundance, studies focussing on their biodiversity or palaeoecology are rare (e.g., Fürsich et al., 2007). This is a direct consequence of the poor state of the clam-shrimp taxonomy (Table 3.1).

Three developmental stages are reported for the Jehol Biota (Chen, 1999b; Chen et al., 2007), each of which are characterized by distinct clam-shrimp faunas (Fig. 4.1): the *Nestoria-Keratestheria* fauna (early Jehol Biota; i.a., Dabeigou Formation), the *Eosestheria* fauna (middle Jehol Biota; Dadianzi Formation, Yixian Formation, Jiufotang Formation), and the widespread *Yanjiestheria* fauna (late Jehol Biota). Chen et al. (2007) mentioned eight clam-shrimp genera for the *Nestoria-Keratestheria* fauna, 20 genera for the *Eosestheria* fauna, and more than 100 species in 16 genera for the *Yanjiestheria* fauna, but acknowledged that many of the 20 genera proposed for the *Eosestheria* fauna were synonyms of either *Eosestheria* or *Diestheria*. Nevertheless, this richness of taxa led authors to refer to a major evolutionary radiation of clam shrimps during late Mesozoic times (Chen et al., 2007; Li et al., 2007). One diversification event was in fact reported for the commencement of the Jianshangou "Beds" of the Yixian Formation (Fig. 2.2), where species of *Eosestheria* and *Diestheria* evolved that thrived until the end of the deposition of the Jiufotang Formation (Li et al., 2007). Li et al. (2007) suggested a total of four families and nine genera in the Jianshangou "Beds" of the Yixian Formation. These interpretations of the clam-shrimp fossil record are given without corrections for sampling biases (e.g., Foote, 2003). Furthermore, resolving true patterns of evolutionary change in clam shrimps requires a more detailed documentation of origination and extinction events, which, at present, is hampered by a very high number of artificial taxa that may even exceed the number of valid taxa. We predict that the quality of the clam-shrimp fossil record of the Jehol Biota is influenced by extensive splitting of taxa, which requires a thorough taxonomic revision at species level.

Confronted with this high number of taxa, it is useful to focus on a geographically constrained subset. Ten species in four genera have been described by Chen (1999a) for western Liaoning (Fig. 1.1; Table 4.4). Descriptions are mostly qualitative and a major shortcoming in the descriptions is that ontogenetic shape variation and associated variation in ornamentation has not been taken into account. Also, even though geometric size has been reported, allometry has never been studied within these clam shrimps.

In general, fossil spinicaudatan taxonomy has suffered from the presence of different schools that assign different weight to different diagnostic characters. This can mainly be summarized in a "battle" between ornamentation and shape (Martens, 1985). Both of which have their benefits and shortcomings. Taxonomists relying on ornamentation often failed to identify ontogenetic shape variation and associated ornamentational variation, which led to splitting of taxa (e.g., Zhang et al., 1976). In contrast, relying on linear measurements led to lumping (Tasch, 1969). On top of that, genus descriptions are often imprecise. A succinct example of this is the description of *Cyzicus* (*Euestheria*): "Carapace generally ovate but with wide variation in shape, size, and ornamentation" (Tasch, 1969). Some processes that lead to lumping cannot be dealt with and refer to the known differences between biological and palaeontological species, the identification of the latter relying mostly on morphological traits. For example, many modern species require males

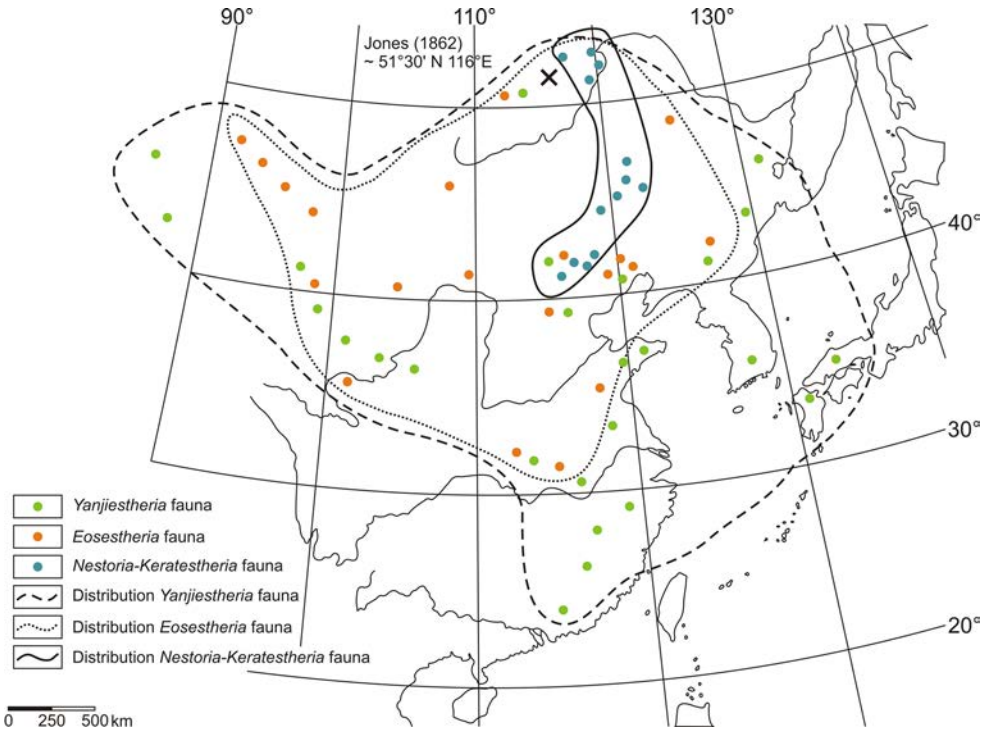

← **Fig. 4.1.** Geographic distribution of the Late Jurassic? to Early Cretaceous clam-shrimp faunas of eastern Asia. Modified after Chen et al. (2007). The *Eosestheria* fauna occupied Transbaikalia, south Mongolia, as well as north China. The cross marks the outcrop position of the syntype series of *Eosestheria middendorfii* collected from Transbaikalia, Russia. (Jones, 1862).

Table 4.1. Terminology based on Raymond (1946), Tasch (1969), and Li and Batten (2005). Some terms have been modified to find a consensus.

Term	Description
General carapace features	
Concentric striation (Raymond, 1946)	Narrow concentric depression, usually marking growth lines
Concentric ridge (Raymond, 1946)	Ridges parallel to growth lines (raised and linear; broad and coarse; low, narrow, and rounded)
Radial costae (Raymond, 1946; Tasch, 1969) = carapace costae in Tasch (1969)	Fine to coarse continuous radial ridges, indicative of the family Estheriellidae (not needed for clam shrimps described in this study)
Growth band	Space between two growth lines (= intervale in Raymond (1946) and Tasch (1969))
Dorsal margin	Junction of two valves
Ornamentational features	
Punctae/nodules	Punctae on carapaces appear as nodules on external moulds
Radial lirae (e.g., Li and Batten, 2005)	= radial markings in Raymond (1946)
Radial striae	Grooves
Reticulation	Polygonal ornamentation on growth bands
Serrated margins	Lower margins of growth bands with notches
Wrinkles	Concentric creases, usually on the lower part of a growth band

for taxonomic identification, and since soft parts are usually not preserved, lumping of fossil taxa can be expected (Frank, 1988).

In the case of eastern Asia, fossil clam-shrimp taxonomy has suffered from extensive splitting over the past decades. Due to the omnipresence of clam shrimps within the Mesozoic continental deposits of eastern Asia, this taxonomic and methodological revision is crucial for further evolutionary, biostratigraphic, biogeographic, and palaeoecological studies.

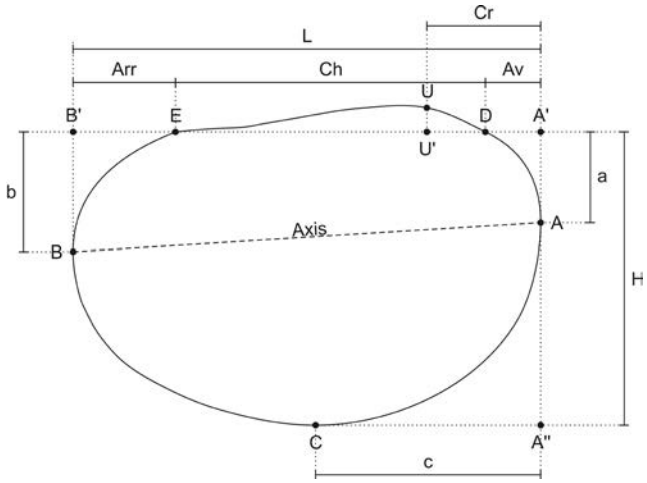

← **Fig. 4.2.** Nine linear measurements. Modified after Defretin-Lefranc (1965). Explanations in the style of Tasch (1987; with small change for U): A – most anterior point of the valve, B – most posterior point of the valve, C – most ventral point of the valve, D – anterior extremity of the dorsal margin, E – posterior extremity of the dorsal margin, U – midpoint of the larval valve (located on the umbo, but not necessarily the midpoint of the umbo). a – vertical distance of A to A', b – vertical distance of B to B', c – horizontal distance of C to A", Arr – horizontal distance of E to B', Av – horizontal distance of D to A', Ch – length of the dorsal margin, Cr – horizontal distance of U' to A', L – valve length, H – valve height. The axis marks the distance between A and B, which was measured in situ during field campaigns (Chapter 7).

Terminology

Fig. 3.1 illustrates some of the clam shrimp terminology listed in Table 4.1. The terminology used herein is a combination of Raymond (1946), Tasch (1969), and Li and Batten (2004a, b; 2005), who each employed different schemes. The most important difference concerns the usage of the term lirae. To Raymond (1946), who introduced the term for clam shrimps, lirae are applied to both, concentric and radial, linear ridges. In his species diagnoses, the term is mostly applied to denote the number of concentric ridges of a carapace (approximating the number of visible growth lines in this study). To Tasch (1969), radial lirae are synonymous with carapace costae. He kept the term "carapace lirae" to denote a type of concentric ridge, but never used the term in any of his generic diagnoses. Except perhaps for one ambiguous species diagnosis in Raymond (1946), the term lirae does not stand for radial ornamentation on the growth bands. In contrast, to Li and Batten (2005) radial lirae refer to radial markings on growth bands. As they have published a number of recent taxonomic works on Chinese clam shrimps, I prefer to follow their definition of the term.

Linear measurements of the carapace (Fig. 4.2) are adopted from Defretin-Lefranc (1965) and Tasch (1987), who established a total of nine variables. It should normally suffice to provide linear measurements of a type specimen in the diagnosis of a species. The conversion of numbers into terms seems to be a complication. But as subjective statements such as "carapace of moderate size" are common practise, there is virtue in the introduction of ratio-based standardized terms as proposed by Goretzki (2003). However, some terms of Goretzki (2003) had to be renamed to more commonly used expressions and some ranges and ratios were adjusted to fit a wider range of clam-shrimp specimens (Table 4.2). For example, the original carapace size groups of Goretzki (2003) did not grasp the full range of carapace sizes, as all of the Cretaceous material studied herein would fall into one single category ("extremely big" at L > 5.5 mm). Furthermore, the size of the larval valve of fossil carapaces is a good guess at best and omitted herein. His subdivision for the position of the umbo (changed to the more precise position of the larval valve) was such that a great majority of clam shrimps would fall into the same category. Therefore, it has also been slightly altered.

Shape versus ornamentation: diagnostic features

Modern systematics are based on soft parts and molecular markers (e.g., Daday de Deés, 1915; Hoeh et al., 2006; Schwentner et al., 2009). Diagnostic criteria for fossil taxa vary with worker. It essentially comes down to shape versus ornamentation (Table 4.3). The various classification schemes in use (Table 3.1) are most likely an immediate result of the different weight workers place on different diagnostic features. The shape of the carapace is subjected to natural variability, ontogenetic shape variation, and deformation, more so than ornamentation, which is unfortunately often not preserved. Type specimens should adequately reflect both, shape and ornamentation, though.

Methods

This chapter is primarily concerned with the taxonomic revision of the ten species described from the Yixian Formation of western Liaoning by Chen (1999a; Table 4.4). Specimens described by Chen

Table. 4.2. Descriptive terms for clam-shrimp carapaces, mostly ratio-based. Modified after Goretzki (2003) and discussed with Frank Scholze, Freiberg.

Feature	Ranges	Descriptive term
Carapace size (*L*)	< 1mm	extremely small
	1-2.5 mm	very small
	2.5-5 mm	small
	5-10 mm	moderate
	10-15 mm	large
	15-20 mm	very large
	> 20 mm	extremely large
Carapace shape (*H*/*L*) of specimens with curved margins	< 0.6	elongate
	0.6-0.75	ovate
	> 0.75	subcircular
Dorsal margin relative size (*Ch*/*L*)	< 0.5	very short
	0.5-0.65	short
	0.65-0.8	long
	> 0.8	very long
Intensity of **curvature** of the **dorsal, anterior, posterior, and ventral margins**		straight
		slightly curved
		curved
Position of **A** (*a*/*H*); Position of **B** (*b*/*H*)	0	dorsal
	0-0.25	dorsal-median
	0.25-0.5	median-dorsal
	0.5	median
	0.5-0.75	median-ventral
	0.75-1	ventral-median
	1	ventral
Position of **C** (*c*/*L*)	0	anterior
	0-0.25	anterior-median
	0.25-0.5	median-anterior
	0.5	median
	0.5-0.75	median-posterior
	0.75-1	posterior-median
	1	posterior
Position of **the larval valve** (*Cr*/*L*)	0-0.25	anterior
	0.25-0.5	submedian
	~ 0.5	median
Growth-line density (growth lines per mm)	< 1-4	wide
	5-7	separate
	8-10	close
	11-15	very close
	16-20	extremely close

(1999a) were chosen over those presented in Wang (1987), who reported a much higher number of taxa from western Liaoning, many of them new. Chen (1999a) discussed some of these in his paper. In ad-

Table 4.3. Diagnostic characters for clam-shrimp taxa as used by selected authors.

Author	Diagnostic characters of fossil taxa
Daday de Deés (1915) Modern clam shrimps	Strong focus on soft parts. **Advantage:** Most likely to capture the true number of biological species. **Shortcoming:** Makes it difficult to correlate modern taxa with fossil taxa.
Kobayashi and Kusumi (1953)	Placed a high value on ornamentation and distinguished new formae and varieties for *Estherites middendorfii* (instead of new species). Since the ornamentation of the formae and varieties was invariable to them, comparison was made through outline, size, and the number of growth lines. **Advantage:** Ornamentation considered before carapace form. **Shortcoming:** Ornamentation not properly quantified.
Tasch (1969, 1987)	Sculpture, carapace shape (ovate, subovate, elliptical, subcircular, etc.), dorsal margin (straight, arched, etc.), umbo placement, number of growth bands (often marked as variable), spacing of growth bands, ornamentation on growth bands (not very differentiated), a set of measurements and ratios analogous to Fig. 4.2. **Advantage:** Circum-descriptive **Shortcoming:** Genus descriptions occasionally too general. Set of measurements not statistically evaluated.
Zhang et al. (1976); Chen (1999a)	Focus on ornamentation. **Advantage:** Ornamentation is species-diagnostic. **Shortcoming:** Misinterpretation of ontogenetic shape variation and associated variation in ornamentation, which led to splitting.
Goretzki (2003)	Focus on size and shape. **Advantage:** Use of more objective statistical methods. A standardized scheme was proposed for formerly subjective descriptions. **Shortcoming:** Landmarks mostly geometrically homologous, instead of biologically homologous. Ornamentation not adequately considered, mainly because materials were mostly poorly preserved. Some species were set apart to avoid a stratigraphical range that is too wide!

dition to type specimens figured by Chen (1999a), the syntype series of *[Estheria] middendorfii* described by Jones (1862) as well as the type species of *Eosestheria*, *E. fuxinensis*, (Zhang et al., 1976) were considered herein. The synonymy list of *Eosestheria middendorfii* is expected to get longer, as more and more holotypes of Zhang et al. (1976) and Wang (1987) are analysed. Most of the type material was investigated at the Nanjing Institute of Geology and Palaeontology, Chinese Academy of Sciences (NIGPAS). The syntype series of Jones (1862) is housed in the Natural History Museum (NHM) and was made available through virtual loan.

Criteria for synonymization rely on methods that are based on geometric morphometrics, which mathematically remove size, as well as traditional morphometrics, which preserve size alongside shape. Linear measurements of various sorts were acquired, which should be assessed with care. Next to a biological signal, they often contain a considerable amount of environmental bias (e.g., growth-band widths). Furthermore, many measurements depend on the exact determination of the relevant number of growth bands, which in most cases can only be approximated, resulting in considerable variation. If, however, measurements diverge significantly, for example by falling outside the 95% confidence interval, the diversion is considered meaningful.

(1) *Radial lirae measurements* were carried out near the distal end of a growth band and compared according to the number of relevant visible growth increment (x-axis in Fig. 4.3). There are two important biases on lirae measurements: (1) Exact growth band counts are impossible due to the usually poor preservation of the umbonal region. (2) Lirae distances do not only vary from one growth band to another, but also along the same growth band, depending on their position near the anterior, ventral, or posterior regions. This results in a high standard deviation within one measurement cohort. The t

test was carried out to check whether mean values of lirae distances of a particular region of a growth band were equal between alleged species. The two-tailed test was employed. Due to the high variability and the uncertainty of the relevant number of growth band, the significance level is set to 0.01. The null hypothesis (H_0) and the alternative hypothesis (H_1) are specified as:

H_0 = Mean radial lirae distances of a particular growth band at a particular part of the carapace are equal between alleged species.

H_1 = Radial lirae distances of a particular growth band at a particular part of the carapace of *Eosestheria middendorfii* exhibit a larger mean than those of *Diestheria yixianensis*.

(2) *Growth-band widths* (Fig. 4.4) were measured along the line connecting U and C (Fig. 4.2). Therefore, measurements do not necessarily represent the widest part of each growth band. Due to the poor outline quality of some type specimens, this line could in some cases only be approximated.

The sample mean of a growth-band width of a particular number of visible growth bands of *Eosestheria* (*Eosestheria* and *Eosestheriopsis*) is an estimate of the true mean μ, but with uncertainty. Therefore, a confidence interval for μ was calculated. This confidence interval is in terms of the true variance of the growth-band widths. As this is unknown, the true variance was replaced by the sample variance, and the *t*-distribution with n-1 degrees of freedom, instead of the normal distribution, was used. The *t*-distribution is wider than the normal distribution taking into account more uncertainty, especially when the sample size, and therefore the number of the degrees of freedom, is small. This is the case, as only a limited number of specimens were considered. Confidence intervals for the 95% level were calculated for growth bands 12 and 14 for *Eosestheria* specimens (shaded in Fig. 4.4), with the exclusion of *Eosestheria fuxinensis* and *Eosestheria jingangshanensis*. At a probability level of 0.05, the two-tailed *t*-value listed in Walser (2011) for 4 degrees of freedom is $t_{0.05,4} = \pm 2.776$.

$$SE_x = \frac{s_x}{\sqrt{n}}$$ (standard error)

$$\left[\bar{x} - t_{0.05,\nu} SE_x, \bar{x} + t_{0.05,\nu} SE_x\right]$$ (95% confidence interval)

n	number of observations
ν	degrees of freedom
s	sample standard deviation
SE_x	standard error of the sample mean
$\bar{x}$	sample mean

(3) *Nine linear measurements* (Fig. 4.2) were measured for 51 type specimens and the following ratios calculated for every type specimen in the style of Defretin-Lefranc (1965) and Tasch (1987): *H*/*L*, *Ch*/*L*, *Cr*/*L*, *Av*/*L*, *Arr*/*L*, *a*/*H*, *b*/*H*, *c*/*L*. All measurements and ratios are listed in Table 4.5. Whether the number of linear measurements can be reduced for a sufficient representation of clam-shrimp proportions will be assessed.

The main goal is to separate taxa on (a) species-level and (b) genus-level and to recognize correlation patterns between variables (size measurements), using a reduced dataset of 16 type specimens (i.e., the first 16 specimens listed in Table 4.5) and the full dataset of 51 type specimens, respectively. The variation in the data is best represented on a reduced number of axes and their associated loadings indicate how to interpret them (e.g., Gingerich, 2003). The standard method is to acquire *principal components* (PC) of a dataset, which are orthogonal, linear combinations of variables that preserve as much variance as possible. *Principal components analysis* (PCA) helps to discover trends in data to cluster in low-dimensional space, which indicates correlation between variables to some degree. The principal components often reflect underlying variables of biological significance (Hammer and Harper, 2006). This method does not make any statistical assumptions, but multivariate normal distribution is recommended (Hammer and Harper, 2006). Multivariate normality was checked using Mardia's multivariate skewness and kurtosis (Mardia, 1970). If the dataset was not multivariate normal, the stability of the principal component vectors was checked with resampling techniques (bootstrapping; Reyment and Savazzi, 1999). The number of significant principal components was estimated using the Jolliffe cut-off value (Jolliffe, 1986); principal components with eigenvalues larger than the cut-off are deemed significant. All variables were measured in mm, so a variance-covariance matrix was employed. PCA was directly applied on the linear measurement dataset. As a result, *PC1* will represent isometric growth, lacking information on shape. *PC2* and *PC3* will be put into perspective for shape variation (Hammer and Harper, 2006). Ratios of linear measurements were created to remove the effects of size. The ratio data was converted to differences by means of log transformation ($\log(a/b) = \log a - \log b$) prior to PCA.

(4) *Fourier shape analysis* investigates two-dimensional form and is a good choice for organisms that

Table 4.6. Linear measurements and number of growth lines for fossil clam shrimps of the Yixian Formation as reported by Chen (1999a). Numbers in bold specify counts that depart from the counts carried out in this study by a considerable number of growth lines (compare with Table 4.4).

Species	Length (mm)	Height (mm)	# reported growth lines
Eosestheria ovata	17-21	12-15	25-32
Eosestheria lingyuanensis	7.5-11.8	6.4-7.5	20-25
Eosestheria aff. *middendorfii*	15	10	25
Eosestheria jingangshanensis	15-17.5	10.5-12.1	**35**
Eosestheria sihetunensis	10-14	7-9	20-25
Eosestheriopsis gujialingensis	16	10-12	**25**
Yanjiestheria? *beipiaoensis*	6-9	4-8	25
Diestheria yixianensis	19-21	12.5-14	**23**-35
Diestheria longinqua	23.5	12.5	31
Diestheria jeholensis	20	12.5-14	30

exhibit only a low number of biologically homologous landmarks (Haines and Crampton, 2000). It should therefore be superior to landmark analysis as proposed by Stoyan et al. (1994) and Goretzki (2003), which is based on mostly constructed, geometrically homologous landmarks. Each of the 51 carapaces measured (Table 4.5) were outlined and right valves were mirrored for the analysis. A comparison of left and right valves in the modern relative *Cyzicus* shows that the mirrored outline of the right valve is matching that of the left perfectly (Fig. 5.1). The outlines were then formatted to be represented by 1500 *xy*-coordinates, using the image capture software tpsDig2 (free software download http://life.bio.sunysb.edu/morph/). In principal, Fourier shape analysis reduced these to a smaller number of parameters, which were further treated with PCA. The first 12 harmonics were chosen to capture the shape of the carapace outlines in all analyses.

Basically, Fourier shape analysis uses an outline that is transformed to a set of *xy*-coordinates and decomposes it into harmonically related sine and cosine curves. There are two Fourier coefficients per harmonic. For computation of the harmonic spectrum, Fast Fourier Transform (FFT), performed by the program Hangle (see below), is used that operates on the tangent angle as a function of arc-length (Haines and Crampton, 2000). For mathematical terms see the appendix of Haines and Crampton (2000).

In contrast to elliptic Fourier analysis (EFA; Kuhl and Giardina, 1982), the method provided by Haines and Crampton (2000) calculates coefficients that are computationally independent of each other. According to Haines and Crampton (2000), harmonics yielded by EFA are increasingly downweighted relative to the first. Therefore, choosing Fourier shape analysis over EFA enhances the discriminatory power of higher-order harmonics (Haines and Crampton, 2000). For example, the biplot in Fig. 4.9 shows that, though *PC1* is driven by low-order harmonic 2, harmonic 5 already contributes significant variance to *PC2*.

Three programs are employed: Hangle, Hmatch, and Hcurve (Crampton and Haines, 1996). High frequency pixel noise due to the automatic tracing of outlines is eliminated with Hangle by smoothing of the outline (prior to the computation of the FFT). This is performed by taking the weighted moving average over three coordinates. The clam-shrimp outlines were subjected to at least five smoothing iterations in the analyses. Calculation of the minimum satisfactory number of smoothing iterations was carried out with the following equation (Haines and Crampton, 2000):

$$\frac{Nsamp}{NFFT} \leq \sqrt{N/2}$$

N	number of smoothing iterations
$Nsamp$	original number of sampled *xy*-coordinates (= 1500)
$NFFT$	number of resampled points (set to 1024)

Fourier methods are sensitive to the starting position. Matching (Hmatch) normalizes for starting position and orientation. In case of clam shrimps, it was unambiguously defined (posterior extremity of the dorsal margin E; Fig. 4.2), but variation already arose from the automatic tracing of outlines that started near E, and not exactly at the point. Therefore, it seemed fit to align the entire set of outlines so that they are as close as possible. This also adjusted the starting position. Running Hmatch adjusts the output of Hangle by taking properties of the

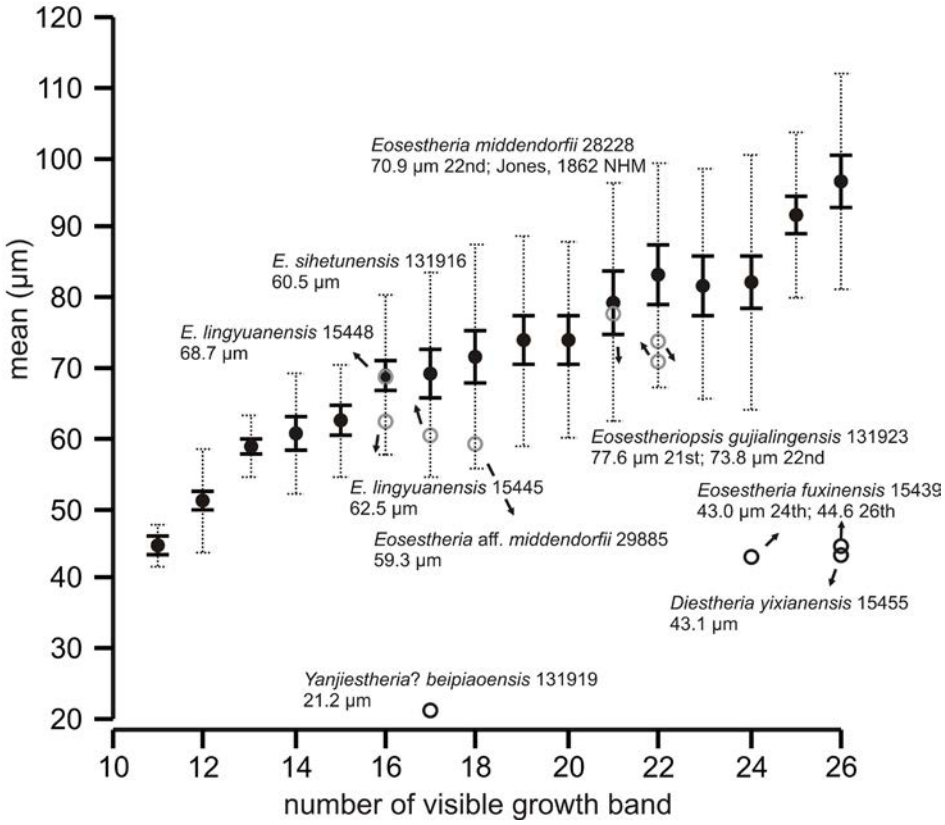

← **Fig. 4.3.** Mean lirae distances at the anteroventral part of growth bands and their associated standard errors (solid lines) and standard deviations (dotted lines) are plotted according to the number of visible growth band. *[Eosestheria ovata]* 131915 serves as the reference specimen. Empty circles indicate specimens of various species described by Jones (1862), Zhang et al. (1976), and Chen (1999a).

entire set of outlines into account and by minimizing the sums of the squares of all differences between the outlines (Haines and Crampton, 2000). In a final step, multivariate statistical analysis of the Fourier coefficients was carried out using PCA on a variance-covariance matrix.

Revision of diagnostic features

Ten species in four genera have been described from the Yixian Formation (Chen, 1999a). They are: *Eosestheria ovata*, *Eosestheria lingyuanensis*, *Eosestheria* aff. *middendorfii*, *Eosestheria jingangshanensis*, *Eosestheria sihetunensis*, *Eosestheriopsis gujialingensis*, *Yanjiestheria*? *beipiaoensis*, *Diestheria yixianensis*, *Diestheria longinqua*, and *Diestheria jeholensis*. Many of the descriptions are qualitative. Quantitative information is restricted to linear measurements of length, height, and the dorsal margin, polygon lengths as well as growth line counts (Table 4.6). This section is putting forward a method for the quantification of ornamentation and it is developing shape characteristics for closely allied late Mesozoic clam shrimps of eastern Asia, listed by order of importance.

Lirae measurements (Fig. 4.3) point at a separation of *Eosestheria* specimens from *Diestheria* and *Yanjiestheria* specimens, with the exception of *Eosestheria fuxinensis* that plots at a similar position as *Diestheria yixianensis*. *E. fuxinensis* will therefore be grouped with *Diestheria* specimens in further analyses. All other *Eosestheria* specimens as well as *Eosestheriopsis gujialingensis* fall at least into the standard deviation of *Eosestheria ovata*. Further lirae measurements from various parts of the carapace are listed in Table 4.7.

Type specimens, whose **growth-band widths** (Fig. 4.4) were measured, are marked with an asterisk in Table 4.4. The genera *Eosestheria*, *Eosestheriopsis*, and *Diestheria* (in blue) cannot be separated with this method, but growth-band widths of the two specimens of *Yanjiestheria*? *beipiaoensis* (orange) are markedly smaller. An exception to this is *Eosestheria lingyuanensis* (15445), where the small values of its 16th and 17th growth bands signify crowding of the carapace, an environmental signal in this case. 95% confidence intervals based on the *t* distribution for the mean growth-band width of *Eosestheria* and *Eosestheriopsis* are shaded in Fig. 4.4 (growth band 12: [390 µm, 554 µm]; growth band 14: [406 µm, 572 µm]). The inclusion of *Diestheria* into the analysis shifts confidence intervals towards higher values (growth band 12: [426 µm, 546 µm]; growth band 14: [435 µm, 638 µm]). 95% confidence intervals for *Y.*? *beipiaoensis* are wide, owing to the very low sample size, but for the sake of completeness they should be mentioned nonetheless: growth band 12: [63 µm, 321 µm]; growth band 14: [12 µm, 432 µm]. There

Tab. 4.7. Lirae measurements for clam shrimps of the Yixian Formation (Zhang et al., 1976; Chen, 1999a) and for the syntype series of Jones (1862). The often low number of measurements is due to a balance between a sufficiently large number of measurements and the introduction of extra bias that results from the change of lirae spacing along single growth bands, which is expressed by a large standard deviation (Fig. 4.3).

Specimen	Number of visible growth band	Mean lirae distance (in µm)
Eosestheria ovata 131915	Fig. 4.3	
Eosestheria lingyuanensis 15445 (Holotype)	16th, anteroventral-ventral	62 (n 3)
Eosestheria lingyuanensis 15448	16th, anteroventral	69 (n 7)
Eosestheria aff. *middendorfii* 29885	18th, anteroventral	59 (n 3)
Estheria middendorfii 28227 NHM (Syntype)	25th, anteroventral	76 (n 10)
	25th, ventral	78 (n 5)
Estheria middendorfii 28228 NHM (Syntype)	22nd, anteroventral	71 (n 11)
	22nd, ventral	75 (n 17)
	22nd, posterior	47 (n 22)
Estheria middendorfii 28229 NHM (Syntype)	27th?, ventral	71 (n 31)
Eosestheria jingangshanensis 15443 (Holotype)	Inspection with SEM needed; specimen inadequate to erect a new species.	
Eosestheria sihetunensis 131917 (Holotype)	Mostly reticulated. A sufficient number of lirae not visible due to crowding.	
Eosestheriopsis gujialingensis 131923	21st, anteroventral	78 (n 4)
	22nd, anteroventral	74 (n 5)
Yanjiestheria? *beipiaoensis* 131919 (Holotype)	17th, anteroventral-ventral	21 (n 6)
Diestheria yixianensis 15455 (Holotype)	26th, anteroventral	43 (n 19)
	30th, ventral	45 (n 17)
	31st, posterior	26 (n 39)
Diestheria yixianensis 15456	19th, anteroventral	52 (n 4)
	21st, ventral	47 (n 13)
Diestheria longinqua 15462 (Holotype)	29th, anteroventral	45 (n 5)
Diestheria jeholensis 15457	25th, anteroventral	47 (n 4)
Eosestheria fuxinensis 15439	24th, anteroventral	43 (n 10)
	26th, anteroventral	45 (n 11)

is a confidence-interval overlap for growth band 14 between *Eosestheria* specimens and *Y.*? *beipiaoensis*, but this is due to the high *t*-value used for the latter. Therefore, the probability of mean growth-band widths of *Y.*? *beipiaoensis* to be of the same range as those of *Eosestheria* or *Diestheria* can be estimated to be low. This separation of *Y.*? *beipiaoensis* from other species described in Chen (1999a) is considered biologically meaningful here, but only because this revision is based entirely on type specimens.

Note that type specimens of fossil clam-shrimp species often exhibit extreme characteristics. In theory they should not do so. Specimens analyzed in Chapter 6 show that growth-band widths strongly depend on environmental parameters (e.g., Fig. 6.1). Their value as a morphological character for systematics is therefore small.

Linear measurements of 16 type specimens (Tables 4.4, 4.6) of *Eosestheria*, *Eosestheriopsis*, *Yanjiestheria*?, and *Diestheria* were subjected to a PCA (Fig. 4.5), with *PC1* explaining 94.9% of the total variance in the dataset. *PC2* and *PC3* explain 3.0% and 1.3%, respectively. All nine variables have positive loadings on *PC1* (Fig. 4.5a, Table 4.8), indicating that *PC1* reflects size. Therefore, as *Diestheria* specimens have high scores on *PC1*, they are generally larger than *Eosestheria*, while *Yanjiestheria*? is generally smaller, because it is occupying the region

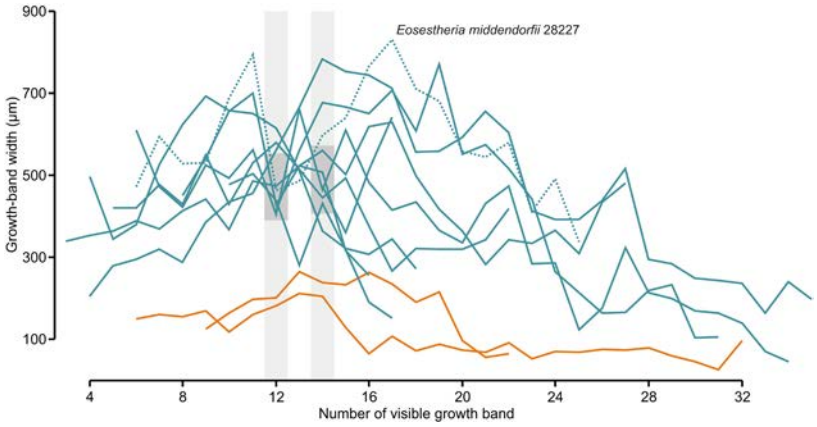

← **Fig. 4.4.** Growth-band widths of selected specimens are marked with an asterisk in Table 4.4. Specimens of *Yanjiestheria*? *beipiaoensis* in orange. Specimens of *Eosestheria*, *Eosestheriopsis*, and *Diestheria* in blue. A representative of the syntype series of *[Estheria] middendorfii* is marked with a dotted line. 95% confidence intervals for *Eosestheria* (excluding *E. fuxinensis* and *E. jingangshanensis*) and *Eosestheriopsis* are shaded for growth bands 12 and 14.

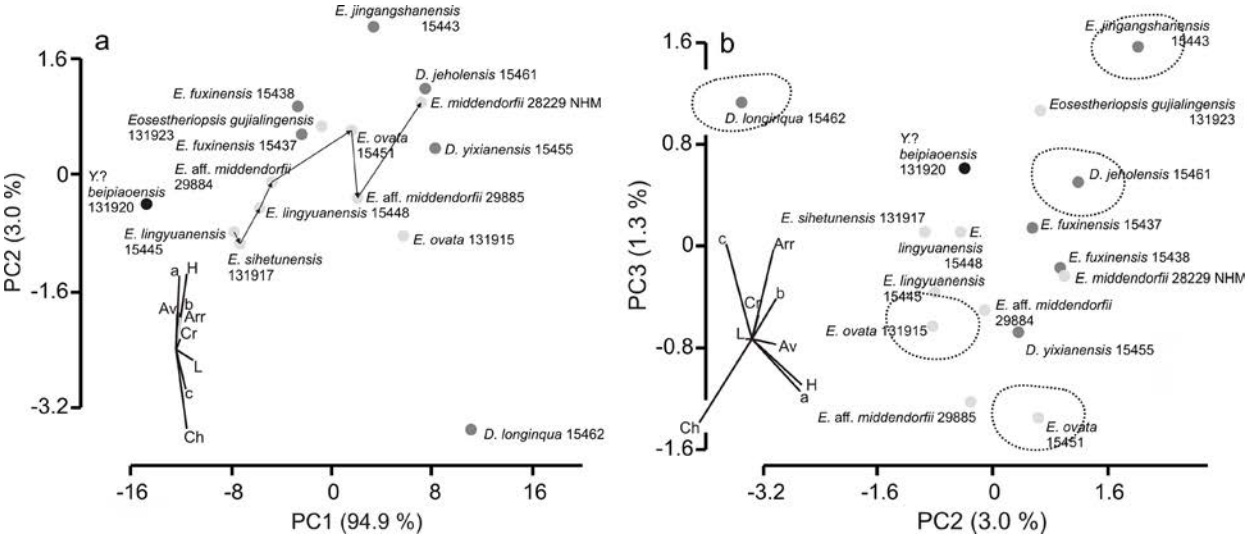

Fig. 4.5. Scores and loadings on (a) *PC1* and *PC2* and (b) *PC2* and *PC3*. Light dots *Eosestheria* and *Eosestheriopsis*, medium-dark dots *Diestheria* (plus *Eosestheria fuxinensis* and *Eosestheria jingangshanensis*), black dots *Yanjiestheria*?. Arrows in (a) correspond to the proposed ontogenetic trajectory of Fig. 4.6.

on the left in Fig. 4.5a. *Eosestheria fuxinensis*, which has been reassigned to *Diestheria* through lirae measurements, plots at an intermediate position.

The main difficulty of size-measurement based taxonomy in fossil clam shrimps is the separation of size differences that follow an allometric model from a truly taxonomic signal. In a true ontogenetic sample that only yields specimens of a single species, *PC1* usually corresponds to the allometric shape component (Mitteroecker et al., 2004). In contrast, *PC1* of multispecies samples will naturally only translate to a common direction of growth and is therefore informally interpreted as a size axis (e.g., Hammer and Harper, 2006). This increase in size can easily be reproduced (Fig. 4.6) by looking at the variable length, which has the highest positive loading of all variables on *PC1* (Table 4.8). Outlines of *Eosestheria* specimens are scaled and arranged according to length in Fig. 4.6 and the proposed ontogenetic trend is indicated with arrows in Fig. 4.5a. For a true ontogenetic trajectory see Chapter 5.

Table. 4.8. Loadings on *PC1-3* for the analysis in Fig. 4.5. Variables contributing most to either component are in bold.

	PC1	*PC2*	*PC3*
a	0.1257	**0.4827**	-0.3045
b	0.1808	0.2449	0.2234
c	0.3751	-0.2587	**0.5349**
Arr	0.1688	0.2182	**0.5054**
Av	0.05311	0.2387	-0.03434
Ch	0.4245	**-0.5242**	**-0.4767**
Cr	0.166	0.07127	0.1365
H	0.3924	**0.5012**	-0.2623
L	**0.6464**	-0.06721	-0.005564

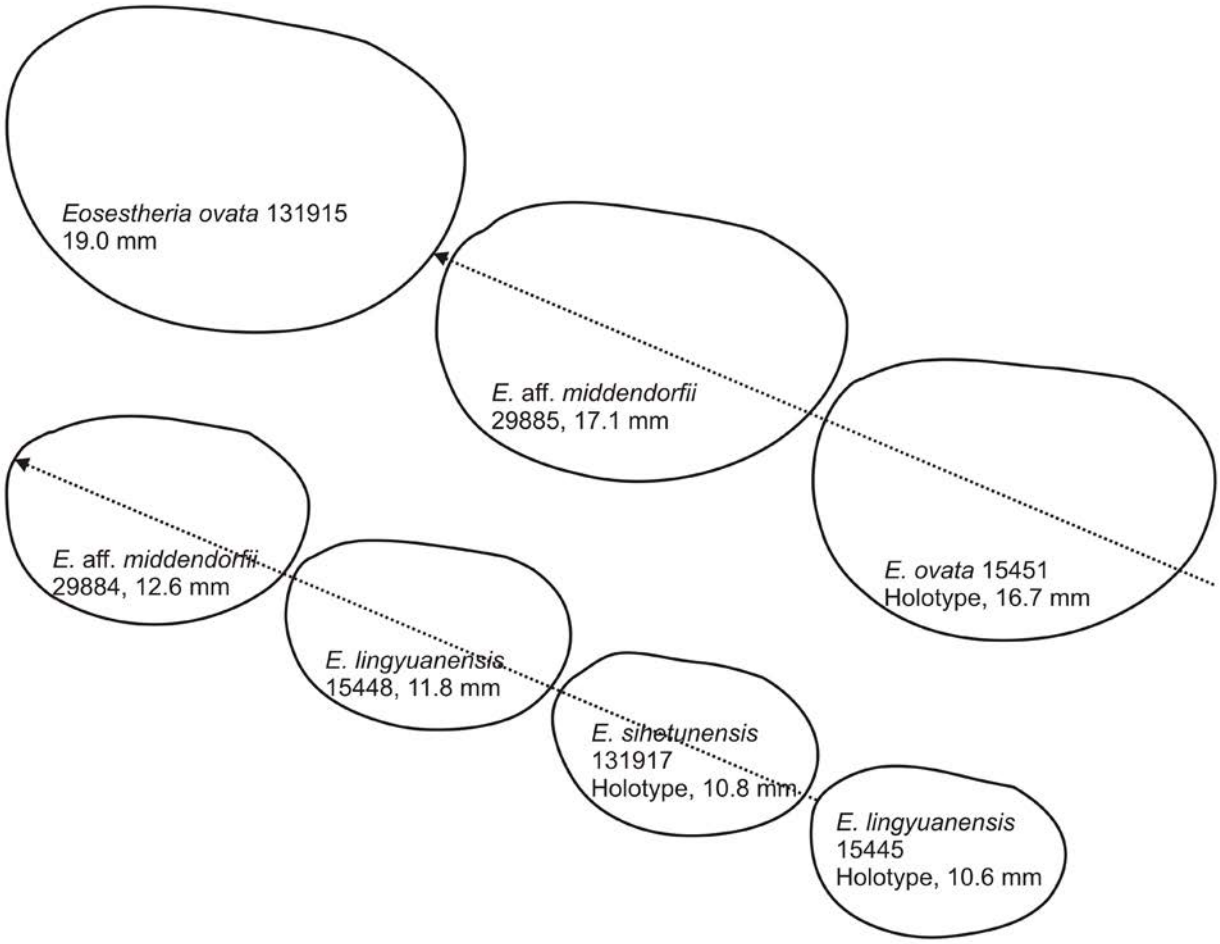

Fig. 4.6. Scaled outlines of type specimens of *Eosestheria* from Chen (1999a) that follow a proposed ontogenetic trajectory.

The plot on *PC2* and *PC3* (Fig. 4.5b) is informative regarding the variation of shape. As scores are increased on *PC2*, length-related variates (*c*, *Ch*, *L*) decrease, while *a*, *b, Arr, Av*, *Cr*, and *H* increase (Table 4.8). *Ch* (negative) as well as *a* and *H* (positive) contribute most to *PC2*. Therefore, specimens with high scores on *PC2* are expected to be more ovate, while those with negative scores should be more elongate. Specimens with high scores on *PC3* have large *c* and *Arr*, while their dorsal margin (*Ch*) is comparatively short.

Specimens of *Eosestheria fuxinensis* are plotting near *Diestheria jeholensis* and *Diestheria yixianensis* in Fig. 4.5, though the separation from *Eosestheria* is poor. *Diestheria longinqua*, in turn, is separated from all other specimens. In conclusion, separation of such closely allied taxa through linear measurements is poor. Alternatively, this could be an indicator for the presence of synonyms.

PCA on linear measurements is problematic for species-level distinction, especially when the number of artificial taxa due to splitting is high, but it might still be useful for genus discrimination. The employed dataset (Table 4.5) was restricted to 51 middle-late Mesozoic type specimens of eastern Asia (Zhang et al., 1976; Shen et al., 2002, 2003; Li and Batten, 2004a, 2005; Chen et al., 2007; Li et al. 2007), including the 16 specimens of Fig. 4.5. Fig. 4.7 illustrates four biplots on *PC1* and *PC2* as well as on *PC2* and *PC3* of linear measurements and their ratios, respectively. Most of the variance is explained by *PC1* and all size measurements increase in value towards higher scores on *PC1*, so it can be interpreted as a size axis (check loadings on principle components in Table 4.9). *PC1* is therefore not informative with regard to shape variation. Shape information can be drawn from the biplot on *PC2* and *PC3* (Fig. 4.7b). *PC2* mainly marks the relative difference between *H* and *Ch*, whereas *PC3* stands for the relative difference between *Cr* and *Arr*. Specimens with higher scores on *PC2* have a short dorsal margin compared to a greater height, appropriate specimens are subcircular to ovate. High scores on *PC3* indicate a long distance between the

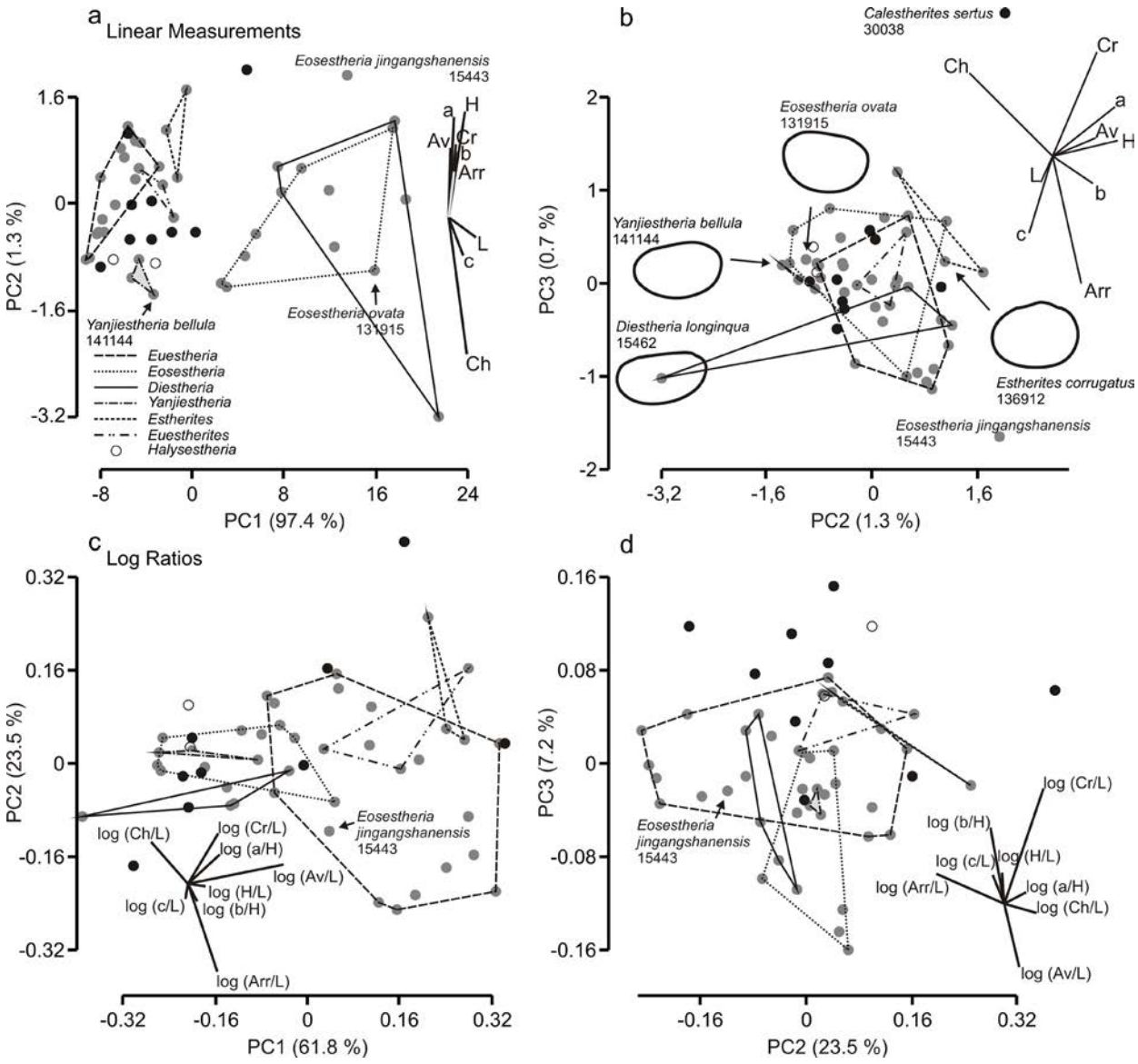

Fig. 4.7. PCA on 51 type specimens of Jurassic and Cretaceous clam shrimps from China. (a, b) PCA on nine linear measurements. (c, d) PCA on the log-transformed ratios. *Yanjiestheria* is shaded in all four plots.

midpoint of the umbo to the most anterior part of the carapace and a comparatively short distance of the posterior extremity to the most posterior part of the carapace.

The separation of genera is partly accomplished in the biplot on *PC2* and *PC3* (Fig. 4.7b), the best perhaps for *Yanjiestheria*, which forms distinct groups in both scatter plots of Figs. 4.7a, b. Due to its comparatively small size (5.4-6.7 cm), *Yanjiestheria* plots in the left region of Fig. 4.7a, far from *Eosestheria*, while it is more similar to *Eosestheria* in Fig. 4.7b, whose convex hull occupies a larger area due to the ontogenetic bias involved (Figs. 4.5, 4.6). The genera *Euestheria* and *Euestherites* do not differ in relative differences between *H* and *Ch* or *Cr* and *Arr*, while *Estherites* can clearly be separated from

Table. 4.9. Loadings on *PC1-3* for the analysis in Fig. 4.7. Variables contributing most to either component are in bold.

	PC1	*PC2*	*PC3*
a	0.1229	**0.4184**	0.2371
b	0.1647	0.274	-0.1294
c	0.3521	-0.1584	-0.3625
Arr	0.1491	0.1928	**-0.6044**
Av	0.05738	0.2904	0.08676
Ch	0.4494	**-0.5616**	0.3952
Cr	0.157	0.3001	**0.4955**
H	0.3891	**0.4378**	0.07726
L	**0.6559**	-0.07828	-0.1227

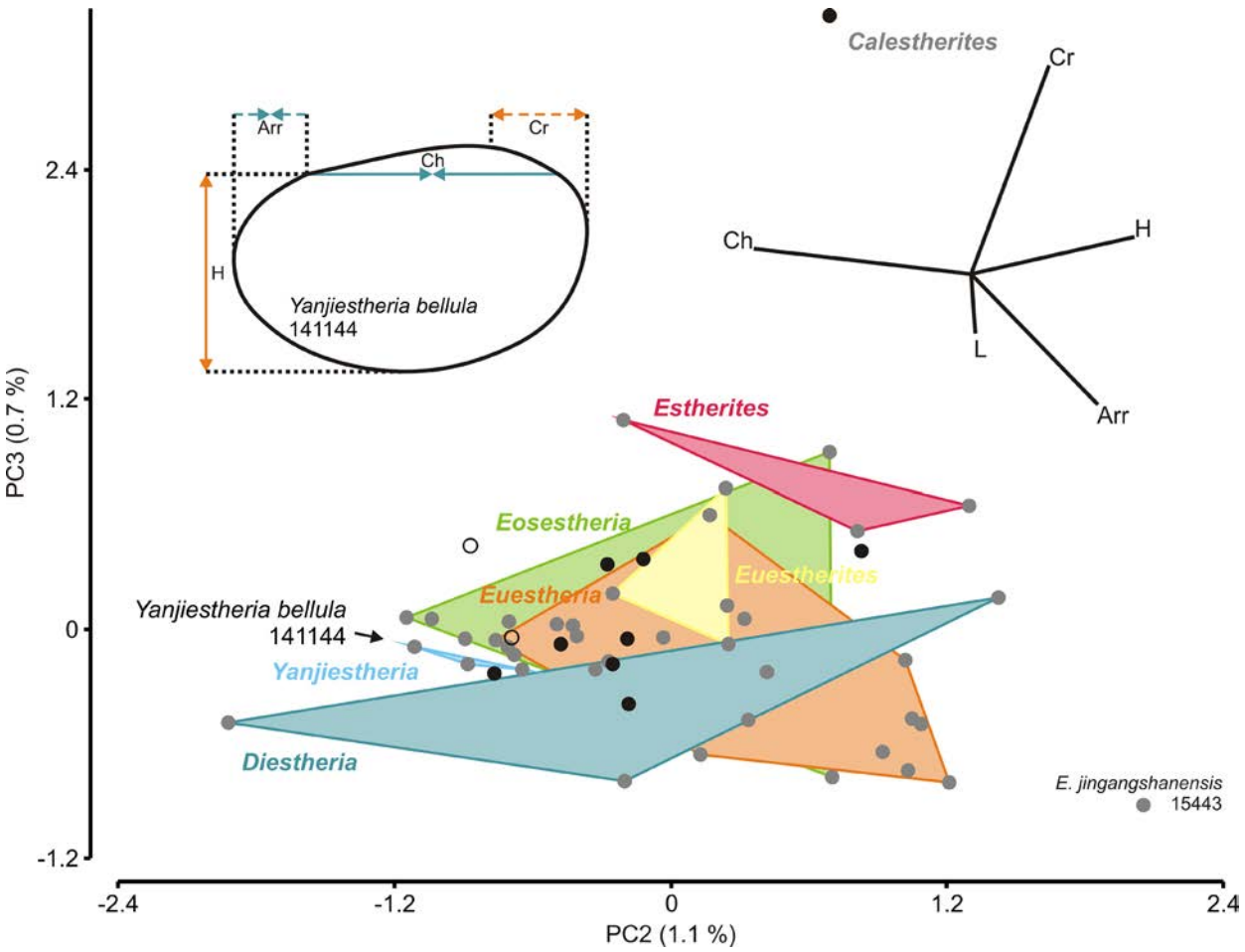

Fig. 4.8. PCA on robust measurements (*Arr*, *Ch*, *Cr*, *H*, and *L*). The outline of *Yanjiestheria bellula* 141144 in the upper left region of the plot illustrates the change of variables as scores are increased on *PC2* (solid lines) and on *PC3* (dashed lines). Positive and negative loadings for principal components are colour-coded in orange and blue, respectively.

Table. 4.10. Loadings on *PC1-3* for the analysis with the reduced dataset comprising only robust variables (Fig. 4.8). Variables contributing most to either component are in bold.

	PC1	*PC2*	*PC3*
Arr	0.1627	0.4099	**-0.5094**
Ch	0.4941	**-0.6995**	0.09749
Cr	0.172	0.2517	**0.8104**
H	0.4267	**0.5283**	0.1445
L	**0.7196**	0.01416	-0.2311

Euestherites. PCA of the log-transformed ratios of the same linear measurements (Fig. 4.7c, d) draws a slightly different picture, in which *Yanjiestheria* cannot be separated from *Eosestheria*. Ratios removed the effects of size, which is often desirable, but it seems size is taxonomically important for clam shrimps. Ratios do not pick up the more subtle differences in shape, which Fourier shape analysis does (see below).

Separation of taxa is mostly accomplished with the help of five variables (*Arr*, *Ch*, *Cr*, *H*, and *L*). *Av* and *b* have comparatively low loadings on *PC 1* to *PC 3* (Table 4.9). Loadings of *a* and *c* are reasonably high, but they are easily rendered meaningless through rotation of the carapace, which occurs because the anterior extremity of the dorsal margin (D; Fig. 4.2) is often not preserved. This affects all nine variables, but it was obvious during data acquisition that *a*, *b*, and *c* are especially sensitive. Misplacement of D naturally strongly affects *Av*, so that most of its variability is probably coming from data acquisition. PCA on the reduced dataset of herein proposed robust variables (*Arr*, *Ch*, *Cr*, *H*, and *L*; Fig. 4.8; Table 4.10) leads to an overall similar picture compared to Fig. 4.7a, b, implying that the collection of only five linear measurements suffices to capture variation in form. The separation of taxa is even slightly enhanced regarding *Euestherites* and *Euestheria*. The

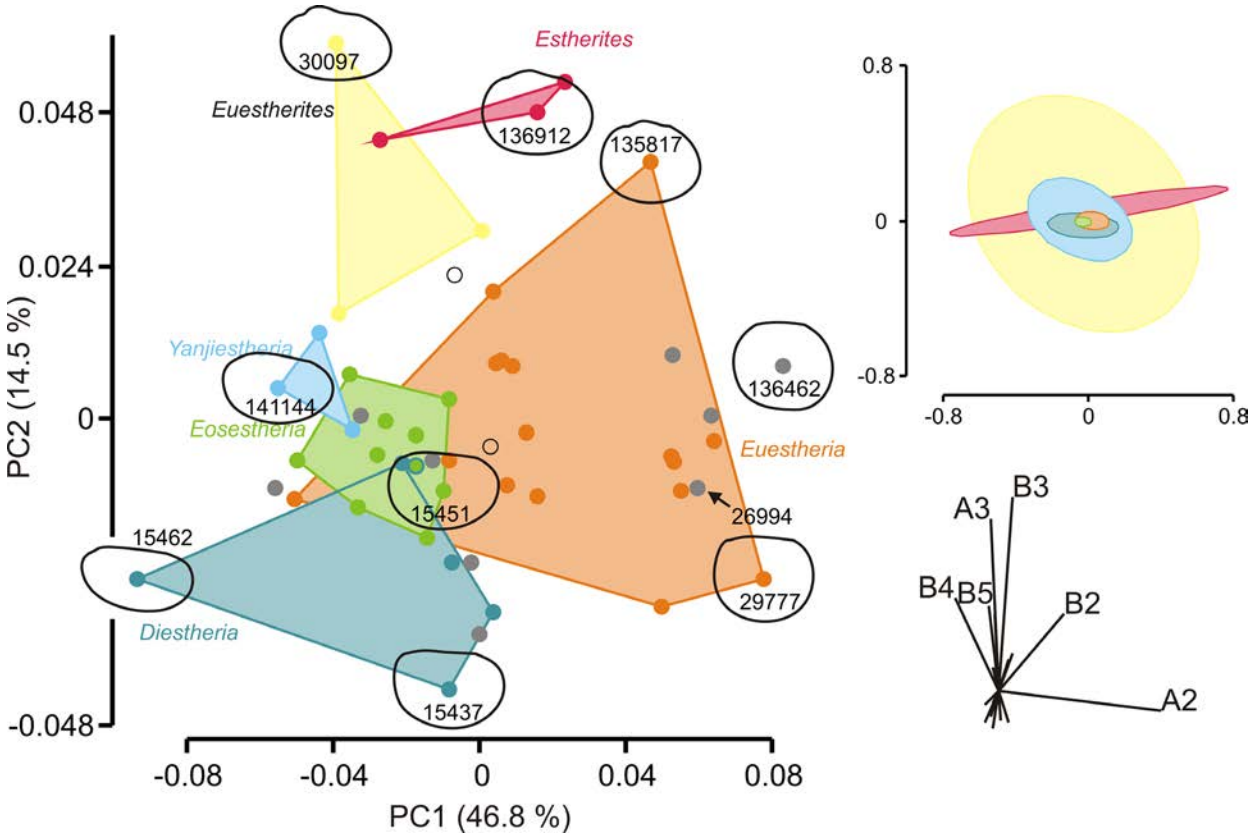

Fig. 4.9. Fourier coefficients on *PC1* and *PC2*. Genera occupy different regions in the scatter plot, but separation is not perfect and sample size too small for the separation of confidence intervals (upper right region of the figure). Corresponding outlines were centred around selected type specimens in shape space. If appropriate, valves were mirrored to show the posterior dorsal extremity on the right side. *Eosestheria jingangshanensis* is marked with a blue circle filled with green to highlight its unclear affinity to either *Eosestheria* or *Diestheria*.

outline in the upper left region of Fig. 4.8 illustrates the most important changes in the clam-shrimp carapace along *PC2* and *PC3*. Correlated variables are *H* and *Ch* as well as *Cr* and *Arr*.

In summary, PCA of linear measurements, less so their ratios, can be a powerful tool for genus-level separation, but will not work for more variable genera. The collection of five robust linear measurements, instead of the nine variables proposed by Defretin-Lefranc (1965) and Tasch (1987), suffices for an appropriate representation of clam-shrimp form.

Ornamentational data suggest that *Eosestheria middendorfii* and *Diestheria jeholensis* are closely related. To clarify whether it is possible to distinguish these two species through shape alone, a *Fourier shape analysis* (Figs. 4.9, 4.10) of 51 type specimens was carried out (Supplementary 4.1). According to the Jolliffe cut-off value *PC1* to *PC6* are considered meaningful. *PC 1* (Fig. 4.9), which explains 46.8% of the variance, depicts carapace shape from elongate (negative scores) to subcircular (positive scores). This corresponds to the *H*/*L* ratio (Table 4.5). *PC2*, *PC3*, *PC4*, *PC5*, and *PC6* (Fig. 4.10) explain 14.5%, 7.7%, 7.0%, 6.0%, and 5.0% of the total variance in the first 12 harmonics. *PC2* marks the prominence of the umbo from smooth (negative scores) to prominent (positive scores). A prominent umbo is diagnostic of genera such as *Euestherites* and *Estherites*. Bias through carapace deformation is involved though, depending on carapace convexity and the way the carapace has been embedded after death. Positive scores on *PC3* (Fig. 4.10a) indicate an anterior displacement of the dorsal margin relative to the lowermost point of the ventral margin (C, Fig. 4.2). *PC4* (Fig. 4.10b), which explains a similar amount of shape variation as *PC3*, stands for the position of B with respect to valve height. B moves upward towards higher scores on *PC4*. Variable *PC4* loosely corresponds to ratio *b*/*H*, but not perfectly. *PC5* (Fig. 4.10c) indicates the position of the umbo, moving from more anterior to median towards higher scores on *PC5*. This should not be confused with the position of the larval valve (U, quantified with *Cr*), which Fourier shape analysis cannot pick up. What variable *PC6* (Fig. 4.10d)

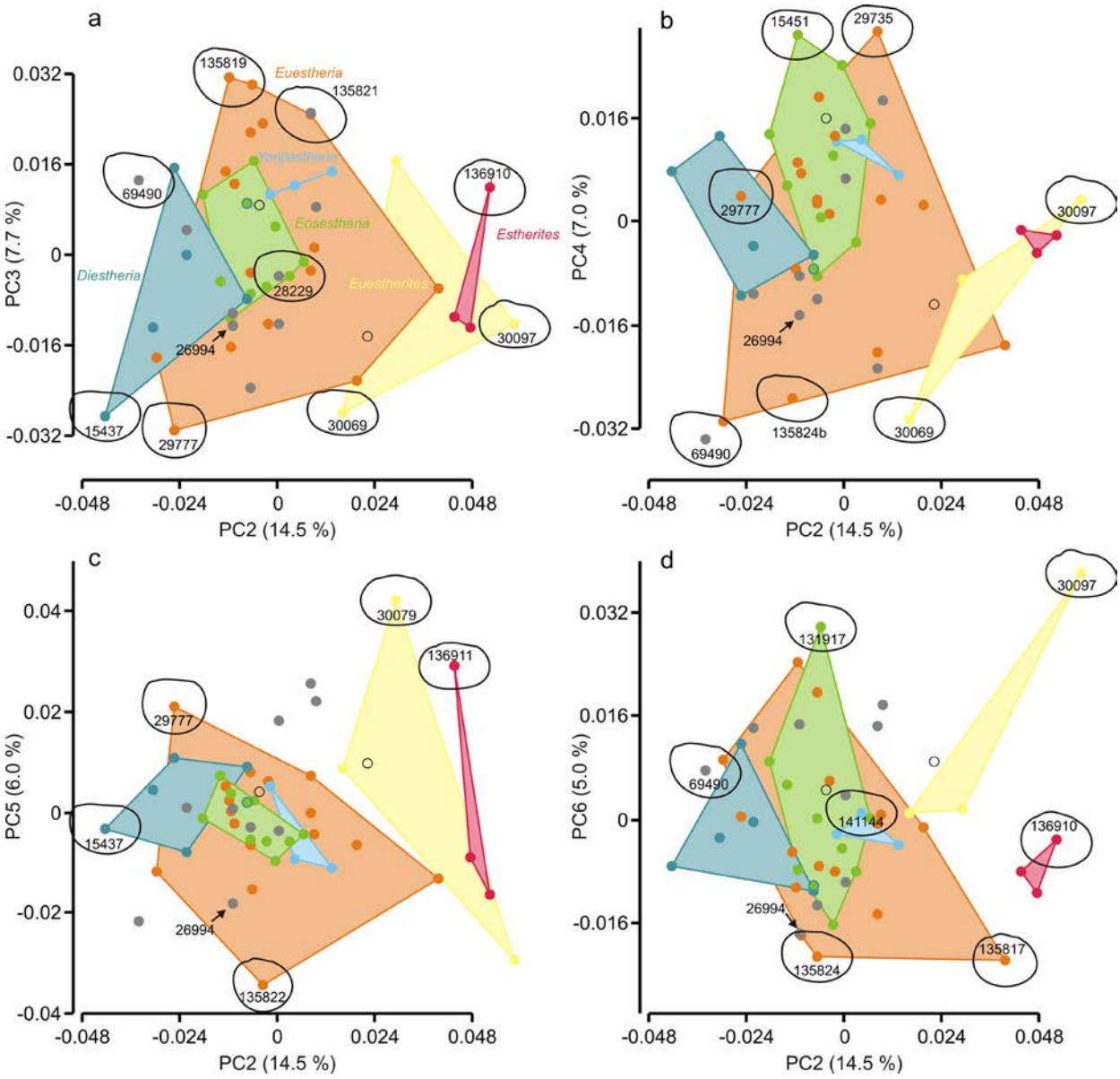

Fig. 4.10. Fourier coefficients on *PC2* and *PC3* to *PC6*. *PC1* to *6* are considered meaningful. *Eosestheria jingangshanensis* is marked with a blue circle filled with green to highlight its unclear affinity to either *Eosestheria* or *Diestheria*.

stands for is not very obvious. Specimens 135817 and 30097 exhibit the most negative and the most positive score on *PC6*, respectively. A cross-check with the ratio data (Table 4.5) yields no conclusive difference, except for their *H*/*L* ratios (0.77 and 0.59), which is clearly driving *PC1*. Therefore, *PC6* must be a variable that is not picked up by the ratios listed. It probably stands for the angularity of the anterior margin, which is more pointed towards higher scores on *PC6*.

In summary, the most important variables characterizing the shape of the clam-shrimp carapace based on the 51 specimens of Table 4.5 are (in descending order of importance): (1) *H*/*L* ratio, (2) prominence of the umbo, (3) displacement of the dorsal margin relative to C, (4) position of B with respect to valve height (similar to ratio *b*/*H*), (5) position of the umbo, and (6) angularity of the anterior margin. During the preparation of the valve outlines, it became clear that the position of the umbo (5) is somewhat variable and the position of the larval valve, defined by the ratio *Cr*/*L*, should be more precise. Fourier shape analysis can be considered the superior analysis, because of a somewhat better separation of genera and because only three out of six shape variables are picked up by ratios. However, the aspect of size is taxonomically important, rendering the acquisition of (robust) linear measurements a significant part of clam-shrimp taxonomy.

Strength of diagnostic features

Modern clam-shrimp species have been distinguished based on ornamentational features (Baird, 1849 [1850]; Grube, 1865), though this is not common practise anymore. Zierold (2007) showed that species distinction with the help of morphometrics was possible when analysing larval valves of limnadiids, while the outline of the entire carapace was indicative for leptestheriids. Unfortunately, the preservation of larval valves is rare and they are usually deformed in more developed specimens. The best representation of the shape of the larval valve is given through preservation of the clam shrimp in butterfly position, but this is not the common case for the type material of this study.

PCA of **robust linear measurements** (*Arr*, *Ch*, *Cr*, *H*, and *L*) leads to a sufficient representation of the proportions of clam shrimps in comparison to PCA of all nine linear measurements (compare Fig. 4.7b and Fig. 4.8). Separation of taxa is enhanced using **Fourier shape analysis**, which is also considered superior to Landmark analysis. Landmarks proposed by Stoyan et al. (1994) rely on the preservation of the shape of the larval valve and on exact growth line counts. The acquisition of both is tricky for the specimens analysed in this study. A number of their "morphological" landmarks are biologically manifested, but they are not practical, because specimens are usually not well enough preserved.

Growth line counts are problematic as a diagnostic character per se. The number of growth lines is correlated with individual life span (Frank, 1988), deformation and poor preservation of the umbo (a well preserved juvenile of 2.2 mm length may yield 17 growth lines, which usually go unrecognized in larger specimens), and growth increment crowding at the carapace margin. Such crowding accounts for up to five extra unrecognized growth lines in Fig. 3.4d. Therefore, the number of growth lines is not an adequate taxonomic character. Tasch (1987) also noted its limited taxonomic value. However, as Chen (1999a) put value into such counts, they are reported nevertheless (Tables 4.4, 4.6). Moreover, the determination of the exact number of an individual growth band is required for the quantification of ornamentational features and for growth-band widths. It should be noted that uncertainty in this number adds extra variance to **radial lirae** and **growth-band widths**. In spite of this uncertainty, the quantification of lirae spacing well delineates *Eosestheria* from *Diestheria*. As mentioned before, considerable variance in the data is expected. Lirae distances also vary on the same growth band depending on their position on the carapace (e.g., more anterior versus more ventral for anteroventral measurements). While differentiation between the two genera *Eosestheria* and *Diestheria* can be accomplished, this method fails to separate *Diestheria* from *Yanjiestheria*?. Growth-band widths need to be used for this. In summary, only with a combination of the various methods described, which quantify carapace size, shape, and ornamentation, it is possible to separate clam-shrimp taxa.

Systematic palaeontology

The classification scheme of higher taxa down to family-level follows that of extant Spinicaudata and ranks listed are adopted from Martin and Davis (2001).

Subphylum **Crustacea Brünnich, 1772**
Class **Branchiopoda Latreille, 1817**
Subclass **Phyllopoda Preuss, 1951**
Order **Diplostraca Gerstaecker, 1866**
Suborder **Spinicaudata Linder, 1945**
Family **Cyzicidae Stebbing, 1910**

Remarks: The suprageneric classification differs from known classification schemes and is a proposal to reconcile modern and fossil spinicaudatan systematics. Braband et al. (2002) declared the Spinicaudata a monophylum based on nuclear and mitochondrial markers. Closest relatives are the Cladoceromorpha (Cladocera, "water fleas", and Cyclestherida), with which the Spinicaudata in turn form a monophylum. This renders the historic taxon "Conchostraca", which combines groups with a laterally compressed body enclosed in a bivalved carapace, paraphyletic (Spinicaudata, Cyclestherida, and Laevicaudata; Tasch, 1969). Three families (Cyzicidae, Leptestheriidae, and Limnadiidae) are distinguished within the suborder Spinicaudata (Martin and Davis, 2001). Family-level distinctions are based mostly on soft part anatomy and genetic data. Monophyly of all three families is not yet clear. The Limnadiidae, for instance, are monophyletic by the exclusion of *Eulimnadia* (Hoeh et al., 2006). Schwentner et al. (2009) distinguished four lineages (Fig. 3.5): Limnadiidae, Leptestheriidae, Cyzicidae (excluding *Eocyzicus*), and *Eocyzicus*. Hence, family-rank distinction of modern taxa is still subject of ongoing research.

There is no classification scheme that can be adopted for fossil taxa per se. The Treatise on Invertebrate Paleontology (Tasch, 1969) presents a comprehensive scheme of fossil and modern taxa, but is out of date regarding the molecular data and the numerous families erected after 1969. This study deals with species that have been published by Zhang et al. (1976), subsequent to the publication of the Treatise (Tasch, 1969). Two of them are name-bearing types for the families Eosestheriidae and Diestheriidae (Chen and Shen, 1985). However, 275 new species of a total of 399 species shed some doubt on the validity of the proposed scheme of Zhang et al. (1976), which may be heavily biased by splitting of taxa. This is hinted at in Figs. 4.5 and 4.6. In view of the genetic data mentioned and the discrepancies between the diverse fossil classification schemes in use (Table 3.1), specimens are assigned to the family Cyzicidae, following Tasch (1969), as close relationship between the Eosestheriidae and the Diestheriidae with the Cyzicidae is assumed (explained below).

Subfamily **Bairdestheriinae Novojilov, 1954**

1976 Eosestheriidae Zhang and Chen
1976 Diestheriidae Zhang and Chen

Remarks: Remarks on the name of the subfamily are linked to the discussion of the valid genus name for *Eosestheria middendorfii* (see below). The starting point for the selection of the Bairdestheriinae as subfamily is the publication of Raymond (1946), in which *Bairdestheria* was segregated from the modern genus *Caenestheriella* Daday de Dées, 1913 by leaving strongly punctate forms in *Caenestheriella* and placing forms that are radially striated into *Bairdestheria*. Importantly, distinctions were based on modern taxa. This subdivision of *Caenestheriella* makes a lot of sense from a palaeontological point of view, as it places more weight on ornamentational features, which are the most diagnostic features of the fossil clam shrimps from Eastern Asia. The approach of Raymond (1946) is probably the best for reconciling modern and fossil classification schemes.

The type species of *Bairdestheria* is *[Estheria] donaciformis* Baird, 1849. Ornamentational features in the original publication (Baird, 1849 [1850]) were described as follows: "…; the ribs are numerous and rather unequal; the spaces between them are striated longitudinally; the striae, …, being irregular and of a somewhat complicated structure, near the edge of the rib frequently forming loops and running one into the other." So, Baird (1849 [1850]) explicitly mentioned radial lirae, but no reticulation. However, in the associated plate, ornamentation of *[Estheria] donaciformis* is clearly figured as a combination of both reticulation and lirae. This is corroborated by the detailed drawings of Grube (1865), who intriguingly noted the close affinity of its ornamentation to that of the fossil species *[Estheria] middendorfii*. Also, Daday de Dées (1915) illustrated the ornamentation of *Caenestheriella donaciformis* as a combination of reticulation and radial lirae, but did not mention it in his species description. Consequently, Raymond (1946) reassigned *[Estheria] middendorfii* to *Bairdestheria*, stating that most indicative of *[Bairdestheria] middendorfii* was the combination of polygons and radial markings on the growth bands.

The drawback is that *Caenestheriella donaciformis*, instead of *[Bairdestheria] donaciformis,* is well established in the classification scheme of modern taxa. Furthermore, Tasch (1969) synonymized *Bairdestheria* with *Cyzicus* (*Euestheria*) in the Treatise on Invertebrate Paleontology, indicative of the latter being reticulations on the growth bands (Depéret and Mazeran, 1912). This is somewhat difficult to understand, because *Bairdestheria* was mainly recognized for its radial lirae before. *Euestheria* itself is a classic waste-basket taxon owing to a very general diagnosis, which is cited in the introduction of this chapter. To confine *Euestheria*, its diagnosis should be restricted to reticulated carapace ornamentation, as is the case in the original article by Depéret and Mazeran (1912). Therefore, there is no reason to discard the genus-group *Bairdestheria*.

In essence, the diagnosis of the genus-group *Bairdestheria* is similar to the family diagnosis of the Eosestheriidae*. This inconsistency in detail between descriptions of different ranks is another problem clam-shrimp classification is facing. Generic diagnoses are much more detailed in Zhang et al. (1976) than they are in Tasch (1969). To place greater emphasis on ornamentation in modern taxa, as has been done by Baird (1849 [1850]), Grube (1865), and Raymond (1946), the genus-group *Bairdestheria* should be elevated to subfamily level (Bairdestheriinae Novojilov, 1954), following No-

*Original diagnosis of Eosestheriidae Zhang and Chen, 1976 (translated from Zhang et al., 1976). – "Moderate to very big size. Growth bands exhibit irregular, shallow reticulation at the anteroventral and the dorsal parts of the carapace. Polygons are small or big. The posterodorsal part of the carapace exhibits narrow or broad lirae (more or less dense). Lirae are branching, curved, and interconnected."

vojilov (1960), Defretin-Lefranc (1965), and Kozur and Seidel (1983).

Unfortunately, the (sub-)family diagnoses provided by these authors restrict the Bairdestheriinae/Bairdestheriidae to radial lirae, probably because Raymond (1946) was focussing his description on them. Publications such as Grube (1865) that state otherwise were neglected. This led to the proposition that the combination of reticulation and radial lirae, herein diagnostic of the Bairdestheriinae, was diagnostic of the Euestheriinae by Defretin-Lefranc (1965). Considering the discussion of the genotype for *Bairdestheria* (*[Estheria] donaciformis*), which clearly shows a combination of both ornamentational features, these (sub-)family diagnoses need to be emended accordingly.

Emended subfamily diagnoses after Defretin-Lefranc (1965):

Euestheriinae Defretin-Lefranc, 1965: Polygonal ornamentation on growth bands.

Bairdestheriinae Novojilov, 1954: Ornamentation marked by a combination of reticulation and radial lirae. Lirae simple or bifurcating.

The allocation of *Caenestheriella donaciformis* to the Bairdestheriinae renders *Caenestheriella* a paraphyletic genus. Genetic data corroborates this, because different *Caenestheriella* species, though closely related, are grouped with *Cyzicus* and *Caenestheria*, respectively (Schwentner et al., 2009; Fig. 3.5). Furthermore, carapace ornamentation among the modern genus-group *Caenestheriella* is variable (Daday de Dées, 1915). The genus name *Caenestheriella* should be kept for its type species *C. variabilis* (see Stoicescu, 2004, for its validity) and it is here proposed to reinstate the genus *Bairdestheria* with its type species *Bairdestheria donaciformis*.

Genus *Eosestheria* Chen, 1976

Originally included species: *Eosestheria fuxinensis* Chen, 1976; *Eosestheria jingangshanensis* Chen, 1976; *Eosestheria lingyuanensis* Chen, 1976; *Eosestheria subrotunda* Chen, 1976; *Eosestheria triformis* Chen, 1976; *Eosestheria elliptica* Chen, 1976; *Eosestheria persculpta* Chen, 1976; *Eosestheria ovaliformis* Chen, 1976; *Eosestheria elongata* (Kobayashi and Kusumi, 1953); *Eosestheria subelongata* (Kobayashi and Kusumi, 1953); *Eosestheria chii* (Kobayashi and Kusumi, 1953); *Eosestheria peipiaoensis* (Kobayashi and Kusumi, 1953); *Eosestheria intermedia* (Kobayashi and Kusumi, 1953); *Eosestheria middendorfii* (Jones, 1862); *Eosestheria* aff. *middendorfii* (Jones, 1862); *Eosestheria takechenensis* (Kobayashi and Kusumi, 1953); *Eosestheria linjiangensis* Zhang, 1976; *Eosestheria dianzhongensis* Chen, 1976; *Eosestheria subovata* Chen, 1976; *Eosestheria semiorbita* Chen, 1976; *Eosestheria subquadrata* Chen, 1976; *Eosestheria qingtanensis* Chen, 1976; *Eosestheria* (?) sp.

Type species: Following Art. 70.3* of the International Code of Zoological Nomenclature (http://www.nhm.ac.uk/hosted-sites/iczn/code/), the type species is now fixed as *Estheria middendorfii* Jones, 1862, misidentified as *Eosestheria fuxinensis* Chen, 1976 in the original designation by Zhang et al. (1976).

Remarks on the new type designation: *Eosestheria fuxinensis* was fixed as the type species of *Eosestheria* by Zhang et al. (1976). However, according to lirae distances and to analyses of shape (e.g., Figs. 4.3, 4.9; specimens 15437-15439), *E. fuxinensis* and *Diestheria yixianensis* are subjective synonyms. The genera *Diestheria* and *Eosestheria* have been simultaneously published by Zhang et al. (1976). As both species are considered type species for the respective genus, both genera would be subjective synonyms as well, if *E. fuxinensis* were kept as the type species for *Eosestheria*. By referring to article 24.2.2* of

*International Code of Zoological Nomenclature (http://www.nhm.ac.uk/hosted-sites/iczn/code/):

"**Art. 24.2.2.** Determination of precedence of names or acts by the First Reviser. If two or more names, different or identical, and based on the same or different types, or two or more nomenclatural acts, are published on the same date in the same or different works, the precedence of the names or acts is fixed by the First Reviser unless Article 24.1 applies."

"**Art. 67.9.** Misidentified type species. If a validly fixed type species is later found to have been misidentified, the provisions of Article 70.3 apply."

"**Art. 70.3.** Misidentified type species. If an author discovers that a type species was misidentified (…), the author may select, and thereby fix as type species, the species that will, in his or her judgment, best serve stability and universality, either 70.3.1. the nominal species previously cited as type species […], or 70.3.2. the taxonomic species actually involved in the misidentification. If the latter choice is made, the author must refer to this Article and cite together both the name previously cited as type species and the name of the species selected."

"**Art. 67.2.** Species eligible for type fixation (originally included nominal species). A nominal species is only eligible to be fixed as the type species of a nominal genus or subgenus if it is an originally included nominal species."

the International Code of Zoological Nomenclature, *D. yixianensis* is selected to have precedence over *E. fuxinensis*.

It would not serve stability to place species of the genus *Diestheria* into *Eosestheria*. The most frequently mentioned clam shrimp of the Yixian Formation, JSG Bed, is not *Eosestheria fuxinensis* but *Eosestheria ovata*, a species originally included in the genus and herein synonymized with *Eosestheria middendorfii* (see below). The new type designation is based upon articles 67.9*, 70.3*, and 67.2*. Because *Eosestheria middendorfii* (Jones, 1862) was originally included in the nominal genus *Eosestheria* by Zhang et al. (1976), it may replace *Eosestheria fuxinensis* as the type species (Art. 67.2*).

Remarks on the genus name: Through time, a number of genus names have been assigned to the original *[Estheria] middendorfii* Jones, 1862. They are *Estheria*, *Bairdestheria*, *Estherites*, *Euestheria*, and *Eosestheria*. *Eosestheria middendorfii* (Jones, 1862), was published as *[Estheria] middendorfii* Jones, 1862. *Estheria* was established as *Estheria dahalacensis* in 1837 (now *Leptestheria dahalacensis*). Subsequently, the genus had been assigned to many spinicaudatans, living or fossil. The first to subdivide "*Estheria*" was Sars (1898), who separated *Leptestheria* from the rest of the estheriids. However, the genus-group name *Estheria* Robineau-Desvoidy, 1830 was first used for a fly from Nova Scotia. It is therefore a junior homonym and must be replaced with a new name. Kobayashi and Huzita (1943) proposed *Estherites* in place of *Estheria* for fossil species, but chose a type species that cannot be grouped with *[Estheria] middendorfii*. According to Li and Batten (2005), the type specimen of *Estherites* was lost. In general, the type species of *Bairdestheria* Raymond (1946) (*[Estheria] donaciformis* Baird, 1849 [1850]), *Estherites* (*[Estheria] mitsuishii* Kobayashi and Huzita, 1942), and *Euestheria* (*[Posidonia] minuta* von Zieten, 1833) do not correspond to the diagnostic features of *[Estheria] middendorfii* Jones, 1862. For this reason, we place *[Estheria] middendorfii* in the next available genus *Eosestheria* Chen, 1976, following Zhang et al. (1976).

Original diagnosis of *Eosestheria*: "Carapace circular or ovate. Medium to large size. The growth bands are usually broad and flat. The number of growth lines is high. Irregular reticulation near the dorsal part as well as the anterior part. Polygons (triangular, squared, pentagonal, hexagonal) of moderate to big size and narrow-walled with a flat bottom. Reticulation is smaller and more regular-hexagonal near the umbo. Near the ventral and the posterior parts, the ornamentation changes from reticulate to wide-spaced radial lirae, which are often branching and curved. Some radial lirae are interconnected. The ornamentation in the central part of the carapace is marked by a transition from reticulation to radial lirae; the upper parts of the growth bands are reticulated, while the lower parts are marked by radial lirae. The change from reticulation near the anterior to radial lirae near the posterior is gradual." (Translated from Zhang et al. 1976.)

Discussion: It is not clear which specimen the diagnosis of *Eosestheria* was based on, but as radial lirae are reported to be wide-spaced, it fits to *Eosestheria middendorfii*-like specimens rather than the obsolete type species *E. fuxinensis,* which is regarded as a junior synonym of *Diestheria yixianensis* in this study.

Emended diagnosis of *Eosestheria*: Carapace very large, mostly ovate, dorsal margin long and slightly curved, position of A median-dorsal, position of B median-dorsal, position of C approximately median, position of the larval valve anterior to submedian, growth lines widely spaced. Mean radial lirae distance of visible growth band 24 in the anteroventral region of the carapace ranging between 74 μm and 90 μm (95% confidence).

Eosestheria middendorfii (Jones, 1862)
Figs. 4.11-4.17, 6.1-6.4

1862 *Estheria middendorfii* sp. nov.; Jones, 1862: 111-114, text-fig. 11, pl. 4: 12-22.
1946 *Bairdestheria middendorfii* (Jones, 1862); Raymond, 1946: 227-228, not figured.
1953 *Estherites middendorfii* (Jones, 1862); Kobayashi and Kusumi, 1953: 16-17, text-fig. 10-11, pl. 1: 1.
1976 *Liaoningestheria ovata* Chen, 1976: 161, pl. 46: 7, pl. 47: 1-7.
1976 *Eosestheria lingyuanensis* Chen, 1976: 154, pl. 41: 1-8.
1987 *Clithrograpta gujialingensis* Wang, 1987: 162, pl. 7: 4-5, pl. 9: 1-3.
1999 *Eosestheria ovata* (Chen, 1976); Chen, 1999: 115-117, pl. 1: 1, pl. 2: 1-3, pl. 3: 7-9.
1999 *Eosestheria* aff. *middendorfii* (Jones, 1862); Chen, 1999: 117-118, pl. 3: 1-3.
1999 *Eosestheria sihetunensis* Chen, 1999: 118, pl. 4: 4-7.
1999 *Eosestheriopsis gujialingensis* (Wang, 1987); Chen, 1999: 119, pl. 4: 8-12.

Name-bearing types: *Estheria middendorfii*
NHM 28227-28230.

Remarks: The syntype series of Jones (1862) is housed in the Natural History Museum, where it is listed as *Cyzicus* (*Euestheria*) *middendorfii*. The material was collected in Siberia (~51°30'N, 116°E; Fig. 4.1). See Table 4.4 for a complete list of analysed syntypes.

Original diagnosis of *[Estheria] middendorfii* Jones, 1862: "Carapace-valves thin, suboblong, straight on the dorsal margin, nearly the whole of which is occupied by

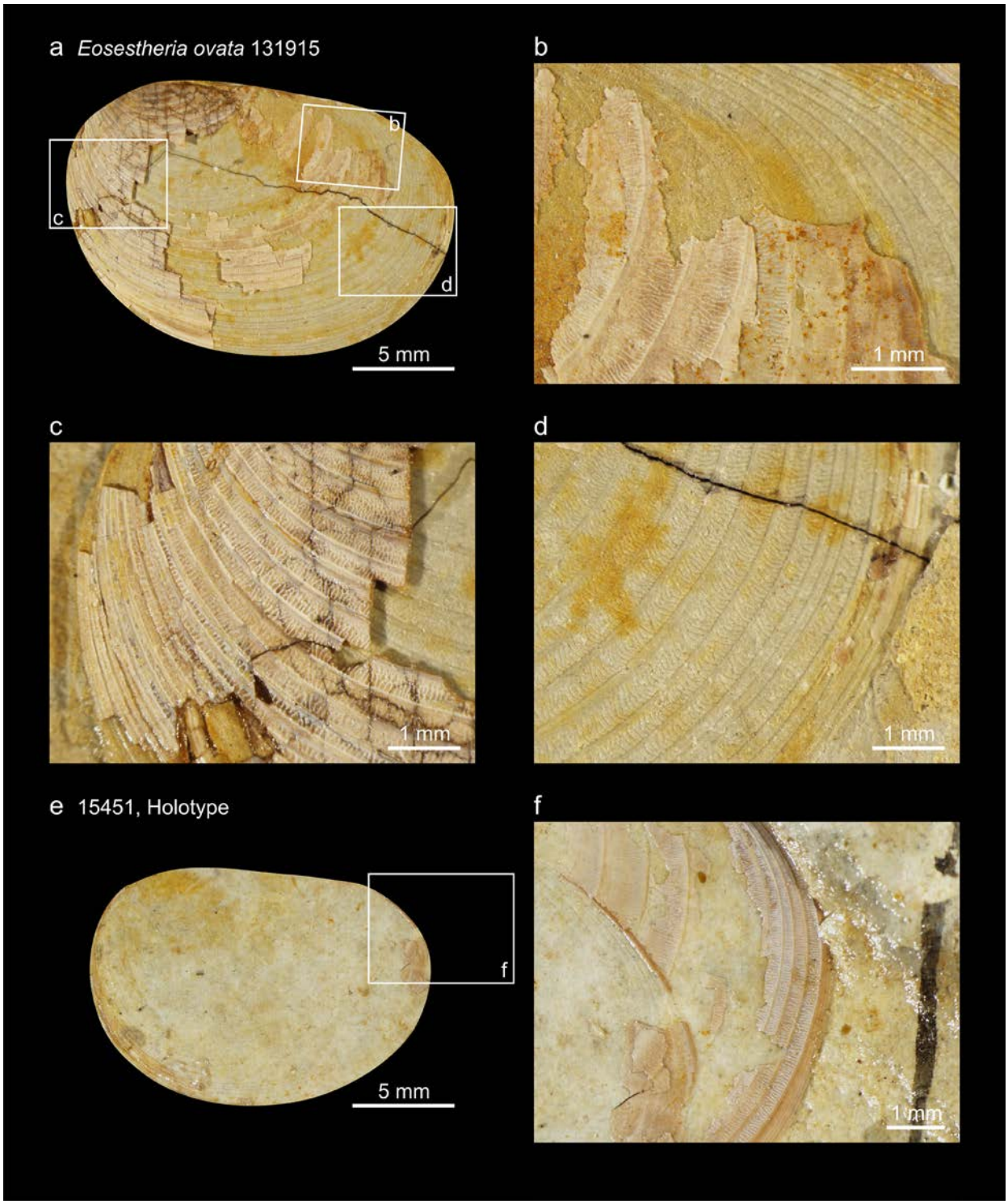

Fig. 4.11. *Eosestheria ovata*, junior synonym of *E. middendorfii*. (a-d) NIGPAS 131915. (a) Right valve traced, mostly preserved as external mould. The anterior dorsal extremity had to be reconstructed, mainly with the help of the left valve, which extends beyond the presented outline. (b) Posterodorsal region. Lirae are branching multiple times, ending in nodules that form a concentric ridge. (c) Anterior region. Carapace ornamentation on the left valve with transition of reticulation to liral ornamentation. (d) Posterior region. Comparatively regular, curved, and branching lirae. (e-f) NIGPAS 15451. (e) Right valve traced, mostly preserved as external mould. (f) Posterodorsal carapace features of the left valve.

the hinge-line; umbo forward, not preserved in the many specimens seen; ends well rounded, and nearly equal; ventral margin gently and nearly symmetrically curved. Ridges distinct, about twenty-four, sometimes more numerous, and crowded towards the ventral edge; interspaces bearing an open, irregular reticulation, often passing

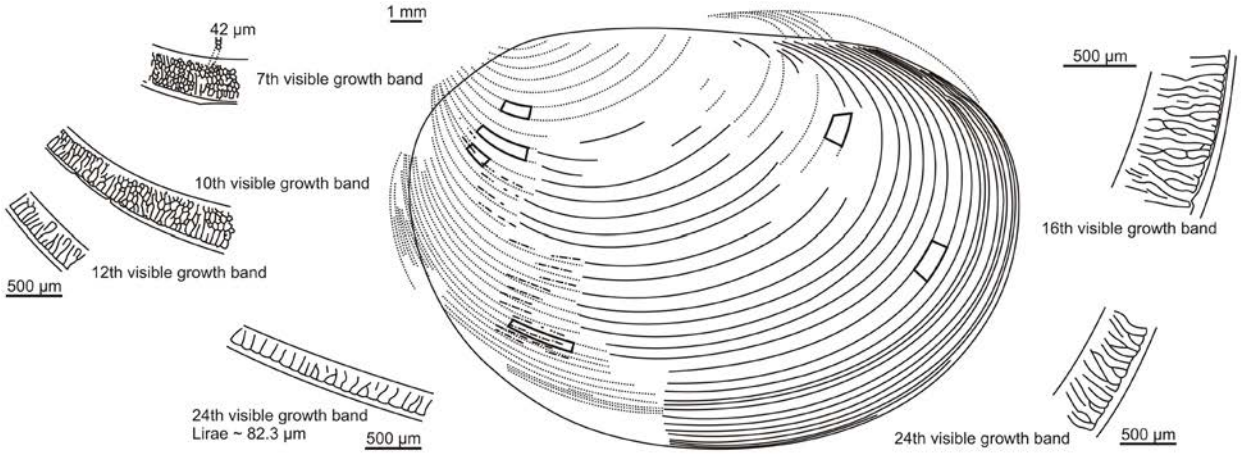

Fig. 4.12. *Eosestheria ovata* (131915) with selected ornamentational features. Radial lirae measurements (Fig. 4.3) at the anteroventral part of consecutive growth bands are marked with dashed lines.

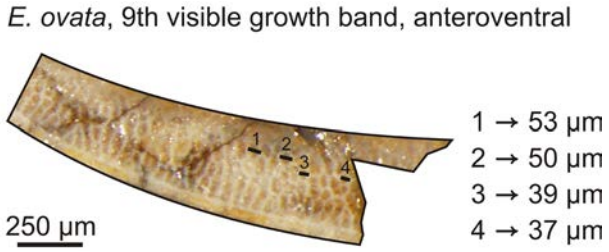

Fig. 4.13. Polygons on the anteroventral part of the 9th visible growth band of *Eosestheria ovata* (131915).

into thin, transverse, somewhat irregular riblets; the irregularly hexagonal areas of the reticulation, when highly magnified, are seen to be delicately punctured." (height 12.7 mm, length 21.2 mm; Jones, 1862)

Discussion: The delicate punctae within the polygons, as described in the original diagnosis of *[Estheria] middendorfii*, were not recognized by Chen (1999a), who examined the syntype material at the NHM in London, nor by Kobayashi and Kusumi (1953) in their material. From the inspection of the photographs of the syntype series, I suggest that either NHM 28228 or NHM 28229 should serve as the lectotype, depending on whether emphasis is placed on ornamentation or outline features. As ornamentation is deemed more diagnostic, NHM 28228 is favoured. A final decision will be made after the personal inspection of the material at the NHM. Nevertheless, the detailed drawings provided by Jones (1862) as well as linear measurements on the syntype series carried out in this study leave no doubt that numerous species of *Eosestheria* should be synonymised with *Eosestheria middendorfii* (Jones, 1862).

Table 4.12. Posterodorsal angles of five specimens of *E. middendorfii, E. ovata*, and *E. lingyuanensis*.

Specimen	Posterodorsal angle
E. middendorfii 28229	160.4°
E. ovata 15451	159.5°
E. ovata 131915	163.7°
E. lingyuanensis 15445	156.6°
E. lingyuanensis 15448	163.9°

Emended diagnosis: Carapace very large, ovate, dorsal margin short to long (ratio very close to the threshold value) and slightly curved, position of A median-dorsal, position of B median-dorsal, position of C median-posterior, submedian position of the larval valve, growth lines widely spaced. Radial lirae in the anteroventral and ventral regions of the carapace are wide-spaced, typical of the genus *Eosestheria*. Mean radial lirae distance at the ventral part of visible growth band 22 is ranging between 70 µm and 81 µm and that of the anteroventral part of the same growth band is ranging between 66 µm and 76 µm (95% confidence; NHM 28228). Radial lirae distance is progressively becoming smaller towards the anterodorsal region of a growth band and reticulation appears on the upper part of a growth band. Growth band 20 is coarsely reticulated anteroventrally. The transition to lirae on the anteroventral part of growth band 22 is fast, on which coarse reticulation is still developed on the upper part. Reticulation is dense near the umbo and becomes coarser on growth bands of later ontogenetic stages. Posterior lirae are more regular and narrower, their mean ranging between 45 µm and 50 µm on growth band 22.

Remarks on junior synonyms: Various new varieties, formae, genera, and species were split from, or allocated to, *[Estheria middendorfii]* (Table 4.11). Chi (1931) erected a new variety *[Estheria] mid-*

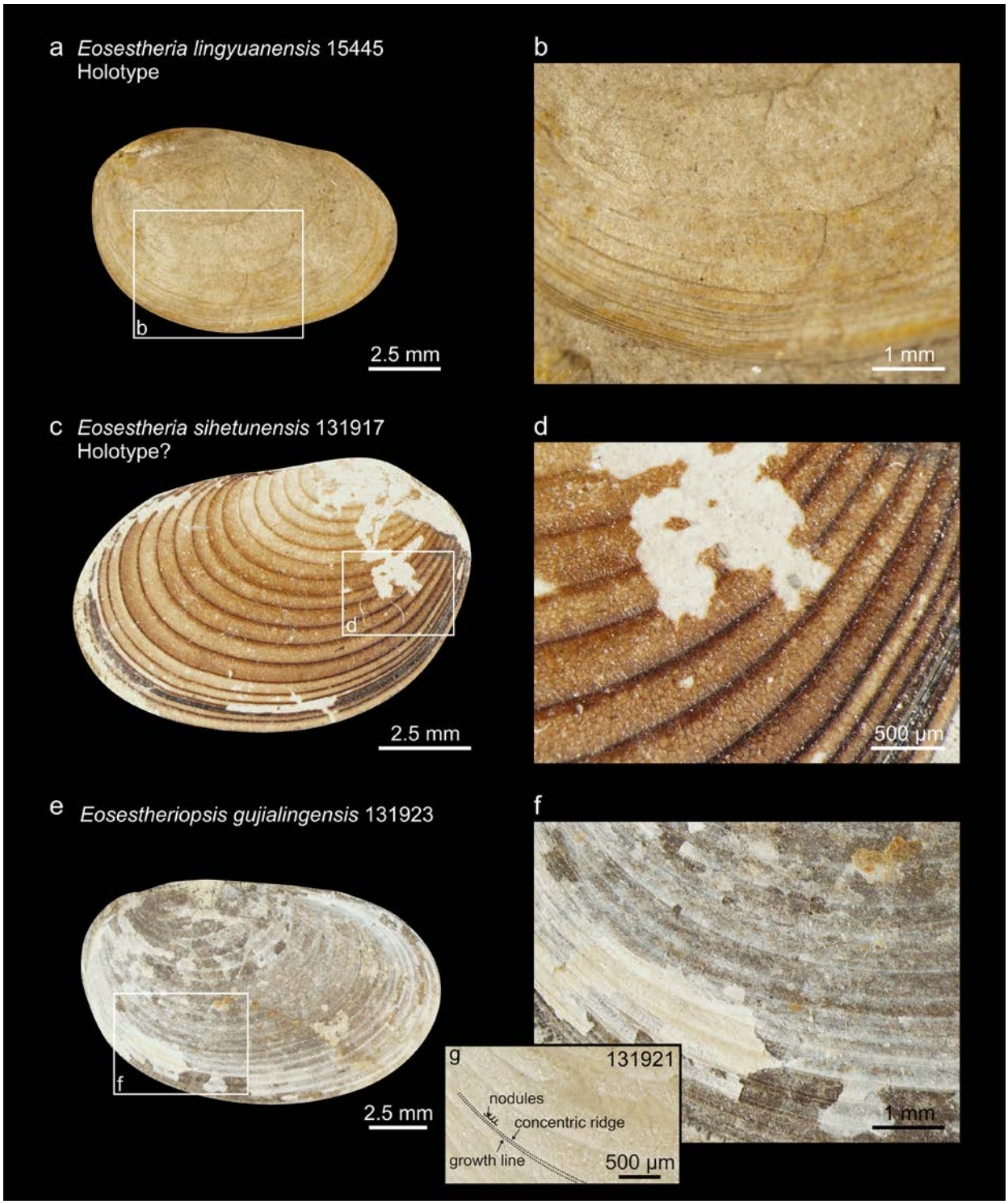

Fig. 4.14. (a, b) *Eosestheria lingyuanensis* NIGPAS 15445. (a) Right valve traced, mostly preserved as external mould. (b) Ventral region. Radial lirae restricted to growth bands of later ontogenetic stages. (c-d) *Eosestheria sihetunensis* NIGPAS 131917. (c) Right valve traced, anterior dorsal extremity reconstructed. (d) Anterior region. Growth bands reticulated and radial lirae appear on the last few growth bands. (e-g) *Eosestheriopsis gujialingensis*. (e, f) NIGPAS 131923. Left valve traced, of which only remnants are left. Interior of right valve mostly visible. Ornamentation is generally poorly preserved. Anteroventral region marked by radial lirae. (g) NIGPAS 131921. Nodular ornamentation on mainly reticulated growth bands.

dendorfii var. *sinensis*, exclusively on the basis of size, with the carapace of the new variety being smaller than *E. middendorfii*. Ornamentation was reported to be the same as the Siberian form described by Jones (1862). Kobayashi and Kusumi (1953) distinguished three varieties (*jeholensis*, *elongata*, *chii*)

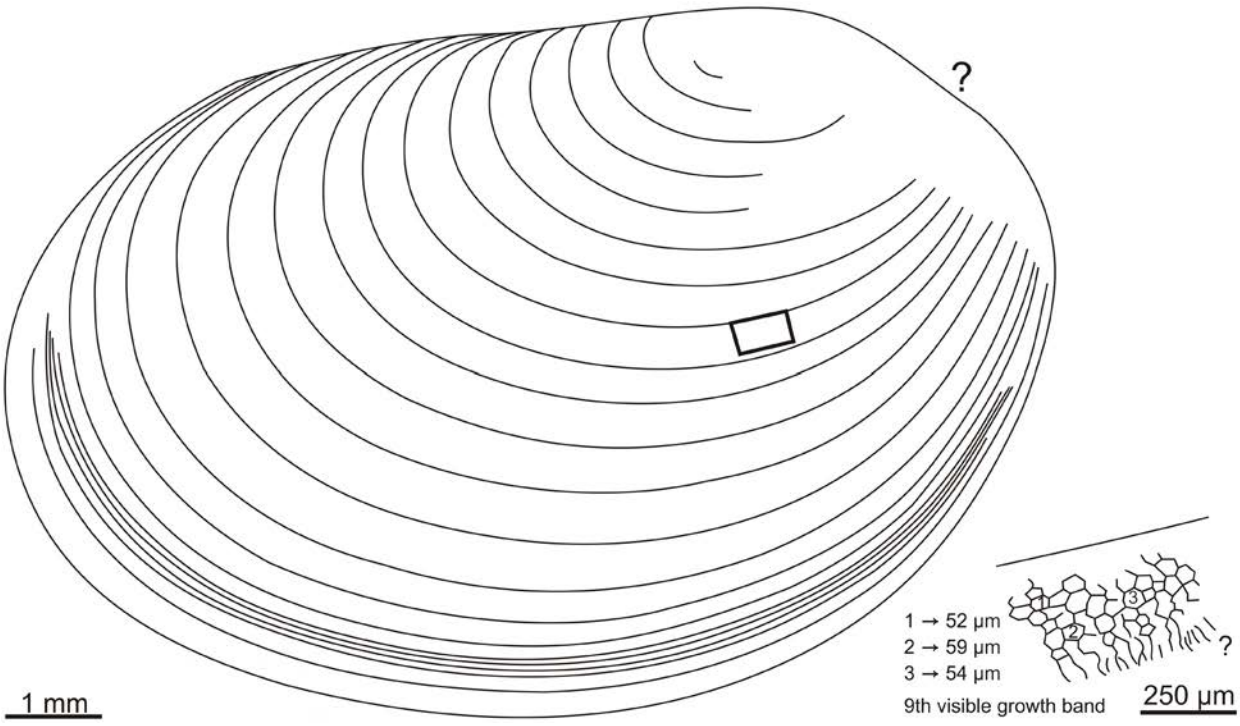

Fig. 4.15. *Eosestheria sihetunensis* (NIGPAS 131917). Original pictured in Fig. 4.14c.

and four formae (*subelongata*, *peipiaoensis*, *intermedia*, *takechenensis*) on top of the typical form. A year later, Kobayashi (1954) corrected the genus name of the leading member of the Jehol clam-shrimp fauna to *[Euestheria] middendorfii*. He claimed *[Euestheria] middendorfii* was a waste-basket taxon, as it was so variable. Varieties and formae of Kobayashi and Kusumi (1953) have been reassigned in Zhang et al. (1976) according to Table 4.11.

Eosestheria middendorfii is the senior synonym of five of the ten species described from the Yixian Formation by Chen (1999a). Species descriptions of Chen (1999a) are often very similar. For example, the main differences of *E.* aff. *middendorfii* (in comparison to *E. ovata* and *E. lingyuanensis*) are smaller polygon width and more closely spaced radial lirae. This is tested herein.

Eosestheria ovata (Chen, 1976). – *E. ovata* is perhaps the most famous clam-shrimp species of the Yixian Formation today. Its ornamentational features (Figs. 4.11-4.13) are analogous to *E. middendorfii*, the senior synonym, which was a well-known clam-shrimp species of the Jehol Biota up to 1976, when Zhang et al. (1976) split the taxon into several species. Identical ornamentation of the two species is corroborated by lirae measurements (Fig. 4.3); the null hypothesis of equal mean lirae distance cannot be rejected at a significance level of 0.01. *E. ovata* and *E. middendorfii* are very similar in shape. The confidence interval of *Eosestheria* is the smallest of all genera analysed (Fig. 4.9), implying very small variation in shape and the presence of only one species.

Eosestheria lingyuanensis Chen, 1976. – The micro-ornamentation of *E. lingyuanensis* (Fig. 14a, b) strongly resembles growth bands of early ontogenetic stages of *E. middendorfii*. The specimens analysed are mostly reticulated and radial lirae appear near the carapace margin on growth bands of later ontogenetic stages. Mean radial lirae distances match those of *E. ovata* specimen 131915 (Fig. 4.3). Anteroventral polygons of the reticulation are on average 48 µm wide on the 10th growth band, which is similar to measurements presented for *E. ovata* in Fig. 4.13. With a length of 10.6 mm (holotype), *E. lingyuanensis* is the smallest of the species assigned to *E. middendorfii* (Table 4.5; Fig. 4.6). Chen (1999a) acknowledged that the ornamentation of *E. lingyuanensis* and *E. ovata* was similar and a more pronounced posterodorsal angle for *E. lingyuanensis* was put forward as the main difference between the two species. However, a closer inspection shows no noteworthy differences between the posterodorsal angles (Table 4.12). *E. lingyuanensis* is a junior synonym that marks juveniles of *E. middendorfii*.

Eosestheria sihetunensis Chen, 1999. – Chen (1999a) pointed out that *E. sihetunensis* (Figs. 4.14c, 4.15, 4.16) was very similar to *E. ovata*. *E. sihetunensis* is smaller and exhibits narrower radial lirae, located only on the lower parts of growth bands. These

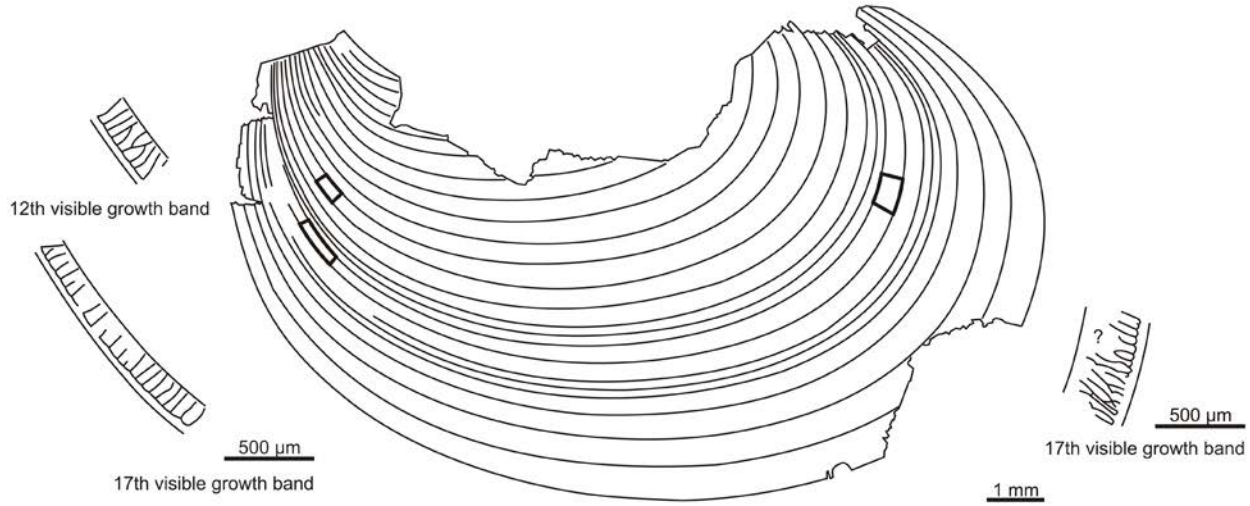

Fig. 4.16. *Eosestheria sihetunensis* (NIGPAS 131916). Ornamentation is excellently preserved.

are generally juvenile features of *E. middendorfii*. It is not clear, which of the two specimens figured by Chen (1999a; 131917, Fig. 4.15; 131916, Fig. 4.16) is the holotype, as photographs of *E. sihetunensis* do not correspond to the figure captions in the publication. The two specimens were apparently swapped. The species description of Chen (1999a) better fits specimen 131917. Radial lirae for instance are clearly developed in specimen 131916. While the ornamentation is well preserved in both specimens, both perimeters are incomplete, rendering growth line counts impossible. A scaled superimposition (Fig. 4.17) of both *E. sihetunensis* specimens and *E. ovata* reveals identical ornamentation for the respective ontogenetic stages. Mean growth-band widths (Fig. 4.4) lie well within the confidence interval established for all *Eosestheria* specimens. *E. sihetunensis* is therefore a juvenile of *E. middendorfii*.

Eosestheriopsis gujialingensis (Wang, 1987). – *Eosestheriopsis gujialingensis* was originally described as *Clithrograpta gujialingensis* by Wang (1987), whose generic diagnosis* matches juvenile specimens of *Eosestheria*. Chen (1999a), however, declared *Clithrograpta* a junior synonym of *Eosestheriopsis* and described specimens from Sihetun, which were inspected in this study (131921-131923; Fig. 4.14e-g). The main diagnostic features reported by Chen (1999a) were irregular reticulation and aligned nodules on the anterior part of the carapace. These nodules result from the termination of lirae (Fig. 4.14g). Similar features can also be recognized in other *Eosestheria* specimens of the same publication. According to Chen (1999a), *E. gujialingensis* is similar in shape to *Eosestheriopsis dianzhongensis* (26994), type species of the genus *Eosestheriopsis*. This is, however, not the case (Figs. 4.9, 4.10): *E. dianzhongensis* plots well outside the 95% confidence interval of *Eosestheria* and *Eosestheriopsis gujialingensis* projected on *PC1* versus *PC2*. Chen (1999a) recognized two morphs in *E. gujialingensis*, which he attributed to sexual dimorphism (Chapter 5). Lirae distance is analogous to that of *Eosestheria* (Fig. 4.3). Considering all data, the specimens described by Chen (1999a) are assigned to *Eosestheria middendorfii*. Although the type material was not available for inspection, the figures provided by Wang (1987) renders *Clithrograpta gujialingensis* a junior synonym of *E. middendorfii*.

Genus *Yanjiestheria* Chen, 1976

Type species: *Yanjiestheria bellula* Chen, 1976

Original Diagnosis: "Carapace of moderate size, ovate, circular, or triangular. Growth bands densely reticulated near the anterior and dorsal regions, with comparatively broad-walled, irregular, and deep polygons. Polygon-diameters are smaller than 0.02 mm. Polygons on the external mould appear as small, irregular, curved, or elongated nodes. Radial lirae form many discontinuous fine lines. The small polygons convert to thin radial lirae towards the ventral and posteroventral regions. Radial lirae are straight or curved, branching upwards or downwards, some are interconnected." (Translated from Zhang et al., 1976 and Chen, 1999a.)

*Original diagnosis of *Clithrograpta* Wang, 1987: "Main sculpture is reticulate on the valve, ridges only on the posterior and anterior ventral region, 0.04-0.10 mm in diameter of mesh." *Clithrograpta gujialingensis* is the type species.

Yanjiestheria? *beipiaoensis* Chen, 1999
Fig. 4.18a

1999 *Yanjiestheria*? *beipiaoensis* sp. nov.; Chen, 1999: 119-120, pl. 2: 10-12.

Name-bearing type: *Yanjiestheria*? *beipiaoensis* NIGPAS 131919.

Original diagnosis: "Carapace small, ovate, almost circular. Length 6-9 mm, height 4-8 mm. Anterior, posterior, and ventral margins rounded, the posterior margin is slightly flattened. The anterior height is much larger than the posterior height. The dorsal margin is long and the umbo is located near the anterior. The total number of growth bands is 25. Growth bands become narrower near the ventral margin. Dorsal region finely reticulated. Reticulation is turning into radial lirae towards the ventral region. Radial lirae are interconnected." (Translated from Chen, 1999a.)

Discussion: Chen et al. (2007) noticed the smaller and denser carapace reticulation and thinner and more closely spaced radial lirae of *Yanjiestheria* (Fig. 4.18a) in contrast to *Eosestheria*, which is corroborated by Fig. 4.3. Growth bands are very narrow-spaced throughout. Growth-band widths (Fig. 4.4; disregarding crowding) fall outside the confidence intervals of both, *Eosestheria* and *Diestheria,* so there might be a biological signal involved. Carapace shape (Figs. 4.8-4.10), though similar to *Eosestheria*, can be separated from both *Eosestheria* and *Diestheria*.

Emended diagnosis: Carapace of moderate size, elongate, dorsal margin short or long (*Ch*/*L* around 0.65) and slightly curved, position of A median-dorsal, position of B median-dorsal, position of C median-posterior, submedian position of the larval valve, growth lines separate. Mean radial lirae distance at the anteroventral to ventral part of visible growth band 17 ranging between 19 µm and 24 µm (95% confidence).

Genus *Diestheria* Chen, 1976

Type species: *Diestheria yixianensis* Chen, 1976

Remarks: It is proposed herein that *Diestheria yixianensis* is a junior synonym of *D. jeholensis*, which was established as *[Estherites] middendorfii* var. *jeholensis* by Kobayashi and Kusumi (1953). The species was reassigned to *Diestheria* by Zhang et al. (1976; Table 4.11). In this study, only the material of Zhang et al. (1976) has been viewed and analysed. The type material of *[E.] middendorfii* var. *jeholensis* was not available for inspection, so only the figures presented by Kobayashi and Kusumi (1953) could be compared with other *Diestheria* specimens. *D. yixianensis* is kept as a discrete species for now. After an inspection of the type material of *D. jeholensis* and verification of synonymy, the type species of the genus *Diestheria* should become *D. jeholensis*.

Original Diagnosis: "Carapace large, ovate, circular, or rectangular. Growth bands have a similar ornamentation as *Eosestheria.* Radial lirae of *Diestheria* are covered by hexagonal ornamentation in the posterior and ventral regions of the carapace. There is a coarse polygonal overprint on the upper part of every growth band, which appears as larger flat nodules on outer moulds." (Translated from Zhang et al., 1976 and Chen, 1999a.)

Discussion: The original diagnosis strongly focusses on the polygonal overprint, which is only displayed, where growth lines are not crowded. It is faint on the ventral part of the carapace. Other robust generic characteristics are lirae distances and carapace shape.

Emended diagnosis: Carapace extremely large, elongate to ovate, dorsal margin mostly long and slightly curved, position of A mainly median-dorsal, position of B median-dorsal, position of C approximately median to median-posterior, position of the larval valve anterior to submedian, growth lines widely spaced. Mean radial lirae distance at the anteroventral part of visible growth band 26 ranging between 40 µm and 46 µm (95% confidence). A coarse polygonal overprint covering narrow-spaced lirae may be developed on the upper part of growth bands near the anterior and posterior regions of the carapace. It is often missing, though, due to its poor preservation potential and possibly because the polygonal overprint was originally not so well developed. The difference between mean radial lirae distances of *Eosestheria middendorfii* and *Diestheria yixianensis* is statistically significant (131915 versus 15455; $p(H0)$ = 1.43E-12 < 0.01; tested for the anteroventral region).

Diestheria jeholensis (Kobayashi and Kusumi, 1953)
Fig. 4.18c

1953 *Estherites middendorfii* var. *jeholensis* sp. nov.; Kobayashi and Kusumi, 1953: 17-19, pl. 1: 2-4, pl. 2: 15-16.
?1976 *Diestheria yixianensis* Chen, 1976*: 176, pl. 57: 1-8.
1976 *Eosestheria fuxinensis* Chen, 1976: 153, pl. 40: 1-4.

**Diestheria yixianensis* is most likely a junior synonym of *D. jeholensis*, but it is treated as a separate species in this study, because the holotype of *D. jeholensis* was not available for examination.

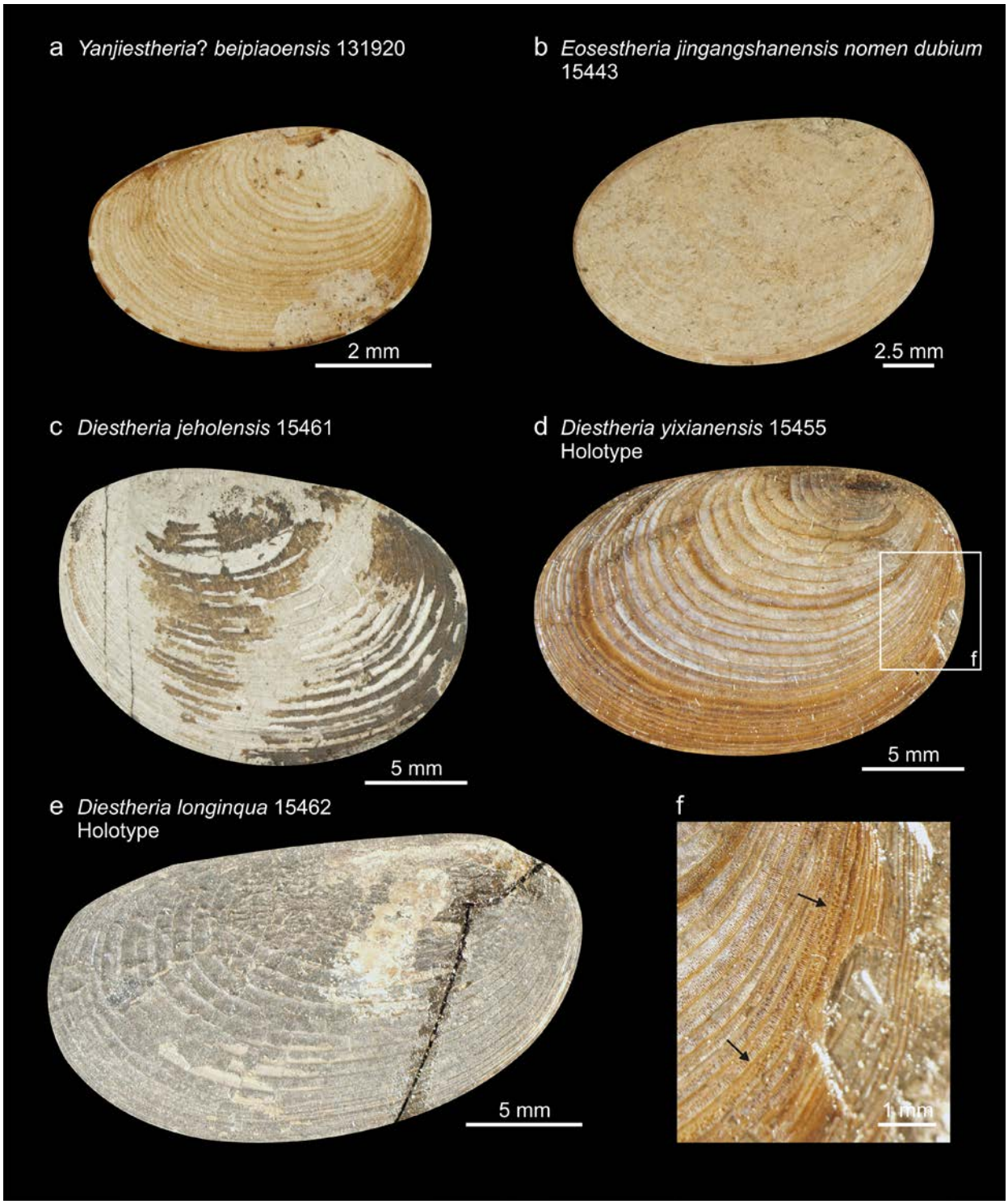

Fig. 4.18. (a) *Yanjiestheria*? *beipiaoensis* NIGPAS 131920. Left valve traced. Ornamentation not preserved on this specimen, but on the holotype NIGPAS 131919. (b) *Eosestheria jingangshanensis* nomen dubium NIGPAS 15443. Left valve traced, preserved mostly as external mould. (c) *Diestheria jeholensis* NIGPAS 15461. Right valve traced, preserved as external mould or interior of valve. (d) *Diestheria yixianensis* NIGPAS 15455, holotype. Right valve traced, carapace ornamentation well preserved. (e) *Diestheria longinqua* NIGPAS 15462, holotype. Left valve traced, mainly preserved as external mould. (f) Anterior of *Diestheria yixianensis*. Ornamentation marked by dense reticulation in early ontogenetic stages, a transitional ornamentation of reticulation and radial lirae on the same growth band, and subsequent radial lirae in older ontogenetic stages. A genus-specific coarse polygonal overprint is arrowed.

Name-bearing type: MA 04754 (Holotype); The University Museum, The University of Tokyo.

Remarks: The homepage of The University Museum (The University of Tokyo) refers to a type series with

three syntypes (MA 04754-56). The type designation can be easily overlooked, but the holotype was fixed within "observations" of *Estherites middendorfii* var. *jeholensis* by Kobayashi and Kusumi (1953), where it became clear that they intended specimen MA 04754 to be the holotype.

Original diagnosis: "Carapace large, subovate; dorsal margin straight or very slightly arcuate; umbo terminal or almost terminal; umbonal angle about 130 degrees; a half to a third of the anterior margin below the umbo nearly straight; ventral margin describing a large arc, more rounded on the antero-ventral than on the postero-ventral side; posterior margin abruptly swings forward above the mid-height and transmits into the dorsal margin gradually. Thus the outline is asymmetrical, expanding anteriorly; carapace becomes tallest in a little anterior to the center; length attains at the maximum above the center. Growth lines distinct, sometimes prominent, generally 27 or more, widely spaced except the vicinity of the periphery where they are close-set. In the umbonal half the intervals ornamented with reticulae, but merges distally with the radial lirae in the peripheral intervals." (Dimensions of MA 04754 H = 14.0 mm; L = 21.4 mm; Kobayashi and Kusumi, 1953.)

Discussion: Unfortunately, it was not possible to examine the type specimen of *D. jeholensis*. The two specimens analysed (15457, 15461) belong to the publications of Zhang et al. (1976) and Chen (1999a). Therefore, an emended diagnosis cannot be presented. From the original figures in Kobayashi and Kusumi (1953), it is suspected that *D. yixianensis* is in fact a junior synonym of *D. jeholensis*. But according to Chen (1999a), the polygonal overprint indicative of *Diestheria* is only faintly developed in the posteroventral region of *D. jeholensis*, setting this species apart from *D. yixianensis*. This difference is, however, most likely a matter of variation in preservation. Lirae in the anteroventral region of the carapace are narrow-spaced (47 µm; ~25th visible growth band; Table 4.7), which is typical of the genus *Diestheria*. *D. yixianensis* is treated as a valid species in this study.

Remarks on junior synonym:

Eosestheria fuxinensis Chen, 1976. – According to Zhang et al. (1976), shape and ornamentation is similar to *E. middendorfii*, with *E. fuxinensis* being shorter and rounder. Lirae measurements (Fig.4.3; Table 4.7) and Fourier shape analysis (Fig. 4.9) associate the analysed specimens of the types series (15437-15439) of *E. fuxinensis* with *Diestheria yixianensis*.

Diestheria yixianensis Chen, 1976
Fig. 4.18d

1976 *Diestheria yixianensis* sp. nov.; Chen, 1976: 176, pl. 57: 1-8.

Name-bearing type: *Diestheria yixianensis* 15455 (Holotype).

Original diagnosis: "Carapace large, short-ovate, almost rectangular. Length 19-21 mm, height 12.5-14 mm. Dorsal margin straight, umbo located near the anterior. Growth lines strong, growth bands broad and flat. Several narrower growth bands located near the ventral region of the carapace. 23-35 growth bands in total. Irregular polygonal ornamentation in the anterior region, polygon diameters become smaller and their shape more regular towards the dorsal region. Likewise, polygon diameters become bigger towards the ventral region with an elongated shape. Radial lirae appear towards the ventral region. Transition from reticulation to radial lirae on the same growth band with polygons on the upper part and lirae on the lower part. The posterior region of the carapace displays almost only radial lirae. The growth bands are crowding near the ventral part and the radial lirae become more pronounced. The growth bands are broad near the dorsal part. In the central part of the carapace, lirae are usually pronounced and regularly curved. Lirae near the posterior are overprinted by coarse polygons. This overprint can also be seen in the anteroventral region of the carapace, where it is not as pronounced, though. It is not present at the anterodorsal part." (Translated from Zhang et al., 1976 and Chen, 1999a.)

Discussion: According to Chen (1999a), the main difference between *Diestheria yixianensis* and *D. jeholensis* is that the coarse polygonal overprint is not as well developed in *D. jeholensis*, where it can only be recognized in the posteroventral part. Apart from it being a very subtle difference, it might well be a taphonomic effect. The polygonal overprint does not seem very resistant to the alteration of the carapace. Therefore, *D. yixianensis* is most likely a junior synonym of *D. jeholensis*. A definite decision on this matter can only be made after the holotype of *D. jeholensis* has been examined. The ornamentation of *D. jeholensis* pictured in Kobayashi and Kusumi (1953) seems identical to that of *D. yixianensis*. In their description for *D. jeholensis*, Kobayashi and Kusumi (1953) mention mainly outline features, stating that ornamentation was of the "same kind" as *Estherites middendorfii*.

Chen (1999a) mentioned 23-35 growth lines, a re-examination of the holotype of *Diestheria yixianensis* (15455) yielded 38 visible growth lines. The diagnosis will be emended for carapace shape based on Table 4.2 and several other properties.

Emended diagnosis: Carapace extremely large and ovate, dorsal margin long and slightly curved, position of A median-dorsal, position of B median-dorsal, position of C nearly median, anterior position of the larval valve, growth lines widely spaced. Radial lirae in the anteroventral region of the carapace narrow-spaced (43 μm; 26th visible growth band; Table 4.7). A coarse polygonal overprint covering close-set lirae is developed on the upper part of growth bands near the anterior and posterior parts of the carapace, respectively. Posterior lirae narrower, their mean ranging between 25 μm and 28 μm (95% confidence; 31st growth band).

Diestheria longinqua Chen, 1976
Fig. 4.18e

1976 *Diestheria longinqua* sp. nov.; Chen, 1976: 177-178, pl. 59: 1-6.

Name-bearing type: *Diestheria longinqua* 15462 (Holotype).

Original diagnosis: "Carapace long to ovate and of large size. Length 23.5 mm, height 12.5 mm. The height-length ratio is almost 1:2. The dorsal margin is straight, almost 16 mm. The dorsal and ventral margins are almost parallel. The umbo is small and located near the anterior. The growth bands are broad and flat, becoming narrow towards the ventral region of the carapace. There are 31 growth bands in total." (Translated from Zhang et al., 1976.)

Discussion: The ornamentation of *Diestheria longinqua* is the same as in *D. yixianensis*, and Chen (1999a) proposed that *D. longinqua* was a male of *D. yixianensis*. If this was true, the holotype of *D. longinqua* 15462 would lose its name-bearing function and become an allotype to the holotype of *D. yixianensis* (15455). Sexual dimorphs can only be recognized with a larger set of specimens, though.

Emended diagnosis: Carapace extremely large, elongate, dorsal margin long and slightly curved, position of A dorsal-median, position of B median-dorsal, position of C median-posterior, anterior position of the larval valve, growth lines widely spaced. Radial lirae in the anteroventral region of the carapace narrow-spaced (45 μm; ~29th visible growth band).

Table. 4.13. Of the ten species in four genera described by Chen (1999a), five species in three genera are kept (in bold). *Diestheria yixianensis* is most likely a junior synonym of *Diestheria jeholensis*, but the holotype of the latter was not available for examination.

Species	Present status
E. middendorfii (Jones, 1862)	Valid species
Eosestheria ovata (Chen, 1976)	Junior synonym
Eosestheria lingyuanensis Chen, 1976	Juvenile; junior synonym
Eosestheria aff. *middendorfii* (Jones, 1862)	Junior synonym
Eosestheria sihetunensis Chen, 1999	Juvenile; junior synonym
Eosestheriopsis gujialingensis (Wang, 1987)	Junior synonym
Yanjiestheria? beipiaoensis Chen, 1999	Valid species
Diestheria jeholensis (Kobayashi and Kusumi, 1953)	Valid species
Diestheria yixianensis Chen, 1976	Valid species, but most likely a junior synonym of *Diestheria jeholensis*
Diestheria longinqua Chen, 1976	Valid species, sexual dimorph?
Eosestheria jingangshanensis Chen, 1976	*nomen dubium*

Nomen dubium

1976 *Eosestheria jingangshanensis* Chen, 1976: 154, pl. 40: 5-8, pl. 41: 9.

Eosestheria jingangshanensis **Chen, 1976.** – The holotype of *Eosestheria jingangshanensis* (15443; Fig. 4.18b) does not display sufficient diagnostic features, neither for the establishment of a species nor for the assignment to *Eosestheria* or *Diestheria* (Figs. 4.5, 4.7, 4.8). Its type specimen bears only little ornamentation, leaving mainly outline features to work with. Fourier shape analysis plots *E. jingangshanensis* into the convex hull spanned by *Eosestheria*, but so close to *D. yixianensis* (Figs. 4.9, 4.10b, d) that they are shown to be almost identical regarding various important shape variables. Lirae measurements remained inconclusive. As such, it becomes a *nomen dubium*.

Conclusions

Five of the ten species described by Chen (1999a) were synonymised with *Eosestheria middendorfii* according to Table 4.13. *Diestheria* species as well as *Yanjiestheria*? *beipiaoensis* are kept, although it can be expected that *D. yixianensis* will be revealed as a junior synonym of *D. jeholensis* once the type specimen of the latter has been examined. *Eosestheria jingangshanensis* is considered a *nomen dubium*.

Diestheria can be separated from *Eosestheria* by the spacing of radial lirae. *Yanjiestheria*? *beipiaoensis*, in turn, exhibits significantly smaller growth-band widths than *Eosestheria* and *Diestheria*. The separation of species through size and shape variables is reasonably good, the most important variables are, in descending order of importance: (1) *H*/*L* ratio, (2) prominence of the umbo, (3) displacement of the dorsal margin relative to C, (4) position of B with respect to valve height (similar to ratio *b*/*H*), (5) position of the umbo, and (6) angularity of the anterior margin. The shape variation in *Eosestheria*-specimens is limited compared to that of other genera, implying the affiliation of the analyzed specimens to just one species. Therefore, a combination of PCA of linear measurements, Fourier shape analysis, and lirae measurements is deemed most diagnostic for the separation of species from the Early Cretaceous Yixian Formation. A reduced dataset of five robust linear measurements (*Arr*, *Ch*, *Cr*, *H*, and *L*), in contrast to all nine linear measurements, is advised for multi-species samples.

The high diversity recognized within Lake Sihetun is artificial. This result questions the proposed major evolutionary radiation within late Mesozoic clam shrimps. Intraspecific variation in size and shape has evidently been misinterpreted within *E. middendorfii*. Sexual dimorphism, ontogenetic variation, and phenotypic variation within *E. middendorfii* of Lake Sihetun will be delineated in the following chapters 5 and 6.

Chapter 5: Sex determination of the Early Cretaceous clam shrimp *Eosestheria middendorfii* of the Yixian Formation (China)

Chapter 5 is a joint project of the following authors:

Manja Hethke[1], Franz T. Fürsich[1], Baoyu Jiang[2]
[1]*GeoZentrum Nordbayern, FG Paläoumwelt, Germany*
[2]*School of Earth Sciences and Engineering, Nanjing University, China*

Introduction

Spinicaudata ("clam shrimps") rival many other taxa concerning the diversity of their sexual systems. There is a wide range of reproductive strategies by which genetic information is passed on to the next generation: (1) obligate sexual reproduction (dioecy), (2) self-fertilization with the occasional presence of males (androdioecy), or (3) unisexuality (self-fertilization or parthenogenesis; Sassaman and Weeks, 1993; Sassaman, 1995; Weeks et al., 2009). Although dioecy is most common, especially among the Cyzicidae and the Leptestheriidae, unisexual reproduction is present in all of the three extant families of the Spinicaudata. Androdioecy evolved within the Limnadiidae (Sassaman, 1995; Roessler, 1995; Weeks et al., 2009). This diversity in breeding systems makes the Spinicaudata a model clade for the study of reproductive system evolution (Astrop et al., 2012). Unisexuality has arisen from an ancestral condition of obligate sexuality. In the Leptestheriidae and the Cyzicidae this happened independently of that in the Limnadiinae, possibly through different evolutionary pathways (Sassaman, 1995). It has been proposed that two discrete sexes are the ancestral state for the fossil family Eosestheriidae (Stigall et al., 2014; see Chapter 4 for a discussion on the family), to which the fossil species analyzed in this study belongs.

The recognition of the sexual system in fossil species is, however, obscured by the incomplete preservation of organismal characters in the fossil record. The sex determination of modern clam shrimps is carried out through the differentiation of modified claspers in males and the presence of oocytes in hermaphrodites or females (Sassaman and Weeks, 1993). However, as oocytes are often not preserved, their absence does not instantly classify a specimen as male. The presence of claspers, in contrast, unambiguously indicates a male individual. While oocytes, or their imprints, are occasionally preserved, claspers are particularly rare. Notable examples of lagerstätten that are marked by the presence of claspers are the Middle Jurassic Jiulongshan Formation of northern Hebei (Zhang et al., 1990) and the Late Carboniferous Castlecomer Fauna of Ireland (Orr and Briggs, 1999).

In order to pinpoint the sexual system of a clam-shrimp species, one has to look for evidence of possible sexual dimorphism in a first step and, if present, 'correctly' allocate a sex to each of the two morphotypes. Subsequently, simple population sex ratio calculation is sufficient to determine the sexual system of a species (~ 50% males → dioecy; 5-30% males → androdioecy; Weeks et al., 2008).

Astrop et al. (2012) pioneered the identification of sexually dimorphic carapace shapes by studying dimorphism in a number of extant species, in which the sex of individuals was known *a priori*. While morphometric separation was excellent for some species, methods were not able to adequately separate sexual morphotypes in all of the extant species studied. Sexual dimorphism was especially subtle in the representative of the Cyzicidae. Astrop et al. (2012) also identified female and male morphotypes in a fossil clam shrimp, the Jurassic *Carapacestheria disgregaris*. However, as will be shown in this study the apparent superb separation within the fossil sample is an artefact and the methodology they employed will always lead to excellent separation. Consequently, the same methodology yielded perfect separation in a subsequent study (Monferran et al., 2013).

In this study, an approach to the identification of sexual morphs and the reproductive system is proposed on the basis of the Early Cretaceous species *Eosestheria middendorfii* from the Yixian Formation of western Liaoning, which is closely related to the Cyzicidae (see Chapter 4). The advantages of this study are (1) that egg clutches are preserved, which pinpoint female and hermaphroditic valves, and (2) that all studied specimens have been obtained

from the same horizon. Fossil-yielding horizons are well separated in the sediments of Lake Sihetun (see Chapter 1). This reduces environmental bias to shape considerably, as all analyzed specimens are considered to have resulted from the same cohort. The main problem is that egg clutches are occasionally only faintly preserved and that there is a gradual transition between their presence and absence. Therefore, the lack of egg clutches does not automatically designate a specimen as male. Consequently, the primary hypothesis to be tested in this study is whether specimens exhibiting egg clutches are morphologically distinct from specimens without.

Discussion of methods

The important contribution of Astrop et al. (2012) was to test whether sexes of Recent clam shrimps exhibit statistically different carapace shapes. They accomplished this through a combination of eigenshape analysis and hierarchical clustering using Ward's method. The equality of multivariate means was tested and discriminant scores were calculated. But the proposed utilization of analogous methodology for the sex determination in Recent and fossil taxa does not work owing to three reasons:

(1) Faced with the lack of egg clutches, Astrop et al. (2012) separated two morphological groups by means of hierarchical cluster analysis (Ward's method) of the first four eigenshapes. However, Ward's method is known to well-separate clusters. It seeks unions of subsets that are associated with the lowest possible error sum of squares (Ward, 1963). This is desirable, but it also assumes the presence of dimorphism and multiple sexes. Importantly, Ward's method tends to produce clusters with comparable numbers of objects (Milligan, 1980; Hammer and Harper, 2006). However, the identification of the reproductive system is sensitive to the sex ratio (Weeks et al., 2008). Therefore, Ward's method is not suitable for identifying reproductive systems.

(2) Although the methods employed for both Recent and fossil specimens were the same, the underlying assumptions were quite different. Recent specimens were grouped *a priori* according to their sexes, while fossil specimens were statistically grouped using Ward's method, which produced two distinct clusters. Multivariate means of these statistical groupings were forced to be different. Consequently, distinction was artificially highly significant. Of course this combination of methods may still separate fossil dimorphs, but one will never know whether groupings are artificially created or whether they are correctly represented by chance.

(3) The third reason relates to general differences in carapace shape between the spinicaudatan families. The between-group (sexual) difference in carapace shape of the cyzicid *Cyzicus mexicanus* was not significant (Astrop et al., 2012). All other specimens analysed were limnadiids, and although most were well separated, there was also a counterexample. This shows that the methods employed identify sexual dimorphism in only a subset of clam-shrimp taxa. Importantly, the brood chamber of limnadiids is located dorsally, while it occupies a more lateral position in the cyzicids. It is obvious from the mean shapes provided by Astrop et al. (2012) that the brood chamber is mostly responsible for the morphological disparity observed within the limnadiids analysed. The poor performance of the proposed methods for the cyzicid species and one limnadiid was ascribed by Astrop et al. (2012) to a smaller sample size and more subtle dimorphism.

Methods

The determination of the reproductive system of *Eosestheria middendorfii* is based on three steps in this study. They include (1) the identification of possible dimorphic carapace shapes in adults, (2) a correct allocation of sexes to either morphotype, and (3) the calculation of the sex ratio. This study of sexual dimorphism involves two *a priori* groups of the same cohort that include 10 individuals with egg clutches (oocytes) and 13 individuals without egg clutches, respectively (Table 5.1). Different shapes are observed, but there are no obvious morphological groups. To keep ontogenetic and environmental bias as low as possible, all analyzed individuals belong to one cohort, namely horizon LXBE S1 (Yixian Formation).

Females or functional hermaphrodites are marked by the presence of egg clutches. They act as the phenotypic archetypes for the entire analysis. In contrast, the sex allocation for specimens without egg clutches is not as simple. They are presumably males, but all sexes (males/females/hermaphrodites) have to be considered. For practical reasons, the group yielding egg clutches is termed "females", while the term "males" marks individuals that do not yield egg clutches. The latter is more imprecise, as some of those individuals may in reality represent a different sex or even juveniles. Therefore, the status of each specimen within the "male" group will have to be reassessed.

Table 5.1. List of specimens chosen for the determination of the reproductive system of *Eosestheria middendorfii*. As the umbo is usually not fully preserved, only minimum numbers of growth lines are given. The perimeter quality is based on the following code: 1 = anterior and posterior extremities of the dorsal margin discernable; 2 = either the anterior or the posterior extremity of the dorsal margin discernable; 3 = perimeter well preserved, but neither anterior nor posterior extremities of the dorsal margin discernable or the dorsal margin, particularly the umbo, not discernable.

Specimen	# visible growth lines	Perimeter quality (1-3)	Egg clutch	Remarks
LXBE				
LXBE S1_77_59	> 33	2	yes	Anterior margin reconstructed
LXBE S1_77_60	> 30	1	no	-
LXBE S1_77_63	NA	3	yes	D and dorsal margin reconstructed
LXBE S1_77_64	NA	3	yes	D and dorsal margin reconstructed
LXBE S1_77_64_19	NA	3	no	D reconstructed
LXBE S1_77_74_1	> 28	1	no	-
LXBE S1_77_74_2	> 30	2	yes	D reconstructed
LXBE S1_77_74_7	> 38	3	no	E reconstructed, hard to discern
LXBE S1_77_74_11	> 34	1	no	-
LXBE S1_77_75_4	> 34	3	yes	D and anterior margin reconstructed
LXBE S1_77_ EO704_24	> 31	1	yes	-
LXBE S1_77_ EO704_29	> 29	3	no	E reconstructed
LXBE S1_77_ EO704_30	> 35	2	no	D reconstructed
LXBE S1_77_ EO704_31	> 35	2	no	Anterior margin deformed
LXBE S1_77_ EO707_23	> 33	3	yes	E and ventral margin reconstructed
LXBE S1 15	> 31	2	yes, egg clutch located near the anterior margin	Dorsal margin reconstructed
LXBE S1 16	> 32	1	no	-
LXBE S1 21	> 28	1	no	-
LXBE S1 24	> 26	2	yes	Anterior margin deformed
LXBE S1 70	> 26	1	no	-
LXBE S1 71	> 34	2	no	Deformation of the posterior margin due to growth
LXBE S1 HS2	> 31	1	no	-
LXBE S1 HS4	> 26	3	yes	E reconstructed; Egg clutch only faintly visible
ZJG				
ZJG H3_493_4	> 33	2	yes	D reconstructed, but easy

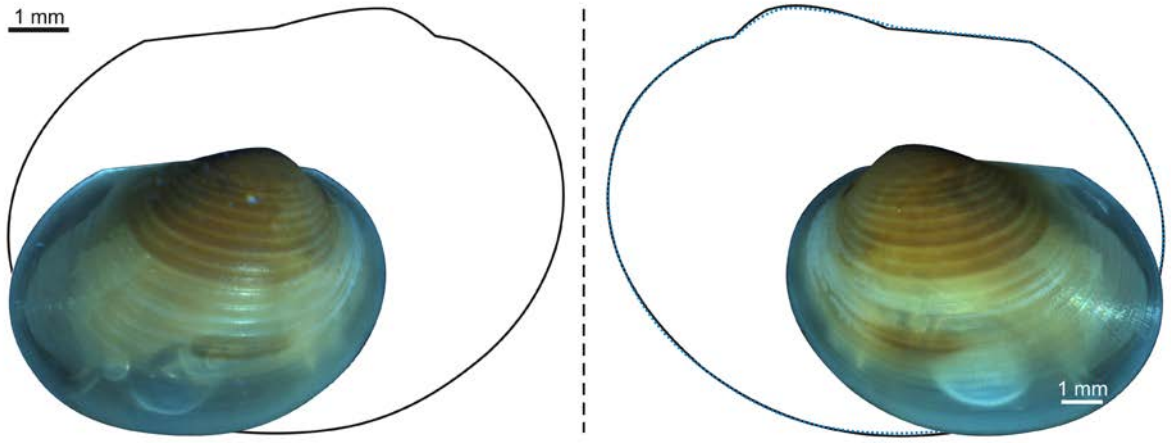

Fig. 5.1. Two photos of the same specimen of *Cyzicus* and the corresponding outlines of both valves. The right valve was mirrored (blue dotted line) and superimposed on the left valve. The almost perfect match shows that both are congruent.

The governing hypothesis tested in this chapter is whether individuals with egg clutches are morphologically distinct from those without egg clutches. A positive result would imply that the absence of egg clutches does not simply reflect preservational bias and that the dimorphic carapace shapes are likely to belong to two discrete sexes. There are two reasons for the comparatively low number of individuals. Only one horizon exhibiting egg clutches has been chosen for this analysis and only specimens whose outlines are well preserved are included. The shape change identified in a preliminary analysis could be entirely ascribed to poor outline qualities, demonstrating that clam-shrimp outlines are very sensitive to too many assumptions during the outlining process.

Morphological variability is mainly quantified by calculating discriminant functions (Fisher, 1936; Hammer and Harper, 2006) on the basis of a linear measurement dataset (Table 5.2; Fig. 4.2) and by Fourier shape analysis of carapace outlines (Supplementary 5.1; Crampton and Haines, 1996; Haines and Crampton, 2000). Possible benefits of growth line counts and of the *H*/*L* ratio for the sex determination in clam shrimps will be assessed.

Discriminant analysis. – Linear functions are calculated to evaluate whether there are two morphologically distinct groups in the adult population of the LXBE-S1 cohort. A multivariate dataset composed of nine linear measurements is analyzed (Table 5.1). In Chapter 4 it has been established that *Arr*, *Ch*, *Cr*, *H*, and *L* are robust variables and a discriminant function is calculated on their basis as well. A percentage of individuals that are classified correctly will be given for each discriminant function. It will be discussed whether the discriminant functions can or cannot be accepted as useful sex discriminators.

Growth line counts. – The number of growth lines is often sex-specific, as the examples of extant species presented in Chapter 3 show (Mattox, 1939; Tasch, 1969). Therefore, it is worth checking, whether growth line counts (Table 5.1) reveal the sex of an adult specimen of *Eosestheria middendorfii*.

H/*L*. – A popular procedure for the sex determination of fossil carapaces is to illustrate length versus height in a linear plot (e.g., Zhang et al., 1990). Values of length and height of *E. middendorfii* are log-transformed to account for possible disproportions between the two variables. It is tested whether there is a statistically significant difference between the means of the *H*/*L* ratios of the two groups. The scatter of log-transformed carapace length versus carapace height is fitted by a reduced major axis (RMA) regression line. It will be assessed whether the two *a priori* groups are well separated by it.

Fourier shape analysis and synthetic shapes. – Clam shrimps are characterized by a profound lack of discrete morphological features, making outline analysis a suitable alternative to landmarks, which are otherwise widely regarded as advantageous (Hammer and Harper, 2006). Fourier shape analysis has been chosen (Crampton and Haines, 1996; Haines and Crampton, 2000). Right valves have been mirrored prior to the analysis. Fig. 5.1 shows that both valves are congruent. The first 12 harmonics are chosen to capture the change in shape. The first harmonic is not significant, as it can be reconstructed from the other harmonics. It is therefore not output by Hangle (Haines and Crampton, 2000). The

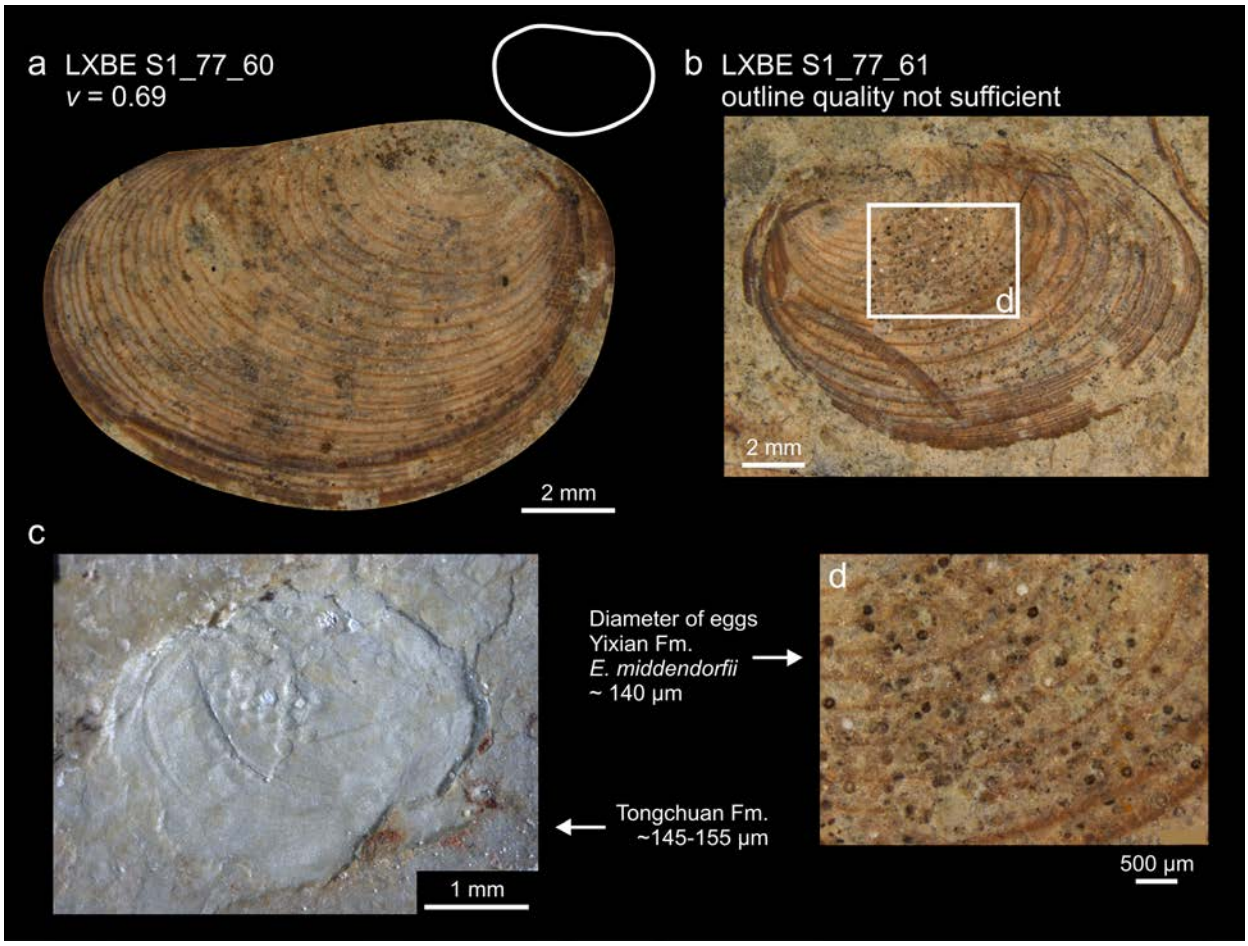

Fig. 5.2. (a, b, d) *Eosestheria middendorfii*, Yixian Formation, horizon LXBE S1. (c) Unidentified specimen from the Triassic Tongchuan Formation. (a) Example of a specimen without egg clutch. The discriminant function (v = 0.69) classifies this specimen as "male". It has an intermediate value close to the cut-off value 0. (b, d) Specimen exhibiting an egg clutch, whose outline quality is not sufficient for further analyses. The lateral position of the egg clutch is similar to the position of egg clutches in modern Cyzicidae. Eggs exhibit a diameter of about 140 µm. (c) Example of a poorly preserved clam shrimp, which nevertheless exhibits the imprint of an egg clutch (diameter of eggs about 145-155 µm). This demonstrates that egg clutches are reasonably often preserved for studies on sex determination. The egg diameters of both species are comparable to that of modern Cyzicidae.

remaining 22 Fourier coefficients (Supplementary 5.1) are projected using principal component analysis (PCA). Refer to the methods described in Chapter 4 for a more detailed description of the procedure.

In addition, synthetic outlines will be calculated to visualize extreme morphologies. Fourier coefficients are processed with the inverse Fourier transform program Hcurve (Crampton and Haines, 1996; Haines and Crampton, 2000). Since eigenvectors correspond to units of standard deviation, PC-loadings must correspond to Fourier coefficients in principal component space. Fourier coefficients of the synthetic outlines are generated by vector addition or subtraction of the eigenvectors from the Fourier coefficients of the mean shape at position (0, 0) (Haines and Crampton, 2000).

Each of the two datasets (linear measurements and Fourier coefficients) has been separated into two groups according to the presence or absence of egg clutches. In line with the prime hypothesis stated in the introduction of this chapter, it will be tested whether "females" and "males" correspond to two different morphotypes using the parametric Hotelling's T^2 and a nonparametric permutation test, respectively. Both methods test whether the two subsets exhibit equal multivariate means. The null hypothesis H_0 for Hotelling's T^2 is specified as:

H_0: Linear measurements are drawn from populations with equal multivariate means.

Multivariate normality, desired for discriminant analysis and Hotelling's T^2 (Hammer and Harper, 2006), is tested using Mardia's measures of multivariate skewness and kurtosis (Mardia, 1970).

Multivariate normality is rejected for the Fourier-coefficient dataset, therefore permutation with 5000 replicates and the Mahalanobis squared distance measure are employed. The test is based on the following null hypothesis:

H_0: Fourier coefficients are drawn from populations with equal multivariate means.

Results

Cohort discriminant analysis with nine linear measurements

The linear measurement dataset (Table 5.2) is multivariate normal and there is only little overlap in the distribution between the two *a priori* groups (Table 5.3; Fig. 5.3), implying that they are morphologically distinct. The discriminant function is $v = (-3.18a + 3.21b + 7.64c - 0.35Arr - 2.79Av - 2.93Ch - 2.87Cr + 9.34H - 5.90L) - 8.885$.

Other adult specimens of *Eosestheria middendorfii* can potentially be classified using this discriminant function by measuring the same variables. Zero should be used as a cut-off between the two groups (Hammer and Harper, 2006). Some degree of error can be expected though, owing to the small dataset employed to obtain the function.

The main difference between the two groups is described by *c*, *H*, and *L*. Coefficients on *a*, *b*, *Av*, *Ch*, and *Cr* show smaller effects, while *Arr* is almost negligible. The discriminant function will yield largely positive values for specimens without egg clutches (blue in Fig. 5.3) and negative values for specimens yielding egg clutches (red in Fig. 5.3). Specimens without egg clutches have large heights and *c* compared with length, a combination of variables that is also picked up by the shape variable *PC4* in Fig. 5.6.

Cohort discriminant analyses with robust linear measurements (*Arr*, *Ch*, *Cr*, *H*, and *L*)

The reduced linear measurement dataset (Table 5.2) is multivariate normal. The discriminant function is $v = (4.37Arr + 4.40Ch - 0.69Cr + 9.18H - 9.01L) - 4.49$.

As with the analysis of all nine measurements, specimens exhibiting $v > 0$ can predominantly be assigned to "males", while "females" are characterized by negative values ($v < 0$). Again, "females" occupy a large part of the distribution not occupied by "males", but there is considerably more overlap between the two groups (Table 5.3).

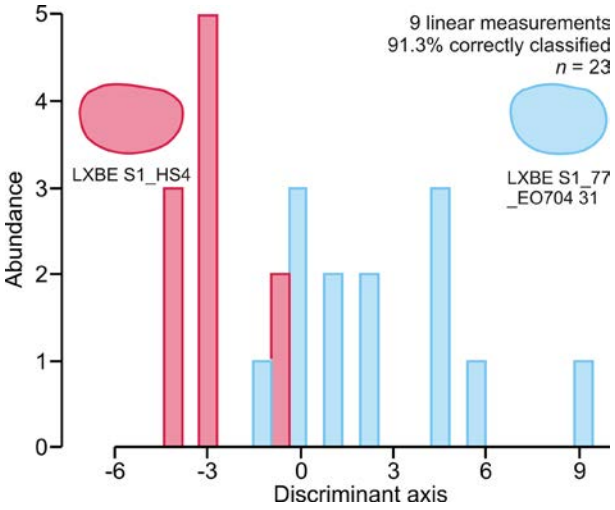

Fig. 5.3. Discriminant analysis of nine linear measurements. Individuals displaying egg clutches (red; "females") and those without (blue; "males") are plotted along their discriminant axis, which maximizes the difference between the two groups with the cut-off point set to 0. 91.3% of the specimens are classified correctly. The two groups occupy different regions of the distribution with only little overlap (Table 5.3). Overlap may be due to misclassification or part of the natural variability.

Coefficients on height and length seem equally important, while the position of the larval valve (*Cr*) does not influence the values for v to a great extent. The main difference between the two groups is that "male" specimens have relatively large heights, dorsal margins, and *Arr* compared with length. The percentage of correctly classified individuals (82.61%) is lower than that of the analysis with all nine measurements. The advantage of the robust dataset is that the hypothesis that both groups are morphologically the same can be rejected ($p \sim 0.041$). Also, this probability is more robust towards sample size. Probabilities range between 0.011 and 0.077, depending on which specimen is left out of the analysis, and most of them indicate a statistically significant dimorphism between the two groups.

Classification of a single specimen using the discriminant functions

The discriminant functions established for LXBE S1 can be put into use by measuring the same variables on any carapace of *Eosestheria middendorfii* and specimens can theoretically be classified as "female" ($v < 0$) or "male" ($v > 0$). But there might be restrictions to this. A second horizon yielding a specimen with egg clutches is ZJG H (ZJG H3_493_4; Table 5.2). Although the presence of egg clutches would predict negative values, the specimen yielded a stag-

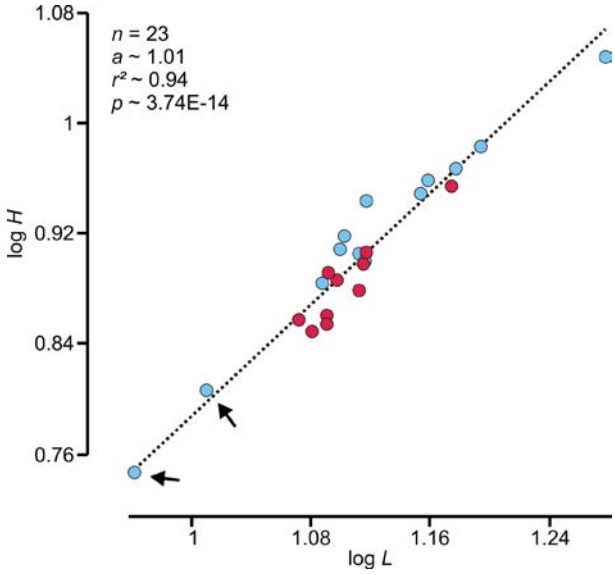

Fig. 5.4. Carapace length versus carapace height. Data are log-transformed and fitted by the RMA regression line (r^2 ~ 0.94; p ~ 3.74E-14). Arrows point towards specimens misclassified as males (Table 5.3), which are possible juveniles.

gering ν = 18.4 for the analysis of all nine measurements and ν = 8.0 for the reduced dataset. Those values are higher than both of the positive extreme "male" archetypes, respectively.

Growth line counts

The null hypothesis of equal means cannot be rejected (31 growth lines in "females" versus 32 in "males", *t* test p = 0.46). Therefore, growth line counts cannot be used for the sex determination in this species.

H/L

There is a statistically significant difference between the means of the *H/L* ratios of the two groups with that of the "females" being lower (Table 5.4; mean *H/L* of specimens yielding egg clutches ~ 0.60; mean *H/L* of specimens without egg clutches ~ 0.63; p = 0.007). The RMA regression line (Fig. 5.4) reveals a moderate visual separation between the two groups. Carapaces of the "female" group are smaller. Separate RMA regression of log *L* against log *H*, reveals *a* = 1.10 for specimens with egg clutches and *a* = 0.96 for specimens without egg clutches. Both slopes are not significantly different from *a* = 1 (p ~ 0.502; p ~ 0.504). Consequently, isometry cannot be rejected for either group. The reason for this is that allometry should be analyzed by the inclusion of juveniles. In Chapter 6, a statistically significant negative allometry in carapace length versus carapace height has, in fact, been detected for 196 specimens of *Eosestheria middendorfii*.

Fourier shape analysis

The Fourier shape analysis on the LXBE S1 cohort is founded on strict requirements concerning the quality of the carapace outline. Variables *PC1-8* represent the most important aspects of shape variation. They explain 24.8%, 19.1%, 13.2%, 9.6%, 7.6%, 5.4%, 4.4%, and 3.6% of the total variation in a dataset comprising 22 Fourier coefficients for each outline (Supplementary 5.1). The equality of multivariate means of the first 10 harmonics cannot be rejected. A permutation test with 5000 replicates yielded p ~ 0.072 with little variation between each run. However, there could still be a difference between the clam shrimps of either group, which would be subtle considering the p-value of 0.072. The power of a test is always dependent on sample size, which had to be kept small in this study. The synthetic outlines show that dimorphism is manifested in shape, but it does not constitute the main variation in the dataset. *PC 1-3* (Fig. 5.5) do not carry discriminatory power for sexual dimorphism. Instead, *PC1* stands for the position of the umbo. Umbones of "elongate" specimens are located more anteriorly, while "rounder" specimens are characterized by more submedian umbones. It is not clear whether this reflects a biological signal or differential compaction (deformation). *PC2* and *PC3* clearly pick up signs of deformation of the carapace through compaction and malformation, respectively.

Sexual dimorphism is represented by *PC4* (Fig. 5.6), which delineates a bulging ventral margin in "males" and a more flattened ventral margin in "females". The "female" interval is more constrained than the "male" interval, which is either due to a lack of egg clutches in the two specimens that were misclassified as "male" (arrowed in Fig. 5.6) and/or owing to the inclusion of juveniles into the analysis. As the two misclassified specimens (Table 5.3) are by far the smallest (Table 5.2), there is reason to assume the latter. An exclusion of these specimens would considerably constrain the "male" 95% confidence interval.

PC5 to *8* (Fig. 5.7) carry a considerable amount of shape variation, but they do not show any discriminatory power towards sexual dimorphism. (Refer to Chapter 6 for an exhaustive discussion on shape variation.)

Mean shapes of alleged female (red) and male (blue) carapaces (Fig. 5.8) are calculated on the basis of a reduced dataset of 10 females and 11 males. The

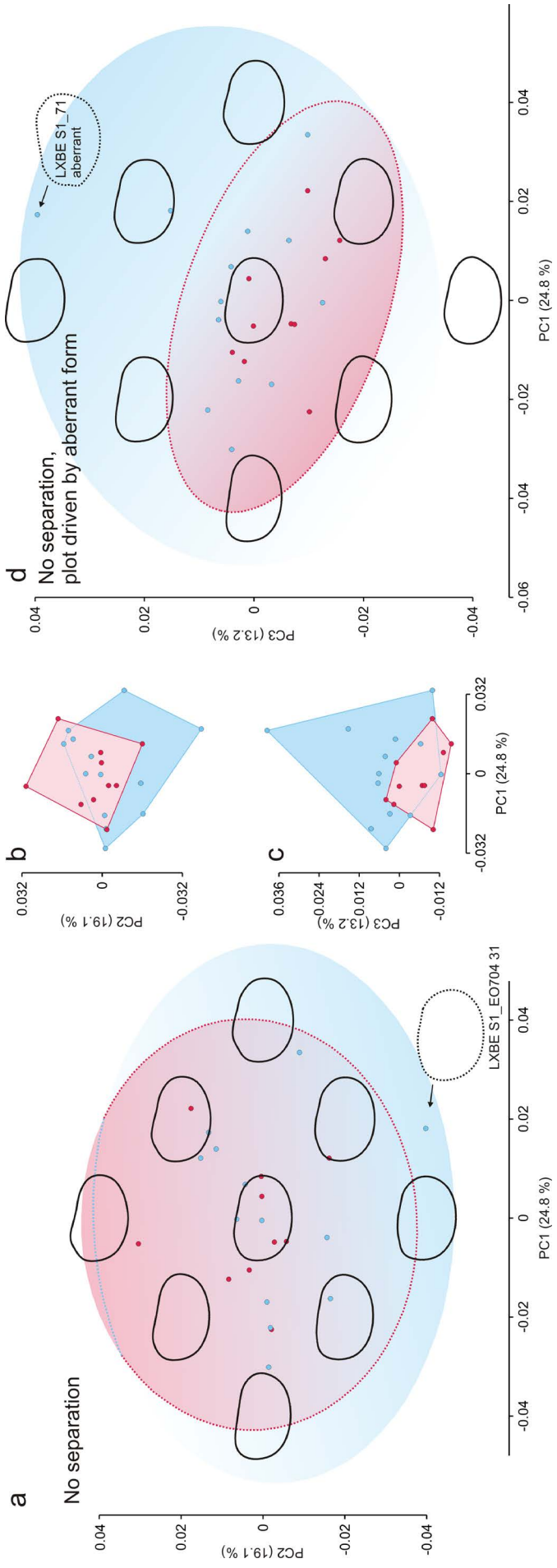

← **Fig. 5.5.** Principal component analysis of the first 12 harmonics (excluding harmonic 1) derived from Fourier shape analysis of 23 specimens of an *Eosestheria-middendorfii* cohort. The first three principal components explain 24.8%, 19.1%, and 13.2% of the total variance, respectively. Synthetic outline shapes illustrate shape change. (a, b) *PC1* against *PC2*. (c, d) *PC1* against *PC3*. 95% confidence intervals are marked in (a) and (d), the transitions from red to blue do not have any quantitative meanings. The shape change exhibited by *PC 1-3* does not separate the group with egg clutches (red) from that without egg clutches (blue). *PC1* captures the position of the umbo, which assumes a more anterior position in elongate specimens (negative scores) and a more submedian position in rounder specimens (positive scores). Plotted against *PC2*, it seems that the corresponding biological change captured by *PC1* is not related to sex. *PC2* and *PC3* carry information on the deformation of the carapace through compaction and malformation, respectively. *PC2* represents change in the prominence of the umbo and *PC3* is spanned by the presence of an aberrant form, whose outline is shown (LXBE S1_71).

two specimens misclassified as "males" (Table 5.3; arrowed Figs. 5.4, 5.6) have been omitted in the calculation. Carapace dimorphism is present but subtle. Females are marked by a more elongate carapace and a flattened ventral margin.

Discussion

Observations

Egg clutches in specimens of *Eosestheria middendorfii* occupy a lateral position and single eggs display a diameter of roughly 140 µm. The eggs of horizon LXBE S1 (Fig. 5.2) are similar in size to those of the modern family Cyzicidae, which are 0.14 mm in diameter. Those of the Limnadiidae exhibit larger diameters of 0.18 mm (Frank, 1988) to 0.25 mm (*Limnadia stanleyana*; Bishop, 1967a). The lateral position of egg clutches (Fig. 5.2b) in *Eosestheria middendorfii* is similar to that of extant Cyzicidae. In addition to the phylogenetic considerations for the family Eosestheriidae discussed in chapters 3 and 4, this is further supporting evidence for a close relationship of this fossil family with the extant Cyzicidae. The Cyzicidae exhibit only subtle

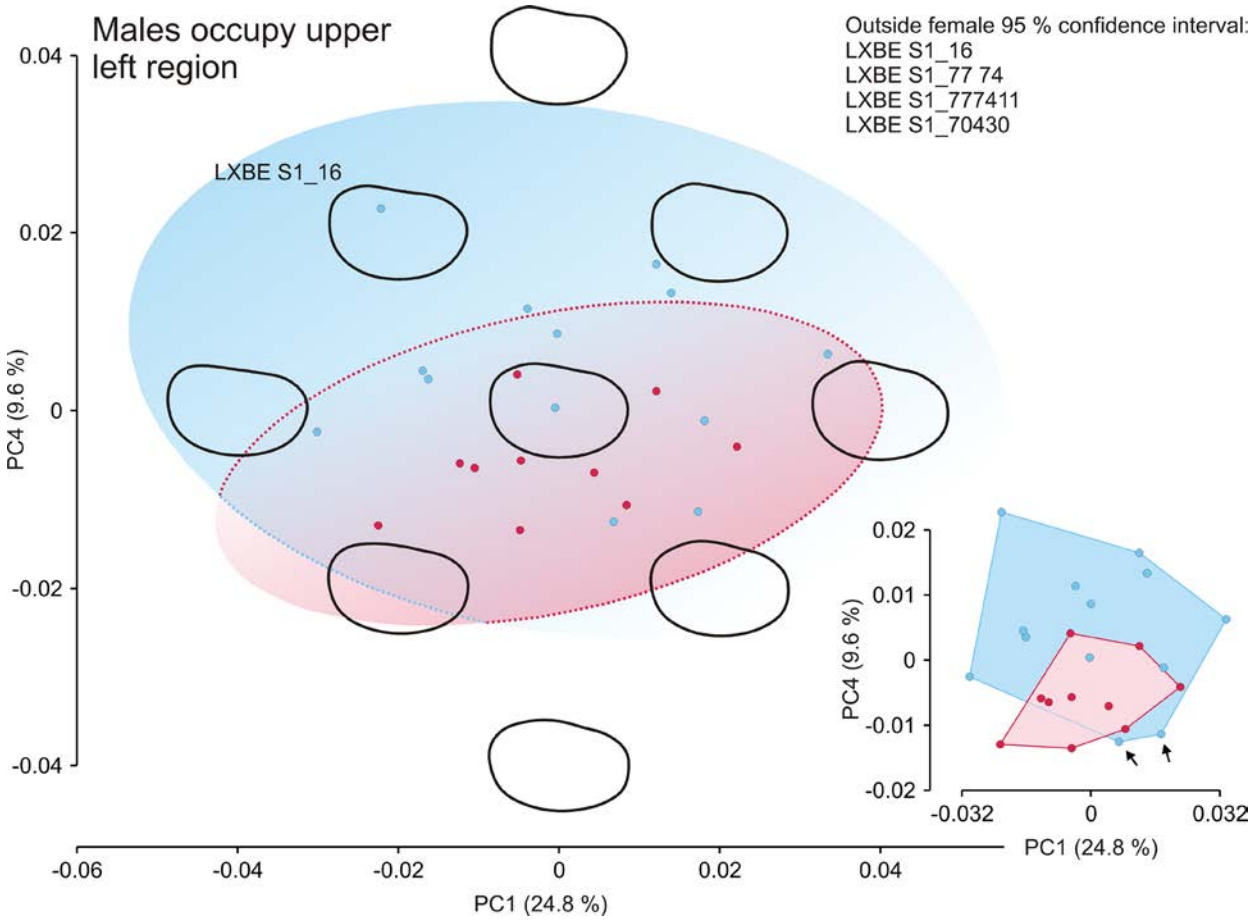

Fig. 5.6. The first and the fourth principal component axes of a dataset comprising Fourier coefficients of 23 specimens of an *Eosestheria-middendorfii* cohort. The two a priori groups are colour-coded in red (females/hermaphrodites; egg clutches visible) and blue (without egg clutches), respectively. Variable *PC4* (9.6% of the total variance) exhibits the most discriminatory power towards sex determination. 95% confidence intervals are shown for both groups and the transitions in colour illustrate progressive female and male carapace shapes. A total of four "male" specimens fall outside the "female" interval, whereas all "females" are part of the "male" interval. The "female" interval is more constrained, because specimens identified as females/hermaphrodites are unambiguous. The "male" interval, in turn, is less constrained, because some of the specimens classified as "male" might in fact represent a different sex or juveniles. The smaller plot in the right hand corner shows the corresponding convex hulls, wherein only one "male" specimen falls into the "female" convex hull. The two arrowed specimens in the bottom corners of the blue convex hull have been misclassified as "male" through discriminant analysis. A set of synthetic outline shapes are ordinated against both axes, facilitating a visualization of the morphospaces "males" and "females" occupy.

differences in sexual morphotypes, as expressed in the modern cyzicid *Cyzicus mexicanus* (Astrop et al., 2012).

Cohort discriminant analysis with nine linear measurements

Specimens with $v > 0$ can predominantly be assigned to "males" and $v < 0$ can predominantly be assigned to "females", while the percentage of correctly classified specimens is 91.3%. The probability that all specimens are morphologically the same is comparatively high ($p \sim 0.079$), though. Therefore it cannot be rejected that all specimens merely stem from a variable population. However, this probability ranges between 0.009 and 0.137 by the exclusion of either one of the 23 specimens, clearly showing the disadvantage of basing the discriminant function on only a small dataset. A second reason for the higher p-value might be that egg clutches are simply not preserved, which can be expected, as they are sometimes hard to discern. The most probable reason is that the two specimens misclassified as males (Table 5.3) are in fact juveniles, as they are markedly smaller than all other specimens (Table 5.2; Fig. 5.4). Therefore, the null hypothesis that specimens of the two groups are morphologically the same is rejected.

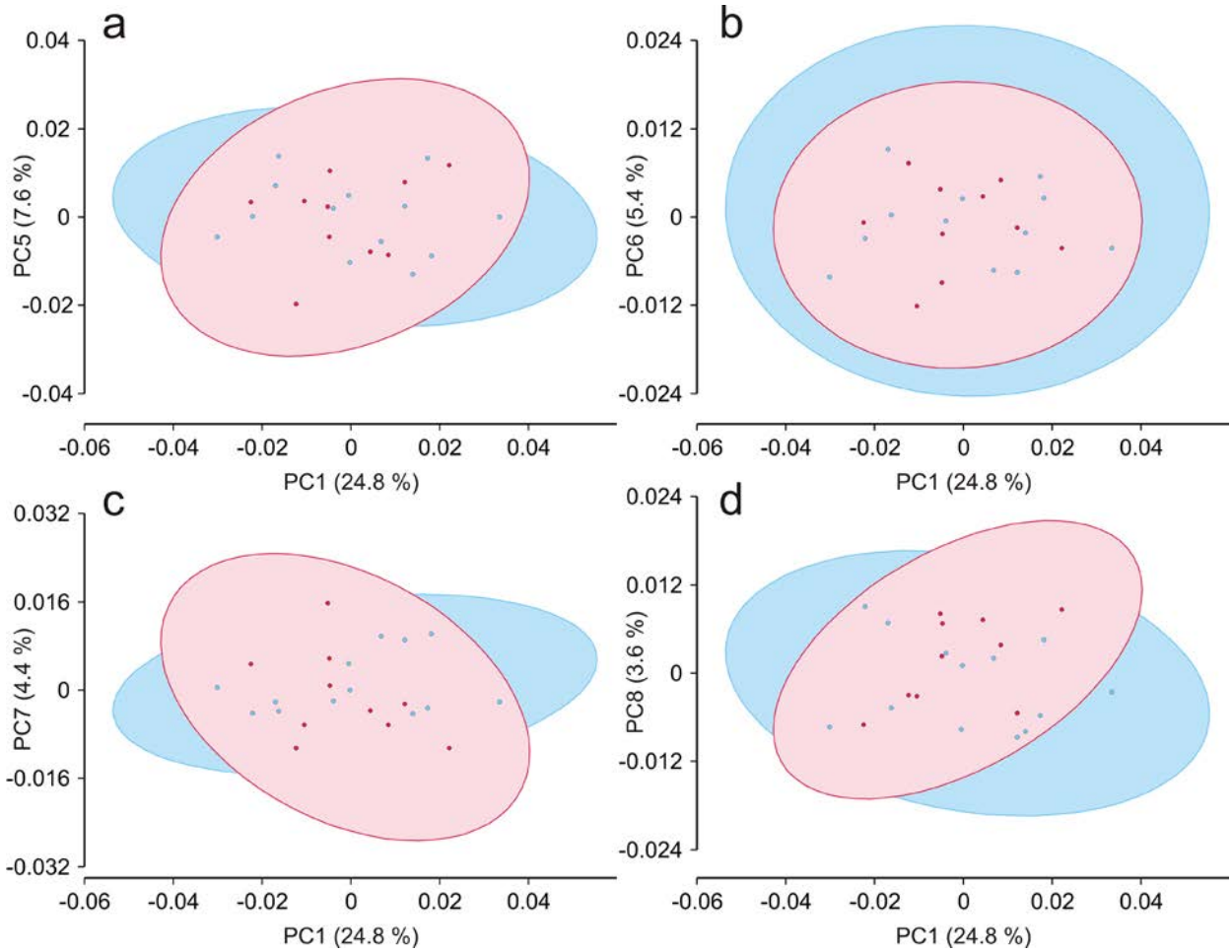

Fig. 5.7. *PC 5-8* explain 7.6%, 5.4%, 4.4%, and 3.6% of the total variance in the Fourier coefficients. None of them separates the two a priori groups. Red (egg clutches visible) and blue (without egg clutches).

It might be convenient to describe the carapace yielding the lowest discriminant score (-4.87 LXBE S1_HS4; Table 5.3, Fig. 5.3) as the "elongate" phenotype and that with the highest discriminant score (9.93, LXBE S1_77_EO704_31) as the "round" phenotype. However, there are strong arguments against this oversimplification: (1) Shapes that are simple to begin with quickly get reduced to such terms. This makes it hard to identify more subtle trends, which can only be pinpointed by looking at multiple variables. (2) Nine variables have been looked at. The most obvious "subtle" difference between the two extreme phenotypes pictured in Fig. 5.3 is that the position of the most posterior point B (Fig. 4.2) is located more dorsally in "female" specimens. This is expressed by a positive coefficient on the variable *b* in the discriminant function.

Cohort discriminant analyses with robust linear measurements

The dataset comprising all nine linear measurements is superior to the reduced one on two accounts. (1) More variables have been considered. (2) A larger sample size is likely to reduce the variability within the probability range. However, if only a small dataset can be sampled, it is advisable to cross-check whether the main trends of the discriminant function established with all nine linear measurements are reflected by that derived from robust measurements.

Classification of a single specimen using the discriminant functions

There are several possible explanations for the obtained results. (1) The ZJG specimen is considerably larger than the specimens the discriminant functions were established with (L ~ 17.55 mm). Allometric growth may render the discriminant functions useless for larger specimens. (Refer to Chapter 6 for the main discussion on allometric growth.) (2) Ecophenotypic variation of the carapace in both settings is another major factor. In general, the position of ZJG within Lake Sihetun is thought to be more oxygen depleted than LXBE (Chapter 2; Hethke

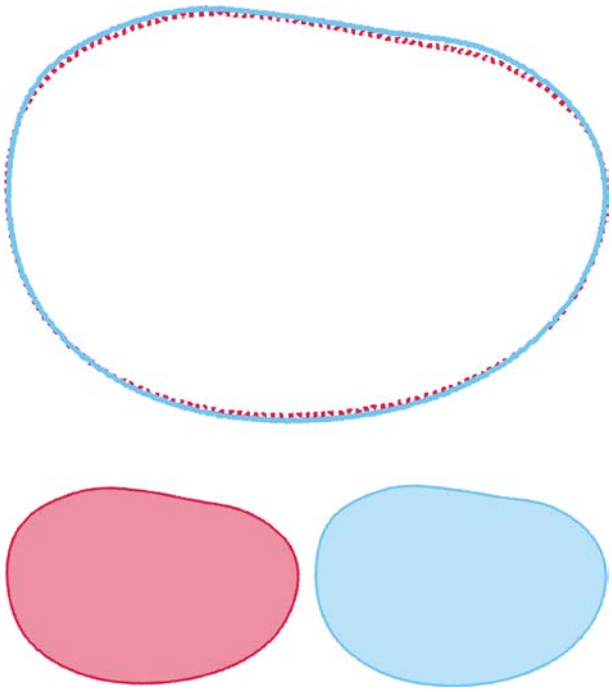

Fig. 5.8. Mean shapes of alleged "female" (red) and "male" (blue) carapaces taking into account the entire morphological variation in the dataset. Misclassified specimens from the discriminant analysis were omitted resulting in a dataset of 10 females and 11 males. Dimorphism in the carapaces is present but very subtle with females being more elongate.

et al., 2013b). (3) Natural variability. There is overlap between both sexual morphs and the analyzed specimen might simply represent an extreme female morphology. (4) A probability of 7.9% was reported for all specimens to be of the same morphotype and a statistical misinterpretation might have led to a type I error; a falsely rejected null hypothesis that all specimens are morphologically invariant. (5) Misleading preservation, however unlikely, might be considered, where egg clutches were originally present in all specimens, but are only preserved within the group classified as "female". The arguments for scenario 5 are weakened by the fact that the specimens the discriminant functions were established with belong to one cohort that was subjected to the same environmental and diagenetic forces.

H/L

The *H*/*L*-ratio may be convenient for a fast sex determination in clam shrimps, but a major weakness is that it does not pick up subtle differences in carapace shape, as only two variables are looked at. The same *H*/*L* ratio may represent anything between a rectangle and a circle. Furthermore, *L* and *H* have already been considered within the discriminant analysis, which facilitates a comparison with other carapace variables. And finally, had there been no *a priori* groupings, almost half of the specimens in Fig. 5.4 would have been misclassified.

Fourier shape analysis

Only one (*PC4*, Fig. 5.6) of eight meaningful shape variables exhibits discriminatory power towards sexual dimorphism, accounting for about 10% of the total variance in the Fourier coefficients. *E. middendorfii* is therefore sexually dimorphic, but differences are subtle (Fig. 5.8) and less obvious than, for example, shape variation resulting from carapace alignment during compaction (Fig. 5.5a) or carapace malformation (Fig. 5.5d).

Sexual dimorphism

Sexual dimorphism in clam shrimps is mainly recognized by dimorphic soft part features. Dimorphic soft parts in *Leptestheria dahalacensis*, for example, are claspers in males as their first two limb pairs, the shape of the cephalic rostrum, the occurrence of bristles at the lower keel of the cephalic rostrum in males, and epipodites in the 10th-15th limbs transformed to ovipositors in females (Scanabissi Sabelli and Tommasini, 1990). Unfortunately, such soft part features are commonly not preserved, bringing morphological traits of the carapace into focus. Carapace dimorphism is expressed by differences in **size** and dimorphic carapace **outlines** (e.g., Daday de Deés, 1915; Bock, 1953; Kobayashi and Kusumi, 1953; Tasch, 1969; Vannier et al., 2003). There may be pronounced sexual dimorphism of carapace surface ornamentation, as commonly observed in ostracods (Ozawa, 2013). A visual examination of ornamentational dissimilarities within the LXBE-S1 cohort did not suggest any such dimorphism, apart from differences that derive from the dissimilar sizes of male and female carapaces. Dimorphism in behavioural traits (courting and mating behaviour) can only be inferred from an analogy with living clam shrimps and is neglected in this study. The focus is therefore placed on the carapace outline and its size. There are numerous accounts on carapace dimorphism in modern species:

Distinctive **female** carapace traits deduced from two species of *Eulimnadia* are (1) a larger carapace and (2) a more convex dorsal margin. Additional characteristics are (3) a more broadly rounded ventral margin and (4) a higher average number of growth lines (Mattox, 1939). In contrast, 85-88% of cyzicid **males** are larger than the females (Bock, 1953). Bock (1953) summarizes the male type to be

less abundant, larger in size, and generally rounder, while the female is more elongate.

These two contrasting views are explained by the fact that Mattox (1939) and Bock (1953) were looking at carapaces of species from two different families. The trend of more elongate but smaller carapaces in cyzicid females is corroborated by *Cyzicus tetracerus,* whose female *L*/*H* ratio is higher (Vannier et al., 2003). There is, however, no significant difference in valve height or valve length between males and females in *Cyzicus grubei* (Machado et al., 1999).

Nevertheless, trends in carapace dimorphism seem to be dependent on the clam-shrimp family. Astrop et al. (2012) report sexual dimorphism for limnadiid specimens with a much more convex dorsal margin in females that is associated with a brood chamber. Sexual dimorphism in the Cyzicidae, exemplified by *Cyzicus mexicanus*, is more subtle with a slightly more elongate female that displays a flattened posteroventral margin.

Eosestheria middendorfii follows the "cyzicid" trend with only subtle sexual dimorphism that is marked by more elongate and slightly smaller females (Figs. 5.6, 5.8). There is a hint of size dimorphism in *E. middendorfii* with larger "males" and smaller "females" (Fig. 5.4). The egg diameter of *E. middendorfii* is about 140 µm, which is in the cyzicid and leptestheriid range. SEM analysis of *Leptestheria dahalacensis* yielded an egg diameter of 133 µm. Diameters of limnadiids are commonly larger (Frank, 1988; Bishop, 1967a). These results along with the lateral position of the egg clutches in *E. middendorfii* imply that the fossil family of the Eosestheriidae is closely related to the Cyzicidae.

Sexual dimorphism in *Eocyzicus mongolianus* (Kobayashi and Kusumi, 1953) is an example that does not follow any particular trend listed above. It is expressed by a generally straight dorsal margin in males and a slightly arched dorsal margin in females, which is reminiscent of limnadiid specimens. In contrast, the male is larger than the female, which in turn is indicative of cyzicids. It is worth noting that the Cyzicidae become monophyletic only by the exclusion of *Eocyzicus* (Schwentner et al., 2009). Kobayashi and Kusumi (1953) visualized sexual dimorphism in a *H*/*L* diagram by drawing what seems to be an arbitrary line between the two morphs. Male and female morphotypes can be visually separated by this line, but separation is not complete.

In practise, the sex determination of modern clam shrimps is carried out by the differentiation of modified claspers in males and by the presence of oocytes in hermaphrodites and females (Sassaman and Weeks, 1993). Such oocytes may also be preserved in the fossil record (Fig. 5.2). Their presence designates female or hermaphroditic specimens, which serve as the archetypes for female or hermaphroditic morphological traits.

There are several accounts of sexual dimorphism in fossil strata from China. According to Chi (1931), who documented specimens of the Eosestheriidae, the "shorter" carapaces of "*Estheria*" are female, as some of them bear eggs. This matches the results presented for *E. middendorfii,* but as the species this statement was based upon was not distinguished by Chi (1931) there is little strength to it.

The sex discrimination of the Middle Jurassic *Euestheria luanpingensis* was carried out using *H*/*L* plots (Zhang et al., 1990). Some of the specimens exhibited either claspers or egg clutches. Sexes of 25 specimens were separated by a line with a slope of about 0.8 (females > 0.8; males < 0.8). The eight specimens yielding claspers fell below and the three specimens yielding egg clutches were found above this line. Specimens displaying neither eggs nor claspers were allocated accordingly. However, Zhang et al. (1990) neglected the relationship between carapace size and shape. A polynomial, instead of a straight line, should have been calculated for the sex discrimination in a scatter plot of length versus height, or the axes should have been log-transformed to illustrate the relationship between height and length. Also, the line was only conveniently drawn. Still there is some discriminatory power to the *H*/*L*-ratio, represented by a significant difference between "males" and "females" in *E. middendorfii*. But it does not identify subtle differences in carapace shape, because only two variables are looked at.

Sex determination in fossil cohorts that cannot be grouped through the presence of egg clutches or claspers should be avoided. Female and male fossil carapaces in Astrop et al. (2012) and Monferran et al. (2013) were statistically predefined. Monferran et al. (2013) identified sexual dimorphism in Late Jurassic specimens from Patagonia, Argentina, using the approach described by Astrop et al. (2012). Their specimens did not exhibit any egg clutches. Seemingly, the morphological distinction between the two sexes was near complete with only very little overlap of the convex hulls indicating female and male specimens in the eigenshape plot. However, sex-groupings were based on the classification through cluster analysis of the first three eigenshapes of the same eigenshape analysis. It is there-

fore not surprising that the distinction between the two groups was that perfect. Cluster analyses of the two datasets generated for *E. middendorfii*, linear measurements and Fourier coefficients, failed to separate "females" and "males".

Sexual dimorphism in *E. middendorfii* is best reconstructed by using a combination of methods on individuals of a single cohort. In this study, group designation is based on the presence or absence of egg clutches. Growth line counts do not discriminate sexes in *E. middendorfii*, while a statistically significant difference between the means of the *H*/*L* ratios of either group has been identified. *H*/*L* ratios seem to work for a fast sex determination, but they do not identify subtle differences in size and shape. The discriminant analysis of linear measurements and a Fourier shape analysis identify such subtle differences that go beyond simple length and height considerations. Importantly, these two methods are based on independent datasets, yet the result of one method corresponds to that of the other.

A discriminant function was calculated based on nine carapace variables. Specimens without egg clutches ("males") have large heights and *c* compared with lengths. This combination of variables is represented by a more bulging ventral margin in "males", defined by the shape variable *PC4* (Fig. 5.6). The high degree of deformational and environmental influence on carapace shape makes it important to check which of the *PC* variables discriminates between sexual dimorphs. Sexual dimorphism in *E. middendorfii* is only subtle and it accounts for about 10% of the shape variation detected by Fourier shape analysis, which means that 90% of the variation in the dataset should be explained by other factors. The percentage of correctly classified specimens is fairly high (91.3%). Misclassified specimens are probably juveniles. Ideally the presented discriminant function can be applied to other specimens of *E. middendorfii*. However, contrasting results presented by a specimen of the same formation but from a different location and horizon show that allometric growth as well as environmental variability, and natural variability are factors that need to be discussed prior to using the function (Chapter 6). Only specimens of the same size range as the cohort the function is based on can be classified with it. In summary, the results presented point to the presence of 21 well-defined dimorphic specimens within the LXBE-S1 cohort: 10 females and 11 males.

Determination of the reproductive mode through sex ratios

In clam shrimps, sex is genetically determined. Genetic analyses of sexual species point out that the male-determining allele is recessive (Sassaman, 1995). Reproductive modes are inferred from the proportional abundance of males in a population (sex ratio; Sassaman, 1995). Spinicaudatans can reproduce (1) obligately sexually (dioecy), (2) through self-fertilization but with the occasional presence of males (androdioecy; Sassaman and Weeks, 1993), or (3) unisexually (self-fertilization or parthenogenesis). These modes correspond to (1) a 1:1 sex ratio, (2) a "female"-biased sex ratio, and (3) an all "female"/hermaphroditic sample. Sexual maturity in *Eulimnadia*, recognized by pairing and brooded clutches, is reached on the eighth or ninth day, and only then species of the same genus can be distinguished from one another. Sexual differentiation between males and females is evident a bit earlier, on the sixth day (e.g., *Eulimnadia texana*; Sassaman and Weeks, 1993).

Both of the misclassified specimens of *Eosestheria middendorfii* (Table 5.3; Figs. 5.4, 5.6) are interpreted as juveniles that cannot be assigned to either sex. The sex ratio determined from the LXBE-S1 cohort was initially "male"-biased, but the misclassification of these two individuals without egg clutches suggests an approximate sex ratio of 1:1 (10 females:11 males). This sex ratio is indicative of the presence of males and females in a dioecious reproductive system. In most extant species, males and females are equally common (Sassaman, 1995). The subfamily Limnadiinae is the notable exception, as it yields many species which are either unisexual or which have a female-biased sex ratio. It should be noted that sex ratios have been found to be variable in cyzicid species (Machado et al., 1999). Considerations how sexes are determined in clam shrimps hint at genetics of the fossil species *E. middendorfii*.

(1) If sex was determined by a single factor in heterozygous condition in one of the parents, then a sex ratio of 1:1 would be expected. Alternatively, if the sex ratio was determined by multiple polymorphic factors or by environmental influences, clutch sex ratios would vary profoundly from generation to generation (Sassaman, 1995). But according to extensive studies on sex ratios of modern clam shrimps, this is not the case. The attributes of obligately sexual clam shrimps, such as proposed for *E. middendorfii*, are: There is no environmental influence and sex is genetically fixed. Females are heterozygous with respect to the sex-determining factor

(S/s = female; s/s = male), so the male-determining genetic factor must be recessive (Sassaman, 1995).

(2) Hermaphroditism is common in lower crustaceans, such as Remipedia (Itô and Schram, 1988) or notostracans (Sassaman, 1991). Hermaphroditic individuals of spinicaudatans lack the male claspers needed to hold on to the margins of the carapace of another individual during pairing, hence they are only able to self-fertilize (Sassaman and Weeks, 1993). Hermaphrodites of androdioecious populations are mixed with males, which increases genetic variability (e.g., *Eulimnadia texana* Packard; Sassaman and Weeks, 1993). There are two types of hermaphrodites in *Eulimnadia texana*, which are morphologically alike: amphigenic and monogenic. The first produces males as well as hermaphrodites and the latter produces only hermaphroditic offspring (Sassaman and Weeks, 1993). Hence, there are three sexual phenotypes (amphigenic, monogenic, and males), which can be explained by a one-locus system of sex determination with the allele s recessive to S. Genotypes are: ss for males, Ss for amphigenic hermaphrodites, and SS for monogenic hermaphrodites (Sassaman and Weeks, 1993).

Populations of *Eulimnadia texana* exhibit a "female"-biased sex ratio with 70-80% "females". Sex ratios vary and some populations are entirely composed of hermaphrodites (Sassaman, 1989). Therefore several populations of one fossil species have to be analyzed in such a case. Generally, pedigrees depend on selfing or crossing of monogenics or amphigenics, resulting in offspring ranging from all-monogenic populations to half amphigenic – half male populations (Sassamen and Weeks, 1993). The ability of self-fertilization would make the loss of males (the loss of the recessive allele) an evolutionary endpoint. Theoretically, the 1:1 sex ratio identified in *E. middendorfii* could represent such a half amphigenic-half male population. But this is an endpoint of a situation that is commonly female-biased. Therefore, dioecy is considered the more likely reproductive system.

In general, the greater the female bias the greater the degree of inbreeding. Inbreeding/self-fertilization gives the animal a fitness advantage and a benefit for the colonization of new habitats in a single wave (Baker, 1955), whereas outcrossing is advantageous for the production of variability. Hypothetically, colonization of new ponds with a single amphigenic individual would lead to a sexual population with males present (Baker 1955; Sassaman and Weeks, 1993). At least one unisexual species can be found in each of the genera *Cyzicus* and *Leptestheria* and the reported species are both of limited geographic distribution (Roessler, 1995; Sassaman, 1995). There are transitions between androdioecy and unisexuality, so unisexual species probably derived from androdioecious species. Sassaman (1995) reports rare males of *Limnadia lenticularis* in populations from Florida, a species whose populations are usually male-free.

Phylogenetic analysis suggests obligate sexual reproduction to be the ancestral condition and unisexual reproduction to be the derived condition that has arisen several times (Sassaman, 1995). The fossil record may corroborate the primitiveness of sexual reproduction within spinicaudatans, as in this study it was established that the Early Cretaceous *E. middendorfii* follows a dioecious reproductive strategy. It would be interesting to examine, whether the high numbers of males of *Limnestheria ardra* from the Late Carboniferous of Ireland (Wright, 1920; Orr and Briggs, 1999), possible ancestor of extant limnadiid species, are indicative of a dioecious system as well. Studies on the evolution of the reproductive system in clam shrimps should progress with the identification of the main reproductive systems in various fossil clam-shrimp families, most notably fossil Limnadiidae, Estheriellidae (both of which are well represented in the Late Carboniferous Castlecomer Fauna; Orr and Briggs, 1999), and Leaiidae.

Conclusions

Soft part features indicative of the sex of a clam-shrimp specimen are commonly not preserved and there have been attempts to allocate sexes to fossil taxa by exclusively employing statistical methods. However, testing the equality of multivariate means of two groups that have been statistically separated in the first place is circular reasoning. The outcome of the test is likely to be statistically significant. Further caution is urged concerning the large documented overlap in female and male morphospaces in a number of extant species. Therefore, the determination of the reproductive system in fossil species is only reasonable if at least one independent *a priori* group can be specified, either through the presence of egg clutches or claspers.

A single cohort of the Early Cretaceous *Eosestheria middendorfii* renders a sufficient amount of egg-clutch-yielding individuals. They are regarded as morphological archetypes for the female/hermaphroditic carapace. The dataset has been divided into two groups according to the presence or absence of egg clutches. Discriminant analysis and

Fourier shape analysis show that carapaces of both *a priori* groups differ in size and shape, confirming the presence of sexual dimorphism. Some degree of overlap between the two morphospaces is observed. Females are characterized by a smaller and slightly more elongate carapace. Males display a more bulging ventral margin. Generally, carapaces show a high degree of deformation, which accounts for a large proportion of the morphological variability in the dataset. *E. middendorfii* follows the "cyzicid" morphological trend, implying that the fossil family Eosestheriidae is closely allied with the extant Cyzicidae.

The separation of dimorphism in *E. middendorfii* by examining the relationship between length and height is not ideal. The female phenotype tends to be smaller in size and it exhibits a significantly smaller *H*/*L* ratio than the male phenotype. This proves that *H*/*L* plots pick up sexual dimorphism to a degree, but by no means should they be used to classify specimens.

A discriminant function that can be used for the classification of individuals is presented with a high percentage of correctly classified specimens. It is advised to use this function only to classify specimens that are of similar size as those of the LXBE-S1 cohort. Allometric growth, environmental variability, and natural variability influence carapace morphology up to a point that may render this function ineligible.

Due to a proposed sex ratio of 1:1, the utilization of dioecy as a reproductive system is inferred for *E. middendorfii*. Further studies on reproductive system evolution using clam shrimps as model organisms are encouraged that factor in the limitations of the fossil record.

Chapter 6: Ontogenetic versus ecophenotypic variation in Early Cretaceous clam shrimps of the Yixian Formation

Chapter 6 is a joint project of the following authors:

Manja Hethke[1], Franz T. Fürsich[1], Baoyu Jiang[2], Simon Schneider[3]
[1]*GeoZentrum Nordbayern, FG Paläoumwelt, Germany*
[2]*School of Earth Sciences and Engineering, Nanjing University, China*
[3]*CASP, Cambridge, UK*

Palaeobiological objectives

Palaeontological species are minimal diagnosable morphological clusters (Gingerich, 1985; Smith, 1994). Ideally, each cluster should contain all representatives of ontogenetic stages and sexes of the same reproductive population (Smith, 1994), however, these can only be inferred in the fossil record. Clam shrimps are morphologically simple and their diagnostic features are bound to the bivalved carapace. Soft parts and genetic characters, on which most extant clam-shrimp species are based (e.g., Sars, 1896; Daday de Deés, 1915; Stoicescu, 2004; Schwentner et al., 2009), are typically not preserved. As a result, there is no consensus on how to deal with fossil clam-shrimp species in taxonomic practice (Table 4.3). Species diagnoses often rely on carapace dimensions (e.g., Tasch, 1987), but they might be unreliable in the light of ontogenetic and phenotypic variation (Kowalewski et al., 1997). Conversely, a focus on the micro-ornamentation of the carapace renders specimens that lack such ornamentation unidentifiable.

A number of clam-shrimp species described from the Yixian Formation by Chen (1999a) have been identified as juveniles of *Eosestheria middendorfii* in Chapter 4. The smallest of those junior synonyms exhibits a length of 10.6 mm and can clearly be assigned to *E. middendorfii* based on its micro-ornamentation. This chapter deals with juveniles of much earlier developmental stages that exhibit lengths of only 1 mm. Diagnostic features established in Chapter 4 cannot be applied to these juveniles, because they are marked by a lack of ornamentation and different carapace morphologies. An identification of these juveniles may nevertheless be rendered possible, as a continuous size spectrum between juveniles and adults is encountered. A visualization of the ontogenetic morphospace occupied by *E. middendorfii* will supplement the taxonomic revision of Chapter 4.

Phenotypic variation in a taxon is an important issue for evolutionary biology, as it is what selection acts upon (Zelditch et al., 2004). To isolate the phenotypic variation, ontogenetic variation and sexual dimorphism need to be considered (Zelditch et al., 2004). Variation resulting from malformation and alignment as well as deformation during compaction has been pinpointed in Chapter 5. While the previous chapter concentrated on a single developmental stage, concluding that about 10 % of the adult shape variation of *E. middendorfii* can be attributed to sexual dimorphism, this chapter considers the full spectrum of carapace growth. The main objective of this chapter is to clarify the diversity of shape within *E. middendorfii* of Lake Sihetun by (1) identifying ontogenetic and phenotypic variation within this species and by (2) assessing whether phenotypic variation is mainly driven by growth or by environmental parameters.

Material and methods

The data consist of three sets of individuals (348 in total) excavated at localities ZJG, LXBE, and JSG (Fig. 2.1), comprising 19, 94, and 235 individuals of various developmental stages, respectively. All are assigned to *Eosestheria middendorfii* (Chapter 4). Individuals of excavation JSG can further be subdivided into 39 specimens that lived during Phase 2 and 196 specimens that lived during Phase 3 of Lake Sihetun. All specimens of ZJG and LXBE belong to Phase 2. Nine linear variables (Fig. 4.2) are chosen to represent the proportions of *E. middendorfii* (Table 6.1). Carapace measurements are overlapping and can be expected to be inter-correlated.

The two main objectives are (1) to identify ontogenetic and phenotypic variation within *E. middendorfii* and (2) to assess the influences of environmental parameters and growth. This will be tackled through a combination of multivariate analyses of the linear measurement data and outline analysis (Fourier shape analysis; Crampton and Haines, 1996; Haines and Crampton, 2000). All measure-

ments have been log-transformed prior to multivariate analyses. There are several reasons for this. Biological variation tends to assume a lognormal distribution rather than a normal distribution (Gingerich, 2000) and the log-transformation of variables adds an aspect of shape on the basis of the allometric equation of Huxley (1932) by generating a scale invariant matrix that preserves allometries (Jolicoeur, 1963; Kowalewski et al., 1997).

Principal component analysis (PCA) on log-transformed linear measurements is carried out to understand the dimensions of the overall observed variability that is derived from a combination of sexual dimorphism, ontogenetic variation, and phenotypic variation (all 348 specimens). Correlations between variables are often well represented on a reduced number of PC axes (Gingerich, 2003). The interpretation of these PC axes happens through associated eigenvector coefficients (loadings).

Ontogenetic variation

Ontogenetic variation is identified through the investigation of allometry in a multivariate morphometric dataset and by identification of the ontogenetic morphospace using Fourier shape analysis (Crampton and Haines, 1996; Haines and Crampton, 2000). The analysis of *allometric relationships* among characters is based on a reduced dataset of 196 specimens of Phase 3 to restrict environmentally-controlled variation as much as possible (excavation JSG). Individuals of Phase 3 are marked by an especially wide size range, displaying lengths of 1.0 mm to 22.9 mm, rendering this dataset suitable for the analysis of growth within *E. middendorfii*. Allometry denotes a change in proportion during ontogeny, described mathematically by Huxley (1932). His model is based on the fact that specific body parts increase in relative size compared with body size. This bivariate relationship is expressed by the following power function

$$y = bx^k$$

(Huxley, 1932)
and can be rewritten as

$$\log y = k \log x + \log b .$$

x is the magnitude of the animal (e.g., carapace length) and y that of a differentially growing body part. b is an arbitrary constant. k is the allometric coefficient and the slope of a straight line on a double logarithmic coordinate system. The ratio of the relative growth rate of an organ to that of the body is constant and expressed by the value of k (Huxley, 1932; Zelditch et al., 2004; Hammer and Harper, 2006). Linear regression (reduced major axis) estimates k. If $k = 1$ there will be isometric growth, if $k \neq 1$ there will be allometry (positive for $k > 1$ or negative for $k < 1$). In the bivariate case pictured in this study, the variable *Ch* is used as a measure of body size.

Multivariate allometry

In the multivariate case, all log-transformed values are subjected to PCA. *PC1* can be regarded as a multivariate allometry vector, if derived from log-transformed measurements in a variance-covariance matrix. *PC1* scores stand for measures of size (Jolicoeur, 1963; Zelditch et al., 2004) and its loadings signify the slope of a straight line in multivariate space (Hammer and Harper, 2006). The allometric coefficient of a variable is thus calculated by the division of its *PC1* loading by the overall mean *PC1* loading. For each allometric coefficient, 95% confidence intervals are calculated by bootstrapping individuals (Kowalewski et al., 1997). If the confidence interval does not include the value 1, allometry is considered significant ($p < 0.05$). The interpretation is essentially the same as for the bivariate case: a significant departure from 1 in coefficients implies allometry. The assumption of size within the *PC1* scores is essential for this analysis and will be evaluated by looking at the total amount of variation it explains.

Ecophenotypic variation

The identification of *ecophenotypic variation* is based on an adult-only dataset of 184 specimens that lived during both phases 2 and 3 (19 ZJG +77 LXBE + 26 JSG, Phase 2 + 62 JSG, Phase 3). Consequently, there are four *a priori* groups that are based on the location of a specimen within Lake Sihetun as well as the time they lived. Prior to the analysis, adult specimens had to be separated from juveniles. In Chapter 5 it was identified that females tend to be smaller than males. The length of the shortest female of the LXBE-S1 cohort is used as a cut-off value (11.8 mm) that artificially separates adults from juveniles in this study. Note that there is certainly overlap in the size distributions of juveniles and adults, but adults of LXBE S1 are already comparatively small considering the length of the overall largest specimen of this study (23.7 mm). Therefore, the bulk of the adult specimens has been captured using this cut-off value. This is the most practical procedure, but it should be stressed that the boundary is artificial and that size by itself holds

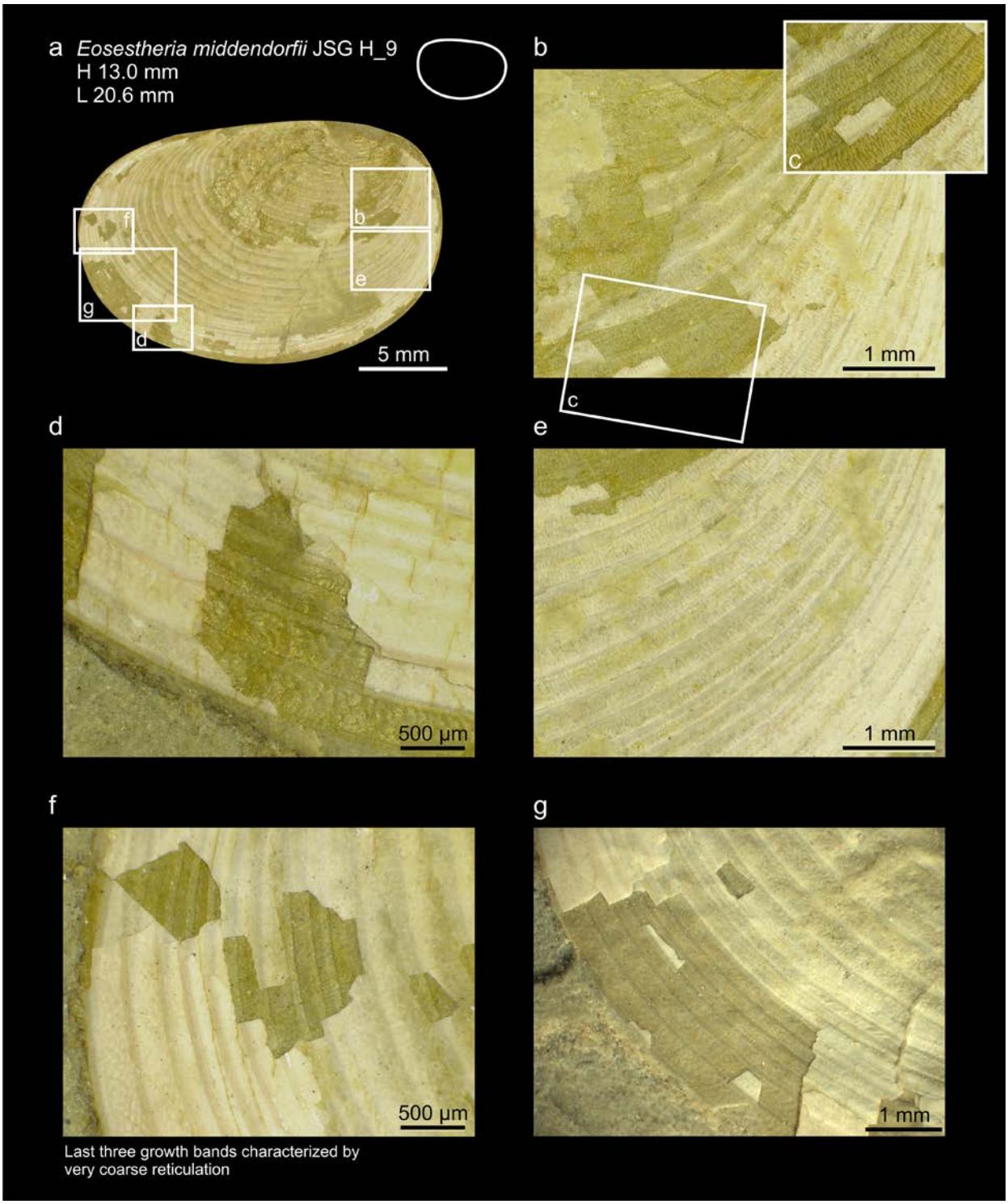

Fig. 6.1. *Eosestheria middendorfii*, JSG H_9, Bed 3. (a) Overview. (b, c) Anteroventral of the respective developmental stages. (d, g) Posteroventral. (e) Anteroventral. (f) Posterior. Radial lirae of intermediate developmental stages are replaced by a coarse and shallow reticulation (d, f-g). Note that there is no crowding of growth increments in this specimen.

environmental information. Also note that the presence of growth-band crowding as a possible criterion for the differentiation between juveniles and adults is not valid, as some of the largest specimens display no such crowding (Fig. 6.1).

It has been suggested by several authors to use Burnaby's method (Burnaby, 1966) for size correction (Rohlf and Bookstein, 1987; Rohlf, 1990; Hammer and Harper, 2006), which eliminates variation parallel to *PC1* by projecting the log-transformed

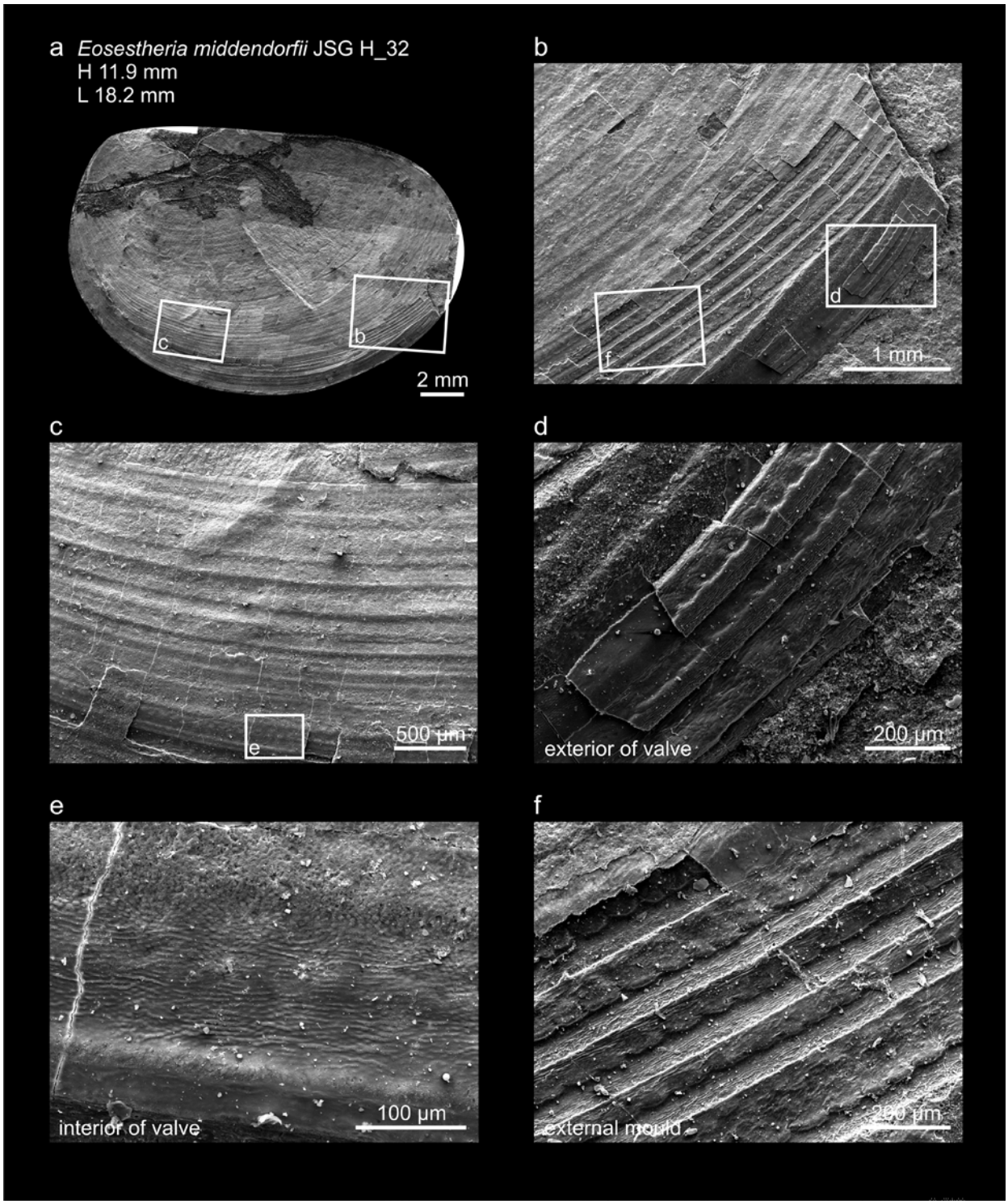

Fig. 6.2. *Eosestheria middendorfii*, SE images of JSG H_32, Bed 3. (a) Overview. (b, c, e) Predominantly interior view that is smooth with hints of concentric ridges and radial lirae. (d) Exterior fragments. The top of an uncovered prolongation of growth band (Fig. 4.1) is visible. (f) External mould with fine concentric striations on the concentric ridges.

measurements onto a plane orthogonal to this axis. This transformation removes the allometric size-dependent shape variation. *Canonical variate analysis* (CVA) is carried out subsequent to the transformation of the data through Burnaby's method, which attempts to maximize separation between the four groups. The presence of different morphological groups observed within the CVA plot is statistically tested by the multivariate analysis of variance

(MANOVA). A *p*-value based on Rao's *F* will be given with the following null hypothesis:

H_0: Individuals of *Eosestheria middendorfii* of Lake Sihetun are morphologically alike, manifested in equal multivariate means.

It is furthermore examined whether the three different localities yield distinct morphogroups and whether Phase-2 clam shrimps are morphologically distinguished from Phase-3 clam shrimps (pairwise comparisons). Hotelling's T^2 is employed with the following null hypothesis:

H_0: Individuals of *Eosestheria middendorfii* of two localities (or alternatively two time intervals) of Lake Sihetun are morphologically alike, manifested in equal multivariate means.

Clam shrimps of Jianshangou

The range of form so far documented for *Eosestheria middendorfii* can be extended. Extreme carapace sizes encountered in Bed 3 of Lake Sihetun are pictured in Figs. 6.1-6.4. The largest clam shrimp of excavation JSG yields a length of 22.9 mm (Fig. 6.3c-e), only one clam shrimp of ZJG surpasses this value (Fig. 6.5). The smallest length measured is 1.0 mm (Fig. 6.4a).

The specimens excavated from Bed 3 allow for emendations to the diagnosis of *E. middendorfii* of Chapter 4, as a change in ornamentation on the last few growth bands of very large forms is revealed (*L* > 20 mm Figs. 6.1-6.3). The radial lirae recognized on growth bands of intermediate to adult developmental stages of specimen 131915 (Figs. 4.12) are replaced by a coarse and shallow reticulation. This feature is best represented by Fig. 6.1d, f, g. This transition does not mark a new species, corroborated by the fact that ornamentational features of intermediate developmental stages are identical to *E. middendorfii* (Fig. 6.1c). Moreover, the broad growth-line width in the specimens of Figs. 6.1-6.3 reveals that radial lirae are restricted to the lower parts of growth bands, which is exemplified by Fig. 6.2d, f. The upper parts of growth bands are smooth and they are normally covered by an earlier growth increment in a crowded carapace margin. Concentric ridges are marked by fine concentric striations (6.2f).

Multivariate analyses of linear measurements

PCA of the complete dataset of 348 specimens

Linear measurements of *E. middendorfii* have been log-transformed and its principal components identified (Fig. 6.5). The dataset is a composite of *E. middendorfii* specimens from all three excavation localities within Lake Sihetun. Overall carapace lengths range between 1 mm and 23.7 mm. The first three principal components explain 99.2% of the variance in the dataset. *PC1* accounts for 97.4 % of the total variance, while *PC2* and *PC3* explain only 1.1 % and 0.7 %, respectively. According to the Jolliffe cut-off, correlation between variables is exhausted beyond *PC1*. Even though variances of *PC2* and *PC3* are small, they are nevertheless meaningful for the detection of shape variation.

All nine linear measurements have positive loadings (Table 6.2) on *PC1* with roughly equal contribution of each variable to this component (Fig. 6.5a). Hence, *PC1* represents a variable related to overall carapace size and can be regarded as an allometric size vector, indicating size variation and size-related shape-variation (Kowalewski et al., 1997). Loadings on *PC2* contrast long *Av, a,* and *Cr* in very young juveniles versus long *Ch, c,* and *L* in juveniles of later developmental stages and adults. The overall smallest specimen (JSG C17_2) yields the highest score on axis 2, as a result of its comparatively small dorsal margin in combination with a submedian location of the larval valve (relatively large *Cr*). *PC3* strongly increases with an increase of *Arr* and decreases with an increase of the dorsal margin (*Ch*), *Av*, or *Cr*. The minimum spanning tree in Fig. 6.5a approximately

Table 6.2. Loadings on *PC1* to *PC3* of a set of linear measurements of 348 specimens.

	PC1	*PC2*	*PC3*
a	0.32	0.29	-0.07
b	0.33	-0.03	0.19
c	0.35	-0.25	0.04
Arr	0.33	0.03	0.82
Av	0.31	0.69	-0.25
Ch	0.36	-0.52	-0.42
Cr	0.32	0.21	-0.21
H	0.33	-0.09	-0.01
L	0.34	-0.22	-0.07

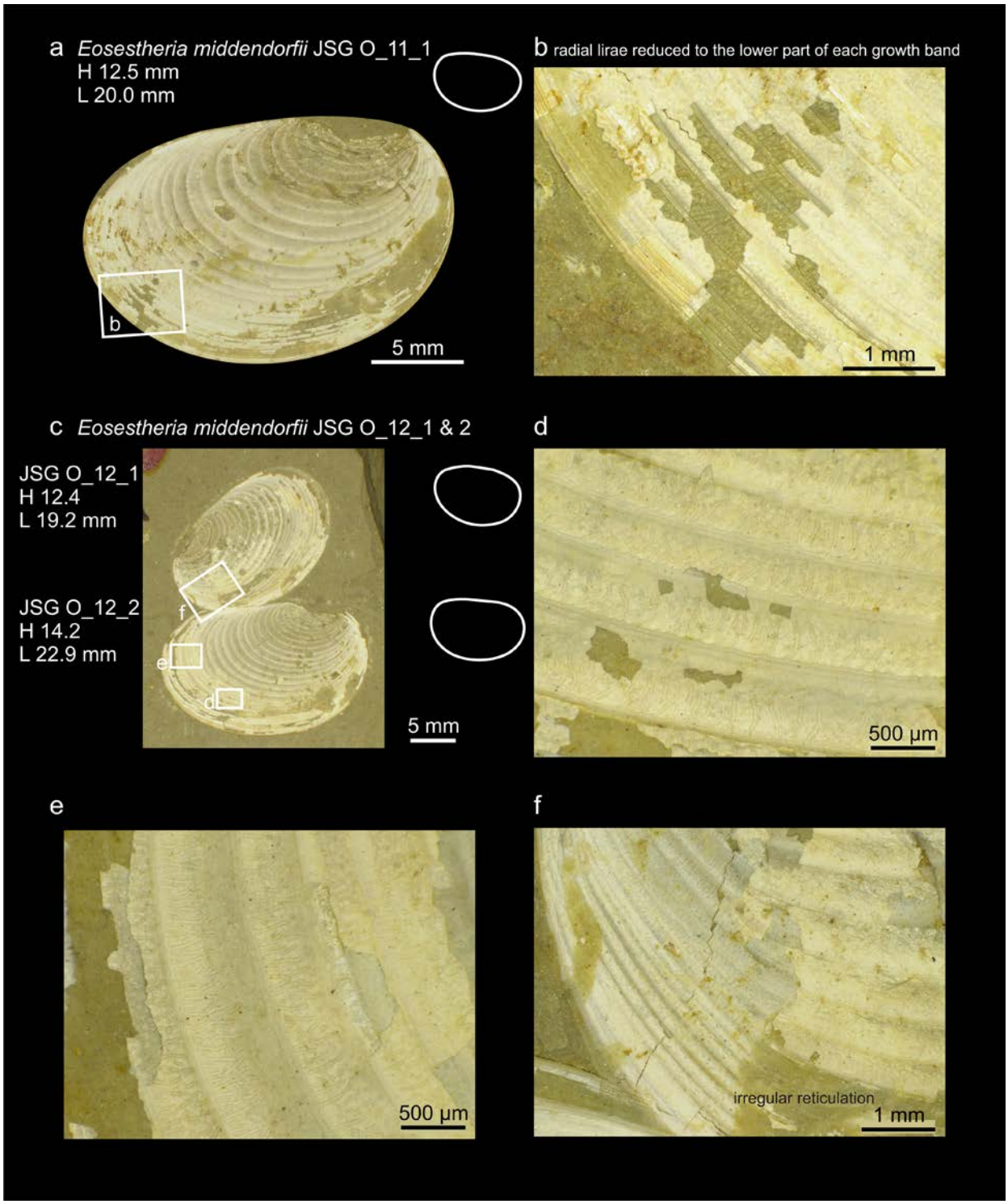

Fig. 6.3. *Eosestheria middendorfii*, Bed 3. JSG O_11_1 (a-b), JSG O_12_1 (c, f), and JSG O_12_2 (c-e). JSG O_12_2 is the largest clam shrimp of excavation JSG. (e) Irregular and branching lirae at the posterior of the valve are in fact restricted to the lower part of growth bands, with smooth upper parts that are otherwise covered by earlier growth increments in crowded carapaces. (f) The transition from lirae to coarse, irregular reticulation is also present within the anteroventral part of the carapace.

follows carapace size. There is a hint that *PC2* scores are high for juveniles that exhibit lengths of less than 1.9 mm. All nine specimens with lengths < 1.9 mm are marked in Fig. 6.5a. *PC2* does not seem to discriminate between juveniles of later developmental stages and adults. Convex hulls of JSG and LXBE occupy a similar area in Fig. 6.5b, while that of ZJG is considerably smaller. This confirms that ZJG is an all-adult sample, while juveniles of diverse ontogenetic stages are present within the latter

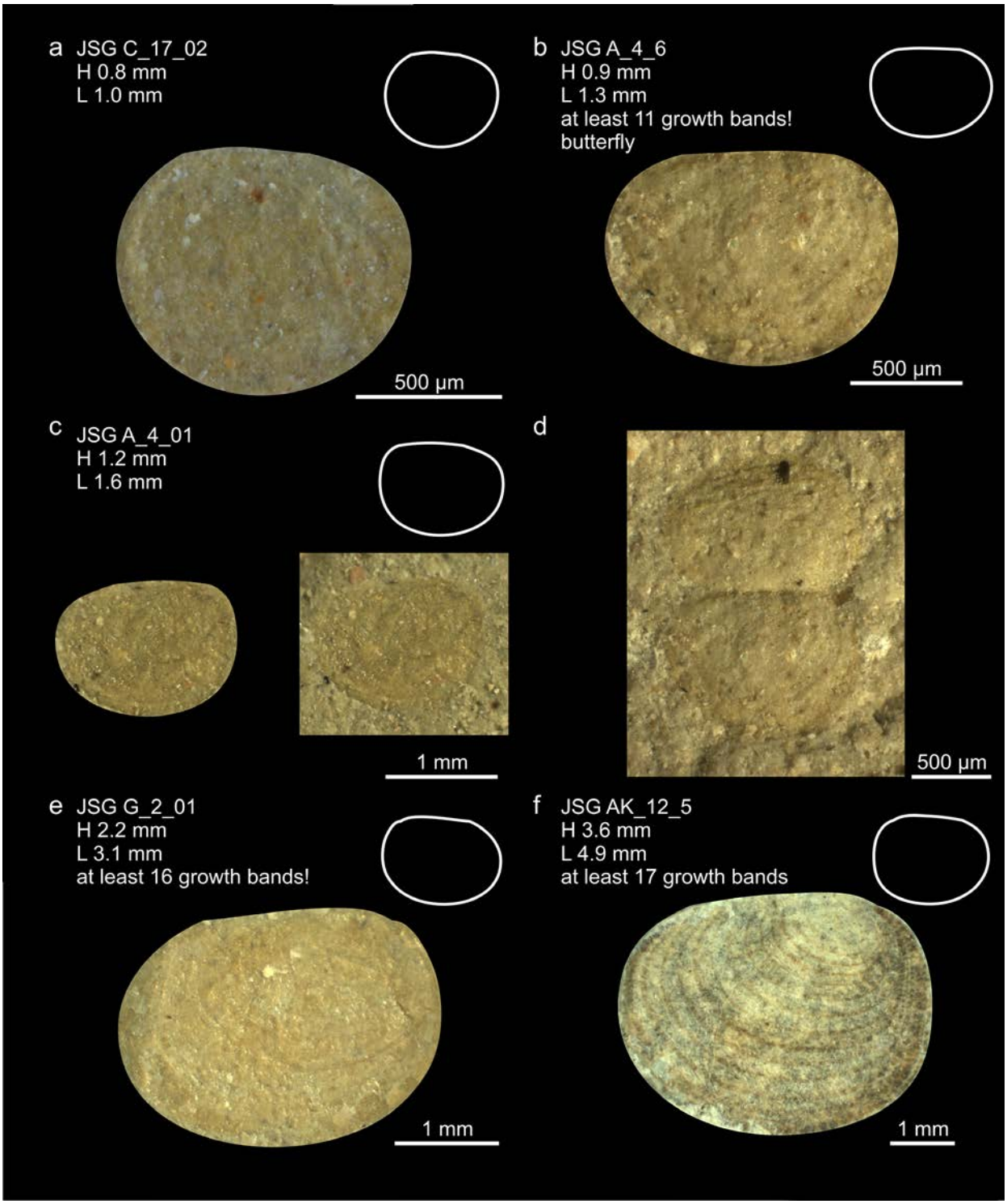

Fig. 6.4. *Eosestheria middendorfii*. Juveniles of Bed 3 (a-e) and Bed 2 (f) from excavation JSG. Micro-ornamentational features needed to identify these juveniles are not preserved, rendering them impossible to determine by current diagnostic criteria. The determination of the growth pattern of these individuals will identify whether these "featureless" juveniles can be assigned to *E. middendorfii*.

two. The higher shape variation within the mixed juvenile-adult samples implies allometry within *E. middendorfii*.

Multivariate allometry

The multivariate morphometric dataset investigated for allometry is composed of nine variables (distance measurements) of 196 individuals that lived during Phase 3 of Lake Sihetun near JSG

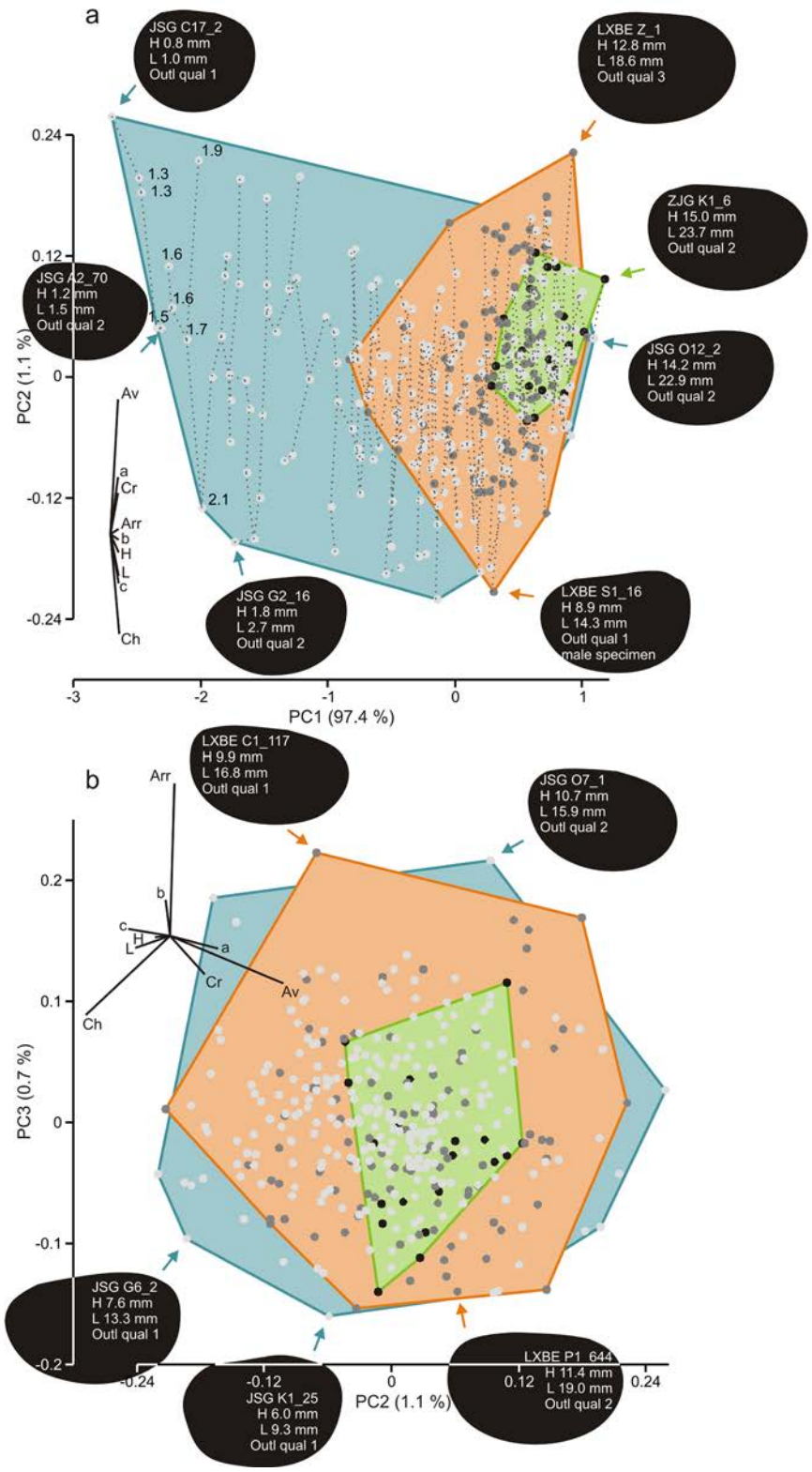

← **Fig. 6.5.** Principal component analysis of log-transformed measurements of a multi-size sample comprising 348 specimens of *Eosestheria middendorfii*. (a) *PC1* versus *PC2* and (b) *PC2* versus *PC3*. The three excavation localities JSG, LXBE, and ZJG are represented by three convex hulls and coded by blue/light dots, orange/medium-dark dots, and green/black dots, respectively. Loadings are rescaled and arbitrarily placed as vectors. Carapace outlines indicating extreme morphologies are not to scale, but their heights and lengths are given. (a) Loadings contribute roughly equally to *PC1*, which increases when carapace variables increase. It therefore represents an allometric size vector. The minimum spanning tree approximately follows size. The lengths of the ten smallest individuals are given in mm. *PC2* decreases as variables such as the dorsal margin (*Ch*) or length (*L*) increase and it increases as *Av*, *a*, and *Cr* increase. (b) *PC3* is also negatively correlated with the dorsal margin (*Ch*), but it sharply increases with an increase of *Arr*. This figure visualizes the presence of juveniles within the excavations. Convex hulls of JSG and LXBE occupy a similar area in (b), owing to the presence of juveniles in the two excavations. Shape variation in the all-adult sample of ZJG (green) is smaller, implying allometry within this species. Outl qual = outline quality.

(Fig. 6.6). Focussing on individuals of a single phase reduces the ecophenotypic variation derived from palaeoenvironmental differences between phases 2 and 3 (chapters 1 and 2).

Allometry relates the increase in size of one variable to that of another and allometric coefficients identify the spatial distribution of relative growth rates. *k* is the growth rate of one variable relative to that of a standard (Zelditch et al., 2004).

97.97% of the variation is captured by *PC1* and correlation between variables is exhausted beyond it, so it can be considered a meaningful size measure. The 95 % confidence interval for variable *Arr* includes value 1, indicating isometry. Length-related

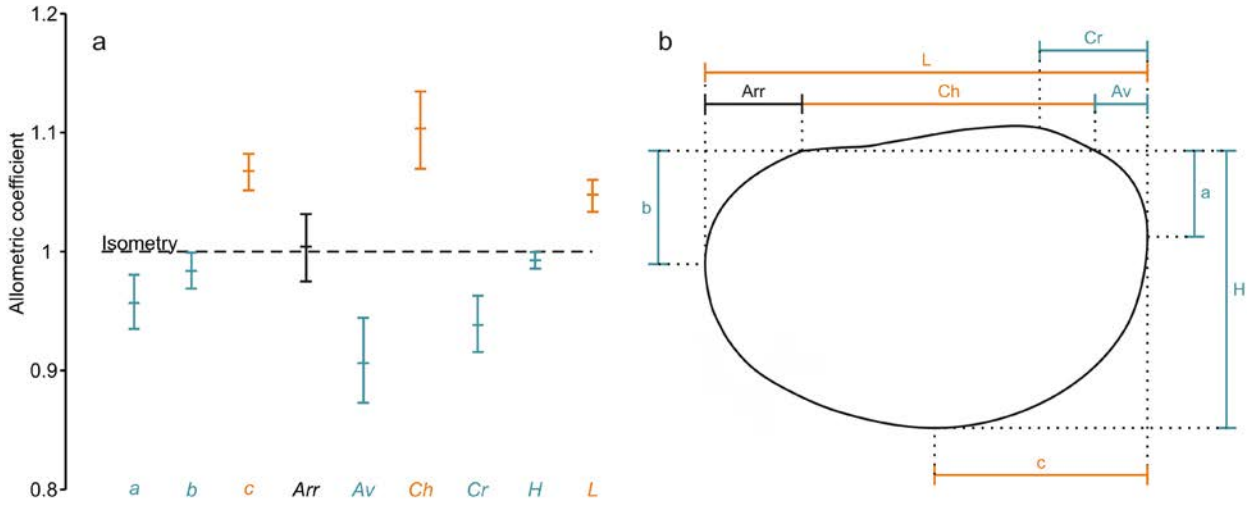

Fig. 6.6. (a) Multivariate allometric coefficients (horizontal bars) for nine carapace characters of *Eosestheria middendorfii* based on 196 specimens that lived during Phase 3 of Lake Sihetun (excavation JSG). Vertical lines mark 95% confidence intervals. *k* is the growth rate of one measurement with respect to overall size represented by *PC1*, which explains 97.97% of the variance. The growth of the isometric variable *Arr* ($k = 1$) keeps pace with that of the entire carapace. Variables displaying positive allometry ($k > 1$) are *c*, *Ch*, and *L*. They increase in size relative to the overall carapace size during growth. Negative allometry has been determined for *a*, *b*, *Av*, *Cr*, and *H* ($k < 1$), which decrease in size relative to overall body size. (b) Schematic representation of variables that relatively increase (orange) and decrease (blue) with increasing overall carapace size during growth.

variates (*c*, *Ch*, *L*) show positive allometry, while allometry for *a*, *b*, *Av*, *Cr*, and *H* is negative. This means, while *E. middendorfii* is growing older, variables colour-coded in orange in Fig. 6.6b (*c*, *Ch*, *L*) are getting relatively larger, while those in blue (*a*, *b*, *Av*, *Cr*, and *H*) are getting relatively shorter compared to carapace size. The allometric coefficient on the dorsal margin (*Ch*) is highest.

Pairs of variables are compared and all inspected bivariate plots reveal no obvious divergences from growth trajectories, exemplified by the bivariate plots of Fig. 6.7 (*Ch* versus *Av* bivariate allometric coefficient a ~ 0.83, $p < 0.001$; *Ch* versus *H* bivariate allometric coefficient a ~ 0.89, $p < 0.001$).

Fourier shape analysis

Ontogenetic shape variation of *E. middendorfii* has been visualized through Fourier shape analysis of carapace outlines (Fig. 6.8). The Fourier coefficients are listed in Supplementary 6.1. The first seven principal components are meaningful and account for 33.5%, 15.8%, 9.5%, 8.6%, 7.0%, 4.9%, and 4.5% of the variation, respectively. *PC1* represents a trend from subcircular juveniles (higher scores) to ovate/elongate adult specimens (lower scores). The smallest specimen of the analysis exhibits the highest score on *PC1*. While juveniles of early developmental stages occupy the right part of Fig. 6.8, specimens of more developed stages disperse along smaller *PC1* scores. The scatter is a result of ecophenotypic variation, ontogenetic variation, and sexual dimorphism in combination with variation resulting from deformation and alignment during diagenesis. The synthetic outlines in Fig. 6.8 give a good representation of the overall morphospace *E. middendorfii* of Phase 3 is occupying. Note that *PC1* does not capture carapace size, as this analysis is entirely based on shape.

The two specimens exhibiting the most negative scores on *PC2* partly yield excellent outline quali-

Table 6.3. Statistical decisions are based on pairwise comparisons using the Hotelling's T^2 test statistic.

Localities	Hotelling's T^2, p-value	Interpretation
ZJG and LXBE	0.112	same
ZJG and JSG (Phase 2)	0.031	different (significant)
ZJG and JSG (Phase 3)	0.001	different (highly significant)
LXBE and JSG (Phase 2)	0.003	different (highly significant)
LXBE and JSG (Phase 3)	0.001	different (highly significant)
JSG (Phase 2) and JSG (Phase 3)	7.11E-5	different (highly significant)

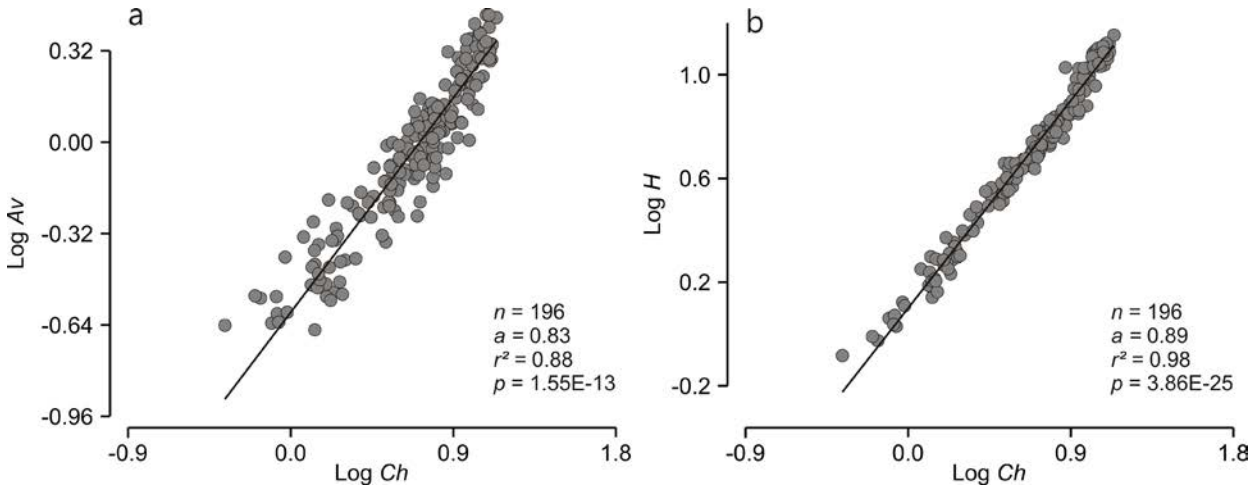

Fig. 6.7. Bivariate allometries. Scatter plots of (a) *Ch* versus *a* and (b) *Ch* versus *H*. Log-transformed data are fitted by RMA regression lines. The departure from isometry is statistically significant in both cases ($p < 0.001$). Individuals follow single growth trajectories, implying the absence of multiple morphs.

ties, so problems with data acquisition can be ruled out. They are marked by relatively long, flattened posteroventral margins. Hence, *PC2* is a variable that is affected by the *b*/*H* ratio. *PC3* (not pictured) picks up the prominence of the umbo. Morphological separation of juveniles and adults is best accomplished along *PC4* (Fig. 6.9), which is driven by the roundness of the posterior margin. Groups in Fig. 6.9 are based on two size classes. Proposed adult specimens are larger than 11.8 mm, following the smallest adult of Chapter 5. Adults exhibit broadly rounded posterior margins (compare with Fig. 6.1, 6.3), opposed to more pointed margins in juveniles.

Canonical variate analysis of adult specimens from three excavations

This section investigates whether adult carapace morphologies yield variation that is not growth-related by testing: (1) whether clam shrimps of the three excavations group by locality and (2) whether Phase-2 clam shrimps are morphologically distinct from Phase-3 clam shrimps. In short, it is testing whether environmentally-controlled variability of the carapace can be identified in time and space. Allometric size-dependent shape variation has been eliminated from the dataset prior to CVA (Fig. 6.10). The vector plot indicates that *Cr* and *Av* are positively correlated with the first canonical axis, while *a*, *b*, *c*, and *Arr* are negatively correlated with this axis. *Ch*, *H*, and *L*, which exhibit only little correlation with the first axis, are positively correlated with CV2.

The four samples are morphologically different (MANOVA $p < 0.001$). Pairwise comparisons (Table 6.3) show that at a significance level of 5%, excavation JSG can be separated from excavations LXBE and ZJG, while there is no significant separation between the latter two. Morphological separation in time (Phase 2 versus Phase 3) is highly significant and, remarkably, most pronounced between clam shrimps of the same excavation (JSG). It should be noted at this point that outliers in the JSG scatter (blue), which are not enclosed in any other convex hull, can also be separated based on their fossil community as documented in the correspondence analysis of Fig. 7.6a. (Refer to Chapter 7 for the palaeocommunity analysis of excavation JSG.) Conversely, all other Phase-2 specimens are morphologically alike to specimens of the remaining two localities.

Discussion

Palaeobiological implications

Palaeontological species are effectively morphological species that tend to change gradually over time (Gingerich, 1985), but change may also be punctuated. Clam shrimps are morphologically simple and diagnostic features are bound to the bivalved carapace. Changes in carapace morphology during the evolutionary history of the spinicaudatans are seemingly only moderate and extant spinicaudatans are marked by an overall low diversity (e.g., Brtek and Thiéry, 1995). There have been considerations that "perceived" taxonomic change was related to morphologic complexity, with more complex forms changing more rapidly over time (Schopf et al., 1975). This resulted in the hypothesis that

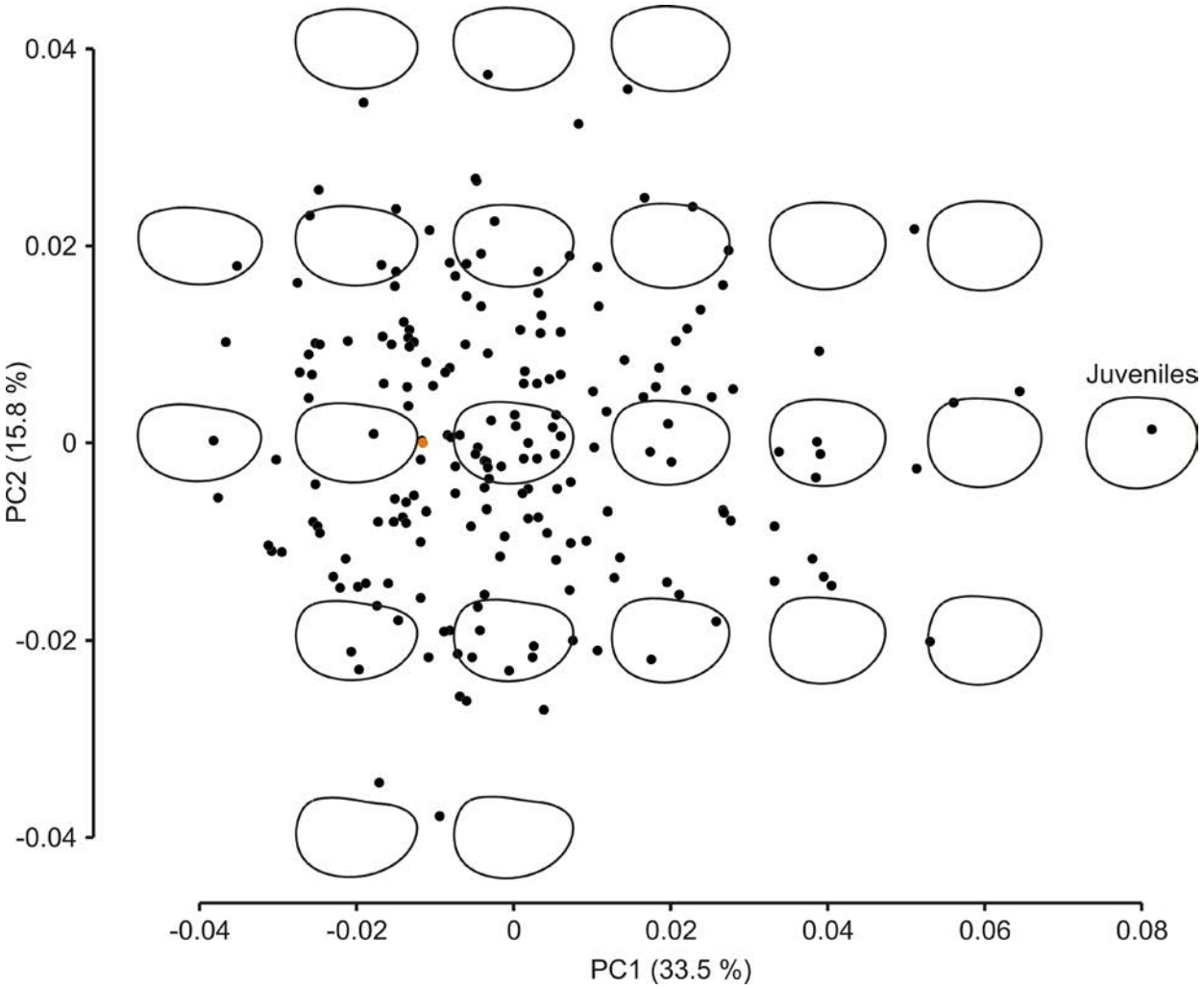

Fig. 6.8. Fourier shape analysis and visualization of the morphospace of *Eosestheria middendorfii* based on 196 individuals that lived in Lake Sihetun during Phase 3. Young juveniles occupy the right part of the diagram, older juveniles and adults cannot be separated within this plot. The largest specimen (JSG O_12_2, orange dot) does not exhibit the most extreme morphology, indicating that *PC1* is not a good discriminator between juveniles of later developmental stages and adults.

slowly evolving species were artefacts and generally under-discriminated. In other words, morphospecies represent numerous biological species in reality. In contrast, careful applications of quantitative methods to one of those "slowly evolving" groups showed that taxonomic diversity was not necessarily a result of morphological complexity (Kowalewski et al., 1997; tested on extant lingulide brachiopods). In their actualistic study, Kowalewski et al. (1997) demonstrated that even morphologically simple species can be discriminated through the use of multivariate morphometric methods based on linear measurement data, contradicting the hypothesis of Schopf et al. (1975). This shows that linear variables of shell morphologies may yield the same taxonomic resolution as modern classification methods. This result is promising for other groups characterized by simple morphologies, such as clam shrimps.

Adult clam shrimps of the three excavations have all been assigned to one species, *Eosestheria middendorfii*, through careful analysis of ornamentational features. However, the lack of diagnostic features within the smaller clam shrimps of Phase 3 (Fig. 6.4) does not permit a taxonomic identification. Their classification needs to be based on the study of carapace growth. The growth of organisms follows simple laws: (1) the rate of growth of a body part is proportional to the size of an organism, (2) growth slows down with increasing age, and (3) it is affected by the environment (Huxley, 1932). After the removal of allometry, environmentally controlled variation can be identified.

In general, variation observed within the clam shrimps of Lake Sihetun is a combination of phenotypic variation, ontogenetic variation, and sexual dimorphism. Variation resulting from malforma-

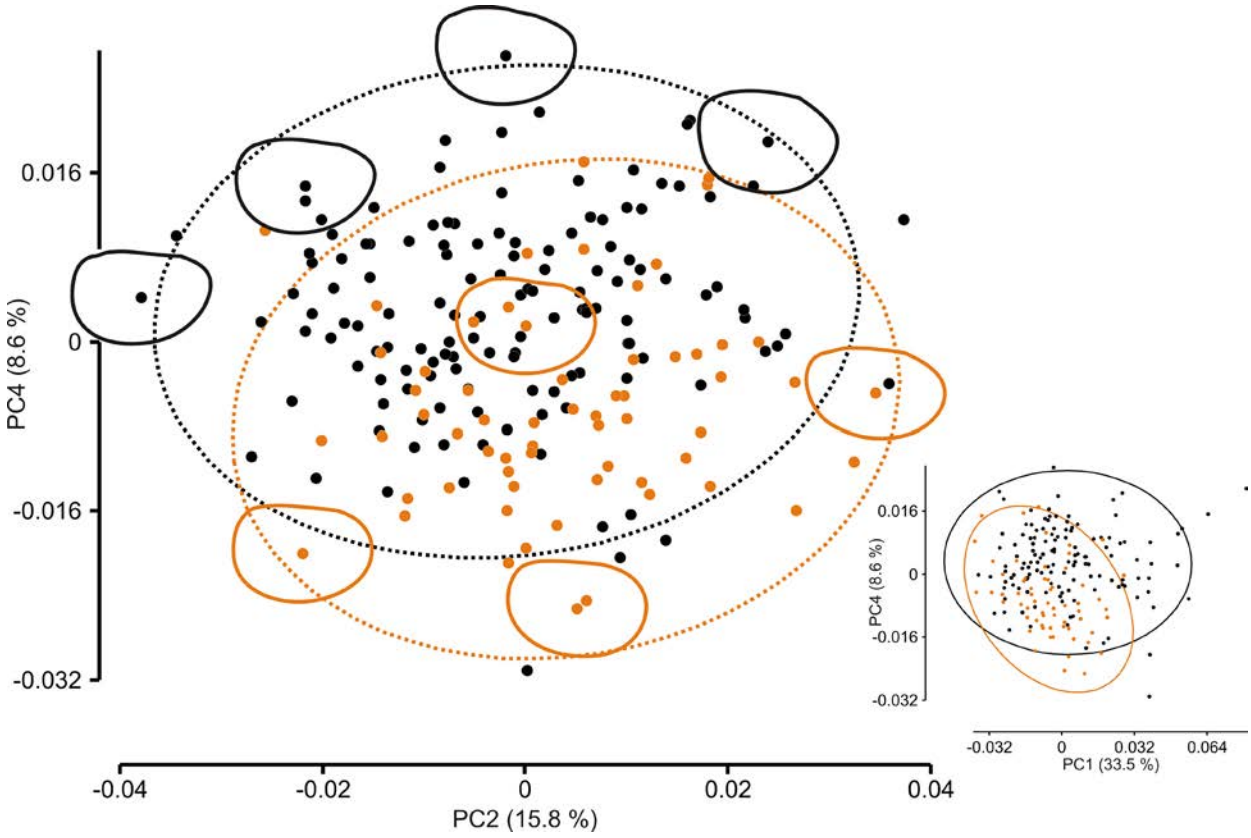

Fig. 6.9. Fourier shape analysis of 196 outlines of *Eosestheria middendorfii*. Morphological separation between juveniles and adults is best represented by the bivariate plot of *PC2* versus *PC4* of the Fourier coefficients. The inset plot shows *PC1* versus *PC4* for comparison. Individuals in orange are proposed adult specimens (L > 11.8 mm). Juveniles are represented by black dots. Selected outlines are centred over their corresponding specimens. The overlap between the two groups is, among other things, due to the arbitrary nature of the cutoff value that classifies specimens as adults and juveniles. Importantly, larger specimens tend to occupy the lower part of the plot, rendering *PC4* the best discriminator between ontogenetic stages and its scores might be used for further analyses. While *PC2* is driven by the *b*/*H* ratio, *PC4* represents the roundness of the posterior margin. Individuals with high scores on *PC4* are marked by pointed posterior margins (juveniles).

tion and deformation as well as alignment during compaction has been dealt with through careful identification of the variation represented by the various principal components of the Fourier-coefficient dataset of Fig. 5.5. More than 30% of the morphological variation within adults is evidently due to carapace deformation, alignment, and malformation. Sexual dimorphism accounts for about 10% of the variation in adult carapaces (Chapter 5).

Ontogenetic and phenotypic variation within *E. middendorfii* (this chapter) has been identified by using two datasets consisting of linear measurements and Fourier coefficients, respectively. In a first step, overall variation has been visualized and growth assessed by looking at allometric coefficients. Subsequently, adult carapace morphology has been corrected for allometry to investigate ecophenotypic variation.

PCA of the complete dataset of 348 specimens

In the scatter plot spanned by the first two PC axes (Fig. 6.5), ZJG samples occupy the right region of the space spanned by excavation JSG, where both adults and juveniles occur alike. There is no separation of excavation localities along *PC1*. It can be interpreted as an allometric size axis, which represents individuals of different ontogenetic ages. Excavation ZJG yields only adult clam shrimps and LXBE is marked by occasional occurrences of juveniles (Fig. 6.5). The high number of juveniles excavated from locality JSG accounts for the extended region the data points occupy in the *PC1-PC2* scatter plot (Fig. 6.5a). There is no separation of localities along *PC2* or *PC3*. The extended convex hulls of JSG and LXBE in comparison to ZJG are largely due to growth-related differences in shape. Growth-unrelated differences in shape cannot be determined from this analysis. It is therefore worthwhile

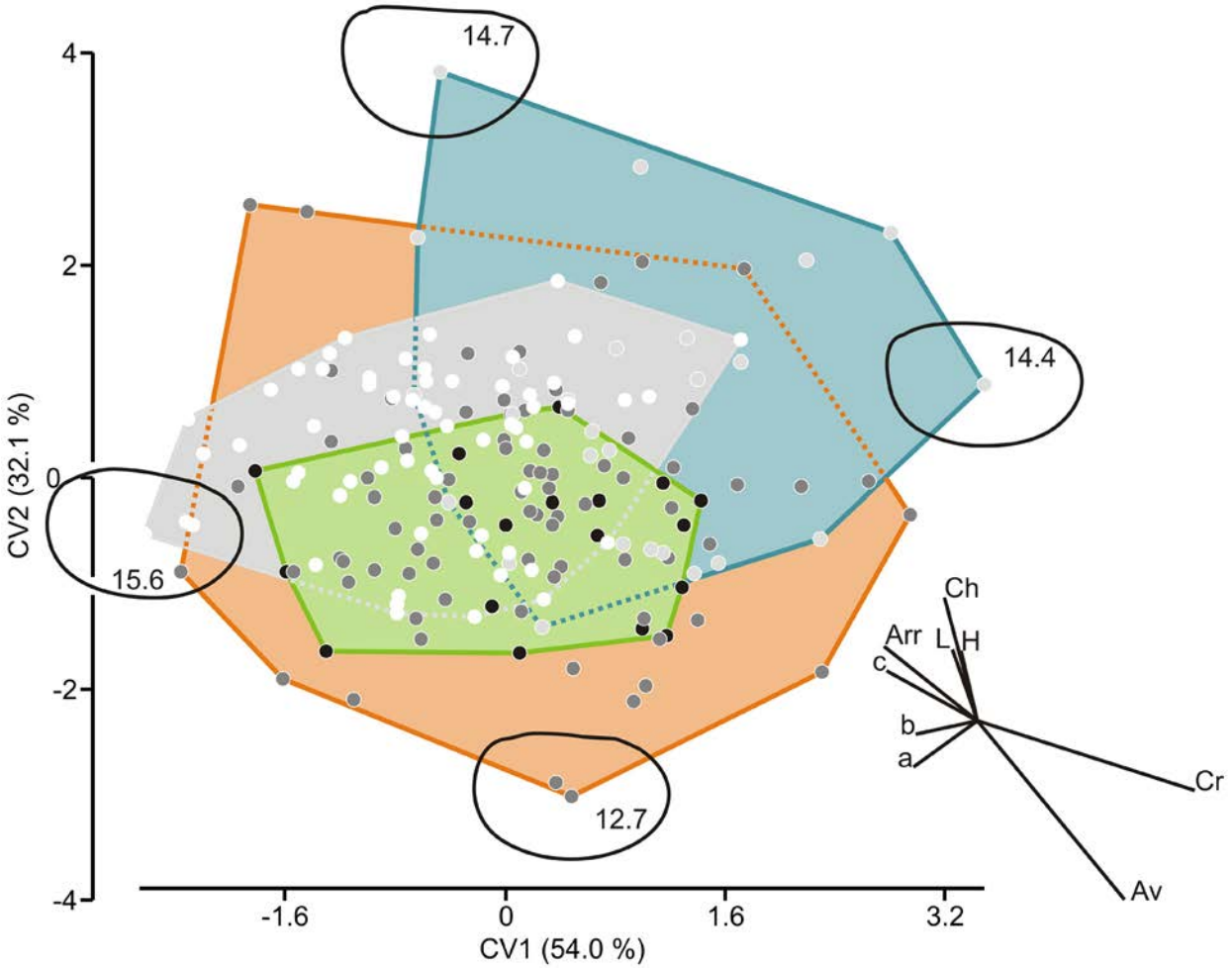

Fig. 6.10. Size-free canonical variates for 184 adult specimens of *Eosestheria middendorfii* from three different localities within Lake Sihetun and two time intervals. The four *a priori* groups are: ZJG, green convex hull/black dots (n = 19); LXBE, orange convex hull/medium-dark dots (n = 77); JSG, Phase 2, blue convex hull/light dots (n = 26); JSG, Phase 3, grey convex hull/white dots (n = 62). Four outline shapes, each centred on their corresponding data point, are sketched and their lengths are given (in mm). The origin of the vector plot is arbitrarily placed and has been rescaled. It indicates that *Cr* and *Av* are positively correlated with CV1, while variables *a*, *b*, *c*, and *Arr* are negatively correlated with this axis. *Ch*, *H*, and *L* are positively correlated with CV2. Even though all four groups exhibit considerable overlap, samples are morphologically distinct (MANOVA p = 1.01E-07). Overall variation in Phase-2 specimens is larger than that of Phase-3 specimens, possibly because Phase-2 specimens are derived from three different localities within Lake Sihetun. Statistical testing indicates that JSG Phase 2 and JSG Phase 3 form distinct morphogroups, respectively, while ZJG and LXBE are indistinguishable.

to examine growth-related changes in the carapace of *Eosestheria middendorfii* prior to identifying the ecophenotypic variation.

Carapace growth

Allometry is pronounced and departure from isometry is partly considerable (Fig. 6.6). With increasing size of *Eosestheria middendorfii*, variables *c*, *Ch*, and *L* increase relative to *a*, *b*, *Av*, *Cr*, and *H*. The negative allometry of *Cr*, for example, means that the larval valve assumes a more anterior position in older individuals. The growth of *Arr* keeps pace with that of the entire carapace, resulting in unvarying proportions relative to size. This growth pattern of positive allometry for length related measurements (*c*, *Ch*, and *L*) most likely reflects that the soft parts of *E. middendorfii* were attached to the carapace near its head, as in extant species. The posterior part of the carapace had to accommodate the increasing thorax and abdomen. Developmental polymorphism, which would have led to a divergence from the growth trajectories in the bivariate plots (Fig. 6.7; Kowalewski et al., 1997), has not been identified. This lack of discontinuities within the bivariate plots confirms the monospecific nature of the analyzed specimens. In summary, variation within indi-

viduals of Bed 3 is mostly growth related, so there is strong evidence for the allocation of the juveniles of Fig. 6.4 to *E. middendorfii*.

Morphological separation between juveniles and adults through Fourier shape analysis is best achieved along *PC4* (Fig. 6.9), which by trend separates individuals with round posterior margins (adults) from those with pointed posterior margins (juveniles).

Canonical variate analysis of adult specimens from three excavations

There is considerable overlap between (1) all three localities and (2) the two time intervals (phases 2 and 3; Fig. 6.10). Nevertheless, pairwise comparisons between localities and phases (Table 3) indicate that *Eosestheria middendorfii* of Phase 3 can be statistically distinguished from Phase-2 individuals of all three locations. Phase-2 clam shrimps of excavations ZJG and LXBE are morphologically alike. The morphogroup of excavation JSG is influenced by the morphological extremes of clam shrimps that are associated with gastropods and bivalves. The vector plot in Fig. 6.10 indicates that after carapace morphology has been corrected for allometry, most of the variation results from *Av* and *Cr* relative to the other variables studied.

Variation caused by sexual dimorphism should be present within Fig. 6.10, but it is comparatively small (Chapter 5) and cannot explain the disparity encountered within this analysis. The statistical separation of the size-free data into three morphogroups implies that there must be parameters influencing carapace shape apart from allometry. They most likely reflect environmentally controlled changes.

Ecophenotypic variation

Different degrees of ecophenotypic variation have been documented in space and time (Fig. 6.10; Table 6.3). For example, *Eosestheria middendorfii* of JSG (Phase 2) exhibit significantly different carapace shapes than those of localities ZJG and LXBE. Ecophenotypic variation in time between phases 2 and 3 is even more pronounced, which reflects a change from an oxygen-controlled lake-floor environment (Phase 2) to a temperature-controlled marginal facies (Phase 3). Both environmental regimes are identified and described in detail in Chapter 7.

Emended adult characters of *Eosestheria middendorfii*

Radial lirae (Fig. 6.1c), a characteristic ornamentational feature of intermediate to late developmental stages, are replaced by a coarse and shallow reticulation in very large specimens (Fig. 6.1d). This change in reticulation is often not visible due to crowding of growth increments. Furthermore, radial lirae on growth bands of late developmental stages are restricted to the lower part of growth bands (Fig. 6.2d, f). Concentric ridges exhibit fine concentric striations (6.2f).

Individuals of *Eosestheria middendorfii* with only 'separate' growth-line densities (as opposed to wide, Table 4.2) have been encountered in several horizons studied, shedding some doubt on the usefulness of growth-band width as a diagnostic feature (Fig. 4.4).

Juvenile characters of *Eosestheria middendorfii*

Even though the shape of *Eosestheria middendorfii* is simple, ontogenetic variation is profound. The juvenile characters identified through a variety of multivariate analyses (Figs. 6.6-6.9) are (1) a submedian position of the larval valve, (2) a subcircular carapace shape, and (3) a more pointed posterior margin that goes along with a flattened posteroventral margin. The ontogenetic growth of *E. middendorfii* is marked by a relative increase in length-related variables (*c*, *Ch*, *L*) and a relative decrease in *a*, *b*, *Av*, *Cr*, and *H*. The allometric coefficient on the dorsal margin (*Ch*) is highest. Therefore, while the larval valve of an individual progressively assumes an 'anterior' position (Table 4.2) during ontogeny (expressed by a relative decrease in *Cr*) the dorsal margin becomes relatively longer. Juveniles of this strongly allometric species were probably ecologically different from older individuals, with transitions in functional demands resulting in transformations between size and shape (Zelditch et al., 2004).

Olesen and Grygier (2004) recognized seven different naupliar larval stages in spinicaudatan species, which range in length between 200 and 850 µm. The nauplius of stage 1 has a lecithotrophic appearance that lacks the characteristic carapace, *anlagen* of which appear in nauplius 4. The carapace is partly free in nauplius stage 6 and generally larger and better-developed in nauplius 7. Therefore, the smallest specimen of *E. middendorfii* recorded in this study (Fig. 6.4a) may have barely completed

the naupliar phase or may even represent one of the last two naupliar stages. There are no visible growth lines in this specimen, except perhaps for one that is faintly visible. Note that the larval stage as defined in this thesis ends when sexual maturity has been reached, expressed by egg clutches.

Conclusions

Ontogenetic and ecophenotypic variation in *Eosestheria middendorfii* have been identified in the present study. Juveniles, which yield no diagnostic features other than their carapace outlines, are morphologically described and compared to more developed stages. Developmental polymorphism has not been identified and the data fit a single allometric model, supporting the presence of a single species in Phase 3. Consequently, all initially featureless juveniles can be assigned to the strongly allometric species *E. middendorfii*.

With increasing overall carapace size, allometry is dominated by an increasing length of the dorsal margin relative to *Cr* and *Av*. Therefore, carapace shapes range from subcircular in juveniles of early ontogenetic stages to ovate in adult specimens. Furthermore, adult specimens exhibit a more anterior position of the larval valve in comparison to a submedian position in juveniles of early ontogenetic stages (*Cr*/*L*). Juveniles are also characterized by pointed posterior margins in comparison with the broadly rounded posterior margins of adults. This feature is expressed in specimens as small as 1.5 mm. The species diagnosis of *E. middendorfii* of Chapter 4 can be emended according to the growth-related shape variation identified.

As *E. middendorfii* is strongly allometric, the analysis of phenotypic variation has to be corrected for allometry. The analysis of ecophenotypic variation classified three distinct morphogroups in time and space. Excavation JSG forms its own morphogroup compared to the morphogroup spanned by LXBE and ZJG. Phase-2 clam shrimps are morphologically distinct from Phase-3 clam shrimps, which signals the presence of palaeoenvironmental – biotic and abiotic – changes to shape. Specifically, this reflects a change from an oxygen-controlled lake-floor environment (Phase 2) to a temperature-controlled marginal facies (Phase 3).

Chapter 7: Benthic community development and palaeoenvironment of an Early Cretaceous lacustrine fossillagerstätte

Chapter 7 is a joint project of the following authors:

Manja Hethke[1], Franz T. Fürsich[1], Baoyu Jiang[2,] Patrick Chellouche[1], Golda Schugmann[1]
[1]*GeoZentrum Nordbayern, FG Paläoumwelt, Germany*
[2]*School of Earth Sciences and Engineering, Nanjing University, China*

Introduction

The most elemental ecological question of this thesis is dealing with what determines the general high abundance and the distribution pattern of the Early Cretaceous clam shrimp *Eosestheria middendorfii* within Lake Sihetun. To answer this question we examine how abiotic and biotic factors combine to determine the population dynamics of this clam-shrimp species. Thus far, abiotic components have been deduced from sedimentological and taphonomic proxies (chapters 1-3). Of the biotic components, only clam-shrimp populations have been looked at (chapters 5 and 6). Herein, they will be viewed in the context of whole communities. For this purpose, the community relicts of 43 horizons of excavation JSG have been quantitatively documented, faunal associations determined, and temporal patterns recognized. Previous studies (Fürsich et al., 2007; Pan et al., 2012) have focussed on a single lake phase (Phase 2). This study presents the first account on Phase-3 lake communities. Importantly, it investigates the community development across the transition of Phase 2 into Phase 3, as recorded in the excavation near Jianshangou (Figs. 1.3, 2.1).

As Lake Sihetun existed at a palaeolatitude of 41.9°N (Enkin et al., 1992; Zhou et al., 2003) during a comparatively cool climatic interval with mean air temperatures of about 10°C (Amiot et al., 2011), it was most likely influenced by seasonally fluctuating abiotic components, expressed in summer hypoxia and winter re-oxygenation of the bottom waters (Fürsich et al., 2007). They must have led to seasonal community successions, which, for example, are manifested in the rhythmic presence of chrysophycean cysts within the sediments of Phase 2 (Chapter 1).

In addition to seasonal successions, pronounced environmental stress due to major disturbances to the ecosystem of Lake Sihetun must have had immense effects on population dynamics and long-term temporal patterns in community composition. Also, clam-shrimp occurrences have frequently been interpreted as mass mortality events, which thus far have only been connected to the abiotic environment. However, death resulting from senescence should be considered for this particular group and the discussion will benefit from a revision of this term. The main disturbances of Phase 2 were most likely connected to volcanic activity (Fig. 1.10; Jiang et al., 2011, 2012; Chapter 1) and recurring anoxia (Fürsich et al., 2007; Chapter 2). During this phase, bottom waters were governed by dysoxia with spells of anoxia, assuming holomictic, eutrophic conditions that episodically alternated with meromictic interludes. Spatial variations in bottom-water redox state were widespread (Chapter 2) and this division into sub-environments most likely led to repeated local extinctions of faunas within Lake Sihetun. Large disturbances to ecosystems are also known from extant lakes; extreme hydrothermal events initiated dramatic sedimentological and biotic changes within Lake Kivu around 5000 years B.P. (Haberyan and Hecky, 1987). In turn, bottom waters of Lake Sihetun were oxygenated during Phase 3 and possible mass mortality events must have been caused by different factors.

In order to understand long-term community successions, it is important to characterize the population ecology of *E. middendorfii*. Of particular interest will be the life cycle of this species, which may explain some of the more puzzling observations, such as the presence of numerous unfossiliferous layers within the sediments of Lake Sihetun (Fürsich et al., 2007; Pan et al., 2012; Chapter 1). It is problematic that interpretations of the population ecology of fossil clam shrimps are often based on an analogy with habitats of extant clam shrimps (Orr and Briggs, 1999; who critically addressed this problem). The presence of clam shrimps is often used as a line of evidence for "shallow and temporary" habitats (e.g., Todd, 1991; Wang, 1999; Fürsich et al., 2007). In particular, *E. middendorfii* has been proposed to have lived in quiet, shallow waters of about 2-50 cm to a maximum of 2 m depth near the lake

coast (Wang, 1999). This stereotypic interpretation of water depth is challenged in this chapter.

In summary, the main objectives of this chapter are (1) the identification of long-term community successions to understand ecological disturbances to the ecosystem of Lake Sihetun and (2) the characterization of the population ecology of *E. middendorfii* to demonstrate similarities as well as possible differences to the habitat of extant clam-shrimp species.

Geological setting

The Early Cretaceous Yixian Formation has been deposited within an interval of about 7 Ma (129.7 ± 0.5 Ma and 122.1 ± 0.3 Ma; $^{40}Ar/^{39}Ar$; Chang et al., 2009; Fig. 2.2b). In the Sihetun area it comprises four units (Lujiatun Unit, Lower Lava Unit, Jianshangou Unit, and Upper Lava Unit; Jiang and Sha, 2007), whose outcrop situation is illustrated in the geological map of Fig. 2.1. Refer to Fig. 2.2 for a schematic litholog of the formation. The worldwide famous fossillagerstätte of the Yixian Formation is formed by the lake sediments of the Jianshangou Unit (125.7 ± 2.6 Ma to 124.2 ± 2.5 Ma; $^{40}Ar/^{39}Ar$; Zhu et al., 2007). Repeated volcano eruptions, manifested in lava flows, magma intrusions, or ash layers (Fig. 1.10; Chapter 1), govern the depositional environment of the Yixian Formation.

The sediments of the so-called Lake Sihetun are represented by the Jianshangou Unit, which can be subdivided into four depositional regimes (beds 1-4; Jiang et al., 2012) that correspond to four general phases of lake evolution. Phase 1 was initiated by a caldera collapse (Jiang et al., 2011) and the subsequent rising of water levels. Phase 2 yields very fine, mainly suspension-derived deposits, while slightly coarser hyperpycnal flows governed Phase 3. A prograding fan delta led to the eventual siltation of the lake during Phase 4. Note that not all of the four beds of the Jianshangou Unit (Fig. 2.2) are present throughout the Sihetun area. Locality LXBE, for example, is lacking the delta deposits of Phase 4 (Fig. 1.3a). This study concentrates on beds 2 and 3 (equivalent to phases 2 and 3), from which the majority of the excellently preserved fossils originate.

Material and methods

This chapter focuses on palaeoenvironmental changes recorded in the excavation near Jianshangou (JSG, Fig. 2.1), which documents the abrupt sedimentological transition from Bed 2 into Bed 3. Bed 3 has not been sampled in any of the two previous excavations (LXBE and ZJG; Fig. 2.3). Thus, this study marks the first examination of palaeoenvironmental changes across the transition between phases 2 and 3. The sedimentological data of excavation JSG is summarized in Table 7.1. Community relicts were quantitatively documented for 30 horizons of Bed 3 and 13 horizons of Bed 2. The abundance data employed in this study consist of 33,226 quantitative specimen counts of nine taxa (Table 7.2).

Biodiversity. – Species richness (*S*) is listed in Table 7.2. To identify whether differences in species richness between horizons are influenced by sample size, richness is rarefied to the same number of individuals. Rarefaction is performed using vegan's rarefy function on the original counts (http://www.r-project.org/; vegan.r-forge.r-project.org) and results are listed in Table 7.2. Another estimate on biodiversity is based on the Shannon-Wiener index (*H'*), which considers the number of species and the relative abundance of taxa. *H'* will be 0 for a monospecific sample.

$$H' = - \Sigma p_i \ln p_i$$

p_i = is the proportion of a species

Orientation patterns of Ephemeropsis larvae. – In situ biostratinomic data for *Ephemeropsis trisetalis* have been obtained during the excavation by defining 12 directions, each of which are separated by 30° (Fig. 7.3; n = 43, 11, 83, 49, 14 for horizons JSG H, J, AA, AB, AP). This directional data is analysed as described by Davis (1986; formulas 5.42, 5.43). Each directional measurement can be thought of as a unit vector. The resultant length R gives the average direction of a set of vectors. Dividing R by the number of observations gives a range between 0 (vectors are randomly dispersed) and 1 (all vectors are pointing towards the same direction). The resultant quantity (, "mean resultant length") can be understood as a measure of dispersion, with larger values indicating orientation in the data and smaller values indicating a wide dispersal of vectors around a circle.

The data collected in the field give the 360° orientation of the larval head as plotted in Fig. 7.3d, where one dot represents one individual. However, if we imagine two individuals of *E. trisetalis* whose heads point towards opposite directions, the resultant vector will have a vector length of 0, even though both individuals exhibit the same orienta-

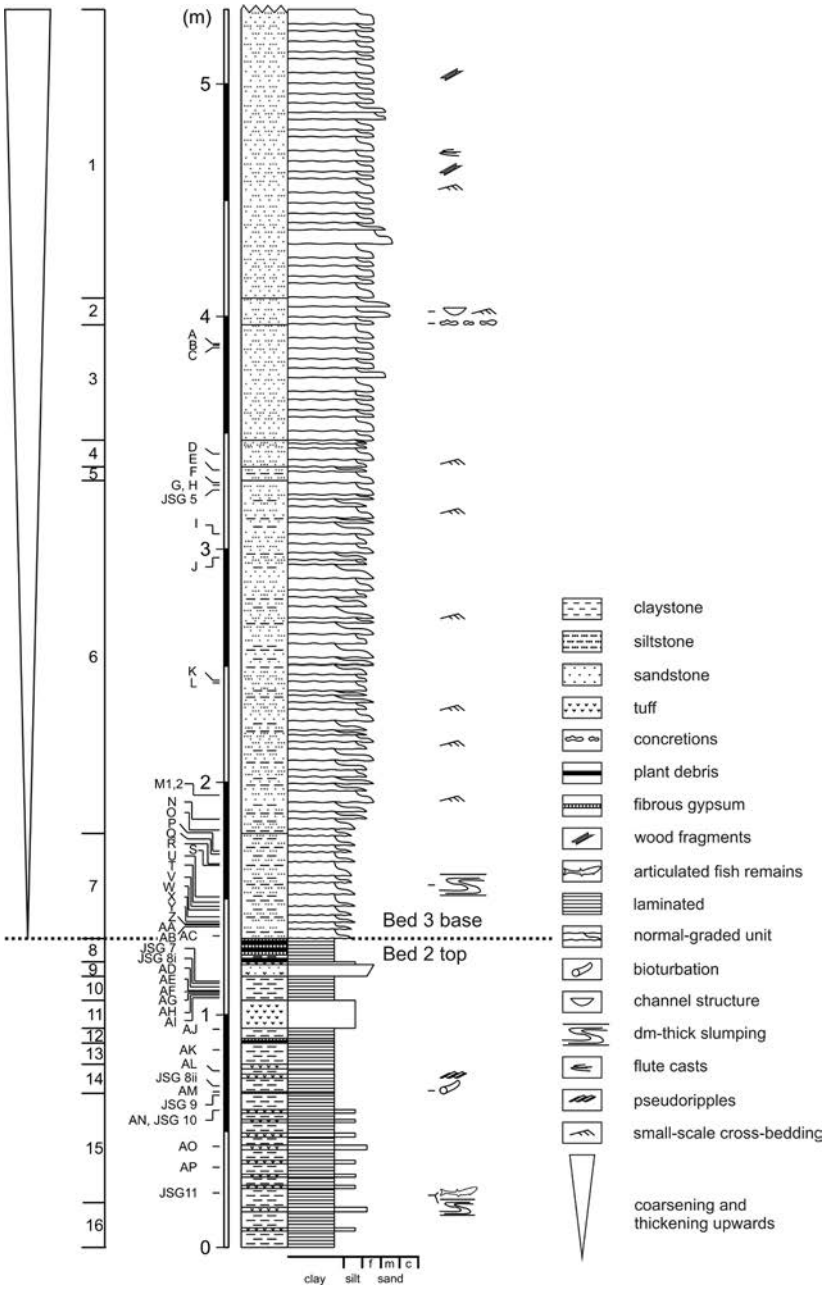

← **Fig. 7.1.** Litholog of excavation JSG, which can roughly be separated into two main beds, whose boundary is designated by a dotted line. 16 segments have been recognized and shortly characterized in Table 7.1. Bed 2 is marked by µm-thick, clay-silt couplets (Mf 1; Chapter 1) and intercalated tuff layers. The uppermost layers of Bed 2 are characterized by cm-thick layers of fibrous gypsum, which are associated with 1-2 cm thick layers of plant remains. Bed 3 is characterized by consecutive units of normal-graded silty fine sandstones that are overlain by biofilms and background sediments. These units are marked by pervasive meiofaunal bioturbation. There is a general coarsening- and thickening-upward trend throughout Bed 3. Thicknesses of normal-graded units in Bed 3 are exaggerated in the litholog.

tion. Hence, instead of signalling a clearly oriented sample, would be falsely low. Therefore, categories 210°-0° have been mirrored (e.g., 210° = 30°, 240° = 60° and so forth) in order to perform Rayleigh's test with only six remaining categories. The probability model used is the circular equivalent of the normal distribution (von Mises; Davis, 1986). The test for randomness is based on the assumption that the data are drawn from a population with the von Mises distribution.

H_0: *Ephemeropsis* larvae are randomly oriented.
H_1: There is a preferred orientation of *Ephemeropsis* larvae.

To substantiate the statistical outcome of Rayleigh's test, the non-parametric Rao's *U* is determined to check for directional patterns as provided in the PAST software (folk.uio.no/ohammer/past/; Hammer et al., 2001).

Determination of associations. – Possible groups in the faunal composition of the different excavated horizons are explored by means of group-average sorting of compositional dissimilarities. The Bray-Curtis measure has been chosen, which is interpreted to have a robust relationship with ecological distance (Faith et al., 1987). The resultant set of dissimilarities has subsequently been hierarchically clustered using the function hclust {stats}.

Correspondence analysis. – The abundance data of 43 horizons (Table 7.2) have been standardized to an excavated area of 10 m^2 and subsequently double-square-root transformed to reduce the strong influence of *Eosestheria middendorfii* on the pattern.

Correspondence analysis (CA) has been chosen to compare associations within the abundance data and to check for underlying environmental signals (Braak, 1985). CA is performed using the function cca as provided in the vegan package (http://www.r-project.org/; vegan.r-forge.r-project.org). In a successful analysis, each of the nine species receives a score close to the scores of the samples it is common in (Braak, 1985). Therefore, species and samples correspond within the plot. Also, species with comparable distributions across samples plot in the vicinity of each other (Hammer and Harper, 2006). Generally, CA axes are interpreted to relate to underlying environmental variables and species are expected to exhibit unimodal responses to the environmental variable by becoming less common at higher and lower values of that variable (Braak, 1985).

Relay plot. – Relays picked up by community relicts relate to variable environmental components that are continuous (Hennebert and Lees, 1991). They are well developed in depositional settings with progressive environmental change. Unimodal response curves of the six most abundant species are plotted along the underlying gradient of CA1. Abundances of taxa in samples are sorted according to their ordinated sequence. The position of horizons in the relay is indicated by the relay index, which is derived from the horizon coordinates on CA1 (Hennebert and Lees, 1991).

Axis measurements. – Clam-shrimp axes (Fig. 4.2) have been measured using a calliper with a precision of ± 0.1 mm. Most of these measurements were taken during the field campaign in Liaoning, where it was impossible to distinguish between closely adjacent, sub-millimetric layers, whose number has subsequently been counted. The data are displayed with a beanplot. Each bean consists of individual observations in form of small lines and a density trace. The advantage of beanplots in comparison to boxplots is that bi- and polymodal distributions can be visualized. The implementation in *R* as provided by Kampstra (2008) is employed.

Sediments

The lithological analysis of excavation JSG yielded 16 segments, which are summarized in Table 7.1. The abrupt sedimentological change that is highlighted by a dotted line in the litholog of Fig. 7.1 marks the transition between beds 2 and 3. The microfacies analysis of Chapter 1 yielded five microfacies for Bed 2, of which very thin allochthonous siliciclastic laminae (Microfacies 1; Fig. 1.5) form the bulk of the sediments. Tuff horizons of varying thicknesses are abundant. Varves, indicated by chrysophycean cysts accumulations, are present but only rarely preserved. Therefore, time is not well constrained within these deposits and a varying number of Mf-1 laminae represents the interval of one year (Fig. 1.6).

The sedimentological transition between Bed 2 and Bed 3 is marked by several tuff layers that are topped by an anomalously large amount of plant debris in association with fibrous gypsum layers (Fig. 7.1). As the fibrous gypsum layers are commonly coupled with plant debris, they are interpreted as products of sulphide (pyrite) oxidization.

Single units of Bed 3 (Fig. 1.11d-g) are made up of horizontally stratified, normal-graded silty fine sandstones that are overlain by microbially fixed argillaceous siltstone layers, which partly form mound-like structures. The sequence is coarsening- and thickening-upward, with sub-millimetric thicknesses in the lower part of Bed 3 to several mm-thick units near horizon JSG K (Fig. 1.11d, e; Fig. 7.4a). Thicknesses of single units are of mainly cm-scale in the upper part of the excavation (segments 1 and 2; Table 7.1). Bed 3 is marked by pervasive meiofaunal bioturbation and several layers exhibit ripple bedding. Even though beds 2 and 3 are interpreted to represent two phases of lake evolution, it should be noted that the onset of Bed-3 sedimentation was most likely not synchronous throughout the lake.

Community composition of beds 2 and 3

Overviews of benthic organisms and their respective horizons are presented in Figs. 7.2-7.5. Figure 7.2 gives an impression of representative Bed-2 horizons. Clam-shrimp density is variable, ranging from pavement-like accumulations (Fig. 7.2a, c) to widely scattered occurrences (Fig. 7.2b, d). An overview of the Transitional Fauna is given in Fig. 7.3. It is characteristic of Bed-3 sediments that immedi-

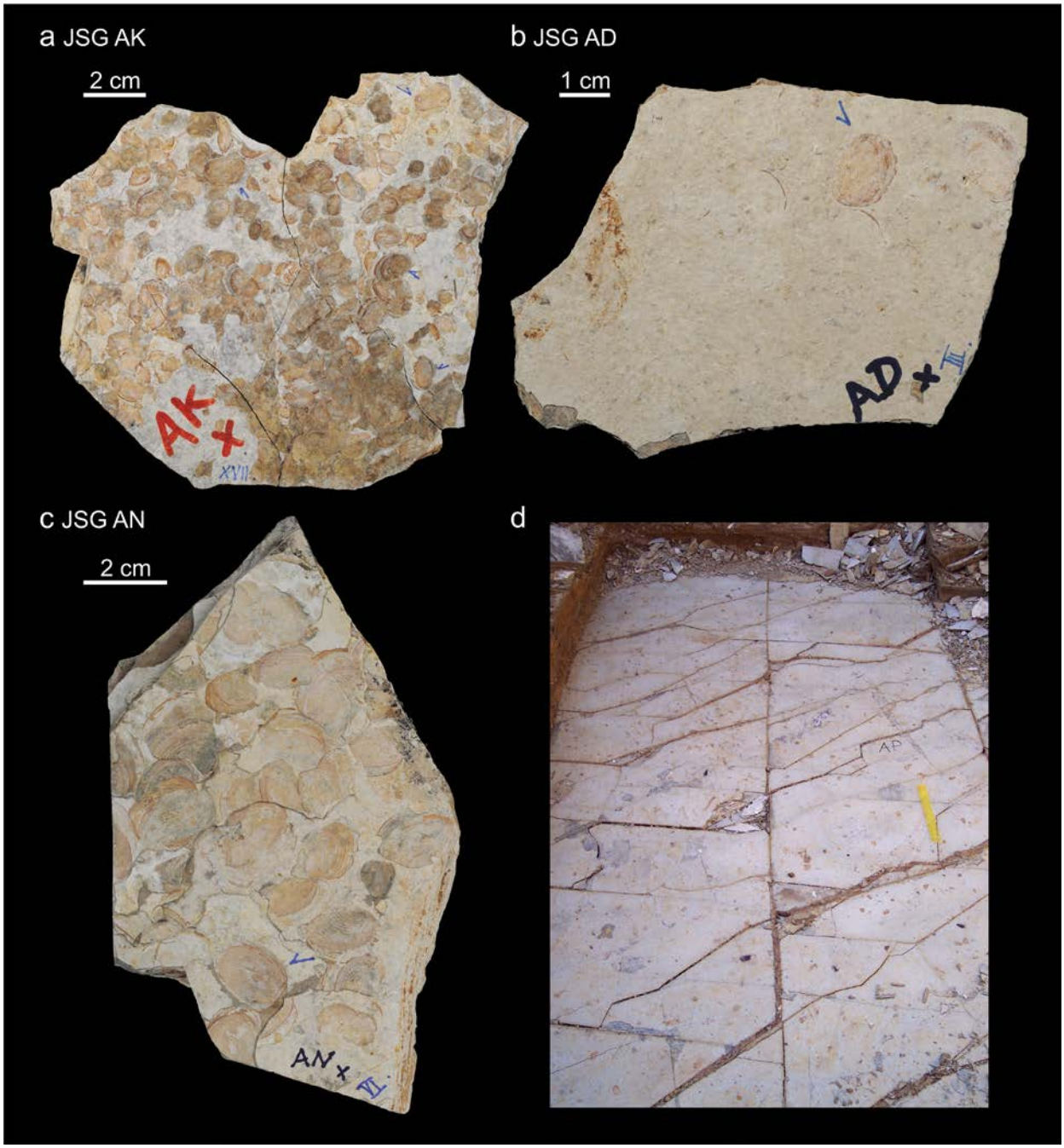

Fig. 7.2. Overview of Bed 2. (a) JSG AK. Concentration of individuals of *Eosestheria middendorfii* of various sizes in multiple laminae. (b) JSG AD. Scattered individuals in a single layer. (c) JSG AN. Concentration of large individuals in multiple laminae. (d) Excavated bedding plane of JSG AP.

ately overlie the major sedimentological transition between beds 2 and 3.

A total of nine benthic taxa has been recognized (*Eosestheria middendorfii*, *Ephemeropsis trisetalis*, *Ephemeropsis* sp. B, *Karataviella* sp. A, naidid oligochaetes, caddisfly larvae, *Liaoningogriphus quadripartitus*, *Probaicalia* sp. A, and *Arguniella ventricosa*; Figs. 7.2-7.5). *Ephemeropsis* sp. B refers to mayfly larvae, whose body is markedly larger and appears somewhat inflated in comparison to *Ephemeropsis trisetalis*. Individuals of *Ephemeropsis* sp. B are particularly prominent in a horizon dominated by mayfly larvae. This study marks the first mention of water boatmen (*Karataviella* sp. A; Fig. 7.5h), otherwise known from the Middle to Upper Jurassic of northeastern China (Zhang, 2010), and naidid oligochaetes (Fig. 7.4d; 7.5f, g) within Lake Sihetun. Both benthics are restricted to Bed 3 in our excavation and they are by far the most common in the Transitional Fauna. The oligochaete 'worms' (Figs.

7.3a, c, 7.5f, g) belong to the Naididae, a family of the Annelida (Clitellata). Figure 7.5f illustrates a specimen that is 19.8 mm long and preserved as a dark stain coated with silica. Its outer body wall is faintly visible and has been traced. The main body is segmented and characterized by a thickened region that can be observed in every specimen. This clitellum-like structure is well preserved in Fig. 7.5f. A sucking organ exists at the anterior part of the specimen, which is often too fragile to be preserved. The naidid oligochaetes are interpreted as vagile benthic worms.

The raw abundance data are compiled in Table 7.2, which also lists species richness (*S*), rarefied richness, and the Shannon index (*H'*), the latter of which is plotted against the litholog in Fig. 7.8. The three diversity indices generally agree. Species richness, however, does not give a good representation of diversity with increasing clam-shrimp dominance. There are 14 monospecific clam-shrimp horizons (disregarding fish coprolites or land insects within these horizons). The occurrence of only one individual of a second species within these horizons would raise species richness by 1. Naturally, the agreement of indices is much better within horizons displaying more evenly distributed counts among taxa, but these horizons are marked by conspicuously less densely scattered populations.

S is generally regarded to be dependent on sample size (e.g., Colwell et al., 2004), but in addition to this sampling effect there is something more subtle. For example, 2205 of 2207 counted individuals of JSG B are clam shrimps. One might think that the vast number of clam-shrimp individuals renders the occurrences of one mayfly larva and one water boatman unimportant. However, this is not the case when looking at specimen counts in a given surface area. Standardized to a surface area of 10 m^2, JSG B exhibits an even higher abundance of *Ephemeropsis trisetalis* (~ 39 ind.) as horizons JSG Q (~ 31 ind.) or JSG Y (~ 25 ind.). Nevertheless, the latter two horizons are marked by much higher relative abundances of *E. trisetalis* (Table 7.2). Clam-shrimp individuals of horizon JSG B (Fig. 7.4b, c) are juvenile and marked by a high population density, while clam shrimps of JSG Y are all large and scattered (Fig. 7.8). JSG Q does not exhibit any clam shrimps.

This raises the question of how reliable diversity indices are in case of a mass occurrence of one species, which undermines the environmental information of co-occurring taxa. As individual counts have always been conducted on a defined area during excavation JSG, taxon occurrences may be regarded not only in relation to the entire community but also to the excavated area (Figs. 7.2d; 7.4f). Therefore, individuals have been standardized to an excavated area of 10 m^2 to enable the comparison of abundances per unit area among horizons.

Common faunal components, or their traces, that have not been included in the palaeocommunity analysis are fish coprolites (Fig. 7.5g) and fish fossils (lowermost horizon JSG 11; marked in Figs. 7.1, 7.8). Clam shrimps were the main food source of fish, as the coprolites (Fig. 7.5g) are entirely made up of disintegrated carapaces. In order for Lake Sihetun to support fish populations, lake size must have been sufficient, as noted by Pan et al. (2012). In addition to the remains of aquatic organisms, there are numerous excellently preserved terrestrial insect fossils in Bed 3, such as spittle bugs (JSG U) or snakeflies (JSG B, JSG Y; Fig. 7.4c).

Orientation patterns of *Ephemeropsis* larvae

The orientation of *Ephemeropsis* larvae has been measured as a proxy for current activity (Fig. 7.3d; Table 7.3). Preferred directions are unambiguously inferred for JSG H, AA, and AB, but according to Rao's *U*, the null hypothesis of a random distribution cannot be rejected for JSG J and JSG AP. This is perhaps a matter of sample size. In contrast, according to Rayleigh's *R* all layers yield a preferred orientation. Studied horizons may in fact consist of several different laminae, introducing an aspect of time-averaging. However, layers of Bed 3 can be separated comparatively well, and JSG H exhibits the clearest pattern with an average orientation of 10-190 (NNE-SSW). In turn, the distribution overlap of two or more sub-millimetric consecutive layers suggests two current directions for JSG AA (Bed 3). The main direction can, however, be summarized as NE-SW.

Benthic palaeocommunities

Three associations and two assemblages have been identified using group-average sorting (Fig. 7.6a). Groupings are driven by diversity, the ratio between *Ephemeropsis trisetalis* and *Eosestheria middendorfii*, and clam-shrimp population density (Fig. 7.8). In contrast, the CA plot is governed by the distribution of species across samples. The following groups can be distinguished:

Association 1 (*n* = 15, "low diversity, high density association", red) comprises mainly monospecific assemblages with possible minor occurrences of *Ephemeropsis trisetalis*, *Karataviella* sp. A, and gas-

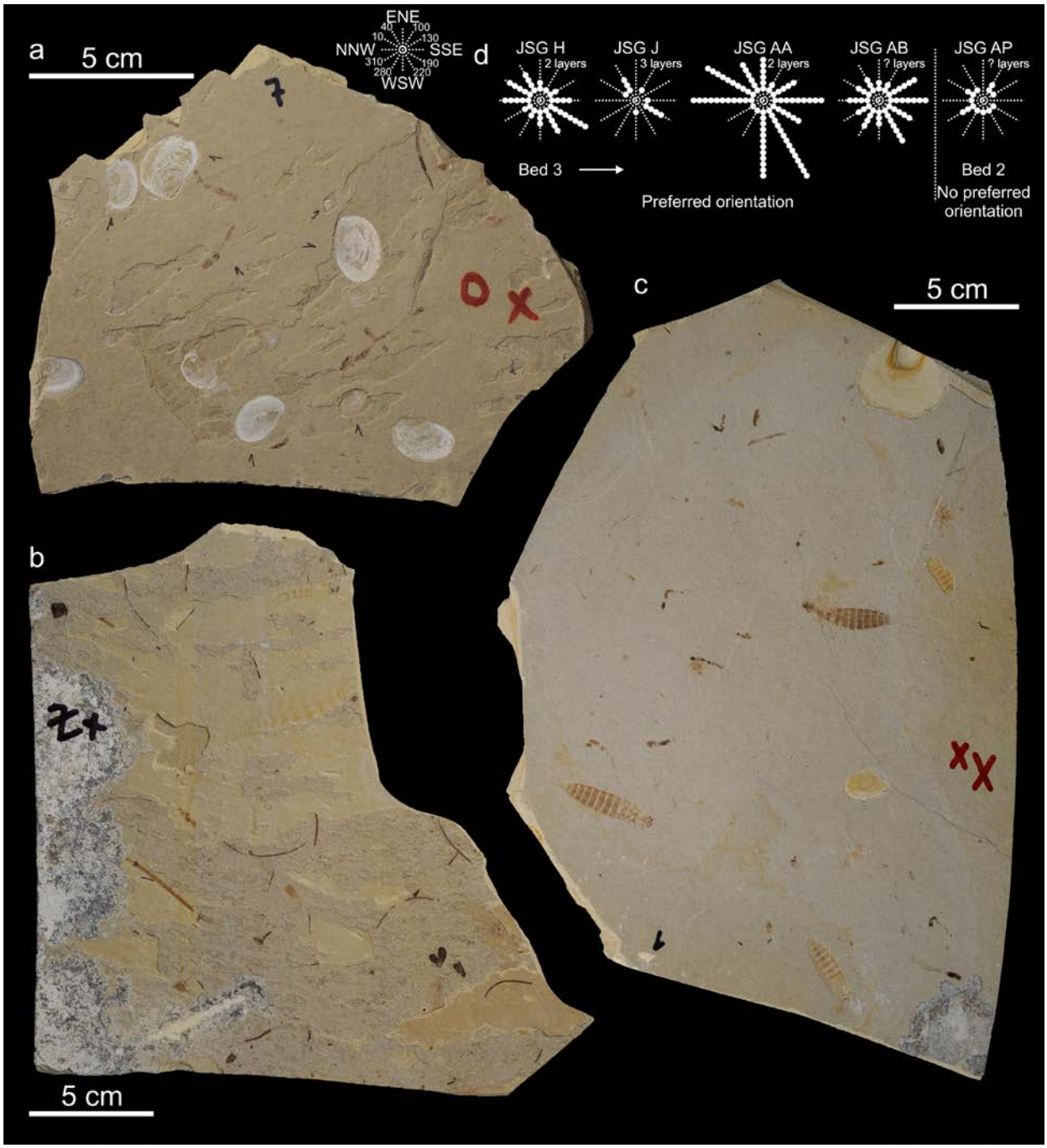

Fig. 7.3. Overview of Bed 3, Transitional Fauna (Association 3 and assemblages Z and Q). (a) JSG O, (b) JSG Z, and (c) JSG X. Bedding planes are well defined. Nevertheless, the exact number of layers within a horizon has been examined to get an estimate of time-averaging. The fauna of JSG X (c) is, for example, distributed over two closely adjacent horizons. (d) The orientation of *Ephemeropsis* larvae within the outcrop is visualized with a dot plot (12 categories). Each dot represents the direction to where the head of one individual points. The column height, therefore, corresponds to the absolute number of observations within a directional category. 360°-180° corresponds to 070-250 (ENE-WSW) and 90°-270° to 160-340 (SSE-NNW) in outcrop position.

tropods. Diversity remains at, or near, *H'* = 0 and does not exceed *H'* = 0.28 (JSG AN; Fig. 7.8).

Association 2 (*n* = 18, "low to medium diversity, low density association", yellow) is made up of 10 horizons of Bed 2 and 8 horizons of Bed 3. This association includes four monospecific horizons (AL, AH, AG, AD), all of which are marked by a distinctly lower clam-shrimp density (individuals per m^2) than horizons of Association 1. The remaining 14 horizons are also dominated by *E. middendorfii*, but they are characterized by an increased importance of mayfly larvae. Except for one specimen

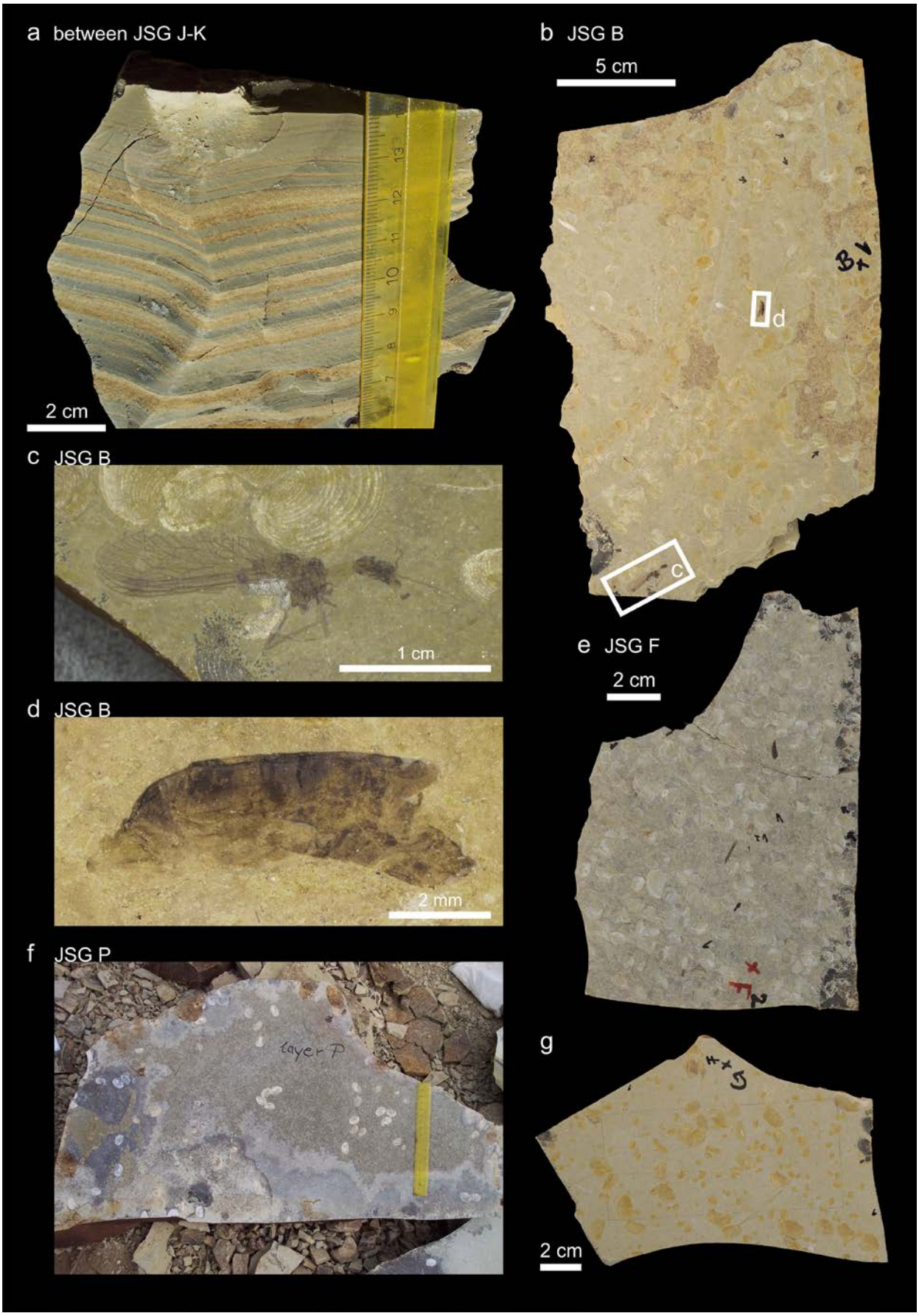

count, Association 2 is devoid of water boatmen. It can be considered an intermediate association that

← **Fig. 7.4.** Overview of Bed 3, shallower facies. (a) Example of normal-graded units, which become progressively coarser throughout Bed 3. (b-d) JSG B. Well defined horizon with excellently preserved insect fossils, such as (c) the snakefly *Alloraphidia* or (d) the water boatman *Karataviella* sp. A. (e) JSG F. Densely distributed clam shrimps of small to medium size. Example horizon of an environmentally induced mass mortality event. (f) JSG P. Horizon with scattered larger clam shrimps. (g) JSG G. Bimodal size distribution with larger individuals being restricted to the lower layer and smaller individuals occurring within the upper layer.

ranges between associations 1 and 3.

Association 3 (n = 8, "medium to comparatively high diversity, low density association", green, Transitional Fauna) consists of horizons yielding varying proportions of *E. middendorfii*, mayfly larvae, water boatmen, and naidid oligochaetes. Naidid oligochaetes are restricted to this association and they form a dominant faunal component in several of its horizons.

Assemblage JSG Z ("low diversity mayfly assemblage", green, Transitional Fauna) is marked by an absence of clam shrimps and a dominance of mayfly larvae with minor occurrences of water boatmen and caddisfly larvae. *Ephemeropsis* sp. B is common in this assemblage.

Assemblage JSG Q ("low diversity water-boatmen assemblage", green, Transitional Fauna) is also marked by an absence of clam shrimps. This assemblage is dominated by the water boatman *Karataviella* sp. A. Mayfly larvae occur in smaller numbers.

Association 3 and assemblages JSG Z and JSG Q (Fig. 7.6a) occur immediately above the sedimentological transition of Bed 2 into Bed 3 (Fig. 7.8). Together they are referred to as the "Transitional Fauna", in which the two assemblages represent end members of Association 3. The presence of bivalves and gastropods does not have a large influence on the groupings owing to the statistical routine employed during clustering. Instead, clam-shrimp population density forms an important determining factor, as illustrated by the density column of Fig. 7.8, which clearly separates Association 1 (red) from Association 2 (yellow). Therefore, depending on their clam-shrimp population density, monospecific horizons may be allocated to either one of the two associations.

While all 14 monospecific clam-shrimp horizons plot in a single spot, horizons yielding the Transitional Fauna (green) are well delimited from all other samples by CA1 (Fig. 7.6). Horizons which are aligned along CA1 are characterized by a progressively higher relative abundance of mayfly larvae with respect to clam shrimps (mainly Association 2). Mollusc-yielding horizons are separated by CA2. They occur within the lowermost three horizons of the profile (Fig. 7.1). The third axis, which explains 14.3 % of the variation in the data, is less informative, but it points out the importance of less abundant taxa, such as caddisfly larvae or a second mayfly species.

Relay plots

CA axes are interpreted to relate to environmental variables and taxa are expected to exhibit unimodal responses to them (Braak, 1985). Continuous environmental gradients are represented by the arrangement of community relicts in a relay (Hennebert and Lees, 1991). Proposed response curves to the environmental gradient underlying CA1 are illustrated in the relay plot of Fig. 7.7. Species abundances should decline at higher or lower values of an environmental variable. An examination of the abundance data in Table 7.2 shows that clam shrimps form the only faunal component that occurs in monospecific assemblages. Therefore, they must have survived environmental conditions that were adverse to all other benthic taxa. In turn, mayfly larvae and water boatman dominated JSG Z and JSG Q, by the exclusion of clam shrimps. Therefore, these two taxa were able to survive conditions that the clam shrimp *E. middendorfii* did not tolerate.

Figure 7.7 shows that the six unimodel response curves to the environmental gradient suggested by CA1 partly overlap. *E. middendorfii* displays the widest response curve, indicating the highest tolerance towards this variable. Conversely, naidid oligochaetes display a comparatively narrow response curve, which, for instance, has nothing in common with that of the bivalve *Arguniella*. Both were specialists with low tolerances towards this environmental variable. Occurrences of *Ephemeropsis* sp. B, caddisfly tubes, and *Liaoningogriphus* are too sporadic to position potential peaks of the respective response curves, which is why they are omitted in the relay plot.

The approximate range of the environmental variable realized within phases 2 and 3 is marked. While the right end of the range is comparatively well constrained, the left end is not. The extrapolation of the response curve for *E. middendorfii* is based on the fact that clam-shrimp abundances peak when they occur in nearly monospecific assemblages (Fig. 7.7a). This indicates that they toler-

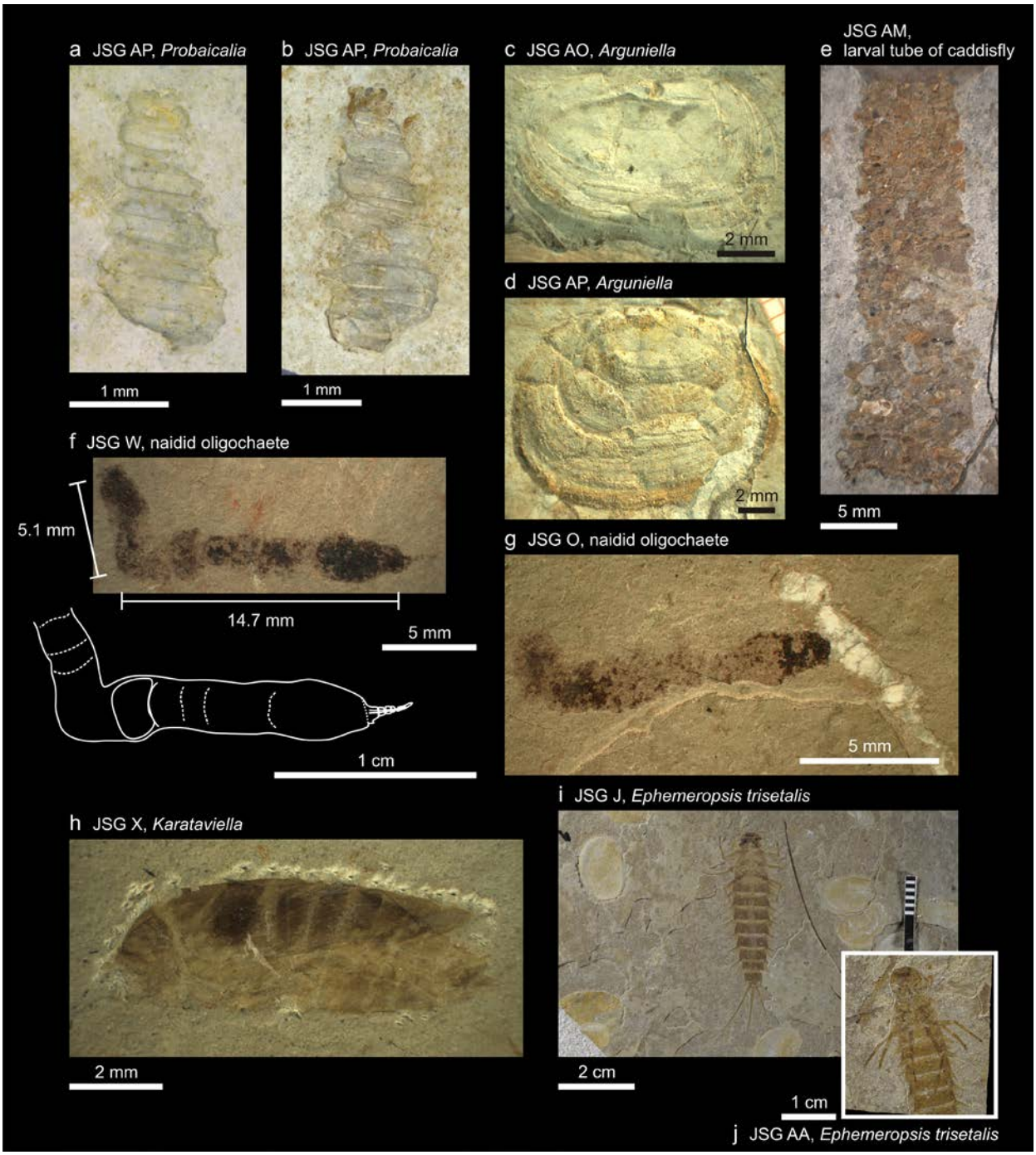

Fig. 7.5. Benthic fauna of excavation JSG. (a-e) Bed 2. (f-j) Bed 3. (a-d) The three stratigraphically lowermost horizons AP-AN yield high-spired gastropods (*Probaicalia* sp. A) and, partially, bivalves (*Arguniella ventricosa*). (e) Caddisfly tubes are occurring in JSG AM and in horizons of the Transitional Fauna. (f, g) Here we present the first record of naidid oligochaetes within Lake Sihetun, which dominate several horizons of the Transitional Fauna (compare with Fig. 7.3c). (g) Fish coprolites made up of clam-shrimp carapaces are common in numerous horizons of Bed 3. (h) Thus far, the water-boatman genus *Karataviella* has been described from Jurassic deposits of northeastern China. This is the first record from the Early Cretaceous Yixian Formation. It is restricted to Bed 3 and dominates several horizons of the Transitional Fauna. (i, j) Mayfly nymphs of the species *Ephemeropsis trisetalis* form the second-most abundant faunal component of this excavation. They occur in varying numbers and their relative abundance peaks in the Transitional Fauna. In contrast, a standardization to area points to more evenly distributed mayfly larvae across associations. Note that the preservation of Bed-3 mayfly larvae is fundamentally different to the iron sulphide replacement of Bed 2.

ated a wider range than that picked up by the relay plot.

Size measurements and clam-shrimp population density

Size measurements are depicted in bean plots (Fig. 7.8). By far the smallest clam-shrimp individuals are found in Association 1. Individuals of Association 2 and the Transitional Fauna are generally large. The largest individual of excavation JSG is from horizon JSG O (L = 22.94 mm; Association 3; Fig. 6.3c-e), followed by two individuals of Association 2 (JSG Y, L = 20.96 mm; JSG H, L = 20.62 mm; Fig. 6.1). By far the highest clam-shrimp density correlates with the overall smallest individuals (Association 1).

There are exceptions to these generalizations, which can mostly be explained by technical limitations. JSG AK consists of multiple µm-thick layers (Fig. 7.2a), rendering it difficult to separate different size classes or taxa. Such a separation is easier in Bed-3 horizons. The community data of JSG D (Association 2) is entirely based on one of the two reported layers; the lower layer that exhibits larger clam shrimps and mayfly larvae. However, the smaller individuals of the upper layer, which can be related to Association 1, have nevertheless been measured. The only exception that cannot be explained by technical limitations is JSG AN (Association 1), which exhibits large clam-shrimp sizes comparable to those of Association 2. However, apart from forming an outgroup within Association 1 (cluster analysis, Fig. 7.6a), JSG AN can be separated from all other horizons and grouped with JSG AO and JSG AP due to the occurrence of the gastropod *Probaicalia* (CA2; Fig. 7.6a).

The sampling distributions of the axis measurements are often tightly clustered around the mean, most notably in JSG F or E, reflecting a smaller amount of variability due to simultaneous hatching. As indicated for each distribution in Fig. 7.8, single horizons are made up of a number of closely adjacent, fossiliferous layers and it is of interest how size classes are distributed among those layers. An inspection of horizons comprising two layers as well as a distinct bimodal distribution shows that there is a marked separation of larger clam shrimps (lower layer) and smaller clam shrimps (upper layer; JSG A, C, D, and G).

Discussion

Abiotic environment during lake phases 2 and 3

Sedimentological analysis

The rapid sedimentological transition between beds 2 and 3 (Fig. 7.1) has been interpreted to reflect a change in climate from dry (Phase 2) to humid (Phase 3; Fig. 1.15; Jiang et al., 2012; Chapter 1). A similar abrupt transition has been identified in the deposits of Lake Khubsugul (Mongolia; Fedotov et al., 2003), in which the Pleistocene (cold and arid) clay-carbonate-dominated sedimentation was abruptly succeeded by a Holocene silt-dominated sedimentation. Raised salinities and drowned palaeo-deltas suggest a shallower Lake Khubsugul during the arid intervals of the Pleistocene with only 70 m lake depth, compared to a modern depth of 262 m. Shallowing was accompanied by a reduction in surface area and an estimated reduced lake volume of 30-40 times the present-day level. At the onset of the Holocene, lake waters rapidly became diluted, putting an end to the prior Pleistocene carbonate build-up and marking the onset of fluvial sedimentation (Fedotov et al., 2003).

The sedimentological shift between beds 2 and 3 of Lake Sihetun is analogous to that of Lake Khubsugul, implying that the transition from a dry Phase 2 to a humid Phase 3 stands for a deepening of the lake and an increased fluvial influx during Phase 3. The abrupt sedimentological transition in Lake Sihetun was most likely accompanied by a shifting of a delta lobe after a flash flood event, which introduced an anomalously large amount of plant debris into the lake, indicated by the prominent organic layers that form the topmost deposits of Bed 2 (Fig. 7.1). In addition to climatic forcing, it may be considered that the transition between phases 2 and 3 was a local event restricted to the excavation site. However, the sedimentological change between beds 2 and 3 was widespread in the Sihetun area (Fig. 1.3a), rendering a climatic forcing plausible. Consequently, in comparison to Phase 3, Phase 2 was marked by lower water levels, a smaller surface area and lake volume, and higher salinities, the latter being indicated by repeated intervals of carbonate precipitation (Mf 4; Fig. 1.9).

Importantly, even though there was a deepening between phases 2 and 3, it does not mean that Phase 2 was shallow, which has often been inferred from the presence of clam shrimps (< 2 m; e.g., Wang, 1999). There is no clear sign of emergence (desic-

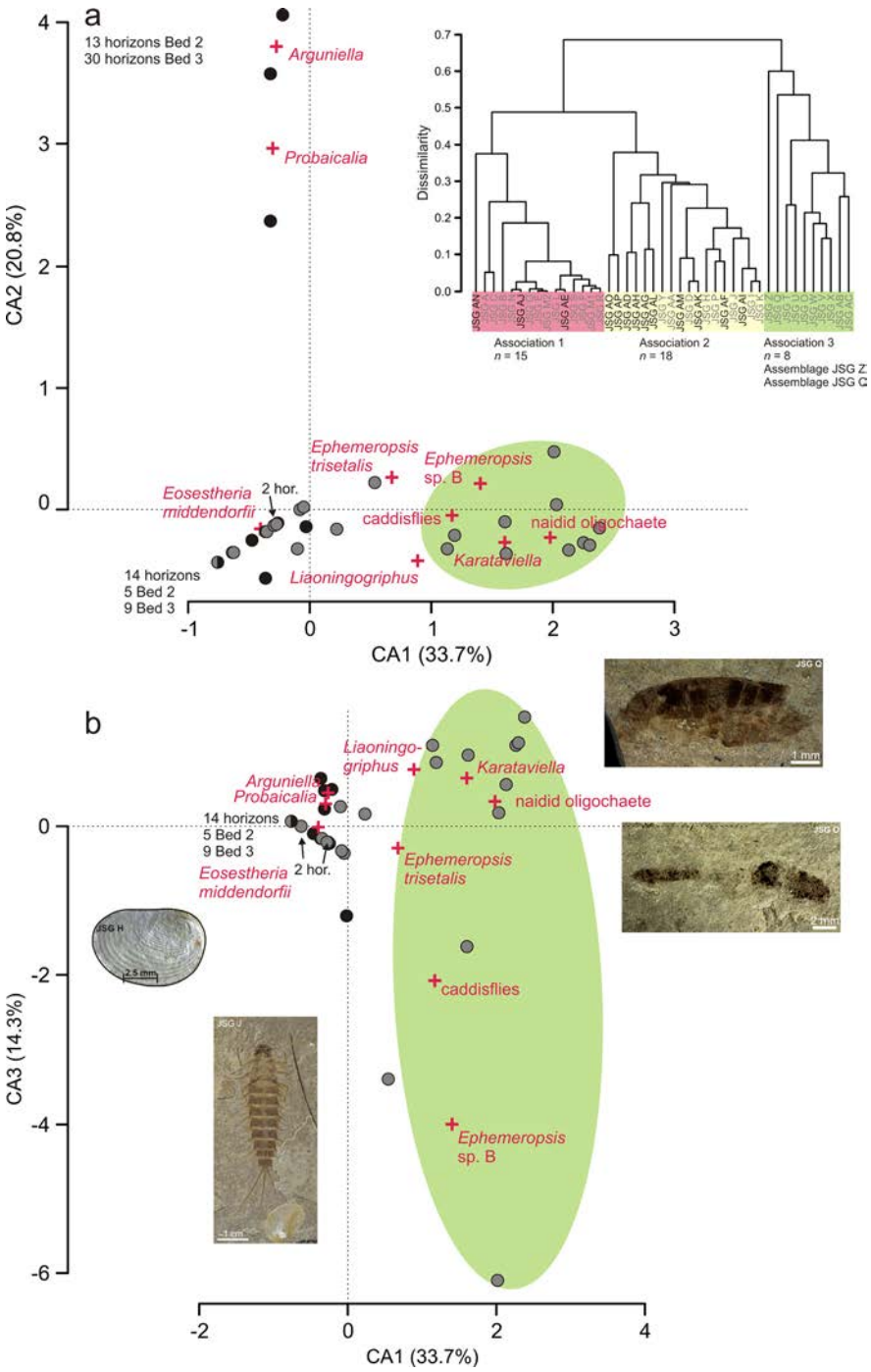

← **Fig. 7.6.** Correspondence analysis. Biplots of horizons and taxa. (a) CA1 versus CA2 and (b) CA1 versus CA3. Black dots indicate horizons of Bed 2, while grey dots mark those of Bed 3. (a) The inset diagram shows the results of the hierarchical cluster analysis (group average sorting), which identified three associations and two assemblages. Association 3 and the two assemblages together form the Transitional Fauna, which is colour-coded in green in the CA plots. Horizons that are aligned along CA1 are driven by an increasing relative abundance of *Ephemeropsis* larvae, while CA2 is governed by the presence of molluscs. (b) Less common taxa, such as caddisflies or *Ephemeropsis* sp. B, span CA3.

cation cracks or salt pseudomorphs) within Phase 2. Even though the transition between both beds is marked by fibrous gypsum layers, they are coupled with plant debris and interpreted as secondary products of sulphide oxidization. Furthermore, the very fine laminae of Bed 2 (clay-silt couplets of Mf 1; Chapter 1) show only little evidence of current or wave action (see below, orientation patterns of mayfly larvae), while the coarser, normal-graded, and partly cross-bedded laminae of Bed 3 imply higher energy levels. The lack of wave action in the bulk of Bed 2 indicates that sediments were deposited well below the storm wavebase, which has been inferred to have lain between <10 m and 5 m water depth in Devonian lakes of Shetland (Allen, 1981). Although allochthonous clam shrimps have been identified in Bed 2 (Fig. 1.8), their bulk is interpreted as autochthonous (Chapter 1). Therefore, the tolerance of the clam shrimp *Eosestheria middendorfii* towards environmental variables connected to water depths becomes one of the central questions to be answered.

The general coarsening-upwards trend within Bed 3 implies an overall shallowing during Phase 3 subsequent to the initial deepening that marks the onset of this phase (Fig. 7.8). Its depositional units are characterized by pervasive meiofaunal bioturbation

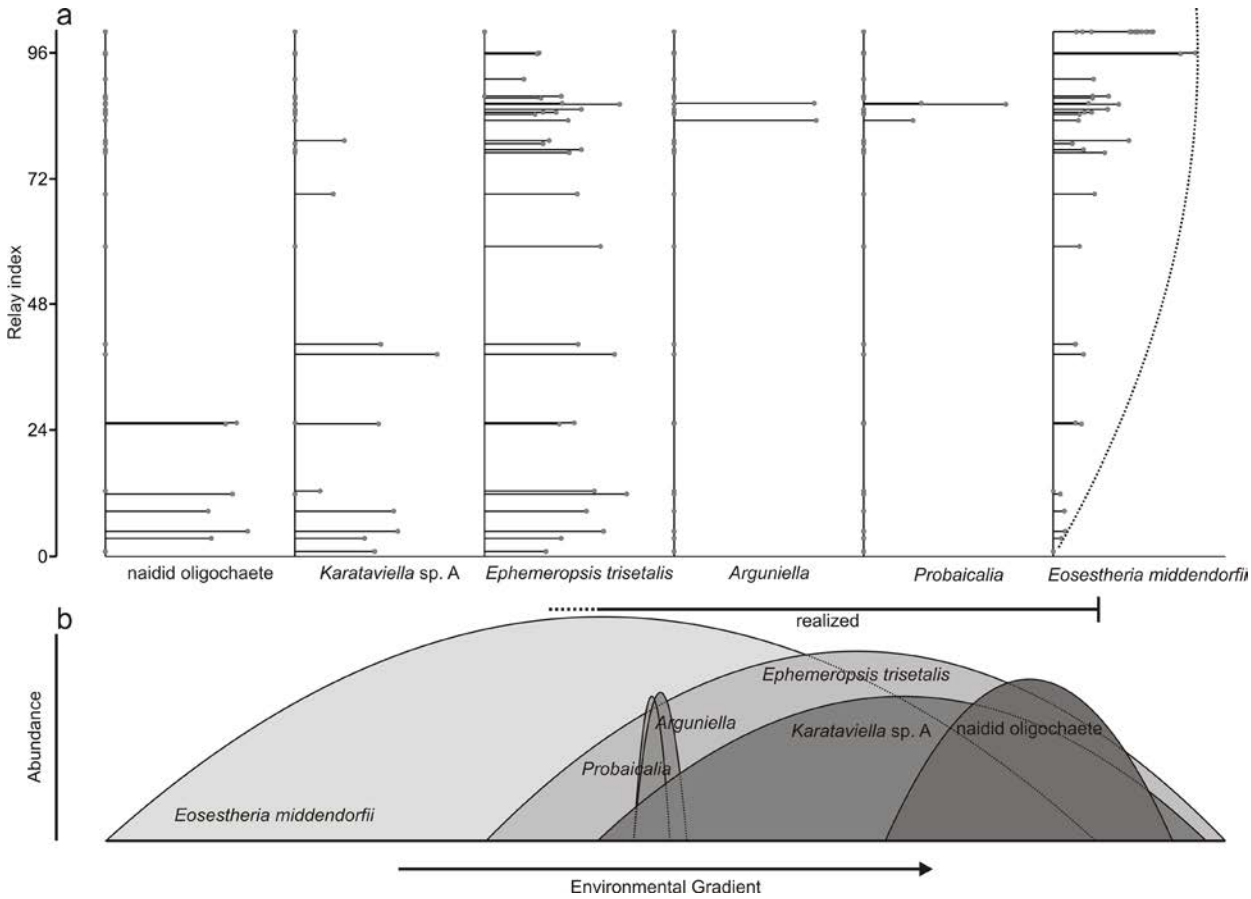

Fig. 7.7. (a) Relay plot based on the correspondence analysis of Fig. 7.6. Only the six principal species are considered. Vertical axes of the relay plot give CA1 scores and the horizontal axes give abundances, which reflect the original abundances that have been standardized to an excavation area of 10 m^2 and subsequently double-square root transformed. This transformation strongly decreases the amplitudes of the ideally unimodal distributions. Taxa are ordered according to their position on the environmental gradient. Peaks are not entirely unimodal, but they give good representations of the respective response curves (dotted line). (b) The resultant schematic response curves of the six benthic invertebrates are overlapping. Clam shrimps, mayfly larvae, and water boatmen were tolerant towards the environmental variable underlying CA1 (generalists), while naidid oligochaetes, bivalves, and gastropods displayed lower tolerances (specialists). The approximate range of the environmental variable realized within phases 2 and 3 is marked.

(Fig. 1.11 d-g), an indicator of generally oxygenated conditions within the sediments and, correspondingly, within the bottom waters of the lake. The top layers of Bed-3 depositional units, which are formed by biofilms, are less disturbed, implying less oxygenated conditions within the upper sediment layers as a result of more tranquil intervals of reduced rainfall within a season. In summary, Bed-3 sediments correspond to an alternation between higher-energy conditions triggered by increased rainfall during the wet season, which produced comparatively thick normal-graded units that quickly became colonized by a meiofauna, and a dry season marked by the draping of bituminous mud. Importantly, there is no evidence for emergence.

Orientation patterns of mayfly larvae

In addition to small-scale cross-bedding, biostratinomic orientation patterns of *Ephemeropsis* larvae are used as a line of evidence for currents or wave action in this study (Fig. 7.3d; Table 7.3). Preferred orientations have unambiguously been verified for three Bed-3 horizons (JSG H, AA, and AB) and the main orientation can be summarized as NE-SW. If wave action had been responsible, the larvae would have been in alignment with the shoreline. However, the presence of current ripples in Bed 3 indicates a directional transport of larvae. According to Rayleigh's test, no preferred orientation has been identified for JSG AP (Bed 2), but this result is based on a very small sample size of only 14 individuals. The pattern of JSG AP (Bed 2) resembles those of *Ephemeropsis trisetalis* and *Liaoningogriphus quadripartitus* from Bed 2 of excavation ZJG

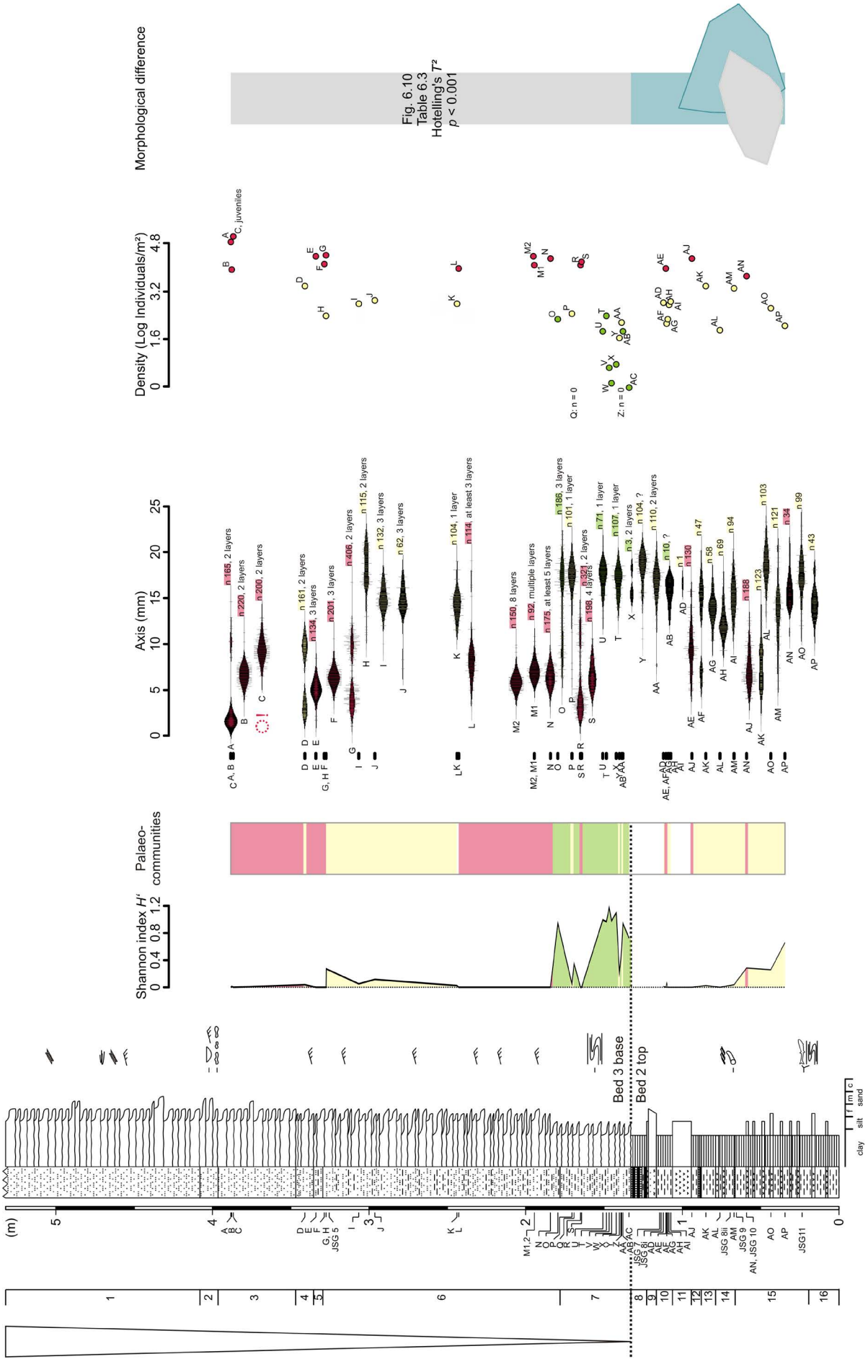
Morphological difference
Fig. 6.10
Table 6.3
Hotelling's T²
p < 0.001
Density (Log Individuals/m²)
0 1.6 3.2 4.8
Axis (mm)
0 5 10 15 20 25
Palaeo-communities
Shannon index H'
0 0.4 0.8 1.2
Bed 3 base
Bed 2 top
clay
silt
sand
(m)

← **Fig. 7.8.** Litholog of excavation JSG and associated environmental proxies. The five columns plotted against the litholog are diversity (Shannon index), palaeocommunities (Fig. 7.6), axis-measurements of *Eosestheria middendorfii*, their density (individuals per m^2 on a log-scale), and the morphological differences between individuals of lake phases 2 and 3 (Chapter 6). The diversity curve has not been smoothed, as horizons are comparatively well-constrained and a sudden drop in diversity is believed to be authentic. Palaeocommunities are colour-coded in red (low diversity, high density association), yellow (low to medium diversity, low density association), and green (Transitional Fauna comprising a medium to comparatively high diversity, low density association, and two low diversity assemblages). Axis measurements of JSG-C clam-shrimp individuals leave out juveniles of ~ 1 mm, which are difficult to measure with a calliper (Fig. 6.4a). The density plot of JSG C, however, includes juvenile counts. The beanplots are sometimes deceptive, as most horizons consist of multiple layers. Horizons A and D, for example, are in fact made up of two layers with smaller individuals being confined to one layer and larger individuals to the other. Therefore, the bimodal size distribution of JSG D is an artefact of two closely adjacent layers that can only be distinguished under the microscope. The number of layers is indicated for each Bed-3 horizon. Correct lamina counts cannot be given for Bed-2 horizons, as lamina thickness is of µm-scale.

(Fürsich et al., 2007). Fürsich et al. (2007) reported invariably random orientations for taxa of Phase 2. However, their interpretation does not correspond to the test statistics they have listed, which indicate a directional pattern for *Ephemeropsis* larvae in at least two horizons of excavation ZJG. Therefore, currents were mostly absent from the lake floor during Phase 2, except for occasional events, corroborated by random occurrences of allochthonous Microfacies-3 layers within Bed 2 (Fig. 1.8; Chapter 1).

Community composition

Eight fossil communities within Bed 2 of excavations ZJG and LXBE were recognized in a previous study (Pan et al., 2012). These communities include a total of ten taxa. However, they do not all belong to the same ecological region. The inclusion of fish, fish coprolites, and plant fragments (Pan et al., 2012) to the analysis is not reasonable in a stratified environment, in which nektonic organisms clearly experienced different environmental conditions than benthic or nektobenthic taxa. Although fish coprolites are abundant, especially in Bed 3 (Fig. 7.5g), they are therefore excluded from the palaeocommunity analysis of this study, which entirely focuses on (nekto-)benthic taxa that are representative of the bottom waters of the lake.

Fürsich et al. (2007) identified three low diversity associations in excavation ZJG, characterized by *Ephemeropsis trisetalis*, *Liaoningogriphus quadripartitus*, and *Eosestheria middendorfii*, respectively. These three previously recognized associations are partly supported by the three associations and two assemblages of this study (Fig. 7.6). Assemblage Z, for example, equals the *E. trisetalis*-Association of Fürsich et al. (2007). The fact that the former belongs to Bed 3 and the latter to Bed 2 implies that *E. trisetalis* was not restricted to a particular lake phase. Neither was the clam shrimp *E. middendorfii*. Both species were generalists with wide response curves towards environmental gradients (Fig. 7.7). This explains why associations 1 and 2 are distributed throughout beds 2 and 3 (Fig. 7.8). It should, however, be noted that Association 1, which comprises mainly small to medium-sized clam shrimps, is especially abundant in the upper part of Bed 3. In addition, even though the associations of beds 2 and 3 are comparable, their clam shrimps exhibit significant differences in carapace shape, identified as ecophenotypic variation in Chapter 6.

Long-term temporal patterns in the community composition of Lake Sihetun have been recognized in excavation JSG. Association 3 and assemblages Z and Q (Transitional Fauna) are restricted to the basal part of Bed 3. The drastic change in community composition from the clam-shrimp dominated associations of Bed 2 to the Transitional Fauna (Fig. 7.8) reflects environmental changes that were connected to a sudden deepening and dilution of bottom waters, as implied by the sedimentological evidence. Apart from *E. trisetalis* and adult individuals of *E. middendorfii*, the main species adapted to this deeper environment were the water boatman *Karataviella* sp. A (Fig. 7.5h) and naidid oligochaetes (Fig. 7.5f). Sporadic occurrences of water boatmen in clam-shrimp dominated associations render their response curve wider than that of the naidid oligochaetes (Fig. 7.7). A gradual shallowing followed the sudden deepening that marked the onset of Phase 3. It was expressed in fluctuating community compositions (Fig. 7.8). Eventually, the shallow-water, low diversity Association 1 dominated the benthic fauna during the late Phase 3.

The response curves of Fig. 7.7 should predict the community composition along the environmental gradient underlying CA1. Even though the overall data fit the proposed scheme of Fig. 7.7b, there are exceptions. In horizon JSG AC (Table 7.2), naidid

oligochaetes occur with mayfly larvae in about equal numbers and only one clam-shrimp specimen has been counted, placing this horizon at the far right side of the environmental gradient depicted. However, even though the response-curve overlap suggests that water boatmen should be present as well, they did not co-exist with the fauna governing this horizon. This can be explained by the presence of seasonalities or some other factor that led to the local extinction of water boatmen during its deposition. Therefore the proposed overlap of response curves (Fig. 7.7b) provides *potential* scenarios. CA1 most likely produces a depth sequence, which itself is related to various environmental gradients, most importantly temperature, light, and oxygen. The right side of the gradient represents deeper waters.

The identified prominent shallowing during Phase 3 renders temperature fluctuations a driving force for community composition, along with progressively increasing energy levels. Substrate preferences, on the other hand, were not a determining factor for the community composition, as fossil communities of beds 2 and 3 are similar with the exception of the Transitional Fauna (Fig. 7.8). The significant shift in the carapace morphology of *E. middendorfii* between phases 2 and 3 (Figs. 6.10, 7.8; Chapter 2) indicates a shift from an oxygen-controlled lake floor environment (Phase 2) to a temperature-controlled environment (Phase 3).

In addition to the response of species to environmental variables, interspecific competition and predation should be considered to explain the separation of species. The malacostracan *Liaoningogriphus quadripartitus* assumes a nektobenthic life style, similar to *Eosestheria middendorfii*, and there is an obvious decline in the abundance of clam shrimps in *Liaoningogriphus*-rich horizons and vice versa (excavation ZJG, Phase 2; Fürsich et al., 2007; Pan et al., 2012). In turn, the mayfly *Ephemeropsis trisetalis* co-occurred with both species in larger numbers. *Eosestheria middendorfii* probably excluded *L. quadripartitus* competitively, accounting for the (near) absence of the latter in excavation JSG. A likely scenario for the presence of scattered individuals of *Liaoningogriphus* in this excavation may be that the prevailing environment was disturbed, creating gaps for *Liaoningogriphus* to settle and the two species to coexist until the eventual exclusion the malacostracan. In turn, niche differentiation was most likely the basis for the coexistence of *E. middendorfii* and *E. trisetalis* (Figs. 7.6, 7.8).

The abundance of coprolites made up of clam shrimps (Fig. 7.5g) shows that *Eosestheria middendorfii* was prey to higher trophic levels, probably fish. Some extant species have also been recognized as important food sources for fish (e.g., *Caenestheriella belfragei*; Donald, 1989). This shows that the food web of Lake Sihetun frequently became more complex.

Population ecology of the benthic fauna

Given that even two freshwater species of the same genus may respond to environmental factors in quite different ways, palaeoecological interpretations cannot entirely be based on analogies with habitats of extant taxa. The approach taken herein is to infer the population ecologies of the fossil taxa identified in excavation JSG from the various proxies gathered in the chapters of this thesis, considering the population ecologies of modern relatives as supporting evidence. Special interest will be placed on the reconstruction of the life history and palaeoecology of *Eosestheria middendorfii*.

Mayfly larvae play an important role in the communities of Lake Sihetun (Fürsich et al., 2007; Table 7.2; Fig. 7.6) and in modern freshwater communities alike. Extant taxa are accepted as bioindicators for water quality and mayfly diversity directly correlates with habitat variety (Bauernfeind and Moog, 2000); undisturbed river sections may yield more than 30 species. Therefore, mayfly species occur in various environments. While one species is dependent on deep pools with macrophytic vegetation, other species are found on dead wood and submerged roots; yet others colonize steep clay banks (Bauernfeind and Moog, 2000). This shows that a correlation with modern species does not serve for the palaeoecological interpretation of *Ephemeropsis trisetalis*. The presence of *E. trisetalis*-dominated associations in Bed 2 (ZJG; Fürsich et al., 2007) and Bed 3 (Assemblage Z; Fig. 7.6; Table 7.2) shows that this species was a generalist and tolerant towards environmental variables related to water depth (Fig. 7.7).

Most Naididae feed on detritus and epiphytic algae (Kaliszewicz, 2003). They are common in shallow to medium depths (Hiltunen, 1967; Löhlein, 1996). In Lake Michigan, for example, they occur in waters of 5.5-18.5 m depth (Hiltunen, 1967). *Stylaria lacustris* is a modern species that displays similar morphological features as the fossil oligochaete of Lake Sihetun (Fig. 7.5f). It is 3.5-12 mm long (Kaliszewicz, 2003) and therefore slightly smaller than that of Lake Sihetun. However, the taxonomy of modern forms is based on chaetae (Hiltunen, 1967), which are not preserved in the sediments of Lake Sihetun. Hence, the Early Cretaceous oligochaete

is left in open nomenclature. The modern species *S. lacustris* dominates oligochaete assemblages associated with *Phragmites* (reed) stems in the littoral zones of northern German lakes (Löhlein, 1996). Individuals do not seek refuge in sediments or self-constructed tubes (Kaliszewicz, 2003), so they act as prey for predators such as insect larvae or leeches. They are able to survive the loss of more than half of their body length by regenerating lost parts after amputation with no impact on the survival rate (Kaliszewicz, 2003). Meiofaunal bioturbation within Bed 3 (diameters ranging between 114 μm and 228 μm; Fig. 1.11d) indicates the presence of an infauna. However, as the Early Cretaceous oligochaetes are about 1.2 – 2 mm thick (Fig. 7.5f), they cannot have been part of it. Instead, they must have assumed a similar epibenthic lifestyle as their modern counterpart *S. lacustris*, inhabiting in the deeper waters of the early Phase 3.

Adult water boatmen are good flyers and they colonize temporary waters by immigration rather than by desiccation-resistant cysts (Batzer and Wissinger, 1996). For food, they gather algae with their legs. Invertebrates are readily consumed by waterfowl and modern water boatmen are important food sources, along with midge larvae or caddisfly larvae (Batzer and Wissinger, 1996). However, the swimming ability of water boatmen does not make them easy prey. Insects are particularly abundant in seasonally flooded and semipermanent marshes, with water boatmen (along with midges, beetles, and mosquitoes) dominating these habitats (Batzer and Wissinger, 1996). A good swimming ability of *Karataviella* sp. A would explain the sporadic occurrences of this species in associations 1 and 2. In general, this Early Cretaceous water boatman must have preferred a similar deeper-water habitat as that of the naidid oligochaetes (Fig. 7.7).

Less common taxa of excavation JSG are gastropods (Fig. 7.5a, b), bivalves (Fig. 7.5c, d), caddisfly larvae (Fig. 7.5e), and the malacostracan *Liaoningogriphus quadripartitus*. In contrast to excavations ZJG and LXBE, in which bivalves are more abundant than gastropods (Pan et al., 2012), the situation is reversed in excavation JSG. Gastropods (*Probaicalia* sp. A) are far more common in this study, but their small size makes them hard to recognize in the field. Subsequent laboratory examinations suggested densities of several individuals per 25 cm^2. CA2 separates horizons yielding molluscs from others (Fig. 7.6a), and the response of both mollusc species to environmental variables underlying water depth seems to be narrow (Fig. 7.7). However, both response curves are based on small sample sizes and should be understood as preliminary.

Caddisfly larvae (Fig. 7.5e) are nowadays widely used in water quality assessments (Bonada et al., 2004). However, the high variability in the ecological profiles of modern taxa (very intolerant to fairly tolerant; Bonada et al., 2004) and their rarity in excavation JSG render the fossil caddisfly larvae of Lake Sihetun insignificant for the environmental characterization of the lake.

In contrast to locations ZJG and LXBE, *Liaoningogriphus quadripartitus* plays only a minor role in excavation JSG. *Eosestheria middendorfii* and the malacostracan were most likely mutually exclusive with the clam shrimp being competitively superior to the latter.

Life-history patterns of *Eosestheria middendorfii*

There are only limited amounts of resources for the growth and reproduction of organisms. Investing in one of the two typically requires some trade-off. Generally, a growth to large size leads to a reduction in reproductive activity. In turn, the growth of an individual slows with the onset of reproduction, due to a diversion of resources (Townsend et al., 2008).

Life-history traits employed for the extant clam-shrimp *Eulimnadia texana* are growth rate, egg production, moult frequency, age at maturity, and lifespan (Weeks et al., 1997). In theory, specific environments induce different combinations of life-history traits in organisms (Stearns, 1976). *Eulimnadia texana* is characterized by an early high growth rate and a significant drop in the rate of growth with the onset of egg production during days 5 and 6. After 17 days, reproductive senescence is reached. The main trade-off that has been recognized between any two life-history traits of this species is between growth and egg production, which are negatively correlated. The identified traits indicate that of an early colonist life history (high initial growth, early reproduction, and early senescence and death). *Eulimnadia texana* is adapted to life in short-lived water bodies, which pose strong natural selection for rapid growth (several days) and early reproduction. This leads to an overall short lifespan of little more than 20 days (Weeks et al., 1997). The average moulting periodicity is about 22 h (~ 1.1 moults per day).

The life history of *Eosestheria middendorfii* has been summarized as opportunistic (Fürsich et

al., 2007). Our data support this view. *Eosestheria middendorfii* lived in an environment that accommodated rapid population growth, favouring large numbers of small progeny. There is considerable variation in adult size among the different populations (horizons) analysed, ranging from < 11.8 mm (LXBE S1; Chapter 5) to 23.7 mm (ZJG K; Table 6.1). Numerous large clam shrimps are marked by a lack of crowding (e.g., Fig. 6.1) or strongly reduced crowding (e.g., Fig. 6.3b), implying fast growth between consecutive moulting events. These faster growing individuals of *E. middendorfii* must have sacrificed increased egg production, as larger individuals of the extant species *E. texana* do (Weeks et al., 1997). The comparatively small adult sizes in combination with crowding in horizon LXBE S1 (Fig. 5.2a, b) were possible, because individuals of *E. middendorfii* were most likely not in competition for resources with other species and able to invest into egg production. Following this hypothesis, environments were suitable for the recruitment of *E. middendorfii* during the deposition of horizon LXBE S1. In turn, competition must have led the larger clam-shrimp individuals of Association 2 and the Transitional Fauna (e.g., JSG H, JSG O; Figs. 6.1, 6.3, 7.8, 7.9) to invest into growth. Associated horizons are marked by reduced population densities and medium to comparatively high diversities (Figs. 7.6, 7.8). However, the trade-off for investing into growth must have been the sacrifice of increased egg production. In turn, clam-shrimp characteristics of Association 1 are small body sizes and high population densities (Fig. 7.8), indicating investment into egg production and less into growth, which is exemplified by JSG G (Fig. 7.4g). Association 1 was therefore marked by a greater reproductive allocation due a comparatively high egg production.

Generally, rapid development, early reproduction, large numbers of progeny, small body sizes, and short life spans are signs for *r*-selecting habitats, which are short-lived and which allow for the rapid colonization and the fast exploitation of its resources (Pianka, 1970). Therefore, the proposed increased investment into egg production of Association-1 clam shrimps, their high population density, their smaller carapace sizes (Fig. 7.8), and their associated shorter life spans imply that habitats were shorter-lived than those of the other two associations. Short-lived habitats are herein interpreted to have suffered from frequent changes in the environment other than desiccation. Such frequent palaeoenvironmental changes were most likely seasonally-induced and most prominent in shallower waters within Lake Sihetun.

In summary, the presence of pronounced differences in carapace size and shape (Figs. 6.5, 6.10, 7.8) indicate that Lake Sihetun was in fact subdivided into shallower *r*-selecting and deeper, slightly more *K*-selecting habitats. The latter favoured higher-diversity associations marked by more intense competition. The environmental variable with the highest effect on *E. middendorfii* will be discussed in the following section.

Modern clam-shrimp population ecology in comparison with *Eosestheria middendorfii*

Great care is needed when drawing conclusions about fossil ecological niches of clam shrimps and the overall environment of a fossil lake. The stereotypic interpretation of sediments yielding spinicaudatans is a "temporary pond filled with freshwater" (e.g., Todd, 1991; Wang, 1999). Such perfunctory generalizations have to be confronted with careful sedimentological and morphometric analyses. Webb (1979) points out that much of the extrapolation of the habitat modern clam shrimps live in to fossil ones seems ill-founded, as the ecology of living species is generally still insufficiently studied.

By far the most abundant faunal component of excavation JSG is the clam shrimp *Eosestheria middendorfii*, which has been subject of the previous three chapters that revised the species taxonomically (Chapter 4), determined its sexual system (Chapter 5), and differentiated between ontogenetic and ecophenotypic variation (Chapter 6). Instead of using *E. middendorfii* as a line of evidence for habitat characteristics, this study will challenge the stereotypic interpretation, revise what is known about modern clam shrimps, and establish the population ecology of *E. middendorfii* by making use of the various proxies presented throughout this thesis.

Life style

Clam shrimps adopt a general life style of resting on their lateral side while being lightly burrowed. Occasionally they swim (Vannier et al., 2003). As shallow burrowers, extant cyzicids usually remain articulated, while more active swimmers, like the limnadiids, are prone to disarticulation (Frank, 1988).

Most clam-shrimp carapaces of Lake Sihetun are preserved articulated near their umbo and both valves are commonly rotated against each other to some extent. There are only few horizons that ex-

hibit disarticulated individuals (e.g., ZJG E). Therefore, *Eosestheria middendorfii* was probably a shallow burrower that occasionally swam.

Eggs, hatching, and early growth

Generally, reproductive adaptations for species restricted to small bodies of standing waters are parthenogenesis as well as dormant and rapidly hatching eggs (Barnes and Harrison, 1992). Hatching is triggered by temperature (see below for details) and the imbibing of water until the breakage of the outer shell (Mattox, 1950). Only a limited proportion of eggs is commonly subjected to a favourable micro-environment when the pool fills and many eggs remain unhatched in the mud, forming a reserve (Bishop, 1967a). Hatching is prevented by a lack of oxygen or light (Bishop, 1967b) and it may take place after several years of drought. However, even though hatching is commonly associated with the filling of a pool, eggs may hatch as readily without having been dried beforehand (Bishop, 1967b). Temperature, oxygen, and light as hatching stimuli are considerably more important. Moreover, drying even retards the development and hatching of eggs (Mattox and Velardo, 1950). A resting period, marked by desiccation and freezing, is therefore not necessary for egg development.

At the time of hatching, nauplii of *Cyzicus gynecia* (formerly *Caenestheriella gynecia*) are 0.37 mm long, growing rapidly to 0.48 mm within three hours. Four days after hatching, their body length averages 1.1 mm. It is enclosed in a carapace of 1.5 mm in length (Mattox, 1950). The development of adults takes several days and is shorter for limnadiids (Bishop, 1968) and a bit longer for cyzicids (Frank, 1988). Temperature strongly influences the post-embryonic development (see below). *Cyzicus mexicanus* hatches from May to August (late spring to summer; Mattox, 1939).

Eosestheria middendorfii of Lake Sihetun must have built up similar egg reserves and the onset of warm conditions during late spring most likely triggered the hatching of nauplii in adequately oxygenated waters. There was no need for the desiccation of larger areas of Lake Sihetun on a seasonal basis, as the dehydration of eggs is not required for egg development (Mattox and Velardo, 1950; Bishop, 1967b). Furthermore, sedimentary features that may corroborate repeated desiccation have not been observed in excavation JSG (Chapter 1). Therefore, micro-environments that triggered the hatching of nauplii were most likely influenced by temperature or oxygen (Chapter 2) instead of desiccation. *Eosestheria middendorfii* was a species capable of hatching several times a year, as indicated by the distinct trend of larger clam shrimps being overlain by smaller clam shrimps in horizons JSG A, C, D, and G (size measurements; Fig. 7.8). The first population of a season grew to maturity, while the second population, although triggered by a similarly favourable micro-environment, suffered from the rapid formation of unfavourable conditions and environmentally-induced mass mortality events. Given that *E. middendorfii* hatched during late spring or early summer, light was probably the same or even better when the second wave was triggered. Oxygen levels must have progressively decreased as the holomictic lake of Phase 3 (chapters 1 and 2) became stagnant during summer. Therefore, the main hatching stimulus must have been temperature.

Hatching in more marginal areas and a subsequent migration of later developmental stages into deeper regions of the lake may be considered. However, juveniles that were only a little larger than the seventh naupliar stage of extant cyzicids (850 μm; Olesen and Grygier, 2004) evidently shared an environment with clam shrimps of later developmental stages (e.g., JSG A; Figs. 6.4b-d, 7.8). Therefore, if nauplii had hatched in marginal areas only, they would have been required to move into deeper waters during their naupliar phase. As nauplii are positively phototactic after hatching (Frank, 1988), this would be a possible scenario. The more sedentary (benthic) mode of life, which was characteristic for adults of *E. middendorfii*, was adopted only after several moults. However, it is more likely that nauplii and adults shared the same environment. Egg production of females (Chapter 5) was probably high, considering the production of two egg clutches per day in extant species (Weeks et al., 1997). As weak swimmers, females presumably did not migrate to shallower waters on a daily basis in order to lay their eggs. In turn, exclusively large clam shrimps of low population density (Fig. 7.8; Transitional Fauna and Association 2) did migrate, indicating that adults were more tolerant towards environmental variables than juveniles (Fig. 7.7).

Co-occurrences

Clam shrimps generally occur in monospecific assemblages, as suggested by several hundred surveyed ponds in Kansas and Oklahoma (Tasch, 1969). Co-occurrences of two species are comparatively common in creek pools, as they are connected to other localities, and they are least common in hyposaline lakes (Timms and Richter, 2002). Syntopic

co-existences of two or more genera occur in 21 % of the collections from the Paroo catchment (Australia; Timms and Richter, 2002). Species are most likely kept separate through salinity, high turbidity, clear short-lived water, and season. For example, both species *Caenestheria* spp. and *Caenestheriella* spp. occur in turbid sites with salinities of < 5000 µS cm^{-1} that tend to fill for 4-8 weeks a year. Both can be found at any time of the year, although *Caenestheria* prefers the warm season and *Caenestheriella* the cooler one. Therefore, one species persists until the late stages of filling, whereas the other occupies the early stages of filling. Different body sizes of co-occurring species that prevent competition have also been suggested, but the feeding behaviour of species is still insufficiently known (Timms and Richter, 2002).

Pinpointing co-occurrences in fossil sites is difficult, as taphocoenoses are commonly preserved. Alleged co-occurrences of fossil spinicaudatans with a diverse marine fauna (e.g., Kummerow, 1939) might merely be the result of allochthonous depositions (Vannier et al., 2003). Two Late Carboniferous species of the Illinois Basin are mostly mutually exclusive and one alleged co-occurrence in fact represents a transported fauna (Petzold and Lane, 1988).

In case of Lake Sihetun, a taxonomic revision demonstrated that five of the alleged ten species of the Yixian Formation actually belong to a single species, *Eosestheria middendorfii* (Chapter 4). This taxonomic revision showed that excavations ZJG, LXBE, and JSG yielded no evidence for co-occurrences of this variable species with any other clam-shrimp species.

Habitat factors

The main ecological factors reported that act on the development of clam shrimps are temperature, food supply, reduced crowding brought about by heavy rainfall, salinity, turbidity, and the relative permanency of sites (Mattox, 1950; Timms and Richter, 2002). They are reviewed in this section. Generally, *Eosestheria middendorfii* exhibits an at least bimodal seasonal distribution (Fig. 7.8) and a high variability of carapace size and shape (Figs. 6.5, 6.10; Chapter 6), indicating a general high tolerance towards environmental variables (Fig. 7.7). The analysis of ecophenotypic variation (Fig. 6.10; Chapter 6) identified three distinct morphogroups. They are (1) Phase-2 clam shrimps of ZJG and LXBE, (2) Phase-2 clam shrimps of JSG, and (3) Phase-3 clam shrimps of JSG (Table 6.3). The difference in shape is most pronounced between Phase-2 and Phase-3 clam shrimps, indicating that the transition from one phase into another brought about significant palaeoenvironmental modifications to Lake Sihetun, which are connected to a change in climate from dry to humid (Chapter 1).

Depth

Most pools of *Limnadia stanleyana* were less than 20 cm deep (Bishop, 1967a). According to Wang (1999), clam shrimps of the Yixian Formation lived in quiet, shallow waters near the lake coast, in depths of about 2-50 cm to a maximum 2 m. This interpretation is clearly based on an analogy with modern clam shrimps.

Excavation JSG yielded fish coprolites in multiple horizons of Bed 3 (Fig. 7.5g; especially abundant in JSG R) as well as fish body fossils in Bed 2 (JSG 11; Fig. 7.1), implying somewhat deeper conditions (Pan et al., 2012). In addition, the sedimentological analysis of excavation JSG suggests that waters of Phase 2 were deeper than <10 m and 5 m. The onset of Phase 3 marks a deepening that led to adverse conditions for the hatching of nauplii. The Transitional Fauna (Fig. 7.6) was therefore a deeper-water fauna that yielded exclusively large individuals of *E. middendorfii*, which immigrated from shallower waters (Fig. 7.8). Association 1 represents a shallower-water fauna and Association 2 corresponds to an intermediate lake depth.

Light intensity

Eggs are more likely to hatch in zones of light penetration in the mud (Bishop, 1967b). In addition to hatching, growth is also accelerated by permanent illumination (Goretzki, 2003). In contrast, Horne (1971) noticed that photoperiod was not the primary environmental stimulus for hatching, as eggs were found to hatch during winter if temperatures permit it.

Light did not play a determining role for the size of *E. middendorfii*, exemplified by generally smaller adult carapace sizes in shallower, better illuminated waters (Association 1; Fig. 7.8). The effect of light was overprinted by environmental variables such as oxygen or temperature.

Oxygen concentration

Oxygen concentration is a limiting factor in extant branchiopod associations (Moore and Burn, 1968; Horne, 1971). Controlled experiments of Bishop (1967b) show that eggs of *Limnadia stanleyana* hatch more readily at higher oxygen concentrations that are close to the equilibrium with

air. Oxygen depletion reduces the amount of nauplii hatching. Therefore, the deeper eggs are buried in the mud the more likely it is that they will not hatch, as oxygen concentrations commonly decrease (Bishop, 1967b). Rainwater saturated with air may stimulate hatching. In contrast, *Caenestheriella setosa* withstands oxygen concentrations as low as 0.1 ppm (Horne, 1971; tap water: 4-7 ppm dissolved oxygen). Therefore, there are clam-shrimp taxa that are exceptionally tolerant to hypoxia. Experiments show that low oxygen concentrations stimulate active swimming, whereas at higher concentrations *C. setosa* lies motionless on the substrate. Concentrations below 0.1 ppm lead to the death of the clam shrimp within 30 minutes time (Horne, 1971). Furthermore, Horne (1971) noticed that at oxygen levels as low as 0.6 ppm no other branchiopods (tadpole shrimps and fairy shrimps) were co-occurring with clam shrimps.

Moore and Burn (1968) surveyed hypoxic ponds (< 1 ppm; 1 m maximum depth) in Louisiana, which commonly fill in December and remain flooded for several months. During wet years they may also fill during summer. One instance of high water temperatures led to the depletion of subsurface oxygen for more than a week, but the pond fauna was not entirely eliminated. Instead, the behaviour of animals changed during this anoxic interval. Anostracans (fairy shrimps), for example, were concentrated in the upper cm of the surface waters. In contrast, the clam shrimp species *Eulimnadia inflecta* was eliminated during anoxia because clam shrimps are only weak swimmers and usually found near the pond floor (Moore and Burn, 1968).

It is likely that *E. middendorfii* was similarly adapted to very low lethal oxygen thresholds, as hypoxia frequently occurred in Lake Sihetun during Phase 2 (Fürsich et al., 2007; Chapter 2). Better swimmers such as mayfly larvae most likely left the habitat in search of more oxygenated regions in the lake. Branchiopods (e.g., fairy shrimps) have also been reported to react to hypoxia with migration (Moore and Burn, 1968). Even though clam shrimps are weak swimmers, *E. middendorfii* probably reacted in a similar way. Disarticulation is rare, but it occurs in several Phase-2 horizons (e.g., ZJG E). It indicates an increased movement of individuals in response to a growing intolerance towards environmental variables. In the above example of ZJG E, swimming was most likely triggered by lethally low oxygen conditions, as this is one of the most oxygen-depleted horizons of all three excavations (Fig. 2.9; Chapter 2). Hence, oxygen ranges

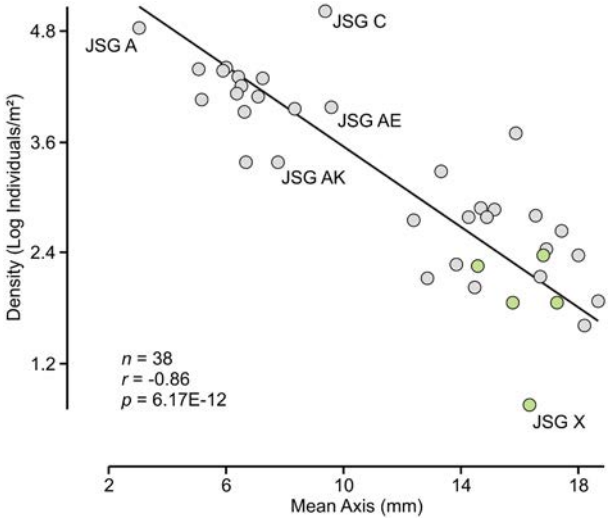

Fig. 7.9. Mean carapace size and population density are significantly negatively correlated at $p < 0.001$ (correlation coefficient $r = -0.86$). Horizons of the Transitional Fauna are marked green. Density has been log-transformed to fit a normal distribution required for the analysis. Note that even though mean values were sometimes calculated from bi- or polymodal distributions (see bean plot of Fig. 7.8), they are regarded as time-averaged estimations of overall size for each horizon. There is a gap between juveniles (left) and adults (right), which possibly represents a mortality threshold and a reaction to crowding as well as worsening environmental conditions. Individuals of later developmental stages exhibited higher chances of survival. Note that small juveniles of JSG C have not been measured, but their density has been counted, rendering the corresponding point an artificial outlier in this plot.

amongst the most important determining variables during Phase 2. The situation was more relaxed during the oxygenated Phase 3, when other factors governed community composition.

pH

According to Goretzki (2003), nauplii only hatch in neutral to weakly alkaline conditions, but there is no report on which and how many species were tested. Tasch (1969) mentions that the preferred pH of clam shrimps ranges between 7 and 9. This corresponds to the alkaline interpretation for the bottom waters of Lake Sihetun (chapters 1 and 2).

Precipitation, crowding, and mass mortality

Cyzicus gynecia (formerly *Caenestheriella gynecia*) occurs in small, shallow, muddy, temporary pools and individuals may survive for six months. Heavy rainfall results in a high food supply and larger, more permanent pools, which greatly reduces crowding of individuals and intraspecific competition. Individuals hatching during such wetter times are distinctly

larger with a higher number of growth lines (10.6 mm as opposed to 7.3 mm in dryer years; Mattox 1950).

The onset of the humid conditions of Phase 3 (Chapter 1) rendered some of the largest clam shrimps of this study (marked green in Fig. 7.9). But as carapaces were similarly large in excavation ZJG (arid Phase 2; Fürsich et al., 2007), a higher food supply resulting from an increased precipitation cannot be put forward as the determining factor of carapace size.

A large proportion of the variance in carapace size can be explained by the population density of *E. middendorfii* (r^2 = 0.74; Fig. 7.9). One would expect that smaller clam shrimps naturally exhibit a higher population density, due to a higher juvenile mortality (e.g., Fig. 7.4b, e). However, the daily survival of a cohort of the extant species *Eulimnadia texana* (captive breeding) remained at 100% survival throughout its juvenile stage. It only started to decrease several days after the individuals have reached maturity (~ day 10). Half of the cohort was still alive during day 15 and the oldest individuals died after little more than 20 days (Weeks et al., 1997). As growth continues in surviving individuals, the resultant taphocoenosis should comprise a wide range of clam-shrimp sizes. (Note that growth slows with the onset of egg production.) So in theory, a small standard deviation within the axis measurements of a horizon should be an estimate for an abrupt death of a cohort of juveniles or young adults, which is exemplified by the small spread of JSG-F individuals in Fig. 7.8 (environmentally-induced mass mortality). In turn, death due to senescence (normal age distribution) should be indicated by a higher standard deviation, exemplified by JSG K. The large clam shrimps of JSG AN (Fig. 7.2c) seem to be exceptionally crowded, however JSG AN is a heavily time-averaged horizon that represents multiple cohorts.

Assuming a survival of 100 % and a restricted habitat, crowding must have increased as the individuals grew. Phase-3 clam shrimps are found on top of depositional units that are associated with biofilms (Chapter 1; Fig. 1.11d, e), implying that they lived during periods of reduced precipitation that probably led to the formation of restricted habitats in shallower areas of Lake Sihetun (later Phase 3). Therefore, crowding in combination with worsening environmental conditions during the dry period of a season (presumably increased temperatures) most likely initiated the repeated environmentally-induced mass mortality events of Association 1. The gap between juveniles and adults in Fig. 7.9 implies the presence of environmental threshold conditions. Chances of survival were increased in less restricted regions that were marked by reduced crowding.

Salinity

The majority of modern spinicaudatans does not tolerate raised salinities. They preferentially inhabit ephemeral inland water bodies; playa lakes, springs, marshes, tundra, and rarely cave pools (Vannier et al., 2003). A study conducted in the Paroo catchment of Australia concluded that most species dwelled in fresh- to subsaline waters (< 250 – 5000 μS/cm; Timms and Richter, 2002). Hence, clam shrimps are generally indicators for freshwater conditions. There are, however, exceptions such as the halophilic species *Eocyzicus parooensis*, which is the most salt tolerant of all spinicaudatans known thus far and it occurs in hyposaline lakes (up to 15 g/l). It has a bimodal seasonal distribution due to fillings of these hyposaline lakes in summer and (mild) winter (Timms and Richter, 2002). *Eocyzicus parooensis* is a variable species with different numbers of growth lines and varying carapace lengths and heights, depending on the specific locality in the Paroo area (Richter and Timms, 2005).

Even though the majority of extant clam shrimps prefers freshwater conditions, exceptions such as the variable species *E. parooensis* show that it is not possible to predict what levels of salinity *E. middendorfii* was able to tolerate. However, *Eocyzicus parooensis* shows that species tolerant towards environmental variables exhibit a high variability in shape, as is the case for *E. middendorfii* (Fig. 6.10; Chapter 6). In addition, the proposed reduced lake volume of Phase 2 (sedimentological analysis) was probably accompanied by an increased salinity marked by carbonate precipitation.

Temperature

There are important temperature effects that influence hatching and the size of the nauplii (Mattox and Velardo, 1950). Hatching takes place after a species-specific temperature has been reached, for example 13°C for wet and 17°C for dried eggs of *Cyzicus gynecia* (formerly *Caenestheriella gynecia*). The optimum temperature for egg development of *C. gynecia* lies between 24°C and 37°C and nauplius size decreases when hatched above this optimum. Post-embryonic development of *Limnadia stanleyana* is strongly dependent on temperature, taking 440 h at 15°C, but only 160 h at 25°C (Bishop, 1967a). Also, growth of *C. gynecia* was found to be distinctly

slower in autumn populations (lower temperatures) than in their summer equivalents, resulting in more closely-spaced growth lines. Emberton (1980) put forward a channelling of energy into egg production as the reason for reduced growth in autumn populations. The appearance of *Caenestheriella setosa* in ponds is driven by temperature as the main factor (Horne, 1971), as populations hatch during particularly warm spells in January (in Texas). Normally this species does not hatch during December to February, even if the respective pools are repeatedly filled.

Water depth and temperature are linked and the inferred shallower waters of the upper part of excavation JSG (upper part of Bed 3) certainly suffered from enhanced temperature fluctuations, such as raised temperatures during summer. Considering the influence of temperature on the post-embryonic development of modern clam shrimps, temperature fluctuations must have had an effect on the size of *E. middendorfii*. High temperatures during summer stagnation and the formation of restricted habitats are held responsible for repeated environmentally induced mass mortality events. Nauplius size decreases when hatched above a temperature optimum; critically high temperatures, in combination with crowding in restricted environments, may explain the presence of numerous horizons yielding only medium-sized individuals (e.g., JSG L, M1, M2, N, R, S; Fig. 7.8). In addition, the influence of temperature on oxygen concentration indirectly led to the elimination of competing taxa in Association 1. In turn, the post-embryonic development of *E. middendorfii* was probably accelerated in slightly cooler intermediate water depths (Association 2), which were nevertheless still located above the thermocline, judging from the accelerated development of extant clam shrimps at 25°C (Bishop, 1967a).

Turbidity

Clam shrimps are rare in highly turbid waters and they prefer clear, well-oxygenated ones. There are exceptions, such as *Caenestheria lutraria* (Timms and Richter, 2002) or *Cyzicus tetracerus* (Stoicescu, 2004). Turbidity is therefore one of the factors that keep species apart. As benthic, non-selective deposit feeders, modern cyzicids burrow into the mud and filter out ingestible material (Vannier et al., 2003). The dislodging of detritus creates enough turbidity to identify ponds carrying clam shrimps and those without (Frank, 1988). The sediment surfaces of Bed 2 of Lake Sihetun are undisturbed (Fig. 1.4; Chapter 1), indicating a shallow foraging of *E. middendorfii* and clear waters.

Temporary versus perennial

Late Carboniferous clam shrimps of the eastern Illinois Basin occur in black shales, which are associated with coal beds and marine units. They are interpreted to have lived in standing water bodies with narrow salinity ranges in the vicinity of coal swamps. Alkalinity was proposed as the determinant habitat factor of the two species identified (Petzold and Lane, 1988). Spinicaudatans of the Westphalian Coal Measures are associated with diverse aquatic habitats, which are proposed to have been temporary by alluding to extant forms (Todd, 1991). In addition to such extrapolations, there are numerous examples of temporary settings yielding clam shrimps that have been recognized as such by the presence of desiccation cracks, footprint horizons, algal laminae, and stromatolites in the associated sediments (e.g., Olempska, 2004; Lucas and Milner, 2006).

Vannier et al. (2003) paralleled the Late Carboniferous Montceau biota with that of temporary aquatic environments, which are marked by the following attributes: a low diversity-high density crustacean fauna, a narrow size range of spinicaudatan assemblages suggesting cohorts, the presence of resting eggs, the dominance of crustaceans as a whole, a high insect diversity in contrast to a relatively low abundance, and the presence of amphibians. These attributes are also reflected by Lake Sihetun.

However, the presence of fishes and syncarid crustaceans at Montceau, which are commonly absent from modern shallow and isolated temporary pools, led Vannier et al. (2003) to reconsider water depth. In addition, they also recognized that sedimentological features of temporary environments are not associated with the clam-shrimp bearing horizons of Montceau. The same arguments can be put forward for Lake Sihetun (Chapter 1). Vannier et al. (2003) reconciled this discrepancy between the observed 'perennial' features and the common 'temporary' interpretation of clam shrimps by proposing flooding and the transportation of faunal components to the depositional area. Thus, the Late Carboniferous Montceau Lagerstätte is characterized as a lake ecosystem with both permanent and temporary niches.

Nevertheless, most fossiliferous layers of Lake Sihetun are interpreted as autochthonous, as clam shrimps are commonly associated with deposits of more tranquil periods of reduced rainfall (Fig. 1.11;

Chapter 1). Examples of clearly transported carapaces are visualized in Fig. 1.8 (Mf 3). We follow the interpretation of Vannier et al. (2003), who divided the palaeolake into various sub-environments. However, the commonly used argument that clam-shrimp eggs require a dry phase has been disproved and temperature has been put forward as the most important hatching stimulus (Mattox and Velardo, 1950; Bishop, 1967b; Horne, 1971). Therefore, instead of interpreting the bulk of Phase-2 clam shrimps as transported to fit the common ecological niche of extant taxa, it is herein proposed that *E. middendorfii* was adapted to life in permanent waters.

Conclusions

Abiotic environment during lake phases 2 and 3

After what must have been the majority of the time of its existence, Lake Sihetun reacted to a climate change from dry to humid with a drastic modification of its depositional regime, which greatly enhanced sediment yield during Phase 3. This transition is marked by an initial deepening of the lake that was accompanied by an increase in the surface area and a dilution of lake waters. A general coarsening upwards trend within Bed 3 implies overall shallowing during Phase 3, which led to the eventual siltation of the lake during Phase 4. Even though lake depth was abruptly increased at the onset of Phase 3, Phase 2 was markedly deeper than inferred in previous studies with minimum water depths of 10 m. Indicators for currents in the lake during Phase 3 are small-scale cross-bedding and the orientation of *Ephemeropsis* larvae, which indicate a preferred direction of NE-SW. Phase 3 was governed by alternations of wet and dry seasons with a well oxygenated lake floor during the wet season that quickly became colonized by a meiofauna. The dry season is represented by a draping of background mud and the formation of microbial structures. Clam shrimps mostly died during this tranquil phase. No evidence of repeated emergence has been identified.

Community development

This study is the first to document the long-term community development across the transition between phases 2 and 3. Three associations and two assemblages have been identified, which are mostly arthropod-dominated, of high-numerical abundance, and of low diversity. Changes in the ancient abiotic environment of Lake Sihetun in response to the climate change event that separates phases 2 and 3 (deepening) are reflected by a sharp modification in the palaeocommunity composition from the clam-shrimp dominated associations 1 and 2 to the insect- and oligochaete-dominated Transitional Fauna, which is marked by comparatively high diversities.

Population ecology of benthics

Response curves to environmental variables are overlapping but of various widths, explaining the exclusion of taxa from certain environments. The clam shrimp *Eosestheria middendorfii* exhibits the widest response curve, indicating high tolerances towards environmental gradients. The high tolerance range is accompanied by a pronounced ecophenotypic variation in carapace morphology, which mainly separates oxygen-driven from temperature-driven environments. Larvae of *Ephemeropsis trisetalis* and the water boatman *Karataviella* sp. A can also be considered as generalists. In contrast, naidid oligochaetes, bivalves, and gastropods displayed comparatively low tolerances towards environmental variables, manifested in narrow response curves.

Life history of *Eosestheria middendorfii*

Eosestheria middendorfii was marked by several generations per year, but the chances of survival were significantly decreased for the second generation of a season, whose individuals often only barely survived its naupliar stage. *Eosestheria middendorfii* did not depend on the imbibing of water for the hatching of eggs. Instead, temperature is proposed as the main trigger for the simultaneous hatching of numerous naupliar larvae. The population dynamics of *E. middendorfii* are predicted to have been dominated by a sudden recruitment, a survival of near 100 % for several days until reproductive maturity was reached, and a subsequent progressive population decline. This was repeatedly interrupted by population crashes due to environmentally induced mass mortality events driven by oxygen depletion during Phase 2 and, more importantly, high temperatures in shallower waters during Phase 3.

Table 1.1 Couplet and varve-thickness measurements in thin-sections of Microfacies 1 to 4.

Mf 1-Couplets (LXBE L1, in µm)		Mf 1-Couplets (LXBE E, in µm)	Mf 1-Couplets (LXBE H, in µm)	Mf 2-Varves (LXBE D, in µm)		Mf 3-Couplets (ZJG S, in µm)	Mf 4-Varves (LXBE K1, in µm)
52.4	34.8	13.5	25.3	235.1	128.4	72.7	149
17.2	22.3	18.3	11.5	110.1	121.6	81.8	383
32.1	17.2	19.6	11.2	114.1	44.8	70.1	187
66.2	13.2	24.0	11.8	110.1	42.1	59.7	212
52.7	14.2	29.1	27.0	101.9	37.4	269.9	230
35.1	17.2	26.4	19.3	103.9	72.0	145.3	107
44.9	21.6	22.6	22.6	112.8	80.8	346.5	156
26.0	38.5	12.8	22.6	84.9	193.6	267.3	162
13.5	20.6	22.3	15.9	103.9	183.4	238.8	134
16.2	18.2	17.6	9.8	195.7	99.9	85.7	119
23.7	16.2	35.5	16.9	152.9	62.5	72.7	129
63.2	17.2	45.3	11.5	135.2	65.9	292.0	179
55.4	12.2	34.1	11.2	66.6	84.9	251.7	
47.0	14.2	16.6	12.2	59.1	62.5		(LXBE J)
28.4	27.4	29.1	12.5	78.1	67.3		240
56.8	15.9	18.9	20.3	79.5	60.5		346
40.5	19.3	20.6	10.5	232.3	297.6		534
37.8	31.4	20.6	14.5	59.1	195.7		
40.2	21.3	26.7	14.5	81.5	85.6		
31.8	19.3		13.5	91.0	76.1		
16.6	26.4		28.0	62.5	99.9		
15.2	33.5		23.3	147.4	88.3		
29.4	27.4		9.5	85.6	104.6		
35.8	32.8		10.1	156.3	78.8		
35.1	33.5		21.0	123.0	46.9		
28.4	19.3		14.2	114.8	59.1		
30.1	17.6			81.5	292.8		
33.5	21.6						
32.1	13.5						
33.1	24.3						
32.8	19.3						
31.1	23.7						
32.0	23.0						
23.0	18.2						
45.6	28.0						
28.0	51.7						

Table 3.1. Compilation of some frequently cited works and treatises dealing with the classification of Spinicaudata. Lower-rank taxa have been included for older publications, as most groups are based on these types. Laevicaudata (Lynceidae), Spinicaudata, and Cyclestherida have been grouped together for a long time, forming the paraphyletic order Conchostraca Sars, 1867. Groups not belonging to the Spinicaudata are put in square brackets. Taxonomic groups marked with an asterisk (*) have been named by the respective worker. Taxonomic groups to which Euestheria has been assigned within the respective classification are underlined.

	Suborder	Superfamily	Family	Subfamily/Genera
Baird, 1849	Phyllopoda (Order)	-	Limnadiadae*	*Limnadia*, *Estheria*
Jones, 1862 "Fossil Estheriae"	-	-	-	Known living genera: *Estheria, Limnadia, Limnadella,* [*Limnetis*]
		-	Estheriae Leaiae (not specified as families)	Fossil genera described: *Estheria, Leaia**
Packard, 1877 North America, modern	Phyllopoda	-	Limnadiadae	Estherianae *Estheria, Limnadia, Eulimnadia, Limnadella** (nov. gen. here, but mentioned by other authors before) [Limnetinae] [*Limnetis*]
Sars, 1896 Norway, modern	Phyllopoda	Conchostraca (not specified as superfamily)	Limnadiidae [Limnetidae*]	-
Sars, 1900 India, modern	Conchostraca (Division)	-	Estheriidae	*Estheria, Leptestheria*
			Limnadiidae	*Limnadia, Eulimnadia, Limnadopsis, Limnadella*
			[Cyclestheriidae]	[*Cyclestheria*]
Stebbing, 1910 South Africa, modern	-	Conchophylla (Tribe)	Cyzicidae	*Cyzicus, Leptestheria*
			[Lynceidae]	[*Lynceus*]
Depéret and Mazeran, 1912 France, Permian, fossil	-	-	-	*Estheria* (*Lioestheria**) *Estheria* (*Euestheria**)
Daday, 1915-1927 modern	Phyllopoda conchostraca	-	Caenestheriidae* Limnadiidae Leptestheriidae* [Lynceidae] [Cyclestheriidae]	-
Linder, 1945 modern	Conchostraca [Laevicaudata*] Spinicaudata*			

	Suborder	Superfamily	Family	Subfamily/Genera
Raymond, 1946 fossil and modern	-	-	Cyzicidae Lioestheriidae* Limnadiidae Leaiadidae* [Lynceidae] [Cyclestheriidae]	-
Kobayashi, 1954 fossil	-	-	Lepidittidae* 1953	-
			Rhabdostichidae	-
			Lioestheriidae	Lioestheriinae* Asmussiinae* Cyclestherioidinae*
			Limnadiidae	Estheriininae*
			[Lynceidae]	-
			Estheriellidae* 1953	-
			Leaiadidae	-
Novojilov, 1960 Treatise, fossil	-	Cyzicoidea	Rhabdostichidae Lioestheriidae [Cyclestheriidae] Glyptoasmussiidae* Ulugkemiidae* 1958 Aquilonoglyptidae* 1958 Cyzicidae Leptestheriidae Estheriinidae Limnadiidae Kontikiidae* 1958 Asmussiidae Bairdestheriidae* 1954 Aphrographidae* 1957	-
		Limnadiopseoidea* 1958	Limnadiopseidae* 1958 Ipsiloniidae* 1958 Vertexiidae	-
		Leaioidea	Amphikoilidae* 1953 Leaiidae Cycloleaiidae* 1952 Estheriellidae	-
		[Lynceioidea]	-	-
		Conchostraca incertae sedis	Lioestheriidae Lepidittidae	-

	Suborder	Superfamily	Family	Subfamily/Genera
Defretin-Lefranc, 1965 USSR, fossil	-	Lioestherioidea	Lioestheriidae	Lioestheriinae Euestheriinae Bairdestheriinae
			Asmussiidae	Orthothemosinae Pseudoasmussiinae Asmussiinae
		Limnadioidea	Palaeolimnadiidae	Estheriinae Palaeolimnadiinae
			Palaeolimnadiopseidae	Palaeolimnadiopseinae Vertexiinae
		[Lynceioidea]		
		Leaioidea	Leaiidae	Leaiinae Hemicycloleaiinae
			Cycloleaiidae	-
Tasch, 1969 Treatise, fossil and modern	Spinicaudata	Limnadioidea	Limnadiidae [Cyclestheriidae] Leptestheriidae	-
		Cyzicoidea	Cyzicidae Asmussiidae	-
		Estherielloidea	Estheriellidae	-
		Leaioidea	Leaiidae	-
		Vertexioidea	Vertexiidae Limnadopsidae* Pemphilimnadiopsidae* 1961 Ipsiloniidae	-
Novojilov, 1970 Russia, treatise	-	Limnadioidea	Limnadiidae	Limnadiinae Metalimnadiinae* Echinolimnadiinae* Novojilov, 1965
			Gabonestheriidae*	Corniinae* Gabonestheriinae*
Kobayashi, 1972 Fossil, revised classification of his 1954 version, taking Novojilov (1960), Defretin-Lefranc (1965), and Tasch (1969) into account	Estheritina	Lioestherioidea	Lioestheriidae Rhabdostichidae Asmussiidae Estheriinidae	-
		Palaeolimnadiopseoidea	Palaeolimnadiopseidae Ipsiloniidae	-
		Vertexioidea	Vertexiidae Pemphilimnadiopsidae	-
	Leaiina	Estherielloidea	Estheriellidae Monoleiolophidae	-
		Leaioidea	Leaiidae Amphikoilidae Rostroleaiidae (?) Echinolimnadiidae	-

	Suborder	Superfamily	Family	Subfamily/Genera
Zhang et al., 1976 China, treatise, fossil	[Laevicaudata]	[Palaeolynceioidea]	[Palaeolynceidae]	-
	Estheritina	Lioestherioidea	Eosestheriidae* Diestheriidae* Euestheriidae Loxomegaglyptidae Lioestheriidae Aquilonoglyptidae Orthothemosiidae Asmussiidae Afrograptidae	-
		Estheriteoidea*	Orthestheriidae* 1975 Dimorphostracidae* 1964 Estheriteidae* Jilinestheriidae* Halysestheriidae*	-
		Vertexioidea	Palaeolimnadiidae Palaeolimnadiopseidae Vertexiidae Ipsiloniidae Perilimnadiidae* 1975	-
	Leaiina	Leaioidea	Monoleiolophidae Leaiidae Praeleaiidae	-
		Estherielloidea	Estheriellidae	-
Kozur, 1982; Kozur and Seidel, 1983 European, fossil	Spinicaudata (the suborder Leaiina does not belong to the Spinicaudata in Kozur, 1982)	Limnadiacea	Kontikiidae	-
		Cyzicacea	Bairdestheriidae Cyzicidae	-
		Lioestheriacea	Vertexiidae	-
		Lepestheriacea or Estheriellacea	Estheriellidae Polygraptidae	-
Zhang et al., 1990 fossil	[Laevicaudata]	-	-	-
	Spinicaudata	-	-	-
	Leaiina	-	-	-
Martin and Davis, 2001 modern	Spinicaudata	-	Cyzicidae Leptestheriidae Limnadiidae	-
Kozur and Weems, 2005 fossil, incomprehensive			Euestheriidae Shipingiidae* Bulbilimnadiidae*	

Table 3.2. Overview of specimens used in this study. Family assignments of the fossil spinicaudatans are deliberately taken from the original study the genus was described in, as numerous new families had been erected since the publication of the Treatise on Invertebrate Paleontology (Tasch, 1969). This applies only to post-Treatise publications. Families of pre-Treatise genera have been synchronized with it (e.g., Depéret and Mazeran, 1912). To increase the Palaeozoic material, Late Carboniferous material described by Orr and Briggs (1999) has been included.

Sample	Sample #	Formation	Age	Family	Family groupings	Carapace mineralogy
1.1 *Euestheria* (Depéret and Mazeran, 1912)	EL 5195	Anstruther Fm., Anstruther Core, Scotland	Early Carboniferous	Cyzicidae Stebbing, 1910 (according to Tasch, 1969)	Cyzicidae *sensu la*to	Organic carbon residues (EDS)
1.2 *Euestheria* (Depéret and Mazeran, 1912)	EL 5844	Anstruther Fm., Anstruther Core, Scotland	Early Carboniferous	Cyzicidae Stebbing, 1910 (according to Tasch, 1969)	Cyzicidae *sensu lato*	Organic carbon residues (EDS)
1.3 *Leaia* Jones, 1862	EL 4985	Anstruther Fm., Anstruther Core, Scotland	Early Carboniferous	Leaiidae Raymond, 1946 (according to Tasch, 1969)	Leaiidae	Organic carbon residues (EDS)
1.4 *Leaia salteriana* Jones	GSE 14091	Anstruther Fm., cottage row, Crail, Scotland	Early Carboniferous	Leaiidae Raymond, 1946 (according to Tasch, 1969)	Leaiidae	Organic carbon residues (EDS)
1.5 *Leaia* Jones, 1862	FG 629/3	El Menizla Fm., Morocco	Carboniferous	Leaiidae Raymond, 1946 (according to Tasch, 1969)	Leaiidae	Dark residue, SiO_2 (XRD)
2.1 *Euestheria* (Depéret and Mazeran, 1912)	GSE 13655	Newarthill Core No.2, Scotland	Late Carboniferous?	Cyzicidae Stebbing, 1910 (according to Tasch, 1969)	Cyzicidae *sensu lato*	Apatitic composition – type 3.2 preservation (EDS)
2.2 *[Estheria]* Rüppell, 1837	I 1043	Coal Measures, South Wales	Late Carboniferous	?	?	Ferroan dolomite, pyrite (EDS)
2.3 *[Estheria] tenella* Bronn, 1850	IN 48885	Carluke, Lanarkshire, Scotland	Late Carboniferous	?	?	Apatitic composition – type 3.2 preservation (EDS)
2.4 *Leaia leidyi* var. *salteriana* Jones, 1862	I 34919	Coal Pit Heath Colliery, Pucklechurch, England	Late Carboniferous	Leaiidae Raymond, 1946 (according to Tasch, 1969)	Leaiidae	Organic carbon residues (EDS)

Sample	Sample #	Formation	Age	Family	Family groupings	Carapace mineralogy
2.5 *Leaia mitchelli* Etheridge, 1892	IN 27153	Wayner's Bay, Lake Macquarrie, Australia	Carboniferous-Permian	Leaiidae Raymond, 1946 (according to Tasch, 1969)	Leaiidae	Organic carbon residues (EDS)
3.1 *Euestheria* (Depéret and Mazeran, 1912)	FG 629/2	Arefino ravine, Russia	Early Triassic	Cyzicidae Stebbing, 1910 (according to Tasch, 1969)	Cyzicidae *sensu lato*	Fluorapatite, SiO_2 (XRD)
3.2 *Estheriella marginostriata*	FG 618/12	Bernburg Fm., Beesenlaublingen	Early Triassic	Estheriellidae Kobayashi, 1954 (according to Tasch, 1969)	Estheriellidae	SiO_2 (XRD)
4 *Euestheria*? (Depéret and Mazeran, 1912)	GZN 2013II TC11_3a	Tongchuan Fm.	Middle Triassic	Cyzicidae Stebbing, 1910 (according to Tasch, 1969)	Cyzicidae *sensu lato*	Fluorapatite, Iron phosphate, SiO_2 (XRD)
5.1 *Euestheria minuta* (von Zieten, 1833)	FG 629/1	Kamysh Bashi Fm., Kyrgyzstan	Late Triassic	Cyzicidae Stebbing, 1910 (according to Tasch, 1969)	Cyzicidae *sensu lato*	Fluorapatite, SiO_2 (XRD)
5.2 *Laxitextella* Kozur, 1982	Coburg 14612	No information	Late Triassic	Cyzicidae Stebbing, 1910 (according to Kozur, 1982)	Cyzicidae *sensu lato*	Fluorapatite, Dolomite (XRD)
6.1 *Carapacestheria* Shen, 1994	IC 697	Carapace Nunatak, Victoria Land, Antarctica	Middle Jurassic	Eosestheriidae Zhang and Chen, 1976 (according to Shen, 1994)	Cyzicidae *sensu lato*	Apatitic composition (EDS)
6.2a *Yanjiestheria* Chen, 1976 (in Zhang et al., 1976)	GZN 2013II WS 8	Wangjiashan Fm.	Middle-Late Jurassic	Eosestheriidae Zhang and Chen, 1976 (according to Zhang et al. 1976)	Cyzicidae *sensu lato*	Fluorapatite (XRD)

Sample	Sample #	Formation	Age	Family	Family groupings	Carapace mineralogy
6.2b *Triglypta*? Wang, 1984	GZN 2013II WS 3	Wangjiashan Fm.	Middle-Late Jurassic	Polygraptidae Novojilov, 1954; Superfamily Lioestherioidea Raymond, 1946 (according to Wang, 1984)	Cyzicidae *sensu lato*	Fluorapatite (XRD)
6.3 *Triglypta* Wang, 1984	GZN 2013II WW 9, 10	Wangjiawan section	Middle-Late Jurassic	Polygraptidae Novojilov, 1954; Superfamily Lioestherioidea Raymond, 1946 (according to Wang, 1984)	Cyzicidae *sensu lato*	Fluorapatite (XRD)
7 *Eosestheria* Chen, 1976	GZN 2013II JSG AN, O, K, 5~H, G, C	Yixian Formation	Early Cretaceous	Eosestheriidae Zhang and Chen, 1976 (according to Zhang et al. 1976)	Cyzicidae *sensu lato*	Fluorapatite, SiO_2, Hematite (XRD)
8.1 *Limnadia lenticularis* (Linnaeus, 1761)	Pulverized	Margraviate Brandenburg, Germany	Recent	Limnadiidae Baird, 1849	Limnadiidae	No biominerals (XRD)
8.2 *Leptestheria dahalacensis* (Rüppell, 1837)	Pulverized	Altenburg near Vienna, Austria	Recent	Leptestheriidae Daday, 1923	Leptestheriidae	Calcite (XRD)
8.3 *Caenestheriella donaciformis* (Baird, 1849)	Pulverized	central Sudan	Recent	Cyzicidae Stebbing, 1910	Cyzicidae *sensu lato*	Calcium phosphates; Calcite (XRD)
8.4 *Cyzicus* sp. A	Pulverized	Captive breeding	Recent	Cyzicidae Stebbing, 1910	Cyzicidae *sensu lato*	Apatitic composition (EDS)
8.5 *Cyzicus* sp. B Azraq Playa, Jordan	Pulverized	Captive breeding	Recent	Cyzicidae Stebbing, 1910	Cyzicidae *sensu lato*	Calcium phosphates (XRD)
Orr and Briggs (1999)						
Limnestheria Wright, 1920			Late Carboniferous	Limnadiidae Baird, 1849 (according to Tasch, 1969; Orr and Briggs, 1999)	Limnadiidae	Organic carbon residues

Sample	Sample #	Formation	Age	Family	Family groupings	Carapace mineralogy
Anomalonema Raymond, 1946			Late Carboniferous	Estheriellidae Kobayashi, 1954 (according to Tasch, 1969; Orr and Briggs, 1999); Limnadiidae Baird, 1849 (according to Raymond, 1946)	Estheriellidae	?Organic carbon residues?

Table 3.3. Explanation for the allocation of genera to the informal group "Cyzicidae" *sensu lato.*

Genus	Explanation "Cyzicidae" ***sensu lato***
Carapacestheria Shen, 1994	The type species of *Carapacestheria* is *C. disgregaris*, formerly known as *Cyzicus (Lioestheria) disgregaris* Tasch, 1987.
Euestheria (Depéret and Mazeran, 1912)	Holub and Kozur (1981) state that Late Mesozoic and Cenozoic Cyzicidae evolved out of *Euestheria*, hence the allocation of this genus to the Cyzicidae. In addition, *Euestheria* is ranked as a subgenus of *Cyzicus* by Tasch (1969).
Laxitextella Kozur, 1982	Kozur (1982) assigned the Late Triassic *Laxitextella* to the family Cyzicidae. Olempska (2004) placed *Laxitextella* into the family Euestheriidae. For this study it suffices to point out that the genus is closely allied with modern cyzicids, as the namesake of the Euestheriidae, *Euestheria*, is regarded a subgenus of *Cyzicus* (Tasch, 1969).
Liograpta Novojilov, 1954	*Liograpta* has been synonymized by Tasch (1969) with *Cyzicus* (*Lioestheria*).
Triglypta Wang, 1984	When Wang (1984) erected the genus *Triglypta*, he placed it into the family Polygraptidae of the superfamily Lioestherioidea. The taxon Polygraptinae has been erected by Novojilov in 1954, who synonymized it with yet another new family Bairdestheriidae in 1960. According to Tasch (1969), Bairdestheriidae as well as Lioestheriidae are synonyms of Cyzicidae. It is therefore difficult to understand why Wang (1984) reinstated the Polygraptidae.
Yanjiestheria Chen, 1976; *Eosestheria* Chen, 1976	The genera *Yanjiestheria* and *Eosestheria* belong to the Eosestheriidae. According to Zhang et al. (1976), this family constitutes, together with the Euestheriidae and other families, the superfamily Lioestherioidea, which should be closely allied with the Cyzicidae, as Tasch (1969) synonymized the Lioestheriidae with the modern Cyzicidae.

Table 3.4. Environmental framework of studied samples. Lithological descriptions are based on field observations. Palaeoenvironmental descriptions of specimens examined at the NHM rely on previously published data.

Sample	Location	Age	Environmental framework
1.1 *Euestheria* (Depéret and Mazeran, 1912)	Anstruther Fm., Anstruther Core, Scotland	Viséan, Early Carboniferous	No field observations on the depositional environment. Material has been investigated by Bennett at the NHM.
1.2 *Euestheria* (Depéret and Mazeran, 1912)	Anstruther Fm., Anstruther Core, Scotland	Viséan, Early Carboniferous	
1.3 *Leaia* Jones, 1862	Anstruther Fm., Anstruther Core, Scotland	Viséan, Early Carboniferous	
1.4 *Leaia salteriana* Jones	Anstruther Fm., cottage row, Crail, Scotland	Viséan, Early Carboniferous	
1.5 *Leaia* Jones, 1862	El Menizla Fm., Morocco	Carboniferous	*Lake environment.* Imprints of leaiaid spinicaudatans in association with leaf fragments and insects have been collected from several dm-thick, horizontally laminated, dark claystone horizons that are indicative of a lacustrine environment.
2.1 *Euestheria* (Depéret and Mazeran, 1912)	Newarthill Core No.2, Scotland	Late Carboniferous?	No field observations on the depositional environment. Material has been investigated by Bennett at the NHM.
2.2 *[Estheria]* Rüppell, 1837	Coal Measures, South Wales	Late Carboniferous	The Coal Measures are interpreted as lacustrine and flood deposits in an upper coastal plain (Hartley, 1993). Spinicaudatans of the Coal Measures occur in a number of lithologies. They are most commonly found in poorly bedded mudstones devoid of plants or they occur associated with abundant lycopod debris (Todd, 1991).
2.3 *[Estheria] tenella* Bronn, 1850	Carluke, Lanarkshire, Scotland	Late Carboniferous	
2.4 *Leaia leidyi* var. *salteriana* Jones, 1862	Coal Pit Heath Colliery, Pucklechurch, England	Late Carboniferous	
2.5 *Leaia mitchelli* Etheridge, 1892	Warner's Bay, Lake Macquarie, Australia	Carboniferous-Permian	
3.1 *Euestheria* (Depéret and Mazeran, 1912)	*Arefino, Russia*	Early Triassic	*Pond on an alluvial plain.* Spinicaudatans have been collected from red, horizontally laminated claystones that are interpreted as pond deposits on an alluvial plain.
3.2 *Estheriella marginostriata*	*Bernburg Formation, Beesenlaublingen, Germany*	Early Triassic	*Playa lake.* The Bernburg Formation comprises fine-grained siliciclastics with intercalations of oolitic limestone horizons of a playa lake environment. Within this succession, spinicaudatans occur in lenticular to flaser-bedded, red and grey coloured claystones to fine-grained sandstones.

Sample	Location	Age	Environmental framework
4 *Euestheria*? (Depéret and Mazeran, 1912)	*Tongchuan Formation, Shaanxi, China*	Middle Triassic	*Lacustrine foreshore.* The Tongchuan Formation at the collection site represents a lacustrine foreshore environment. Ostracods, spinicaudatans, and bivalves have been collected from a 2-m-thick unit of rubbly bedded dark, bituminous siltstones (Fig. 3.8e) that are grading into fine sandstones. A several-dm-thick horizon with convolute-bedding follows, topped by a parallel- to low-angle bedded sandstone. The Tongchuan Formation is generally highly carbonaceous and lacustrine oil shales have been found in the vicinity of the studied outcrop. The investigated specimens are tentatively assigned to *Euestheria*?.
5.1 *Euestheria minuta* (von Zieten, 1833)	*Kamysh Bashi Formation, Kyrgyzstan*	Late Triassic	*Pond within a fluvial plain.* The lithofacies of the 14-cm-thick, spinicaudatan-yielding horizon consists of fine-sandy siltstones interpreted as ephemeral ponds in a sparsely vegetated floodplain. Spinicaudatans are associated with insects, ostracod imprints, horsetail leaves, and stem fragments.
5.2 *Laxitextella* Kozur, 1982	Bayreuth, Southern Germany	Late Triassic	The samples, housed in the Naturkunde-Museum Coburg, have been collected at the Bodenmühle near the city of Bayreuth, northern Bavaria. Clam shrimps are embedded in grey marlstone and have been identified as *Laxitextella laxitexta*.
6.1 *Carapacestheria* Shen, 1994	Carapace Nunatak, Victoria Land, Antarctica	Middle Jurassic	*Lake environment.* Fossiliferous interbeds in a volcanic environment, interpreted as shallow, ephemeral ponds by Stigall et al. (2008). This interpretation is, however, based on an analogy with the life cycle of modern clam shrimps.
6.2a *Yanjiestheria* Chen, 1976 (in Zhang et al., 1976)	*Wangjiashan Formation*	Middle-Late Jurassic	*Deep, permanent lake.* The thickness of the Wangjiashan lake sediments is comparatively great (80.5 m) and the succession begins with a palaeosol horizon that is overlain by mostly laminated clay and silt with few intercalations of fine-grained sandstone. Three depositional facies in the clay to silty clay fraction have been identified: Facies A is non-layered, facies B is irregularly laminated due to the presence of microbial mats, and facies C is facies B, reworked by meiofaunal bioturbation. Clam shrimps of facies C are associated with darwinulid ostracods, freshwater gastropods, and fish remains. Oxygen deficiency at the sediment-water interface was thought to have been highest in facies B, implied by the occurrence of pyrite framboids and monospecific associations. The investigated specimens (Fig. 3.10) are assigned to *Yanjiestheria* (facies B) and *Triglypta*? (facies C).
6.2b *Triglypta*? Wang, 1984	*Wangjiashan Formation*	Middle-Late Jurassic	
6.3 *Triglypta* Wang, 1984	*Wangjiawan section*	Middle-Late Jurassic	*Shallow lake.* The thickness of the lacustrine deposits of the Wangjiawan section is distinctly smaller (about 2.5 m). Thin-section analysis reveals rhythmic, sub-millimetric, graded laminae, each of them sealed at the top by a layer rich in organic matter, possibly a microbial mat. Smaller coherent mat-like filaments occur scattered within the laminae. These rhythmites represent a lacustrine facies governed by seasonal changes in precipitation. The lake was governed by monospecific assemblages of *Triglypta* (Fig. 3.11).

Sample	Location	Age	Environmental framework
7 *Eosestheria* Chen, 1976	*Early Cretaceous Yixian Formation (Jianshangou Unit), Liaoning, China*	Early Cretaceous	*Volcanic lake.* The sediments of the Jianshangou Unit are subdivided into four beds (Jiang et al. 2012), of which beds 2 and 3 yield most of the exceptionally preserved fossils known from the Yixian Formation, a famous Mesozoic fossillagerstätte. Bed 2 is governed by siliciclastic clay-silt couplets (thickness commonly 15-60 µm), into which numerous conformable ash-tuff layers are intercalated. This represents a phase during which bottom waters were mostly dysoxic with occasional anoxic spells. Bed 3 comprises comparatively thick, partly bioturbated fine-sandy silt layers that formed in shallow-water, oxygenated environments (Hethke et al., 2013a, b). Specimens from both phases of lake evolution have been chosen to account for oxygen restricted and oxygenated environments, respectively. They are assigned to *Eosestheria*.
8.1 *Limnadia lenticularis* (Linnaeus, 1761)	Margraviate Brandenburg in 1956	Recent	Freshwater
8.2 *Leptestheria dahalacensis* (Rüppell, 1837)	Altenburg near Vienna in 1959	Recent	Freshwater
8.3 *Caenestheriella donaciformis* (Baird, 1849)	Kordofan (central Sudan) before 1911	Recent	Freshwater
8.4 *Cyzicus* sp. A	-	Recent	Captive breeding in freshwater
8.5 *Cyzicus* sp. B Azraq Playa, Jordan	-	Recent	Captive breeding in freshwater
Orr and Briggs (1999)			
Limnestheria Wright, 1920		Late Carboniferous	Reducing conditions; paralic environment
Anomalonema Raymond, 1946		Late Carboniferous	Reducing conditions; paralic environment

Table 3.5. EDS results for three modern species that belong to the three extant spinicaudatan families, respectively.

Species	Element	Weight-%				Atomic-%			
		M1	M2	M3	M4	M1	M2	M3	M4
Limnadia lenticularis Measured in cross-section	C	48.35	46.34	49.27	47.50	56.15	53.94	57.05	54.99
	N	16.79	19.12	16.87	17.70	16.72	19.08	16.75	17.57
	O	28.16	28.02	27.25	29.04	24.55	24.48	23.69	25.25
	Al	0.39	0.31	0.22	0.22	0.20	0.16	0.11	0.12
	Cl	3.88	3.84	3.98	3.37	1.53	1.51	1.56	1.32
	Ca	2.43	2.36	2.41	2.17	0.85	0.82	0.84	0.75
Caenestheriella donaciformis Measured in cross-section	C	34.54	20.45	32.35	43.07	45.25	32.99	43.78	54.23
	N	14.08	-	7.66	-	15.82	-	8.89	-
	O	30.45	37.06	35.98	41.63	29.95	44.89	36.55	39.35
	Mg	0.29	0.57	0.49	0.53	0.19	0.46	0.33	0.33
	P	5.87	12.58	7.62	4.58	2.98	7.87	4.00	2.24
	Ca	14.78	27.94	15.90	10.20	5.81	13.51	6.45	3.85
	Nb	-	1.39	-	-	-	0.29	-	-
Leptestheria dahalacensis Measured in cross-section	C	52.03	57.22	-	-	61.95	67.44	-	-
	O	38.65	32.40	-	-	34.55	28.67	-	-
	Mg	0.35	0.21	-	-	0.21	0.12	-	-
	Cl	2.04	3.73	-	-	0.82	1.49	-	-
	Ca	6.93	6.45	-	-	2.47	2.28	-	-

Table 3.6. Quantitative determination using EMP analysis provides a fluorapatite composition for sample JSG H, confirming results from EDS (compare Supplementary 3.1).

Element	Weight-%	Atomic-%
$Ca_5(PO_4)_3F$		
Ca	41.9	25.5
O	36.4	55.3
P	17.2	13.5
F	4.5	5.7

Table 4.4. Information on the type specimens revised.

Specimen	Specimen#	Nature of type specimen	# visible growth lines	Perimeter quality	Ornamentation visible?	Remarks
Chen, 1999 (complete) and Zhang et al., 1976 (parts)						
Eosestheria ovata	15451	Holotype	NA	2	some	Ch reconstructed
*Eosestheria ovata**	131915	-	34	2	yes	D and anterior margin reconstructed
*Eosestheria lingyuanensis**	15445	Holotype	~ 25	3	yes	D and anterior margin reconstructed
Eosestheria lingyuanensis	15447	-	-	Perimeter incomplete	yes	-
Eosestheria lingyuanensis	15448	-	> 21	1	some	-
Eosestheria lingyuanensis	131918	-	-	perimeter quality poor	very little	-
Eosestheria aff. *middendorfii*	29884	-	~ 22	1	no	-
Eosestheria aff. *middendorfi*i	29885	-	~ 24	2	some	Anterior margin reconstructed
*Eosestheria jingangshanensis**	15443	Holotype	~ 29?	2	some	Unsure about ventral margin
Eosestheria sihetunensis	131916	-	-	Perimeter incomplete	yes	-
*Eosestheria sihetunensis**	131917	Holotype	22	3	yes	D, E and anterior margin reconstructed
Eosestheriopsis gujialingensis	131921	-	> 29	Perimeter incomplete	yes	-
Eosestheriopsis gujialingensis	131922	-	> 30	Perimeter incomplete	yes	-
*Eosestheriopsis gujialingensis**	131923	-	25 (no crowding)	3	some	E reconstructed
Yanjiestheria? *beipiaoensis**	131919	Holotype	~ 25	Perimeter overlap	some	-
Yanjiestheria? *beipiaoensis**	131920	-	~ 34	3	no	D reconstructed

Specimen	Specimen#	Nature of type specimen	# visible growth lines	Perimeter quality	Ornamentation visible?	Remarks
*Diestheria yixianensis**	15455	Holotype	~ 38	3	yes	D and anterior margin reconstructed
Diestheria yixianensis	15456	-	-	Perimeter incomplete	yes	-
*Diestheria longinqua**	15462	Holotype	~ 33	2	yes	D and dorsal margin reconstructed
*Diestheria jeholensis**	15457	-	~ 32	Perimeter incomplete	yes	-
Diestheria jeholensis	15461	-	> 32	2	yes	Dorsal margin reconstructed
Zhang et al. (1976)						
*Eosestheria fuxinensis**	15437	Syntype?	~ 30	1	yes	-
Eosestheria fuxinensis	15438	Syntype?	~ 30	2	some	E reconstructed
Eosestheria fuxinensis	15439	Syntype?	~ 36	Perimeter incomplete	yes	-
Jones, 1862						
*Estheria middendorfii**	28227 NHM	Syntype	26	Perimeter incomplete	yes, but deformed	-
Estheria middendorfii (with egg clutch)	28228 NHM	Syntype (proposed Lectotype)	~ 26	Perimeter incomplete	yes	-
Estheria middendorfii (with egg clutch)	28229 NHM	Syntype	~ 30	3	yes	D, E, and anterior margin reconstructed
Estheria middendorfii	28230 NHM	Syntype	~ 36 (very hard to count)	Perimeter incomplete	yes	-
	JSG A_8		17	1		juvenile

Table 4.5. Linear measurements and ratios for 51 specimens. Specimens of *Eosestheria fuxinensis* had been assigned to *Diestheria* in the analyses. Most of the material is stored at NIGPAS, except for the specimen described by Jones (1862), which is housed in the NHM, London.

Sample	Outl. Qual.	*a*	*b*	*c*	*Arr*	*Av*	*Ch*	*Cr*	*H*	*L*	*H/L*	*Ch/L*	*Cr/L*	*Av/L*	*Arr/L*	*a/H*	*b/H*	*c/L*
Chen, 1999a																		
Eosestheria ovata 15451	2	4.24	4.24	7.90	3.50	2.07	11.12	3.87	10.87	16.70	0.65	0.67	0.23	0.12	0.21	0.39	0.39	0.47
Eosestheria ovata 131915	2	3.50	4.86	10.33	4.10	1.61	13.33	4.69	12.05	19.04	0.63	0.70	0.25	0.08	0.22	0.29	0.40	0.54
Eosestheria lingyuanensis 15445	3	1.96	2.81	5.01	2.16	0.83	7.59	2.81	6.25	10.58	0.59	0.72	0.27	0.08	0.20	0.31	0.45	0.47
Eosestheria lingyuanensis 15448	1	2.43	3.25	6.31	2.68	1.11	8.04	3.04	7.18	11.83	0.61	0.68	0.26	0.09	0.23	0.34	0.45	0.53
Eosestheria aff. *middendorfii* 29884	1	2.50	3.05	6.14	2.50	1.73	8.33	3.16	7.96	12.56	0.63	0.66	0.25	0.14	0.20	0.31	0.38	0.49
Eosestheria aff. *middendorfii* 29885	2	4.07	3.88	8.36	3.52	1.80	11.74	4.15	10.35	17.06	0.61	0.69	0.24	0.11	0.21	0.39	0.38	0.49
Eosestheria jingangshanensis 15443	2	4.34	5.63	9.79	5.60	2.25	9.77	4.58	11.48	17.62	0.65	0.55	0.26	0.13	0.32	0.38	0.49	0.56
Eosestheria sihetunensis 131917	3	1.68	3.15	5.65	2.26	0.85	7.66	2.88	6.43	10.76	0.60	0.71	0.27	0.08	0.21	0.26	0.49	0.52
Eosestheriopsis gujialingensis 131923	3	3.19	4.23	8.18	4.31	2.29	8.87	3.86	9.13	15.46	0.59	0.57	0.25	0.15	0.28	0.35	0.46	0.53
Yanjiestheria? *beipiaoensis* 131920	3	1.22	1.51	3.16	1.44	0.66	3.82	1.65	3.45	5.92	0.58	0.65	0.28	0.11	0.24	0.35	0.44	0.53
Diestheria yixianensis 15455	3	4.77	6.10	10.76	4.97	2.17	13.91	4.53	13.12	21.05	0.62	0.66	0.22	0.10	0.24	0.36	0.46	0.51
Diestheria longinqua 15462	2	2.67	5.56	13.90	5.39	1.43	16.17	5.65	11.95	22.98	0.52	0.70	0.25	0.06	0.23	0.22	0.47	0.60
Diestheria jeholensis 15461	2	4.30	6.17	10.73	5.54	1.79	12.61	5.86	13.42	19.94	0.67	0.63	0.29	0.09	0.28	0.32	0.46	0.54
Jones, 1862																		
Eosestheria middendorfii 28229 NHM	3	4.88	5.86	10.53	4.69	2.31	12.91	6.32	12.87	19.90	0.65	0.65	0.32	0.12	0.24	0.38	0.46	0.53
Zhang et al., 1976																		
Eosestheria fuxinensis 15437	1	2.98	4.08	7.26	3.58	1.33	8.85	3.25	9.32	13.75	0.68	0.64	0.24	0.10	0.26	0.32	0.44	0.53
Eosestheria fuxinensis 15438	2	3.30	3.91	7.02	3.24	1.79	8.58	3.33	9.35	13.60	0.69	0.63	0.24	0.13	0.24	0.35	0.42	0.52

Sample	Outl. Qual.	*a*	*b*	*c*	*Arr*	*Av*	*Ch*	*Cr*	*H*	*L*	*H/L*	*Ch/L*	*Cr/L*	*Av/L*	*Arr/L*	*a/H*	*b/H*	*c/L*
Chen et al., 2007																		
Halysestheria biformis 27106 holotype	2	1.43	2.09	3.89	1.23	0.52	4.71	2.26	4.04	6.46	0.63	0.73	0.35	0.08	0.19	0.35	0.52	0.60
Halysestheria biformis 27107 paratype	3	0.98	1.31	2.33	0.95	0.34	2.95	1.29	2.80	4.24	0.66	0.70	0.30	0.08	0.22	0.35	0.47	0.55
Nestoria reticulata 29871	1	1.70	1.73	2.56	0.97	0.73	3.44	1.77	3.96	5.13	0.77	0.67	0.34	0.14	0.19	0.43	0.44	0.50
Calestherites sertus 30038 holotype	2	3.78	3.82	5.40	1.55	2.17	7.48	6.11	8.47	11.20	0.76	0.67	0.55	0.19	0.14	0.45	0.45	0.48
Euestherites bifurcatus 30069 holotype	3	1.79	2.55	4.35	1.91	0.97	4.78	2.62	4.58	7.66	0.60	0.62	0.34	0.13	0.25	0.39	0.56	0.57
Migransia xiaqiaoensis 42274 holotype	3	1.59	2.11	3.38	1.62	0.47	4.28	1.89	4.09	6.37	0.64	0.67	0.30	0.07	0.25	0.39	0.52	0.53
Linhaiella longiformis specimen co-occurring with 55202	3	0.82	1.02	1.80	0.89	0.29	2.45	1.02	2.18	3.63	0.60	0.67	0.28	0.08	0.25	0.38	0.47	0.50
Monilestheria ovata 69490	1	0.96	1.91	2.97	1.55	0.30	3.24	1.30	3.64	5.08	0.72	0.64	0.26	0.06	0.30	0.26	0.53	0.58
Eosestheriopsis dianzhongensis 26994 holotype	2	1.84	2.34	3.13	1.45	0.45	4.27	2.15	4.78	6.17	0.77	0.69	0.35	0.07	0.23	0.39	0.49	0.51
Li and Batten, 2004a																		
Cratostracus? *cheni* 136462	1	1.79	2.11	3.01	1.36	1.10	2.29	2.10	4.08	4.75	0.86	0.48	0.44	0.23	0.29	0.44	0.52	0.63
Li and Batten, 2005																		
Euestherites quadratus 30079 holotype	2	1.78	1.86	2.93	1.35	1.27	3.20	2.75	3.83	5.82	0.66	0.55	0.47	0.22	0.23	0.46	0.49	0.50
Euestherites regularis 30097 holotype	1	1.77	2.35	3.73	2.14	1.29	3.98	2.50	4.36	7.42	0.59	0.54	0.34	0.17	0.29	0.41	0.54	0.50
Estherites corrugatus 136910	1	2.67	3.07	4.40	2.43	1.66	4.26	3.53	5.97	8.36	0.71	0.51	0.42	0.20	0.29	0.45	0.51	0.53
Estherites corrugatus 136911	3	2.28	2.33	3.66	1.42	1.70	4.95	3.48	4.84	8.08	0.60	0.61	0.43	0.21	0.18	0.47	0.48	0.45
Estherites corrugatus 136912	1	2.24	2.52	3.60	2.05	1.42	3.85	3.04	5.06	7.33	0.69	0.53	0.42	0.19	0.28	0.44	0.50	0.49
Li et al., 2007																		

Sample	Outl. Qual.	*a*	*b*	*c*	*Arr*	*Av*	*Ch*	*Cr*	*H*	*L*	*H/L*	*Ch/L*	*Cr/L*	*Av/L*	*Arr/L*	*a/H*	*b/H*	*c/L*
Yanjiestheria bellula 141144	3	1.08	1.64	3.46	1.39	0.55	4.79	1.83	3.77	6.74	0.56	0.71	0.27	0.08	0.21	0.29	0.43	0.51
Yanjiestheria bellula 141145	2	1.04	1.37	2.96	1.16	0.51	3.74	1.41	3.23	5.41	0.60	0.69	0.26	0.09	0.21	0.32	0.42	0.55
Shen et al., 2002																		
Sinokontikia lianmuqinensis 130637	2	1.88	2.47	5.06	2.32	1.22	5.57	2.62	5.27	9.12	0.58	0.61	0.29	0.13	0.25	0.36	0.47	0.56
Turfanograpta chowmincheni 130639	1	1.40	2.58	4.17	1.92	0.56	4.91	2.15	5.09	7.39	0.69	0.66	0.29	0.08	0.26	0.27	0.51	0.56
Euestheria jingyuanensis same slab as 130643	1	0.74	0.88	1.42	0.59	0.35	1.99	0.89	2.00	2.93	0.68	0.68	0.30	0.12	0.20	0.37	0.44	0.48
Shen et al., 2003																		
Euestheria luanpingensis same slab as 135817	2	1.30	1.48	1.81	1.06	0.80	1.72	1.53	2.75	3.58	0.77	0.48	0.43	0.22	0.30	0.47	0.54	0.51
Euestheria luanpingensis same slab as 135818	1	1.54	1.80	2.76	1.59	1.02	2.96	2.00	3.85	5.57	0.69	0.53	0.36	0.18	0.29	0.40	0.47	0.50
Euestheria luanpingensis 135819	1	1.27	2.15	2.64	2.02	0.74	2.10	1.33	3.84	4.86	0.79	0.43	0.27	0.15	0.42	0.33	0.56	0.54
Euestheria luanpingensis 135820	1	1.63	2.17	3.14	2.50	0.93	2.49	1.59	4.39	5.93	0.74	0.42	0.27	0.16	0.42	0.37	0.49	0.53
Euestheria luanpingensis 135821	1	1.54	2.38	3.14	2.12	1.01	2.35	1.68	4.17	5.48	0.76	0.43	0.31	0.18	0.39	0.37	0.57	0.57
Euestheria haifanggouensis 135822	2	1.57	2.13	2.59	1.75	1.09	2.35	1.72	4.38	5.19	0.84	0.45	0.33	0.21	0.34	0.36	0.49	0.50
Euestheria jingyuanensis same slab as 135824	1	0.81	1.34	2.35	1.53	0.58	1.74	1.00	2.44	3.86	0.63	0.45	0.26	0.15	0.40	0.33	0.55	0.61
Euestheria jingyuanensis same slab as 135824	2	1.44	1.76	2.61	2.13	1.03	1.74	1.39	3.47	4.90	0.71	0.36	0.28	0.21	0.43	0.42	0.51	0.53
Euestheria ziliujingensis 135825	1	1.80	2.20	2.54	1.93	1.04	2.12	1.45	4.20	5.10	0.82	0.42	0.28	0.20	0.38	0.43	0.52	0.50
Zhang et al., 1976																		
Euestheria minuta 20020	2	0.69	0.90	1.26	0.57	0.30	1.89	0.93	1.77	2.76	0.64	0.69	0.33	0.11	0.20	0.39	0.51	0.46
Euestheria ziliujingensis 20029	2	0.88	1.38	1.77	0.86	0.36	2.09	0.91	2.61	3.31	0.79	0.63	0.27	0.11	0.26	0.34	0.53	0.54

Sample	Outl. Qual.	*a*	*b*	*c*	*Arr*	*Av*	*Ch*	*Cr*	*H*	*L*	*H/L*	*Ch/L*	*Cr/L*	*Av/L*	*Arr/L*	*a/H*	*b/H*	*c/L*
Euestheria minuta 29735	2	1.01	0.89	1.56	0.82	0.56	2.09	1.19	2.36	3.48	0.68	0.60	0.34	0.16	0.24	0.43	0.38	0.45
Euestheria shandanensis 29777	3	2.27	2.31	3.33	1.32	0.90	4.26	2.35	5.31	6.48	0.82	0.66	0.36	0.14	0.20	0.43	0.43	0.51
Euestheria haifanggouensis 29778	3	1.28	1.52	2.24	1.06	0.70	2.49	1.34	3.32	4.26	0.78	0.59	0.31	0.16	0.25	0.39	0.46	0.53
Euestheria ziliujingensis 29779	1	1.03	1.25	1.99	0.70	0.57	2.38	1.12	2.83	3.65	0.77	0.65	0.31	0.16	0.19	0.36	0.44	0.54

Table 4.11. Splitting of *Estheria middendorfii*.

Jones, 1862	**Chi, 1931**	**Raymond, 1946**	**Kobayashi and Kusumi (1953)**	**Zhang et al., 1976**	**Chen, 1999a**
Estheria middendorfii	*Estheria middendorfii*	*Bairdestheria middendorfii*	*Estherites middendorfii*	*Eosestheria middendorfii*; *Eosestheria* aff. *middendorfii*	*Eosestheria* aff. *middendorfii*
–	*Estheria middendorfii* var. *sinensis*	*Bairdestheria sinensis*	*Euestheria middendorfii* var. *sinensis* (Chi, 1931; in part)	*Yanjiestheria* (?) *chii*	–
–	–	–	*Estherites middendorfii* var. *jeholensis*	*Diestheria jeholensis*	*Diestheria jeholensis*
–	–	–	*Estherites middendorfii* var. *elongata*	*Eosestheria elongata*	–
–	–	–	*Estherites middendorfii* forma *subelongata* = forma *orientalis* Eichwald in Kobayashi (1954)	*Eosestheria subelongata*	–
–	–	–	*Estherites middendorfii* var. *chii*	*Eosestheria chii*	–
–	–	–	*Estherites middendorfii* forma *peipiaoensis*	*Eosestheria peipiaoensis*	–
–	–	–	*Estherites middendorfii* forma *intermedia* = *Estheria middendorfii* as figured by Chi (1931)	*Eosestheria intermedia*	–

Jones, 1862	Chi, 1931	Raymond, 1946	Kobayashi and Kusumi (1953)	Zhang et al., 1976	Chen, 1999a
–	–	–	*Estherites middendorfii* forma *takechenensis*	*Eosestheria takechenensis*	–
–	–	–	–	*Liaoningestheria ovata*	*Eosestheria ovata*
–	–	–	–	*Eosestheria lingyuanensis*	*Eosestheria lingyuanensis*
–	–	–	–	*Eosestheria jingangshanensis*	*Eosestheria jingangshanensis*
–	–	–	–	–	*Eosestheria sihetunensis*
–	–	–	–	–	*Eosestheriopsis gujialingensis* (Wang, 1987)
–	–	–	–	–	*Yanjiestheria* ? *beipiaoensis*
–	–	–	–	*Diestheria yixianensis*	*Diestheria yixianensis*
–	–	–	–	*Diestheria longinqua*	*Diestheria longinqua*

Table 5.2. Nine linear measurements of 23 specimens of the LXBE-S1 cohort and of an additional specimen from horizon ZJG H.

Specimen	*a*	*b*	*c*	*Arr*	*Av*	*Ch*	*Cr*	*H*	*L*
LXBE S1_77_60	2.372	3.128	5.884	2.677	1.446	8.101	2.975	7.654	12.224
LXBE S1_77_64_19	3.356	4.542	9.259	4.193	1.569	13.198	4.628	11.170	18.960
LXBE S1_77_74_1	3.387	4.130	7.423	3.711	1.621	9.744	3.790	9.271	15.052
LXBE S1_77_74_7	1.629	2.471	4.682	2.199	0.899	6.052	2.482	5.585	9.150
LXBE S1_77_74_11	2.766	3.436	6.327	3.312	1.482	7.769	3.153	8.105	12.564
LXBE S1_77_EO704_29	3.760	3.937	7.866	3.727	2.111	9.789	4.312	9.606	15.627
LXBE S1_77_EO704_30	2.448	3.722	6.572	3.223	1.179	8.535	3.570	8.040	12.937
LXBE S1_77_EO704_31	2.970	4.133	6.720	2.733	1.744	8.630	3.475	8.786	13.106
LXBE S1_16	2.599	3.547	6.906	3.214	1.048	9.988	2.542	8.882	14.250
LXBE S1_21	3.182	3.658	5.968	2.989	2.099	7.583	3.351	8.273	12.671
LXBE S1_70	3.518	3.663	6.939	3.381	1.568	9.455	3.315	9.097	14.403
LXBE S1_71	2.127	2.918	4.948	2.202	1.191	6.829	2.681	6.402	10.222
LXBE S1_HS2	2.694	3.210	7.054	2.847	1.242	8.981	2.848	7.946	13.070
LXBE S1_15	2.471	3.160	6.572	2.593	1.256	9.097	2.836	7.557	12.947
LXBE S1_24	3.151	3.288	5.783	2.817	1.819	7.713	3.525	7.784	12.348
LXBE S1_HS4	2.543	2.584	5.673	2.196	1.364	8.246	2.921	7.199	11.806
LXBE S1_77_EO704_24	2.172	2.758	6.025	2.548	1.270	8.498	2.643	7.248	12.316
LXBE S1_77_EO707_23	2.812	3.005	6.451	2.881	1.809	8.355	3.665	7.905	13.046
LXBE S1_77_59	2.468	3.247	5.724	2.907	1.499	8.109	3.343	7.703	12.514
LXBE S1_77_63	2.526	2.943	5.957	2.761	1.393	7.876	3.170	7.061	12.031
LXBE S1_77_64	2.173	3.125	6.060	2.547	1.154	8.611	3.273	7.152	12.312
LXBE S1_77_74_2	3.126	3.830	7.076	3.998	1.231	9.712	3.747	8.998	14.940
LXBE S1_77_75_4	2.765	3.286	6.177	3.394	1.675	8.030	4.018	8.052	13.099
ZJG H3_493_4	4.177	5.285	9.574	4.479	1.978	11.093	4.848	11.514	17.549

Table 5.3. Discriminant scores for all nine linear variables and for the subset (*Arr*, *Ch*, *Cr*, *H*, *L*). Numbers in red mark misclassified specimens.

Specimen	1 - no eggs, 2 - eggs	Score (9 var.)	Classification (9 var.)	Score (5 var.)	Classification (5 var.)
LXBE S1_77_60	1	0.69	1	0.87	1
LXBE S1_77_64_19	1	0.41	1	0.33	1
LXBE S1_77_74_1	1	2.85	1	1.41	1
LXBE S1_77_74_7	1	-0.31	2	-1.17	2
LXBE S1_77_74_11	1	6.15	1	3.13	1
LXBE S1_77_EO704_29	1	1.18	1	-0.79	2
LXBE S1_77_EO704_30	1	4.58	1	1.87	1
LXBE S1_77_EO704_31	1	9.93	1	5.53	1
LXBE S1_16	1	5.25	1	4.81	1
LXBE S1_21	1	2.12	1	1.35	1
LXBE S1_70	1	1.91	1	3.26	1
LXBE S1_71	1	-0.78	2	-0.04	2
LXBE S1_HS2	1	4.89	1	0.63	1
LXBE S1_15	2	-1.41	2	-2.43	2
LXBE S1_24	2	-3.09	2	-0.54	2
LXBE S1_HS4	2	-4.87	2	-0.96	2
LXBE S1_77_EO704_24	2	-2.80	2	-2.28	2
LXBE S1_77_EO707_23	2	-3.08	2	-2.70	2
LXBE S1_77_59	2	-3.02	2	-0.52	2
LXBE S1_77_63	2	-4.02	2	-3.59	2
LXBE S1_77_64	2	-4.05	2	-3.06	2
LXBE S1_77_74_2	2	-0.62	2	1.04	1
LXBE S1_77_75_4	2	-2.93	2	-1.26	2

Table 5.4. *H*/*L* ratios for specimens with egg clutches and those without.

Specimen	H/L	Specimen	H/L
LXBE S1_77_60	0.63	LXBE S1_15	0.58
LXBE S1_77_64_19	0.59	LXBE S1_24	0.63
LXBE S1_77_74_1	0.62	LXBE S1_HS4	0.61
LXBE S1_77_74_7	0.61	LXBE S1_77_EO704_24	0.59
LXBE S1_77_74_11	0.65	LXBE S1_77_EO707_23	0.61
LXBE S1_77_EO704_29	0.61	LXBE S1_77_59	0.62
LXBE S1_77_EO704_30	0.62	LXBE S1_77_63	0.59
LXBE S1_77_EO704_31	0.67	LXBE S1_77_64	0.58
LXBE S1_16	0.62	LXBE S1_77_74_2	0.60
LXBE S1_21	0.65	LXBE S1_77_75_4	0.61
LXBE S1_70	0.63		
LXBE S1_71	0.63		
LXBE S1_HS2	0.61		

Table 6.1. Linear measurement data of 348 individuals from the three excavations ZJG, LXBE, and JSG, all conducted in the Sihetun area. All values are in mm. The nine variables are explained in Fig. 4.2. Carapace measurements are overlapping and most likely intercorrelated to some extent. Variable pairs a and b as well as Arr and Av are negatively correlated when the carapace is biased by rotation due to the misplacement of one of the extremities of the dorsal margin. This bias has however been minimized through careful examination of the outline quality of each specimen. Ratios between variables that are well established in taxonomic works on clam shrimps are also listed.

Sample	Outl. Qual.	a	b	c	Arr	Av	Ch	Cr	H	L	H/L	Ch/L	Cr/L	Av/L	Arr/L	a/H	b/H	c/L
LXY (NIGPAS)																		
ZJG A1_2	3	3.045	4.173	7.838	3.016	1.994	9.795	4.104	9.400	14.805	0.635	0.662	0.277	0.135	0.204	0.324	0.444	0.529
ZJG C_3	2	3.519	4.138	7.843	3.507	1.796	10.532	4.095	9.799	15.834	0.619	0.665	0.259	0.113	0.221	0.359	0.422	0.495
ZJG C5_493 1	3	4.403	5.894	11.459	4.951	2.717	13.631	6.364	13.156	21.299	0.618	0.640	0.299	0.128	0.232	0.335	0.448	0.538
ZJG D3_2	2	4.308	4.890	8.844	4.524	2.497	10.549	5.163	11.329	17.570	0.645	0.600	0.294	0.142	0.257	0.380	0.432	0.503
ZJG D>5_1	2	3.857	4.485	9.395	3.186	2.093	12.036	4.175	10.525	17.315	0.608	0.695	0.241	0.121	0.184	0.366	0.426	0.543
ZJG E_6	2	3.429	4.200	8.107	3.936	2.147	8.890	4.265	9.352	14.973	0.625	0.594	0.285	0.143	0.263	0.367	0.449	0.541
ZJG E_7	2	3.870	4.824	8.876	4.899	2.088	10.834	4.190	10.875	17.821	0.610	0.608	0.235	0.117	0.275	0.356	0.444	0.498
ZJG E3_2	3	2.747	3.105	6.549	3.043	1.664	8.578	3.293	7.606	13.285	0.573	0.646	0.248	0.125	0.229	0.361	0.408	0.493
ZJG G1_1	3	4.945	5.000	9.851	4.272	2.410	13.356	5.091	12.705	20.038	0.634	0.667	0.254	0.120	0.213	0.389	0.394	0.492
ZJG H3_493_4	2	4.177	5.285	9.574	4.479	1.978	11.093	4.848	11.514	17.549	0.656	0.632	0.276	0.113	0.255	0.363	0.459	0.546
ZJG Ixia_3	3	3.666	4.417	7.899	4.375	1.515	9.543	3.513	9.718	15.432	0.630	0.618	0.228	0.098	0.283	0.377	0.455	0.512
ZJG Ixia_6	1	3.222	4.550	8.625	4.375	1.731	10.246	4.036	10.193	16.352	0.623	0.627	0.247	0.106	0.268	0.316	0.446	0.527
ZJG K1_4	3	4.625	5.660	10.209	4.546	2.040	12.493	4.743	11.957	19.079	0.627	0.655	0.249	0.107	0.238	0.387	0.473	0.535
ZJG K1_6	2	5.520	6.702	12.385	5.899	3.259	14.579	6.875	14.979	23.737	0.631	0.614	0.290	0.137	0.249	0.369	0.447	0.522
ZJG K2_5	1	4.389	5.503	9.571	4.664	2.325	11.344	5.314	11.915	18.332	0.650	0.619	0.290	0.127	0.254	0.368	0.462	0.522
ZJG N_15+2	1	3.216	3.466	6.354	3.319	1.711	8.064	3.467	8.506	13.094	0.650	0.616	0.265	0.131	0.254	0.378	0.408	0.485
ZJG N_16+5	2	3.953	4.963	8.438	5.610	2.259	8.723	4.311	10.710	16.592	0.646	0.526	0.260	0.136	0.338	0.369	0.463	0.509
ZJG O_1	2	3.445	4.402	8.102	4.053	2.428	8.881	4.402	9.990	15.362	0.650	0.578	0.287	0.158	0.264	0.345	0.441	0.527
ZJG O_2	3	2.761	3.599	6.138	2.645	1.394	8.132	3.716	7.908	12.171	0.650	0.668	0.305	0.115	0.217	0.349	0.455	0.504

Sample	Outl. Qual.	a	b	c	Arr	Av	Ch	Cr	H	L	H/L	Ch/L	Cr/L	Av/L	Arr/L	a/H	b/H	c/L
LXBE (NIGPAS)																		
LXBE E	3	2.245	2.331	4.356	2.361	1.099	5.918	2.772	5.619	9.379	0.599	0.631	0.296	0.117	0.252	0.400	0.415	0.464
LXBE G	2	2.853	2.989	6.100	2.896	1.357	8.044	2.624	7.753	12.297	0.630	0.654	0.213	0.110	0.236	0.368	0.385	0.496
LXBE H_1	3	2.138	2.564	4.840	2.608	1.053	6.225	2.223	6.001	9.886	0.607	0.630	0.225	0.106	0.264	0.356	0.427	0.490
LXBE H_3	3	2.152	2.821	5.451	2.905	0.967	6.017	2.364	6.110	9.889	0.618	0.608	0.239	0.098	0.294	0.352	0.462	0.551
LXBE H_52_EO096	3	3.186	3.864	7.821	4.230	1.941	8.646	4.597	8.984	14.817	0.606	0.584	0.310	0.131	0.285	0.355	0.430	0.528
LXBE L	3	2.881	3.524	6.134	3.188	1.963	6.714	3.415	7.612	11.866	0.641	0.566	0.288	0.165	0.269	0.378	0.463	0.517
LXBE M_54_EO151 110	2	3.275	4.068	7.535	3.743	1.781	8.809	3.455	9.074	14.332	0.633	0.615	0.241	0.124	0.261	0.361	0.448	0.526
LXBE M_54_EO152 108	2	3.377	4.219	8.359	4.207	2.004	9.499	4.112	9.404	15.710	0.599	0.605	0.262	0.128	0.268	0.359	0.449	0.532
LXBE M_54_EO154 101	1	3.858	4.523	7.441	5.547	1.964	7.379	3.647	9.652	14.890	0.648	0.496	0.245	0.132	0.373	0.400	0.469	0.500
LXBE M_54_EO155 104	1	2.959	4.886	9.122	5.064	1.576	9.783	3.812	10.187	16.424	0.620	0.596	0.232	0.096	0.308	0.290	0.480	0.555
LXBE P_28	2	4.058	3.996	7.466	3.636	2.026	9.618	4.009	9.912	15.280	0.649	0.629	0.262	0.133	0.238	0.409	0.403	0.489
LXBE P_37	2	3.680	4.451	8.475	4.423	2.055	10.178	4.336	9.645	16.657	0.579	0.611	0.260	0.123	0.266	0.382	0.462	0.509
LXBE P_120	2	3.047	4.179	7.870	3.402	1.626	10.386	3.987	9.371	15.415	0.608	0.674	0.259	0.106	0.221	0.325	0.446	0.511
LXBE P_122	2	2.903	3.351	6.947	3.175	1.305	9.965	3.363	8.448	14.444	0.585	0.690	0.233	0.090	0.220	0.344	0.397	0.481
LXBE P_125	2	3.537	4.414	8.600	4.514	1.721	10.190	4.381	9.780	16.425	0.595	0.620	0.267	0.105	0.275	0.362	0.451	0.524
LXBE P_55_EO198 108	1	3.788	3.932	8.207	5.158	2.055	8.907	4.246	9.813	16.121	0.609	0.553	0.263	0.127	0.320	0.386	0.401	0.509
LXBE P_55_EO200 104	3	3.993	4.927	8.169	5.972	2.128	7.857	4.538	10.460	15.957	0.655	0.492	0.284	0.133	0.374	0.382	0.471	0.512
LXBE P_55_EO206 107	1	2.452	3.409	6.087	3.424	1.557	6.471	3.261	6.907	11.452	0.603	0.565	0.285	0.136	0.299	0.355	0.494	0.532
LXBE P_55_EO216 18	2	2.495	2.969	6.138	3.910	1.344	7.882	2.993	7.756	13.136	0.590	0.600	0.228	0.102	0.298	0.322	0.383	0.467
LXBE P_55_EO229 2	2	4.146	4.193	7.790	3.851	2.224	10.146	3.966	9.520	16.220	0.587	0.625	0.245	0.137	0.237	0.436	0.440	0.480
LXBE R_20	2	2.595	3.968	8.021	3.820	1.576	9.392	3.217	8.794	14.787	0.595	0.635	0.218	0.107	0.258	0.295	0.451	0.542
LXBE R_24	2	3.861	4.691	8.426	4.296	1.739	10.037	4.273	10.432	16.072	0.649	0.624	0.266	0.108	0.267	0.370	0.450	0.524
LXBE R_26	2	4.026	4.281	7.551	3.844	2.140	9.549	4.016	10.193	15.534	0.656	0.615	0.259	0.138	0.247	0.395	0.420	0.486
LXBE R_144	1	3.181	4.149	8.596	3.614	1.627	10.657	3.981	10.015	15.899	0.630	0.670	0.250	0.102	0.227	0.318	0.414	0.541
LXBE R_146	1	3.659	3.745	8.449	3.724	1.826	10.883	3.897	10.150	16.433	0.618	0.662	0.237	0.111	0.227	0.360	0.369	0.514

Sample	Outl. Qual.	a	b	c	Arr	Av	Ch	Cr	H	L	H/L	Ch/L	Cr/L	Av/L	Arr/L	a/H	b/H	c/L
LXBE R_149	2	3.876	3.991	8.081	4.020	1.874	9.790	4.297	9.518	15.684	0.607	0.624	0.274	0.119	0.256	0.407	0.419	0.515
LXBE R_211	1	3.488	4.100	7.716	3.909	1.626	10.525	3.983	9.875	16.060	0.615	0.655	0.248	0.101	0.243	0.353	0.415	0.480
LXBE R_57_EO267 7	1	3.355	4.173	8.007	3.847	1.957	9.660	3.313	9.404	15.464	0.608	0.625	0.214	0.127	0.249	0.357	0.444	0.518
LXBE R_57_EO267 8	1	4.177	3.908	7.137	3.891	2.239	8.574	3.412	9.158	14.703	0.623	0.583	0.232	0.152	0.265	0.456	0.427	0.485
LXBE R_57_EO268 1	1	3.379	4.124	7.749	3.726	2.142	9.757	3.534	9.910	15.625	0.634	0.624	0.226	0.137	0.238	0.341	0.416	0.496
LXBE R_57_EO283 126	1	4.005	4.743	8.632	3.700	2.238	10.803	3.947	10.795	16.742	0.645	0.645	0.236	0.134	0.221	0.371	0.439	0.516
LXBE R_57_EO309 15	1	3.485	3.950	7.308	3.200	2.646	9.626	4.498	9.519	15.473	0.615	0.622	0.291	0.171	0.207	0.366	0.415	0.472
LXBE R_58_EO330 109	2	4.042	3.860	7.292	4.053	2.284	8.964	3.844	9.733	15.300	0.636	0.586	0.251	0.149	0.265	0.415	0.397	0.477
LXBE R_58_EO336 110	2	3.572	4.431	8.343	3.775	1.988	10.528	3.694	10.130	16.292	0.622	0.646	0.227	0.122	0.232	0.353	0.437	0.512
LXBE S_58_EO355 4	2	1.531	1.793	3.662	1.604	1.106	4.648	2.081	4.387	7.358	0.596	0.632	0.283	0.150	0.218	0.349	0.409	0.498
LXBE U_58_EO364 3	2	3.464	4.244	6.723	4.317	1.862	6.721	3.355	8.972	12.882	0.697	0.522	0.260	0.145	0.335	0.386	0.473	0.522
LXBE U_58_EO367 108	2	1.893	2.016	4.183	2.226	0.951	5.403	1.848	5.344	8.580	0.623	0.630	0.215	0.111	0.259	0.354	0.377	0.488
LXBE W2_61_EO409 4	2	3.123	3.466	7.123	3.080	2.151	9.023	4.037	8.658	14.254	0.607	0.633	0.283	0.151	0.216	0.361	0.400	0.500
LXBE W3_60_EO404 4	2	2.919	3.216	7.502	4.166	1.547	9.010	2.574	8.961	14.723	0.609	0.612	0.175	0.105	0.283	0.326	0.359	0.510
LXBE X_60_EO386 105	3	1.444	1.615	2.858	1.780	0.661	3.452	1.279	3.840	5.893	0.652	0.586	0.217	0.112	0.302	0.376	0.421	0.485
LXBE Z_62_19	2	3.715	4.024	6.999	3.596	2.367	10.103	3.889	9.999	16.067	0.622	0.629	0.242	0.147	0.224	0.371	0.402	0.436
LXBE Z_62_114	3	3.141	3.706	7.184	3.707	1.357	9.134	3.134	8.241	14.197	0.580	0.643	0.221	0.096	0.261	0.381	0.450	0.506
LXBE Z_62_151	1	3.920	4.263	7.696	3.691	1.875	9.545	3.554	10.063	15.112	0.666	0.632	0.235	0.124	0.244	0.390	0.424	0.509
LXBE Z_62_160	2	4.291	5.336	9.538	4.873	2.725	12.725	4.245	12.269	20.324	0.604	0.626	0.209	0.134	0.240	0.350	0.435	0.469
LXBE Z_62_161	1	3.510	4.167	7.664	3.868	2.028	10.618	3.667	9.983	16.515	0.605	0.643	0.222	0.123	0.234	0.352	0.417	0.464
LXBE Z_62_EO455 1	3	4.972	5.630	8.660	5.457	3.226	9.912	5.858	12.751	18.595	0.686	0.533	0.315	0.173	0.293	0.390	0.442	0.466
LXBE Z_6	2	4.554	5.856	9.813	5.500	2.245	12.534	5.113	12.696	20.279	0.626	0.618	0.252	0.111	0.271	0.359	0.461	0.484
LXBE Z_139	2	3.270	3.831	7.139	3.509	1.571	8.262	3.478	8.946	13.349	0.670	0.619	0.261	0.118	0.263	0.366	0.428	0.535
LXBE Z_152	2	4.761	6.270	11.007	6.054	2.524	12.939	5.928	14.445	21.517	0.671	0.601	0.275	0.117	0.281	0.330	0.434	0.512
LXBE C1_63_117	1	3.135	4.614	9.010	6.479	1.437	8.857	3.976	9.944	16.772	0.593	0.528	0.237	0.086	0.386	0.315	0.464	0.537
LXBE C1_63_EO462 11	1	3.249	3.141	5.423	3.787	1.458	7.052	3.298	7.745	12.298	0.630	0.573	0.268	0.119	0.308	0.420	0.406	0.441
LXBE C1_63_EO466 13	2	3.637	4.532	8.618	6.436	2.426	7.343	5.115	10.041	16.205	0.620	0.453	0.316	0.150	0.397	0.362	0.451	0.532

Sample	Outl. Qual.	a	b	c	Arr	Av	Ch	Cr	H	L	H/L	Ch/L	Cr/L	Av/L	Arr/L	a/H	b/H	c/L
LXBE C1_63_EO485 106	2	2.797	4.074	6.695	4.048	1.383	7.134	3.067	8.255	12.565	0.657	0.568	0.244	0.110	0.322	0.339	0.494	0.533
LXBE C1_63_EO485 107	1	4.165	5.163	8.861	4.281	1.937	11.754	4.674	11.316	17.971	0.630	0.654	0.260	0.108	0.238	0.368	0.456	0.493
LXBE D1_63_9	1	4.156	4.877	7.718	5.306	2.409	8.592	4.866	10.266	16.308	0.630	0.527	0.298	0.148	0.325	0.405	0.475	0.473
LXBE I1_67_EO543 126	3	3.198	3.765	7.204	5.099	1.976	6.766	3.672	8.992	13.841	0.650	0.489	0.265	0.143	0.368	0.356	0.419	0.520
LXBE I1_67_EO548 14	3	3.170	3.721	6.806	3.661	1.666	7.638	3.519	8.816	12.965	0.680	0.589	0.271	0.128	0.282	0.360	0.422	0.525
LXBE I1_67_EO549 18	3	2.820	3.729	7.365	4.560	1.565	7.156	3.587	8.249	13.281	0.621	0.539	0.270	0.118	0.343	0.342	0.452	0.555
LXBE I1_67_EO554 4	1	2.175	2.744	5.167	2.177	1.545	6.854	3.009	6.552	10.576	0.620	0.648	0.285	0.146	0.206	0.332	0.419	0.489
LXBE I1_67_EO555 10	2	2.130	2.337	5.010	2.110	1.218	6.272	2.834	6.176	9.600	0.643	0.653	0.295	0.127	0.220	0.345	0.378	0.522
LXBE I1_67_EO556 105	2	2.563	2.515	4.375	2.863	1.343	4.583	2.642	5.896	8.788	0.671	0.521	0.301	0.153	0.326	0.435	0.427	0.498
LXBE I1_67_EO558 2	2	3.233	3.621	6.358	3.472	2.028	7.244	3.869	7.868	12.749	0.617	0.568	0.303	0.159	0.272	0.411	0.460	0.499
LXBE I1_124	2	2.266	2.699	5.419	2.427	1.378	6.210	2.821	6.306	10.016	0.630	0.620	0.282	0.138	0.242	0.359	0.428	0.541
LXBE I1_140	2	1.561	1.825	3.676	1.523	0.765	4.854	2.007	4.575	7.142	0.641	0.680	0.281	0.107	0.213	0.341	0.399	0.515
LXBE I1_HS2	3	2.749	2.972	6.040	2.672	1.332	8.575	3.295	7.820	12.579	0.622	0.682	0.262	0.106	0.212	0.351	0.380	0.480
LXBE I1_HS4	3	2.552	3.304	5.553	3.352	1.224	6.525	3.015	7.293	11.101	0.657	0.588	0.272	0.110	0.302	0.350	0.453	0.500
LXBE I1_HS5_13	3	2.874	3.059	5.229	3.068	1.804	6.571	3.477	7.272	11.443	0.635	0.574	0.304	0.158	0.268	0.395	0.421	0.457
LXBE I1_HS5_19	2	3.313	3.179	6.874	3.076	1.706	8.781	3.940	8.834	13.563	0.651	0.647	0.291	0.126	0.227	0.375	0.360	0.507
LXBE P1_73_EO640_8	1	2.487	3.119	5.989	3.385	1.582	7.245	3.250	7.473	12.212	0.612	0.593	0.266	0.130	0.277	0.333	0.417	0.490
LXBE P1_73_EO644	2	4.401	4.591	9.517	3.718	2.615	12.706	4.939	11.441	19.039	0.601	0.667	0.259	0.137	0.195	0.385	0.401	0.500
LXBE S1_77_59	2	2.468	3.247	5.724	2.907	1.499	8.109	3.343	7.703	12.514	0.616	0.648	0.267	0.120	0.232	0.320	0.422	0.457
LXBE S1_77_60	1	2.372	3.128	5.884	2.677	1.446	8.101	2.975	7.654	12.224	0.626	0.663	0.243	0.118	0.219	0.310	0.409	0.481
LXBE S1_77_63	3	2.526	2.943	5.957	2.761	1.393	7.876	3.170	7.061	12.031	0.587	0.655	0.264	0.116	0.230	0.358	0.417	0.495
LXBE S1_77_64	3	2.173	3.125	6.060	2.547	1.154	8.611	3.273	7.152	12.312	0.581	0.699	0.266	0.094	0.207	0.304	0.437	0.492
LXBE S1_77_64_19	3	3.356	4.542	9.259	4.193	1.569	13.198	4.628	11.170	18.960	0.589	0.696	0.244	0.083	0.221	0.300	0.407	0.488
LXBE S1_77_74_1	1	3.387	4.130	7.423	3.711	1.621	9.744	3.790	9.271	15.052	0.616	0.647	0.252	0.108	0.247	0.365	0.445	0.493
LXBE S1_77_74_2	2	3.126	3.830	7.076	3.998	1.231	9.712	3.747	8.998	14.940	0.602	0.650	0.251	0.082	0.268	0.347	0.426	0.474
LXBE S1_77_74_7	3	1.629	2.471	4.682	2.199	0.899	6.052	2.482	5.585	9.150	0.610	0.661	0.271	0.098	0.240	0.292	0.442	0.512
LXBE S1_77_74_11	1	2.766	3.436	6.327	3.312	1.482	7.769	3.153	8.105	12.564	0.645	0.618	0.251	0.118	0.264	0.341	0.424	0.504

Sample	Outl. Qual.	a	b	c	Arr	Av	Ch	Cr	H	L	H/L	Ch/L	Cr/L	Av/L	Arr/L	a/H	b/H	c/L
LXBE S1_77_75_4	3	2.765	3.286	6.177	3.394	1.675	8.030	4.018	8.052	13.099	0.615	0.613	0.307	0.128	0.259	0.343	0.408	0.472
LXBE S1_77_EO704_24	1	2.172	2.758	6.025	2.548	1.270	8.498	2.643	7.248	12.316	0.589	0.690	0.215	0.103	0.207	0.300	0.380	0.489
LXBE S1_77_EO704_25	2	1.277	1.268	2.576	1.101	0.708	3.385	1.523	3.303	5.194	0.636	0.652	0.293	0.136	0.212	0.387	0.384	0.496
LXBE S1_77_EO704_29	3	3.760	3.937	7.866	3.727	2.111	9.789	4.312	9.606	15.627	0.615	0.626	0.276	0.135	0.239	0.391	0.410	0.503
LXBE S1_77_EO704_30	2	2.448	3.722	6.572	3.223	1.179	8.535	3.570	8.040	12.937	0.621	0.660	0.276	0.091	0.249	0.304	0.463	0.508
LXBE S1_77_EO704_31	2	2.970	4.133	6.720	2.733	1.744	8.630	3.475	8.786	13.106	0.670	0.658	0.265	0.133	0.208	0.338	0.470	0.513
LXBE S1_77_EO707_23	3	2.812	3.005	6.451	2.881	1.809	8.355	3.665	7.905	13.046	0.606	0.640	0.281	0.139	0.221	0.356	0.380	0.494
LXBE S1_15	2	2.471	3.160	6.572	2.593	1.256	9.097	2.836	7.557	12.947	0.584	0.703	0.219	0.097	0.200	0.327	0.418	0.508
LXBE S1_16	1	2.599	3.547	6.906	3.214	1.048	9.988	2.542	8.882	14.250	0.623	0.701	0.178	0.074	0.226	0.293	0.399	0.485
LXBE S1_21	1	3.182	3.658	5.968	2.989	2.099	7.583	3.351	8.273	12.671	0.653	0.598	0.265	0.166	0.236	0.385	0.442	0.471
LXBE S1_24	2	3.151	3.288	5.783	2.817	1.819	7.713	3.525	7.784	12.348	0.630	0.625	0.285	0.147	0.228	0.405	0.422	0.468
LXBE S1_70	1	3.518	3.663	6.939	3.381	1.568	9.455	3.315	9.097	14.403	0.632	0.656	0.230	0.109	0.235	0.387	0.403	0.482
LXBE S1_71	2	2.127	2.918	4.948	2.202	1.191	6.829	2.681	6.402	10.222	0.626	0.668	0.262	0.116	0.215	0.332	0.456	0.484
LXBE S1_HS2	1	2.694	3.210	7.054	2.847	1.242	8.981	2.848	7.946	13.070	0.608	0.687	0.218	0.095	0.218	0.339	0.404	0.540
LXBE S1_HS4	3	2.543	2.584	5.673	2.196	1.364	8.246	2.921	7.199	11.806	0.610	0.698	0.247	0.116	0.186	0.353	0.359	0.481
JSG (GZN2013 II)																		
JSG A1_3	3	0.767	0.696	1.149	0.713	0.466	1.178	0.821	1.781	2.357	0.755	0.500	0.348	0.198	0.303	0.431	0.391	0.488
JSG A2_70	2	0.423	0.492	0.761	0.506	0.233	0.784	0.436	1.150	1.523	0.755	0.515	0.286	0.153	0.332	0.368	0.427	0.500
JSG A4_1	2	0.479	0.507	0.795	0.530	0.251	0.841	0.477	1.179	1.622	0.727	0.519	0.294	0.155	0.327	0.406	0.430	0.490
JSG A4_6	2	0.377	0.402	0.617	0.343	0.284	0.680	0.499	0.943	1.306	0.721	0.520	0.382	0.218	0.262	0.400	0.426	0.472
JSG A4_73	1	2.170	2.310	4.591	2.298	1.309	5.802	2.349	5.881	9.415	0.625	0.616	0.249	0.139	0.244	0.369	0.393	0.488
JSG A5_80	1	1.884	2.254	4.408	2.125	0.701	6.141	2.033	5.700	8.967	0.636	0.685	0.227	0.078	0.237	0.330	0.395	0.492
JSG A6_84	2	2.406	2.448	5.288	2.797	1.353	6.321	2.599	6.377	10.471	0.609	0.604	0.248	0.129	0.267	0.377	0.384	0.505
JSG A7_ 85	3	2.082	3.204	5.930	3.419	0.853	6.097	2.170	6.568	10.369	0.633	0.588	0.209	0.082	0.330	0.317	0.488	0.572
JSG A8_1	1	0.735	0.702	1.072	0.490	0.373	1.363	0.766	1.502	2.227	0.675	0.612	0.344	0.168	0.220	0.489	0.467	0.481

Sample	Outl. Qual.	a	b	c	Arr	Av	Ch	Cr	H	L	H/L	Ch/L	Cr/L	Av/L	Arr/L	a/H	b/H	c/L
JSG A8_2	2	2.409	3.262	6.427	2.995	1.160	7.773	2.473	7.370	11.928	0.618	0.652	0.207	0.097	0.251	0.327	0.443	0.539
JSG A8_92	2	2.578	3.288	6.205	3.116	1.255	7.679	2.795	7.378	12.051	0.612	0.637	0.232	0.104	0.259	0.349	0.446	0.515
JSG A10_3	1	2.496	2.386	4.516	2.591	1.248	5.759	2.203	6.301	9.599	0.656	0.600	0.230	0.130	0.270	0.396	0.379	0.470
JSG B1_3	3	1.311	1.607	2.986	1.456	0.614	3.541	1.249	3.791	5.612	0.676	0.631	0.222	0.109	0.260	0.346	0.424	0.532
JSG B2_25	1	0.939	1.108	2.091	1.041	0.553	2.425	1.016	2.689	4.019	0.669	0.603	0.253	0.138	0.259	0.349	0.412	0.520
JSG B2_27	1	1.261	1.494	2.823	1.658	0.575	3.771	1.234	3.698	6.005	0.616	0.628	0.205	0.096	0.276	0.341	0.404	0.470
JSG B2_31	1	1.388	2.039	4.197	2.233	0.863	5.307	2.337	4.965	8.403	0.591	0.631	0.278	0.103	0.266	0.279	0.411	0.499
JSG B2_32	2	1.015	1.383	2.677	1.202	0.447	3.359	1.174	3.268	5.008	0.653	0.671	0.234	0.089	0.240	0.311	0.423	0.535
JSG B2_43	1	1.412	1.536	2.940	1.885	0.726	3.404	1.488	3.791	6.015	0.630	0.566	0.247	0.121	0.313	0.373	0.405	0.489
JSG B2_44	1	1.214	1.339	2.617	1.573	0.591	3.276	1.364	3.530	5.440	0.649	0.602	0.251	0.109	0.289	0.344	0.379	0.481
JSG B3_45	1	1.585	1.879	3.491	2.280	0.715	4.009	1.831	4.535	7.003	0.647	0.572	0.261	0.102	0.326	0.350	0.414	0.499
JSG B4_48	1	1.433	1.799	3.376	2.020	0.794	3.783	1.598	4.243	6.597	0.643	0.574	0.242	0.120	0.306	0.338	0.424	0.512
JSG B4_49	2	1.009	1.341	2.405	1.531	0.667	2.447	1.188	3.002	4.644	0.646	0.527	0.256	0.144	0.330	0.336	0.447	0.518
JSG B5_51	2	1.346	1.665	3.216	1.844	0.678	3.903	1.571	4.153	6.425	0.646	0.607	0.244	0.105	0.287	0.324	0.401	0.501
JSG B5_54	2	1.299	1.375	2.751	1.635	0.646	2.875	1.432	3.400	5.156	0.659	0.558	0.278	0.125	0.317	0.382	0.404	0.534
JSG B5_56	2	1.481	1.652	3.216	2.256	0.786	3.675	1.539	4.285	6.717	0.638	0.547	0.229	0.117	0.336	0.346	0.385	0.479
JSG B5_57	2	1.799	1.587	3.231	1.842	1.016	4.433	1.777	4.651	7.290	0.638	0.608	0.244	0.139	0.253	0.387	0.341	0.443
JSG B6_60	2	1.051	1.297	2.124	1.530	0.598	2.199	1.148	2.883	4.326	0.666	0.508	0.265	0.138	0.354	0.365	0.450	0.491
JSG B6_61	1	1.771	1.963	3.880	2.042	0.889	4.735	2.050	4.858	7.666	0.634	0.618	0.267	0.116	0.266	0.365	0.404	0.506
JSG B6_62	1	1.809	1.689	3.621	1.815	1.124	4.804	2.180	4.832	7.742	0.624	0.620	0.282	0.145	0.234	0.374	0.350	0.468
JSG B7_64	1	1.586	1.902	3.370	2.319	0.972	3.407	1.834	4.552	6.698	0.680	0.509	0.274	0.145	0.346	0.348	0.418	0.503
JSG B8_2	1	1.594	1.994	3.547	1.908	0.918	4.334	2.052	4.714	7.159	0.658	0.605	0.287	0.128	0.266	0.338	0.423	0.495
JSG B9_1	1	1.108	1.447	2.418	1.654	0.563	2.385	1.254	3.091	4.601	0.672	0.518	0.273	0.122	0.359	0.358	0.468	0.525
JSG B9_2	1	1.674	1.725	3.461	1.636	0.803	4.833	1.554	4.435	7.272	0.610	0.665	0.214	0.110	0.225	0.378	0.389	0.476
JSG B9_3	1	1.770	2.218	4.366	2.545	0.915	5.133	1.818	5.384	8.593	0.627	0.597	0.212	0.107	0.296	0.329	0.412	0.508
JSG C1a_1	2	1.821	1.901	4.283	2.444	0.914	5.329	1.895	5.367	8.688	0.618	0.613	0.218	0.105	0.281	0.339	0.354	0.493
JSG C1a_2	1	1.493	1.767	3.562	1.876	0.746	4.835	1.315	4.766	7.457	0.639	0.648	0.176	0.100	0.252	0.313	0.371	0.478

Sample	Outl. Qual.	a	b	c	Arr	Av	Ch	Cr	H	L	H/L	Ch/L	Cr/L	Av/L	Arr/L	a/H	b/H	c/L
JSG C1a_3	2	2.016	2.279	4.590	2.949	0.948	5.480	1.542	6.030	9.377	0.643	0.584	0.164	0.101	0.315	0.334	0.378	0.490
JSG C1a_4	1	1.816	1.984	3.966	2.269	0.774	4.916	1.711	5.117	7.959	0.643	0.618	0.215	0.097	0.285	0.355	0.388	0.498
JSG C1a_5	2	2.078	2.341	5.002	2.480	0.953	6.623	2.018	6.110	10.055	0.608	0.659	0.201	0.095	0.247	0.340	0.383	0.497
JSG C1_77	1	2.265	2.725	5.414	3.163	1.260	6.464	2.466	6.858	10.887	0.630	0.594	0.226	0.116	0.291	0.330	0.397	0.497
JSG C1_79	1	2.010	2.077	4.452	2.422	1.158	5.580	1.872	5.610	9.161	0.612	0.609	0.204	0.126	0.264	0.358	0.370	0.486
JSG C1_82	1	1.686	2.125	4.106	2.103	0.927	5.029	2.018	5.266	8.059	0.653	0.624	0.250	0.115	0.261	0.320	0.404	0.509
JSG C1_84	1	2.102	2.693	4.794	3.017	1.420	5.191	2.822	6.076	9.628	0.631	0.539	0.293	0.147	0.313	0.346	0.443	0.498
JSG C2_88	2	1.854	2.036	3.843	2.290	1.055	4.895	2.170	5.125	8.240	0.622	0.594	0.263	0.128	0.278	0.362	0.397	0.466
JSG C6_100	1	1.723	2.279	4.714	2.036	0.947	6.070	2.229	5.324	9.053	0.588	0.671	0.246	0.105	0.225	0.324	0.428	0.521
JSG C8_107	1	2.142	2.283	4.782	2.555	1.349	6.371	2.216	6.112	10.275	0.595	0.620	0.216	0.131	0.249	0.350	0.373	0.465
JSG C10_109	2	2.049	2.054	4.198	2.264	1.193	5.317	1.830	5.382	8.774	0.613	0.606	0.209	0.136	0.258	0.381	0.382	0.479
JSG C12_1	1	1.938	2.301	4.338	2.558	1.093	7.014	2.481	6.289	10.666	0.590	0.658	0.233	0.103	0.240	0.308	0.366	0.407
JSG C12_2	3	2.196	2.490	4.917	2.653	1.369	6.037	2.375	6.155	10.060	0.612	0.600	0.236	0.136	0.264	0.357	0.405	0.489
JSG C14_6	2	1.615	2.148	4.470	1.878	0.753	6.119	1.885	5.449	8.749	0.623	0.699	0.215	0.086	0.215	0.296	0.394	0.511
JSG C14_9	1	1.622	1.698	3.269	2.080	0.831	3.589	1.407	4.338	6.501	0.667	0.552	0.216	0.128	0.320	0.374	0.391	0.503
JSG C15_10	2	2.157	2.366	4.639	2.249	0.878	6.188	1.759	5.788	9.315	0.621	0.664	0.189	0.094	0.241	0.373	0.409	0.498
JSG C15_13	2	1.709	2.052	4.022	2.458	0.819	4.997	1.675	5.288	8.273	0.639	0.604	0.203	0.099	0.297	0.323	0.388	0.486
JSG C15_14	3	1.976	2.086	4.523	2.572	1.065	5.570	1.870	5.691	9.207	0.618	0.605	0.203	0.116	0.279	0.347	0.366	0.491
JSG C17_02b	1	0.364	0.351	0.495	0.347	0.228	0.432	0.443	0.826	1.008	0.820	0.429	0.439	0.227	0.344	0.441	0.425	0.491
JSG C18_1	1	1.641	2.157	4.355	2.353	1.052	5.494	2.241	5.311	8.899	0.597	0.617	0.252	0.118	0.264	0.309	0.406	0.489
JSG C19_1	1	1.898	2.290	4.397	2.420	1.108	5.472	1.925	5.604	9.000	0.623	0.608	0.214	0.123	0.269	0.339	0.409	0.489
JSG C20_6	2	2.315	3.084	6.188	3.204	1.282	7.834	2.489	7.696	12.320	0.625	0.636	0.202	0.104	0.260	0.301	0.401	0.502
JSG 4_1	1	1.589	2.004	4.193	1.967	1.229	5.356	2.235	5.160	8.552	0.603	0.626	0.261	0.144	0.230	0.308	0.388	0.490
JSG 4alpha_1	2	1.356	1.274	2.572	1.458	0.733	3.362	1.529	3.495	5.553	0.629	0.606	0.275	0.132	0.263	0.388	0.365	0.463
JSG 4alpha_2	1	1.371	1.480	2.899	1.618	0.821	3.534	1.709	3.974	5.973	0.665	0.592	0.286	0.137	0.271	0.345	0.372	0.485
JSG 4alpha_3	2	1.250	1.592	2.766	1.503	0.617	3.479	1.244	3.699	5.598	0.661	0.621	0.222	0.110	0.268	0.338	0.431	0.494
JSG 4alpha_4	2	1.907	2.237	4.345	2.122	1.137	5.721	2.361	5.761	8.980	0.642	0.637	0.263	0.127	0.236	0.331	0.388	0.484

Sample	Outl. Qual.	a	b	c	Arr	Av	Ch	Cr	H	L	H/L	Ch/L	Cr/L	Av/L	Arr/L	a/H	b/H	c/L
JSG 4alpha_5	1	1.623	1.515	2.886	1.703	0.701	3.561	1.257	3.969	5.966	0.665	0.597	0.211	0.118	0.286	0.409	0.382	0.484
JSG 4alpha_6	3	0.899	0.972	1.691	1.044	0.499	1.784	1.098	2.257	3.327	0.679	0.536	0.330	0.150	0.314	0.398	0.430	0.508
JSG 4alpha_7	2	1.563	1.470	3.041	1.642	0.881	3.990	1.441	4.143	6.513	0.636	0.613	0.221	0.135	0.252	0.377	0.355	0.467
JSG 4ualpha_1	2	0.370	0.415	0.633	0.328	0.290	0.634	0.483	0.978	1.252	0.781	0.506	0.385	0.231	0.262	0.378	0.425	0.506
JSG 4ualpha_4	1	0.456	0.471	0.757	0.361	0.234	0.859	0.456	1.071	1.454	0.736	0.591	0.314	0.161	0.248	0.425	0.440	0.520
JSG D2_105	1	2.284	2.366	4.854	2.715	1.281	6.207	2.384	6.107	10.204	0.599	0.608	0.234	0.126	0.266	0.374	0.387	0.476
JSG D4_117	2	2.574	2.983	5.040	2.414	1.191	6.888	2.170	6.676	10.493	0.636	0.656	0.207	0.114	0.230	0.386	0.447	0.480
JSG D4_118	2	1.955	2.282	4.709	2.240	1.139	6.585	2.078	6.256	9.964	0.628	0.661	0.209	0.114	0.225	0.312	0.365	0.473
JSG D6_1b	2	1.677	2.511	5.046	2.227	0.817	6.274	2.590	5.730	9.319	0.615	0.673	0.278	0.088	0.239	0.293	0.438	0.542
JSG D7_2	1	0.722	0.730	1.168	0.513	0.298	1.719	0.646	1.706	2.531	0.674	0.679	0.255	0.118	0.203	0.423	0.428	0.461
JSG E1_1	2	1.359	1.908	2.921	1.706	0.814	2.885	1.663	3.665	5.405	0.678	0.534	0.308	0.151	0.316	0.371	0.521	0.541
JSG E2_2	1	0.447	0.500	0.775	0.485	0.288	0.832	0.478	1.090	1.605	0.679	0.518	0.298	0.179	0.302	0.410	0.459	0.483
JSG E3_137	2	1.128	1.389	2.383	1.445	0.546	2.780	1.325	3.115	4.771	0.653	0.583	0.278	0.114	0.303	0.362	0.446	0.499
JSG F1_3	1	0.847	0.890	1.498	0.744	0.454	1.762	0.949	1.937	2.960	0.654	0.595	0.321	0.153	0.251	0.437	0.460	0.506
JSG F2_6	1	1.340	1.678	2.498	1.682	0.615	2.683	1.261	3.548	4.981	0.712	0.539	0.253	0.124	0.338	0.378	0.473	0.502
JSG F2_8	2	1.681	2.036	3.642	2.352	0.998	3.663	1.703	4.566	7.013	0.651	0.522	0.243	0.142	0.335	0.368	0.446	0.519
JSG F3_3	3	0.592	0.579	0.828	0.529	0.396	0.931	0.651	1.326	1.856	0.714	0.502	0.351	0.213	0.285	0.447	0.437	0.446
JSG F5_3	2	1.021	1.055	1.679	1.178	0.628	1.619	1.200	2.354	3.425	0.687	0.473	0.350	0.183	0.344	0.434	0.448	0.490
JSG F6_2	2	1.305	1.773	2.556	1.352	0.678	3.535	1.313	3.544	5.565	0.637	0.635	0.236	0.122	0.243	0.368	0.500	0.459
JSG F7_1	1	1.951	1.899	3.240	2.003	0.947	4.460	1.725	4.738	7.411	0.639	0.602	0.233	0.128	0.270	0.412	0.401	0.437
JSG G1_2	1	0.647	0.954	1.602	0.836	0.324	1.865	0.705	2.074	3.025	0.686	0.616	0.233	0.107	0.276	0.312	0.460	0.530
JSG G1_4	1	0.701	0.829	1.262	0.684	0.364	1.635	0.713	1.900	2.683	0.708	0.609	0.266	0.136	0.255	0.369	0.436	0.470
JSG G1_7	2	0.752	0.732	1.135	0.759	0.365	1.314	0.793	1.730	2.439	0.709	0.539	0.325	0.150	0.311	0.435	0.423	0.466
JSG G2_1	1	0.895	1.047	1.613	0.817	0.469	1.815	0.803	2.172	3.100	0.701	0.585	0.259	0.151	0.263	0.412	0.482	0.520
JSG G2_12	2	0.493	0.626	0.919	0.508	0.254	0.956	0.581	1.285	1.718	0.748	0.557	0.338	0.148	0.296	0.383	0.487	0.535
JSG G2_13	2	1.709	2.689	5.352	2.803	1.073	6.501	2.485	6.441	10.378	0.621	0.626	0.239	0.103	0.270	0.265	0.417	0.516
JSG G2_14	2	0.604	0.882	1.422	0.872	0.288	1.580	0.736	1.842	2.740	0.672	0.577	0.269	0.105	0.318	0.328	0.479	0.519

Sample	Outl. Qual.	a	b	c	Arr	Av	Ch	Cr	H	L	H/L	Ch/L	Cr/L	Av/L	Arr/L	a/H	b/H	c/L
JSG G2_16	2	0.528	0.793	1.449	0.788	0.279	1.663	0.526	1.787	2.731	0.654	0.609	0.193	0.102	0.289	0.296	0.444	0.531
JSG G3_2	2	2.421	2.797	5.356	2.503	1.170	7.758	2.749	6.958	11.438	0.608	0.678	0.240	0.102	0.219	0.348	0.402	0.468
JSG G3_20	1	2.145	2.693	5.605	2.521	0.952	7.448	2.608	6.357	10.921	0.582	0.682	0.239	0.087	0.231	0.337	0.424	0.513
JSG G3_21a	3	1.006	1.096	1.743	0.907	0.613	2.053	0.902	2.409	3.573	0.674	0.575	0.252	0.172	0.254	0.418	0.455	0.488
JSG G3_21b	3	0.741	1.171	1.726	1.081	0.386	2.001	0.788	2.497	3.469	0.720	0.577	0.227	0.111	0.312	0.297	0.469	0.497
JSG G3_28	1	1.737	2.220	5.473	2.167	0.775	7.218	2.181	5.694	10.160	0.560	0.710	0.215	0.076	0.213	0.305	0.390	0.539
JSG G3_29	1	1.742	2.248	5.107	2.284	0.884	6.395	2.489	5.777	9.563	0.604	0.669	0.260	0.092	0.239	0.302	0.389	0.534
JSG G3_30	1	0.772	0.918	1.355	0.994	0.526	1.333	0.929	1.986	2.854	0.696	0.467	0.325	0.184	0.348	0.389	0.462	0.475
JSG G4_2	1	0.737	0.908	1.498	1.030	0.438	1.427	0.949	1.948	2.895	0.673	0.493	0.328	0.151	0.356	0.378	0.466	0.517
JSG G4_3	1	0.601	0.634	1.085	0.623	0.317	1.300	0.796	1.542	2.240	0.689	0.581	0.356	0.141	0.278	0.390	0.411	0.484
JSG G4_4	2	2.566	2.890	5.264	2.575	1.354	7.071	2.445	7.160	11.000	0.651	0.643	0.222	0.123	0.234	0.358	0.404	0.479
JSG G4_5	3	0.881	0.864	1.451	0.864	0.452	1.692	0.776	2.047	3.008	0.681	0.563	0.258	0.150	0.287	0.430	0.422	0.483
JSG G4_6	2	1.337	1.412	2.605	1.453	0.727	3.295	1.377	3.818	5.475	0.697	0.602	0.251	0.133	0.265	0.350	0.370	0.476
JSG G4_7	1	0.912	1.017	1.805	1.020	0.391	2.290	0.935	2.500	3.701	0.675	0.619	0.253	0.106	0.276	0.365	0.407	0.488
JSG G4_8	3	0.444	0.683	1.098	0.513	0.220	1.359	0.652	1.384	2.092	0.662	0.650	0.312	0.105	0.245	0.321	0.494	0.525
JSG G5_1	2	2.073	2.387	4.698	2.506	1.209	6.265	2.329	6.000	9.980	0.601	0.628	0.233	0.121	0.251	0.345	0.398	0.471
JSG G5_2	2	1.733	1.306	2.718	1.359	0.974	3.968	1.680	3.990	6.302	0.633	0.630	0.267	0.155	0.216	0.434	0.327	0.431
JSG G5_3	2	0.740	0.857	1.336	0.840	0.319	1.571	0.732	1.931	2.729	0.708	0.576	0.268	0.117	0.308	0.383	0.444	0.489
JSG G5_4	2	0.783	0.846	1.500	0.830	0.381	1.883	0.727	1.983	3.095	0.641	0.609	0.235	0.123	0.268	0.395	0.426	0.485
JSG G5_5	1	0.658	0.674	1.037	0.540	0.417	1.354	0.762	1.604	2.311	0.694	0.586	0.330	0.181	0.234	0.410	0.420	0.449
JSG G5_6	2	0.659	0.748	1.154	0.659	0.309	1.405	0.714	1.630	2.373	0.687	0.592	0.301	0.130	0.278	0.404	0.459	0.486
JSG G6_2	1	2.326	2.803	6.460	2.546	1.016	9.740	3.078	7.582	13.302	0.570	0.732	0.231	0.076	0.191	0.307	0.370	0.486
JSG G7_1	2	0.564	0.580	1.063	0.501	0.330	1.449	0.623	1.456	2.280	0.639	0.636	0.273	0.145	0.220	0.388	0.398	0.466
JSG G7_2	1	0.625	0.858	1.486	0.898	0.293	1.934	0.653	2.005	3.125	0.642	0.619	0.209	0.094	0.287	0.312	0.428	0.475
JSG G8_1	1	2.401	2.776	6.116	3.386	1.587	7.171	2.528	7.331	12.143	0.604	0.591	0.208	0.131	0.279	0.328	0.379	0.504
JSG G9_2	2	1.091	1.329	2.293	1.294	0.471	3.206	1.037	3.166	4.972	0.637	0.645	0.209	0.095	0.260	0.345	0.420	0.461
JSG G9_3	3	2.178	2.781	4.832	2.281	1.088	6.707	2.165	6.608	10.077	0.656	0.666	0.215	0.108	0.226	0.330	0.421	0.480

Sample	Outl. Qual.	a	b	c	Arr	Av	Ch	Cr	H	L	H/L	Ch/L	Cr/L	Av/L	Arr/L	a/H	b/H	c/L
JSG H1_32	1	3.032	4.448	8.032	4.352	1.473	9.687	3.605	9.630	15.512	0.621	0.624	0.232	0.095	0.281	0.315	0.462	0.518
JSG H2_34	3	5.313	5.381	9.605	5.053	2.787	12.121	4.889	12.969	19.962	0.650	0.607	0.245	0.140	0.253	0.410	0.415	0.481
JSG H9_1	1	4.990	5.449	10.180	5.528	2.526	12.557	4.657	12.978	20.621	0.629	0.609	0.226	0.123	0.268	0.384	0.420	0.494
JSG H10_01b	1	3.759	4.252	7.881	3.753	2.303	9.835	3.815	10.082	15.891	0.634	0.619	0.240	0.145	0.236	0.373	0.422	0.496
JSG H11_01	1	4.092	5.531	10.055	4.814	1.951	12.902	4.956	12.546	19.667	0.638	0.656	0.252	0.099	0.245	0.326	0.441	0.511
JSG H18_55	2	4.200	5.292	10.186	4.542	2.089	12.705	5.016	12.257	19.336	0.634	0.657	0.259	0.108	0.235	0.343	0.432	0.527
JSG I2_1	1	2.858	3.951	8.198	3.871	1.355	10.149	3.236	9.246	15.375	0.601	0.660	0.210	0.088	0.252	0.309	0.427	0.533
JSG I4_1	1	3.714	4.358	7.916	4.426	1.624	9.437	3.126	9.951	15.487	0.643	0.609	0.202	0.105	0.286	0.373	0.438	0.511
JSG I6_117	2	2.062	2.577	4.949	2.939	1.001	6.171	2.341	6.298	10.111	0.623	0.610	0.232	0.099	0.291	0.327	0.409	0.489
JSG I9_127	1	2.876	2.674	5.376	2.732	1.426	8.167	3.101	7.705	12.325	0.625	0.663	0.252	0.116	0.222	0.373	0.347	0.436
JSG J1_4	1	3.807	4.286	7.556	4.103	1.675	9.120	3.200	9.546	14.898	0.641	0.612	0.215	0.112	0.275	0.399	0.449	0.507
JSG J1_18	1	3.494	3.320	6.859	3.838	1.979	8.457	3.356	8.918	14.274	0.625	0.592	0.235	0.139	0.269	0.392	0.372	0.481
JSG J2_1	2	4.634	4.110	7.884	4.378	2.242	9.731	3.798	10.635	16.350	0.650	0.595	0.232	0.137	0.268	0.436	0.386	0.482
JSG J2_3	2	4.069	4.589	7.445	4.860	1.886	8.789	3.313	10.558	15.535	0.680	0.566	0.213	0.121	0.313	0.385	0.435	0.479
JSG J3_1	2	3.569	4.622	9.291	4.212	1.701	11.588	4.263	10.854	17.501	0.620	0.662	0.244	0.097	0.241	0.329	0.426	0.531
JSG J3_3	1	3.843	4.177	7.463	3.444	1.607	10.059	3.074	9.955	15.110	0.659	0.666	0.203	0.106	0.228	0.386	0.420	0.494
JSG J3_4	1	2.514	2.872	6.209	2.377	1.174	8.742	3.086	7.085	12.293	0.576	0.711	0.251	0.095	0.193	0.355	0.405	0.505
JSG J3_5	1	3.217	4.055	7.540	4.088	1.704	9.289	3.095	9.209	15.082	0.611	0.616	0.205	0.113	0.271	0.349	0.440	0.500
JSG K1_24	1	2.516	2.222	4.848	2.761	1.327	6.522	2.431	6.463	10.610	0.609	0.615	0.229	0.125	0.260	0.389	0.344	0.457
JSG K1_25	1	1.881	2.336	4.576	1.682	1.072	6.582	2.453	6.014	9.336	0.644	0.705	0.263	0.115	0.180	0.313	0.388	0.490
JSG K1_26	1	3.725	3.924	6.977	3.258	1.856	10.126	3.549	9.400	15.240	0.617	0.664	0.233	0.122	0.214	0.396	0.417	0.458
JSG K2_2	1	2.867	3.423	7.044	3.539	1.411	9.506	2.834	8.663	14.439	0.600	0.658	0.196	0.098	0.245	0.331	0.395	0.488
JSG K2_3	2	3.668	4.321	7.394	4.924	1.580	8.529	3.374	9.642	15.032	0.641	0.567	0.224	0.105	0.328	0.380	0.448	0.492
JSG K2_31	1	3.101	3.640	7.190	4.361	1.767	8.288	3.498	8.842	14.416	0.613	0.575	0.243	0.123	0.303	0.351	0.412	0.499
JSG K4_53	3	3.173	3.916	8.572	3.393	1.304	10.877	3.492	9.052	15.575	0.581	0.698	0.224	0.084	0.218	0.351	0.433	0.550
JSG K8_1	2	3.844	4.611	8.484	5.251	2.121	9.425	3.882	10.491	16.797	0.625	0.561	0.231	0.126	0.313	0.366	0.440	0.505
JSG L1_1	2	1.810	2.025	3.884	2.333	0.769	5.108	2.320	5.244	8.210	0.639	0.622	0.283	0.094	0.284	0.345	0.386	0.473

Sample	Outl. Qual.	a	b	c	Arr	Av	Ch	Cr	H	L	H/L	Ch/L	Cr/L	Av/L	Arr/L	a/H	b/H	c/L
JSG L1_46	2	1.578	2.098	3.910	2.330	0.908	4.774	1.916	4.958	8.012	0.619	0.596	0.239	0.113	0.291	0.318	0.423	0.488
JSG L2_48	1	1.662	2.193	3.904	1.856	0.834	4.888	2.114	5.048	7.579	0.666	0.645	0.279	0.110	0.245	0.329	0.434	0.515
JSG L6_1	2	2.002	2.284	4.317	2.583	1.193	4.994	2.524	5.306	8.769	0.605	0.569	0.288	0.136	0.295	0.377	0.430	0.492
JSG L6_4	2	1.247	2.184	3.726	2.422	0.548	3.938	1.644	4.540	6.908	0.657	0.570	0.238	0.079	0.351	0.275	0.481	0.539
JSG L6_5	3	2.045	3.003	5.638	3.486	1.031	6.092	2.703	6.682	10.608	0.630	0.574	0.255	0.097	0.329	0.306	0.449	0.531
JSG Mb1_2	3	2.077	2.196	4.272	3.105	1.278	4.861	2.253	5.511	9.244	0.596	0.526	0.244	0.138	0.336	0.377	0.399	0.462
JSG Mb2_1	3	1.382	1.882	3.153	1.851	0.598	3.514	1.403	4.006	5.963	0.672	0.589	0.235	0.100	0.310	0.345	0.470	0.529
JSG Mb2_4	2	1.559	1.755	3.620	2.152	0.801	4.268	1.779	4.360	7.220	0.604	0.591	0.246	0.111	0.298	0.357	0.402	0.501
JSG Mb2_5	2	1.787	2.305	4.248	2.109	1.133	5.095	2.087	5.263	8.337	0.631	0.611	0.250	0.136	0.253	0.340	0.438	0.510
JSG N1_56	3	1.873	1.979	3.944	2.272	0.887	5.217	2.307	5.134	8.376	0.613	0.623	0.275	0.106	0.271	0.365	0.385	0.471
JSG N2_61	2	1.385	1.971	3.861	1.917	0.618	5.203	1.834	4.812	7.737	0.622	0.672	0.237	0.080	0.248	0.288	0.409	0.499
JSG N3_1	2	1.322	1.486	2.912	1.641	0.713	3.601	1.470	3.577	5.955	0.601	0.605	0.247	0.120	0.276	0.370	0.415	0.489
JSG N3_2	2	1.413	1.711	3.560	1.554	0.552	5.017	1.780	4.337	7.123	0.609	0.704	0.250	0.077	0.218	0.326	0.395	0.500
JSG N5_1	3	1.416	1.828	3.373	1.994	0.772	4.280	2.013	4.335	7.046	0.615	0.607	0.286	0.110	0.283	0.327	0.422	0.479
JSG O1_64	2	4.068	4.840	9.139	3.489	1.979	12.185	4.428	10.909	17.654	0.618	0.690	0.251	0.112	0.198	0.373	0.444	0.518
JSG O2_66	1	4.560	5.405	10.526	4.995	2.177	12.895	4.150	12.250	20.067	0.610	0.643	0.207	0.108	0.249	0.372	0.441	0.525
JSG O2_67	2	4.105	5.082	9.336	5.822	1.674	10.973	4.256	11.320	18.469	0.613	0.594	0.230	0.091	0.315	0.363	0.449	0.506
JSG O7_1	2	3.277	5.527	9.053	6.390	2.072	7.416	4.383	10.659	15.878	0.671	0.467	0.276	0.130	0.402	0.307	0.518	0.570
JSG O7_2	3	4.252	6.310	11.228	5.118	1.923	12.692	5.067	12.655	19.733	0.641	0.643	0.257	0.097	0.259	0.336	0.499	0.569
JSG O7_3	2	5.636	5.704	9.460	4.946	2.205	12.993	4.652	13.248	20.144	0.658	0.645	0.231	0.109	0.246	0.425	0.431	0.470
JSG O7_5	2	1.706	2.040	3.903	2.257	0.830	5.439	2.435	5.376	8.526	0.631	0.638	0.286	0.097	0.265	0.317	0.379	0.458
JSG O11_1	1	4.262	5.769	10.652	6.361	2.068	11.548	4.910	12.530	19.977	0.627	0.578	0.246	0.104	0.318	0.340	0.460	0.533
JSG O11_2	2	4.547	5.537	10.208	5.556	2.250	10.523	4.440	12.105	18.329	0.660	0.574	0.242	0.123	0.303	0.376	0.457	0.557
JSG O12_1	1	4.001	5.761	10.656	5.986	2.302	10.930	4.505	12.432	19.218	0.647	0.569	0.234	0.120	0.311	0.322	0.463	0.554
JSG O12_2	2	5.037	6.360	11.873	6.443	2.731	13.768	5.643	14.221	22.942	0.620	0.600	0.246	0.119	0.281	0.354	0.447	0.518
JSG P1_88	3	4.940	5.073	9.153	4.839	2.196	13.030	5.436	12.266	20.065	0.611	0.649	0.271	0.109	0.241	0.403	0.414	0.456
JSG P2_1	1	3.020	4.619	8.505	4.535	1.961	9.332	4.362	9.710	15.828	0.613	0.590	0.276	0.124	0.287	0.311	0.476	0.537

Sample	Outl. Qual.	a	b	c	Arr	Av	Ch	Cr	H	L	H/L	Ch/L	Cr/L	Av/L	Arr/L	a/H	b/H	c/L
JSG P4_1	2	4.308	5.119	8.935	4.404	2.423	11.025	4.364	11.682	17.853	0.654	0.618	0.244	0.136	0.247	0.369	0.438	0.501
JSG P6_1	2	5.142	5.893	10.764	6.216	2.397	11.197	5.745	12.646	19.811	0.638	0.565	0.290	0.121	0.314	0.407	0.466	0.543
JSG R1_1	1	2.815	3.678	7.216	3.463	1.670	8.804	3.293	8.256	13.937	0.592	0.632	0.236	0.120	0.248	0.341	0.445	0.518
JSG R3_2	2	0.479	0.738	1.337	0.701	0.346	1.423	0.736	1.602	2.470	0.649	0.576	0.298	0.140	0.284	0.299	0.461	0.541
JSG R4_1	1	2.230	2.702	6.053	3.070	1.229	7.703	2.330	7.069	12.003	0.589	0.642	0.194	0.102	0.256	0.315	0.382	0.504
JSG R4_2	1	1.982	2.884	6.541	3.363	1.036	8.374	2.968	7.289	12.773	0.571	0.656	0.232	0.081	0.263	0.272	0.396	0.512
JSG R6_7	1	2.216	2.742	6.117	2.765	1.167	8.834	2.486	7.268	12.766	0.569	0.692	0.195	0.091	0.217	0.305	0.377	0.479
JSG S1_1	1	1.529	1.845	3.241	1.800	0.785	4.012	1.747	4.235	6.597	0.642	0.608	0.265	0.119	0.273	0.361	0.436	0.491
JSG S3_2	2	1.719	1.925	3.690	2.103	1.104	4.470	1.749	4.748	7.677	0.618	0.582	0.228	0.144	0.274	0.362	0.406	0.481
JSG T1_1	1	3.769	5.290	9.278	4.280	2.157	10.653	4.493	11.886	17.090	0.695	0.623	0.263	0.126	0.250	0.317	0.445	0.543
JSG T1_2	2	4.164	5.447	9.681	5.106	1.984	10.936	4.715	11.637	18.026	0.646	0.607	0.262	0.110	0.283	0.358	0.468	0.537
JSG T2_1	3	3.931	5.278	10.257	5.003	2.024	12.303	4.732	11.753	19.329	0.608	0.636	0.245	0.105	0.259	0.334	0.449	0.531
JSG U1_93	3	3.678	4.300	9.691	4.464	1.969	11.517	4.762	10.760	17.950	0.599	0.642	0.265	0.110	0.249	0.342	0.400	0.540
JSG U2_1	3	4.384	4.759	9.180	5.173	2.285	9.397	5.186	10.610	16.855	0.629	0.558	0.308	0.136	0.307	0.413	0.449	0.545
JSG V5_1	1	2.450	3.366	6.432	2.583	1.511	8.116	2.788	7.942	12.210	0.650	0.665	0.228	0.124	0.212	0.309	0.424	0.527
JSG X_5	2	4.224	5.570	9.996	5.491	2.187	11.632	4.857	12.069	19.310	0.625	0.602	0.252	0.113	0.284	0.350	0.461	0.518
JSG Y6_1	1	4.304	5.534	9.763	5.593	2.599	10.441	5.093	11.711	18.633	0.629	0.560	0.273	0.139	0.300	0.367	0.473	0.524
JSG Y7_1	1	5.398	5.638	11.081	5.687	2.785	12.492	5.098	13.217	20.964	0.630	0.596	0.243	0.133	0.271	0.408	0.427	0.529
JSG Y8_1	1	4.807	5.742	10.349	5.336	1.999	11.966	4.792	12.875	19.301	0.667	0.620	0.248	0.104	0.276	0.373	0.446	0.536
JSG Y8_2	1	4.628	4.679	9.533	4.143	2.077	12.667	4.852	11.531	18.895	0.610	0.670	0.257	0.110	0.219	0.401	0.406	0.505
JSG Y9_1	1	4.046	4.640	8.148	3.905	1.580	10.621	3.449	10.779	16.105	0.669	0.659	0.214	0.098	0.242	0.375	0.430	0.506
JSG AA1_110	2	4.299	4.677	9.401	4.637	1.964	11.350	4.578	11.036	17.951	0.615	0.632	0.255	0.109	0.258	0.389	0.424	0.524
JSG AA2_113	2	4.314	4.830	9.340	3.984	1.958	12.540	4.776	11.905	18.482	0.644	0.679	0.258	0.106	0.216	0.362	0.406	0.505
JSG AA3_1	1	4.738	5.005	9.108	4.393	2.249	12.068	4.790	12.192	18.715	0.651	0.645	0.256	0.120	0.235	0.389	0.410	0.487
JSG AB1_114	1	3.250	3.824	7.034	3.132	1.658	8.792	3.860	8.760	13.582	0.645	0.647	0.284	0.122	0.231	0.371	0.437	0.518
JSG AD1_118	1	3.836	3.865	7.856	3.959	2.494	8.563	4.192	9.526	15.020	0.634	0.570	0.279	0.166	0.264	0.403	0.406	0.523
JSG AD1_119	2	3.582	4.436	8.841	3.934	2.095	10.673	4.418	10.166	16.701	0.609	0.639	0.265	0.125	0.236	0.352	0.436	0.529

Sample	Outl. Qual.	a	b	c	Arr	Av	Ch	Cr	H	L	H/L	Ch/L	Cr/L	Av/L	Arr/L	a/H	b/H	c/L
JSG AD3_1	2	3.670	3.705	7.552	3.579	2.183	8.969	4.208	9.432	14.731	0.640	0.609	0.286	0.148	0.243	0.389	0.393	0.513
JSG AE1_1	3	2.080	2.575	4.961	2.119	0.990	6.676	2.272	6.213	9.785	0.635	0.682	0.232	0.101	0.217	0.335	0.415	0.507
JSG AE2_1	2	1.860	2.401	4.345	2.286	1.050	5.193	2.228	5.631	8.529	0.660	0.609	0.261	0.123	0.268	0.330	0.426	0.509
JSG AF1_1	2	4.347	4.572	8.947	4.502	2.130	12.079	4.739	11.360	18.710	0.607	0.646	0.253	0.114	0.241	0.383	0.403	0.478
JSG AF2_1	3	3.229	3.876	7.101	3.741	1.709	9.183	3.729	9.627	14.633	0.658	0.628	0.255	0.117	0.256	0.335	0.403	0.485
JSG AJ1_1	2	1.997	2.669	4.784	2.558	1.182	6.043	2.310	5.989	9.783	0.612	0.618	0.236	0.121	0.261	0.334	0.446	0.489
JSG AJ2_1	2	1.635	2.135	4.407	1.894	0.898	5.942	1.729	5.467	8.735	0.626	0.680	0.198	0.103	0.217	0.299	0.390	0.504
JSG AK_1b1	3	1.475	1.445	2.466	1.638	0.742	2.533	1.544	3.453	4.913	0.703	0.516	0.314	0.151	0.333	0.427	0.418	0.502
JSG AK7_1	1	1.474	2.142	4.091	1.897	1.000	5.504	2.325	5.399	8.401	0.643	0.655	0.277	0.119	0.226	0.273	0.397	0.487
JSG AK8_1	1	1.657	1.919	3.854	1.790	0.841	4.760	1.614	4.719	7.391	0.638	0.644	0.218	0.114	0.242	0.351	0.407	0.521
JSG AK12_2	2	2.122	2.482	4.953	2.724	0.988	7.183	2.608	6.505	10.896	0.597	0.659	0.239	0.091	0.250	0.326	0.382	0.455
JSG AK12_5	2	1.533	1.555	2.376	1.125	0.849	2.894	1.270	3.559	4.868	0.731	0.594	0.261	0.174	0.231	0.431	0.437	0.488
JSG AK12_6	3	1.567	1.952	3.538	1.494	0.972	4.680	1.793	4.676	7.146	0.654	0.655	0.251	0.136	0.209	0.335	0.418	0.495
JSG AK14_1	2	2.728	2.895	6.143	2.960	1.441	8.220	2.651	7.776	12.621	0.616	0.651	0.210	0.114	0.235	0.351	0.372	0.487
JSG AK15_1	2	3.748	4.165	8.225	3.928	1.951	10.361	4.006	9.982	16.241	0.615	0.638	0.247	0.120	0.242	0.376	0.417	0.506
JSG AK17_1	1	2.050	3.483	6.856	2.869	1.094	9.763	3.520	8.096	13.726	0.590	0.711	0.256	0.080	0.209	0.253	0.430	0.499
JSG AK17_2	2	2.412	2.844	5.066	2.699	1.177	6.497	2.308	6.687	10.374	0.645	0.626	0.223	0.113	0.260	0.361	0.425	0.488
JSG AK18_1	1	1.954	2.079	4.141	2.202	1.204	5.408	1.907	5.617	8.815	0.637	0.614	0.216	0.137	0.250	0.348	0.370	0.470
JSG AL1_123	3faint	3.525	4.777	9.406	4.218	1.665	11.676	3.729	11.621	17.559	0.662	0.665	0.212	0.095	0.240	0.303	0.411	0.536
JSG AM1_1	2	3.846	4.283	7.642	4.019	2.466	9.012	4.470	10.138	15.496	0.654	0.582	0.288	0.159	0.259	0.379	0.422	0.493
JSG AM1_2	2	2.716	3.378	5.665	3.262	1.580	6.582	3.343	7.734	11.424	0.677	0.576	0.293	0.138	0.286	0.351	0.437	0.496
JSG AM2_2	2	2.228	3.105	6.160	3.077	1.218	8.389	3.239	7.567	12.684	0.597	0.661	0.255	0.096	0.243	0.294	0.410	0.486
JSG AM3_3	1	2.299	3.325	7.253	2.778	1.571	9.918	3.810	7.931	14.268	0.556	0.695	0.267	0.110	0.195	0.290	0.419	0.508
JSG AM3_4	1	2.589	2.827	5.632	3.492	1.536	7.590	3.085	7.853	12.618	0.622	0.601	0.245	0.122	0.277	0.330	0.360	0.446
JSG AN1_125	2	2.990	3.616	6.826	3.386	1.300	9.974	3.801	8.619	14.661	0.588	0.680	0.259	0.089	0.231	0.347	0.420	0.466
JSG AN1_126	2	2.748	3.247	6.302	3.720	1.412	8.855	2.910	8.780	13.987	0.628	0.633	0.208	0.101	0.266	0.313	0.370	0.451
JSG AN1_127	2	3.655	4.218	6.674	4.244	1.930	8.082	4.018	9.419	14.457	0.652	0.559	0.278	0.133	0.294	0.388	0.448	0.462

Sample	Outl. Qual.	a	b	c	Arr	Av	Ch	Cr	H	L	H/L	Ch/L	Cr/L	Av/L	Arr/L	a/H	b/H	c/L
JSG AN1_128	3	4.105	4.452	8.230	3.932	1.997	10.346	4.064	10.903	16.275	0.670	0.636	0.250	0.123	0.242	0.377	0.408	0.506
JSG AN1_129	2	2.733	3.173	7.278	3.414	1.373	9.927	2.619	9.370	14.714	0.637	0.675	0.178	0.093	0.232	0.292	0.339	0.495
JSG AN1b_2	2	4.064	4.775	8.194	5.385	2.415	8.443	4.787	10.638	16.243	0.655	0.520	0.295	0.149	0.332	0.382	0.449	0.504
JSG AN2_1	2	3.135	4.559	7.764	4.336	1.459	9.761	3.747	9.895	15.556	0.636	0.627	0.241	0.094	0.279	0.317	0.461	0.499
JSG AN4_1	2	3.821	4.996	8.634	4.429	1.983	10.925	4.523	11.025	17.337	0.636	0.630	0.261	0.114	0.255	0.347	0.453	0.498
JSG AN4_2	2	4.021	4.650	9.210	3.936	2.224	12.274	5.223	12.530	18.434	0.680	0.666	0.283	0.121	0.214	0.321	0.371	0.500
JSG AO2_3	2	3.680	5.406	10.806	5.635	2.020	12.599	5.421	12.079	20.254	0.596	0.622	0.268	0.100	0.278	0.305	0.448	0.534
JSG AO3_1	2	4.209	4.502	7.924	4.316	2.454	10.039	5.307	10.648	16.808	0.633	0.597	0.316	0.146	0.257	0.395	0.423	0.471
JSG AP1_133	3	2.185	3.441	7.017	3.036	1.221	10.181	4.599	8.230	14.438	0.570	0.705	0.319	0.085	0.210	0.265	0.418	0.486
JSG AP3_1	1	3.143	3.561	6.283	3.455	1.550	8.809	3.447	8.557	13.815	0.619	0.638	0.250	0.112	0.250	0.367	0.416	0.455

Table 7.1. Excavation JSG is subdivided into 16 segments and the corresponding litholog can be found in Fig. 7.1. Note that segments are numbered in reversed order according to the strata first excavated (top segment = #1; bottom-most segment = #16).

	Sediments	**Interpretation**
General remarks	- Sediments are generally coarsening and thickening upwards. - Clam shrimps occur throughout the section, mostly forming pavements on top of consecutive layers. Some are scattered within the matrix. - Gentle dip of strata (3-4°) with a variable but generally eastward direction. - Thin tuff horizons of µm and mm-scale are intercalated throughout Bed 2. Thicker units are marked in the litholog of Fig. 7.1. - Most of the material of Bed 3 is reworked.	- From base to top: Increasing energy level due to drainage of a river into Lake Sihetun. - Shallow level of wave activity. - Repeated volcano eruptions throughout Phase 2. Volcanic activity did not necessarily cease during Phase 3. However, there is only little evidence for volcanic activity during this phase, due to the reworking of sediments. - The silty claystones of Bed 2 correspond to environments of at least 5 m and most likely more than 10 m water depth. - The onset of Bed-3 sedimentation was probably not synchronous throughout the lake, but it is interpreted to represent a deepening of the lake due to a change in climate from dry to humid conditions. - Bed 3 stands for an intermediate environment characterized by intermittent wave agitation. Allen (1981) interpreted a water depth of 3-10 m for a similar environment.
Bed 2		
Segment 16	- Alternation of tuff layers (several mm to cm thick) and brownish-blackish mudstone rich in plant debris.	- Distal facies. The storm wave-base did not reach the basin floor. - The dark colour indicates less weathered conditions (Fig. 1.4).
Segment 15 (horizons AP-AN)	- µm-thick, allochthonous siliciclastic laminae, tuffaceous. - Occurrence of fish fossils within a slumping horizon.	- Distal facies. The storm wave-base did not reach the basin floor.
Segment 14 (horizons AL, AM)	- Heterogeneous sediments. - Pseudoripples between JSG AL and JSG 8ii. - Horizontal burrowing system infilled with tuff. - Organic-rich fibrous gypsum layer.	- Pseudoripples are created through quick tuff deposition.
Segment 13 (Horizon AK)	- Alternation of µm-thick, allochthonous siliciclastic laminae and calcareous mudstones.	- Distal facies. The storm wave-base did not reach the basin floor.
Segment 12 (Horizon AJ)	- Wavy-bedded laminae. - Laminae underlying segment 11 are folded for several cm before they die out downwards. - There is a 1 cm thick wood layer in association with fibrous gypsum (also 1 cm thick) that is mostly overlying the wood layer	- The wavy structures were generated through load-derived deformation as a result of fast sedimentation of the overlying tuff horizon.
Segment 11	- Ash-tuff layer	- Volcano eruption.

	Sediments	Interpretation
Segment 10 (horizons AI-AD)	- µm-thick, allochthonous siliciclastic laminae, tuffaceous	- Distal facies. The storm wave-base did not reach the basin floor.
Segment 9	- Alternation of tuff and reworked material. - Transition from Segment 10 to 9 marked by alleged desiccation cracks.	- Possible explanation for the desiccation cracks: Lake Sihetun has been interpreted as a caldera lake by Jiang et al. (2011). The considerably rapid shallowing of the lake was a consequence of the filling of a magma chamber and the resultant formation of a topographic high within the centre of the lake.
Segment 8 (Sedimentological transition)	- Finely laminated layers that are associated with prominent organic layers made up of wood fragments and plant remains. - cm-thick fibrous gypsum layers are associated with the organic layers. They are not stratiform.	- Gypsum layers are interpreted as secondary products of sulphide (pyrite) oxidization. - A lack of root horizons is indicative of an allochthonous origin of the plant material.
Bed 3		
Segment 7 (Horizons AC-P)	- Regular alternation of normal-graded siltstone and claystone. - 10.5 cm thick slumping horizon.	
Segment 6 (Horizons O-F)	- Normal-graded µm to mm-thick, fine sandstone to siltstone. Layers are notably thicker than those of segment 7. - Channel fills occurring.	- The increased sediment thickness is indicative of a shallowing of the lake.
Segment 5 (Horizon E)	- Tuff intercalated with wavy-bedded tuffaceous mudstone.	
Segment 4 (Horizon D)	- Same as segment 3, but finer.	
Segment 3 (Horizons A-C)	- Alternation of graded sandstone beds (0.2-5 cm thick) and claystones. - Collapse structures.	
Segment 2	- Interbedding of normal-graded coarser sandstone (Fsst < 1.9 cm thick) and siliciclastic mudstone. The basal parts of the sandstone layers are marked by mm-long mudclasts of the same grain size as the underlying mudstone. The sandstones are cross-bedded forming channels. - The base of segment 2 is marked by a concretionary layer. Concretions are oblate and cm-thick.	- High energy levels and the proximity to a river mouth are inferred. - Mudclasts are indicative of transportation.
Segment 1	- Normal-graded fine sandstone to siliciclastic mudstone, interbedded by sandstone layers. The basal parts of the sandstone layers are marked by mm-long mudclasts. - Scattered wood fragments. - Single layer with aligned flute casts of cm- to dm-scale.	- Sedimentary structures point to comparatively high energy levels that are associated with currents in the vicinity of a river mouth.

Table 7.2. Abundance matrix of 9 species in 43 sampled horizons, comprising 33226 quantitative specimen counts. The two counts of Ephemeropsis trisetalis in horizons A and C have each been scaled to an area of 50 cm^2. The area counted is given for each horizon and varies according to fossil density. Sample sizes range between 73 and 7251. Selected diversity indices (species richness, rarefied richness, and the Shannon index) are given for each horizon. The last column gives the number of mayfly larvae standardized to an excavated area of 10 m^2. Numbers in green indicate horizons of the Transitional Fauna.

	Eosestheria middendorfii	*Ephemeropsis trisetalis*	*Ephemeropsis* sp. B	*Karataviella* (water boatman)	oligochaete	caddisfly tube	*Liaoningogriphus*	gastropods	bivalves	Area (in cm^2)	Species Richness (*S*)	Rarefied Richness	Shannon *H'*	*Ephemeropsis trisetalis* per $10m^2$
JSG A	347	0.008	0	0	0	0	0	0	0	50	2	1	0.000	16
JSG B	2205	1	0	1	0	0	0	0	0	2560	3	1.07	0.008	39
JSG C	533	0.01	0	0	0	0	0	0	0	50	2	1	0.000	20
JSG D	886	7	0	0	0	0	0	0	0	3743	2	1.45	0.046	187
JSG E	83	0	0	0	0	0	0	0	0	34	1	1	0	0
JSG F	7251	0	0	0	0	0	0	0	0	5355	1	1	0	0
JSG G	309	0	0	0	0	0	0	0	0	121	1	1	0	0
JSG H	606	50	0	0	0	0	0	0	0	26257	2	2	0.269	190
JSG I	422	4	0	0	0	0	0	0	0	6985	2	1.53	0.053	57
JSG J	533	11	0	1	0	0	0	0	0	6955	3	1.93	0.112	158
JSG K	272	1	0	0	0	0	0	0	0	4418	2	1.27	0.024	23
JSG L	1775	0	0	0	0	0	0	0	0	1925	1	1	0	0
JSG M1	136	0	0	0	0	0	0	0	0	110	1	1	0	0
JSG M2	818	0	0	0	0	0	0	0	0	338	1	1	0	0
JSG N	176	0	0	0	0	0	0	0	0	86	1	1	0	0
JSG O	718	26	0	120	239	0	0	0	0	39250	4	3.83	0.941	66
JSG P	958	9	0	0	0	0	0	0	0	35600	2	1.51	0.053	25
JSG Q	0	9	0	74	0	0	0	0	0	28850	2	2	0.343	31
JSG R	1160	0	0	0	0	0	0	0	0	1000	1	1	0	0
JSG S	167	0	0	0	0	0	0	0	0	104	1	1	0	0
JSG T	305	81	0	335	0	0	0	0	0	13150	3	3	0.966	616
JSG U	86	20	0	41	0	0	2	0	0	12085	4	3.74	0.100	165

	Eosestheria middendorfii	*Ephemeropsis trisetalis*	*Ephemeropsis* sp. B	*Kataviella* (water boatman)	oligochaete	caddisfly tube	*Liaoningogriphus*	gastropods	bivalves	Area (in cm^2)	Species Richness (*S*)	Rarefied Richness	Shannon *H'*	*Ephemeropsis trisetalis* per $10m^2$
JSG V	14	73	0	191	107	1	1	0	0	31550	6	4.33	1.169	231
JSG W	3	17	0	33	84	0	0	0	0	22500	4	3.9	0.985	76
JSG X	11	88	0	143	240	0	0	0	0	20000	4	3.84	1.104	440
JSG Y	194	12	0	0	0	0	0	0	0	47100	2	2	0.222	25
JSG Z	0	127	16	1	0	1	0	0	0	40150	4	3.01	0.428	316
JSG AA	295	82	5	0	0	0	0	0	0	21200	3	2.66	0.587	387
JSG AB	232	45	3	0	281	0	0	0	0	32300	4	3.34	0.942	139
JSG AC	1	91	0	0	81	0	0	0	0	10400	3	2.42	0.723	875
JSG AD	1446	0	0	0	0	0	2	0	0	22400	2	1.1	0.010	0
JSG AE	1521	0	0	0	0	0	0	0	0	1595	1	1	0	0
JSG AF	365	4	0	0	0	0	0	0	0	27200	2	1.59	0.060	15
JSG AG	464	0	0	0	0	0	0	0	0	24600	1	1	0	0
JSG AH	854	0	0	0	0	0	0	0	0	15200	1	1	0	0
JSG AI	1409	1	0	0	0	0	0	0	0	19100	2	1.05	0.006	5
JSG AJ	1130	0	0	0	0	0	0	0	0	572	1	1	0	0
JSG AK	638	2	0	0	0	0	0	0	0	2600	2	1.22	0.021	77
JSG AL	142	0	0	0	0	0	0	0	0	18900	1	1	0	0
JSG AM	1355	8	0	0	0	1	0	0	0	7000	3	1.41	0.042	114
JSG AN	68	1	0	0	0	0	0	4	0	138	3	3	0.284	725
JSG AO	220	4	0	0	0	0	0	4	4	5000	4	3.35	0.260	80
JSG AP	267	27	0	0	0	0	0	11	21	25300	4	3.94	0.661	107

Table. 7.3. Test results for the randomness of the biostratinomic observations of *Ephemeropsis* larvae.

	n	**Rao's *U***	***p*(random)**	**Rayleigh's *R***	***p*(random)**
JSG H	43	259.5	0	0.771	1.96E-11
JSG J	11	169.1	0.056	0.8187	0.000119
JSG AA	83	308	0	0.760	2.1688E-20
JSG AB	49	271.8	0	0.7071	3.1407E-11
JSG AP	14	102.9	0.855	0.684	0.000696

References

Albrecht, C., Wilke, T. 2008. Ancient Lake Ohrid: biodiversity and evolution. – *Hydrobiologia* **615**: 103-140.

Allen, P.A. 1981. Devonian lake margin environments and processes, SE Shetland, Scotland. – *Journal of the Geological Society, London* **138**: 1-14.

Allison, P.A. 1988. *Konservat-Lagerstätten*: cause and classification. – *Paleobiology* **14**: 331-344.

Amiot, R., Wang, X., Zhou, Z., Wang, X., Buffetaut, E., Lécuyer, C., Ding, Z., Fluteau, F., Hibino, T., Kusuhashi, N., Mo, J., Suteethorn, V., Wang, Y., Xu, X., Zhang, F. 2011. Oxygen isotopes of East Asian dinosaurs reveal exceptionally cold Early Cretaceous climates. – *Proceedings of the National Academy of Sciences of the United States of America* **108**: 5179-5183.

Anderson, R.Y., Kirkland, D.W. 1960. Origin, varves, and cycles of Jurassic Todilto Formation, New Mexico. – *American Association of Petroleum Geologists Bulletin* **44**: 37-52.

Anderson, R.Y. 1964. Varve calibration of stratification. – *Kansas Geological Survey, Bulletin* **169**: 1-20.

Anderson, R.Y., Dean, W.E. 1988. Lacustrine varve formation through time. – *Palaeogeography, Palaeoclimatology, Palaeoecology* **62**: 215-235.

Anderson, R.Y., Dean, W.E., Bradbury, J.P. 1993. Elk Lake in perspective. *In:* Bradbury, J.P., Dean, W.E. (eds). Elk Lake, Minnesota: Evidence for rapid climate change in the North-Central United States: Boulder, Colorado, Geological Society of America Special Paper **276**: 1-6.

Andrews, S.D., Trewin, N.H., Hartley, A.J., Weedon, G.P. 2010. Solar variance recorded in lacustrine deposits from the Devonian and Proterozoic of Scotland. – *Journal of the Geological Society* **167**: 847-856.

Astin, T.R. 1990. The Devonian lacustrine sediments of Orkney, Scotland; implications for climate cyclicity, basin structure and maturation history. – *Journal of the Geological Society, London* **147**: 141-151.

Astrop, T.I., Park, L.E., Brown, B., Weeks, S.C. 2012. Sexual discrimination at work: Spinicaudatan 'Clam Shrimp' (Crustacea: Branchiopoda) as a model organism for the study of sexual system evolution. – *Palaeontologia Electronica* **15**: 1-15.

Audouin, M. 1837. Sèance du 1er fèvrier 1837. – *Annales de la Société Entomologique de France*, Tome 6: IX-XII.

Baas Becking, L.G.M, Kaplan, I.R., Moore, D. 1960. Limits of the natural environment in terms of pH and oxidation-reduction potentials. – *The Journal of Geology* **68**: 243-284.

Bailey, J.V., Raub, T.D., Meckler, A.N., Harrison, B.K., Raub, T.M.D., Green, A.M., Orphan, V.J. 2010. Pseudofossils in relict methane seep carbonates resemble endemic microbial consortia. – *Palaeogeography, Palaeoclimatology, Palaeoecology* **285**: 131-142.

Baird, G.C., Sroka, S.D., Shabica, C.W., Beard, T.L. 1985. Mazon Creek-type fossil assemblages in the U.S. midcontinent Pennsylvanian: their recurrent character and palaeoenvironmental significance. – *Philosophical Transactions of the Royal Society of London* **B 311**: 87-99.

Baird, W. 1849. Monograph of the family Limnadiadae, a family of entomostracous Crustacea. – *Proceedings of the Zoological Society of London* **17**: 84-90.

Baker, H. G. 1955. Self-compatibility and establishment after "long-distance" dispersal. – *Evolution* **9**: 347-349.

Balian, E.V., Segers, H., Lévèque, C., Martens, K. 2008. The freshwater animal diversity assessment: an overview of the results. – *Hydrobiologia* **595**: 627-637.

Barnes, R.D., Harrison, F.W. 1992. Introduction. *In:* Harrison, F.W., Humes, A.G. (eds.). Microscopic anatomy of invertebrates, Volume 9, Crustacea. – Wiley-Liss, New York.

Barrett, P.M. 2000. Evolutionary consequences of dating the Yixian Formation. – *Trends in Ecology and Evolution* **15**: 99-103.

Batzer, D.P., Wissinger, S.A. 1996. Ecology of insect communities in nontidal wetlands. – *Annual Review of Entomology* **41**: 75-100.

Bauernfeind, E., Moog, O. 2000. Mayflies (Insecta: Ephemeroptera) and the assessment of ecological integrity: a methodological approach. – *Hydrobiologia* **422/423**: 71-83.

Behr, H.-J. 2002. Magadiite and Magadi chert: a critical analysis of the silica sediments in the Lake Magadi Basin, Kenya. – *SEPM Special Publication* **73**: 257-273.

Berner, R.A. 1981. A new geochemical classification of sedimentary environments. – *Journal of sedimentary petrology* **51**: 359-365.

Berner, R.A. 1984. Sedimentary pyrite formation: An update. – *Geochimica et Cosmochimica Acta* **48**: 605-615.

Bishop, J.A. 1967a. Seasonal occurrence of a branchiopod crustacean, *Limnadia stanleyana* King (Conchostraca) in eastern Australia. – *Journal of Animal Ecology* **36**: 77-95.

Bishop, J.A. 1967b. Some adaptations of *Limnadia stanleyana* King (Crustacea: Branchiopoda: Conchostraca) to a temporary freshwater environment. – *Journal of Animal Ecology* **36**: 599-609.

Bishop, J.A. 1968. Aspects of the post-larval life history of *Limnadia stanleyana* King (Crustacea: Conchostraca). – *Australian Journal of Zoology* **16**: 885-895.

Blakemore, R. 1975. Magnetotactic Bacteria. – *Science* **190**: 377-379.

Bock, W. 1953. American Triassic estherids. – *Journal of Paleontology* **27**: 62-76.

Bonada, N., Zamora-Muñoz, C., Rieradevall, M., Prat, N. 2004. Ecological profiles of caddisfly larvae in Mediterranean streams: implications for bioassessment methods. – *Environmental Pollution* **132**: 509-521.

Bond, D., Wignall, P.B., Racki, G. 2004. Extent and duration of marine anoxia during the Frasnian-Famennian (Late Devonian) mass extinction in Poland, Germany, Austria and France. – *Geological Magazine* **141**: 173-193.

Bond, D., Wignall, P.B. 2005. Evidence for Late Devonian (Kellwasser) anoxic events in the Great Basin, western United States. *In:* Over, D.J., Morrow, J.R., Wignall, P.B. (eds). Understanding Late Devonian and Permian-Triassic biotic and climatic events: Towards an integrated approach. – *Developments in Palaeontology and Stratigraphy* **20**: 225-262.

Bond, D., Wignall, P.B. 2010. Pyrite framboid study of marine Permian-Triassic boundary sections: A complex anoxic event and its relationship to contemporaneous mass extinction. – *Geological Society of America Bulletin* **122**: 1265-1279.

Bourrelly, P. 1963. Loricae and cysts in the Chrysophyceae. – *Annals of the New York Academy of Sciences* **108**: 421-429.

Braak, C.J.F. ter 1985. Correspondence analysis of incidence and abundance data: properties in terms of a unimodal response model. – *Biometrics* **41**: 859-873.

Braband, A., Richter S., Hiesel, R., Scholtz, G. 2002. Phylogenetic relationships within the Phyllopoda (Crustacea, Branchiopoda) based on mitochondrial and nuclear markers. – *Molecular Phylogenetics and Evolution* **25**: 229-244.

Briggs, D.E.G., Raiswell, R., Bottrell, S.H., Hatfield, D., Bartels, C. 1996. Controls on the pyritization of exceptionally preserved fossils: an analysis of the Lower Devonian Hun-

srück Slate of Germany. – *American Journal of Science* **296**: 633-663.

Briggs, D.E.G., Stankiewicz, B.A., Meischner, D., Bierstedt, A., Evershed, R.P. 1998. Taphonomy of arthropod cuticles from Pliocene lake sediments, Willershausen, Germany. – *Palaios* **13**: 386-394.

Briggs, D.E.G. 1999. Molecular taphonomy of animal and plant cuticles: selective preservation and diagenesis. – *Philosophical Transactions of the Royal Society of London: Biological Sciences* **354**: 7-17.

Brtek, J., Thiéry, A. 1995. The geographic distribution of the European Branchiopods (Anostraca, Notostraca, Spinicaudata, Laevicaudata). – *Hydrobiologia* **298**: 263-280.

Burnaby, T.P. 1966. Growth-invariant discriminant functions and generalized distances. – *Biometrics* **22**: 96-110.

Burrows, M.T., Schoeman, D.S., Buckley, L.B., Moore, P., Poloczanska, E.S., Brander, K.M., Brown, C., Bruno, J.F. et al. 2011. The pace of shifting climate in marine and terrestrial ecosystems. – *Science* **334**: 652-655.

Butler, I.B., Rickard, D. 2000. Framboidal pyrite formation via the oxidation of iron (II) monosulfide by hydrogen sulphide. – *Geochimica et Cosmochimica Acta* **64**: 2665-2672.

Calvert, S.E., Thode, H.G., Yeung, D., Karlin, R.E. 1996. A stable isotope study of pyrite formation in the Late Pleistocene and Holocene sediments of the Black Sea. – *Geochimica et Cosmochimica Acta* **60**: 1261-1270.

Canfield, D.E., Raiswell, R. 1991. Pyrite formation and fossil preservation. *In:* Allison, P.A., Briggs, D.E.G. (eds). Taphonomy, Releasing the data locked in the fossil record. – Plenum Press, New York, pp. 337-388.

Chang, S., Zhang, H., Renne, P.R., Fang, Y. 2009. High-precision $^{40}Ar/^{39}Ar$ age for the Jehol Biota. – *Palaeogeography, Palaeoclimatology, Palaeoecology* **280**: 94-104.

Chen, I., Hill, J.K., Ohlemüller, R., Roy, D.B., Thomas, C.D. 2011. Rapid range shifts of species associated with high levels of climate warming. – *Science* **333**: 1024-1026.

Chen, P., Shen, Y. 1985. Fossil Conchostraca. – Science Press, Beijing. (in Chinese)

Chen, P. 1999a. Fossil conchostracans from the Yixian Formation of western Liaoning, China. – *Palaeoworld* **11**: 114-130. (in Chinese)

Chen, P. 1999b. Distribution and spread of the Jehol Biota. – *Palaeoworld* **11**: 1-6. (in Chinese)

Chen, P. 2003. Jurassic biostratigraphy of China. *In:* Zhang, W.-T., Chen, P.-J., Palmer, A.R. (eds.). Biostratigraphy of China. – Beijing, Science Press, pp. 423-463.

Chen, P., Li, G., Batten, D.J. 2007. Evolution, migration and radiation of late Mesozoic conchostracans in East Asia. – *Geological Journal* **42**: 391-413.

Cheng, R.H., Liu, Z.J., Wang, D.P. 1997. Types of filling sequences in the continental basins, examples from Mesozoic basins, western Liaoning province. – *Acta Sedimentologica Sinica* **15**: 166-170. (in Chinese)

Chi, Y.S. 1931. On the occurrence of fossil *Estheria* in China, and its geological significance. – *Bulletin of the Geological Society of China* **10**: 189-228.

Cloud, P. 1976. Beginnings of biospheric evolution and their biogeochemical consequences. – *Paleobiology* **2**:351-387.

Colwell, R.K., Mao, C.X., Chang, J. 2004. Interpolating, extrapolating, and comparing incidence-based species accumulation curves. – *Ecology* **85**: 2717-2727.

Crampton, J.S., Haines, A.J. 1996. Users' manual for programs Hangle, Hmatch, and Hcurve for the Fourier shape analysis of two-dimensional outlines. – Institute of Geological & Nuclear Sciences, Science Report.

Daday de Deés, E. 1915. Monographie systématique des Phyllopodes Conchostracés. – *Annales des Sciences Naturelles, Zoologie*, série 9, **20**: 39-330. (in Latin and French)

Dalingwater, J.E., Mutvei, H. 1990. Arthropod exoskeletons. *In:* Carter, J.G. (ed.). Skeletal biomineralization: Patterns, processes and evolutionary trends. – Van Nostrand Reinhold, New York, pp. 83-96.

Damgaard, J., Olesen, J. 1998. Distribution, phenology and status for the larger Branchiopoda (Crustacea: Anostraca, Notostraca, Spinicaudata and Laevicaudata) in Denmark. – *Hydrobiologia* **377**: 9-13.

Davis, J.C. 1986. Statistics and data analysis in geology. – John Wiley & Sons, New York.

Deevey, Jr., E.S. 1984. Stress, strain, and stability of lacustrine ecosystems. *In:* Haworth, E.Y., Lund, J.W.G. (eds). Lake sediments and environmental history, studies in palaeolimnology and palaeoecology in honour of Winifred Tutin. – University of Minnesota Press, Minneapolis, pp. 203-229.

Defretin-Lefranc, S. 1965. Etude et révision de Phyllopodes Conchostracés en provenance d'U.R.S.S. – *Annales de la Société Géologique du Nord* **85**: 15-48.

Degens, E.T., Okada, H., Honjo, S., Hathaway, J.C. 1972. Microcrystalline sphalerite in resin globules suspended in Lake Kivu, East Africa. – *Mineralium Deposita* **7**: 1-12.

Depéret, M.C., Mazeran, M.P. 1912. Les Estheria du Permien d'Autun. – *Bulletin de la Société d'Histoire Naturelle d'Autun* **25**: 165-174.

Ding, Q., Zhang, L., Guo, S., Zhang, C., Peng, Y., Jia, B., Chen, S., Xing, D. 2003. Paleoclimatic and palaeoenvironmental proxies of the Yixian Formation in the Beipiao area, western Liaoning. – *Geological Bulletin of China* **22**:186-191. (in Chinese)

Dixit, A.S., Dixit, S.S. 1989. Surface-sediment chrysophytes from 35 Quebec lakes and their usefulness in reconstructing lake-water pH. – *Canadian Journal of Botany* **67**: 2071-2076.

Donald, D.B. 1989. First Canadian record for the clam shrimp *Caenestheriella belfragei* (Crustacea: Conchostraca). – *The Canadian Field-Naturalist* **103**: 593-594.

Duff, K.E., Zeeb, B.A., Smol, J.P. 1995. Atlas of chrysophycean cysts. *In:* Dumont, H.J. (ed.). Developments in Hydrobiology. – Kluwer Academic Publishers, Dordrecht, pp. 1-189.

Elliott, J.C. 2002. Calcium phosphate biominerals. *In:* Kohn, M.J., Rakovan, J., Hughes, J.M. (eds.). Phosphates: Geochemical, geobiological, and materials importance. – *Reviews in Mineralogy and Geochemistry* **48**: 427-453.

Eloranta, P. 1995. Biogeography of chrysophytes in Finnish lakes. *In:* Sandgren, C.D., Smol, J.P., Kristiansen, J. (eds). Chrysophyte algae, ecology, phylogeny and development. – Cambridge University Press, Cambridge, pp. 214-231.

Emberton, K.C. 1980. Ecology of a fall population of the clam shrimp *Caenestheriella gynecia* Mattox (Crustacea: Conchostraca). – *Ohio Journal of Science* **80**: 156-159.

Enkin, R.J., Yang, Z., Chen, Y., Courtillot, V. 1992. Paleomagnetic constraints on the geodynamic history of the major blocks of China from the Permian to the Present. – *Journal of Geophysical Research* **97**: 13953-13989.

Faith, D.P., Minchin, P.R., Belbin, L. 1987. Compositional dissimilarity as a robust measure of ecological distance. – *Vegetatio* **69**: 57-68.

Farina, M., Esquivel, D.M.S., Lins de Barros, H.G.P. 1990. Magnetic iron-sulphur crystals from a magnetotactic microorganism. – *Nature* **343**: 256-258.

Farrand, M. 1970. Framboidal sulphides precipitated synthetically. – *Mineralium Deposita* **5**: 237-247.

Fassbinder, J.W.E., Stanjek, H., Vali, H. 1990. Occurrence of magnetic bacteria in soil. – *Nature* **343**: 161-163.

Fedotov, A.P., Semenov, M.Y., Osipov, E.Y., Vorobyova, S.S., Golobokova, L.P. 2003. Evidence of Lake Khubsugul volume decrease due to climate aridization in Upper Pleistocene. *In:* Ivanov, A., Coulter, G., Timoshkin, O., Riedel, F. (eds.). Speciation in ancient lakes, SIAL III, Proceedings of the International Symposium. – *Berliner Paläobiologische Abhandlungen* **4**: 89-95.

Fisher, R.A. 1936. The use of multiple measurements in taxonomic problems. – *Annals of Eugenics* **7**: 179-188.

Foote, M. 2003. Origination and extinction through the Phanerozoic: A new approach. – *The Journal of Geology* **111**: 125-148.

Frank, P.W. 1988. Conchostraca. – *Palaeogeography, Palaeoclimatology, Palaeoecology* **62**: 399-403.

Frankel, R.B., Blakemore, R.P., Torres de Araujo, F.F., Esquivel, D.M.S., Danon, J. 1981. Magnetotactic Bacteria at the Geomagnetic Equator. – *Science* **212**: 1269-1270.

Fry, B., Jannasch, H.W., Molyneaux, S.J., Wirsen, C.O., Muramoto, J.A., King, S. 1991. Stable isotope studies of the carbon, nitrogen and sulfur cycles in the Black Sea and the Cariaco Trench. – *Deep-Sea Research* **38**: S1003-S1019.

Fryer, G. 1987. A new classification of the branchiopod Crustacea. – *Zoological Journal of the Linnean Society* **91**: 357-383.

Fürsich, F.T., Sha, J., Jiang, B., Pan, Y. 2007. High resolution palaeoecological and taphonomic analysis of Early Cretaceous lake biota, western Liaoning (NE-China). – *Palaeogeography, Palaeoclimatology, Palaeoecology* **253**: 434-457.

Gall, J.-C., Grauvogel-Stamm, L. 2005. The early Middle Triassic 'Grès à Voltzia' Formation of eastern France: a model of environmental refugium. – *Comptes Rendus Palevol* **4**: 637-652.

Gingerich, P.D. 1985. Species in the fossil record: concepts, trends, and transitions. – *Paleobiology* **11**: 27-41.

Gingerich, P.D. 2000. Arithmetic or geometric normality of biological variation: an empirical test of theory. – *Journal of Theoretical Biology* **204**: 201-221.

Gingerich, P.D. 2003. Land-to-sea transition in early whales: evolution of Eocene Archaeoceti (Cetacea) in relation to skeletal proportions and locomotion of living semiaquatic mammals. – *Paleobiology* **29**: 429-454.

Goretzki, J. 2003. Biostratigraphy of conchostracans: A key for the interregional correlations of the continental Palaeozoic and Mesozoic – Computer-aided pattern analysis and shape statistics to classify groups being poor in characteristics. Dissertation, Technische Universität Bergakademie Freiberg.

Grabau, A.W. 1928. Stratigraphy of China, Part 2, Mesozoic. – Geological Survey of China, Peking.

Grube, E. 1865. Ueber die Gattungen *Estheria* und *Limnadia* und einen neuen *Apus*. – Nicolaische Verlagsbuchhandlung, Berlin.

Gu, Z. 1962. The Jurassic and Cretaceous of China. – Science Press, Beijing. (in Chinese)

Haberyan, K.A., Hecky, R.E. 1987. The late Pleistocene and Holocene stratigraphy and paleolimnology of Lakes Kivu and Tanganyika. – *Palaeogeography, Palaeoclimatology, Palaeoecology* **61**: 169-197.

Haines, A.J., Crampton, J.S. 2000. Improvements to the method of fourier shape analysis as applied in morphometric studies. – *Palaeontology* **43**: 765-783.

Hairston, N.G., Fussmann, G.F. 2014. Lake ecosystems. *In:* Encyclopaedia of Life Sciences (eLS). – Wiley, Chichester.

Hammer, Ø., Harper, D.A.T., Ryan, P.D. 2001. PAST: Paleontological statistics software package for education and data analysis. – *Palaeontologia Electronica* **4**: 1-9.

Hammer, Ø., Harper, D. 2006 Paleontological data analysis. – Blackwell Publishing.

Hartley, A.J. 1993. A depositional model for the Mid-Westphalian A to late Westphalian B Coal Measures of South Wales. – *Journal of the Geological Society, London*, **150**: 1121-1136.

He, H.Y., Wang, X.L., Zhou, Z.H., Jin, F., Wang, F., Yang, L.K., Ding, X., Boven, A., Zhu, R.X. 2006. $^{40}Ar/^{39}Ar$ dating of Lujiatun Bed (Jehol Group) in Liaoning, northeastern China. – *Geophysical Research Letters* **33**: L04303.

Hennebert, M., Lees, A. 1991. Environmental gradients in carbonate sediments and rocks detected by correspondence analysis: examples from the Recent of Norway and the Dinantian of southwest England. – *Sedimentology* **38**: 623-642.

Hethke, M., Fürsich, F.T., Jiang, B., Pan, Y. 2013a. Seasonal to sub-seasonal palaeoenvironmental changes in Lake Sihetun (Lower Cretaceous Yixian Formation, NE China). – *International Journal of Earth Sciences* **102**: 351-378.

Hethke, M., Fürsich, F.T., Jiang B., Klaus R. 2013b. Oxygen deficiency in Lake Sihetun; formation of the Lower Cretaceous Liaoning Fossillagerstätte (China). – *Journal of the Geological Society, London*, **170**: 817-831.

Hiltunen, J.K. 1967. Some oligochaetes from Lake Michigan. – *Transactions of the American Microscopical Society* **86**: 433-454.

Hoeh, W.R., Smallwood, N.D., Senyo, D.M., Chapman, E.G., Weeks, S.C. 2006. Evaluating the monophyly of *Eulimnadia* and the Limnadiinae (Branchiopoda: Spinicaudata) using DNA sequences. – *Journal of Crustacean Biology* **26**: 182-192.

Holub, V., Kozur, H. 1981. Revision einiger Conchostracen-Faunen des Rotliegenden und biostratigraphische Auswertung der Conchostracen des Rotliegenden. – *Geologisch-Paläontologische Mitteilungen Innsbruck* **11**: 39-94.

Horne, F.R. 1971. Some effects of temperature and oxygen concentration on phyllopod ecology. – *Ecology* **52**: 343-347.

Hu, Y., Meng, J., Wang, Y., Li, C. 2005. Large Mesozoic mammals fed on young dinosaurs. – *Nature* **433**: 149-152.

Huxley, J.S. 1932. Problems of relative growth. – Methuen & Co. LTD., London.

Itô, T., Schram, F.R. 1988. Gonopores and the reproductive system of nectiopodan Remipedia. – *Journal of Crustacean Biology* **8**: 250-253.

Jiang, B., Sha, J. 2006. Late Mesozoic stratigraphy in western Liaoning, China: A review. – *Journal of Asian Earth Sciences* **28**: 205-217.

Jiang, B., Sha, J. 2007. Preliminary analysis of the depositional environments of the Lower Cretaceous Yixian Formation in the Sihetun area, western Liaoning, China. – *Cretaceous Research* **28**: 183-193.

Jiang, B., Fürsich, F.T., Sha, J., Wang, B., Niu, Y. 2011. Early Cretaceous volcanism and its impact on fossil preservation in Western Liaoning, NE China. – *Palaeogeography, Palaeoclimatology, Palaeoecology* **302**: 255-269.

Jiang, B., Fürsich, F.T., Hethke, M. 2012. Depositional evolution of the Early Cretaceous Sihetun Lake and implications for regional climatic and volcanic history in western Liaoning, NE China. – *Sedimentary Geology* **257-260**: 31-44.

Jolicoeur, P. 1963. The multivariate generalization of the allometry equation. – *Biometrics* **19**: 497-499.

Jolliffe, I.T. 1986. Principal Component Analysis. – Springer.

Jones, B., Manning, D.A.C. 1994. Comparison of geochemical indices used for the interpretation of palaeoredox conditions in ancient mudstones. – *Chemical Geology* **111**: 111-129.

Jones, T.R. 1862. A monograph of the fossil Estheriae. – *The Palaeontographical Society, London*.

Kaliszewicz, A. 2003. Sublethal predation on *Stylaria lacustris*: a study of regenerative capabilities. – *Hydrobiologia* **501**: 83-92.

Kampstra, P. 2008. Beanplot: A boxplot alternative for visual comparison of distributions. – *Journal of Statistical Software* **28**: 1-9.

Kelts, K., Hsü, K.J. 1978. Freshwater carbonate sedimentation. *In:* Lerman, A. (ed.). Lakes - chemistry, geology, physics. – Springer, New York, pp. 295-323.

Kile, D.E., Eberl, D.D., Hoch, A.R., Reddy, M.M. 2000. An assessment of calcite crystal growth mechanisms based on crystal size distributions. – *Geochimica et Cosmochimica Acta* **64**: 2937-2950.

Kirkland, D.W. 2003. An explanation for the varves of the Castile evaporites (Upper Permian), Texas and New Mexico, USA. – *Sedimentology* **50**: 899-920.

Kobayashi, T., Huzita, A. 1943. On *Estherites*, new genus. – *The Journal of the Geological Society of Japan* **50**: 196-202. (in Japanese, with English abstract)

Kobayashi, T., Kusumi, H. 1953. A study on *Estherites middendorfii* (Jones). – *Japanese Journal of Geology and Geography* **23**: 1-24.

Kobayashi, T. 1954. Fossil estherians and allied fossils. – Journal of the Faculty of Science, University of Tokyo, vol. 9, pp. 1-192.

Kobayashi, T. 1972. On the two discontinuities in the history of the order Conchostraca. – *Proceedings of the Japan Academy* **48**: 725-729.

Kowalewski, M., Dyreson, E., Marcot, J.D., Vargas, J.A., Flessa, K.W., Hallman, D.P. 1997. Phenetic discrimination of biometric simpletons: paleobiological implications of morphospecies in the lingulide brachiopod *Glottidia*. – *Paleobiology* **23**: 444-469.

Kozur, H. 1982. Beiträge zur Taxonomie und stratigraphischen Auswertung der untertriassischen Conchostracen. – *Geologisch-Paläontologische Mitteilungen Innsbruck* **11**: 355-398.

Kozur, H., Seidel, G. 1983. Revision der Conchostracen-Faunen des unteren und mittleren Buntsandsteins. Teil I. – *Zeitschrift für geologische Wissenschaften* **11**: 295-423.

Kozur, H.W., Weems, R.E. 2005. Conchostracan evidence for a late Rhaetian to early Hettangian age for the CAMP volcanic event in the Newark Supergroup, and a Sevatian (late Norian) age for the immediately underlying beds. – *Hallesches Jahrbuch für Geowissenschaften, Reihe B: Geologie, Paläontologie, Mineralogie* **27**: 21-51.

Kozur, H.W., Weems, R.E. 2010. The biostratigraphic importance of conchostracans in the continental Triassic of the northern hemisphere. *In:* Lucas, S.G. (ed.). The Triassic Timescale. – *Geological Society, London, Special Publications* **334**: 315-417.

Krauskopf, K.B., Bird, D.K. 1995. Introduction to geochemistry. McGraw-Hill, 3rd edition, 647 pp.

Kuhl, F.P., Giardina, C.R. 1982. Elliptic fourier features of a closed contour. – *Computer Graphics and Image Processing* **18**: 236-258.

Kummerow, E.H.E. 1939. Die Ostrakoden und Phyllopoden des deutschen Unterkarbons. – *Abhandlungen der Preußischen Geologischen Landesanstalt* **194**: 1-107.

Langbein, W.B., Schumm, S.A. 1958. Yield of sediment in relation to mean annual precipitation. – *Transactions American Geophysical Union* **39**:1076-1084.

Leng, Q., Yang, H. 2003. Pyrite framboids associated with the Mesozoic Jehol Biota in northeastern China: Implications for microenvironment during early fossilization. – *Progress in Natural Science* **13**: 206-212.

Li, G., Batten, D.J. 2004a. *Cratostracus*? *cheni*, a new conostracan species from the Yixian Formation in western Liaoning, north-east China, and its age implications. – *Cretaceous Research* **25**: 577-584.

Li, G., Batten D.J. 2004b. Revision of the conchostracan genera *Cratostracus* and *Porostracus* from Cretaceous deposits in north-east China. – *Cretaceous Research* **25**: 919-926.

Li, G., Batten, D.J. 2005. Revision of the conchostracan genus *Estherites* from the Upper Cretaceous Nenjiang Formation of the Songliao Basin and its biogeographic significance in China. – *Cretaceous Research* **26**: 920-929.

Li, G., Shen, Y., Batten, D.J. 2007. *Yanjiestheria*, *Yanshania* and the development of the *Eosestheria* conchostracan fauna of the Jehol Biota in China. – *Cretaceous Research* **28**: 225-234.

Li, J., Batten, D.J. 2007: Palynological evidence of an Early Cretaceous age for the Yixian Formation at Sihetun, western Liaoning, China. – *Cretaceous Research* **28**: 333-338.

Li, W., Liu, Z. 1999. Sporomorph assemblage from the basal Yixian Formation in western Liaoning and its geological age. – *Palaeoworld* **11**: 68-79. (in Chinese)

Linder, F. 1945. Affinities within the Branchiopoda, with notes on some dubious fossils. – *Arkiv för Zoologi* **37**: 1-28.

Lindqvist, J.K., Lee, D.E. 2009. High-frequency paleoclimate signals from Foulden Maar, Waipiata Volcanic Field, southern New Zealand: An Early Miocene varved lacustrine diatomite deposit. – *Sedimentary Geology* **222**: 98-110.

Link, E., Fürsich, F.T. 2001. Hochauflösende Feinstratigraphie und Mikrofaziesanalyse der Oberjura-Plattenkalke von Painten, Südliche Frankenalb. – *Archaeopteryx* **19**: 71-88.

Liu, T., Liu, J., Chu, G., 2002. Early Cretaceous maars, depositional environments and their relationship to the fossil preservation in Sihetun, Liaoning, Northeast China. *In:* Zhou, Z., Zhang, F. (eds). Proceedings of the 5th Symposium of the Society of Avian Paleontology and Evolution, pp. 307-311.

Löhlein, B. 1996. Seasonal dynamics of aufwuchs Naididae (Oligochaeta) on *Phragmites australis* in a eutrophic lake. – *Hydrobiologia* **334**:115-123.

Lotter, A.F. 1989. Evidence of annual layering in Holocene sediments of Soppensee, Switzerland. – *Aquatic Sciences* **51**: 19-30.

Lucas, S.G., Milner, A.R.C. 2006. Conchostraca from the Lower Jurassic Whitmore Point Member of the Moenave Formation, Johnson Farm, southwestern Utah. *In:* Harris et al. (eds). The Triassic-Jurassic terrestrial transition. – *New Mexico Museum of Natural History and Science Bulletin* **37**: 421-423.

Machado, M., Cristo, M., Reis, J., Cancela da Fonseca, L. 1999. Biological data on *Triops cancriformis mauritanicus* (Ghigi, 1921) and *Cyzicus grubei* (Simon, 1886) – Crustacea, Branchiopoda – in SW Portugal temporary ponds. – *Limnetica* **16**: 1-7.

Mann, S., Sparks, N.H.C., Frankel, R.B., Bazylinski, D.A., Jannasch, H.W. 1990. Biomineralization of ferrimagnetic greigite (Fe_3S_4) and iron pyrite (FeS_2) in a magnetotactic bacterium. – *Nature* **343**: 258-261.

Marcus, V., Weeks, S.C. 1997. The effects of pond duration on the life history traits of an ephemeral pond crustacean, *Eulimnadia texana*. – *Hydrobiologia* **359**: 213-221.

Mardia, K.V. 1970. Measures of multivariate skewness and kurtosis with applications. – *Biometrika* **57**: 519-530.

Martens, K. 1997. Speciation in ancient lakes. – *TREE* **12**: 177-182.

Martens, K., Schön, I. 1999. Crustacean biodiversity in ancient lakes: A review. – *Crustaceana* **72**: 899-910.

Martens, T. 1985. Taxonomische Probleme der Conchostraca (Crustacea, Phyllopoda) unter besonderer Berücksichtigung der Variabilität des Carapax. – *Freiberger Forschungshefte* **C400**: 44-76. (in German)

Martin, J.W. 1992. Branchiopoda. *In:* Harrison, F.W., Humes, A.G. (eds.). Microscopic anatomy of invertebrates, Volume 9, Crustacea. – Wiley-Liss, New York.

Martin, J.W., Davis, G.E. 2001. An updated classification of the recent Crustacea. – *Natural History Museum of Los Angeles County, Science Series* **39**: 1-124.

Mathias, P. 1937. Biologie des Crustacés Phyllopodes. – Hermann et Cie, Paris.

Mattox, N.T. 1939. Description of two new species of the genus *Eulimnadia* and notes on the other Phyllopoda of Illinois. – *American Midland Naturalist* **22**: 642-653.

Mattox, N.T. 1950. Notes on the life history and description of a new species of conchostracan phyllopod, *Caenestheriella gynecia*. – *Transactions of the American Microscopical Society* **69**: 50-53.

Mattox, N.T., Velardo, J.T. 1950. Effect of temperature on the development of the eggs of a conchostracan phyllopod, *Caenestheriella gynecia*. – *Ecology* **31**: 497-506.

Merinero, R., Lunar, R., Somoza, L., Díaz-Del-Río, V., Martínez-Frías, J. 2009. Nucleation, growth and oxidation of framboidal pyrite associated with hydrocarbon-derived submarine chimneys: lessons learned from the Gulf of Cadiz. – *European Journal of Mineralogy* **21**: 947-961.

Milligan, G.W. 1980. An examination of the effect of six types of error perturbation on fifteen clustering algorithms. – *Psychometrika* **45**: 325-342.

Mitteroecker, P., Gunz, P., Bernhard, M., Schaefer, K., Bookstein, F.L. 2004. Comparison of cranial ontogenetic trajectories among great apes and humans. – *Journal of Human Evolution* **46**: 679-698.

Monferran, M.D., Gallego, O.F., Astrop, T.I., Cabaleri, N. 2013. Autecology of *Wolfestheria smekali* (Spinicaudata) from the Upper Jurassic (Cañadón Asfalto Formation), Patagonia, Argentina. – *Palaeogeography, Palaeoclimatology, Palaeoecology* **392**: 52-61.

Moore, W.G., Burn, A. 1968. Lethal oxygen thresholds for certain temporary pond invertebrates and their applicability to field situations. – *Ecology* **49**: 349-351.

Müller, G., Irion, G., Förstner, U. 1972. Formation and diagenesis of inorganic Ca-Mg carbonates in the lacustrine environment. – *Naturwissenschaften* **59**: 158-164.

Muramoto, J.A., Honjo, S., Fry, B., Hay, B.J., Howarth, R.W., Cisne, J.L. 1991. Sulfur, iron and organic carbon fluxes in the Black Sea: sulfur isotopic evidence for origin of sulfur fluxes. – *Deep-Sea Research* **38**: S1151-S1187.

Nayar, A. 2009. A lakeful of trouble. – *Nature* **460**: 321-323.

Nielsen, J.K., Shen, Y. 2004. Evidence for sulfidic deep water during the Late Permian in the East Greenland Basin. – *Geology* **32**: 1037-1040.

Novojilov, N. 1960. Subclass Gnathostraca. *In:* Orlov, J.A. (ed.). Osnovy paleontologii: Členistonogie – trilobitoobraznye i rakoobraznye (N.E. Černyševa, ed.). – Gosudarstvennoe Naučno-Tehničeskoe Izdatel'stvo Literatury po Geologii i Ohranie Nedr, Moskva, pp. 216-253. (in Russian)

Novojilov, N. 1970. Conchostraca, Limnadioidea. – Nauka, Moscow. (in Russian)

Ohfuji, H., Rickard, D. 2005. Experimental syntheses of framboids – a review. – *Earth-Science Reviews* **71**: 147-170.

Olempska, E. 2004. Late Triassic spinicaudatan crustaceans from southwestern Poland. – *Acta Palaeontologica Polonica* **49**: 429-442.

Olesen, J., Grygier, M.J. 2004. Larval development of Japanese 'conchostracans': part 2, larval development of *Caenestheriella gifuensis* (Crustacea, Branchiopoda, Spinicaudata, Cyzicidae), with notes on homologies and evolution of certain naupliar appendages within the Branchiopoda. – *Arthropod Structure & Development* **33**: 453-469.

Olsen, P.E. 1986. A 40-million-year lake record of Early Mesozoic orbital climatic forcing. – *Science* **234**: 842-848.

Orr, P.J., Briggs, D.E.G. 1999. Exceptionally preserved conchostracans and other crustaceans from the Upper Carboniferous of Ireland. – *Special Papers in Palaeontology* **62**: 1-68.

Orr, P.J., Briggs, D.E.G., Kearns, S.L. 2008. Taphonomy of exceptionally preserved crustaceans from the Upper Carboniferous of southeastern Ireland. – *Palaios* **23**: 298-312.

Ozawa, H. 2013. The history of sexual dimorphism in Ostracoda (Arthropoda, Crustacea) since the Palaeozoic. *In:* Moriyama, H. (ed.). Sexual dimorphism. – InTech, doi: 10.5772/55329. Available from www.intechopen.com/books/sexual-dimorphism/

Packard, A.S. 1877. A monograph of the phyllopod Crustacea of North America, with remarks on the order Phyllocarida. – *Geological Survey of the Territories*: 295-809.

Pan, Y., Sha, J., Fürsich, F.T., Wang, Y., Zhang, X., Yao, X. 2012. Dynamics of the lacustrine fauna from the Early Cretaceous Yixian Formation, China: implications of volcanic and climatic factors. – *Lethaia* **45**: 299-314.

Pan, Y., Sha, J., Zhou, Z., Fürsich, F.T. 2013. The Jehol Biota: Definition and distribution of exceptionally preserved relicts of a continental Early Cretaceous ecosystem. – *Cretaceous Research* **44**: 30-38.

Parmesan, C., Yohe, G. 2003. A globally coherent fingerprint of climate change impacts across natural systems. – *Nature* **421**: 37-42.

Peckmann, J., Reimer, A., Luth, U., Luth, C., Hansen, B.T., Heinicke, C., Hoefs, J., Reitner, J. 2001. Methane-derived carbonates and authigenic pyrite from the northwestern Black Sea. – *Marine Geology* **177**: 129-150.

Petzold, D.D., Lane, N.G. 1988. Stratigraphic distribution and paleoecology of Pennsylvanian conchostracans (Crustacea: Branchiopoda) on the east side of the Illinois Basin. – *Journal of Paleontology* **62**: 799-808.

Pianka, E.R. 1970. On *r*- and *K*-selection. – *The American Naturalist* **104**: 592-597.

Poloczanska, E.S., Brown, C.J., Sydeman, W.J., Kiessling, W., Schoeman, D.S., Moore, P.J., Brander, K., Bruno, J.F., Buckley, L.B. *et al*. 2013. Global imprint of climate change on marine life. – *Nature Climate Change* **3**: 919-925.

Ragotzkie, R.A. 1978. Heat Budgets of lakes. *In:* Lerman, A. (ed.). Lakes - chemistry, geology, physics. – Springer, New York.

Raymond, P.E. 1946. The genera of fossil Conchostraca – an order of bivalved Crustacea. – *Bulletin of the Museum of Comparative Zoology at Harvard College* **96**: 217-307.

Reed, S.J.B. 2005. Electron microprobe analysis and scanning electron microscopy in geology. – Cambridge University Press, Cambridge.

Reyment, R.A., Savazzi, E. 1999. Aspects of multivariate statistical analysis in Geology. – Elsevier, Amsterdam.

Richter, S., Timms, B.V. 2005. A list of the Recent clam shrimps (Crustacea: Laevicaudata, Spinicaudata, Cyclestherida) of Australia, including a description of a new species of *Eocyzicus*. – *Records of the Australian Museum* **57**: 341-354.

Rickard, D.T. 1970. The origin of framboids. – *Lithos* **3**: 269-293.

Rieder, N., Abaffy, P., Hauf, A., Lindel, M., Weishäupl, H. 1984. Funktionsmorphologische Untersuchungen an den Conchostracen *Leptestheria dahalacensis* und *Limnadia lenticularis* (Crustacea, Phyllopoda, Conchostraca). – *Zoologische Beiträge Neue Folge* **28**: 417-444.

Roessler, E.W. 1995. Review of Colombian Conchostraca (Crustacea) – ecological aspects and life cycles – families Lynceidae, Limnadiidae, Leptestheriidae and Metalimnadiidae. – *Hydrobiologia* **298**: 125-132.

Rohlf, F.J., Bookstein, F.L. 1987. A comment on shearing as a method for "size correction". – *Systematic Zoology* **36**: 356-367.

Rohlf, F.J. 1990. Morphometrics. – *Annual Review of Ecology and Systematics* **21**: 299-316.

Ross, D.A., Degens, E.T. 1974. Recent sediments of Black Sea. *In:* Degens, E.T., Ross, D.A. (eds). The Black Sea – Geology, chemistry, and biology. – *The American Association of Petroleum Geologists*, Tulsa, Memoir **20**: 183-199.

Sars, G.O. 1896. Fauna Norvegiae. Descriptions of the Norwegian species at present known, belonging to the sub-orders Phyllocarida and Phyllopoda. – *Christiania*, pp. 1-140.

Sars, G.O. 1898. Description of two additional South African Phyllopoda. – *Archiv for Mathematik og Naturvidenskab* **20**: 1-23.

Sars, G.O. 1900. On some Indian Phyllopoda. – *Archiv for Mathematik og Naturvidenskab* **22**: 1-30.

Sassaman, C. 1989. Inbreeding and sex ratio variation in female-biased populations of a clam shrimp, *Eulimnadia texana*. – *Bulletin of Marine Science* **45**: 425-432.

Sassaman, C. 1991. Sex ratio variation in female-biased populations of notostracans. – *Hydrobiologia* **212**: 169-179.

Sassaman, C. and Weeks, S.C. 1993. The genetic mechanism of sex determination in the conchostracan shrimp *Eulimnadia texana*. – *The American Naturalist* **141**: 314-328.

Sassaman, C. 1995. Sex determination and evolution of unisexuality in the Conchostraca. – *Hydrobiologia* **298**: 45-65.

Scanabissi Sabelli, F., Tommasini, S. 1990. Occurrence of *Leptestheria dahalacensis* Rüppell, 1837 and *Eoleptestheria ticinensis* (Balsamo-Crivelli, 1859) (Conchostraca, Leptestheriidae) in Emilia-Romagna, Italy; new morphological data. – *Crustaceana* **59**: 259-264.

Schäfer, A. 2005. Klastische Sedimente, Fazies und Sequenzstratigraphie. – Spektrum, München.

Schieber, J. 2002. The role of an organic slime matrix in the formation of pyritized burrow trails and pyrite concretions. – *Palaios* **17**: 104-109.

Schopf, T.J.M, Raup, D.M., Gould S.J, Simberloff, D.S. 1975. Genomic versus morphologic rates of evolution: influence of morphologic complexity. – *Paleobiology* **1**: 63-70.

Schwentner, M., Timms, B.V., Bastrop, R., Richter, S. 2009. Phylogeny of Spinicaudata (Branchiopoda, Crustacea) based on three molecular markers – An Australian origin for *Limnadopsis*. – *Molecular Phylogenetics and Evolution* **53**: 716-725.

Seilacher, A., Reif, W.E., Westphal, F. 1985. Sedimentological, ecological and temporal patterns of fossil Lagerstätten. – *Philosophical Transactions of the Royal Society of London B* **311**: 5-23.

Shen, Y. 1994. Jurassic conchostracans from Carapace Nunatak, southern Victoria Land, Antarctica. – *Antarctic Science* **6**: 105-113.

Shen, Y., Li, Z., Chen, P. 2002. Some Jurassic and Cretaceous conchostracans from Gansu Province, NW China. – *Palaeoworld* **14**: 123-135. (in Chinese, English summary)

Shen, Y., Chen, P., Huang, D. 2003. Age of the fossil conchostracans from Daohugou of Ningcheng, Inner Mongolia. – *Journal of Stratigraphy* **27**: 311-314. (in Chinese)

Siver, P.A. 1988. Morphology and ecology of *Mallomonas galeiformis* (Chrysophyceae), a potentially useful paleolimnological indicator. – *Transactions of the American Microscopical Society* **107**: 152-161.

Siver, P.A. 1995. The distribution of chrysophytes along environmental gradients: their use as biological indicators. *In:* Sandgren, C.D., Smol, J.P., Kristiansen, J. (eds). Chrysophyte algae, ecology, phylogeny and development. – Cambridge University Press, Cambridge, pp. 232-268.

Smith, A.B. 1994. Systematics and the fossil record: documenting evolutionary patterns. – Blackwell Science, London.

Smith, R.M.H. 1986. Sedimentation and palaeoenvironments of Late Cretaceous crater-lake deposits in Bushmanland, South Africa. – *Sedimentology* **33**: 369-386.

Soliman, M.F., El Goresy, A. 2012. Framboidal and idiomorphic pyrite in the upper Maastrichtian sedimentary rocks at Gabal Oweina, Nile Valley, Egypt: Formation processes, oxidation products and genetic implications to the origin of framboidal pyrite. – *Geochimica et Cosmochimica Acta* **90**: 195-220.

Stankiewicz, B.A., Briggs, D.E.G., Evershed, R.P., Flannery, M.B., Wuttke, M. 1997. Preservation of chitin in 25-million-year-old fossils. – *Science* **276**: 1541-1543.

Stearns, S.C. 1976. Life-history tactics: A review of the ideas. – *The Quarterly Review of Biology* **51**: 3-47.

Stebbing, T.R.R. 1910. General catalogue of South African Crustacea. – *Annals of the South African Museum* **6**: 481-494.

Stevenson, J.R. 1985. Dynamics of the Integument. *In:* Bliss, D.E., Mantel, L.H. (eds). The Biology of Crustacea, Vol.9. Integument, Pigments, and Hormonal Processes. – Orlando, FL: Academic Press.

Stigall, A.L., Babcock, L.E., Briggs, D.E.G., Leslie, S.A. 2008. Taphonomy of lacustrine interbeds in the Kirkpatrick Basalt (Jurassic), Antarctica. – *Palaios* **23**: 344-355.

Stigall, A.L., Hembree, D.I., Gierlowski-Kordesch, E.H., Weismiller, H.C. 2014. Evidence for a dioecious mating system in Early Jurassic *Hardapestheria maxwelli* gen. et sp. nov. (Crustacea, Branchiopoda, Spinicaudata) from the Kalkrand Formation of Namibia. – *Palaeontology* **57**: 127-140.

Stoicescu, A. 2004. *Caenestheriella variabilis* (Daday) (Conchostraca: Crustacea) espèce nouvelle pour la faune de Roumanie et sa validité. – *Revue Roumaine de Biologie, série de Biologie Animale* **49**: 11- 18.

Stoyan, D., Frenz, M., Goretzki, J., Schneider, J.W. 1994. Tests zur formstatistischen Klassifikation von Conchostraken (Crustacea, Branchiopoda) mittels Prokrustesanalyse. – *Freiberger Forschungsheft* **C452**: 153-162.

Strayer, D.L., Dudgeon, D. 2010. Freshwater biodiversity conservation: recent progress and future challenges. – *Journal of the North American Benthological Society* **29**: 344-358.

Sturm, M. 1979. Origin and composition of clastic varves. *In:* Schlüchter, C. (ed.). Moraines and varves. – Balkema, Rotterdam, pp. 281-285.

Sun, G., Ji, Q., Dilcher, D.L., Zheng, S., Nixon, K.C., Wang, X. 2002. Archaefructaceae, a new basal angiosperm family. – *Science* **296**: 899-904.

Sweeney, R.E., Kaplan, I.R. 1973. Pyrite framboid formation: Laboratory synthesis and marine sediments. – *Economic Geology* **68**: 618-634.

Swisher III, C.C., Wang, Y., Wang, X., Xu, X., Wang, Y. 1999. Cretaceous age for the feathered dinosaurs of Liaoning, China. – *Nature* **400**: 58-61.

Tansley, A.G. 1935. The use and abuse of vegetational concepts and terms. – *Ecology* **16**: 284-307.

Tappan, H. 1980. The paleobiology of plant protists. – WH Freeman and Company, San Francisco.

Tasch, P. 1969. Branchiopoda. *In:* Moore, R.C. (ed.): Treatise on Invertebrate Paleontology, Part R, Arthropoda 4 (I). – University of Kansas Press and The Geological Society of America, Inc., Lawrence, pp. R128-R191.

Tasch, P. 1987. Fossil Conchostraca of the southern hemisphere and continental drift, paleontology, biostratigraphy, and dispersal. – *The Geological Society of America Memoir* **165**: 1-290.

Tassi, F., Vaselli, O., Tedesco, D., Montegrossi, G., Darrah, T., Cuoco, E., Mapendano, M.Y., Poreda, R., Delgado Huertas, A. 2009. Water and gas chemistry at Lake Kivu (DRC): Geochemical evidence of vertical and horizontal heterogeneities in a multibasin structure. – *Geochemistry, Geophysics, Geosystems* **10**: Q02005.

Timms, B.V., Richter, S. 2002. A preliminary analysis of the conchostracans (Crustacea: Spinicaudata and Laevicaudata) of the middle Paroo catchment of the Australian aridzone. – *Hydrobiologia* **486**: 239-247.

Todd, J.A. 1991. A forest-litter animal community from the Upper Carboniferous?: notes on the association of animal body fossils with plants and lithology in the Westphalian D Coal Measures at Writhlington, Avon. – *Proceedings of the Geologists' Association* **102**: 179-184.

Townsend, C.R., Begon, M., Harper, J.L. 2008. Essentials of ecology. – Blackwell Publishing.

Vannier, J., Thiéry, A., Racheboeuf, P.R. 2003. Spinicaudatans and ostracods (Crustacea) from the Montceau Lagerstätte (Late Carboniferous, France): Morphology and palaeoenvironmental significance. – *Palaeontology* **46**: 999-1030.

Virtasalo, J.J., Löwemark, L., Papunen, H., Kotilainen, A.T., Whitehouse, M.J. 2010. Pyritic and baritic burrows and microbial filaments in postglacial lacustrine clays in the northern Baltic Sea. – *Journal of the Geological Society, London* **167**: 1185-1198.

Virtasalo, J.J., Whitehouse, M.J., Kotilainen, A.T. 2013. Iron isotope heterogeneity in pyrite fillings of Holocene worm burrows. – *Geology* **41**: 39-42.

Walser, H. 2011. Statistik für Naturwissenschaftler. – Haupt Verlag, Bern.

Wang, B., Li, J., Fang, Y., Zhang, H. 2009. Preliminary elemental analysis of fossil insects from the Middle Jurassic of Daohugou, Inner Mongolia and its taphonomic implications. – *Chinese Science Bulletin* **54**: 783-787.

Wang, H., Yang, S., Li, S. 1983. Mesozoic and Cenozoic basin formation in east China and adjacent regions and development of the continental margin. – *Acta Geologica Sinica* **57**: 213-223. (in Chinese)

Wang, S. 1984. New Jurassic-Cretaceous conchostracans from northern Hebei and Nei Mongol. – *Acta Palaeontologica Sinica* **23**: 726-737. (in Chinese)

Wang, S. 1999. Palaeoecology and Palaeoenvironment of the Jehol Biota. – *Acta Geologica Sinica* **73**: 289-301. (in Chinese)

Wang, W. 1987. Mesozoic conchostracans from western Liaoning Province, China. – Geological Publishing House, Beijing, China, pp. 134-179. (in Chinese)

Wang, X., Zhou, Z. 2006. Pterosaur assemblages of the Jehol Biota and their implication for the Early Cretaceous pterosaur radiation. – *Geological Journal* **41**: 405-418.

Ward, J.H. 1963. Hierarchical grouping to optimize an objective function. – *Journal of the American Statistical Association* **58**: 236-244.

Webb, J.A. 1979. A reappraisal of the palaeoecology of conchostracans (Crustacea: Branchiopoda). – *Neues Jahrbuch für Geologie und Paläontologie, Abhandlungen*, **158**: 259-275.

Weeks, S.C., Marcus, V., Alvarez, S. 1997. Notes on the life history of the clam shrimp, *Eulimnadia texana*. – *Hydrobiologia* **359**: 191-197.

Weeks, S.C., Sanderson, T.F., Zofkova, M., Knott, B. 2008. Breeding systems in the clam shrimp family Limnadiidae (Branchiopoda, Spinicaudata). – *Invertebrate Biology* **127**: 336-349.

Weeks, S.C., Chapman, E.G., Rogers, D.C., Senyo, D.M., Hoeh, W.R. 2009. Evolutionary transitions among dioecy, androdioecy and hermaphroditism in limnadiid clam shrimp (Branchiopoda: Spinicaudata). – *Journal of Evolutionary Biology* **22**: 1781-1799.

Westrich, J.T., Berner, R.A. 1984. The role of sedimentary organic matter in bacterial sulfate reduction: The *G* model tested. – *Limnology and Oceanography* **29**: 236-249.

Wignall, P.B., Hallam, A. 1991. Biofacies, stratigraphic distribution and depositional models of British onshore Jurassic black shales. *In:* Tyson, R.V., Pearson, T.H. (eds). Modern and ancient continental shelf anoxia. – *Geological Society Special Publication* **58**: 291-309.

Wignall, P.B., Twitchett, R.J. 1996. Oceanic anoxia and the end Permian mass extinction. – *Science* **272**: 1155-1158.

Wignall, P.B., Newton, R. 1998. Pyrite framboid diameter as a measure of oxygen deficiency in ancient mudrocks. – *American Journal of Science* **298**: 537-552.

Wignall, P.B., Newton, R., Brookfield, M.E. 2005. Pyrite framboid evidence for oxygen-poor deposition during the Permian-Triassic crisis in Kashmir. – *Palaeogeography, Palaeoclimatology, Palaeoecology* **216**: 183-188.

Wignall, P.B., Bond, D.P.G., Kuwahara, K., Kakuwa, Y., Newton, R.J., Poulton, S.W. 2010. An 80 million year oceanic redox history from Permian to Jurassic pelagic sediments of the Mino-Tamba terrane, SW Japan, and the origin of four mass extinctions. – *Global and Planetary Change* **71**: 109-123.

Wilkin, R.T., Barnes, H.L. 1996. Pyrite formation by reactions of iron monosulfides with dissolved inorganic and organic sulfur species. – *Geochimica et Cosmochimica Acta* **60**: 4167-4179.

Wilkin, R.T., Barnes, H.L., Brantley, S.L. 1996. The size distribution of framboidal pyrite in modern sediments: An indicator of redox conditions. – *Geochimica et Cosmochimica Acta* **60**: 3897-3912.

Wilkin, R.T., Arthur, M.A., Dean, W.E. 1997. History of water-column anoxia in the Black Sea indicated by pyrite framboid size distributions. – *Earth and Planetary Science Letters* **148**: 517-525.

Wright, M.C. 1920. *Limnestheria*: a new conchostracan genus from the Kilkenny Coal-Measures. – *Proceedings of the Royal Irish Academy* **35B**: 187-204.

Wu, H., Zhang, S., Jiang, G., Yang, T., Guo, J., Li, H. 2013. Astrochronology for the Early Cretaceous Jehol Biota in northeastern China. – *Palaeogeography, Palaeoclimatology, Palaeoecology* **385**: 221-228.

Xu, X., Tang, Z., Wang, X. 1999a. A therizinosauroid dinosaur with integumentary structures from China. – *Nature* **399**: 350-354.

Xu, X., Wang, X., Wu, X. 1999b. A dromaeosaurid dinosaur with a filamentous integument from the Yixian Formation of China. – *Nature* **401**: 262-266.

Xu, X., Zhou, Z., Wang, X. 2000. The smallest known non-avian theropod dinosaur. – *Nature* **408**: 705-708.

Xu, X., Zhou, Z., Prum, R.O. 2001. Branched integumental structures in *Sinornithosaurus* and the origin of feathers. – *Nature* **410**: 200-204.

Xu, X., Norell, M.A., Kuang, X., Wang, X., Zhao, Q., Jia, C. 2004. Basal tyrannosauroids from China and evidence for protofeathers in tyrannosauroids. – *Nature* **431**: 680-684.

Yang, W., Li, S., Jiang, B. 2007. New evidence for Cretaceous age of the feathered dinosaurs of Liaoning: zircon U-Pb SHRIMP dating of the Yixian Formation in Sihetun, northeast China. – Cretaceous Research **28**: 177-182.

Zelditch, M.L., Swiderski, D.L., Sheets, H.D., Fink, W.L. 2004. Geometric morphometrics for biologists: A primer. – Elsevier, Amsterdam.

Zhang, J. 2010. Revision and description of water boatmen from the Middle-Upper Jurassic of northern and northeastern China (Insecta: Hemiptera: Heteroptera: Corixidae). – *Paleontological Journal* **44**: 515-525.

Zhang, W., Chen, P., Shen, Y. 1976. Fossil Conchostraca of China. – Science Press, Beijing. (in Chinese)

Zhang, W., Shen, Y., Niu S. 1990. Discovery of Jurassic conchostracans with well-preserved soft parts and notes on its biological significance. – *Palaeontologia Cathayana* **5**: 311-352.

Zhou, Z., Barrett, P.M., Hilton, J. 2003. An exceptionally preserved Lower Cretaceous ecosystem. – *Nature* **421**: 807-814.

Zhou, Z. 2006. Evolutionary radiation of the Jehol Biota: chronological and ecological perspectives. – *Geological Journal* **41**: 377-393.

Zhu, R., Pan, Y., Shi, R., Liu, Q., Li, D. 2007. Palaeomagnetic and $^{40}Ar/^{39}Ar$ dating constraints on the age of the Jehol Biota and the duration of deposition of the Sihetun fossil-bearing lake sediments, northeast China. – *Cretaceous Research* **28**: 171-176.

Ziegler, B. 1998. Einführung in die Paläobiologie Teil 3, Spezielle Paläontologie, Würmer, Arthropoden, Lophophoraten, Echinodermen. – E. Schweizerbart'sche Verlagsbuchhandlung Stuttgart.

Zierold, T. 2007. Der Carapax der Muschelschaler – (ein) Werkzeuge für die Paläontologie? – *Veröffentlichungen des Museums für Naturkunde Chemnitz* **30**: 83-96.

Zolitschka, B. 1989. Jahreszeitlich geschichtete Seesedimente aus dem Holzmaar und dem Meerfelder Maar. – *Zeitschrift der Deutschen Geologischen Gesellschaft* **140**: 25-33.

Online Resources

http://life.bio.sunysb.edu/morph/

http://www.nhm.ac.uk/hosted-sites/iczn/code/

http://www.r-project.org/

IUCN (International Union for Conservation of Nature and Natural Resources) 2013. IUCN Red List of Threatened Species. – Available from http://www.iucnredlist.org.

vegan.r-forge.r-project.org

Supplementary 1.1. Overview of 50 horizons examined from three different excavations near Zhangjiagou (ZJG). Erdaogou (LXBE). and Jianshangou (JSG). The presence of a microfacies (Mf) within a horizon is marked (+ present. - not present). Framboids. commonly related to Mf 1 and Mf 4. are listed separately. Their mode of occurrence (S-scattered and/or C-concentrated) is distinguished and their abundance estimated on a 4-point scale of abundance: abundant (a). common (c). occurring (o). and rare (r). The degree of alteration is estimated on a three-point scale (1-minimal. 2-moderate. and 3-profound). Discontinuous Mf 3-lenses (dc) are distinguished from continuous layers.

Horizon	Mf 1	Mf 2	Mf 3	Mf 4	Mf 5	Mf 6	Framboids	Alteration	Phase
JSG ~H	–	–	–	–	–	+	–	1	3
JSG K	–	–	–	–	–	+	–	1	3
JSG ~L	–	–	–	–	–	+	–	1	3
JSG ~O	–	–	–	–	–	+	–	1	3
JSG AC	+?	–	–	–	–	+	–	1	3
JSG AD-AC	+	–	+(dc)	–	–	–	–	1-2	2
JSG AD-AC	+	–	+	–	–	–	+(o) C	2	2
JSG ~AH, AG	+?	–	?	–	–	–	?	3	2
JSG ~AK	+	–	+	–	+	–	?	2-3	2
JSG AN	+	–	+	–	+	–	–	2-3	2
JSG AO-AN	+	–	+	–	+	–	+(r) C	3	2
JSG AP	+	–	+(o)	–	–	–	+(o) SC	2-3	2
JSG 11 cm-AP	–	–	+	–	+	–	+(o) SC	1	2
JSG 14 cm-AP	–	–	+	–	+	–	+(o-c) SC	1	2
JSG 26 cm-AP	–	–	+	–	–	–	+(c) SC	1	2
LXBE Aabove	+	+?	+	–	+	–	+(r) C	2-3	2
LXBE C	+	–	+	–	+	–	–	3	2
LXBE D	+	+	+	–	+	–	–	1-2	2
LXBE E	+	–	+(dc)	–	+	–	+(c) SC	2-3	2
LXBE F	+	–	+	–	+?	–	+(r) C	3	2
LXBE H	+	–	+	–	+	+	+(o) C	3	2
LXBE I	–	–	+	–	+	–	+(o) C	2-3	2
LXBE J	–	–	–	+	+	–	+(o-c) C	1	2
LXBE K	–	–	–	+	–	–	?C	3	2
LXBE L	+	–	+	–	+	–	–	2-3	2
LXBE S	+	–	+	–	–	–	?	3	2
LXBE V	+	–	+	–	+?	–	?	3	2
LXBE X	–	–	–	+?	+	–	–	2	2
LXBE Y	–	–	–	+	+	–	–	1	2
LXBE A1	+	–	+	–	–	–	?	3	2
LXBE B1	+	–	+	–	–	–	+(a) SC	3	2
LXBE C1	+	–	–	–	+	–	+(r) C	3	2
LXBE F1	+	–	+	–	–	–	+(o-c) SC	3	2
LXBE G1	+	–	+	–	+?	–	+(c-a) SC	2-3	2
LXBE H1	+	–	+	–	+?	–	+(r) C	2	2
LXBE K1	–	–	–	+	–	–	+(r) C	1-2	2
LXBE L1	+	–	+(dc)	–	+	–	+(a) SC	1	2
LXBE N1	+	–	+	–	–	–	+(c-a) SC	2-3	2
ZJG D	+	–	+(o)	–	–	–	+(a) SC	3	2
ZJG E	+	–	+	–	+	–	+(r) C	3	2
ZJG G	+	–	–	–	–	–	+(a) SC	3	2
ZJG I	+	–	–	–	–	–	+(a) SC	3	2
ZJG K	+	–	+(dc)	–	+	–	+(a) SC	3	2
ZJG M	+	–	+(dc)	–	+?	–	+(a) SC	3	2
ZJG O	+	–	–	–	+	–	+(a) SC	3	2
ZJG P	+	–	–	–	–	–	+(a) SC	3	2
ZJG Q	+	–	+(dc)	–	–	–	+(a) SC	3	2
ZJG $S_{Thin\text{-}section\ 1}$	+	–	+(dc)	–	–	–	+(a) SC	3	2
ZJG $S_{Thin\text{-}section\ 2}$	–	–	+(a)	–	–	–	–	2	2
ZJG T	+	–	+(dc)	–	–	–	+(a) SC	3	2

Supplementary 3.1. EDS results for specimens of all measured horizons. The term "apatitic composition" is used, as EDS only provides qualitative elemental compositions. See separate file.

Supplementary 3.2. Data used for the transect in Fig. 3.6.

Transect *Cyzicus*	Weight-%	C	N	O	P	Ca	Mg	Al	Si	Cl
M1		70.14	0	18.28	3.06	8.52	0	0	0	0
M2		55.02	0	11.92	8.9	24.15	0	0	0	0
M3		51.63	0	12.72	10.44	24.9	0.31	0	0	0
M4		56.07	0	10.44	10.85	21.72	0.32	0.24	0.36	0
M5		64.27	0	23.24	4.03	7.82	0.29	0	0.34	0
M6		50.88	19.64	23.87	1.89	3.27	0.25	0	0	0.2
M7		57.97	16.85	20.37	1.6	2.84	0.17	0	0	0.2
M8		55.27	18.49	23.58	0.83	1.56	0.15	0	0	0.12
M9		53.59	20.15	25.18	0.27	0.62	0.11	0	0	0.08
M10		48.23	24.76	26.44	0.18	0.33	0	0	0	0.05
M11		50.52	21.22	27.35	0.27	0.55	0	0	0	0.08
M12		46.26	24.42	28.71	0.19	0.37	0	0	0	0.05

Supplementary 3.3. Data used for the transect in Fig. 3.11.

Transect *Triglypta*	Weight-%	O	F	Al	Si	P	Ca	Na	Mg	S	Br	Nd	Ce	Fe	K
M1		53.94	3.18	0.28	30.86	4.84	6.9	0	0	0	0	0	0	0	0
M2		48.06	7.04	0	13.94	10.82	19.12	0.29	0	0.22	0.5	0	0	0	0
M3		46.2	9.55	0.2	5.28	13.14	24.65	0	0	0.23	0	0.76	0	0	0
M4		45.92	9.36	0	2.49	13.81	27.39	0	0	0.21	0	0	0.82	0	0
M5		45.86	10.3	0	0.84	14.12	27.75	0	0	0.29	0	0	0.85	0	0
M6		47.01	8.98	0.42	0.83	13.86	27.07	0	0	0.26	0	0	0.99	0.57	0
M7		46.85	10.07	0.71	1.08	13.66	26.79	0	0	0.29	0	0	0	0.36	0.19
M8		47.46	9.32	1.47	2.45	12.59	24.23	0.36	0.35	0	0	0	0.84	0.55	0.38
M9		50.45	7.7	3.52	6.38	10.07	18.87	0	0.63	0.24	0	0	0	1.07	1.06
M10		53	5.55	6.68	13.37	5.83	10.35	0	1	0.17	0	0	0	2.01	2.04

Supplementary 4.1. Fourier coefficients of 51 type specimens (Figs. 4.9, 4.10).

	A2	A3	A4	A5	A6	A7	A8	A9	A10	A11	A12	B2	B3	B4	B5	B6	B7	B8	B9	B10	B11	B12
130637Si	-0.172	-0.009	-0.008	-0.004	0.001	-0.007	-0.010	0.000	-0.008	-0.009	-0.009	-0.069	-0.034	-0.012	-0.005	0.007	0.013	-0.005	-0.001	0.005	0.004	-0.000
130639Tu	-0.117	-0.025	-0.009	0.002	-0.004	-0.008	-0.005	-0.001	0.008	0.005	0.000	-0.056	-0.039	-0.015	-0.011	0.008	0.009	0.000	-0.001	-0.001	0.003	0.002
130643Eu	-0.112	-0.001	0.001	0.003	-0.012	-0.015	-0.002	0.003	-0.005	-0.012	-0.004	-0.030	-0.040	-0.018	-0.005	-0.001	-0.003	-0.011	-0.006	0.001	-0.002	-0.005
135817Eu	-0.080	0.017	-0.011	-0.004	-0.012	-0.021	-0.021	-0.016	-0.002	0.010	0.011	-0.014	-0.007	-0.002	-0.012	0.007	-0.000	-0.007	-0.016	-0.022	-0.017	-0.006
135818Eu	-0.116	0.011	0.001	0.002	-0.003	-0.002	-0.008	-0.002	0.005	0.004	0.001	-0.037	-0.032	-0.009	-0.011	0.005	0.009	0.002	-0.010	-0.007	-0.002	-0.001
135819Eu	-0.095	-0.007	-0.020	-0.010	-0.005	-0.000	0.008	0.006	0.008	-0.002	-0.003	-0.043	-0.036	0.001	-0.007	-0.005	-0.007	0.003	0.003	0.003	0.008	0.005
135820Eu	-0.109	0.002	-0.001	-0.019	-0.009	0.002	-0.002	-0.001	-0.000	-0.007	-0.006	-0.039	-0.043	-0.006	-0.009	-0.010	-0.001	-0.003	-0.003	0.003	0.005	-0.003
135821Eu	-0.106	-0.005	-0.017	-0.009	-0.009	-0.002	0.002	0.002	-0.001	-0.004	-0.005	-0.041	-0.009	0.005	-0.013	-0.008	-0.003	-0.003	0.001	0.003	0.001	0.004
135822Eu	-0.050	-0.012	-0.009	-0.005	0.002	-0.009	-0.011	-0.016	-0.017	-0.014	-0.008	-0.027	-0.039	0.002	0.005	0.007	0.015	0.010	0.008	-0.003	-0.009	-0.011
135824E2	-0.163	-0.006	-0.022	-0.021	-0.004	0.002	-0.001	-0.003	-0.007	-0.005	-0.003	-0.068	-0.021	-0.007	-0.018	-0.011	0.003	0.010	0.011	0.008	0.004	0.004
135824Eu	-0.125	0.010	-0.006	-0.017	0.003	0.005	0.003	0.010	0.001	-0.003	0.002	-0.040	-0.033	-0.004	-0.025	-0.015	-0.003	0.006	0.008	0.007	-0.006	-0.005
135825Eu	-0.064	0.010	0.006	-0.001	0.001	0.004	0.005	-0.004	-0.007	-0.010	-0.010	-0.022	-0.041	-0.001	-0.021	-0.001	-0.000	0.010	0.012	0.012	0.010	0.005
136462Cr	-0.047	-0.003	-0.006	-0.006	0.017	0.008	0.008	-0.001	0.001	0.008	0.007	-0.020	0.006	-0.043	-0.005	-0.004	0.003	0.004	-0.001	-0.002	-0.003	0.004
136910Es	-0.097	0.028	0.007	-0.003	-0.014	-0.008	-0.013	-0.013	-0.005	-0.000	0.000	-0.025	0.000	0.010	0.005	0.011	0.009	0.008	-0.009	-0.007	-0.004	0.003
136911Es	-0.154	0.013	0.005	-0.002	-0.024	-0.009	0.002	-0.002	-0.010	-0.004	0.005	-0.036	0.001	-0.010	0.014	0.003	-0.016	-0.011	-0.002	-0.006	-0.013	-0.008
136912Es	-0.109	0.028	-0.000	-0.008	-0.013	-0.019	-0.022	-0.009	0.002	0.004	-0.002	-0.024	-0.009	-0.004	0.009	0.013	0.003	-0.015	-0.020	-0.012	-0.004	-0.000
141144Ya	-0.164	0.009	-0.003	-0.008	-0.010	-0.012	0.005	0.004	0.000	-0.003	0.005	-0.059	-0.044	0.013	-0.004	0.011	0.008	0.006	0.008	0.007	0.001	-0.001
141145Ya	-0.148	-0.003	0.007	-0.014	-0.010	-0.006	0.001	0.007	-0.001	-0.002	-0.002	-0.054	-0.039	0.003	0.004	-0.001	0.002	-0.002	0.003	0.004	0.003	-0.002
20020Eu	-0.124	0.033	-0.005	-0.001	-0.012	-0.018	-0.003	-0.007	-0.007	-0.011	-0.001	-0.030	-0.026	-0.031	-0.020	0.017	0.004	-0.001	0.003	0.004	0.002	-0.002
20029Eu	-0.078	-0.015	-0.025	0.001	-0.002	-0.013	-0.019	-0.016	-0.006	-0.002	-0.008	-0.037	-0.036	-0.051	-0.026	0.004	0.008	0.006	-0.002	-0.004	0.004	0.008
26994Eop	-0.067	0.007	-0.017	-0.015	-0.004	-0.013	-0.021	-0.013	-0.009	-0.005	-0.014	-0.022	-0.037	-0.034	-0.021	-0.004	0.004	-0.009	-0.009	-0.003	0.005	0.005
27106Hal	-0.132	0.006	-0.003	-0.003	-0.010	-0.016	-0.010	-0.004	-0.004	-0.006	-0.004	-0.042	-0.007	-0.022	-0.001	0.018	-0.004	-0.007	-0.004	0.002	0.007	0.001
27107Hal	-0.115	-0.001	0.008	0.004	-0.003	-0.001	-0.007	0.003	0.005	-0.002	-0.001	-0.041	-0.041	-0.008	0.000	0.002	-0.008	0.006	0.001	0.007	0.005	0.003
29735Eu	-0.120	0.018	0.016	0.003	0.003	-0.002	-0.007	0.007	-0.002	-0.008	-0.002	-0.029	-0.042	-0.012	-0.002	-0.005	0.012	-0.005	-0.006	0.003	-0.006	-0.008
29777Eu	-0.061	-0.024	0.008	0.011	-0.005	-0.014	-0.010	-0.003	-0.003	-0.008	-0.009	-0.013	-0.038	-0.058	-0.017	-0.005	-0.008	-0.016	-0.012	-0.006	-0.004	-0.009
29778Eu	-0.075	-0.001	0.008	0.003	0.004	0.002	-0.012	-0.008	-0.003	-0.009	-0.012	-0.028	-0.029	-0.037	-0.010	0.004	0.019	0.007	0.001	-0.002	0.000	-0.006
29779Eu	-0.074	-0.012	0.014	0.005	-0.001	-0.012	-0.013	0.002	-0.003	-0.014	-0.010	-0.027	-0.031	-0.043	-0.011	0.017	0.015	-0.002	-0.001	0.008	0.001	-0.008

	A2	A3	A4	A5	A6	A7	A8	A9	A10	A11	A12	B2	B3	B4	B5	B6	B7	B8	B9	B10	B11	B12
29871Nes	-0.069	0.003	0.009	0.008	0.006	-0.002	0.000	0.005	0.004	-0.000	0.004	-0.014	-0.030	-0.039	-0.009	0.002	-0.001	-0.014	-0.003	0.000	-0.003	-0.006
30038Cal	-0.076	-0.009	0.031	0.012	-0.010	-0.004	0.004	-0.004	-0.003	0.002	-0.000	-0.022	-0.015	-0.027	0.006	0.002	-0.010	0.010	0.011	0.004	-0.001	0.005
30069Ebi	-0.164	0.000	-0.019	0.005	-0.014	-0.015	-0.016	-0.007	-0.002	-0.010	-0.009	-0.053	-0.005	-0.018	-0.016	0.007	0.000	-0.003	-0.013	-0.004	-0.003	-0.010
30079Equ	-0.123	0.004	0.001	-0.004	0.002	0.001	0.013	0.019	0.006	-0.002	0.000	-0.037	0.012	-0.012	0.002	-0.001	-0.008	-0.013	-0.003	0.005	0.001	-0.001
30097Ere	-0.158	0.036	0.006	0.018	-0.001	-0.021	-0.017	-0.015	-0.007	-0.009	-0.010	-0.049	-0.006	0.007	0.016	0.039	0.028	0.011	0.002	-0.002	0.001	0.000
42274Mig	-0.137	0.002	-0.013	0.000	-0.006	-0.017	-0.015	-0.010	-0.005	-0.010	-0.012	-0.043	-0.034	-0.019	-0.024	-0.002	-0.006	-0.008	-0.009	-0.001	0.004	0.001
55202Lin	-0.153	0.018	-0.003	-0.002	-0.008	-0.009	-0.013	-0.004	-0.001	-0.007	-0.004	-0.047	-0.040	-0.012	-0.014	-0.004	-0.001	-0.001	0.000	0.008	0.005	-0.000
69490Mon	-0.111	-0.022	-0.023	-0.022	0.002	-0.006	-0.014	-0.017	-0.006	0.004	-0.003	-0.064	-0.038	-0.018	-0.018	-0.003	0.020	0.011	0.006	-0.003	0.009	0.015
DiJ15461	-0.124	-0.013	-0.005	-0.009	-0.007	-0.007	-0.018	-0.008	0.001	-0.000	-0.005	-0.053	-0.045	-0.014	-0.006	-0.007	0.006	0.001	0.000	0.006	0.008	0.003
DiL15462	-0.197	-0.021	-0.016	-0.017	-0.004	0.002	0.001	0.009	0.015	0.003	0.007	-0.089	-0.045	0.003	0.001	0.002	0.007	0.010	-0.001	0.009	0.004	-0.004
DiY15455	-0.143	0.000	-0.008	-0.010	-0.005	-0.011	-0.006	0.003	-0.001	-0.005	-0.002	-0.046	-0.032	-0.018	-0.018	-0.005	-0.003	-0.004	-0.002	0.006	-0.001	-0.003
EFu15437	-0.133	-0.021	0.008	-0.007	-0.013	-0.015	-0.014	-0.008	-0.002	-0.011	-0.012	-0.047	-0.064	-0.033	-0.025	-0.010	0.001	0.003	-0.008	-0.004	0.002	-0.002
EFu15438	-0.120	-0.013	0.008	-0.007	-0.006	-0.004	-0.007	-0.002	-0.001	-0.008	-0.009	-0.042	-0.057	-0.029	-0.012	-0.006	0.001	-0.006	-0.007	0.003	0.004	-0.004
EG131923	-0.165	-0.004	-0.009	-0.013	-0.010	-0.013	-0.005	-0.005	-0.004	-0.005	-0.007	-0.061	-0.037	-0.006	-0.009	0.004	0.009	0.002	0.003	-0.004	-0.004	-0.003
EJi15443	-0.136	0.000	-0.007	-0.010	0.008	-0.002	-0.005	-0.003	-0.003	0.000	-0.002	-0.049	-0.032	-0.005	-0.019	-0.010	-0.000	0.001	0.000	-0.001	-0.001	0.002
ELi15445	-0.151	0.018	-0.005	-0.003	-0.014	-0.016	-0.001	0.007	-0.003	-0.002	0.004	-0.048	-0.043	-0.008	-0.000	0.006	0.009	-0.002	0.010	0.013	0.001	0.000
ELi15448	-0.151	-0.008	0.004	-0.007	-0.008	-0.012	0.000	-0.001	-0.002	-0.005	-0.001	-0.056	-0.041	-0.017	-0.002	-0.004	0.005	-0.001	0.003	0.005	0.006	0.004
EMi28229	-0.126	0.004	-0.003	-0.016	-0.009	-0.015	-0.012	-0.005	-0.000	-0.012	-0.007	-0.044	-0.029	-0.010	-0.005	-0.001	0.004	-0.004	-0.005	0.005	0.004	-0.002
EMi29884	-0.134	0.004	0.001	-0.015	-0.019	-0.022	-0.010	0.005	-0.014	-0.006	0.002	-0.043	-0.041	-0.007	-0.011	-0.005	0.006	-0.008	0.008	0.008	-0.003	-0.000
EMi29885	-0.142	0.013	0.013	-0.006	0.000	-0.010	-0.002	0.005	-0.006	-0.005	0.001	-0.044	-0.047	0.003	-0.014	0.001	0.013	-0.004	0.003	0.009	0.002	0.007
EO131915	-0.128	-0.007	0.005	-0.013	0.003	-0.005	-0.007	0.008	0.006	-0.003	0.001	-0.053	-0.049	-0.012	0.003	0.000	0.010	0.003	0.001	0.011	0.005	0.001
EO15451	-0.133	0.003	0.013	0.001	-0.004	-0.007	-0.007	0.004	-0.006	-0.006	0.001	-0.036	-0.058	-0.016	-0.007	-0.003	-0.004	-0.005	-0.001	0.003	-0.009	-0.004
ES131917	-0.141	0.005	-0.017	0.008	0.007	0.008	0.010	0.010	0.001	0.001	0.004	-0.060	-0.039	-0.015	0.001	0.017	0.017	0.008	0.009	0.008	0.001	0.002
YB131920	-0.154	0.015	0.003	-0.018	-0.003	-0.008	-0.012	0.003	0.001	-0.008	-0.000	-0.055	-0.027	0.014	-0.003	0.001	0.011	0.005	0.003	0.014	0.006	-0.001

Supplementary 5.1. Fourier coefficients of 23 specimens of the LXBE-S1 cohort. The corresponding plots can be found in Figs. 5.5-5.8.

	A2	A3	A4	A5	A6	A7	A8	A9	A10	A11	A12	B2	B3	B4	B5	B6	B7	B8	B9	B10	B11	B12
LXS1_15	-0.155	0.008	0.008	-0.013	-0.017	-0.014	-0.008	0.000	-0.003	0.000	0.004	-0.056	-0.037	-0.005	0.003	-0.007	0.002	0.001	0.007	0.006	0.004	0.002
LXS1_16	-0.145	0.008	0.016	-0.011	-0.004	-0.013	-0.005	0.000	-0.003	-0.007	-0.000	-0.058	-0.069	-0.029	-0.011	-0.006	0.005	-0.002	0.006	0.010	0.003	0.002
LXS1_21	-0.125	0.018	0.008	-0.000	-0.013	-0.023	-0.018	-0.003	-0.001	-0.010	-0.010	-0.042	-0.036	0.003	0.008	0.005	0.005	0.001	0.004	0.010	0.008	-0.002
LXS1_24	-0.137	0.017	0.012	-0.009	-0.009	-0.018	-0.007	-0.004	-0.009	-0.010	-0.008	-0.040	-0.037	-0.003	-0.003	0.002	0.001	-0.003	0.002	-0.001	-0.003	-0.006
LXS1_70	-0.143	0.007	0.011	-0.005	-0.005	-0.006	-0.006	-0.000	-0.003	-0.008	-0.002	-0.049	-0.051	-0.018	-0.014	-0.015	-0.003	-0.004	-0.008	0.002	-0.004	-0.001
LXS1_71	-0.135	0.021	0.006	0.013	-0.026	0.006	-0.005	0.006	0.006	-0.018	0.011	-0.059	-0.045	-0.015	0.002	0.008	-0.005	0.026	-0.006	0.021	-0.002	0.005
LXS1_HS2	-0.152	0.003	0.020	-0.007	-0.006	-0.007	-0.010	0.009	-0.002	-0.009	-0.001	-0.059	-0.047	-0.019	-0.012	-0.006	0.013	-0.003	0.003	0.008	0.001	-0.004
LXS1_HS4	-0.146	0.011	0.017	-0.013	-0.011	-0.010	-0.006	0.002	-0.003	-0.010	-0.003	-0.049	-0.046	-0.006	0.002	-0.014	0.006	0.003	0.002	0.008	-0.007	-0.004
S170424	-0.151	0.019	0.019	-0.001	-0.003	-0.005	-0.001	0.006	0.006	0.005	0.011	-0.064	-0.061	-0.003	0.007	0.006	0.017	0.010	0.009	0.006	0.000	0.005
S170429	-0.147	0.009	0.011	0.004	0.005	-0.008	-0.012	0.005	-0.006	-0.006	0.003	-0.054	-0.041	-0.005	-0.000	0.007	0.011	-0.006	-0.001	0.001	-0.011	-0.006
S170430	-0.137	0.013	-0.000	-0.000	-0.005	-0.014	-0.014	-0.005	-0.004	-0.008	-0.008	-0.062	-0.051	-0.007	-0.000	0.013	0.014	0.010	0.005	0.010	0.013	0.005
S170431	-0.114	-0.004	-0.002	-0.011	-0.020	-0.017	-0.002	0.002	-0.002	-0.006	-0.001	-0.047	-0.030	-0.023	0.004	0.003	-0.011	-0.004	0.001	0.007	-0.002	-0.005
S170723	-0.144	0.011	0.003	-0.016	-0.012	-0.010	-0.010	0.006	-0.006	-0.012	-0.004	-0.055	-0.042	0.005	0.005	0.004	0.013	-0.006	-0.003	0.010	-0.000	0.003
S17759	-0.144	0.020	-0.005	-0.007	-0.012	-0.009	-0.008	0.009	-0.001	-0.002	-0.001	-0.055	-0.043	-0.014	0.005	0.001	0.010	-0.002	0.004	0.011	0.000	-0.001
S17760	-0.143	0.009	0.008	0.003	-0.015	-0.013	-0.008	0.005	-0.005	-0.007	-0.004	-0.059	-0.062	-0.010	0.008	0.002	0.006	0.000	0.009	0.014	0.003	-0.002
S17763	-0.163	0.004	0.005	-0.008	-0.007	-0.007	0.000	0.007	-0.002	-0.004	-0.004	-0.059	-0.045	-0.004	-0.010	-0.014	0.002	-0.001	0.006	0.002	-0.004	-0.005
S17764	-0.163	0.009	0.001	-0.009	-0.017	-0.012	-0.007	0.001	-0.008	-0.011	-0.004	-0.067	-0.055	-0.016	0.005	0.010	0.008	-0.000	0.000	0.007	-0.004	-0.002
S1776419	-0.163	0.006	0.005	-0.010	-0.013	-0.006	-0.004	-0.003	-0.004	0.002	0.001	-0.061	-0.061	-0.016	-0.009	-0.009	-0.006	-0.002	0.002	0.001	0.000	-0.001
S17774	-0.140	0.017	0.018	0.003	0.001	-0.011	-0.002	-0.007	-0.003	-0.006	-0.009	-0.054	-0.050	-0.002	0.004	0.008	0.008	0.011	0.012	0.007	0.013	0.005
S1777411	-0.136	0.009	0.009	-0.008	-0.009	-0.012	-0.014	0.000	-0.004	-0.004	-0.001	-0.048	-0.051	-0.024	-0.005	-0.002	-0.003	-0.002	0.006	0.005	-0.003	-0.000
S177742	-0.153	0.019	0.003	-0.008	-0.013	-0.002	-0.010	0.001	-0.003	-0.002	-0.002	-0.056	-0.051	-0.012	-0.004	-0.011	0.001	0.007	-0.000	0.004	0.003	0.006
S177747	-0.139	0.008	0.003	-0.013	-0.015	-0.000	-0.003	-0.003	0.006	-0.002	-0.003	-0.062	-0.042	-0.004	0.007	0.000	0.008	0.011	-0.000	0.006	0.003	-0.000
S177754	-0.141	0.035	0.016	-0.008	-0.014	-0.007	-0.011	0.004	0.000	-0.009	-0.007	-0.050	-0.039	0.000	0.002	0.007	0.020	0.012	0.001	0.009	0.005	0.001

Supplementary 6.1. Fourier coefficients of 196 carapace outlines (excavation JSG). The corresponding plot can be found in Fig. 6.8.

	A2	A3	A4	A5	A6	A7	A8	A9	A10	A11	A12	B2	B3	B4	B5	B6	B7	B8	B9	B10	B11	B12
4alp_1_1	-0.149	0.007	0.016	-0.022	-0.009	-0.006	-0.011	0.000	-0.002	-0.005	-0.004	-0.031	-0.060	-0.006	-0.014	-0.015	0.006	-0.003	-0.008	0.001	0.000	-0.002
4alp_1_2	-0.130	0.002	0.013	-0.021	-0.013	-0.010	-0.014	-0.002	0.004	-0.008	-0.006	-0.031	-0.062	-0.010	-0.009	-0.011	0.009	-0.004	-0.007	0.001	0.001	-0.004
4alp_1_3	-0.129	-0.002	0.008	-0.006	-0.012	-0.009	-0.002	-0.004	-0.004	-0.004	-0.005	-0.038	-0.059	-0.014	-0.005	0.003	0.002	0.002	-0.001	-0.003	0.001	-0.000
4alp_1_4	-0.144	-0.006	0.010	-0.018	-0.018	-0.017	-0.008	0.001	-0.006	-0.008	-0.003	-0.038	-0.064	-0.021	-0.007	-0.006	0.001	-0.009	-0.003	-0.001	-0.002	-0.003
4alp_1_5	-0.135	0.006	0.022	-0.008	-0.025	-0.003	-0.013	-0.007	-0.000	-0.007	-0.008	-0.032	-0.056	-0.021	-0.013	-0.019	-0.001	0.010	-0.005	0.006	0.005	0.005
4alp_1_6	-0.124	0.006	0.009	-0.024	-0.009	0.001	-0.008	-0.005	-0.002	-0.001	-0.002	-0.033	-0.038	-0.016	-0.007	-0.018	0.007	0.004	-0.002	-0.006	0.001	0.004
4alp_1_7	-0.149	0.005	0.017	-0.017	-0.008	-0.003	-0.008	0.005	-0.001	-0.005	-0.002	-0.029	-0.067	-0.011	-0.017	-0.012	0.009	-0.007	-0.008	-0.002	-0.003	-0.005
4_1_1	-0.157	-0.007	-0.008	-0.030	-0.006	-0.019	-0.016	0.004	0.001	-0.009	-0.000	-0.046	-0.053	-0.004	-0.012	-0.005	0.011	-0.003	0.000	0.009	-0.003	-0.009
A2_70	-0.092	-0.005	-0.000	-0.019	0.003	0.011	-0.002	-0.003	0.003	0.004	0.006	-0.028	-0.052	-0.021	-0.013	-0.015	0.001	0.002	-0.005	-0.003	-0.003	-0.001
A4_73	-0.148	-0.004	0.003	-0.020	-0.001	-0.006	-0.008	0.005	0.003	-0.006	-0.004	-0.038	-0.046	-0.006	-0.009	-0.013	0.007	-0.006	-0.006	0.005	-0.001	-0.006
A5_80	-0.140	0.004	0.011	-0.018	-0.018	-0.013	-0.015	-0.002	0.001	-0.007	-0.002	-0.038	-0.061	-0.020	-0.009	-0.006	0.008	0.001	-0.005	0.008	0.008	0.001
A6_84	-0.166	-0.010	0.011	-0.022	-0.008	-0.011	-0.012	0.001	-0.001	-0.004	-0.003	-0.042	-0.055	-0.015	-0.016	-0.019	-0.002	-0.009	-0.004	0.003	-0.000	-0.002
A7_85	-0.151	-0.006	-0.012	-0.031	-0.007	-0.008	-0.009	-0.004	0.002	0.000	0.004	-0.048	-0.037	0.001	-0.017	-0.012	0.005	0.009	0.002	0.003	0.001	-0.001
A8_92	-0.154	-0.004	-0.008	-0.016	-0.019	-0.016	-0.017	-0.004	-0.001	-0.004	-0.004	-0.046	-0.036	-0.006	-0.004	-0.011	0.003	-0.001	-0.001	0.004	0.006	0.003
AA1_110	-0.153	-0.006	0.009	0.002	-0.002	0.003	-0.013	-0.006	-0.001	-0.005	-0.008	-0.045	-0.045	-0.003	-0.003	-0.012	0.000	0.007	-0.001	0.007	0.007	0.006
AA2_113	-0.136	-0.006	0.006	-0.015	-0.014	-0.011	-0.012	-0.001	-0.001	-0.005	-0.004	-0.035	-0.047	-0.018	-0.013	-0.012	-0.002	-0.004	-0.002	0.003	0.000	-0.004
AB1_114	-0.127	0.008	0.019	0.001	-0.002	-0.006	-0.003	0.002	0.005	-0.001	-0.003	-0.033	-0.036	-0.003	0.003	0.007	0.012	0.006	0.004	0.008	0.007	-0.000
A_01_03	-0.095	-0.004	0.027	0.006	0.009	0.007	-0.002	0.000	0.003	0.001	-0.002	-0.021	-0.061	-0.013	-0.011	-0.003	0.005	0.004	-0.003	-0.000	0.004	0.002
A_10_03	-0.144	-0.003	0.012	-0.012	-0.009	-0.001	-0.011	-0.003	0.003	-0.004	-0.005	-0.033	-0.064	-0.025	-0.014	-0.020	-0.005	-0.006	-0.011	-0.001	0.001	-0.004
B2_25	-0.123	-0.003	0.009	-0.022	0.000	-0.002	-0.010	-0.001	0.006	-0.001	-0.005	-0.036	-0.050	-0.017	-0.004	0.003	0.007	-0.005	-0.005	0.003	0.005	-0.001
B2_27	-0.157	0.004	0.008	-0.011	0.003	0.007	-0.002	0.002	0.007	0.004	-0.001	-0.039	-0.072	-0.017	-0.012	-0.010	0.004	0.004	0.000	0.005	0.009	0.005
B2_31	-0.157	0.008	-0.004	-0.032	-0.009	-0.015	-0.012	0.001	-0.001	-0.004	-0.006	-0.049	-0.053	0.004	-0.010	0.003	0.023	0.007	0.006	0.009	0.007	0.005
B2_32	-0.129	-0.008	0.001	-0.014	-0.019	-0.007	-0.019	-0.002	-0.000	-0.004	-0.007	-0.046	-0.046	-0.010	-0.007	-0.004	0.011	0.005	-0.004	0.004	0.009	0.001
B2_43	-0.150	0.009	0.012	-0.031	-0.010	-0.011	-0.016	-0.008	-0.004	-0.004	-0.006	-0.034	-0.054	-0.008	-0.021	-0.015	0.013	0.004	-0.002	-0.000	0.003	0.005
B2_44	-0.137	0.004	0.018	-0.021	-0.009	-0.002	-0.006	-0.001	-0.000	-0.001	-0.001	-0.034	-0.068	-0.014	-0.009	-0.010	0.008	-0.000	-0.006	0.001	0.003	0.002
B3_45	-0.137	0.007	0.004	-0.025	-0.007	0.002	-0.016	-0.007	-0.000	-0.000	0.000	-0.042	-0.059	-0.008	0.001	-0.011	0.009	0.006	0.000	0.005	0.006	0.006
B4_48	-0.140	0.002	0.003	-0.025	-0.011	-0.000	-0.012	-0.007	0.002	-0.000	-0.003	-0.042	-0.051	-0.004	-0.009	-0.012	0.008	0.006	-0.007	-0.006	0.003	0.002

	A2	A3	A4	A5	A6	A7	A8	A9	A10	A11	A12	B2	B3	B4	B5	B6	B7	B8	B9	B10	B11	B12
B4_49	-0.142	0.001	0.001	-0.025	-0.012	-0.005	-0.006	-0.004	-0.001	0.003	0.000	-0.043	-0.044	-0.006	-0.009	-0.009	0.008	0.007	-0.000	-0.004	-0.001	0.004
B5_51	-0.136	0.001	0.003	-0.029	-0.007	-0.004	-0.011	-0.001	0.001	-0.001	-0.001	-0.038	-0.056	-0.012	-0.010	-0.011	0.004	-0.003	-0.004	0.001	0.001	-0.001
B5_54	-0.139	-0.012	0.009	-0.029	-0.006	-0.001	-0.016	-0.011	-0.002	-0.002	-0.003	-0.041	-0.052	-0.014	-0.019	-0.025	0.001	0.004	-0.007	-0.002	0.004	0.005
B5_56	-0.149	0.003	0.008	-0.032	-0.006	-0.006	-0.015	-0.009	-0.006	-0.008	-0.005	-0.038	-0.068	-0.014	-0.021	-0.019	0.007	0.003	-0.001	0.002	0.002	0.001
B5_57	-0.142	0.008	0.016	-0.024	0.002	-0.011	-0.012	0.007	-0.003	-0.006	-0.000	-0.026	-0.069	0.003	-0.009	-0.011	0.006	-0.011	-0.004	0.006	-0.004	-0.004
B6_60	-0.137	0.005	-0.004	-0.029	-0.008	0.001	-0.007	-0.005	-0.003	-0.002	-0.000	-0.034	-0.045	-0.013	-0.013	-0.015	0.008	-0.001	-0.007	-0.003	-0.004	-0.003
B6_61	-0.144	-0.005	0.008	-0.019	-0.005	-0.009	-0.014	-0.003	-0.003	-0.006	-0.008	-0.040	-0.049	-0.008	-0.011	-0.012	0.009	-0.001	-0.004	0.003	0.004	-0.001
B6_62	-0.153	0.000	0.015	-0.014	-0.009	-0.011	-0.016	0.004	0.001	-0.007	-0.001	-0.037	-0.063	-0.003	-0.004	-0.012	0.004	-0.006	-0.009	0.004	-0.002	-0.004
B7_64	-0.130	-0.007	0.007	-0.013	-0.012	0.002	-0.003	-0.002	-0.004	0.002	0.003	-0.039	-0.063	-0.023	-0.008	-0.008	-0.003	0.002	-0.002	-0.004	-0.006	0.002
B_01_03	-0.113	0.005	0.006	-0.025	-0.017	-0.006	-0.009	-0.006	0.003	-0.006	-0.003	-0.035	-0.033	-0.007	-0.007	-0.003	0.006	0.006	-0.007	0.001	0.004	0.002
B_08_02	-0.133	-0.006	-0.003	-0.023	-0.012	-0.007	-0.012	-0.008	0.000	-0.005	-0.007	-0.039	-0.055	-0.014	-0.016	-0.013	-0.001	0.001	-0.010	-0.003	0.001	-0.004
B_09_01	-0.135	0.002	-0.004	-0.021	-0.007	0.001	-0.009	-0.006	-0.007	-0.005	-0.001	-0.038	-0.046	-0.012	-0.015	-0.012	0.007	0.010	0.001	0.001	-0.002	0.003
B_09_02	-0.152	0.010	0.012	-0.016	-0.011	-0.014	-0.014	-0.000	0.001	-0.005	-0.003	-0.034	-0.058	0.002	-0.012	-0.004	0.003	0.001	-0.001	0.010	0.007	0.004
B_09_03	-0.156	-0.014	-0.005	-0.021	-0.000	-0.004	-0.010	0.003	0.002	-0.000	-0.004	-0.047	-0.061	-0.022	-0.014	-0.011	0.007	-0.009	-0.011	-0.005	-0.003	-0.002
C10_109	-0.159	-0.000	0.009	-0.013	-0.003	-0.012	-0.009	0.003	0.006	-0.002	-0.001	-0.034	-0.064	0.006	-0.015	-0.003	0.004	-0.010	-0.012	-0.002	0.001	-0.003
C12_1	-0.159	0.016	0.003	-0.030	-0.003	-0.011	-0.013	0.005	0.001	0.000	0.003	-0.041	-0.065	-0.005	0.011	-0.004	0.007	-0.002	0.004	0.007	0.002	-0.000
C12_2	-0.150	0.005	0.002	-0.026	-0.003	-0.011	-0.012	-0.003	-0.001	-0.003	-0.001	-0.041	-0.042	-0.001	-0.005	-0.009	0.013	-0.003	0.001	0.006	0.006	0.003
C14_6	-0.138	-0.005	-0.001	-0.032	-0.019	-0.019	-0.013	-0.002	-0.005	-0.007	-0.004	-0.045	-0.052	-0.009	-0.005	-0.005	0.004	-0.006	0.001	0.009	0.007	0.004
C14_9	-0.131	-0.007	0.007	-0.025	-0.008	-0.001	-0.012	-0.007	-0.002	-0.001	-0.002	-0.039	-0.064	-0.006	-0.009	-0.016	0.004	0.001	-0.007	-0.004	0.000	0.004
C15_10	-0.147	0.007	0.014	-0.020	-0.011	-0.011	-0.010	-0.001	0.000	-0.005	-0.003	-0.035	-0.045	-0.023	-0.008	-0.012	0.004	-0.002	-0.004	0.003	0.002	-0.002
C15_13	-0.149	-0.002	0.005	-0.022	-0.015	-0.004	-0.013	-0.008	-0.006	-0.004	-0.002	-0.040	-0.072	-0.024	-0.015	-0.009	0.003	-0.003	-0.007	0.000	0.002	0.003
C15_14	-0.158	-0.004	0.016	-0.019	-0.006	-0.003	-0.015	-0.006	-0.002	-0.005	-0.008	-0.043	-0.074	-0.010	-0.011	-0.012	0.002	0.003	-0.002	0.002	0.004	0.003
C1_77	-0.152	-0.009	-0.006	-0.022	-0.012	-0.003	-0.011	-0.001	-0.000	-0.002	0.000	-0.043	-0.055	-0.013	-0.012	-0.017	0.003	-0.004	-0.007	-0.000	-0.003	-0.002
C1_79	-0.160	-0.003	0.008	-0.025	-0.011	-0.011	-0.010	-0.000	-0.008	-0.005	-0.004	-0.039	-0.065	-0.007	-0.013	-0.007	0.003	-0.010	-0.006	0.004	-0.005	0.000
C1_82	-0.134	-0.009	-0.007	-0.025	-0.002	-0.006	-0.016	-0.002	0.006	-0.008	-0.005	-0.043	-0.052	-0.016	-0.012	-0.011	0.007	0.003	-0.011	0.006	0.006	-0.001
C1_84	-0.147	0.000	-0.013	-0.025	-0.004	-0.006	-0.013	-0.002	-0.002	-0.002	-0.001	-0.043	-0.038	0.003	-0.007	-0.013	0.013	0.004	-0.004	0.000	-0.001	0.001
C2_88	-0.158	0.008	0.001	-0.012	-0.004	-0.003	-0.014	-0.004	0.008	-0.000	-0.008	-0.035	-0.074	0.003	-0.024	-0.007	0.006	0.002	-0.010	-0.005	0.006	-0.001
C6_100	-0.158	-0.003	-0.008	-0.023	-0.012	-0.020	-0.014	0.001	0.000	-0.008	-0.003	-0.048	-0.035	0.005	-0.003	-0.000	0.010	-0.001	0.005	0.010	0.005	-0.002
C8_107	-0.170	-0.002	0.007	-0.021	-0.002	-0.013	-0.015	-0.001	-0.001	-0.005	-0.003	-0.044	-0.064	-0.007	-0.009	-0.008	0.007	-0.002	-0.003	0.007	0.003	-0.002

	A2	A3	A4	A5	A6	A7	A8	A9	A10	A11	A12	B2	B3	B4	B5	B6	B7	B8	B9	B10	B11	B12
C_17_02b	-0.063	-0.002	0.021	0.007	0.004	0.006	-0.000	-0.000	0.003	0.003	-0.001	-0.021	-0.040	-0.012	0.009	-0.002	0.005	0.005	0.002	0.000	0.005	0.006
C_18_01	-0.160	0.002	-0.001	-0.029	-0.013	-0.018	-0.018	-0.002	-0.000	-0.006	-0.004	-0.048	-0.051	-0.005	-0.006	-0.007	0.015	0.000	-0.001	0.001	0.002	-0.003
C_19_01	-0.156	-0.013	-0.005	-0.015	-0.008	-0.006	-0.001	0.001	0.003	-0.004	-0.002	-0.045	-0.066	-0.008	-0.008	-0.008	-0.003	-0.006	-0.006	0.001	0.002	-0.003
D2_105	-0.167	0.001	0.006	-0.021	-0.001	-0.008	-0.009	0.004	0.002	-0.004	-0.004	-0.039	-0.055	-0.005	-0.017	-0.014	0.008	-0.006	-0.005	0.004	0.003	-0.002
D4_117	-0.140	0.002	-0.004	-0.010	-0.009	-0.010	-0.007	-0.005	-0.001	-0.009	-0.009	-0.035	-0.045	-0.015	-0.006	-0.005	-0.003	-0.008	-0.005	0.002	0.005	-0.002
D4_118	-0.141	0.007	0.009	-0.022	-0.014	-0.005	-0.009	0.001	0.002	-0.005	-0.002	-0.040	-0.061	-0.009	-0.002	-0.007	0.010	0.005	-0.000	0.005	0.005	-0.003
D_06_01b	-0.143	0.003	0.002	-0.023	-0.009	-0.011	-0.006	0.005	0.003	0.002	-0.002	-0.042	-0.039	-0.007	-0.007	0.005	0.012	-0.002	-0.003	0.004	0.006	0.003
D_07_02	-0.113	0.013	0.011	-0.008	-0.008	-0.020	-0.007	-0.004	-0.009	-0.009	-0.005	-0.016	-0.048	-0.019	-0.011	0.002	-0.004	-0.009	0.005	0.005	0.003	0.001
E3_137	-0.141	-0.008	-0.004	-0.012	-0.011	-0.007	-0.013	-0.012	-0.005	-0.001	-0.005	-0.046	-0.054	-0.020	-0.008	-0.013	0.001	0.007	0.001	0.000	0.006	0.007
E_01_01	-0.128	0.000	-0.023	-0.020	0.002	-0.003	-0.006	-0.004	-0.004	0.003	0.002	-0.037	-0.023	-0.000	-0.018	-0.010	0.005	0.004	0.005	-0.001	-0.000	0.005
E_02_02	-0.124	0.011	-0.003	-0.014	-0.008	-0.002	-0.007	-0.004	0.001	-0.002	-0.000	-0.028	-0.031	-0.007	-0.013	-0.011	0.001	0.006	-0.006	-0.004	-0.003	0.002
F_01_03	-0.134	0.005	0.004	-0.006	-0.006	-0.010	-0.008	-0.002	0.001	-0.002	-0.007	-0.024	-0.026	-0.009	-0.022	-0.006	-0.001	-0.004	-0.007	-0.005	-0.002	-0.002
F_02_06	-0.118	-0.006	-0.007	-0.019	-0.007	-0.006	-0.006	-0.004	-0.004	0.002	0.001	-0.029	-0.049	-0.013	-0.037	-0.021	0.006	0.003	0.001	-0.007	-0.003	-0.001
F_02_08	-0.143	-0.007	-0.002	-0.017	0.007	0.001	-0.006	-0.005	-0.004	-0.001	0.002	-0.040	-0.052	-0.007	-0.019	-0.006	0.002	0.003	-0.004	-0.004	-0.006	-0.004
F_03_03	-0.112	0.011	0.008	0.005	0.001	-0.001	-0.011	-0.003	0.007	0.003	-0.000	-0.022	-0.041	-0.010	0.001	-0.005	-0.000	0.000	-0.009	-0.003	0.001	-0.003
F_05_03	-0.126	0.009	0.013	-0.014	0.012	0.003	-0.002	-0.004	-0.004	0.001	0.001	-0.023	-0.041	-0.016	-0.019	-0.014	0.006	0.001	-0.001	-0.006	-0.005	-0.001
F_06_02	-0.142	0.015	-0.018	-0.007	-0.008	-0.011	-0.008	0.001	0.005	-0.002	-0.005	-0.030	-0.031	-0.027	-0.017	0.001	0.003	-0.003	-0.006	0.001	0.004	-0.002
F_07_01	-0.148	0.014	0.010	-0.006	-0.011	-0.012	-0.006	-0.001	0.006	-0.004	-0.004	-0.024	-0.061	-0.006	-0.011	-0.011	-0.005	-0.005	-0.011	-0.005	-0.002	-0.003
G1_2	-0.113	0.003	-0.012	-0.039	0.002	-0.013	-0.014	0.000	0.000	0.000	-0.002	-0.034	-0.041	-0.014	-0.028	0.002	0.021	-0.001	-0.002	0.003	0.002	0.009
G1_4	-0.104	0.003	-0.003	-0.013	0.002	-0.008	-0.009	-0.003	0.003	-0.002	-0.007	-0.024	-0.055	-0.017	-0.015	-0.002	0.005	-0.004	-0.007	-0.002	0.006	0.001
G1_7	-0.111	0.010	0.014	-0.014	-0.002	0.001	-0.005	-0.004	-0.001	0.002	0.000	-0.018	-0.045	-0.020	-0.011	-0.019	-0.001	-0.001	-0.004	-0.005	-0.004	-0.003
G2_12	-0.094	-0.000	-0.009	-0.015	-0.007	0.000	-0.011	-0.012	-0.004	-0.002	-0.002	-0.030	-0.027	-0.023	-0.013	-0.006	0.004	0.008	-0.003	-0.005	-0.002	0.002
G2_13	-0.143	0.001	-0.006	-0.027	-0.022	-0.005	-0.010	0.003	0.005	-0.003	-0.003	-0.052	-0.055	-0.007	-0.001	0.000	0.012	0.008	-0.000	0.006	0.004	0.000
G2_14	-0.130	-0.006	-0.013	-0.028	-0.001	-0.013	-0.011	-0.007	-0.005	0.001	-0.003	-0.040	-0.045	-0.009	-0.024	-0.014	0.015	0.003	0.004	-0.003	-0.000	0.007
G2_16	-0.131	-0.007	-0.011	-0.031	0.008	-0.005	-0.012	-0.001	0.001	0.004	-0.000	-0.041	-0.055	-0.003	-0.023	-0.004	0.015	0.006	0.000	0.002	0.006	0.006
G3_20	-0.160	0.005	0.005	-0.013	-0.017	-0.011	-0.004	0.011	0.003	-0.001	0.000	-0.046	-0.037	-0.000	0.002	-0.005	0.009	0.003	0.002	0.009	0.002	0.000
G3_21a	-0.129	-0.007	-0.007	0.004	0.008	-0.012	-0.009	0.004	0.004	0.000	-0.005	-0.028	-0.040	-0.007	-0.021	-0.004	0.005	-0.010	-0.004	0.003	0.007	0.001
G3_21b	-0.107	-0.001	-0.015	-0.025	-0.010	0.000	-0.010	-0.009	0.006	0.007	0.005	-0.037	-0.054	-0.003	-0.023	-0.016	0.010	0.018	-0.001	-0.003	0.004	0.008
G3_28	-0.173	-0.006	0.002	-0.028	-0.007	-0.006	-0.008	0.003	0.001	-0.002	0.003	-0.053	-0.044	-0.001	-0.003	-0.006	0.010	0.001	0.000	0.011	0.003	0.001

	A2	A3	A4	A5	A6	A7	A8	A9	A10	A11	A12	B2	B3	B4	B5	B6	B7	B8	B9	B10	B11	B12
G3_29	-0.150	-0.000	0.010	-0.018	-0.009	-0.008	-0.012	0.009	0.009	-0.007	0.001	-0.049	-0.043	0.000	0.002	-0.003	0.018	0.008	-0.001	0.014	0.006	-0.003
G3_30	-0.121	0.007	-0.007	-0.019	-0.001	-0.001	0.000	-0.002	-0.001	0.003	0.003	-0.027	-0.047	-0.002	-0.019	-0.012	0.001	0.002	-0.000	-0.006	-0.004	0.000
G_03_02	-0.147	0.014	0.012	-0.019	-0.013	-0.010	-0.006	0.005	0.004	-0.001	-0.002	-0.034	-0.041	-0.012	-0.001	-0.007	0.006	0.004	0.002	0.007	0.001	-0.000
G_04_02	-0.135	-0.005	-0.017	-0.029	-0.011	-0.008	-0.015	-0.004	-0.010	-0.004	0.000	-0.038	-0.038	-0.008	-0.015	-0.024	-0.000	0.004	-0.005	-0.002	-0.005	0.003
G_04_03	-0.116	0.007	0.008	-0.020	0.003	-0.002	-0.012	-0.001	0.008	0.001	-0.004	-0.023	-0.051	-0.005	-0.016	-0.009	-0.000	-0.002	-0.009	-0.007	-0.002	-0.001
G_04_04	-0.137	-0.003	0.004	-0.013	-0.010	-0.010	-0.008	0.004	-0.000	-0.004	-0.005	-0.033	-0.054	-0.020	-0.008	-0.008	-0.002	-0.010	-0.006	0.002	0.000	-0.004
G_05_01	-0.165	0.006	-0.003	-0.012	-0.011	0.003	-0.007	0.005	0.001	-0.008	-0.003	-0.043	-0.064	-0.006	-0.007	-0.004	0.007	-0.001	-0.006	0.004	0.005	-0.002
G_05_02	-0.152	0.010	0.031	-0.019	-0.008	-0.013	-0.015	-0.002	-0.007	-0.012	-0.001	-0.025	-0.069	-0.009	-0.009	-0.013	-0.002	-0.009	-0.008	0.002	-0.006	-0.008
G_05_03	-0.116	-0.000	0.002	-0.009	-0.005	0.007	-0.006	-0.008	-0.001	0.001	-0.004	-0.027	-0.058	-0.026	-0.020	-0.017	-0.003	0.002	-0.004	-0.010	-0.001	-0.001
G_05_04	-0.138	0.012	0.005	-0.011	-0.001	-0.005	-0.012	-0.001	0.002	-0.000	-0.002	-0.031	-0.047	-0.005	-0.014	-0.005	0.011	0.001	-0.001	0.003	0.005	0.003
G_05_05	-0.114	0.008	-0.000	-0.013	-0.001	-0.007	-0.002	0.002	0.004	-0.004	0.000	-0.020	-0.042	-0.018	-0.013	-0.004	-0.001	-0.011	-0.004	0.003	0.003	-0.004
G_05_06	-0.120	0.004	-0.004	-0.012	0.001	-0.007	-0.011	-0.007	0.001	0.000	-0.003	-0.027	-0.041	-0.020	-0.020	-0.012	0.010	-0.004	-0.008	-0.002	0.006	0.006
G_06_02	-0.167	0.001	0.007	-0.017	-0.010	-0.012	-0.007	0.006	-0.002	-0.004	0.004	-0.044	-0.056	0.003	-0.006	-0.011	0.011	0.002	0.005	0.007	-0.000	0.003
G_07_01	-0.141	0.004	0.003	-0.012	-0.000	-0.006	-0.006	0.007	-0.003	-0.009	-0.001	-0.029	-0.047	-0.015	-0.015	-0.001	0.009	-0.009	-0.007	0.005	-0.002	-0.007
G_07_02	-0.141	-0.001	-0.009	-0.019	-0.009	-0.005	-0.009	-0.006	0.002	-0.003	-0.005	-0.043	-0.066	-0.015	-0.008	-0.010	0.000	0.003	-0.005	-0.001	0.004	0.003
G_08_01	-0.167	-0.014	0.007	-0.019	-0.014	-0.004	-0.008	0.001	0.007	0.000	-0.001	-0.055	-0.065	-0.008	-0.001	-0.015	0.003	0.002	-0.008	-0.001	0.002	-0.002
H18_55	-0.132	-0.003	0.008	-0.010	-0.013	-0.015	-0.009	-0.004	-0.002	-0.001	-0.002	-0.044	-0.040	0.001	0.011	0.003	0.000	0.006	0.003	0.006	0.003	0.004
H1_32	-0.151	-0.008	-0.009	-0.011	-0.012	-0.004	-0.004	-0.003	0.001	-0.001	-0.004	-0.049	-0.048	-0.017	-0.004	-0.006	-0.001	0.005	-0.003	-0.002	-0.001	0.000
H2_34	-0.142	-0.006	0.007	-0.003	-0.003	-0.014	-0.010	-0.002	-0.002	-0.006	-0.006	-0.031	-0.054	-0.015	-0.015	-0.008	-0.003	-0.011	-0.008	0.001	-0.001	-0.002
H_09_01	-0.150	-0.003	0.002	-0.004	-0.013	-0.009	-0.011	-0.002	-0.001	-0.002	-0.003	-0.040	-0.046	-0.014	-0.008	-0.013	-0.001	-0.001	-0.001	0.002	0.002	0.002
H_10_01b	-0.141	0.003	0.013	-0.002	-0.007	-0.009	-0.003	0.002	-0.005	-0.005	-0.005	-0.039	-0.047	-0.008	0.002	0.010	0.011	-0.002	0.002	0.004	0.004	0.001
H_11_01	-0.140	-0.009	-0.005	-0.015	-0.006	-0.009	-0.016	-0.004	0.006	-0.003	-0.008	-0.042	-0.044	-0.012	-0.008	-0.011	0.006	-0.003	-0.015	-0.000	0.007	-0.003
I6_117	-0.150	0.004	-0.003	-0.020	-0.009	-0.003	-0.009	-0.004	0.000	-0.006	-0.003	-0.043	-0.063	-0.010	-0.003	-0.007	0.006	-0.001	-0.006	0.002	0.005	0.004
I9_127	-0.147	0.010	0.018	-0.023	-0.005	-0.007	-0.007	0.005	-0.001	-0.007	-0.001	-0.028	-0.068	-0.007	-0.008	-0.012	0.001	-0.004	-0.002	0.005	-0.000	-0.003
I_02_01	-0.150	0.006	0.004	-0.025	-0.012	-0.011	-0.012	-0.007	0.002	-0.003	-0.001	-0.048	-0.041	0.004	-0.003	0.005	0.014	0.008	0.003	0.009	0.010	0.001
I_04_01	-0.145	-0.006	0.010	-0.013	-0.008	-0.010	-0.005	-0.011	-0.003	-0.004	-0.003	-0.038	-0.047	-0.025	-0.011	-0.012	0.000	-0.000	-0.001	-0.005	-0.002	-0.003
J1_18	-0.149	0.005	0.009	-0.011	-0.006	-0.007	-0.011	-0.000	0.000	-0.002	-0.001	-0.036	-0.053	-0.000	-0.008	-0.007	0.003	0.000	-0.003	0.004	0.002	0.004
J1_4	-0.148	-0.004	0.000	-0.010	-0.002	-0.007	-0.010	-0.006	0.004	-0.001	-0.005	-0.035	-0.042	-0.019	-0.024	-0.015	0.000	-0.004	-0.007	-0.004	0.002	-0.002
JSG4u1_1	-0.077	-0.009	0.008	0.000	-0.002	-0.003	-0.006	0.003	0.002	-0.004	-0.005	-0.028	-0.047	-0.024	-0.004	0.008	0.011	0.002	0.002	0.005	0.005	-0.000

	A2	A3	A4	A5	A6	A7	A8	A9	A10	A11	A12	B2	B3	B4	B5	B6	B7	B8	B9	B10	B11	B12
JSG4u1_4	-0.095	-0.005	0.008	0.004	-0.006	-0.003	-0.013	-0.008	-0.001	-0.004	-0.010	-0.025	-0.032	-0.028	-0.006	-0.013	0.004	0.000	-0.008	-0.002	0.005	0.003
JSGA4_1	-0.110	-0.004	0.007	-0.012	-0.014	0.003	-0.005	-0.007	-0.001	0.002	0.001	-0.028	-0.049	-0.035	-0.014	-0.022	-0.009	-0.001	-0.008	-0.007	-0.002	0.000
JSGA4_6	-0.112	-0.004	0.012	0.002	-0.005	-0.003	0.000	0.003	0.002	-0.001	-0.003	-0.030	-0.052	-0.033	-0.008	-0.001	-0.001	-0.003	-0.000	0.004	0.006	0.003
JSGAA_3	-0.135	-0.003	0.012	-0.006	-0.002	-0.008	-0.013	-0.001	0.005	-0.005	-0.007	-0.032	-0.053	-0.009	-0.004	-0.009	0.001	-0.003	-0.007	0.002	0.005	-0.006
JSGA_8	-0.125	0.008	0.008	0.013	0.004	-0.014	-0.008	0.004	0.004	-0.001	-0.002	-0.011	-0.021	-0.020	-0.022	-0.001	0.000	-0.015	-0.010	-0.005	-0.001	-0.008
JSGA_8_2	-0.146	-0.004	-0.003	-0.015	-0.011	-0.009	-0.014	-0.003	0.001	-0.003	-0.003	-0.048	-0.037	-0.008	0.001	-0.002	0.009	0.002	-0.002	0.004	0.005	0.003
JSGC1a_1	-0.156	-0.005	0.018	-0.026	-0.007	-0.005	-0.016	-0.002	-0.000	-0.006	-0.006	-0.045	-0.070	-0.010	-0.007	-0.018	0.003	0.001	-0.004	0.003	0.005	-0.002
JSGC1a_2	-0.142	0.002	0.009	-0.022	-0.012	-0.008	-0.013	0.001	0.002	-0.005	-0.001	-0.038	-0.072	-0.018	-0.012	-0.007	0.007	-0.001	-0.007	0.004	0.003	-0.000
JSGC1a_3	-0.144	-0.006	0.013	-0.026	-0.007	-0.002	-0.006	-0.007	0.003	-0.001	-0.003	-0.043	-0.073	-0.015	-0.008	-0.019	0.004	0.001	-0.008	-0.003	0.004	0.004
JSGC1a_4	-0.142	-0.003	0.013	-0.023	-0.008	-0.010	-0.015	-0.008	-0.003	-0.004	-0.005	-0.038	-0.065	-0.013	-0.015	-0.011	0.004	0.001	-0.006	-0.000	0.002	0.002
JSGC1a_5	-0.160	-0.004	0.011	-0.018	-0.013	-0.013	-0.017	-0.005	-0.005	-0.010	-0.006	-0.045	-0.060	-0.016	-0.004	-0.007	0.006	-0.003	-0.006	0.004	0.001	-0.000
JSGC20_6	-0.142	-0.002	0.001	-0.025	-0.008	-0.011	-0.009	0.003	0.002	-0.001	0.001	-0.044	-0.058	-0.003	-0.008	-0.005	0.011	0.002	0.006	0.012	0.010	0.008
JSGG2_1	-0.116	-0.004	-0.004	0.006	0.002	-0.006	-0.012	-0.003	0.003	-0.001	-0.007	-0.028	-0.031	-0.030	-0.018	-0.004	0.002	-0.002	-0.006	0.001	0.003	0.002
JSGG4_5	-0.124	0.008	0.012	-0.006	0.004	0.004	-0.011	-0.000	0.006	0.002	-0.003	-0.024	-0.042	-0.014	-0.014	-0.015	0.007	0.001	-0.010	-0.002	0.003	0.003
JSGG4_6	-0.116	-0.003	0.010	-0.013	-0.005	0.002	-0.009	0.002	0.009	-0.002	-0.002	-0.031	-0.064	-0.021	-0.006	-0.012	0.003	-0.000	-0.011	0.001	0.003	-0.005
JSGG4_7	-0.122	0.004	0.018	-0.012	-0.011	-0.003	-0.009	-0.008	0.002	-0.000	-0.005	-0.033	-0.056	-0.018	-0.001	-0.010	0.001	0.006	-0.005	-0.002	0.003	0.000
JSGG4_8	-0.126	0.003	-0.016	-0.009	-0.005	-0.015	-0.012	-0.001	0.001	-0.006	-0.007	-0.038	-0.037	-0.021	-0.015	0.016	0.013	0.002	-0.002	0.008	0.010	0.005
JSGGneu2	-0.138	0.014	0.003	-0.017	-0.012	-0.009	-0.009	0.000	0.004	-0.001	-0.001	-0.032	-0.059	-0.012	-0.009	-0.006	0.003	0.002	0.000	0.009	0.009	0.003
JSGGneu3	-0.142	-0.007	-0.000	-0.002	-0.020	-0.005	-0.005	0.001	0.002	-0.004	-0.002	-0.038	-0.071	-0.025	-0.011	-0.006	-0.009	-0.004	-0.006	0.002	-0.000	-0.005
JSGO12_2	-0.157	-0.012	-0.001	-0.006	-0.007	-0.007	-0.006	-0.005	-0.000	-0.003	-0.002	-0.048	-0.050	-0.018	-0.004	-0.003	-0.003	-0.004	-0.003	-0.001	-0.000	-0.002
JSGX_5	-0.146	-0.002	-0.001	-0.006	-0.000	-0.013	-0.006	-0.000	-0.001	-0.005	-0.006	-0.045	-0.042	-0.005	-0.004	0.003	0.009	0.001	0.006	0.010	0.008	0.007
J_02_01	-0.140	0.004	0.021	-0.008	-0.016	-0.005	-0.014	-0.008	-0.001	-0.003	-0.002	-0.031	-0.048	-0.016	0.001	-0.015	-0.008	-0.006	-0.009	-0.004	-0.005	-0.007
J_02_03	-0.130	0.002	0.006	-0.016	-0.010	-0.003	-0.006	-0.006	0.003	0.001	-0.006	-0.029	-0.051	-0.027	-0.017	-0.018	-0.004	0.000	-0.010	-0.010	-0.002	-0.002
J_03_01	-0.149	-0.010	-0.003	-0.023	-0.019	-0.016	-0.014	-0.005	-0.008	-0.009	-0.006	-0.046	-0.047	-0.008	-0.012	-0.002	0.003	-0.006	-0.002	0.002	0.001	-0.002
J_03_03	-0.135	-0.005	0.007	-0.007	-0.007	-0.016	-0.012	-0.003	-0.003	-0.006	-0.003	-0.027	-0.052	-0.022	-0.021	-0.003	0.002	-0.012	-0.008	-0.003	-0.004	-0.008
J_03_04	-0.164	0.003	0.005	-0.023	-0.018	-0.023	-0.007	0.005	-0.002	-0.006	0.002	-0.040	-0.036	0.006	-0.010	-0.008	0.000	-0.006	0.004	0.007	-0.001	-0.003
J_03_05	-0.155	0.005	0.001	-0.009	-0.013	-0.004	-0.011	-0.007	-0.001	-0.003	-0.008	-0.041	-0.048	0.001	-0.007	-0.003	0.005	0.004	-0.002	-0.003	0.003	-0.001
K1_24	-0.159	0.011	0.030	-0.017	-0.004	0.001	-0.008	0.004	-0.001	-0.004	-0.003	-0.031	-0.071	-0.002	-0.001	-0.009	0.007	-0.005	-0.007	0.001	-0.003	-0.002
K1_25	-0.128	-0.008	0.014	-0.022	-0.019	-0.020	-0.003	0.001	-0.008	-0.001	0.003	-0.045	-0.042	-0.032	0.024	-0.007	0.009	-0.012	0.006	-0.003	-0.008	-0.001

	A2	A3	A4	A5	A6	A7	A8	A9	A10	A11	A12	B2	B3	B4	B5	B6	B7	B8	B9	B10	B11	B12
K1_26	-0.152	0.007	-0.003	-0.009	-0.004	-0.013	-0.011	0.002	-0.003	-0.007	0.001	-0.030	-0.044	-0.014	-0.012	-0.004	-0.001	-0.010	-0.004	0.003	-0.005	-0.006
K2_31	-0.159	0.004	0.011	-0.020	-0.011	0.000	0.001	-0.003	0.003	0.001	0.000	-0.043	-0.060	-0.010	-0.007	-0.005	0.001	-0.001	-0.005	-0.009	0.003	0.002
K4_53	-0.158	0.005	0.010	-0.016	-0.006	-0.009	-0.006	-0.004	0.000	-0.006	-0.006	-0.045	-0.034	0.001	-0.003	0.001	0.005	0.005	0.001	0.004	0.006	-0.001
K_02_02	-0.160	0.005	0.013	-0.022	-0.016	0.000	-0.003	-0.007	0.002	-0.002	-0.005	-0.044	-0.060	-0.012	-0.003	-0.009	-0.002	0.006	0.001	0.000	0.005	-0.000
K_02_03	-0.149	0.005	-0.005	-0.014	-0.009	-0.007	-0.016	-0.009	-0.008	-0.006	-0.001	-0.032	-0.054	-0.015	-0.023	-0.003	0.003	-0.005	-0.010	0.000	-0.007	0.001
K_08_01	-0.154	0.002	0.002	-0.016	-0.009	-0.006	-0.009	-0.003	-0.007	0.000	-0.003	-0.038	-0.044	-0.014	-0.011	-0.004	0.008	-0.007	-0.003	-0.003	-0.006	0.000
L1_46	-0.157	0.005	0.003	-0.010	-0.009	-0.001	-0.011	0.001	0.002	0.001	-0.001	-0.044	-0.061	-0.018	-0.010	-0.001	0.007	0.008	-0.002	0.008	0.005	0.005
L2_48	-0.124	-0.002	0.001	-0.020	-0.008	-0.015	-0.013	0.000	0.003	-0.004	-0.004	-0.034	-0.048	-0.013	-0.019	0.003	0.012	-0.002	-0.001	0.008	0.007	0.001
L_01_01	-0.134	0.012	0.005	-0.030	-0.011	-0.009	-0.016	-0.001	-0.000	-0.008	-0.007	-0.039	-0.060	-0.003	-0.001	-0.011	0.012	0.002	-0.002	0.009	0.012	0.006
L_06_01	-0.160	0.001	-0.003	-0.018	-0.022	-0.016	-0.014	-0.008	-0.003	0.000	-0.005	-0.046	-0.044	0.009	0.001	-0.007	-0.003	-0.005	-0.005	-0.000	0.002	0.004
L_06_04	-0.137	-0.001	-0.017	-0.034	-0.007	-0.005	-0.008	-0.003	0.001	0.002	0.004	-0.048	-0.053	-0.003	-0.013	-0.009	0.005	0.012	0.002	0.004	-0.001	0.004
L_06_05	-0.146	0.005	0.001	-0.030	-0.022	-0.009	-0.010	-0.010	-0.004	-0.002	-0.002	-0.049	-0.046	-0.006	-0.003	-0.004	0.004	0.010	0.004	0.003	0.002	0.006
M2_01_02	-0.175	0.005	0.004	-0.019	-0.004	-0.004	-0.008	0.003	-0.001	0.000	-0.002	-0.041	-0.056	-0.010	-0.013	-0.012	0.009	-0.004	-0.006	0.000	-0.004	-0.001
M2_02_01	-0.126	-0.003	-0.012	-0.030	-0.003	-0.005	-0.012	-0.008	-0.007	-0.001	-0.003	-0.038	-0.041	-0.006	-0.019	-0.013	0.006	-0.000	0.000	-0.002	-0.001	0.004
M2_02_04	-0.159	0.003	0.005	-0.031	-0.012	-0.017	-0.017	-0.005	-0.007	-0.005	-0.002	-0.042	-0.052	0.004	-0.012	-0.008	0.012	-0.002	-0.002	0.004	0.004	0.004
M2_02_05	-0.135	0.000	-0.000	-0.018	-0.004	-0.017	-0.003	0.003	-0.002	-0.007	-0.008	-0.043	-0.040	0.007	0.003	0.011	0.015	-0.002	0.004	0.009	0.011	0.005
N1_56	-0.157	-0.002	0.003	-0.025	0.006	-0.004	-0.013	-0.002	-0.000	-0.002	0.002	-0.039	-0.058	-0.011	-0.011	-0.019	0.007	-0.004	-0.003	0.006	0.003	-0.002
N2_61	-0.148	-0.005	-0.001	-0.022	-0.009	-0.015	-0.011	0.001	-0.002	-0.005	-0.004	-0.046	-0.061	-0.019	-0.014	-0.005	0.012	0.001	0.002	0.008	0.006	0.005
N_03_01	-0.169	0.002	0.003	-0.010	-0.007	-0.009	-0.017	0.000	0.001	-0.006	-0.006	-0.043	-0.053	-0.011	-0.017	-0.009	0.010	0.003	-0.007	0.005	0.007	0.004
N_03_02	-0.149	-0.002	0.001	-0.022	-0.016	-0.019	-0.015	0.006	-0.001	-0.010	-0.004	-0.039	-0.047	-0.003	-0.012	-0.012	0.009	-0.003	-0.001	0.011	0.004	-0.001
N_05_01	-0.153	0.007	-0.010	-0.020	-0.012	-0.004	-0.017	-0.003	0.002	-0.008	-0.004	-0.044	-0.052	-0.006	-0.003	-0.005	0.009	0.003	-0.009	0.004	0.002	-0.004
O1_64	-0.143	-0.007	0.004	0.000	-0.008	-0.014	-0.004	-0.001	-0.003	-0.007	-0.003	-0.037	-0.035	0.000	-0.006	0.004	-0.001	-0.002	0.001	0.008	-0.001	-0.005
O2_66	-0.154	-0.009	-0.007	-0.014	-0.010	-0.013	-0.013	-0.002	-0.001	-0.008	-0.003	-0.044	-0.040	-0.003	-0.013	-0.006	-0.002	-0.005	-0.006	0.005	0.004	0.000
O2_67	-0.160	0.001	-0.004	-0.016	-0.006	-0.008	-0.015	-0.012	-0.007	-0.005	-0.000	-0.042	-0.054	-0.008	-0.012	-0.006	0.001	0.000	-0.005	-0.001	0.001	0.005
O_07_01	-0.143	-0.022	-0.023	-0.019	-0.014	-0.002	0.001	-0.001	-0.005	-0.004	-0.003	-0.055	-0.038	-0.014	-0.005	-0.005	-0.003	0.000	0.002	-0.000	-0.002	-0.002
O_07_02	-0.136	-0.006	-0.010	-0.009	-0.005	-0.009	-0.006	0.005	0.005	0.005	0.000	-0.041	-0.018	-0.003	-0.010	-0.003	0.010	-0.001	-0.002	0.001	0.005	0.005
O_07_03	-0.138	0.004	0.011	0.003	-0.007	-0.008	-0.004	0.001	0.003	0.002	0.000	-0.023	-0.053	-0.026	-0.020	-0.010	-0.006	-0.006	-0.005	-0.003	-0.004	-0.006
O_07_05	-0.140	0.010	-0.007	-0.029	-0.013	-0.010	-0.014	-0.002	-0.004	-0.008	-0.002	-0.035	-0.063	-0.002	-0.008	-0.006	0.003	-0.002	-0.006	0.004	-0.003	-0.002
O_11_01	-0.152	-0.011	-0.005	-0.017	-0.005	-0.006	-0.004	-0.005	-0.003	-0.001	-0.001	-0.044	-0.047	-0.001	-0.013	-0.004	-0.000	-0.005	-0.005	-0.004	-0.002	-0.001

	A2	A3	A4	A5	A6	A7	A8	A9	A10	A11	A12	B2	B3	B4	B5	B6	B7	B8	B9	B10	B11	B12
O_11_02	-0.139	-0.020	-0.001	-0.007	-0.002	-0.003	-0.006	-0.003	-0.004	0.000	-0.000	-0.044	-0.038	-0.025	-0.010	-0.014	-0.005	-0.005	-0.004	-0.003	-0.002	0.001
O_12_01	-0.139	-0.020	-0.009	-0.014	-0.006	-0.006	-0.011	-0.009	-0.002	-0.001	-0.000	-0.056	-0.036	0.000	0.006	-0.007	0.011	0.002	-0.002	-0.004	-0.000	-0.000
P1_88	-0.152	0.010	0.005	-0.015	-0.004	-0.004	-0.007	-0.003	-0.000	-0.002	-0.003	-0.031	-0.044	-0.011	-0.007	-0.014	-0.002	-0.003	-0.006	-0.002	0.001	-0.001
P_02_01	-0.154	-0.010	-0.021	-0.021	-0.004	-0.013	-0.010	-0.007	-0.004	-0.004	-0.005	-0.055	-0.037	-0.002	-0.016	0.003	0.017	0.002	0.000	0.002	0.008	0.006
P_04_01	-0.136	-0.007	-0.001	-0.006	-0.012	-0.011	-0.001	0.003	-0.000	-0.008	-0.002	-0.036	-0.039	-0.022	-0.009	-0.008	-0.002	-0.008	-0.003	0.004	0.000	-0.001
P_06_01	-0.146	-0.004	-0.002	-0.020	0.006	-0.004	-0.017	-0.007	-0.004	0.001	0.001	-0.039	-0.032	0.006	-0.021	-0.022	0.010	0.004	0.001	0.003	0.003	0.008
R_01_01	-0.159	-0.007	-0.012	-0.015	-0.004	-0.007	-0.014	-0.003	0.005	-0.008	-0.004	-0.054	-0.042	0.009	0.005	-0.000	0.011	-0.001	-0.006	0.007	0.012	0.000
R_03_02	-0.133	-0.004	-0.016	-0.032	-0.010	-0.019	-0.026	-0.014	-0.008	-0.009	-0.013	-0.047	-0.033	0.003	-0.017	0.002	0.019	0.010	0.001	-0.001	0.002	-0.002
R_04_01	-0.171	-0.013	-0.002	-0.023	-0.010	-0.009	-0.012	0.003	0.001	-0.007	-0.003	-0.050	-0.068	0.001	-0.010	-0.003	0.004	-0.006	-0.009	0.002	0.002	-0.005
R_04_02	-0.166	0.003	-0.008	-0.026	-0.002	-0.003	-0.009	0.008	-0.000	-0.005	0.004	-0.052	-0.051	0.009	-0.002	-0.000	0.021	0.008	0.007	0.015	-0.001	0.002
R_06_07	-0.169	0.008	-0.007	-0.029	-0.015	-0.007	-0.007	0.003	-0.004	-0.010	0.002	-0.048	-0.063	0.004	-0.003	0.007	0.007	-0.005	-0.008	0.007	-0.001	-0.004
S_01_01	-0.135	0.008	0.005	-0.021	-0.007	-0.012	-0.008	-0.003	0.003	-0.000	-0.009	-0.032	-0.045	0.001	-0.016	-0.010	0.009	0.005	0.003	0.002	0.009	0.004
S_03_02	-0.157	-0.000	0.004	-0.013	-0.007	-0.005	-0.009	0.003	0.007	0.001	-0.000	-0.044	-0.055	-0.008	-0.005	-0.007	0.002	0.000	-0.007	0.000	0.001	0.001
T_01_01	-0.112	-0.017	-0.008	-0.014	-0.006	-0.006	-0.011	0.000	0.003	-0.004	-0.006	-0.041	-0.039	-0.018	-0.016	-0.004	0.011	0.005	-0.005	0.003	0.006	0.000
T_01_02	-0.147	-0.016	-0.007	-0.014	-0.007	-0.002	-0.005	-0.010	-0.004	-0.004	-0.007	-0.044	-0.041	-0.024	-0.022	-0.015	-0.002	0.003	-0.007	-0.008	-0.000	0.000
T_02_01	-0.156	-0.013	-0.008	-0.010	0.000	-0.003	-0.009	-0.009	-0.002	-0.003	-0.004	-0.052	-0.045	-0.004	-0.011	-0.010	0.008	0.010	0.002	0.000	0.006	-0.000
U1_93	-0.161	-0.018	-0.003	-0.022	-0.007	-0.004	-0.012	-0.001	-0.002	-0.008	-0.004	-0.053	-0.053	-0.000	-0.009	-0.008	0.001	0.002	-0.006	0.004	0.002	-0.002
U_02_01	-0.151	-0.002	0.010	-0.008	-0.001	-0.006	-0.015	-0.013	-0.005	-0.004	-0.005	-0.040	-0.035	0.002	-0.014	-0.009	0.003	0.009	0.004	-0.001	0.003	0.007
V_05_01	-0.128	-0.014	-0.000	-0.010	-0.023	-0.013	-0.006	0.002	-0.002	-0.006	-0.001	-0.049	-0.050	-0.007	0.012	0.007	-0.004	-0.003	0.006	0.010	0.004	0.000
Y_0601	-0.151	-0.008	-0.011	-0.006	-0.007	-0.003	-0.005	-0.004	-0.000	-0.000	-0.001	-0.046	-0.039	-0.002	-0.011	-0.006	0.001	0.001	0.002	0.003	0.005	0.005
Y_07_01	-0.147	-0.005	0.014	-0.006	-0.001	-0.003	-0.006	-0.000	-0.000	0.001	-0.001	-0.034	-0.039	0.001	-0.015	-0.010	0.000	-0.003	-0.003	-0.004	-0.001	0.000
Y_08_01	-0.129	-0.009	0.004	-0.011	0.000	0.001	-0.014	-0.005	0.003	0.003	-0.002	-0.036	-0.042	-0.009	-0.020	-0.012	0.004	0.003	-0.005	-0.001	0.000	0.001
Y_08_02	-0.153	-0.002	0.015	-0.014	-0.016	-0.011	-0.012	-0.008	-0.000	-0.006	-0.011	-0.037	-0.050	0.001	-0.002	-0.011	-0.011	-0.004	-0.001	-0.002	0.001	-0.006
Y_09_01	-0.125	-0.009	-0.003	-0.009	-0.006	-0.003	-0.014	-0.010	-0.003	-0.005	-0.006	-0.033	-0.050	-0.021	-0.015	-0.011	-0.004	-0.004	-0.008	-0.000	0.003	-0.001

Sample	Age	Interpretation (XRD results taken into account)	Coating	Weight-%	C	N	O	F	Na	Mg	Al	Si	P	S	Cl	K	Ca	Ti	Mn	Fe	Cu	Nb	Tc	La	Ce	Nd	Atomic-%	C	N	O	F	Na	Mg	Al	Si	P	S	Cl	K	Ca	Ti	Mn	Fe	Cu	Nb	Tc	La	Ce	Nd
Collection GZN 2013 II, except for *Laxitextella*																																																
Euestheria ? Tongchuan interior TC10 5_2	Middle Triassic	Apatitic composition; Fe	Gold		25.63	-	26.51	3.27	-	-	-	-	14.07	-	-	-	30.08	-	-	0.45	-	-	-	-	-	-		41.23	-	32.01	3.33	-	-	-	-	8.78	-	-	-	14.50	-	-	0.15	-	-	-	-	-	-
Euestheria ? Tongchuan exterior TC10 5_2	Middle Triassic	Apatitic composition	Gold		40.06	-	23.65	-	-	-	-	-	11.41	-	-	-	24.87	-	-	-	-	-	-	-	-	-		57.48	-	25.48	-	-	-	-	-	6.35	-	-	-	10.69	-	-	-	-	-	-	-	-	-
Euestheria ? Tongchuan TC10_7	Middle Triassic	Apatitic composition; Fe	Gold		32.73	-	36.98	4.51	-	-	0.46	0.55	8.29	-	-	0.13	15.89	-	-	0.45	-	-	-	-	-	-		45.52	-	38.61	3.97	-	-	0.29	0.33	4.47	-	-	0.06	6.62	-	-	0.14	-	-	-	-	-	-
Euestheria ? Tongchuan near umbo	Middle Triassic	Apatitic composition; Fe	Gold		24.83	-	35.70	4.92	-	-	0.19	0.67	11.03	-	-	-	21.86	-	-	0.78	-	-	-	-	-	-		37.56	-	40.54	4.71	-	-	0.13	0.44	6.47	-	-	-	9.91	-	-	0.25	-	-	-	-	-	-
Euestheria ? Tongchuan	Middle Triassic	Apatitic composition; Fe	Gold		25.51	-	35.89	4.43	-	-	0.29	0.35	11.21	-	-	-	21.90	-	-	0.44	-	-	-	-	-	-		38.34	-	40.50	4.21	-	-	0.19	0.22	6.53	-	-	-	9.86	-	-	0.14	-	-	-	-	-	-
Euestheria ? Tongchuan exterior	Middle Triassic	Apatitic composition; Fe	Gold		30.69	-	38.55	3.62	-	0.21	0.63	0.79	8.30	-	-	-	16.13	-	-	0.52	-	0.58	-	-	-	-		43.30	-	40.83	3.23	-	0.15	0.40	0.47	4.54	-	-	-	6.82	-	-	0.16	-	0.11	-	-	-	-
Euestheria ? Tongchuan interior	Middle Triassic	Apatitic composition; Rare earth elements	Gold		42.48	-	30.89	2.98	-	-	0.11	-	7.59	-	-	-	15.34	-	-	0.29	-	-	0.33	-	-	-		56.46	-	30.82	2.51	-	-	0.07	-	3.91	-	-	-	6.11	-	-	0.08	-	-	-	0.04	-	-
Laxitextella Coburg 14612	Late Triassic	Apatitic composition; calcium carbonates; with S	Gold		14.03	-	27.00	3.21	0.66	-	-	-	15.92	1.96	-	-	37.22	-	-	-	-	-	-	-	-	-		25.63	-	37.03	3.71	0.63	-	-	-	11.28	1.34	-	-	20.38	-	-	-	-	-	-	-	-	-
Laxitextella Coburg 14612	Late Triassic	Apatitic composition; calcium carbonates; with S	Gold		12.79	-	36.97	5.54	0.87	-	-	-	13.60	1.62	0.14	-	28.46	-	-	-	-	-	-	-	-	-		21.69	-	47.08	5.94	0.78	-	-	-	8.95	1.03	0.08	-	14.47	-	-	-	-	-	-	-	-	-
Laxitextella Coburg 14612 cross-section	Late Triassic	Apatitic composition; calcium carbonates; silicates; with S	Gold		11.92	-	47.90	1.63	0.59	1.00	1.83	3.89	9.09	1.06	0.15	0.70	19.61	-	-	0.63	-	-	-	-	-	-		19.11	-	57.63	1.65	0.50	0.79	1.3	2.67	5.65	0.63	0.08	0.35	9.42	-	-	0.22	-	-	-	-	-	-
Laxitextella Coburg 14612 cross-section	Late Triassic	Apatitic composition; calcium carbonates; silicates; with S	Gold		15.29	-	43.78	4.20	0.76	0.41	0.64	1.24	10.55	1.2	0.14	0.24	21.38	-	-	0.16	-	-	-	-	-	-		24.14	-	51.89	4.19	0.63	0.32	0.45	0.84	6.46	0.71	0.07	0.12	10.12	-	-	0.06	-	-	-	-	-	-
Laxitextella Coburg 14612 cross-section	Late Triassic	Apatitic composition; calcium carbonates; silicates; with S	Gold		16.66	-	40.41	3.08	0.67	0.50	0.96	2.07	11.02	1.29	0.18	0.42	22.42	-	-	0.32	-	-	-	-	-	-		26.62	-	48.47	3.11	0.56	0.39	0.68	1.42	6.83	0.77	0.10	0.21	10.74	-	-	0.11	-	-	-	-	-	-
Yanjiestheria WS 8	Middle-Late Jurassic	Apatitic composition; silicates	Gold		19.68	-	37.19	6.21	1.79	0.80	2.10	4.13	8.76	-	-	0.74	17.01	-	-	1.58	-	-	-	-	-	-		30.46	-	43.21	6.07	1.45	0.61	1.45	2.73	5.25	-	-	0.35	7.89	-	-	0.53	-	-	-	-	-	-
Yanjiestheria WS 8	Middle-Late Jurassic	Apatitic composition; silicates	Gold		19.36	-	38.90	4.60	1.64	0.83	0.84	1.15	10.40	-	0.19	0.20	21.07	-	-	0.82	-	-	-	-	-	-		30.14	-	45.45	4.53	1.33	0.64	0.58	0.76	6.28	-	0.10	0.10	9.83	-	-	0.27	-	-	-	-	-	-
Yanjiestheria WS 8	Middle-Late Jurassic	Apatitic composition	Gold		17.09	-	40.33	6.55	1.50	0.36	0.17	-	11.21	-	-	-	22.04	-	-	0.75	-	-	-	-	-	-		26.84	-	47.56	6.51	1.23	0.28	0.12	-	6.83	-	-	-	10.38	-	-	0.25	-	-	-	-	-	-
Yanjiestheria WS 8 external mould (matrix or silica?)	Middle-Late Jurassic	Matrix minerals (silicates)	Gold		10.60	-	43.45	-	0.52	1.62	11.13	21.71	-	-	-	3.50	0.60	0.57	-	6.29	-	-	-	-	-	-		17.30	-	53.23	-	0.44	1.31	8.09	15.15	-	-	-	1.75	0.29	0.23	-	2.21	-	-	-	-	-	-
Triglypta ? WS 3 exterior, anterior	Middle-Late Jurassic	Apatitic composition; with S	Gold		16.03	-	27.19	3.49	1.22	0.36	0.40	-	15.35	2.59	0.30	-	32.35	-	-	0.72	-	-	-	-	-	-		28.36	-	36.12	3.91	1.13	0.31	0.32	-	10.53	1.72	0.18	-	17.16	-	-	0.27	-	-	-	-	-	-
Triglypta ? WS 3 exterior, near umbo	Middle-Late Jurassic	Apatitic composition; with S	Gold		15.77	-	30.96	4.30	1.51	0.40	0.17	-	14.64	2.40	0.25	-	28.66	-	0.32	0.61	-	-	-	-	-	-		27.07	-	39.90	4.66	1.36	0.34	0.13	-	9.75	1.55	0.15	-	14.74	-	0.12	0.22	-	-	-	-	-	-
Triglypta ? WS 3 mid-carapace	Middle-Late Jurassic	Apatitic composition; with S; some silicates	Gold		16.14	-	27.65	3.19	1.22	0.33	0.56	0.68	15.19	2.53	0.27	-	31.57	-	-	0.67	-	-	-	-	-	-		28.43	-	36.55	3.55	1.12	0.28	0.44	0.51	10.37	1.67	0.16	-	16.66	-	-	0.25	-	-	-	-	-	-
Triglypta ? WS 3 posteroventral	Middle-Late Jurassic	Apatitic composition; with S	Gold		14.52	-	23.71	2.31	1.13	0.42	0.33	-	16.68	3.01	0.33	-	36.93	-	-	0.62	-	-	-	-	-	-		27.08	-	33.19	2.72	1.10	0.38	0.27	-	12.06	2.10	0.21	-	20.63	-	-	0.25	-	-	-	-	-	-
Triglypta WW 9_2 exterior	Middle-Late Jurassic	Apatitic composition; silicates; rare earth elements	Gold		16.11	-	36.57	5.81	0.34	-	0.36	0.45	12.68	-	-	-	26.42	-	-	0.47	-	-	0.79	-	-	-		26.51	-	45.18	6.04	0.29	-	0.26	0.32	8.09	-	-	-	13.03	-	-	0.17	-	-	-	0.11	-	-
Triglypta WW 10_4 exterior	Middle-Late Jurassic	Apatitic composition	Gold		19.74	-	30.45	5.87	-	-	0.33	-	14.78	-	-	-	28.40	-	-	0.43	-	-	-	-	-	-		32.47	-	37.60	6.10	-	-	0.24	-	9.43	-	-	-	14.00	-	-	0.15	-	-	-	-	-	-
Triglypta WW 10_4 external mould	Middle-Late Jurassic	Silicates; iron minerals	Gold		25.64	-	29.05	-	-	1.11	9.34	25.02	-	-	-	3.57	0.41	0.27	-	5.59	-	-	-	-	-	-		39.24	-	33.37	-	-	0.84	6.36	16.37	-	-	-	1.68	0.19	0.10	-	1.84	-	-	-	-	-	-
LXBE V cross-section of welded growth increments (heavily weathered)	Early Cretaceous, Phase 2	Apatitic composition; iron oxides	Gold		14.73	-	34.60	4.81	0.26	0.42	-	-	13.94	-	-	-	30.15	-	-	0.26	-	0.83	-	-	-	-		25.10	-	44.25	5.18	0.23	0.35	-	-	9.21	-	-	-	15.39	-	-	0.10	-	0.18	-	-	-	-
LXBE V cross-section of welded growth increments (heavily weathered)	Early Cretaceous, Phase 2	Apatitic composition; iron oxides	Gold		13.08	-	38.19	7.60	0.30	0.38	0.14	-	12.99	-	-	-	26.98	-	-	0.33	-	-	-	-	-	-		21.74	-	47.66	7.99	0.26	0.31	0.11	-	8.37	-	-	-	13.44	-	-	0.12	-	-	-	-	-	-
JSG AN exterior	Early Cretaceous, Phase 2	Apatitic composition; iron oxides	Gold		16.31	-	39.88	6.18	-	-	0.32	0.84	12.40	-	-	-	23.80	-	-	0.27	-	-	-	-	-	-		26.03	-	47.78	6.24	-	-	0.23	0.57	7.67	-	-	-	11.38	-	-	0.09	-	-	-	-	-	-
JSG AN exterior	Early Cretaceous, Phase 2	Apatitic composition; iron oxides	Gold		16.25	-	33.98	5.54	-	-	0.30	-	14.55	-	-	-	29.12	-	-	0.26	-	-	-	-	-	-		27.17	-	42.64	5.86	-	-	0.22	-	9.43	-	-	-	14.59	-	-	0.09	-	-	-	-	-	-
JSG AN cross-section of intact growth increments	Early Cretaceous, Phase 2	Apatitic composition; iron oxides	Carbon		-	-	46.34	7.59	-	-	1.02	-	14.69	-	-	-	30.06	-	-	0.30	-	-	-	-	-	-		-	-	63.47	8.76	-	-	0.83	-	10.39	-	-	-	16.44	-	-	0.12	-	-	-	-	-	-
JSG AN cross-section of intact growth increments	Early Cretaceous, Phase 2	Apatitic composition; iron oxides	Carbon		-	-	41.44	6.21	-	-	-	-	16.08	-	-	-	35.90	-	-	0.37	-	-	-	-	-	-		-	-	59.70	7.54	-	-	-	-	11.97	-	-	-	20.65	-	-	0.15	-	-	-	-	-	-
JSG AN cross-section2 of intact growth increments	Early Cretaceous, Phase 2	Apatitic composition; iron oxides	Carbon		-	-	42.60	8.19	-	-	-	-	15.91	-	-	-	32.95	-	-	0.36	-	-	-	-	-	-		-	-	60.03	9.72	-	-	-	-	11.58	-	-	-	18.54	-	-	0.14	-	-	-	-	-	-
JSG AN cross-section2 of intact growth increments	Early Cretaceous, Phase 2	Apatitic composition; iron oxides	Carbon		-	-	36.47	4.41	-	-	-	-	17.90	-	-	-	40.63	-	-	0.58	-	-	-	-	-	-		-	-	55.41	5.64	-	-	-	-	14.05	-	-	-	24.64	-	-	0.25	-	-	-	-	-	-
JSG AN cross-section3 of intact growth increments	Early Cretaceous, Phase 2	Apatitic composition; iron oxides	Carbon		-	-	46.61	8.87	-	-	-	-	14.76	-	-	-	29.52	-	-	0.24	-	-	-	-	-	-		-	-	63.37	10.16	-	-	-	-	10.36	-	-	-	16.02	-	-	0.09	-	-	-	-	-	-
JSG AN cross-section3 of intact growth increments	Early Cretaceous, Phase 2	Apatitic composition; silicates; iron oxides	Carbon		-	-	43.53	6.33	-	0.25	0.66	1.30	15.23	-	-	-	32.18	-	-	0.51	-	-	-	-	-	-		-	-	61.30	7.51	-	0.23	0.55	1.04	11.08	-	-	-	18.09	-	-	0.21	-	-	-	-	-	-
JSG O exterior	Early Cretaceous, Phase 3	Apatitic composition	Gold		15.49	-	38.69	7.24	-	-	-	-	12.78	-	-	-	25.81	-	-	-	-	-	-	-	-	-		25.06	-	47.00	7.40	-	-	-	-	8.02	-	-	-	12.52	-	-	-	-	-	-	-	-	-
JSG O	Early Cretaceous, Phase 3	Apatitic composition; rare earth elements	Gold		15.24	-	41.93	7.11	0.30	-	-	-	11.58	-	-	-	23.26	-	-	-	-	-	0.59	-	-	-		24.24	-	50.06	7.15	0.25	-	-	-	7.14	-	-	-	11.09	-	-	-	-	-	-	0.08	-	-
JSG O internal chords (compare Fig. 6c)	Early Cretaceous, Phase 3	Apatitic composition	Gold		16.34	-	44.74	8.58	0.33	-	0.19	0.30	9.81	-	-	-	19.13	-	-	0.58	-	-	-	-	-	-		24.98	-	51.36	8.29	0.26	-	0.13	0.20	5.81	-	-	-	8.77	-	-	-	-	-	-	-	0.19	-
JSG K exterior	Early Cretaceous, Phase 3	Apatitic composition; Na, rare earth elements	Gold		15.23	-	39.19	6.95	0.30	-	-	-	12.25	-	-	-	23.76	-	-	0.18	-	-	0.64	0.85	0.64		24.85	-	48.00	7.17	0.26	-	-	-	7.75	-	-	-	11.61	-	-	0.06	-	-	-	0.09	0.12	0.09
JSG K exterior of internal growth increment	Early Cretaceous, Phase 3	Apatitic composition; Na, rare earth elements	Gold		13.76	-	39.34	7.23	0.32	-	-	-	12.25	-	-	-	24.46	-	-	-	0.28	-	0.73	0.91	0.72		22.79	-	48.93	7.57	0.27	-	-	-	7.87	-	-	-	12.14	-	0.09	-	-	-	-	0.10	0.13	0.10
JSG K interior	Early Cretaceous, Phase 3	Apatitic composition; Na, rare earth elements	Gold		17.09	-	36.41	6.17	0.39	-	-	-	12.42	-	-	-	25.36	-	-	-	-	-	0.65	0.97	0.56		27.96	-	44.72	6.38	0.33	-	-	-	7.88	-	-	-	12.43	-	-	-	-	-	-	0.09	0.14	0.08
JSG K interior	Early Cretaceous, Phase 3	Apatitic composition; Na, rare earth elements	Gold		17.75	-	38.24	5.50	0.39	-	-	-	11.96	-	-	-	24.03	-	-	-	-	-	0.70	0.90	0.54		28.56	-	46.18	5.60	0.33	-	-	-	7.46	-	-	-	11.58	-	-	-	-	-	-	0.10	0.12	0.07
JSG 5−H cross-section	Early Cretaceous, Phase 3	EMP: Fluorapatite																																															
JSG 5−H cross-section of welded growth increments	Early Cretaceous, Phase 3	Apatitic composition; silicates; rare earth elements	Carbon		-	-	29.18	2.15	0.24	-	0.45	1.18	17.92	-	-	-	47.30	-	-	-	-	-	1.58	-	-	-		-	-	48.30	3.00	0.28	-	0.44	1.11	15.32	-	-	-	31.25	-	-	-	-	-	-	0.30	-	-
JSG 5−H cross-section of welded growth increments	Early Cretaceous, Phase 3	Apatitic composition; silicates; rare earth elements	Carbon		-	-	37.33	3.74	0.32	-	0.24	0.53	17.82	-	-	-	38.47	-	-	0.29	-	-	1.26	-	-	-		-	-	56.62	4.78	0.33	-	0.22	0.46	13.96	-	-	-	23.29	-	-	0.13	-	-	-	0.22	-	-
JSG 5−H cross-section of intact growth increments	Early Cretaceous, Phase 3	Apatitic composition	Carbon		-	-	46.92	8.26	-	-	-	-	14.71	-	-	-	30.11	-	-	-	-	-	-	-	-	-		-	-	63.84	9.47	-	-	-	-	10.34	-	-	-	16.35	-	-	-	-	-	-	-	-	-
JSG 5−H cross-section of intact growth increments	Early Cretaceous, Phase 3	Apatitic composition; rare earth elements	Carbon		-	-	36.10	4.62	-	-	-	-	18.03	-	-	-	38.14	-	-	-	-	-	1.10	1.13	0.89		-	-	55.64	6.00	-	-	-	-	14.35	-	-	-	23.46	-	-	-	-	-	0.20	0.20	0.20	0.15
JSG G juvenile, carapace extremely thin	Early Cretaceous, Phase 3	Apatitic composition; rare earth elements; partly silicified	Gold		14.57	-	37.52	6.77	0.34	-	0.69	5.24	11.48	-	-	0.33	21.54	-	-	0.65	-	0.20	-	0.67	-		23.89	-	46.20	7.02	0.29	-	0.51	3.68	7.30	-	-	0.17	10.59	-	-	0.23	-	0.04	-	-	0.09	-
JSG G	Early Cretaceous, Phase 3	Apatitic composition; rare earth elements	Gold		10.60	-	37.38	5.20	-	-	0.16	-	14.46	-	-	-	29.47	-	-	0.21	-	0.46	0.07	0.68	1.31		18.67	-	49.46	5.80	-	-	0.13	-	9.88	-	-	-	15.57	-	-	0.08	-	0.11	0.01	0.10	0.20	-
JSG G exterior	Early Cretaceous, Phase 3	Apatitic composition; rare earth elements	Gold		11.49	-	38.32	4.68	-	-	0.12	-	14.26	-	-	-	29.30	-	-	0.21	-	0.51	0.06	-	1.06		19.88	-	49.78	5.12	-	-	0.09	-	9.57	-	-	-	15.19	-	-	0.08	-	0.11	0.01	-	0.16	-
JSG C exterior	Early Cretaceous, Phase 3	Apatitic composition; rare earth elements	Gold		18.79	-	32.80	3.98	0.34	-	-	-	15.06	-	-	-	28.13	-	-	-	-	-	-	0.89	-		31.07	-	40.73	4.17	0.30	-	-	-	9.66	-	-	-	13.95	-	-	-	-	-	-	-	0.13	-
JSG C interior	Early Cretaceous, Phase 3	Apatitic composition; silicates; iron minerals	Gold		23.80	-	24.48	3.70	-	-	3.75	11.79	9.55	-	-	2.60	15.87	-	-	4.01	0.46	-	-	-	-		38.74	-	29.91	3.81	-	-	2.72	8.21	6.03	-	-	1.30	7.74	-	-	1.40	0.14	-	-	-	-	-
JSG C Sediment (no carapace measurement!)	Early Cretaceous, Phase 3	Silicates; iron minerals	Gold		18.43	-	37.64	-	2.05	0.59	7.25	24.33	-	-	-	2.49	1.03	-	-	5.77	0.42	-	-	-	-		28.77	-	44.10	-	1.67	0.45	5.04	16.24	-	-	-	1.20	0.48	-	-	1.94	0.12	-	-	-	-	-
					-	-	-	-	-	-	-	-	-	-	-	-	-	-	-	-	-	-	-	-	-		-	-	-	-	-	-	-	-	-	-	-	-	-	-	-	-	-	-	-	-	-	-	-
Cyzicus cross-section	modern	Calcium phosphate biominerals	Gold		39.04	-	46.61	-	-	0.53	0.06	-	5.52	-	-	-	8.06	-	-	-	-	0.19	-	-	-	-		49.48	-	44.35	-	-	0.33	0.03	-	2.71	-	-	-	3.06	-	-	-	0.03	-	-	-	-	-
Cyzicus exterior	modern	Calcium phosphate biominerals	Gold		42.05	-	34.85	-	-	0.52	0.34	-	8.47	-	-	-	13.78	-	-	-	-	-	-	-	-	-		55.30	-	34.41	-	-	0.34	0.20	-	4.32	-	-	-	5.43	-	-	-	-	-	-	-	-	-
Cyzicus exterior	modern	Calcium phosphate biominerals; organic material	Gold		47.49	13.34	18.64	-	-	0.29	0.13	-	6.95	-	-	-	13.17	-	-	-	-	-	-	-	-	-		59.55	14.34	17.54	-	-	0.18	0.07	-	3.38	-	-	-	4.95	-	-	-	-	-	-	-	-	-
Cyzicus exterior of an internal growth increment	modern	Calcium phosphate biominerals	Gold		40.61	-	42.21	-	-	0.60	-	-	6.45	-	0.21	-	9.75	-	-	-	0.16	-	-	-	-	-		51.98	-	40.56	-	-	0.38	-	-	3.20	-	0.09	-	3.74	-	-	0.04	-	-	-	-	-	-
Caenestheriella donaciformis cross-section	modern	Calcium phosphate biominerals; ?calcium carbonates (from XRD, p	Gold		34.54	14.08	30.45	-	-	0.29	-	-	5.87	-	-	-	14.78	-	-	-	-	-	-	-	-	-		45.25	15.82	29.95	-	-	0.19	-	-	2.98	-	-	-	5.81	-	-	-	-	-	-	-	-	-
Caenestheriella donaciformis cross-section	modern	Calcium phosphate biominerals; ?calcium carbonates (from XRD, p	Gold		20.45	-	37.06	-	-	0.57	-	-	12.58	-	-	-	27.94	-	-	-	-	1.39	-	-	-	-		32.99	-	44.89	-	-	0.46	-	-	7.87	-	-	-	13.51	-	-	0.29	-	-	-	-	-	-
Caenestheriella donaciformis cross-section	modern	Calcium phosphate biominerals; ?calcium carbonates (from XRD, p	Gold		32.35	7.66	35.98	-	-	0.49	-	-	7.62	-	-	-	15.90	-	-	-	-	-	-	-	-	-		43.78	8.89	36.55	-	-	0.33	-	-	4.00	-	-	-	6.45	-	-	-	-	-	-	-	-	-
Limnadia lenticularis cross-section	modern	Organic material (proteins, chitin)	Gold		48.35	16.79	28.16	-	-	-	0.39	-	-	-	3.88	-	2.43	-	-	-	-	-	-	-	-	-		56.15	16.72	24.55	-	-	-	0.20	-	-	-	1.53	-	0.85	-	-	-	-	-	-	-	-	-
Limnadia lenticularis cross-section	modern	Organic material (proteins, chitin)	Gold		46.34	19.12	28.02	-	-	-	0.31	-	-	-	3.84	-	2.36	-	-	-	-	-	-	-	-	-		53.91	19.08	24.48	-	-	-	0.16	-	-	-	1.51	-	0.82	-	-	-	-	-	-	-	-	-
Limnadia lenticularis cross-section	modern	Organic material (proteins, chitin)	Gold		47.50	17.70	29.04	-	-	-	0.22	-	-	-	3.37	-	2.17	-	-	-	-	-	-	-	-	-		54.99	17.57	25.25	-	-	-	0.12	-	-	-	1.32	-	0.75	-	-	-	-	-	-	-	-	-